A venture into the epigenetics of aging and Alzheimer's Disease

A VENTURE INTO THE EPIGENETICS OF AGING AND ALZHEIMER'S DISEASE

Roy Lardenoije

GRAPHIC DESIGN: Eric Lardenoije
PUBLISHED BY: Roy Lardenoije
ISBN: 978-90-9030435-9
PRINTED BY: Drukkerij De Bink

A VENTURE INTO THE EPIGENETICS OF AGING AND ALZHEIMER'S DISEASE

Dissertation

To obtain the degree of Doctor at Maastricht University, on authority of the Rector Magnificus Prof. dr. Rianne M. Letschert, in accordance with the decision of the Board of Deans, to be defended in public on:
Thursday 7 September 2017, at 16:00 hrs.

by

ROY **LARDENOIJE**

PROMOTORS

Prof. dr. Bart P. F. Rutten
Prof. dr. Harry W. M. Steinbusch

CO-PROMOTORS

Dr. Daniël L. A. van den Hove
Dr. Cynthia A. Lemere (Harvard Medical School, USA)

ASSESSMENT COMMITTEE

Prof. dr. Bert Smeets (Chair)
Dr. Alfredo Ramirez (University of Cologne, Germany)
Dr. Bas Heijmans (Leiden University Medical Center)
Prof. dr. Frans Verhey
Prof. dr. Klaus-Peter Lesch

To mom and dad, for their unwavering faith in me.

Contents

GENERAL INTRODUCTION

Alzheimer's disease (AD) is devastating for mind and body, and aging, something all humans do, is the most important risk factor [1]. AD is mainly feared for the development of cognitive problems such as memory loss, of which it is the most common cause, although clinical symptoms may also include a wide array of aberrations in other functional abilities of the brain and other organs [2, 3]. Apart from the heavy burden on patients, caregivers and/or loved ones, it also presents a massive economic burden, which can be deduced from the estimated 36.5 million cases of dementia worldwide, most of which due to AD [4, 5]. As a consequence of the lack of treatment options and the progressive, yet relatively slow, course of disease, patients with AD require long-time care. This results in high healthcare expenses; amounting to annual costs of $215 billion in 2010 in the United States, which is expected to double by 2040 [6]. However, it is interesting to note that a study found that the prevalence of dementia actually has decreased in recent years, which is thought to be the result of increased education levels [7]. Nevertheless, while breakthroughs in other clinical fields have led to a decrease in deaths due to common age-related diseases such as heart failure, stroke, and cancer, death due to AD has risen to the sixth most common cause of death in the United States [8]. With the increasing geriatric population, AD thus presents a titanic problem for modern society. To understand why no viable strategies to halt or slow disease progression have been developed since the discovery of the disease over a century ago, it is important to get an idea of the complexity of the disease.

AD as it is currently defined, actually comprises two distinct forms of dementia, linked by the occurrence of protein aggregates, the extracellular senile or amyloid plaques, and the intracellular neurofibrillary tangles. The first form, which was originally described by Alzheimer in 1906, is early onset AD, characterized by the development of dementia before the age of 65 years [9]. Although the clinical manifestations of AD dementia had already been described by the ancient Greeks [10], and plaques were first observed by Redlich [11], Alzheimer is thought to be the first to describe tangles [12]. Alzheimer's description of the disease led his colleague Kraepelin to name the disease after him [13]. Interestingly, since this early onset variant of AD is quite rare, it did not receive much scientific attention [14], as did late-onset senile dementia, which was thought to be caused by stiffening of the blood vessels [10]. The second type of AD, late-onset AD, was not defined until the late 1960s, made possible by the discovery of AD pathology in most cases of senile dementia [15, 16]. Thus, with the additional identification of late-onset AD and the technical advances of the last decades, the brunt of AD research was actually performed in the past 25-30 years [14].

Naturally, its diagnosis being based on the presence of plaques and tangles, initial research widely focused on these lesions, leading to the identification of amyloid-β (Aβ) and phosphorylated tau as the main constituents of plaques and tangles, respectively [10]. In parallel, causative genes in families with familial, usually early-onset, AD were investigated, leading to the identification of mutations in the gene encoding the precursor protein of Aβ, *APP*, and in the presenilin genes *PSEN1* and *PSEN2*, which are involved in Aβ processing [10]. These early-onset familial variants of AD can already start to manifest in the late 30s [17]. Although familial AD is much less common than sporadic, usually late-onset, AD, the implication of the *APP* and *PSEN* genes in familial AD has been pivotal for the development of transgenic animal models of AD and mechanistic studies of Aβ and tau neurotoxicity [10]. Of note, no mutations in *MAPT*, the gene encoding tau, have been associated with AD, although other forms of dementia are associated with *MAPT* mutations [10].

Sporadic AD has a much less obvious genetic origin, however, as no mutations in *APP*, *PSEN1*, or *PSEN2* are associated with this form of AD. For some time *APOE* allele 4 was the only genetic risk factor associated with sporadic AD [18], and remains the factor conveying the highest risk for developing sporadic AD [19]. The advent of large-scale genome-wide association studies (GWAS) has led to the identification of several additional loci associated with sporadic AD [20, 21], the largest of which included 74,046 subjects and identified 20 AD-associated loci in genes involved in Aβ and tau processing, immune system function, endocytosis, and lipid transport [22]. Even though early- and late-onset AD are both associated with plaques and tangles, it remains largely unknown how most of the genetic risk factors associated with late-onset AD lead to these pathological hallmarks [1].

Apart from genetic susceptibility, there are likely also other factors at play that affect the manifestation of AD. Indeed, a wide array of conditions and environmental exposures have been identified that may influence, either in a negative or positive sense, the development of AD [1, 23]. Pre-existing conditions increasing the risk for developing AD include obesity, hypertension, stroke, and diabetes [1]. In general, vascular risk factors, factors affecting the brain's glucose metabolism, and stress can also be considered as risk factors for AD [24–26]. The link between stress and AD is thought to be mediated through the immune system [1, 27]. In line with these risk factors, it was found that regular physical activity and a healthy diet, including fish (omega-3), but with limited sugar and saturated fat intake, may be protective against AD dementia [28–31]. Another protective lifestyle factor is being frequently engaged in mentally complex and demanding activities [32]. This may lead to more extensive

dendritic connections than required for normal functioning. Such a 'cognitive reserve' may reinforce the threshold for cognitive impairment in the face of progressive neurodegeneration, and may explain why the presence of AD pathological hallmarks in the brain is no guarantee for clinical dementia.

Interestingly, the exceedingly complex and possibly life-long etiopathogenesis of AD is exemplified by a study showing a decrease in the prevalence of late-onset AD due to an increase in education levels [7]. Even more perplexing may be the finding that having a high sense of purpose in life is associated with lower AD pathology and cognitive impairment [33]. Indeed, general psychological well-being is associated with lower AD pathology [34]. It has furthermore been found that symptoms of affective psychopathology precede cognitive problems in patients with AD [35]. Affective issues may thus drive neuropathology, be an early sign of neuropathology, or both. The first possibility raises the critical question whether treatment strategies based solely on the neuropathology, neglecting the affective component of AD, are ineffective by design. Could, in case of late-onset AD, the pre-clinical identification of patients at risk of conversion to AD dementia, followed by psychological and behavioral therapy, possibly complemented with pharmacotherapeutic interventions focused on affective dysregulation, aid in forestalling the development of AD dementia?

To investigate such questions and advance the field of AD research, it must first be possible to identify people who will develop AD dementia, which in turn requires insight into the pre-clinical stages of the disease. From the brief history of AD research above, it appears that sporadic AD may arise due to the concerted effects of genetic susceptibility and exposure to environmental risk factors [36]. Recent years have seen an extensive deepening of our understanding of epigenetic regulation of gene expression, followed by a widespread invasion of epigenetics studies in complex afflictions such as depression, psychosis, and neurodegeneration [37–39]. Epigenetics has moved from being regarded as a programmed process of gene silencing during cell differentiation and development, to being identified as a delicate, crucial regulatory system involved in translating environmental exposures to changes in gene expression and even poses a means of transgenerational inheritance that transcends genetic mutations [40, 41]. Such complex regulation is established through multiple layers of effector mechanisms, including DNA and chromatin modifications, and non-coding RNAs [39]. As a mediator between genetic and environmental factors, epigenetic markers may thus offer a unique window into the etiopathogenesis of sporadic AD before the onset of clinical signs. With age being the most important risk factor for developing AD, it will also be critical to investigate how

age-related epigenetic alterations may facilitate age-related diseases and, thus, how healthy aging differs epigenetically from pathologic aging leading to diseases such as AD.

Overview of thesis

The research compiled in this thesis can be divided in three parts. The first two chapters comprise reviews providing a broad introduction to epigenetics, aging, AD, and the study thereof. The following three chapters involve investigations of global levels of epigenetic markers in relation to aging and AD, making use of animal models. Finally, three epigenome-wide association studies (EWAS) in relation to AD are presented, covering both the brain and the blood.

While this general introduction only briefly touches epigenetic regulation itself, **CHAPTER 2** offers an in-depth discussion of the various layers of epigenetic control over transcription and translation. Additionally, it provides an overview of epigenetic dysregulation in aging and neurodegeneration, specifically in AD, Parkinson's disease, and Huntington's disease, as well as an outlook on therapeutic strategies based on epigenetic principles. It concludes with an exploration of the challenges the field of epigenetics research currently faces and how these may be tackled in future research.

As many critical insights into cognitive dysfunction, as observed in AD, and the exploration of therapeutic interventions can be attributed to animal model research, **CHAPTER 3** constitutes a concise overview of available rodent animal models for the study of cognitive impairment and neurodegenerative diseases. The chapter covers both pharmacological and transgenic animal models and also presents options beyond AD.

With aging being the principal risk factor for AD, **CHAPTER 4** investigates age-related changes in global DNA methylation and hydroxymethylation levels in mouse cerebellar Purkinje cells, cells that are particularly vulnerable to aging. It was also studied whether the known interference of caloric restriction and increased anti-oxidant levels with age-related deterioration might be mediated through epigenetic mechanisms, as reflected in the global DNA methylation and hydroxymethylation levels.

Global age-related epigenetic alterations in rodent animal models expressing mutant *APP*, both mutant *APP* and *PSEN1*, or a combination of mutant *APP*, *PSEN1* and *MAPT*, and a nonhuman primate model of sporadic AD are investigated in **CHAPTER 5**. This study focused on the hippocampus, one of the primary brain regions affected in AD.

In **CHAPTER 6** the epigenetic ramifications of active Aβ immunotherapy in APPswe/PS1dE9 mice are investigated. Specifically, the effects of lowering Aβ plaque pathology on global DNA methylation and hydroxymethylation levels, as well as DNA methyltransferase (DNMT) 3A, responsible for *de novo* DNA methylation, were determined in the hippocampus. Correlations between these epigenetic players and measures of cognition were also established.

CHAPTER 7 moves from animal models to the human brain, comparing the methylome and hydroxymethylome of AD patients and age-matched healthy controls. Differentially methylated, hydroxymethylated, and unmodified cytosine positions were investigated, as well as altered genomic regions.

CHAPTER 8 features an exploration of the blood methylome associated with AD, while also looking at the overlap with methylomic changes observed in subjects with mild cognitive impairment (MCI). The relationship of the AD methylomic profile with other established measures of clinical AD, including cognitive performance, levels of Aβ and tau in the cerebrospinal fluid, and hippocampal volume, was also investigated.

The final study included within this thesis, as described in **CHAPTER 9**, ventured into the pre-clinical stage of AD and identified the blood methylomic signature associated with conversion to AD dementia. Additionally, methylomic markers showing differential time-related changes in converters and non-converters were observed, which may represent signs of vulnerability or resilience to conversion to AD dementia. The identified markers not only offer mechanistic insight into AD etiopathogenesis, but may also act as potential biomarkers.

In its totality, the work gathered in this thesis covers a wide spectrum of studies, including multiple species, tissues, and techniques, geared towards advancing our understanding of the epigenetic involvement in AD versus healthy aging, and in addition provide novel diagnostic candidates.

REFERENCES

[1] Robinson M, Lee BY, Hane FT. Recent Progress in Alzheimer's Disease Research, Part 2: Genetics and Epidemiology. *J Alzheimers Dis* 2017; 57: 317–330.

[2] Bediou B, Ryff I, Mercier B, et al. Impaired Social Cognition in Mild Alzheimer Disease. *J Geriatr Psychiatry Neurol* 2009; 22: 130–140.

[3] Budson AE, Solomon PR. New criteria for Alzheimer disease and mild cognitive impairment: implications for the practicing clinician. *Neurologist* 2012; 18: 356–363.

[4] Ferri CP, Prince M, Brayne C, et al. Global prevalence of dementia: a Delphi consensus study. *Lancet* 2005; 366: 2112–2117.

[5] Sosa-Ortiz AL, Acosta-Castillo I, Prince MJ. Epidemiology of dementias and Alzheimer's disease. Arch Med Res 2012; 43: 600–608.

[6] Hurd MD, Martorell P, Delavande A, et al. Monetary Costs of Dementia in the United States. *N Engl J Med* 2013; 368: 1326–1334.

[7] Langa KM, Larson EB, Crimmins EM, et al. A Comparison of the Prevalence of Dementia in the United States in 2000 and 2012. *JAMA Intern Med* 2017; 177: 51–58.

[8] Alzheimer's Association. 2015 Alzheimer's disease facts and figures. *Alzheimers Dement* 2015; 11: 332–84.

[9] Alzheimer A. Über eine eigenartige Erkrankung der Hirnrinde. *Allg Zeitschrift fur*

Psychiatr und Psych Medizin 1907; 64: 146–148.

[10] Hardy J, Saura CA, Choi SY, et al. A hundred years of Alzheimer's disease research. *Neuron* 2006; 52: 3–13.

[11] Redlich F. Uber miliare Sklerose der Hirnrinde bei seniler Atrophie. *Jarbucher fur Psychiatr und Neurol*; 17.

[12] Perusini G. The nosographic value of some characteristic histopathologic findings in senility. *Riv Ital di Neuropathol Psichiatr ed Elettroterapia* 1991; 4: 193–213.

[13] Kraepelin E. Das senile und prasenile Irreseine. *Psychiatr ein Lehrb fur Stud und Arzte* 1910; 593–632.

[14] Altman J. Alzheimer: 100 Years and Beyondhttp://www.alzforum.org/news/conference-coverage/alzheimer-100-years-and-beyond (2007, accessed 11 May 2017).

[15] Blessed G, Tomlinson BE, Roth M. The association between quantitative measures of dementia and of senile change in the cerebral grey matter of elderly subjects. *Br J Psychiatry 1968*; 114: 797–811.

[16] Tomlinson BE, Blessed G, Roth M. Observations on the brains of demented old people. *J Neurol Sci* 1970; 11: 205–42.

[17] Martin JJ, Gheuens J, Bruyland M, et al. Early-onset Alzheimer's disease in 2 large Belgian families. *Neurology* 1991; 41: 62–8.

[18] Corder EH, Saunders AM, Strittmatter WJ, et al. Gene dose of apolipoprotein E type 4 allele and the risk of Alzheimer's disease in late onset families. *Science* 1993; 261: 921–3.

[19] Farrer LA, Adrienne Cupples L, Van Duijn CM, et al. Apolipoprotein E genotype in patients with alzheimer's disease: Implications for the risk of dementia among relatives. *Ann Neurol* 1995; 38: 797–808.

[20] Medway C, Morgan K. Review: The genetics of Alzheimer's disease; putting flesh on the bones. *Neuropathol Appl Neurobiol* 2014; 40: 97–105.

[21] Tosto G, Reitz C. Genome-wide Association Studies in Alzheimer's Disease: A Review. *Curr Neurol Neurosci Rep* 2013; 13: 381.

[22] Lambert J-C, Ibrahim-Verbaas CA, Harold D, et al. Meta-analysis of 74,046 individuals identifies 11 new susceptibility loci for Alzheimer's disease. *Nat Genet* 2013; 45: 1452–1458.

[23] Chouliaras L, Rutten BPF, Kenis G, et al. Epigenetic regulation in the pathophysiology of Alzheimer's disease. *Prog Neurobiol* 2010; 90: 498–510.

[24] Li J, Wang YJ, Zhang M, et al. Vascular risk factors promote conversion from mild cognitive impairment to Alzheimer disease. *Neurology* 2011; 76: 1485–1491.

[25] Baker LD, Cross DJ, Minoshima S, et al. Insulin Resistance and Alzheimer-like Reductions in Regional Cerebral Glucose Metabolism for Cognitively Normal Adults With Prediabetes or Early Type 2 Diabetes. *Arch Neurol* 2011; 68: 51–7.

[26] Sotiropoulos I, Catania C, Pinto LG, et al. Stress acts cumulatively to precipitate Alzheimer's disease-like tau pathology and cognitive deficits. *J Neurosci* 2011; 31: 7840–7.

[27] Cohen S, Janicki-Deverts D, Doyle WJ, et al. Chronic stress, glucocorticoid receptor resistance, inflammation, and disease risk. *Proc Natl Acad Sci U S A* 2012; 109: 5995–9.

[28] Buchman AS, Boyle PA, Yu L, et al. Total daily physical activity and the risk of AD and cognitive decline in older adults. *Neurology* 2012; 78: 1323–1329.

[29] Hardman RJ, Kennedy G, Macpherson H, et al. Adherence to a Mediterranean-Style Diet and Effects on Cognition in Adults: A Qualitative Evaluation and Systematic Review of Longitudinal and Prospective Trials. *Front Nutr* 2016; 3: 22.

[30] Francis H, Stevenson R. The longer-term impacts of Western diet on human cognition and the brain. *Appetite* 2013; 63: 119–28.

[31] Huang TL. Omega-3 Fatty Acids, Cognitive Decline, and Alzheimer's Disease: A Critical Review and Evaluation of the Literature. *J Alzheimer's Dis* 2010; 21: 673–690.

[32] Stern Y. Cognitive reserve in ageing and Alzheimer's disease. *Lancet Neurol* 2012; 11: 1006–1012.

[33] Boyle PA, Buchman AS, Wilson RS, et al. Effect of purpose in life on the relation between Alzheimer disease pathologic changes on cognitive function in advanced age. *Arch Gen*

Psychiatry 2012; 69: 499–505.
[34] Chen ST, Siddarth P, Saito NY, et al. Psychological well-being and regional brain amyloid and tau in mild cognitive impairment. *Am J Geriatr Psychiatry* 2014; 22: 362–9.
[35] Babulal GM, Ghoshal N, Head D, et al. Mood Changes in Cognitively Normal Older Adults are Linked to Alzheimer Disease Biomarker Levels. *Am J Geriatr Psychiatry* 2016; 24: 1095–1104.
[36] Lahiri DK, Maloney B, Zawia NH. The LEARn model: an epigenetic explanation for idiopathic neurobiological diseases. *Mol Psychiatry* 2009; 14: 992–1003.
[37] Januar V, Saffery R, Ryan J. Epigenetics and depressive disorders: a review of current progress and future directions. *Int J Epidemiol* 2015; 44: 1364–1387.
[38] Pishva E, Kenis G, van den Hove D, et al. The epigenome and postnatal environmental influences in psychotic disorders. *Soc Psychiatry Psychiatr Epidemiol* 2014; 49: 337–348.
[39] Lardenoije R, Iatrou A, Kenis G, et al. The epigenetics of aging and neurodegeneration. *Prog Neurobiol* 2015; 131: 21–64.
[40] Goldberg AD, Allis CD, Bernstein E. Epigenetics: A Landscape Takes Shape. *Cell* 2007; 128: 635–638.
[41] Nagy C, Turecki G. Transgenerational epigenetic inheritance: an open discussion. *Epigenomics* 2015; 7: 781–790.

THE EPIGENETICS OF AGING AND NEURODEGENERATION

ROY **LARDENOIJE**[A], ARTEMIS **IATROU**[A], GUNTER **KENIS**[A], KONSTANTINOS **KOMPOTIS**[B], HARRY W. M. **STEINBUSCH**[A], DIEGO **MASTRONI**[A, C], PAUL **COLEMAN**[C], CYNTHIA A. **LEMERE**[D], PATRICK R. **HOF**[E], DANIËL L. A. VAN **DEN HOVE**[A, F, *], BART P. F. **RUTTEN**[A, *]

[A] SCHOOL FOR MENTAL HEALTH AND NEUROSCIENCE (MHENS), DEPARTMENT OF PSYCHIATRY AND NEUROPSYCHOLOGY, MAASTRICHT UNIVERSITY, UNIVERSITEITSSINGEL 50, 6200 MD MAASTRICHT, THE NETHERLANDS

[B] CENTER FOR INTEGRATIVE GENOMICS, UNIVERSITY OF LAUSANNE, GENOPODE BUILDING, 1015 LAUSANNE-DORIGNY, SWITZERLAND

[C] L.J. ROBERTS ALZHEIMER'S DISEASE CENTER, BANNER SUN HEALTH RESEARCH INSTITUTE, 10515 W. SANTA FE DRIVE, SUN CITY, AZ 85351, USA

[D] CENTER FOR NEUROLOGIC DISEASES, DEPARTMENT OF NEUROLOGY, BRIGHAM AND WOMEN'S HOSPITAL, HARVARD MEDICAL SCHOOL, 77 AVENUE LOUIS PASTEUR, BOSTON, MA 02115, USA

[E] FISHBERG DEPARTMENT OF NEUROSCIENCE AND FRIEDMAN BRAIN INSTITUTE, ICAHN SCHOOL OF MEDICINE AT MOUNT SINAI, ONE GUSTAVE L. LEVY PLACE, NEW YORK, NY 10029, USA

[F] LABORATORY OF TRANSLATIONAL NEUROSCIENCE, DEPARTMENT OF PSYCHIATRY, PSYCHOSOMATICS AND PSYCHOTHERAPY, UNIVERSITY OF WUERZBURG, FUECHSLEINSTRASSE 15, 97080 WUERZBURG, GERMANY

[*] THESE AUTHORS CONTRIBUTED EQUALLY TO THIS WORK.

Progress in Neurobiology 131:21-64
(2015)

Abstract

Epigenetics is a quickly growing field encompassing mechanisms regulating gene expression that do not involve changes in the genotype. Epigenetics is of increasing relevance to neuroscience, with epigenetic mechanisms being implicated in brain development and neuronal differentiation, as well as in more dynamic processes related to cognition. Epigenetic regulation covers multiple levels of gene expression; from direct modifications of the DNA and histone tails, regulating the level of transcription, to interactions with messenger RNAs, regulating the level of translation. Importantly, epigenetic dysregulation currently garners much attention as a pivotal player in aging and age-related neurodegenerative disorders, such as Alzheimer's disease, Parkinson's disease, and Huntington's disease, where it may mediate interactions between genetic and environmental risk factors, or directly interact with disease-specific pathological factors. We review current knowledge about the major epigenetic mechanisms, including DNA methylation and DNA demethylation, chromatin remodeling and noncoding RNAs, as well as the involvement of these mechanisms in normal aging and in the pathophysiology of the most common neurodegenerative diseases. Additionally, we examine the current state of epigenetics-based therapeutic strategies for these diseases, which either aim to restore the epigenetic homeostasis or skew it to a favorable direction to counter disease pathology. Finally, methodological challenges of epigenetic investigations and future perspectives are discussed.

KEYWORDS: Epigenetics; aging; neurodegeneration; Alzheimer's disease; Parkinson's disease; Huntington's disease

2.1 Epigenetics

Conrad Hal Waddington coined the term “epigenetics” in 1942, an event commonly viewed as the birth of epigenetics as it developed from a phenomenon to an immensely studied branch of science [1]. A merger between the terms “genetics” and “epigenesis”, the concept of epigenetics in a way represents the association of two views on development that have been clashing at least since the time of Hippocrates and Aristotle [2]. Hippocrates proposed what became known as the preformationist view of development; all parts of a mature organism are already present at the embryonic stage, albeit in a miniature stage, and they simply grow during development. Aristotle argued against this preformationist view, providing an alternative explanation that lies at the foundation of the epigenesis concept: embryonic development involves the formation of new parts. After numerous scientific discoveries, these views evolved over the centuries. A contemporary preformationist would hold that all that is needed to generate a mature organism is its genetic code, whereas a supporter of epigenesis would argue that the genome only holds the information of building blocks – but that how these are put together depends on environmental influences. The contemporary perspective of “epigenetics” is that of the field of science that studies how changes in gene expression occur without changes in the DNA sequence [1]. Such changes can be induced by environmental factors, while some are more programmed, as seen during cell differentiation. As such, these epigenetic alterations can be highly stable, such as those resulting from genetic imprinting, or dynamic such as the epigenetic changes associated with memory. Many epigenetic modifications can be inherited through mitosis and some have even found to be transgenerational [3–6]. Thus, whereas genetic alterations usually reflect permanent changes of the DNA sequence, epigenetic changes are mediated through processes that are in principle reversible [7]. While environmental influences can potentially alter the phenotype of an organism by interacting with and by acting on both the genome and epigenome [8], the reversible nature of epigenetic changes makes them more suitable as candidates for clinical interventions [9]. Over the past decade there have been ample studies investigating the contributions of epigenetic modifications to aging and age-related neurodegenerative diseases, including Alzheimer’s disease (AD), Parkinson’s disease (PD) and Huntington’s disease (HD). The epigenetic machinery covers multiple levels of control, including DNA methylation and hydroxymethylation, chromatin remodeling, and non-coding RNA (ncRNA) regulation [10]. See Figure 1 for a general overview of the epigenetic mechanisms discussed below.

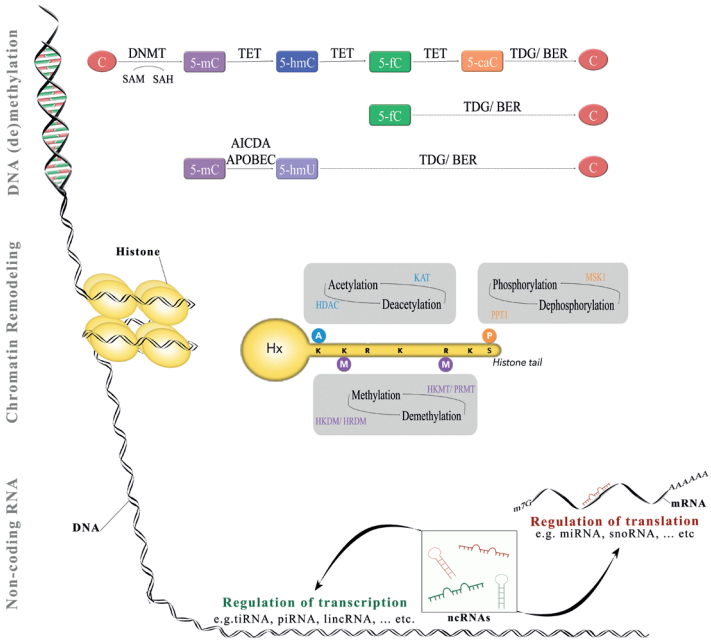

FIGURE 1. The three levels of epigenetic regulation. The upper section summarizes DNA methylation and demethylation processes, the middle section summarizes the most important chromatin remodeling processes, and the bottom section summarizes non-coding RNA regulation.
ABBREVIATIONS: *5*-caC, *5*-carboxylcytosine; *5*-fC, *5*-formylcytosine; *5*-hmC, *5*-hydroxymethylcytosine; *5*-hmU, *5*-hydroxymethyluracil; *5*-mC, *5*-methylcytosine; A, acetyl modification; AICDA, activation-induced cytidine deaminase; APOBEC, apolipoprotein B mRNA editing enzyme, catalytic polypeptide-like protein; BER, base excision repair; C, cytosine; DNMT, DNA methyltransferase; H, histone; HDAC, histone deacetylase; HKDM, histone lysine demethylase; HKMT, histone lysine methyltransferase; HRDM, histone arginine demethylase; K, lysine; KAT, lysine acetyltransferase; lincRNA, large intergenic non-coding RNA; M, methyl modification; miRNA, micro RNA; MSK1, mitogen- and stress-activated protein kinase 1; ncRNA, non-coding RNA; P, phosphate modification; piRNA, piwi-interacting RNA; PPT1, protein phosphatase 1; PRMT, protein arginine methyltransferase; R, arginine; SAH, S-adenosylhomocysteine; SAM, S-adenosylmethionine; snoRNA, small nucleolar RNA; TDG, thymine DNA glycosylase; TET, ten-eleven translocation; tiRNA, transcription initiation RNA; tRNA, transfer RNA.

2.1.1. DNA methylation

The best characterized epigenetic modification, DNA methylation involves the addition of a methyl group at the 5 position on the pyrimidine ring of cytosines, creating 5-methylcytosine (5-mC) [11]. These modifications primarily occur at cytosine-phosphate-guanine (CpG) islands. Recently, however, non-CpG methylation has received increased attention [12]. Apart from cytosines, there are also reports of guanine and adenine methylation, resulting in 7-methylguanine (7-mG) and 3-methyladenine, respectively [13]. In this review, however, DNA methylation refers exclusively to 5-mC, unless mentioned otherwise. Generally, DNA methylation is associated with transcriptional repression and is mostly found in heterochromatin [14], while the euchromatin typically contains low amounts of methylated DNA. Some genes, however, are suspected to show enhanced expression when hypermethylated [15]. Additionally, DNA methylation within gene bodies (the transcribed portion of a gene) has been implicated in alternative splicing [16, 17]. How DNA methylation exactly affects gene transcription is highly dependent on the location in or around the gene [18]. In promoter regions, methylated DNA can directly disrupt the transcriptional process by interfering with the binding of transcription factors [19]. Additional repression can be established through the attraction of methyl-CpG-binding domain proteins (MBDs) and subsequent activation of the histone tail modifying machinery,

leading ultimately to chromatin compaction [20]. How gene expression is enhanced through methylation of gene bodies remains unclear.

Although DNA methylation is the most stable epigenetic modification, the DNA methylation profile, or 'methylome', is highly dynamic [21–23]. DNA methylation profiles are, at least partly, heritable, both after cell division, as well as in a transgenerational fashion [24, 25]. Heritable DNA methylation needs to be copied to the newly synthesized DNA strand, a process that is referred to as maintenance DNA methylation. The addition of completely new DNA methylation marks is called *de novo* DNA methylation. DNA methyltransferases (DNMT) are responsible for maintenance and *de novo* DNA methylation [26]. There are four known types of DNMTs; DNMT1, DNMT2, DNMT3A and DNMT3B, all of which use S-adenosylmethionine (SAM) as the methyl donor [19, 26]. Note, however, that DNMT2 was actually found to be a RNA methyltransferase [27]. Furthermore, there is another DNMT, DNMT3-like (DNMT3L), which exhibits no enzymatic activity, but detects unmethylated lysine 4 of histone H3 tails (H3K4) and recruits or activates DNMT3A [28]. Interestingly, the DNMT3B splice variants DNMT3B3 and DNMT3B4 are also inactive and play a regulatory role in *de novo* DNA methylation [29]. DNMT1 is the most common variant in somatic cells and primarily involved in maintenance DNA methylation, and DNMT3A and DNMT3B are responsible for *de novo* DNA methylation [30]. DNMT3A and DNMT3B isoforms are expressed in a more cell-type-specific manner [12, 30].

It is worth mentioning that the methyl donor of the DNMTs, SAM, is generated through a complex cycle and is the methyl donor of numerous additional transmethylation reactions [31, 32]. This cycle starts with the conversion of tetrahydrofolate (THF) to 5,10-methylenetetrahydrofolate (MTHF) by vitamin B6-dependent serine hydroxymethyltransferase (SHMT), and the subsequent conversion of 5,10-MTHF to 5-MTHF by B2-dependent MTHF reductase (MTHFR). 5-MTHF acts as the methyl donor for the methylation of homocysteine (Hcy), producing methionine, by cobalamin-dependent methionine synthase (MetH). SAM is subsequently generated from methionine by methionine adenosyltransferase (MAT). During methyltransferase reactions SAM is converted to S-adenosylhomocysteine (SAH), which is further hydrolyzed to Hcy and adenosine by SAH hydrolase (SAHH). Folate serves as cardinal input for this cycle and the proper elimination of Hcy and adenosine is important to maintain homeostasis. For instance, global DNA hypomethylation could be induced through folate deficiency and high levels of Hcy [31].

As DNA methylation can be relatively simple and robustly assessed using genomic DNA, it has been the primary focus of human epidemiological epigenetic research [33]. Early investigations into DNA methylation

showed its cardinal importance in the proliferation and differentiation of neural stem cells [34]. More recently, it has been established that DNA methylation is pivotal for synaptic plasticity, neuronal repair, neuronal survival, and learning and memory [35–37]. Such dynamic processes are more dependent on *de novo* methylation, although the importance of maintenance DNA methylation should not be underestimated, as a loss of DNMT1 was shown to result in increased histone acetylation, a disruption of the nuclear organization and eventually cell death [35, 38–41]. Since these are factors disturbed in a neurodegenerative state, DNA methylation is a valid target when investigating neurodegeneration.

2.1.2. DNA demethylation

While DNA methylation is a well-established epigenetic mechanism, the existence of active DNA demethylation in animals has long been a point of controversy [42]. Observations such as high levels of DNMTs in nondividing cells [43] and a significant decrease in methylated DNA levels when DNA methylation is blocked [14, 22], despite the stability of the 5-mC mark, have led to an avid search for the players responsible for an active demethylation process. This search generated several mechanisms, including an RNA-dependent pathway by which the methyl group is removed from 5-mC, a pathway involving the nucleotide excision repair mechanism, and a base excision repair based pathway [21, 44–47].

Although still a point of discussion, the base excision repair pathway is a prime candidate as the primary road to demethylation in post-mitotic neurons [45], which does not exclude the possibility of multiple overlapping demethylation pathways. DNA demethylation is thought to be initiated by the oxidation of 5-mC into 5-hydroxymethylcytosine (5-hmC) by the ten-eleven translocation (TET) proteins [48, 49]. There are 3 TET proteins, TET1, TET2 and TET3, which are differentially expressed and regulated throughout the body [50]. Interestingly, in the last few years 5-hmC was shown to be an important epigenetic marker that is functionally different from 5-mC [51]. While DNA hydroxymethylation is generally associated with increased gene activity, work by Jin et al. [52] indicates that this correlation does not always hold and depends on the location of 5-hmC in the gene and the CpG content. 5-hmC is present in most tissues and cell types, but is especially enriched in the brain [53], with cerebellar Purkinje cells exhibiting some of the highest levels [54]. Furthermore, in the frontal cortex, 5-hmC is selectively enriched in promoter and intragenic regions [52]. Interestingly, 5-hmC levels are particularly low in stem cell-rich areas [53, 55]. In addition to the formation of 5-hmC, it has recently been discovered that TET enzymes can further oxidize 5-hmC to 5-formylcytosine (5-fC), and 5-fC to 5-carboxylcytosine

(5-caC) [49]. Although it is generally accepted that 5-hmC is a functional epigenetic marker, such a role remains to be established for 5-fC and 5-caC [56, 57]. Apart from oxidation, 5-mC and 5-hmC can be deaminated instead, by either activation-induced cytidine deaminase (AICDA) or apolipoprotein B mRNA editing enzyme, catalytic polypeptide-like protein (APOBEC), resulting in thymidine or 5-hydroxymethyluracil (5-hmU) [48, 58]. 5-caC, thymidine or 5-hmU present a mismatch in the base pairing of the DNA sequence (5-caC:G, T:G or 5-hmU:G, respectively). Such a mismatch can be detected and mended through the removal of the transformed bases by thymidine or uracil glycosylases [48, 59–61]. Alternatively, 5-fC and 5-caC can be changed back to cytosine by removal of formic acid or decarboxylation, respectively [49]. In addition to the aforementioned enzymes, the growth arrest and DNA damage 45 (GADD45) proteins are crucially involved in directing the activity of these enzymes, thereby assisting in the localization of demethylation activity to specific gene promoters [44, 62–64]. Clearly, the exact mechanisms underlying DNA demethylation remain to be elucidated.

2.1.3. Chromatin remodeling

Chromatin can be seen as a string of nucleosomes, which mainly consist of DNA and the histones around which it is wrapped. There are five types of histone proteins; H2A, H2B, H3, and H4 forming the octameric core of the nucleosome, and H1 serving as a linker and stabilizer, binding to DNA among nucleosomes [32, 65]. The conformation of these histones largely determines the accessibility of the DNA for transcription, and can be adjusted through reversible modifications of their N-terminal tails. Such modifications include lysine (K), arginine (R) or histidine (His) methylation [66], K acetylation [67], serine (S), threonine (T) or tyrosine (Y) phosphorylation [68], ubiquitination [69], adenosine diphosphate (ADP)-ribosylation [70], crotonylation [71], hydroxylation [72], proline isomerization [73] and K SUMOylation [74], which together constitute the histone code. A specific state of the histone code may either lead to gene activation or silencing [75]. The endless possible combinations of the various modifications and target sites, allows the histone code for highly versatile fine tuning of gene expression, but is also critically involved in DNA repair and replication [76]. Owing to the attention that chromatin-modifying enzymes have received over the past years, many enzymes that had been identified as modifying histones, were later found to have many additional substrates. In view of this, Allis et al. [77] have proposed an updated nomenclature that better reflects the full spectrum of functions of these enzymes. For instance, histone (lysine) acetyltransferases

(HATs) were renamed to lysine acetyltransferases (KATs). As, however, this new nomenclature has only sporadically been adopted, both old and new names will be stated to avoid confusion.

Acetyl coenzyme A serves as donor of the acetyl group, which is transferred to lysines of histone tails by KATs [78]. There are a multitude of proteins with KAT activity, which can be divided into five main groups, comprising KAT2A (or general control of amino acid synthesis [GCN] 5), KAT2B (or P300/CBP-associated factor [PCAF]), KAT6-8, cyclic adenosine monophosphate (cAMP) response element-binding protein binding protein (CREBBP or CBP) and adenovirus early region 1A (E1A)-binding protein P300 (EP300 or P300) [79].

Currently, there are 18 known histone deacetylases (HDACs) in humans, generally subdivided into four classes; class I (HDACs 1, 2, 3 and 8), class IIa (HDACs 4, 5, 7 and 9), class IIb (HDACs 6 and 10), class III (sirtuins [SIRTs] 1, 2, 3, 4, 5, 6 and 7) and class IV (HDAC11) [80]. Although their name suggests that histones are the primary targets of HDACs, phylogenetic analysis indicates that the evolutionary development of HDACs preceded that of histones [81]. Indeed, over 50 non-histone targets of HDACs have been identified, including proteins important for proliferation, migration, and cell death [82–84]. Thus, as for HATs, it was suggested that HDACs should be more appropriately referred to as lysine deacetylases [85]. The different HDACs fulfill many different roles, either by affecting gene expression or by directly regulating protein functioning. Class I HDACs for instance, are thought to play a general role in cell survival and proliferation, whereas class II HDACs have a more tissue-specific role [86–92]. The SIRTs further differ from the other HDACs in that their activity is nicotine adenine dinucleotide (NAD+)-dependent, whereas the other classes require the presence of zinc. Not all SIRTs are even primarily deacetylases. This has led to the suggestion that SIRTs should be classified as deacylases, as opposed to deacetylases [93]. Although class I and class IV HDACs are mainly nuclear, class IIa shuttles between the nucleus and cytoplasm, and class IIb is primarily cytoplasmic. The SIRTs of class III are most varied in their localization, and can be either expressed in the nucleus (SIRTs 1, 2, 6 and 7), cytoplasm (SIRTs 1 and 2) or mitochondria (SIRTs 3, 4 and 5) [94]. The expression of the different HDACs is also highly region- and cell-type-specific, for instance, while HDAC2 is expressed in most brain regions, it is predominantly active in mature neurons and weakly or not in progenitor and glial cells [95, 96].

Methylation of histone tails happens at K or R residues of H3 or H4, and is executed by histone lysine methyltransferases (HKMTs) and protein arginine methyltransferase (PRMT), respectively, whereas demethylation

is performed by histone lysine demethylases (HKDMs) and histone arginine demethylases (HRDMs) [97, 98]. The other histone modifications are less well characterized. Phosphorylation and dephosphorylation of histones is executed by protein kinases, such as mitogen- and stress-activated protein kinase (MSK)-1, and protein phosphatases, such as protein phosphatase (PPT) 1, respectively [99, 100]. Histone phosphorylation is dynamic in function; H3 phosphorylation, for instance, marks open chromatin during active gene expression, whereas during mitosis this marker associates with condensed chromatin [101]. Ubiquitination can either enhance or inhibit gene expression, whereas SUMOylation is primarily thought to suppress transcription [98].

The actual effect and interplay between these modifications are complex, and depend on the type of histone protein and the specific amino acid that is modified, and a combination of certain modifications can even have a function that is different from that of these modifications in isolation [75, 101–104]. For instance, acetylation of K 9 (H3K9ac) and 14 (H3K14ac) of H3, or tri-methylation at K 4 of H3 (H3K4me3), H3K36me, H3K79me, H3R2me, H3R17me, H3R26me and H4R3me are associated with gene activation, whereas H3K9me2/3, H3K27me3, H3R8me, H4K20me3 and H4R3me are generally associated with gene repression [98]. Interestingly, in case of histone methylation, the number of attached methyl groups also matters, as the previously mentioned H3K9me3, H3K27me3 and H4K20me3 marks that are associated with gene repression, all have monomethylated counterparts that are associated with gene activation [105]. Of note, recent studies mapping histone tail modifications to genomic regions found that many transposable elements (TEs) are enriched with certain histone marks [106–108] and it has therefore been suggested that TEs may attract certain histone marks to induce heterochromatic and euchromatic states, or serve as boundary elements that prevent the propagation of such states [109].

In addition to histone modifications, chromatin remodeling also occurs through adenosine triphosphate (ATP)-dependent multi-protein chromatin remodeling complexes. Four distinct remodeling complex families have been identified, including the Brg1/hBrm associated factor (BAF; previously known as switching defective/sucrose nonfermenting [SWI/SNF]), imitation SWI (ISWI), chromodomain, helicase, DNA-binding (CHD) and inositol requiring 80 (INO) families [110–112]. These complexes, or remodelers, can bind nucleosomes, disrupt nucleosome-DNA binding, and then move, destabilize, eject or restructure them, using ATP hydrolysis as energy source. In doing this, remodelers can either induce transcriptional activation or repression, through the recruitment of coactivator or corepressor complexes. The different remodeling complexes are defined by their ATPase subunits, but variation in their

remaining subunit composition, possibly altering the DNA and protein binding properties of the complex, allows for great diversity, leading to cell-type specific roles [113, 114]. Furthermore, multiple functionally different versions of a complex may be present within one cell [115]. The BAF complex, consisting of at least 15 subunits, is of particular interest, as it is the only chromatin remodeling complex with a neuron-specific subunit, BAF53b. The BAF complex is thought to play an important role in neuronal development and functioning, with unique subunit compositions in embryonic stem cells, neuronal progenitors and mature neurons [112]. The BAF53b subunit was shown to be important for dendritic development *in vitro* and long term memory in mice [116]. See the excellent review by Hargreaves and Crabtree [111] for a detailed discussion of the different chromatin remodeling complexes.

2.1.4. Non-coding RNAs

Until recently, it was widely believed that most of the human genome consisted of so-called 'junk', or nonfunctional DNA. It was later revealed that almost the whole genome is transcribed, but that only about 2% is actually translated into proteins [117]. Most of the 'junk' is functional and is primarily involved in the regulation of gene expression, usually in the form of ncRNAs. There are many types of ncRNAs, including microRNAs (miRNAs), small interfering RNAs (siRNAs), small nuclear RNAs (snRNAs), small nucleolar RNAs (snoRNAs), small Cajal body-specific RNAs (scaRNAs), piwi-interacting RNAs (piRNAs), splice junction-associated RNAs (spliRNAs), small modulatory RNAs (smRNAs), repeat-associated small interfering RNAs (rasiRNAs), transcription initiation RNAs (tiRNAs), promoter-associated short RNAs (PASRs), transcription start site-associated RNAs (TSSa-RNAs), promoter upstream transcripts (PROMPTS), ribosomal RNAs (rRNAs), transfer RNAs (tRNAs), and small double-stranded RNAs (dsRNAs) [118–122]. These are small ncRNAs (sncRNAs), of <200 nucleotides, whereas there are also long ncRNAs (lncRNAs), which can exceed 100,000 nucleotides, often including TE-derived sequences that may confer specific protein or nucleic acid interacting properties [123]. Examples of lncRNAs are intergenic ncRNAs (lincRNAs), natural antisense transcripts (NATs), ncRNA expansion repeats, promoter-associated RNAs (PARs), and enhancer RNAs (eRNAs) [124–128]. The sncRNAs fulfill various functions, including infrastructural (rRNAs, tRNAs and snRNAs) and regulatory roles (miRNAs, siRNAs, snoRNAs, piRNAs and spliRNAs), whereas the lncRNAs are primarily regulatory. Interestingly, lncRNAs are expressed in a highly cell-specific manner, may undergo alternative splicing, and may even have protein-coding isoforms [129–132]. Alternatively, some mRNAs may function as trans-acting regulatory RNAs [133–135]. In terms of

epigenetics, ncRNAs are cardinally involved in gene expression control, in the silencing of TEs, X-chromosome inactivation, alternative splicing, and DNA imprinting [136–138]. Additionally, some lncRNAs have been proposed to direct epigenetic enzymes to their target sites [125, 139, 140], while others are thought to bind and sequester other epigenetic players, such as DNMTs and miRNAs, thereby hampering their activity [132, 140, 141].

The best characterized of the ncRNAs are miRNAs. These begin their lives as primary miRNAs, after which they are cleaved by ribonuclease type III Drosha to form precursor miRNAs (pre-miRNAs) [142]. These pre-miRNAs are then transported from the nucleus to the cytosol by Exportin-5, where Dicer makes the final adjustment to produce double-stranded mature miRNAs. Mature miRNAs span 21-25 nucleotides and regulate protein production through an RNA interference pathway, involving the association of one of the strands of the miRNA duplex with the RNA-induced silencing complex (RISC) [143, 144]. They interfere with gene expression through binding to messenger RNA (mRNA), usually to the 3' untranslated region (UTR), which hampers the initiation of translation and affects mRNA stability. MiRNAs can potentially regulate the translation of multiple genes, whereas genes can also be regulated by several miRNAs, as the sequences of the miRNA and its target are not required to be a perfect match for interference to take effect [145, 146]. While siRNAs are processed and function similarly, they require stricter matching with their target sequence when compared to miRNAs [147]. Apart from interacting with RISC, some miRNAs have been observed to promote mRNA translation and gene transcription, by binding to gene promoter regions [148, 149]. There are numerous miRNAs, many of which are expressed according to strict spatial and temporal patterns. Currently, there are 1881 precursors and 2588 mature human miRNAs registered in the fast growing miRBase [150]. While expressed throughout the whole human body, the brain is especially enriched in miRNAs, suggesting an important role for them in neuronal development, functioning, and aging [151, 152]. Their biological role has been further characterized, and reviewed by Santosh and colleagues, as well as Qu and Adelson [153, 154]. Both the reviews extend beyond the aforementioned functions, and present the key role of ncRNA in RNA splicing, transcriptional, post-transcriptional, and translational regulation by either binding directly to transcriptional factors or by generating siRNAs, that consequently interact with the translational machinery.

2.1.5. Additional epigenetic mechanisms

DNA methylation, chromatin remodeling, and ncRNAs represent the best-studied epigenetic mechanisms, especially in relation to aging and neurodegenerative diseases. Epigenetic regulation goes much deeper, however, and also includes the rising subfields of RNA editing, RNA methylation and mitochondrial epigenetics, which will be briefly touched upon in this section, but will not be further discussed in relation to aging and neurodegeneration due to the as of yet extremely limited findings in this respect. Clearly, more studies on the role of these additional layers of epigenetic regulation in aging and neurodegeneration are warranted.

2.1.5.1. RNA editing

The observation of discrepancies in genomic and cDNA sequences led to the discovery of RNA editing [155]. The finding that RNA can be edited, a process that seems particularly important in the brain, adds another layer to the transcriptional and post-transcriptional regulation of gene expression. It has even been proposed that a dramatically increased RNA editing capacity was crucial for the evolution of the mammalian brain as it may function as a mechanism driving phenotypic adaptability, which ultimately led to the superior cognitive abilities of humans [156, 157]. In support of this, roughly 35 times more RNA editing is observed in humans compared to mice. This surplus appears to be mainly directed to retrotransposed *Alu* elements that are primate-specific and constitute 10.5% of the human genome [158–162].

In contrast to RNA and DNA modifications, RNA editing involves a change in RNA sequence by deamination of either adenosine (A) or cytosine (C), to inosine (I) [155, 163] or uracil (U) [164, 165], respectively. A to I editing is performed by adenosine deaminases that act on RNA (ADARs), while C to U editing is carried out by APOBECs. APOBECs are related to AICDAs, which targets DNA and is pivotal in the generation of the immunoglobulin repertoire [166]. Although not much is known about the targeting, regulation and functional impact of ADARs and APOBECs, they are thought to be evolved from adenosine deaminases that act on tRNAs (ADATs) and thus bind double-stranded RNA regions, such as those seen in hairpin formations that are also present in tRNAs [155, 164].

ADAR1 and ADAR2 are ubiquitously expressed and they appear to be enriched in the brain, while the expression of ADAR3 seems to be restricted to the brain. A to I RNA editing has been observed in coding

transcripts, for instance leading to changes in the amino acid sequence of glutamate and serotonin receptors. Most editing, however, happens to noncoding sequences, such as miRNAs [167–169] and transposon-derived repetitive sequences [170], suggesting that RNA editing not only directly affects gene expression, but also indirectly by regulating other epigenetic players [156]. APOBECs, together with overall RNA editing, appear to have undergone a substantial expansion over the course of evolution, with APOBEC3 being especially favored in humans with eight orthologs, compared to one in mice [165, 171, 172]. Although it has been suggested that these enzymes have evolved to combat retrotransposons and endogenous retroviruses [173, 174], there is also evidence indicating that these elements actually have been harnessed as epigenetic regulators involved in growth and differentiation, including the generation of neuronal diversity [175–177].

Recently, the implication of RNA editing in the etiopathogenesis and progression of neurodegenerative disorders as well as normal aging processes has gained momentum and the few available studies begin to elucidate this connection. The majority of these studies are focusing on aging. Sebastiani et al. [178] observed that 5 single nucleotide polymorphisms (SNPs) in the ADAR encoding genes *ADARB1* and *ADARB2* are associated with extreme longevity in 4 independent human studies. The observation of the critical role of ADARs in aging was also verified in a *CAENORHABDITIS ELEGANS* (*C. ELEGANS*) model with loss of function of *ADR1* and *ADR2* (*ADARB1* and *ADARB2* orthologues), which had a 50% decrease in lifespan. After this study a lot of RNA editing targets were discovered, such as *Gabra2*, *Cyfip2*, *Kcnal*, *Flna*, *Blcap*, *Cog3*, *Neat1*, *Neat2*, *Malat1* and *Pisd-ps1* that are differentially edited in the aging murine and human brain. Among them, *Cyfip2* and *Pisd-ps1* have gained considerable attention [179–181]. Nicholas et al. [180] demonstrated that A to I editing declines with age in humans, in a gene-specific manner, resulting in downregulation of an ADAR2 target gene, *Cyfip2*, which is responsible for synaptic maintenance. In the hippocampal formation of aged mice Stilling et al. [181] showed that the altered RNA editing levels of *Pisd-ps1* results in higher editing frequency with age and thus upregulation of gene expression.

In case of AD, Akbarian et al. [182] observed a decrease in the RNA editing levels of glutamate receptor (GluR) 2 in the prefrontal cortex of AD human brains. Rechavi's team [183] following the aforementioned research line, examined the GluR2 Q/R RNA editing levels in the hippocampus of AD human brains, where they found a decrease in the aforementioned levels in AD samples in comparison to controls. Additionally, they showed lower GluR2 Q/R RNA editing in the hippocampi of APOEε4 carriers. The mRNA expression of ADARs was

also investigated in this specific study; unexpectedly no differences were found in the hippocampus but a 37% decrease of ADAR2 mRNA expression was noticed in the caudate. Finally, Akbarian et al. [182] extended the study on HD where they also showed a decrease in GluR2 RNA editing levels in the striatum.

2.1.5.2. RNA methylation

Although the discovery of methylated RNA was done decades ago [184, 185], over a hundred RNA nucleotide modifications have been identified across different organisms [186, 187]. In eukaryotes the best-studied mRNA modifications are N6-methyladenosine (m6A) and 5-mC, which mainly occur at 3' UTRs and stop codon sites [188]. As in DNA, 5-hmC has also been observed in RNA [189]. m6A is the most prevalent mRNA modification in mammals and has also been observed in tRNAs, rRNAs and snoRNAs [190–197]. In humans the m6A modification shows high tissue specificity, with the highest levels occurring in the brain, in transcripts such as *Bdnf*, *Dscam*, *Lis1* and *Ube3a* [198]. In mice and humans m6A methyltransferase-like protein (METTL) 3 is responsible for the post-transcriptional m6A RNA modification [199]. Additionally, METTL14 and Wilm's tumor-associated protein (WTAP) have been shown to interact with METTL3 and are thought to be additional components involved in RNA methylation [200, 201]. Just as DNA methylation, the identification of m6A demethylases fat mass and obesity-associated protein (FTO) and AlkB, alkylation repair homolog (ALKBH) 5 [202, 203], indicates that RNA methylation is a dynamic regulatory mechanism. FTO, a dioxygenase, demethylates RNA via a similar oxidation procedure as is employed by the TET enzymes that are thought to be involved in DNA demethylation, namely through the generation of intermediates N6-hydroxymethyladenosine (hm6A) and N6-formyladenosine (f6A), before being reversed to A [204]. Although these intermediates remain stable for several hours, no separate regulatory roles for hm6A and f6A have been reported yet. ALKBH5 is thought to remove m6A directly, without the generation of intermediates [203]. Although the exact regulatory functions of m6A RNA methylation remain to be elucidated, its main occurrence at 3' UTRs and stop codons has been suggested to indicate a role in switching genes on or off [205]. Alternatively, the observation that players involved in m6A RNA methylation were located at splice sites suggests that the m6A RNA modification may modulate splicing [188]. More recent findings show a relation between the m6A modification and mRNA degradation, as m6A selectively binds human YTH domain family (YTHDF) 2 proteins, which can bind and target mRNA to decay sites, such as processing bodies (P-bodies) [206]. Other members of the YTH domain family, YTHDF1 and YTHDF3 also selectively bind m6A modified

RNA. Another study, however, indicated that m6A does not lead to RNA decay through the YTHDF2 pathway, but by interacting with miRNAs, and that the removal of m6A promotes human antigen R (HuR) binding, a protein that protects against RNA decay [201]. These studies suggest that the m6A mark may dynamically regulate mRNA lifetime.

An alternative pathway of RNA methylation involves the versatile regulatory ncRNAs snoRNAs, which can guide 2'-O-methylation and pseudo-uridylation of RNA transcripts, including mRNAs [207]. 2'-O-methylation is important for the functioning of certain rRNAs [208], but also determines the guide strand and targeting specificity of siRNAs [209]. Apart from their role in RNA modifications, snoRNAs can be further processed into snoRNA-derived small RNAs (sdRNAS), which are similar to miRNAs [210–213].

The pathway that most closely resembles DNA methylation involves DNMT2, which, despite its name, transfers methyl groups to cytosines in RNA [27, 214]. Apart from tRNA, the exact substrates of DNMT2 still need to be identified. Nevertheless, DNMT2 has been implicated in brain development and retrotransposon silencing [215, 216]. Other known RNA methylation modifications include N1-methyladenosine (m1A) and N1-methylguanine (m1G), which occur mainly in tRNAs and are thought to enhance tRNA stability, and m1G also decoding accuracy [217–220].

The only reported studies connecting RNA methylation to aging, as well as neurodegenerative disorders, were performed by Giordano et al. [221] and Thomas et al. [13], respectively. Bellizzi's team studied the methylated cytosine residues in two mitochondrial genes, 12S and 16S rRNA and they showed that the methylation levels of 12S rRNA are decreased with age in males. Thomas et al. [13], while attempting to develop a novel method for detecting trace amounts of 7-mG in biological samples, observed differential methylation patters in murine HD models and significantly increased levels of 7-mG in postmortem human HD brain samples.

2.1.5.3. Mitochondrial epigenetics

Apart from the nuclear genome, human cells can harbor thousands of copies of the mitochondrial genome. Both the nuclear and mitochondrial genome consist of DNA, but there are some striking differences [222]. The mitochondrial genome is only 16 kb long, contains 37 genes without introns and is much more prone to mutations than the nuclear genome. With respect to epigenetics, its regulation seems to be less complex, as mitochondrial DNA (mtDNA) is thought not to be wrapped around histones

and not to contain CpG islands; the 435 CpG sites in the mitochondrial genome are almost evenly dispersed.

Over 40 years ago, methylated mtDNA was discovered in loaches, and it was shown there is DNMT activity in mitochondria that is independent from DNMT activity outside mitochondria [223, 224]. Later, mtDNA methylation was also observed in humans [225], and a mitochondrial DNMT (mtDNMT) was discovered [226]. Of note, however, more recent studies cast doubt on the general notion that DNA methylation is the prime epigenetic mechanism at work in mitochondria. For instance, Hong et al. [227] were unable to detect CpG methylation in the genome of human mitochondria, whereas Choi et al. [228] report on the possible existence of mitochondrial histones, and Barrey et al. [229] found miRNAs in mitochondria. Nevertheless, there are also many recent reports supporting the presence of methylated mtDNA and even hydroxymethylated mtDNA [230–233], showing that it is not always located at CpG sites [234, 235], and that mtDNA methylation plays a role in mitochondrial gene regulation [236, 237]. Clearly, these rapid developments within the field of mitochondrial epigenetics warrant further attention. In the recent study of Dzitoyeva et al. [231] not only the hydroxymethylation of mtDNA was reported but they also demonstrated that solely the levels of hydroxymethylated mtDNA reduce with age in the frontal cortex of mice. This decrease in 5-hmC is associated with an increase in complex I components (ND2, ND4, ND4L, ND5, ND6) in the same area. Furthermore, they observed region-specific differential expression of epigenetic players; the mRNA levels of TET2 and TET3, which are also responsible for the hydroxymethylation of mtDNA, are only increased in the cerebellum, whereas the mRNA levels of mtDNMT1 decrease solely in the frontal cortex.

2.1.6. Epigenetic processes are interdependent

The epigenetic processes of DNA (de)methylation, chromatin remodeling, and miRNAs do not act independently, but closely interact to form a complex, multilayered regulatory system that can dynamically fine-tune gene expression. DNA methylation stability in promoter regions, for instance, is enforced by methyl CpG binding protein (MeCP) 1, which also binds the nucleosome remodeling and histone deacetylase (NuRD) core and cyclin-dependent kinase 2 associated protein (CDK2AP) 1; forming a protein complex not only able to stabilize DNA methylation, but also to modify the histone code [238, 239]. MeCP1 is attracted to methylated DNA through its affinity for MBD2, which directly binds to

DNA methylated at CpG sites. As such, DNA methylation and histone modifications act in concert to regulate gene expression, through interference with transcription factor binding and chromatin compaction [19]. Another interesting interplay, between DNMT3A-dependent DNA methylation and Polycomb-group (PcG)-dependent H3K27me3 marks was discovered by Wu et al. [240]. They showed that DNMT3A activity at non-promoter regions correlated with increased expression of neurogenic genes, by interfering with PcG binding and H3K27me3-mediated gene repression. In contrast, DNMT3A activity at the promoter regions inhibited gene expression. Alternatively, MBD1 can antagonize H3K4me3, leading to chromatin compaction. DNA methylation can thus in a bottom-up fashion induce changes on the chromatin level [241]. The other way around is also possible, as exemplified by Detich et al. [242]. They showed that increases in H3 acetylation can induce DNA demethylation, and thereby gene expression *in vitro*. Conversely, HDAC activity is thought to inhibit gene expression through the induction of DNA methylation [243]. There are additional complex interactions between miRNAs and other components of the epigenetic machinery. Where some miRNAs regulate the expression of proteins involved in epigenetic regulation, the expression of various miRNAs themselves is also subject to factors such as DNA methylation and histone modifications [244]. For example, miRNA 184 (miR-184), involved in the regulation of proliferation and differentiation of neural stem cells, is surrounded by CpG islands, attracting MBD1, which can suppress its expression as described above [241].

2.2. Aging

Before delving into the aberrant epigenetic processes associated with neurodegeneration, it is important to consider the epigenetic changes associated with normal aging and related hallmarks, such as oxidative stress, as these can already be quite dramatic. Bocklandt et al. [245] for instance, devised a method to determine the age of an individual based on the methylation of specific sites in the *EDARADD*, *TOM1L1* and *NPTX2* genes. At these sites a linear correlation between methylation and age was observed, allowing for a prediction of age with an average accuracy of 5.2 years. Horvath later devised an even more accurate method to determine the ‘DNAm age’, based on the methylation status of 353 CpGs [246]. The DNAm age of Horvath has a chronological age correlation of about 0.96 and an error of 3.6 years and is applicable in many different tissue and cell-types. Note, however, that epigenetic processes are not the only players involved in aging. According to the “free radical theory of aging”, oxidative stress is thought to play an integral role in the aging process [247]. Oxidative stress refers to the

generation of reactive oxygen species (ROS), which are damaging to proteins, nucleic acids and lipids and are known to also affect epigenetic players [248]. Furthermore, as aging is the prime risk-factor of most neurodegenerative diseases, it is possible that age-related processes, including epigenetic alterations and oxidative stress, facilitate the development of these illnesses.

2.2.1. DNA (de)methylation in aging

Early research established that DNA methylation plays a crucial role during development. Later studies identified aging to be a pivotal modulator of the epigenome. The DNAm age of Horvath offers some interesting insights in this respect [246]. Of the 353 CpG sites used to predict the DNAm age, 193 got hypermethylated and 160 got hypomethylated with age, and most are associated with genes involved in cell death and survival, cell growth and proliferation, organismal and tissue development, and cancer. Additionally, DNAm age shows a logarithmic relationship with chronological age until adulthood, and a linear relationship later in life, indicating that the epigenetic clock 'ticks' faster during growth and development. While highly accurate in most tissues, Horvath found that the DNAm age was consistently lower in tissues which may be renewed through the presence of stem cells, such as skeletal and heart muscle. It was, however, also observed that DNAm age does not reflect cellular senescence, as it highly correlated with chronological age in short and long lived cells, as well as immortal cells. As could be expected, embryonic stem cells appeared to have a DNAm age close to zero. Interestingly, the DNAm age of induced pluripotent stem cells did not differ significantly from that of embryonic stem cells. While the clock CpGs used for Horvath's DNAm age are enriched in cancer genes, there are some important differences between normally aging and cancerous tissue. In general, cancer tissue exhibits an accelerated DNAm age. Due to the heterogeneity of cancer types, however, general statements about its use should be interpreted with caution, as for example thyroid cancer progression negatively correlates with age acceleration. Additionally, Horvath observed that an increased DNAm age may promote genomic stability, as he found in several cancer types a negative relation between DNAm age acceleration and somatic mutations. He proposes that cancer triggers a hypothetical epigenetic maintenance system that promotes genetic stability, a process that is dependent on P53, as mutations in the *TP53* gene are associated with a lower DNAm age acceleration. Interestingly, in glioblastoma multiforme *TP53* mutations appear to be associated with an increased DNAm age

acceleration. While it thus seems that in general cancer is associated with an increased DNAm age profile and aging with global DNA hypermethylation, neurodegenerative diseases such as AD and PD are associated with global DNA hypomethylation [26, 249]. Note, however, that the DNAm age itself has not yet been assessed in neurodegenerative tissue. Nevertheless, despite having age as a common risk factor, cancer and age-related neurodegenerative diseases seem to involve (at least partly) different epigenetic dysregulation or compensatory mechanisms.

Taking a more specific approach, Siegmund et al. [250] investigated the DNA methylation status of 50 CpG islands associated with genes involved in brain growth and development in subjects of various ages, and they observed a robust and progressive increase in DNA methylation of multiple genes with age (Table 1). They also confirmed that a rise in DNA methylation typically results in a decline of corresponding mRNA levels. In addition, it was observed that DNMT3A was expressed across all ages, supporting the notion that DNA methylation can be dynamically altered throughout the lifespan. Interestingly, in relation to AD, the promoter region of the amyloid-β precursor protein (APP) gene becomes hypomethylated with age [251]. Additionally, binding sites for granulocyte chemotactic factor (GCF), known to repress CG-rich promoters, and interaction sites for specificity factor (SP) 1, which enhances gene expression in the tau promoter, became hypo- and hypermethylated, respectively, with age, decreasing its overall expression. This finding suggests that certain age-related epigenetic changes might facilitate the development of AD. Although expressed across all ages, levels of DNMT3A and 5-mC actually increase with age in the dentate gyrus (DG), cornu ammonis (CA) 1-2, and CA3 regions of the mouse hippocampus [252, 253], which is in line with previous reports [254]. An interesting study by Oliveira et al. [255] showed that hippocampal levels of DNMT3A2, an isoform of DNMT3A, decrease with age and that this decrease correlated with age-related cognitive decline in mice. Importantly, experimental restoration of DNMT3A2 levels alleviated this age-related cognitive impairment. Additionally, Hernandez et al. [256] investigated 27,000 CpG sites in brain samples of varying ages and detected a general positive correlation between age and methylation levels. In contrast, it was found that expression levels of DNMT1 decrease with aging in human fetal lung fibroblasts, which would be in support of reports of global DNA hypomethylation with aging and cell senescence, including non-coding regions and repetitive sequences in the blood [254, 257, 258]. Mazin [259] put forward an interesting hypothesis, proposing a DNA methylation-dependent aging process. This model is based on the observation that methylation of cytosines may induce C > T mutations, which is suggested to result in age-related genome disintegration, and eventually cell apoptosis, organism aging and

death. Due to the age-related increase in 5-mC > T transitions, this model predicts an age-related depletion of 5-mC.

Note, however, that DNA methylation profiles are not only known to be different between different tissues, regions and cell-types, but that these also seem to be differentially affected by the aging process [260–262]. An interesting study by Fraga et al. [263], investigating DNA methylation and histone acetylation during the lifetime of monozygotic twins, illustrates that the epigenome not only changes with age, but also that differences in the epigenome might explain phenotypic disparity in genotypically identical individuals.

In addition to the age-related increases of DNMT3A and 5-mC levels, a significant age-related increase in 5-hmC levels was found in the DG, CA1-2, and CA3 regions of the mouse hippocampus [264], which is in line with previous investigations into the spatial and temporal distribution of 5-hmC in the brain [265, 266]. While some of the genes that exhibit age-related increases in 5-hmC levels are associated with age-related neurodegenerative diseases [266], further investigations are required to elucidate the functional consequences of these findings, taking into account the differential functions of the 5-mC and 5-hmC markers. Table 1 summarizes the age-related alterations regarding DNA (de)methylation.

2.2.2. Chromatin remodeling in aging

Apart from widespread changes in the neuronal DNA methylation profile throughout the lifespan, the neuronal histone code also undergoes age-related alterations (Table 2). An example is the observation of lower levels of histone acetylation with aging *in vitro* [270], and an age-related progressive decline of H3 and H4 methylation [271] and monoacetylated H4 levels, discovered in neurons from the rat cerebral cortex [272]. Apart from detecting decreased levels of H3K9ac and increased levels of H3S10p [273], Nakamura et al. [274] detected decreased acetylation of extranuclear proteins. In senescence-accelerated prone mouse 8 (SAMP8) brains it was shown that many histone marks are altered with age [275] (Table 2). In rats, however, some of these markers were observed not to undergo significant age-related changes [276]. These not always compatible findings between species illustrate the necessity of translating results regarding epigenetic changes to the human situation. Apart from changes in specific histone methylation marks, the HKMTs polycomb repressive complex member Bmi1 (PRC1) and polycomb repressive complex member enhancer of zeste homolog

TABLE 1. Epigenetic dysregulation in aging: DNA (de)methylation. ↑ indicates increased levels and ↓ indicates decreased levels.
ABBREVIATIONS: 5-hmC, 5-hydroxymethylcytosine; 5-mC, 5-methylcytosine; BS, bisulfite sequencing; CA, cornu ammonis; ChIP; chromatin immunoprecipitation; DG, dentate gyrus; DNMT, DNA methyltransferase; HPLC: high-performance liquid chromatography; IHC, immunohistochemistry; MS-PCR, methylation specific-PCR; PCR, polymerase chain reaction; RT-PCR, real time-PCR.

(EZH) 2 (*Drosophila*) (PRC2) have been observed to decrease with cell senescence, a common, but limited, *in vitro* model of aging, while the HKDM jumonji domain containing (JMJD) 3 increased [277, 278]. The balance between PcG and JMJD3 gene expression is in turn thought to be regulated by HDAC activity.

The finding that HDAC2 expression increases with age in the mouse hippocampus is in line with findings of decreased acetylation levels [279]. Age-associated reduction in acetylated H4 is thought to reduce chromatin structural plasticity and may result in a decreased accessibility of the DNA for repairing enzymes and other regulatory factors [272, 280].

table 1.

Gene	Regulation	Epigenetic modification	Observed in	Sample size	Approach	Methods	Reference
GABRA2	↑	Methylation (promoter region)	Human	125	Targeted (50 loci)	BSeq	[250]
GAD1	↑						
HOXA1	↑						
NEUROD1	↑						
NEUROD2	↑						
PGR	↑						
STK11	↑						
SYK	↑						
IFN-γ	↑ ↑			784	Targeted (9 loci)		[267]
RUNX3	↑ ↑			26	Targeted (7 loci)	BSeq, MS-PCR	[268]
ERβ	↑ ↑			7-10	Targeted (1 locus)	BSeq, MS-PCR, Pyrosequencing, ChIP	[269]
APP	↓	Methylation		16	Targeted (18 loci)	BSeq	[251]
GCF	↓	Methylation (binding sites)					
SP1	↑ ↑	Methylation (interaction sites)					

Protein/ (Hydroxy) Methylated base	Regulation	Modification in	Observed in	Sample size	Methods	Reference
DNMT1	↓	Expression	Fibroblasts (fetal lung)	-	DNMT assay ChIP, RT-PCR	[254, 258]
DNMT3A2	↓		Mice (12 month old)	15	IHC	[255]
DNMT3A	↑		Mouse hippocampus (DG, CA1-2 and 3)	240	IHC	[252]
5-mC	↑					[253]
5-hmC	↑			4	HPLC	[265, 266]

Other studies are more specific, pointing towards a role of deregulated H4K12ac in age-related memory impairment [281], a negative influence of HDAC2 on synaptic plasticity and memory formation through the suppression of neuronal gene transcription [95, 282], and a dependence of histone acetylation on citrate levels [283], which decline in the aging brain [284]. Furthermore, the KAT CREBBP is important for long-term memory formation and late-phase long-term potentiation in the hippocampus of mice [285, 286]. Apart from histone acetylation, H3K4me3 [287] and H3 phosphorylation [288] are also involved in memory formation. The SIRT HDACs have also been implicated in aging. In contrast to HDAC2, SIRT1 levels were found to drop with age, a change not limited to the brain [289, 290] and also observed in senescent cells [291]. Reduced levels of SIRT1 have been associated with increased levels of H4K16ac *in vitro* [292]. SIRT1 can in addition directly deacetylate the HKMT suppressor of variegation 3-9 homologue (SUV39H) 1, which increases the activity of SUV39H1 [293]. This HKMT is responsible for H3K9me3, which is important for the formation of facultative heterochromatin. Despite the association between senescence and decreased H3K9me3 levels, H3K9me3 is thought to accumulate in senescence-associated heterochromatin foci (SAHF), a form of facultative heterochromatin, which are thought to induce senescence through the repression of the pro-proliferation E2F transcription factor family [294, 295]. Alternatively, in *C. elegans*, it has been observed that sir-2.1, the ortholog of mammalian SIRT1, can extend lifespan through its product nicotinamide [296]. Nicotinamide can be methylated by nicotinamide-N-methyltransferase-1, producing 1-methylnicotinamide, and 1-methylnicotinamide in turn is processed by aldehyde oxidase gastrulation defective 3 (GAD-3) to generate hydrogen peroxide. This hydrogen peroxide is thought to play a mitohormetic role, inducing longevity [297]. Reinstating SIRT levels, for instance through caloric restriction, has in addition been reported to increase lifespan in yeast, invertebrates, and vertebrates [298, 299], and has been argued to facilitate healthy aging in humans, thereby slowing the development of age-related neurodegenerative diseases such as AD [300, 301].

2.2.3. Non-coding RNAs in aging

One of the first ncRNAs reported to affect the aging process was miRNA lin-4, whose expression was observed to modulate lifespan in *C. elegans* [302]. In neurons of *C. elegans*, miR-71 promotes longevity through the dauer 16/forkhead box O (DAF-16/FOXO) pathway, increasing resistance towards heat shock and oxidative stress [303]. Other studies

TABLE 2. Epigenetic dysregulation in aging: chromatin remodeling. ↑ indicates increased levels, ↓ indicates decreased levels, and ≠ indicates altered, not further specified.
ABBREVIATIONS: ChIP-Seq, chromatin immunoprecipitation sequencing; H, histone; hAD-MSC, human adipose tissue-derived mesenchymal stem cells; HDAC, histone deacetylase; HPLC, high-performance liquid chromatography; hUCB-MSC, human umbilical cord blood-derived MSCs; ICC, immunocytochemistry; IHC, immunohistochemistry; K, lysine; MALDI-TOF, matrix assisted laser desorption/ionization time-of-flight; Nano-LC, nano liquid chromatography; NS, not specified; p, phosphorylation, PRC; polycomb repressive complex; RT-PCR, real-time PCR; S, serine; SAMP8, senescence-accelerated prone mouse 8; SIRT, sirtuin; SOD, copper-zinc superoxide dismutase 1; TOF MS, time-of-flight mass spectrometry; WB, western blot.

found increased levels of some miRNAs with age, but did not detect any significantly downregulated miRNAs in mice [304] (Table 3). In human blood mononuclear cells, however, various miRNAs were significantly decreased in older participants [305] (Table 3). Altered expression of various miRNAs, has been linked to age-related cardiovascular problems [306–310] (Table 3). Moreover, various members of the miR-17-92 cluster were reported to be downregulated in humans [311] (Table 3). Another study in human endothelial cells detected additional miRNAs affected by age [310] (Table 3). Increased ROS levels in human endothelial cells were observed to induce miR-200c and concomitant initiation of apoptosis and senescence [312]. Several studies have recently shown the importance of certain miRNAs specific to the aging brain and their roles in the development of neurodegenerative diseases [313, 314].
In the cortex and cerebellum of humans, chimpanzees, and macaque monkeys, miR-144 was observed to be upregulated [315]. This miRNA targets the ataxin-1 gene, which is critically involved in the development

table 2.

Chromatin remodeling target	Regulation	Epigenetic modification	Observed in	Sample size	Methods	Reference
H3	↓	Methylation	Rat cerebral cortex	12-18	WB	[271]
H3K9	↓	Acetylation	Rat (liver)	NS		[273]
H3K27	↑	Methylation	SAMP8 mice	6	Nano-LC, MALDI-TOF/TOF MS, WB, IHC	[275]
H3K36	↓	Tri-methylation				
H3K79	↑	Tri-methylation				
H3S10p	↑	Phosphorylation	Rat cerebral cortex	NS	WB	[273]
H4	↓	Methylation		12-18		[271]
		Monoacetylation				[272]
H4K12	≠	Acetylation	16-months old mice	12	ChIP-Seq-PCR, HAT/HDAC assay	[281]
H4K16	↑	Acetylation	SIRT-1 transfected cell lines	-	ChiP	[292]
H4K20	↓	Methylation	SAMP8 mice	6	Nano-LC, MALDI-TOF/TOF MS, WB, IHC	[275]
H4K20	↑	Tri-methylation	Rats (kidney, liver)	NS	HPLC	[276]

Enzyme	Regulation	Modification in	Observed in	Sample size	Methods	Reference
HDAC2	↑	Expression	SOD mice	48	IHC	[279]
SIRT1	↓		Rat brain, senescent cells	24-45,-	WB, IHC, RT-PCR	[289 - 291]
PRC1, PRC2	↑		hAD-MSCs, hUCB-MSCs	-	ICC, WB, RT-PCR	[278]

of spinocerebellar ataxia type 1, and its age-related dysregulation could thus facilitate the development of this disease. Li et al. [316] forged a link between aberrant miRNA expression and age-related declines in mitochondrial respiration rates. They found 70 miRNAs to be upregulated in the aging mouse brain, 27 of which were implicated in the downregulation of mitochondrial complexes III, IV and F0F1-ATPase that are all pivotal to the oxidative phosphorylation process. Interestingly, in the SAMP8, a mouse model of accelerated aging, miR-16 was found to be dysregulated. This miRNA modulates AD-related APP protein expression and with age APP levels were shown to drastically increase in the hippocampus of SAMP8 mice, leading to the suggestion that this model might serve as a model for AD [317]. Table 3 provides an overview of some of the ncRNAs that undergo age-related changes.

TABLE 3. Epigenetic dysregulation in aging: non-coding RNAs. ↑ indicates increased expression levels, ↓ indicates decreased expression levels, and ≠ indicates altered expression, not further specified.

ABBREVIATIONS: C57BL/6J mice, C57 black 6 inbred mouse strain; *C. elegans*, *Caenorhabditis elegans*; HAEC, human aortic endothelial cells; HCAEC, human coronary artery endothelial cells; HUVEC, human umbilical vein endothelial cells; IHC, immunohistochemistry; ISH, *in situ* hybridization; miR(NA), micro RNA; NB, northern blot; NS, not specified; PCR, polymerase chain reaction; RFLP, restriction fragment length polymorphism; SAMP8 mouse, senescence-accelerated prone mouse 8; SB, Southern blot; WB, western blot.

table 3.

Regulation	ncRNA	Observed in	Sample size	Approach	Methods	Reference
≠	miRNA lin-4	*C.elegans*	NS	Targeted	RFLP mapping, SB, NB	[302]
↑	miR-34	C57BL/6J mice	NS	Genome-wide	microRNA microarray	[304]
↑	miR-93					
↑	miR-214					
↑	miR-669c					
↑	miR-709					
↓	miR-24	Human (blood)	10-14	Targeted (800 miRNAs)	miRNome miRNA profiling	[305]
↓	miR-103					
↓	miR-107					
↓	miR-128					
↓	miR-130a					
↓	miR-155					
↓	miR-221					
↓	miR-496					
↓	miR-1538					
≠	miR-29	C57BL/6J mice and human	Mice: 4 Human: 30, 79	Genome-wide	PCR, microRNA microarray	[307]
	miR-34a	Sirt1+/–, Ku80–/– and miR-34a–/– mice	≥ 4	Targeted (570 miRNAs)	PCR, ISH	[306]
	miR-146a	HUVEC	-	Genome-wide	microRNA microarray	[310]
		HUVEC, HAEC, HCAEC	-	Targeted (367 miRNAs)	microRNA microarray, PCR	[309]
	miR-217	HUVEC, HAEC, HCAEC	-	Targeted (10 miRNAs)	microRNA microarray, PCR, NB	[308]
↓	miR-17	Human cell lines	-	Targeted (599 miRNAs)	microRNA microarray, PCR	[311]
↓	miR-19c					
↓	miR-20a					
↓	miR-106a					
↓	miR-146a	HUVEC	-	Genome-wide	microRNA microarray	[301]
↑	miR-26a					
↑	miR-181a					
↑	miR-221					
↑	miR-200b					
↑	miR-200c	Human cell lines	-	Targeted (1 miRNA)	WB	[312]
↑	miR-144	Human (cortex and cerebellum)	8	Genome-wide	microRNA microarray	[315]
		Chimpanzees	4			
		Macaque monkeys	5			
≠	miR-16	SAMP8 mouse	N.S.	Targeted (7 miRNAs)	PCR, ISH, IHC	[317]

2.3. Neurodegeneration

Neurodegenerative diseases typically involve a progressive loss of neuronal integrity and function, followed by neuronal death. Depending on where in the brain the loss of integrity and neuronal loss occur, various functional disabilities may arise and which gradually worsen as the neurodegeneration spreads. The underlying cause and localization of the neurodegenerative processes, however, often vary between different neurodegenerative disorders. Some of the most common include AD, PD and HD, but also amyotrophic lateral sclerosis and prion diseases are well studied forms of neurodegeneration [318]. Multiple sclerosis is more recently also being investigated as a neurodegenerative disease [319]. The exact etiology of most neurodegenerative diseases is far from clear, while in some cases, such as for HD [320], it is clear that the origin is largely genetic, for others, including sporadic AD and PD, the link between genetics and disease development is much more complex, possibly involving gene-gene and gene-environment interactions [321–323]. Numerous studies have, where genetics did not give simple answers, investigated other possible instigators, of which epigenetic mechanisms seem to be most promising. Although it remains to be elucidated whether dysfunctional epigenetic machinery plays a causal role, it has been critically implicated in various neurodegenerative processes. Additionally, environmental factors enjoy much attention as either direct modulators of disease development, or indirect via genetic or epigenetic pathways [321, 322, 324, 325].

2.3.1. Alzheimer's disease

The most ubiquitous neurodegenerative disorder and form of dementia is AD, with an estimated worldwide prevalence of over 35 million cases [326]. Mainly characterized by cognitive decline, late-stage AD concomitantly involves progressive motor aberrancies, mood instabilities and other behavioral and physical abnormalities [327, 328]. Although most of these symptoms arise as a result of cortical degeneration, others are due to degeneration of subcortical or autonomic function-related areas. It should be noted, however, that AD pathology does not equally affect the whole brain, as certain brain areas and cell types are specifically vulnerable to AD pathology [329]. Among the areas mainly affected by degeneration in AD are the frontal cortex, temporal and parietal lobes, including the hippocampus and entorhinal cortex (EC), and the cingulate gyrus, whereas the cerebellum is largely spared [330]. Interestingly, there is some evidence indicating that, while the cerebellum is mostly spared, the Purkinje cells are specifically targeted by AD pathology [331]. Despite numerous pre-clinical and clinical

trials for AD treatments, only basic symptom management therapies are currently Food and Drug Administration (FDA)-approved (some acetylcholinesterase inhibitors and an *N*-methyl-D-aspartic acid [NMDA] receptor antagonist), which cannot halt, or slow down the progressive neurodegeneration and the associated decline of memory, cognitive and executive functions. Apart from being a scourge among the elderly and the relatives of patients, dementia also incurs a tremendous socioeconomic burden; amounting to an estimated $200 billion in 2013 in the United States of America alone [332].

AD is a complex, multifaceted disorder, involving dysregulated homeostasis on various fronts, including energy metabolism, inflammation, and cell cycle control [26], likely resulting from a complex interplay between genetic, epigenetic and environmental factors [31, 318]. Despite much research into the pathophysiology of AD, including amyloid (Aβ) and phosphorylated tau proteins [333], its exact etiology remains to be elucidated [334]. Aβ, which exists in monomeric, oligomeric, and aggregated forms (senile plaques), is the product of APP cleavage by the β- and γ-secretases [335, 336]. APP cleavage by γ-secretases can result in either Aβ40 or Aβ42, of which Aβ42 is thought to be especially neurotoxic. APP can also be cleaved by α-secretases such as a disintegrin and metalloproteases domain (ADAM) 10 and tumor necrosis factor alpha (TNF-α) converting enzyme (TACE), but this cleavage does not result in Aβ, but generates APPs-α, which is thought to be neuroprotective [337]. One of the most prominent theories of AD pathology is the amyloid hypothesis, which states that Aβ is responsible for initiating the pathogenic pathway that leads to neurodegeneration and dementia in AD. Generally, this theory proposes that neurodegeneration is the result of impaired Aβ homeostasis, which leads to aberrant calcium homeostasis, triggering - and sensitizing cells to - damaging processes, including excitotoxicity and the formation of neurofibrillary tangles (NFTs) [338–340]. This hypothesis is applicable especially to early onset familial types of AD (fAD), which have a much more evident genetic component than the far more common late onset sporadic AD (sAD) [341]. Mutations in the APP gene and the presenilin (PS) genes *PS1* and *PS2*, have been observed in fAD cases [323, 338, 342–346]. PS1 and PS2 are γ-secretase-associated proteins involved in the generation of Aβ from APP, and PS mutations are able to bias this process towards Aβ42 production, the 42 amino acid-long Aβ isoform that is more prone to aggregate then the shorter Aβ40 isoform, by either increasing Aβ42 production, or lowering Aβ40 production [347]. This relation has been corroborated by the detection of elevated Aβ42 levels in the blood and brains of fAD cases with PS mutations [342]. Their major impact on disease development has led to the widespread use of mutant forms of the APP and PS genes to generate animal models of AD [348]. Although

some mutations in the PS and APP genes seem to play a large role in disease development in fAD cases, most of the sAD susceptibility genes, including the risk factor with the highest population-attributable risk, the ε4 allele of the apolipoprotein E (APOE) gene and those identified through genome-wide association studies (*ABCA7*, *CLU*, *CR1*, *CD33*, *PICALM*, *MS4A6A*, *MS4A4E*, *CD2AP*) have a relatively minor influence on AD progression when altered [349–351]. Moreover, despite the robust association with sAD of some of these common sequence variants, it remains largely unknown how they influence the development and course of sAD [352–355]. The same applies to the rare mutations recently discovered in the *TREM2* gene, although they confer a much larger increase in risk to develop sAD than the common sequence variants [356–358]. Although these genetic risk factors may be informative in screening for populations at risk to develop sAD, it has not yet been discovered how they exactly affect AD development [351]. Most is known about the involvement of the major risk factor APOEε4. For instance, increased levels of brain APOEε4 mRNA in AD cases, compared to controls with the same allele, were detected [359]. Interestingly, the APOEε3 allele is thought to protect against Aβ neurotoxicity [360]. Additionally, a study with a transgenic mouse model of AD expressing human APOE isoforms indicated that different APOE alleles might influence clearing soluble Aβ from the brain [361]. This is in line with evidence indicating that sAD is characterized by an inability to clear Aβ from the brain and not an increase Aβ production [362]. A similar effect is suggested for the *CLU* gene, another important risk gene associated with sAD, implicating it in the aggregation and clearance of Aβ, thereby mainly influencing age of onset and progression [363]. Apart from the gene, clusterin (CLU) levels were shown to be elevated in the cerebrospinal fluid and brains of AD patients and CLU plasma levels were associated with several AD hallmarks [364, 365].

Besides an abnormal Aβ homeostasis, dysfunctional tau has also been pointed out as a pivotal player in AD pathology. Tau, a microtubule-associated protein that promotes microtubule assembly [366], becomes hyperphosphorylated in AD. This causes it to dissociate from microtubules and aggregate, which induces cytoskeletal disorganization, neuronal dysfunction and cell death [367, 368]. This pathological process of aggregation is thought to play a part in the neurodegeneration and memory deficits as seen in AD [369, 370]. Interestingly, while a similar process occurs in other tauopathies, diseases involving pathological tau aggregation, these generally involve mutations of the tau encoding *MAPT* gene, whereas such mutations are usually not found in AD cases [367, 371]. Mitochondrial abnormalities have also been investigated as contributors to AD pathogenesis, mainly in relation to energy imbalances and increased ROS levels [372].

Aβ and tau have long been the direct focus of treatment strategies, involving potential aggregation inhibitors, immunotherapy, and enzyme modulators [373]. More recently, however, while the epigenetic involvement in neurodegeneration is being explored, the epigenetic machinery has become an attractive target for novel intervention strategies. That minor aberrancies in the epigenetic machinery can have widespread consequences on gene expression, combined with the sporadic and complex nature of AD, has led to a recent interest in the role of epigenetic factors in the etiology of AD [31, 374].

2.3.2. Parkinson's disease

PD is the second most common progressive neurodegenerative disorder, affecting the dopaminergic neurons of the midbrain substantia nigra. Because the dopaminergic projections from the substantia nigra are crucially involved in the initiation of motor events, PD is mainly known for symptoms such as tremor, rigidity, bradykinesia, and gait disturbances [375]. These motor disturbances are, however, complemented by psychiatric symptoms, autonomic impairments, sleep disturbances, and cognitive dysfunctions, including dementia, that are intrinsic to the disease pathology and may even precede the motor symptoms [376–378]. These non-motor symptoms are related to imbalances in other neurotransmitter systems, including serotonergic, noradrenergic, and cholinergic malfunctions [379]. Furthermore, cognitive impairments in PD are generally accompanied by the occurrence of Lewy bodies in brain areas including the midbrain and cortex [380]. Lewy bodies are cytoplasmic protein aggregates, consisting mainly of α-synuclein, parkin, and ubiquitin [381]. Exactly what part Lewy bodies play in PD pathophysiology warrants additional investigation. As with AD, PD exists as a familial (fPD) and a sporadic (sPD) variant, of which the former is again much rarer. *SNCA*, the gene encoding the presynaptic protein α-synuclein, is one of the cardinal risk genes for PD; increased expression of only this gene (through point mutations and multiplications) can already induce familial parkinsonian syndromes [382, 383]. In addition to *SNCA*, *MAPT*, *PARK16* and *LRRK2* are also indicated as risk genes, with *SNCA* and *MAPT* SNPs conferring the highest risk [384, 385]. Although genetic predisposition remains a high risk factor for sPD, age and environmental variations are also thought to be highly influential [386–388], with factors such as a rural environment increasing the risk to develop PD and factors such as smoking and the consumption of coffee decreasing the risk [389]. Additionally, the development of sPD has often been linked with exposure to environmental toxins, of which 1-methyl-4-phenyl-1,2,3,6-tetrahydropyridine (MPTP) has the most prominent link to developing PD, leading to its widespread use to

induce PD-like symptoms in animal models [390, 391]. A causal role in the development of PD of most other toxins, however, remains a point of controversy [392]. Nevertheless, evidence is accumulating pointing towards a cardinal role of the epigenetic machinery in mediating the effect of chronic environmental exposures on alterations in gene expression that can lead to the development of late-onset neurodegenerative diseases [393]. At least for some genes a mechanism of DNA methylation-induced allelic skewing is proposed as the underlying mechanism of how an epigenetic process can modulate the interaction between genotype and environment. DNA methylation-induced allelic skewing is the process by which the paternal and maternal alleles are differentially methylated, leading to the preferential expression of either one.

2.3.3. Huntington's disease

In contrast to AD and PD, HD is primarily a genetic, autosomal-dominant neurologic disorder, with the sporadic variant being rarer. When symptoms start to occur progress can be fast and will result in death, with no treatment options currently available to change this devastating process [394]. The most characteristic symptom of HD is chorea, but other prominent symptoms include cognitive deterioration and psychiatric disturbances. It is known that HD pathology is ignited by an expansion of a cytosine-adenine-guanine (CAG) repeat section, coding for glutamine, in the coding region of the huntingtin (HTT) gene on chromosome 4p16.3 [395]. Note that the familial and sporadic variants have the same genetic origin. A CAG repeat number of 36 units leads to the development of HD and sporadic cases are caused by *de novo* mutations that increase the repeat number to above the critical number, with high repeat numbers leading to a younger age of onset [396, 397]. The primary risk factor for developing HD is thus having family members with HD, or members with a high CAG repeat number. The expansion results in a dysfunctional HTT protein, which has been shown to disrupt transcription via multiple pathways [398, 399]. It remains, however, unclear exactly how the production of mutant HTT leads to the lethal neurodegeneration associated with HD [400]. Curiously, HD neurodegeneration is very region and cell-type specific, mainly affecting the medium-sized spiny neurons of the neostriatal nuclei, caudate nucleus and putamen, explaining the grave motor symptoms [401–408]. Despite the specificity of neurodegeneration in HD, the HTT protein can be found in neurons throughout the whole brain [409]. Wildtype HTT is mainly situated in the cytoplasm, its exact function, however, remains elusive, with proposed roles in intracellular transport, autophagy, transcription, mitochondrial functioning and signal transduction [410–413]. Nevertheless, HTT is critical for survival, as complete deletion of the HTT gene results on nonviable offspring [414].

Mutant HTT was shown to impair fast axonal transport, destabilize microtubules, and through its interactions with a multitude of proteins it disrupts important cellular pathways leading to hampered proteolysis, mitochondrial dysfunction, oxidative damage, inflammatory reactions, excitotoxicity and induction of apoptosis [415–417]. Additionally, evidence indicates that mutant HTT has a widespread impact on gene expression, through interactions with specific transcription factors [418], interference with the core transcriptional machinery and posttranscriptional modifications of histones, skewing the chromatin towards a more condensed state [419].

2.4. DNA (de)methylation in neurodegeneration

2.4.1. DNA (de)methylation in Alzheimer's disease

Early epigenetic investigations related to AD by West et al. [420] focused on DNA methylation, reporting an AD-specific hypomethylation of the APP gene promoter region in a single patient. This was confirmed by another study and linked to elevated Aβ levels [251]. A later study with a larger sample was, however, unable to replicate this finding, nor find any other significant AD-related abnormalities in *MAPT*, *APP* and *PS1* methylation [421]. Others also did not find significant AD-related methylation changes in the *APP* promoter. Barrachina et al. [421] did report the presence of low and high methylated CpG sites in and close to the *APP* promoter region, as did Fuso et al. for the *APP*, *PS* and *BACE* genes [422]. Conversely, Brohede et al. [423] observed no methylation at the investigated CpG site of the APP gene in a small sample of fAD patients, in all brain areas investigated, including the frontal cortex, parietal cortex, temporal cortex and cerebellum, concluding that *APP* is not transcriptionally regulated by methylation. All in all, these studies provide inconclusive evidence of whether APP methylation is involved in AD, raising the need for studies clearly separating between sAD and fAD, investigating multiple CpG sites and ideally also differentiate between cell types instead of using homogenates of whole regions. Wang et al. [424] observed a high interindividual variance in promoter methylation of *PS1*, *APOE*, *MTHFR*, and *DNMT1*, and a particularly marked epigenetic drift in AD cases.

A finding relevant not only to global DNA methylation, but also for many other biochemical pathways, is a severe AD-associated reduction of

SAM (up to 85%) and its demethylated metabolite SAH (up to 79%) in several neocortical areas, the hippocampus and putamen [425]. Additionally, cerebrospinal fluid levels of folate and SAM, and levels of SAM in the frontal cortex, occipital cortex, temporal cortex, putamen and hippocampus, were found to be decreased in AD cases [425–427], concomitant with an increase in brain SAH levels [428]. Accordingly, lower serum folate levels and increased plasma Hcy levels were observed in sAD patients versus controls [429]. Cell culture work has indicated that increased Hcy levels can be linked to enhanced tau hyperphosphorylation and subsequent NFT formation [430], which may be the result of the inhibitory effect of Hcy on methyltransferases, thereby preventing the methylation of protein phosphatase 2A (PP2A), which is required for its proper activation. PP2A can dephosphorylate phosphorylated tau and its decreased activity thus promotes the hyperphosphorylation of tau. In both mouse Neuro-2a (N2a) cells expressing human mutant APP and transgenic mice expressing human mutant PS1 and APP, PP2A was also found to be hypomethylated, resulting in elevated tau phosphorylation [431]. Furthermore, antagonizing folate with methotrexate in rat primary neuron cultures heightened phosphorylated tau, APP and BACE levels [432]. Interestingly, hypomethylated PP2A, but not normally methylated PP2A colocalized with hyperphosphorylated tau in the hippocampus of rats and AD cases [433].

The apparent importance of folate and vitamins B12 and B6 in maintaining SAM levels has stimulated investigations into the potentially protective effects of supplementing these vitamins to counteract cognitive decline and possibly the onset of dementia [434]. *In vitro* folate deprivation was able to induce global DNA hypomethylation, leading to an increased expression of BACE and PS1, but unaltered TACE, ADAM10 and APP expression [422]. SAM supplementation successfully restored the folate deficiency-induced abnormalities. In a follow-up study, mutant human APP transgenic mice deprived of folate, vitamin B12 and vitamin B6 [435], showed increased SAH to SAM ratios and increased PS1 and BACE levels, thus corroborating the *in vitro* findings. These increases in PS1 and BACE expression were paired with elevated Aβ aggregation, early appearance of intraneuronal Aβ and mild spatial learning and memory impairments. In a similar study, it was later shown that SAM supplementation was also able to remedy the B vitamin deficiency-induced detrimental effects in mice, resulting in a reduction in PS1 and BACE1 expression, amyloid production, tau phosphorylation, and subsequent enhanced spatial memory [436]. Vitamin B deficiency induced hypomethylation of CpG sites near the *PS1* promoter, indicating that PS1 expression is indeed regulated by methylation [437]. Another group also found beneficial effects of dietary SAM supplementation in the 3xTg-AD mouse model [438]. Additionally, a vitamin/nutriceutical formulation

including folate and vitamin B was shown to delay the progression of dementia in a small sample of early stage [439], and moderate to late stage AD [440].

Observations of an overall reduction in DNA methylation in AD patients are in line with these findings and further stress the importance of DNA methylation in AD [26, 31, 424]. Interestingly, despite this AD-associated global DNA hypomethylation, specific loci of the MTHFR gene, which is crucial for SAM synthesis, were found to be hypermethylated, in both postmortem prefrontal cortex and peripheral lymphocyte samples of AD patients [424].

Studies focusing on the hippocampus, one of the brain areas early affected by AD and aging, have observed that levels of 5-mC [253] and DNMT3A [252] increase with age in mice, whereas these levels are significantly decreased in the hippocampus of AD patients [441].

Siegmund et al. [250] found an increase in the methylation of *SORBS3* and a decrease in the methylation of *S100A2* in AD subjects, compared to controls of 60 years and older. Interestingly, although a progressive increase in *SORBS3* and decrease in *S100A2* methylation is normal with aging, this process is accelerated in AD. *SORBS3* encodes a cell adhesion molecule and the product of *S100A2* is observed in *corpora amylacea*, which are a hallmark of human brain aging and, in greater numbers, of neurodegenerative diseases [442]. A decline in *SORBS3* expression might have a hand in the synaptic abnormalities associated with AD [443]. Intriguingly, recent epigenome-wide association studies identified another gene that encodes an adaptor protein and its methylation signature is highly associated with AD pathology. More specifically, a differential cortex-specific hypermethylated region of *ANK1* was found to be associated with the early stages as well as the progression of AD neuropathology [444, 445].

Remarkably, Aβ has also been implicated as a trigger of epigenetic changes. Chen et al. [446] found that Aβ induces global DNA hypomethylation, while promoting hypermethylation of *NEP*, a gene that encodes neprilysin. Neprilysin is one of the enzymes involved in Aβ degradation and its expression is known to decrease with aging and AD. This finding indicates that Aβ is able to induce a vicious cycle that depends on epigenetic processes and favors Aβ deposition. Other regulatory players may further enforce this cycle, for instance, TNF-α and cysteine-dependent aspartate-directed protease (caspase)-3 were found to increase Aβ production, and they are increasingly expressed in response to hypomethylation [447–450].

Tau gene expression is also subject to complex epigenetic regulation, involving differentially methylated binding sites for transcription factors. It was found that with age, the activator-binding site for transcription factor SP1 became hypermethylated in the tau gene promoter region, whereas the repressor-binding site for GCF was hypomethylated in the human cerebral cortex [251], which might be relevant to AD and other age-related tauopathies. This points toward an age-related decrease in tau expression, which has indeed been detected in the human frontal cortex and hippocampus, but this did not correlate with NFT pathology [451].

The *APOE* gene promoter has a low CpG count and generally exhibits low levels of DNA methylation. There is, however, a CpG island located at the 3' end that is usually heavily methylated, and which contains the sequence of the *APOE* ε4-haplotype, the prime genetic risk factor for sAD [424]. It has been suggested that the ε4 allele might disturb the epigenetic regulation of the *APOE* gene, as this allele is associated with a C > T transition, preventing this site from being methylated. The *CLU* gene is more clearly regulated by epigenetic mechanisms, as its promoter regions contain a CpG island, the demethylation of which after 5-aza-2'-deoxycytidine (decitabine; DAC) treatment was shown to enhance CLU expression in cancer cell lines [452]. A similar demethylating treatment in addition to the administration of HDAC inhibitors (HDACIs) has also been observed to increase CLU expression and secretion in human neurons and retinal pigment epithelial cells [453, 454].

There is increasing evidence of disturbed cell-cycle control and subsequent induction of apoptosis in degenerating AD neurons and, although not directly investigated, many of the proteins involved in these processes that have been shown to be upregulated in these neurons and are also known to be regulated through DNA methylation [447, 455–458]. In addition to genes involved in cell-cycle control, the promoter regions of *COX-2* and *NF-κB* were found to be hypomethylated, while the promoter regions of *BDNF* and *CREB* were hypermethylated in the frontal cortex of AD patients [459].

Bollati et al. [460] specifically investigated blood for the methylation status of repetitive elements, including *Arthrobacter luteus* elements (*Alu*), long interspersed element 1 (LINE-1) and satellite-α (SAT-α), which comprise a large portion of the human genome and are known to contain large numbers of CpG sites. Interestingly, they found that LINE-1 methylation was increased in AD patients and that within the AD group enhanced LINE-1 methylation was associated with a better cognitive performance.

Although not as well studied in relation to AD as DNA methylation, the DNA demethylation process is receiving increased attention. As for

5-mC, 5-hmC levels were also found to be greatly decreased in the hippocampus of AD patients [441]. This is in line with previous findings indicating a global DNA hypomethylation in EC NFT-bearing neurons of AD patients [26]. Additionally, it was found that global 5-hmC levels were decreased in the EC and cerebellum of AD subjects, while no significant disease-related changes in 5-mC, 5-fC and 5-caC were detected [461]. In contrast, levels of 5-mC and 5-hmC were immunohistochemically found to be increased in the middle frontal gyrus and middle temporal gyrus of AD patients and positively correlated with Aβ, NFT, and ubiquitin load [462]. This study included a cell-type specific analysis and found that 5-hmC and 5-mC were mainly present in Neuronal Nuclei (NeuN; a neuronal marker)-positive cells, with glial fibrillary acidic protein (GFAP; an astrocyte marker)-positive cells and ionized calcium-binding adapter molecule 1 (IBA1; a microglial/macrophage maker)-positive cells only presenting with weak or no immunoreactivity. This latter study is in line with findings from Bradley-Whitman and Lovell [463], who observed increased levels of TET1, 5-mC and 5-hmC in the hippocampus and parahippocampal gyrus in subjects with preclinical and late-stage AD. In addition, it was found that 5-fC and 5-caC levels were significantly decreased. Another study detected global hypermethylation in the frontal cortex of AD patients [459]. Whether global 5-mC and 5-hmC levels are thus decreased or increased in AD remains to be conclusively determined. Possible factors contributing to the discordant findings have been suggested and include differences in the brain regions studied, tissue processing, and detection methods and protocols [462]. An additional factor that could influence readings is whether a cell type-specific analysis is conducted, or different cell types are grouped together. Considering the uncertainty regarding global 5-mC and 5-hmC changes in relation to AD it might be a bit too early to speculate about the consequences of such changes. Nevertheless, Coppieters et al. [462], who detected a global DNA hypermethylation and hyperhydroxymethylation argue that these changes may facilitate cell death, as the methylation of cytosines is thought to enhance the mutation rate of these cytosines and this increased mutation rate could facilitate the loss of neurons in AD. There are, however, also studies indicating that DNA hypomethylation leads to neuronal degeneration [35, 464], suggesting that no simple conclusions can be drawn from observations of globally increased or decreased DNA methylation levels.

Münzel et al. [265] observed an age-related increase in 5-hmC levels, which seemed to be especially prominent in genes associated with neurodegeneration. Another finding indicating DNA demethylation to play a role in the development of AD is a SNP in the TET1 gene that was associated with sAD [465]. See Table 4 for an overview of the aberrant DNA (de)methylation in AD.

2.4.2. DNA (de)methylation in Parkinson's disease

Obeid et al. [249] explored the relation between the methylation potential, represented by the SAM/SAH ratio, and cognitive performance in PD patients, and found that a higher methylation potential correlated with better cognitive capabilities. In addition, it was found that α-synuclein can associate with DNMT1, sequestering it in the cytoplasm, resulting in global DNA hypomethylation. This property of α-synuclein was not only found in PD cases, but also in dementia with Lewy bodies and a transgenic mouse model expressing human α-synuclein [466]. Because α-synuclein can also be observed in AD [467], this mechanism might also contribute to the global DNA hypomethylation observed there. *In vitro* overexpression of DNMT1, as well as in transgenic mice, was able to normalize the nuclear localization of DNMT1. Jowaed et al. [468] specifically investigated methylation of human *SNCA* and showed that expression of this gene is regulated through methylation of the first intron.

Interestingly, a negative correlation between *SNCA* intron 1 methylation and *SNCA* expression has also been identified, and that *SNCA* methylation is decreased in the substantia nigra, putamen, and cortex of sPD patients [468, 469]. Another study, investigating the high-resolution methylome of Lewy body disease cases, including PD, found, however, no overall differences in *SNCA* intron 1 methylation [470]. Although this study reported some differences at the single CpG level, it signifies that the extent of erroneous DNA methylation in PD warrants additional research efforts. Apart from *SNCA*, however, additional genes, including *PARK16*, *GPNMB* and *STX1B* have also reported to be differentially methylated in PD [471]. A very recent EWAS in blood from PD patients, using a discovery and replication cohort, identified additional differentially methylated genes, with the most reliable differentially methylated CpGs being located in the *FANCC* and *TNKS2* genes [472]. How this aberrant DNA methylation exactly affects gene expression and ultimately influences PD pathology remains to be unveiled.

Interestingly, although a mutation in *PARK2*, the gene encoding parkin, has been associated with a juvenile form of PD, deviant methylation patterns in the promoter of this gene have been observed in myelogenous leukemia and acute lymphoblastic leukemia, but not PD [473, 474]. Similar observations were made for *UCHL1*, a gene associated with PD, and *ATP13A2*, which causes a recessive form of parkinsonism, failing to establish a relation between abnormal promoter methylation and PD, although the promoter of *UCHL1* was found to be hypermethylated in cancer [383, 421, 475]. Table 5 summarizes the findings regarding dysregulated DNA (de)methylation in PD.

TABLE 4. Epigenetic dysregulation in Alzheimer's disease: DNA (de) methylation.
↑ indicates increased levels, ↓ indicates decreased levels, and ≠ indicates altered, not further specified.
ABBREVIATIONS: 450K BeadChip, Illumina Infinium HumanMethylation 450K BeadChip; 5-caC, 5-carboxylcytosine; 5-fC, 5-formylcytosine; 5-hmC, 5-hydroxymethylcytosine; 5-mC, 5-methylcytosine; Aβ, amyloid-β; AD, Alzheimer's disease; BSeq, bisulfite sequencing; CEC, cerebral endothelial cell; CiEC, circulating endothelial cells; CpG, cytosine-phosphate-guanine; EC, entorhinal cortex; FC, frontal cortex; GCF, granulocyte chemotactic factor; HPLC, high-performance liquid chromatography; IHC, immunohistochemistry; LINE-1, long interspersed element 1; MFG, middle frontal gyrus; MS-PCR, methylation, specific PCR; MTG, middle temporal gyrus; N2a, neuro-2a cell line; NS, not specified; PFC, prefrontal cortex; SB, Southern blot; SK-N-BE, SK-N-SH, human neuroblastoma cell lines; SP, specificity factor; STC, superior temporal cortex; TET1, ten-eleven translocation 1.

table 4.

Gene	Regulation	Epigenetic modification	Observed in	Sample size	Approach	Methods	Reference
APP	↓	Methylation (promoter region)	AD patients	16	Targeted (18 loci)	BSeq	[251]
				1	Targeted (1 locus)	SB	[420]
	≠	Methylation (CpG sites in and close to the promoter region)	AD patients	AD stages I to II (n = 17), AD stages III to IV (n = 15), AD stages V to VI (n = 12)	Targeted (6 loci)	BSeq	[421, 422]
PS1	≠	Methylation (CpG sites in and close to the promoter region)	SK-N-SH and SK-N-BE cell lines	-	Targeted (5 loci)	HPLC/Nucleic acid analysis	[422]
BACE	≠	Methylation (CpG sites in and close to the promoter region)					
	↓	Expression due to folate deptivation -induced global DNA hypomethylation					
PS1	≠	Methylation (promoter region)	AD patients	24	Targeted (12 loci)	BSeq	[424]
	↑	Expression due to folate deptivation -induced global DNA hypomethylation	SK-N-SH and SK-N-BE cell lines	-	Targeted (5 loci)	HPLC/Nucleic acid analysis	[422]
APOE	≠	Methylation (promoter region)	AD patients (PFC, peripheral lymphocytes)	24	Targeted (12 loci)	BSeq	[424]
MTHFR	≠	Methylation (promoter region)					
	↑	Methylation					
DNMT1	≠	Methylation (promoter region)					
PP2A	↓	Inhibition of methylation due to increase of Hcy levels	N2a cells, AD mouse model (APP/PS1)	NS	Targeted (1 locus)	IHC	[431]
SORBS3	↑	Methylation	AD patients	18	Targeted (50 loci)	BSeq	[250]
S100A2	↓						
NEP	↑	Methylation	CEC cell line exposed to Aβ	-	Targeted (1 locus)	MS-PCR	[446]
MAPT	↑	Methylation (SP1 activator binding site)	Human (cerebral cortex)	16	Targeted (18 loci)	BSeq	[251]
	↓	Methylation (GCF repressor binding site)					
APOE	↑	Methylation (CpG island located at the 3' end)	AD patients (postmortem)	24	Targeted (12 loci)	BSeq	[424]
COX-2	↓	Methylation (promoter region)	AD patients (FC)	10	Targeted (8 loci)	Promoter region-specific CpG methylation assay	[459]
NF-κB	↓						
BDNF	↑						
CREB	↑						
LINE-1	↑	Methylation	AD patients (blood)	43	Targeted (3 loci)	BSeq	[460]
ANK1	↑ ↑	Methylation	AD patients (EC, STC, PFC)	62, 122, 144	Genome-wide	BSeq	[445]

Protein/ (Hydroxy) Methylated base	Regulation	Modification in	Observed in	Sample size	Approach	Reference
5-hmC	↓	Expression	AD patients (EC, cerebellum)	10	IHC	[441]
5-mC, 5-hmC	↑		AD patients (MFG, MTG, hippocampus)	7 late-stage AD 5 preclinical AD		[463]
				13 MFG 29 MTG		[462]
5-fC, 5-caC	↓		AD patients (hippocampus)	7 late-stage AD, 5 preclinical AD		[463]
DNMT3A	↓		AD patients	10		[441]
DNMT3A2	↓		Mice (12 months old)	15		[255]
TET1	↑		AD patients (hippocampus)	7 late-stage AD, 5 preclinical AD		[463]

table 4. (continued)

2.4.3. DNA (de)methylation in Huntington's disease

DNA methylation states have been investigated in transgenic models, and to a lesser extend in HD patients [476–478] (Table 6). Promoter regions of genes important for neurogenesis were found to be hypermethylated in the presence of mutant HTT [476] (Table 6). Although these findings need to be replicated in HD patients, reduced hippocampal neurogenesis might partially underlie the cognitive impairments seen in HD [407]. Decreased expression of the adenosine A2a receptor in HD patients is also epigenetically regulated. In both HD patients and transgenic mice adenosine A2a receptor expression was observed to be downregulated [478]. However, in patients this was associated with increased 5' UTR DNA methylation, whereas in the mouse model with decreased 5' UTR DNA hydroxymethylation of the adenosine A2a receptor gene (*ADORA2A*). This finding indicates that epigenetic regulation might differ between species and illustrates the importance of replicating findings in human cases. The widely neglected 7-mG form of DNA methylation, which also occurs in RNA, was found to be disturbed in HD mouse models and patients, in both the nucleus and cytoplasm, the latter primarily reflecting methylated RNA [13].

TABLE 5. Epigenetic dysregulation in Parkinson's disease: DNA (de) methylation.
↓ indicates decreased levels, and ≠ indicates altered, not further specified.
ABBREVIATIONS: 450K BeadChip, Illumina Infinium HumanMethylation 450K BeadChip; (s)PD, (sporadic) Parkinson's disease; SN, substantia nigra; BSeq, bisulfite sequencing; methQTL, methylation quantitative trait locus.

TABLE 6. Epigenetic dysregulation in Huntington's disease: DNA (de) methylation.
↑ indicates increased levels and ≠ indicates altered, not further specified.
ABBREVIATIONS: 7-mG, 7-methylguanine; CAG140 KI mice, transgenic mouse model overexpressing human HTT with 140 cytosine-adenine-guanine repeats; HD, Huntington's disease; HTT, Huntingtin; R6/2 mice, transgenic mouse model overexpressing exon 1 of human HTT with an expanded cytosine-adenine-guanine repeat length; NS, not specified; RRBS, reduced representation bisulfite sequencing; MeDIP-Seq, methylated DNA immunoprecipitation sequencing; ECD, electrochemical detection; HPLC, high-performance liquid chromatography; ChIP-Seq, chromatin immunoprecipitation sequencing.

2.5. Chromatin remodeling in neurodegeneration

2.5.1. Chromatin remodeling in Alzheimer's disease

Going from the DNA to the chromatin level, additional epigenetic dysregulation can be observed in AD (Table 7). Histone acetylation was found to be drastically decreased in the temporal lobe of AD patients when compared to aged controls [479], but also in animal models of AD [480]. The importance of gene-specific investigations apart from global changes in epigenetic markers is exemplified by the observation of increased H3 acetylation at the promoter region of the *BACE1* gene in AD patients [481]. The increase in H3 acetylation enhanced promoter accessibility and subsequent gene expression. Importantly, it was found that indirectly enhancing histone acetylation through chronic treatment with HDACIs was able to reverse cognitive deficits in double transgenic mice overexpressing human APP isoform 695 with the double KM670/671NL Swedish mutation (APPswe) and the human PS1 deleted in exon 9 mutation (PS1dE9) (APPswe/PS1dE9 mice) [482]. The mechanism of action of HDACI treatment might be related to the

table 5.

Gene	Regulation	Epigenetic modification	Observed in	Sample size	Approach	Methods	Reference
SNCA	↓	Methylation	sPD patients (SN, putamen, cortex)	6, 14	Targeted (1 locus)	BSeq	[468]
				11	Targeted (1 locus)	BSeq	[469]
PARK16 *GPNMB* *STX1B*	≠	Methylation	PD patients	12, 386	Genome-wide	methQTL	[471]
FANCC *TNKS2*	≠	Methylation	PD patients	30	Genome-wide	450K BeadChip	[472]

table 6.

Gene	Regulation	Epigenetic modification	Observed in	Sample size	Approach	Methods	Reference
Ap-1	↑	Methylation of promoter region	Mouse striatal neurons overexpressing HTT	-	Targeted (10 loci)	RRBS, MeDIP-Seq, ChIP-Seq assay	[476]
Sox2	↑						
Pax6	↑						
Nes	↑						
	≠	7-mG DNA and RNA methylation	HD mouse models (R6/2, CAG140 KI mice)	10		ECD/HPLC	[13]
			HD patients	NS			

finding that dysregulation of H4K12ac is implicated in mediating cognitive impairment seen in aged mice, impairments which were alleviated through HDACI administration [281]. Another study using transgenic APP/PS1 mice observed diminished acetylation of H4 and linked this to memory impairments, which could be alleviated through trichostatin A (TSA), an HDACI, administration [483]. Decreased histone acetylation is in line with the discovery of elevated nuclear translocation of EP300 interacting inhibitor of differentiation 1 (EID1) in cortical neurons of AD subjects [484]. EID1 inhibits EP300 and CREBBP, important KATs, and the overexpression of EID1 in mice resulted in learning and memory impairments thought to be the result of this inhibition. In the triple transgenic mouse model of AD, expressing human mutant APPK670N/M671L, PS1M146V, and TauP301L, (3xTg-AD mice) CREBBP expression was also decreased, while overexpression of CREBBP elevated brain-derived neurotrophic factor (BDNF) levels and restored memory function in this AD model [485]. Additionally, expression of a truncated inhibitory form of EP300 impaired memory in transgenic mice [486, 487]. Curiously, while knock-out of KAT2B resulted in memory impairments in mice [488], such mice were resistant to the neurotoxic effects of Aβ injected into the lateral ventricles in another study [489].

Conversely, cultured neurons from 3xTg-AD mice and non-transgenic controls, harvested at different ages, revealed increased H3 and H4 acetylation levels from an age of 4 months, which is before the onset of memory impairments in this model of AD [490]. With normal aging, H3 acetylation levels seem to remain unchanged, whereas H4 acetylation levels decreased, but administration of Aβ to the non-transgenic neurons increased acetylation levels. The repressive H3K9 mark in these same neurons increased with age in both the transgenic and non-transgenic neurons, but was more prominent in the transgenic cells. This later finding has been corroborated in humans; comparing two monozygotic twins discordant for AD it was found that the one with AD exhibited higher levels of H3K9me3 in the temporal cortex and hippocampus [491]. Using transgenic mice overexpressing APPswe (Tg2576 mice), increased H3 acetylation levels were found in the prefrontal cortex, as well as increased H4 acetylation levels in the CA1 region of the hippocampus [492]. Additionally, they also reported elevated levels of H3 phosphorylation and methylation in the prefrontal cortex, but decreased H3 methylation in the striatum.

While the use of non-selective HDACIs is a promising strategy for the treatment of cognitive problems, it might be even better to target the specific HDACs that induce the memory problems. Currently, HDAC2 is a prime suspect [95, 493]. Especially the group of Gräff and Tsai has contributed significantly in this respect, starting with their detection of

increased levels of HDAC2 in the hippocampus and prefrontal cortex of a mouse model of AD, while levels of the related HDAC1 and HDAC3 were not affected. Note, however, that recently it was reported that MS-275 treatment, an HDACI that favors HDAC1, was able to partially alleviate behavioral deficits, neuroinflammation and plaque load in transgenic mice overexpressing APPswe and human PS1 with the L166P mutation, line 21 (APP/PS1-21 mice) [494], and that HDAC3 inhibition enhanced long-term memory formation in the C57 black 6 inbred mouse strain (C57BL/6 mice) [495]. To study the effects of this HDAC2 dysregulation at the gene level, Gräff et al. [493] focused on genes involved in learning, memory and synaptic plasticity that were previously shown to be downregulated in the AD brain and found that HDAC2 was significantly enriched at the promoter and coding regions of these genes, in their mouse model. In addition, they found several acetylation marks, associated with neuroplasticity, to be hypoacetylated (Table 7). Subsequently, it was shown that increased localization of HDAC2 to the investigated genes and hypoacetylation negatively correlated with RNA polymerase (RNAP) II binding and mRNA expression. Interestingly, knock-down of HDAC2 ameliorated the cognitive problems and aberrant synaptic plasticity. It was then investigated how HDAC2 could be induced in AD, by testing *in vitro* the effect of the AD-associated neurotoxic stimuli hydrogen peroxide and Aβ in primary hippocampal neurons. Both stimuli were found to enhance HDAC2 mRNA levels through activation of glucocorticoid receptor (GR) 1. Importantly, HDAC2 was also investigated in human postmortem brain samples from AD patients revealing that in AD cases HDAC2 was markedly increased in the hippocampus and EC. Already at Braak stages I and II HDAC2 levels were found to be significantly elevated in hippocampal area CA1 and the EC, indicating that increased HDAC2 activity might be involved in the early stages of AD. In addition to HDAC2, HDAC6 levels were found to be significantly higher in the hippocampus of AD cases when compared to controls [496]. Interestingly, HDAC6 is thought to interact with tau, affecting its phosphorylation and aggregation [497]. HDAC6 has been suggested to make tau vulnerable to phosphorylation through deacetylation, a finding relevant to tauopathies in general [498]. HDAC6 also indirectly affects tau clearance through deacetylation of chaperone protein heat shock protein (HSP) 90, which affects its drive towards refolding or degradation [499]. It has been reported that tau can actually act as a HDAC6 inhibitor [500]. Accordingly, in a mouse model for AD, reduction of HDAC6 levels mitigated learning and memory problems [501]. Studies on HDAC6 suggest that the role of HDACs in neurodegeneration might not solely depend on the deacetylation of histones, but also on the deacetylation of other targets, such as α-tubulin in the case of HDAC6 [497, 501, 502]. The same holds true for KATs, as the KAT human immunodeficiency virus type 1 transactivating protein interactive protein (TIP60/KAT5), the proposed

counterpart of HDAC6 [503] that has been associated with microtubule acetylation [504], has been shown to guard against Aβ toxicity [505]. KAT5 in addition regulates the expression of genes involved in apoptosis [505], axonal transport [506] and DNA damage control [507], and was found to interact with the APP intracellular domain [508].

Not all HDACs have a detrimental effect on learning and memory, as inhibition of the class IIa HDACs HDAC4 and HDAC5 impair these processes [509, 510]. Moreover, SIRT1, also an HDAC, was found to be decreased in the parietal cortex of AD patients [511]. SIRT1 has been linked to neurogenesis, DNA repair, apoptosis, cell stress responses, and various other vital signaling pathways [512]. SIRT1 expression is suggested to be beneficial in case of AD [513], as it induces ADAM10 expression, an α-secretase that can cleave APP without producing Aβ [514]. Additionally, SIRT1 is able to deacetylate tau and its deficiency in AD is thus thought to enhance tau expression and pathology [511, 515]. Note that this is in conflict with more recent findings regarding HDAC6, which is thought to increase tau pathology through deacetylation of tau, as stated above [498], although the SIRT1 study investigated global tau acetylation, whereas the HDAC6 study specifically investigated the acetylation of KXGS motifs. Nevertheless, enhancing SIRT1 expression attenuated axonal neurodegeneration and microglia-dependent Aβ toxicity [513, 516, 517]. Interestingly, SIRT1 was found to be upregulated in AD mouse models, but which might be a defense mechanism [512, 513], although it was found to be decreased in AD patients [511]. Histone modification abnormalities in AD also include histone phosphorylation, as H3 phosphorylation was found to be increased in the frontal cortex of AD patients [459]. Phosphorylation of histone protein H2A member X (H2AX) at S139, a marker of DNA damage, was shown to be increased in the AD hippocampus, but specifically in astrocytes [518].

Accumulating evidence indicates that dysfunctional protein localization might be a chief player in the incapacitation of the epigenetic machinery in AD, and possibly in neurodegeneration in general. Ogawa et al. [519] made some fundamental observations in this respect. As some neurons in AD erroneously exhibit signs of cell cycle activation, they investigated H3S10 phosphorylation, a histone modification critical for chromosome compaction during cell division. Strikingly, it was not only found that H3 phosphorylation was increased in hippocampal AD neurons, but also that this epigenetic marker was abnormally restricted to the cytoplasm in these neurons. In addition, it has also been shown that the mitogen-activated protein kinase (MAPK) pathway involved in the phosphorylation of H3 is upregulated in degeneration vulnerable neurons in AD [520–522]. Furthermore, the presence of high levels of histones in the cytoplasm of neurons in the HD brain [523] suggests that incapacitated nuclear

transport might be a common denominator for neurodegenerative processes. In support of this, Mastroeni et al. [524] found that Aβ could reduce rat sarcoma (Ras)-related nuclear protein (RAN) expression, a pivotal player in nucleocytoplasmic transport. As an apparent result, they observed DNMT1 and RNAPII to be erroneously sequestered in the cytoplasm of neurons from AD patients.

Histone 1 ADP-ribosylation has not been directly investigated in relation to AD, but the observations that a loss of poly[ADP]-ribose polymerase (PARP) 1 induces memory problems in mice [525] and that a dysregulation of PARP-1 is associated with amyloid pathology and sAD [526–528] suggests that ADP-ribosylation might be a relevant target for future studies. Although various histone methylation marks and histone methylation and demethylation enzymes have been linked to cognitive functioning in mice and humans (shortly reviewed in [503]), no links with AD have been firmly identified yet.

2.5.2. Chromatin remodeling in Parkinson's disease

α-Synuclein normally localizes to the nucleus and presynaptic nerve terminals, but increased nuclear targeting is neurotoxic, possibly contributing to PD-related neurodegeneration [529]. This nuclear toxicity of α-synuclein is supported by the finding that fPD α-synuclein mutations A30P and A53T result in an increased nuclear targeting of α-synuclein. Kontopoulos et al. [529] found that nuclear toxicity of α-synuclein might be the result of direct binding of α-synuclein to histones, reducing the levels of acetylated histone H3 and acetylation in general in cultured cells through interactions with SIRT2. In cell cultures and transgenic flies, it was further shown that a rescue of α-synuclein toxicity could be achieved through HDACIs [530, 531]. Similar findings were found after exposure to oxidative stress, which induces the relocation of α-synuclein to the nucleus, where it subsequently binds to the *PGC1-α* promoter element [532]. This binding of α-synuclein causes histone deacetylation, lowering peroxisome p roliferator receptor gamma coactivator-1 alpha (PGC1-α) expression, which is deleterious for mitochondrial functioning. Interestingly, levels of PGC1-α were significantly reduced in postmortem substantia nigra neurons of PD patients [533].

Curiously, not only does α-synuclein interact with the epigenetic machinery, the KAT EP300 interacts with protein aggregation in Lewy bodies. A specific domain of EP300, reminiscent of prion-like domains, was found to serve as a potential interaction site for misfolded proteins,

Chromatin remodelling target	Regulation	Epigenetic modification	Observed in	Sample size	Methods	Reference
Histones (globally)	↓	Acetylation	AD patients	5-6	Targeted proteomics assay	[479]
H3	↑	Acetylation (*BACE1* promoter region)	AD patients	31	FAIRE/ChIP	[481]
		Acetylation	AD mouse model (3xTg-AD mice; 4 months of age)	6	IF	[481]
			AD mouse model (Tg2576 mice; PFC)	N.S.	N.S.	[492]
	↑	Phosphorylation	AD mouse model (Tg2576 mice; PFC)			
	↓		AD patients (hippocampus)			
	↑	Methylation	AD mouse model (Tg2576 mice; PFC)			
	↓	Methylation	AD mouse model (Tg2576 mice; striatum)			
H3K9	↑	Tri-methylation	AD monozygotic twin (temporal cortex and hippocampus)	1	IHC	[491]
H4	↓	Acetylation	AD mouse model (APP/PS1 mice)	4	WB	[483]
	↑	Acetylation	AD mouse model (3xTg-AD mice; 4 months of age)	6	IF	[490]
	↑	Acetylation	AD mouse model (Tg2576 mice; CA1)	N.S.	N.S.	[492]
H2AX (S139)	↑	Phoshorylation	AD patients (hippocampus and astrocytes)	13	ICC	[518]
HDAC2	↑	Expression	AD mouse models (CK-p25, 5xFAD, Cdk5cKO mice; hippocampus and PFC)	6-9	IHC, WB,Co-IP, ChIP, PCR	[493]
			AD patients (hippocampus and EC)	4-8		
H2BK5	↓	Acetylation	AD mouse models (CK-p25, 5xFAD, Cdk5cKO mice; hippocampus and PFC)	6-9		
H3K14	↓	Acetylation	AD mouse models (CK-p25, 5xFAD, Cdk5cKO mice; hippocampus and PFC)	6-9		
H4K5	↓	Acetylation				
H4K12	↓	Acetylation	Mice (16 months old)	4-5	ChIP, PCR, HAT/ HDAC assay	[281]
SIRT1	↓	Expression	AD patients (parietal cortex)	19	WB, ISH	[511]
	↑	Expression	AD mouse model (3×Tg-AD mice)	NS		

table 7.

such as α-synuclein found in Lewy bodies, and enhance their aggregation [534]. Conversely, α-synuclein was found to have neuroprotective actions via its interactions with EP300 and nuclear transcription factor kappa B (NF-κB), downregulating the proapoptotic protein kinase Cδ (PKCδ) [535].

In PD patients, most of the aforementioned findings regarding the involvement of histone modifications still need to be replicated, but there is a report of an fPD case with a heterozygous A53T *SNCA* mutation, in which the affected allele was epigenetically silenced through histone modifications and the normal allele displayed expression levels exceeding those of two normal alleles in controls [536].

Previously, the mechanism of DNA methylation-induced allelic skewing was described as a mediator between the genotype and environment. Histone modifications, however, are the most common epigenetic modality affected by environmental toxins such as pesticides, herbicides and industrial agents [386]. MPTP, for instance, has been shown to lower H3K4me3 levels in the striatum of mice and non-human primates [537]. Interestingly, H3K4me3 levels could be restored through chronic L-3,4-dihydroxy-phenylalanine (L-DOPA) treatment. Additionally, the herbicide paraquat and the insecticide dieldrin, which have both been associated with the development of PD, were found to affect histone acetylation, with exposure to paraquat increasing H3 acetylation and hampering overall HDAC activity, and exposure to dieldrin increasing H3 and H4 acetylation, in N27 dopaminergic cells [538, 539]. Dieldrin induces apoptosis in neurons and is thought to enhance histone acetylation through its inhibitory interaction with the proteasome system, leading to the build-up of CREBBP, an important KAT. Administration of the KAT inhibitor anacardic acid in a mouse model exposed to dieldrin, decreased histone acetylation and apoptosis, suggesting that the neurotoxic effect of dieldrin leading to apoptosis might be the result of detrimental histone acetylation [538]. See Table 8 for an overview of the aberrant chromatin remodeling seen in PD.

TABLE 7. Epigenetic dysregulation in Alzheimer's disease: chromatin remodeling.
↑ indicates increased levels and ↓ indicates decreased levels.
ABBREVIATIONS: 3xTg-AD mice, triple transgenic mouse model of AD expressing human mutant amyloid precursor protein (APPK670N/M671L), presenilin 1 (PS1M146V), and tau (TauP301L); 5xFAD mice, transgenic mouse model overexpressing mutant human APP (695) with the Swedish (K670N and M671L), Florida (I716V), and London (V717I) mutations, and mutant PS1 with the M146L and L286V familial AD mutations; AD, Alzheimer's disease; APP/PS1 mice, transgenic mouse model expressing mutant human APPK670N/M671L and PS1M146V; CA, cornu ammonis; Cdk5cKO mice, cyclin-dependent kinase 5 knock-out mouse model; ChIP, chromatin immunoprecipitation; CK-p25 mice, transgenic mouse model overexpressing p25 under control of an inducible calcium/calmodulin-dependent protein kinase II a promoter; Co-IP, protein complex immunoprecipitation; EC, entorhinal cortex; FAIRE, formaldehyde-assisted isolation of regulation; H, histone; HAT, histone acetyltransferase; HDAC, histone deacetylase; ICC, immunocytochemistry; IF, immunofluorescence; IHC, immunohistochemistry; ISH, *in situ* hybridization; K, lysine; NS, not specified; PCR, polymerase chain reaction; PFC, prefrontal cortex; S, serine; SIRT, sirtuin; Tg2576 mice, transgenic mice overexpressing human APP isoform 695 with the double KM670/671NL Swedish mutation; WB, western blot.

Chromatin remodeling target	Regulation	Epigenetic modification	Observed in	Sample size	Methods	Reference
Histones (globally)	↑	Deacetylation via binding of α-synuclein to *PGC1-α* promoter element	PD patients (SN)	16	GWES	[533]
H3	↓	Acetylation via the interaction of α-synuclein with SIRT1	α-Synuclein-transfected SH-SY5Y cells	-	WB	[529]
			PD *Drosophila* model	NS		
	↑	Acetylation due to paraquat and/or dieldrin exposure	N27 dopaminergic cells	-	WB	[538, 539]
H3K4	↓	Tri-methylation due to MPTP-induced toxicity	Mice (striatum)	5	WB	[537]
			Non-human primates (striatum)	18		
H4	↑	Acetylation due to dieldrin exposure	N27 dopaminergic cells	-	WB	[539]
Heterozygous A53T *SNCA* mutation	×	Epigenetically silenced affected allele via histone modifications	fPD patient	1	PCR	[536]

table 8.

2.5.3. Chromatin remodeling in Huntington's disease

In general, HD is associated with hypoacetylated and hypermethylated histones [75, 540, 541] (Table 9). The mechanism underlying histone hypoacetylation has been fairly well characterized and is thought to center around the deleterious interaction between CREBBP and mutant HTT [285, 286]. The polyglutamine section of mutant HTT is thought to physically interact and sequester CREBBP, hampering its KAT activity [407]. Besides its KAT activity, CREBBP has additional integral functions in the regulation of transcription, interacting with various transcription factors and the RNAPII complex. Sequestration of CREBBP by mutant HTT thus disrupts transcription at multiple levels [540, 542–545]. Interestingly, a study using transgenic mice expressing a form of CREBBP without KAT activity found that this modification specifically affected the consolidation of short-term memory into long-term memory, leaving short-term memory unaffected [286]. A similar study with inactive EP300, a homolog of CREBBP, found long-term recognition and contextual fear memory to be impaired [487].

It has been proposed that disruption of CREBBP functioning by mutant HTT is also indirectly responsible for the induction of histone hypermethylation and the subsequent formation of large abnormal heterochromatin domains [546]. CREBBP is normally thought to repress the expression of *Drosophila* Su(var)3-9 and enhancer of zeste proteins

TABLE 8. Epigenetic dysregulation in Parkinson's disease: chromatin remodeling.
↑ indicates increased expression levels, ↓ indicates decreased expression levels, and × indicates a genetic mutation affecting epigenetic regulation.
ABBREVIATIONS: fPD, familial PD; H, histone; K, lysine; MPTP, 1-methyl-4-phenyl-1,2,3,6-tetrahydropyridine; PD, Parkinson's disease; PGC1-a, peroxisome proliferator receptor gamma coactivator-1 alpha; SH-SY5Y cells, human neuroblastoma cell line; SIRT1, sirtuin 1; SN, substantia nigra; SNCA, synuclein alpha; N.S., not specified; GWES, genome-wide epistasis study; WB, Western blot; PCR, polymerase chain reaction.

(SET) domain, bifurcated 1 (SETDB1), an HKMT that methylates H3K9. Due to the shutdown of CREBBP by mutant HTT, the repression of SETDB1 is released and SETDB1 levels increase, subsequently resulting in H3K9 hypermethylation. This mechanism is corroborated by observations of increased levels of *SETDB1* and H3K9me3 in striatal neurons of both transgenic HD mice and HD cases [544]. Additionally, H3K9me3 induced chromatin remodeling has been directly associated with altered gene expression profiles in HD [407, 546, 547]. Among the genes thought to be affected by this aberrant chromatin condensation is *CHRM1* [548]. Decreased expression of muscarinic acetylcholine receptor 1 (CHRM1) has been proposed to induce synaptic dysfunction and CHRM1 levels are indeed lowered in the HD striatum [549, 550]. Deregulation of striatal cholinergic signaling has been identified as a pivotal factor in the pathophysiology of HD, especially affecting medium spiny neurons [551].

table 9.

Chromatin remodeling target	Regulation	Epigenetic modification	Observed in	Sample size	Methods	Reference
histones (Globally)	≠	Acetylation	HD mouse model (R6/2 mice)	NS	WB	[540]
H3K9	↑	Tri-methylation	HD mouse model (R6/2 mice; striatal neurons)	10	RT-PCR, histone methylation assay	[544]
			HD patients (striatum)	6		

TABLE 9. Epigenetic dysregulation in Huntington's disease: chromatin remodeling.
↑ indicates increased levels and ≠ indicates altered, not further specified.
ABBREVIATIONS: H, histone; HD, Huntington's disease; K, lysine; NS, not specified; R6/2 mice, transgenic mouse model overexpressing exon 1 of human *HTT* with an expanded cytosine-adenine-guanine repeat length; RT-PCR, real-time polymerase chain reaction; WB, western blot.

2.6. Non-coding RNAs in neurodegeneration

2.6.1. Non-coding RNAs and Alzheimer's disease

In addition to DNA methylation and chromatin remodeling, ncRNAs, and especially miRNAs, have more recently been identified as possible contributors to AD pathology [552] (Table 10). Interestingly, miRNA profiling studies have found several miRNAs to be upregulated in peripheral blood mononuclear cells of AD patients [553]. Apart from the blood, many brain region-specific imbalances in miRNA expression have been identified in relation to AD (for review see [554]), including those with candidate binding sites in the 3' UTRs of β-secretase (BACE), PS1 and APP mRNA. More specifically, miR-16, -17, -20a, -101, -106a, -106b, -107, -124, -137, -147, -153, -195, -323-3p, -520c, -644, -655 and

let-7 are thought to regulate APP metabolism and Aβ production [313, 317, 555–561]. MiR-16 overexpression was found to reduce APP levels in SAMP8 mice [317]. In human neurons, miR-106a, -153 and -520c were found to target APP mRNA, downregulating APP and Aβ levels [561, 562]. Others, however, could not corroborate the involvement of miR-106a and miR-520c in the regulation of APP expression [313, 556]. Inhibiting miR-101 in hippocampal neurons proved to decrease APP expression and Aβ load, indicating a possible detrimental role of the miRNA in AD [559]. Conversely, miR-124, a miRNA involved in adult neuronal differentiation [563], is reported to be downregulated in some AD patients [564]. MiR-124 is thought to, together with polypyrimidine tract binding protein (PTBP) 1, modulate the alternative splicing of *APP* exons 7 and 8. Additionally, miR-124, but also miR-9, -29a/b-1, -29c, -107, -195, -298, -328 and -485-5p, affect Aβ indirectly by modulating BACE1 mRNA translation [313, 565–567]. In addition, in SAMP8 mice miR-195 expression was found to be decreased, whereas BACE1 levels were heightened [567]. The involvement of all these miRNAs in AD might, however, not be a general phenomenon. For instance, the miR-29a/b-1 cluster was found to be lowered in the anterior temporal cortex of sAD patients, coupled with high BACE1 protein levels, but only in approximately 30% of the examined cases [566]. In a transgenic AD mouse model miR-29c was observed to be highly expressed and was found to hamper BACE1 expression [568]. Levels of miR-107 were found to be lowered in the temporal cortex of AD cases, which was suggested to facilitate AD progression as a result of diminished *BACE1* repression [569–571]. MiR-195, -298, and -328 also reduce Aβ production by inhibiting BACE1 mRNA translation [567, 572]. Interestingly, while most of the miRNAs affecting BACE1 expression repress translation by binding to the 3' UTR of its mRNA, miR-485-5p represses BACE1 by binding to the open reading frame in exon 6 [573]. The involvement of post-transcriptional regulation of BACE1 is further supported by the observation that in AD brains BACE1 protein levels are increased, whereas mRNA levels remain unchanged [313]. Serine palmitoyltransferase (SPT) is an enzyme crucial for ceramide synthesis, which is thought to facilitate Aβ production. MiR-9, -29a/b-1, -137 and -181c negatively modulate SPT production and their levels were lowered in the frontal cortex of AD patients [574]. MiR-137 is known to additionally promote proliferation of neural stem cells through the inhibition of differentiation and dendrite formation [575, 576].

MiRNAs can thus affect Aβ production, but Aβ can also affect the expression of some miRNAs *in vitro*, for example inducing miR-106b expression [577] but repressing miR-9 and miR-181c [578]. Curiously, Hébert et al. [579] found miR-106b to be downregulated in the anterior temporal cortex of AD brains. Furthermore, miR-106 was reported to

not only directly bind to and inhibit the translation of APP mRNA, but also affect APP trafficking and Aβ clearance. Additionally, by regulating ATP binding cassette subfamily A member 1 (ABCA1), which transports cholesterol, it is thought to influence BACE and γ-secretase functioning. ABCA1 expression in the hippocampus has been positively correlated with cognitive impairments in AD [580]. Normally, miR-106b is thought to promote neurogenesis through its regulation of the insulin-like growth factor (IGF) 1 pathway [581]. MiR-9 has been reported to be a pivotal player in the differentiation and migration of neural stem cells [582, 583].

Furthermore, while there are generally no AD-associated mutations in tau, miR-15, -16, -132, and -497 are thought to regulate tau expression and might play a role in AD. In example, a decrease in miR-132 is suggested to mediate the alternative splicing of tau exon 10, through a lowered repression of PTBP2, which hampers physiological phosphorylation of tau [584, 585]. Alternative splicing of tau influences whether it contains 3 or 4 microtubule-binding repeats (3R-tau and 4R-tau, respectively) [586]. Furthermore, changes in the 3R:4R tau ratio are thought to be related to neurodegeneration [587]. Apart from miR-132, miR-9, -124 and -137 have also been reported to affect the 3R:4R tau ratio. MiR-212 and miR-454 have also been implicated in NFT pathology in AD [570, 588]. Note that dysregulated miRNA expression in relation to tau is probably not unique for AD and likely also occurs in other tauopathies. For instance, miR-132 was found to be downregulated in progressive supranuclear palsy and frontotemporal lobar degeneration [585, 589].

Phosphorylation of tau is performed by extracellular signal-regulated kinase (ERK) 1, which in turn is regulated by members of the miR-16 family (miR-15, -16, -195 and -495), of which miR-15 was found to be downregulated in AD [584]. Tau can also be phosphorylated by glycogen synthase kinase GSK 3β, which has been implicated in Aβ and NFT formation, and has been reported to be negatively regulated by miR-26a, a miRNA that is dysregulated in AD [588, 590]. As stated above, SIRT1 negatively regulates tau expression, while miR-9, -34c and -181c, however, have been shown to inhibit SIRT1 production, thereby enhancing tau production in AD [578, 591]. MiR-128 has been suggested to affect tau clearance, through its regulation of cochaperone B-cell chronic lymphocytic leukemia/lymphoma 2-associated athanogene 2 (BAG2), and has been reported to be altered in AD [592, 593]. There is additional indirect evidence for the involvement of miRNAs in the regulation of tau metabolism, as studies knocking out Dicer, which is crucial for miRNA processing, observed increased hyperphosphorylation of tau, alternate splicing of tau and neurodegeneration [594, 595].

Next to miRNAs impacting on Aβ and tau metabolism, various miRNAs that were found to be dysregulated in AD also affect other pathological hallmarks of AD. MiR-146a, is for instance a regulator of inflammatory processes through its interaction with interleukin-1 receptor-associated kinase (IRAK) 1 that is upregulated in AD brains [596, 597]. In addition to IRAK1, miR-146a was reported to bind to the 3' UTR of complement factor H, a suppressor of inflammation which is downregulated in AD [598]. Another regulator of inflammation is miR-101, which normally inhibits (COX)-2, but its levels were shown to be lowered in AD, whereas levels of COX-2 were increased [559]. MiR-132 and miR-125b have been linked to synaptic plasticity, and miR-132 was lower in the hippocampus, cerebellum and medial frontal gyrus of AD patients, whereas miR-125b levels were higher in these areas [599]. Brain cytoplasmic RNA 200 (BC200) was initially reported to be decreased in the temporal neocortex of AD cases [600], but later studies reported increased BC200 levels in the hippocampus and superior frontal gyrus, but erroneously located in the neuronal soma [601]. BC200 is thought to enhance long-term synaptic plasticity by interacting with protein synthesis in postsynaptic microdomains. In transgenic mice overexpressing a combination of APPswe and human APP with the V717F Indiana mutation (APPind; Tg19959 mice) miR-103 and miR-107 were found to be decreased, which was linked to increased cofilin expression [602]. Cofilin is a pivotal player in cytoskeletal integrity and is thought to influence microtubule stability, neuronal transport and synaptic functioning [603].

Compared to miRNAs, evidence for the involvement of other ncRNAs in AD pathology is sparse. RNAPIII-dependent ncRNA neuroblastoma differentiation marker (NDM) 29 was found to facilitate the production and secretion of Aβ by influencing APP processing [604], whereas the lncRNA BACE1-antisense (BACE1-AS) positively affects BACE1 expression [313]. BACE1-AS has a length of about 2 kb and is transcribed from the DNA strand complementary to the BACE1 gene [605]. It is thought to enhance the stability of BACE1 mRNA, facilitating BACE1 protein production. Interestingly, BACE1-AS transcription is enhanced in response to Aβ exposure, initiating a vicious cycle, as its positive effects on BACE1 expression in turn enhances Aβ production. In both AD patients and Tg19959 mice, BACE1-AS was indeed found to be overexpressed. Although only confirmed for the nonconventional miR-485-5p, evidence suggests that the binding of BACE1-AS to BACE1 mRNA enhances mRNA stability by competing with miRNA binding [573]. The ncRNA 17a has been observed to promote Aβ secretion and accumulation and is elevated in the cerebral cortex of AD cases, which is thought to be the result of inflammatory factors [606].

2.6.2. Non-coding RNAs and Parkinson's disease

Apart from epigenetic transcriptional regulation of *SNCA*, some miRNAs have been identified that regulate its function on a translational level. One of these is miR-7, which negatively regulates α-synuclein expression through binding to the 3' UTR of α-synuclein mRNA and is mainly expressed in neurons [607]. Through its suppression of α-synuclein, including cytotoxic mutant forms, it is thought to have a neuroprotective role in PD. Interestingly, miR-7 levels were shown to be decreased *in vitro* and in animal models after exposure to the toxic metabolite of MPTP, 1-methyl-4-phenyl-pyridinium ion (MPP+), increasing α-synuclein expression. Downregulation of miR-7 might thus, at least in part, explain how MPTP induces PD-like pathology.

Another miRNA, miR-153, represses α-synuclein production both at a mRNA and protein level [608]. Indirectly, miR-433 has also been implicated in SNCA expression, via its regulation of the fibroblast growth factor 20 (FGF20). FGF20 expression has been positively correlated with α-synuclein expression, and a 3' UTR SNP (rs1270208) has been linked to an increased risk to develop PD. This SNP interferes with miR-433 binding, increasing FGF20 expression [609]. Conversely, α-synuclein has been shown to affect the expression levels of certain miRNAs in in vivo models were α-synuclein was overexpressed. Levels of various miRNAs were affected in a transgenic mouse model overexpressing human A30P α-synuclein [610] (Table 11). In a transgenic *C. elegans* model expressing human α-synuclein, alterations in levels of 12 miRNAs were found [611]. The significance for the human situation, however, remains to be elucidated as the human orthologs of these miRNAs remain to be identified.

In addition to *SNCA*, the expression of *LRRK2*, a gene implicated in both fPD and sPD, is also regulated by miRNAs. MiR-205 targets the 3' UTR of *LRRK2* mRNA and was found to be downregulated in sPD cases in which leucine-rich repeat kinase 2 (LRRK2) protein levels were increased, whereas miR-205 was able to mitigate the aberrant neurite growth induced by LRRK2 mutation R1411G *in vitro* [612]. Conversely, mutant LRRK2 (I1915T or G2019S) was observed to inhibit the actions of let-7 and miR-184*. These miRNAs regulate E2F transcription factor 1 (E2F1) and differentiation regulated transcription factor protein (DP) levels, transcription factors associated with cell cycle regulation and cell survival. LRRK2 thus induces E2F1 and DP expression, which is associated with reduced dopaminergic neuron numbers and locomotor activity in *Drosophila*, effects that have also been linked to mutant LRRK2 [613].

table 10.

Regulation	ncRNA	Observed in	Sample size	Approach	Methods	Reference
↓	miR-124	AD patients	11	Targeted	WB, RT-PCR	[564]
↓	miR-195	AD mouse model (SAMP8 mice)	N.S.	Targeted (5 miRNAs)	RT-PCR	[567]
↓	miR-29a/b-1	sAD patients (ATC)	34	Genome-wide	miRNA microarray	[566]
↑	miR-29c	AD mouse model (APP/PSdE9 mice)	6	Targeted	RT-PCR	[568]
↓	miR-107	AD patients	7, 10	Genome-wide	miRNA microarray, rna22 algorithm	[569, 570]
		AD mouse model (Tg19959 mice)	7	Targeted	RT-PCR	[602]
↓	miR-106b	AD patients (ATC)	19	Targeted (200 miRNAs)	miRNA microarray, NB	[579]
↓	miR-9, miR-181c	AD patients	15 (brain) 10 (CSF)	Targeted (48 miRNAs)	PCR	[588]
↓	miR-132	AD patients (hippocampus, cerebellum, MedFG)	6	Targeted (15 miRNAs)	NB	[599]
↓	miR-15	Dicer cKO mice	8-10	Targeted (200 miRNAs)	miRNA microarray	[595]
≠	miR-26a	AD patients	15 (brain) 10 (CSF)	Targeted (48 miRNAs)	PCR	[588]
↓	miR-101	HeLa, HEK293T, U373, SK-N-SH, PC12 cells	-	Targeted (1 miRNA)	PCR	[559]
↑	miR-125b	AD patients (hippocampus, cerebellum, medial frontal gyrus)	6	Targeted (15 miRNAs)	NB	[599]
↑	BC200	AD patients (hippocampus, SFG)	12	Targeted (2 miRNAs)	NB, ISH	[601]
↓		AD patients (temporal neocortex)				
↓	miR-103	AD mouse model (Tg19959 mice)	7	Targeted (2 miRNAs)	RT-PCR	[602]
↑	BACE1-AS	AD patients	2	Targeted (48 probes)	HTS, ECA	[573]
↑	ncRNA 17a	AD patients	11	Targeted (5 probes)	RT-PCR	[606]

TABLE 10. Epigenetic dysregulation in Alzheimer's disease: non-coding RNAs.

↑ indicates increased levels, ↓ indicates decreased levels, and ≠ indicates altered, not further specified.

ABBREVIATIONS: (s)AD, (sporadic) Alzheimer's disease; APP/PS1dE9 mice, transgenic mice overexpressing human APP isoform 695 with the double KM670/671NL Swedish mutation and human PS1 with the deleted exon 9 mutation; ATC, anterior temporal cortex; BACE1-AS, b-secretase 1-antisense; BC200, brain cytoplasmic RNA 200; CSF, cerebrospinal fluid; Dicer cKO mice, conditional Dicer1 knockout mouse model; ECA, enzyme complementation assay; HEK293 cells, human embryonic kidney 293 cell line; HeLa cells, cell line established from cervical cancer cells; HTS, high-throughput sequencing; ISH, *in situ* hybridization; MedFG, medial frontal gyrus; miR (NA), micro RNA; NB, northern blot; ncRNA, non-coding RNA; NS, not specified; PC12 cells, rat pheochromocytoma-derived cell line; PCR, polymerase chain reaction; RT-PCR, real-time PCR; SAMP8 mouse, senescence-accelerated prone mouse 8; SFG, superior frontal gyrus; SK-N-SH cells, human neuroblastoma cell line; Tg19959 mice, transgenic mouse model overexpressing mutant human APP with the double KM670/671NL Swedish and V717F Indiana mutations; U373 cells, human glioblastoma astrocytoma-derived cell line; WB, western blot.

Overexpression of let-7 or miR-184* reversed the deleterious effects of mutant LRRK2 expression. Note, however, that let-7b was also found to progressively inhibit neural stem cell proliferation in the subventricular zone with age [614]. Interestingly, the disruption of let-7 and miR-184*

activity by mutant LRRK2 is thought to be an indirect effect, as the increased activity of mutant LRRK2 increases the phosphorylation of eukaryotic translation initiation factor 4E binding protein (4E-BP). 4E-BP interacts with Argonaute 2, a pivotal constituent of the RISC, which in turn is required for proper let-7 and miR-184* functioning [615]. The negative regulation of these miRNAs by LRRK2 thus depends on gain of function mutations, such as I1915T and G2019S [615, 616]. Indeed, mutant LRRK2 without enzymatic activity does not affect miRNA repression [613]. Additionally, LRRK2 might also affect Dicer, another protein integral to the RNA interference (RNAi) pathway, as knocking down LRRK2 was able to attenuate some of the pathology in the *Drosophila* model related to decreased Dicer activity.

MiRNA profiling of PD brains at different stages of the disease pointed towards a miR-34b/c downregulation, mainly at the early premotor stages (1-3) [617]. MiR-34b/c is thought to modulate mitochondrial functioning via its modulation of deglycase DJ-1 and E3 ubiquitin-protein ligase parkin, proteins that have both been associated with fPD. In the blood, comparing healthy individuals with untreated PD patients, miR-1, -22*, and -29 were found to be differentially expressed, while miR-16-2*, -26a2*, and -30a were differentially expressed comparing treated and untreated PD patients [618]. Table 11 contains the most important findings regarding ncRNAs associated with PD.

table 11.

Regulation	ncRNA	Observed in	Sample size	Approach	Methods	Reference
↓	miR-7	HEK293T, SH-SY5Y, NS20Y cell lines	-	Targeted (2 miRNAs)	PCR	[607]
≠	miR-10a	Mouse model (overexpressing A30P α-synuclein)	3	Targeted (266 miRNAs)	miRNA expression profiling (microfluidic chips)	[610]
≠	miR-10b					
≠	miR-132					
≠	miR-212					
≠	miR-495					
↓	miR-205	sPD patients	8	Targeted (1 miRNA)	PCR	[612]
≠	miR-1	Healthy individuals and untreated PD patients	8	Targeted (85 miRNAs)	PCR	[618]
≠	miR-22*					
≠	miR-29					
≠	miR-16-2*	Treated and untreated PD patients	7 treated 8 untreated			
≠	miR-26a2*					
≠	miR-30a					

TABLE 11. Epigenetic dysregulation in Parkinson's disease: non-coding RNAs.
↓ indicates decreased levels and ≠ indicates altered, not further specified.
ABBREVIATIONS: HEK293T cells, human embryonic kidney cell line; miR, micro RNA; NS20Y, mouse cholinergic neuroblastoma cell line; PCR, polymerase chain reaction; SH-SY5Y cells, human neuroblastoma cell line; (s)PD, (sporadic) Parkinson's disease.

2.6.3. Non-coding RNAs and Huntington's disease

In accordance with the widespread dysregulation of gene expression, the expression of miRNAs is also affected in HD (Table 12). In HD models and patients neuronal miRNA expression was found to be decreased in general, resulting in an upregulation of their target mRNAs [144, 619, 620] (Table 12). In addition, it was observed that mutant HTT expression decreased miR-125b and miR-150 expression [621]. These miRNAs have P53 among their targets, which is known to repress NF-κB and miR-146a expression. Further interactions between P53 and mutant HTT mediate nuclear and mitochondrial damage in HD models and patients [622].

2.7. Epigenetic-based diagnostics and therapies

The available treatment strategies for most progressive neurodegenerative diseases only provide symptomatic relief, stressing the need to develop innovative, realistic therapeutic approaches that can effectively modulate the disease process. The factor common to all of the conditions discussed in this review is their neurodegenerative nature. Treatments providing a general neuroprotective effect could thus potentially be beneficial for any of them. Among such treatments, HDAC and DNMT inhibitors represent interesting options to act upon the epigenetic machinery. These are already used in the treatment of other disorders such as epilepsy and cancer [623]. The versatile and reversible nature of epigenetic changes makes epigenetic mechanisms ideal targets for the development of efficient, novel treatment strategies [624]. The adverse role of HDAC2 in memory facilitation has, for instance, led to the investigation of HDACIs as a potential treatment for memory impairment, for example in AD [95].

2.7.1. Strategies targeting DNA methylation

Neurodegenerative disorders may involve a dysregulated SAM metabolism, resulting in global DNA hypomethylation, as well as the hypermethylation of some crucial genes. It is thus not surprising that strategies aiming to increase or decrease DNA methylation have been investigated. Enhancing DNA methylation can be achieved by boosting

table 12.

Regulation	ncRNA / protein	Observed in	Sample size	Approach	Methods	Reference
↓	miR-22	HD murine models (YAC128, R6/2 mice, 3NP-induced rat model; striatum)	12 (mouse model) 18 (rat model)	Targeted (567 miRNAs)	miRNA microassay	[620]
↓	miR-29c					
↓	miR-125b					
↓	miR-128					
↓	miR-132					
↓	miR-139					
↑	miR-146a					
↓	miR-150					
↓	miR-218					
↓	miR-222					
↓	miR-344					
↓	miR-674					
↓	Drosha					

TABLE 12. Epigenetic dysregulation in Huntington's disease: non-coding RNAs.
↑ indicates increased levels and ↓ indicates decreased levels.
ABBREVIATIONS: 3NP, 3-nitro-propionic acid; HD, Huntington's disease; miR(NA), micro RNA ; R6/2 mice, transgenic mice overexpressing exon 1 of human huntingtin with an expanded cytosine-adenine-guanine repeat length; YAC128 mice, transgenic mouse model expressing the human huntingtin gene with 128 cytosine-adenine-guanine repeats.

SAM metabolism, for example through the administration of SAM itself, and by vitamin B12 and folate supplementation was shown to be effective [625–627]. Reducing the levels of methylated DNA can be accomplished with DNA demethylating agents, such as DAC [32]. However, these treatment options are highly unspecific, which may, especially in the case of DNA demethylating compounds, result in considerable adverse effects. Apart from therapies targeting DNA methylation, it has also been suggested that differential genomic and mtDNA methylation patterns may serve as diagnostic biomarkers [628, 629].

2.7.1.1. Alzheimer's disease

Scarpa et al. [627] argued that the Hcy accumulation often seen in AD might be an indication for an abnormal SAM metabolism. The resulting decrement in SAM levels could explain a global decrease in DNA methylation, which in turn could lead to an overexpression of multiple genes, including ones involved in AD pathology. Interestingly, *in vitro* SAM administration led to a repression of PS1 gene expression and Aβ production. Accordingly, folate and vitamin B12 supplementation have been found to enhance cognitive functioning and slow the development of dementia [625, 626]. There are, however, also other studies that could not detect a positive effect of folate and vitamin B12 supplementation [630, 631], and it has been reported that folic acid supplementation, in addition to other side-effects, might exacerbate neuropathology in patients with low vitamin B12 levels [632]. The observation that some crucial genes are hypermethylated in AD has led to the suggestion that the DNA demethylating agent DAC could be used to restore normal expression

levels of these genes. AD, however, is also associated with general hypomethylation and due to the non-specific nature of DAC it might in fact cause more harm than good [32].

2.7.1.2. Parkinson's disease

Similarly to AD, a disturbed SAM metabolism has also been associated with PD, and decreased methylation was linked to cognitive decline [249]. A viable option to counteract this decline would be to increase the levels of SAM, through administration of methionine, choline, folates or vitamin B12, among other possibilities [623].

2.7.2. Strategies targeting chromatin modifications

One of the most promising epigenetics-based treatment options in relation to neurodegeneration are HDACIs. There are many HDACIs, which can be subdivided into four classes, including short-chain fatty acids, hydroxamic acids, epoxyketones and benzamides. Of these, sodium butyrate (SB) has received most of the attention for clinical use. The bioavailability of SB in the central nervous system has been characterized and is well tolerated in animals and in humans due to its low toxicity [633–635]. Chen et al. [636] investigated the short-chain fatty acid valproate (valproic acid, VPA), a drug used as a mood stabilizer and anti-epileptic that was found to be an HDACI. VPA is thought to enhance H3 acetylation indirectly, possibly through the recruitment of the KAT EP300 [637]. This study found that VPA exerts a neurotrophic effect, involving the repression of pro-inflammatory factors released by microglia and a stimulation of neurotropic factor expression, including glial cell line-derived neurotrophic factor (GDNF) and BDNF, by astrocytes. VPA may thus represent a viable treatment option to counteract neurodegeneration. Comparable effects have been attributed to other HDACIs, including TSA, suberoylanilide hydroxamic acid (SAHA) and SB, as well as MS-275 and apicidin, which specifically inhibit class I HDACs [637–642]. Some HDACIs, such as 4-phenylbutyrate (4PBA), VPA, and urocortin, might also exert some of their neuroprotective effects independent of their effects on HDACs [643–645].

The use of HDACIs in the treatment of neurodegenerative diseases is thus promising and deserves attention. However, several issues, especially concerning the non-specific action of most tested HDACIs, must be overcome for HDACIs to be ready for clinical use. For example,

as some HDACIs are already being used in cancer therapy, it was observed that they induce cell death and cell-cycle arrest, which has also been reported to affect neurons [646–649]. HDACIs have additionally been observed to disturb the immune system [650, 651]. It has thus been found that targeting specific HDACs would be more preferable over the more general HDACIs. Some examples of specific HDACIs are tubacin, a selective HDAC6 inhibitor, and suramin, a selective SIRT1 and SIRT2 inhibitor [652, 653].

2.7.2.1. Alzheimer's disease

A decrease in BDNF expression, a pivotal player in memory processes [654], has been implicated as an early marker in the development of AD [490] and TSA treatment has been shown to enhance BDNF expression *in vitro*, possibly through restoring BDNF promoter histone acetylation levels [655, 656]. Another HDACI, VPA, can counter Aβ production in human embryonic kidney 293 (HEK293) cells expressing APPswe isoform 751 and in a transgenic mouse model overexpressing APPind (PDAPP mice) [657]. Using a transgenic mouse model with a 7-fold overexpression of APPswe (APP23 mice), this decrease in Aβ was shown to be due to an inhibition of GSK-3β-mediated γ-secretase cleavage of APP by VPA, which was also found to improve behavioral impairments [658]. Another HDACI, 4PBA, was shown to reverse learning and memory problems in Tg2576 mice, without affecting Aβ levels, but decreasing tau phosphorylation [659]. This was accompanied by increases in GSK-3β, histone acetylation, as well as GluR1, postsynaptic density protein (PSD) 95 and microtubule-associated protein (MAP) 2, the later three being involved in synaptic plasticity [659]. A subsequent study using the same mouse model showed that 4PBA elevated intraneuronal Aβ clearance, paired with an increase in plasticity-related proteins and subsequent restoring of dendritic spine densities in the hippocampus [660]. Treatment in mice with the HDACI SAHA achieved an increase in H4K12 acetylation levels and accordingly restored expression levels of genes associated with learning [281]. VPA and SAHA were also reported to restore CLU expression *in vitro* [661]. Effective VPA, SB, and SAHA treatment in AD models has additionally been linked to elevating H4 acetylation levels and alleviation of memory deficits [482]. Interestingly, although VPA, SB, and SAHA by elevating H4 acetylation are likely to generally affect gene expression, the HDACI TSA was found to specifically enhance expression of those genes involved in memory consolidation [662]. Curiously, inhibition of SIRTs, the class III HDACs, with nicotinamide was observed to restore cognitive impairments in 3xTg-AD mice, by indirectly promoting microtubule stability, which is affected by hyperphosphorylated tau in AD [663]. Recently, Forum Pharmaceuticals compound 0334 (FRM-0334),

a class I HDACI specifically designed to cross the blood-brain barrier (BBB) was developed, addressing the problem of BBB permeability [664]. FRM-0334 is one the first HDACI that is specifically being tested for the treatment of AD, with most others having an approved indication in cancer treatment. In relation to specific HDAC inhibition, the selective HDAC6 tubacin has been reported to affect tau phosphorylation *in vitro* [496]. In addition to HDACIs, KAT agonists are being developed [665] and it has also been suggested that targeting HKMTs and HKDMs may prove to be a viable treatment strategy for AD [503].

2.7.2.2. Parkinson's disease

As stated above, preventing histone deacetylation may alleviate memory problems, such as those associated with AD [95]. Similar approaches in PD models suggest that HDAC inhibition could be neuroprotective. In *in vitro* and *Drosophila* models the HDACIs SB and SAHA attenuated α-synuclein-induced toxic effects [529], illustrating the prominent role of disrupted histone acetylation in the neurotoxic effects of α-synuclein, caused by its direct binding to histones. TSA was able to rescue mitochondrial fragmentation and cell death induced by MPP+ in human neuroblastoma cells [666]. Similar results were obtained when inhibiting the HDAC SIRT2 with 2-cyano-3-(5-(2,5-dichlorophenyl)-2-furanyl)-N-5-quinolinyl-2-propenamide (AGK2) [530]. Additionally, pretreatment with VPA has been shown to protect midbrain dopaminergic neurons from inflammation and α-synuclein-induced neurotoxicity [636, 667–669].

Currently, one of the main treatments for PD is the dopamine precursor L-DOPA, which provides some symptom alleviation. Although not intended as such, chronic L-DOPA treatment was observed to induce epigenetic alterations. Specifically, the development of L-DOPA-induced dyskinesia presented with decreased H3K4me3 levels, whereas L-DOPA induced hyperkinesia was associated with decreased acetylation levels of H4K5, H4K8, H4K12 and H4K16, in the striatum of animal models [537]. Additionally, it was shown that L-DOPA-induced dyskinesia paralleled H3 phosphoacetylation, suggesting that the inhibition of striatal H3 phosphoacetylation when using L-DOPA might prevent the development of dyskinesia [670].

2.7.2.3. Huntington's disease

In HD, reversing the reduced expression of crucial genes due to histone hypoacetylation has been attempted through the application of HDACIs, showing promising results, both in terms of neuropathology

and motor symptoms [419, 540, 542, 543, 545, 671–673]. HDACIs improved memory and behavior in CREBBP deficiency or KAT deletion animal models [285, 286, 674]. Additionally, in an *in vitro* model based on the administration of toxic polyglutamine, a model that also exhibits histone hypoacetylation, HDACIs were able to mitigate the toxic effects of polyglutamine [675]. As in PD, SAHA, and SB also were effective in transgenic HD mice [676]. HDAC inhibition, either through SAHA or SB administration, or HDAC2 knock-out, improved memory in mice [677]. SB-treated transgenic mice overexpressing exon 1 of human HTT with an expanded CAG repeat length (R6/2 mice), however showed improved motor performance and decreased neuropathology, and survived significantly longer than non-treated mice [678]. Alternatively, 4PBA may represent a promising candidate treatment for HD, as it is already FDA-approved and data about pharmacokinetics, toxicity, and dosing are available. Although 4PBA itself has no inhibitory effect on HDACs, its metabolite phenylacetate does, in addition to having a high bioavailability in the brain [679]. As with SB, treatment with 4PBA improved motor symptoms and neuropathology in a transgenic HD mouse model [542]. Unfortunately, a multicenter, double-blind, placebo-controlled clinical trial of 4PBA to determine safety and tolerability in HD, patients showed that its efficacy was very low, necessitating the use of high doses [680, 681]. Therefore, although promising in animal models, the use of 4PBA in the treatment of HD is not optimal. A novel HDACI, the pimelic diphenylamide HDACI 4b, has also shown to be effective in R6/2 mice, improving the HD-related transcriptional abnormalities, including H3 acetylation and mRNA levels, and behavioral phenotype [419]. Additionally, in a different HD model, that expresses the first 171 amino acids of HTT with 82 CAG repeats at a relatively low steady-state level (N171-82Q mice), HDACI 4b enhanced body weight, motor function and cognitive performance, which may be mediated by modulatory effects of HDACI 4b on post-translational mechanisms, such as protein phosphorylation and ubiquitination [682]. Accordingly, activation of inhibitor of kappaB kinase (IKK) by HDACI 4b enhanced phosphorylation and acetylation of HTT, and subsequent clearance effected by the ubiquitin-proteasomal and autophagy systems. The selectivity of HDACI 4b to inhibit class I and class II HDACs, and restore proper gene expression, was also explored in various HD models, including mice, flies, and cells [683]. Targeted inhibition of HDAC1 and HDAC3 was observed to mitigate mutant HTT-induced degeneration of the eyes and brain in Drosophila, and subdued some of the metabolic defects seen in STHdhQ111 mutant HTT knock-in striatal cells. In addition to HDACI 4b, some additional compounds were tested, revealing that one of them, compound 136, could effectively inhibit HDAC3 and restore proper gene expression in HD models. Although the exact targeting mechanisms remain elusive, HDACIs upregulate pro-survival genes selectively, while downregulating pro-death genes [684].

Apart from drugs targeting HDACs, DNA-binding drugs have also received some attention in the context of HD. These efforts are mainly focused on the DNA intercalating anthracyclines, such as mithramycin A and chromomycin A3, which were isolated from *Streptomyces argillaceus* and *Streptomyces griseus*, respectively [685–687]. Mithramycin A and chromomycin A3 inhibit the replication and translation processes in cells, processes that are especially indispensable to tumors. Mithramycin A has already been used to treat Paget's disease, hypercalcemia in malignancy, and various types of cancer [688–690]. These DNA intercalating agents specifically block the binding of transcription activators and repressors that bind to GC-rich regions of gene promoters, thereby affecting gene expression [688, 691, 692]. Their interference with transcription factors SP1 and SP3 are thought to be neuroprotective, as these induce detrimental responses after oxidative stress and DNA damage [693]. In R6/2 mice, mithramycin A was found to reduce clinical and neuropathological symptoms, as well as significantly increase survival rate, probably via the reduction of pericentromeric heterochromatin condensation through an epigenetic mechanism [540, 544]. Mithramycin A can repress the HKMT SETDB1 and thereby reverse the H3K9 hypermethylation seen in R6/2 mice [540]. The effects of chromomycin A3 have been investigated in both N171-82Q and R6/2 mice, showing that it can beneficially tip the methylation-acetylation balance at H3K9 in favor of acetylation, reactivating the chromatin and improving the HD phenotype [547]. Despite already being used as chemotherapy in cancer, mithramycin A and chromomycin A3 are not well-suited for chronic use, which would be required for HD treatment, due to their relatively high, dose-dependent, toxicity in humans. Nevertheless, they may serve as a template in the development of less toxic DNA-binding compounds to treat HD.

2.7.3. Strategies targeting non-coding RNAs

Due to their relatively high specificity, miRNAs have been investigated as potential therapeutic targets for the treatment of neurodegenerative disorders. Alternatively, miRNA mimics, miRNA precursor analogs, and anti-miRNAs could also be employed to restore miRNA homeostasis in such conditions [694]. Although these RNA-based strategies are specific, a major obstacle, as with HDACIs, remains access and distribution to the brain. For instance, simple intravenous administration of anti-miRNAs conjugated to cholesterol molecules ("antagomirs"), while showing promise, failed to cross the BBB [695]. Additionally, although cholesterol facilitates cell entry, it might induce undesirable side effects [694]. More invasive, direct injections into the ventricles may represent

an effective way of circumventing the BBB to enhance the performance of such treatments [696, 697]. Packaging siRNAs into exosomes has been suggested as a less invasive strategy to pass the BBB [698, 699].

2.7.3.1. Alzheimer's disease

Suggested miRNA targets for the treatment of AD include miR-124 and miR-195, which, when increased, could lower the levels of BACE1 and subsequently Aβ [565, 567]. Alternatively, miR-323-3p, which is associated with inflammatory responses, has been proposed as a target for therapy in AD [700]. Apart from being promising treatment targets, miRNA levels have also been investigated as potential diagnostic and prognostic markers for AD. For instance, Schipper et al. [553] investigated miRNA expression in blood mononuclear cells of mild sAD patients, finding miR-34a and miR-181b to be upregulated in these patients. Although it remains to be elucidated whether these miRNAs play a significant role in AD pathology, they might serve as valuable prognostic biomarkers, especially as they can be relatively easily measured in the blood. Identifying changes in miRNA expression in very early, non-symptomatic stages of AD will substantially enhance AD diagnostic and treatment efficacy.

2.7.3.2. Huntington's disease

Because HD is caused by the expression of mutant HTT, directly targeting its mRNA through RNAi is an attractive treatment strategy [701–703]. Due to the cardinal role of normal HTT in neuronal survival and functioning, it is crucial that such a treatment specifically target only mutant HTT. Choosing for adeno-associated virus short hairpin RNA (shRNA)-mediated RNAi, Harper et al. [704] were able to improve motor function and neuropathology in transgenic N171-82Q mice. Subsequently, studies using adenovirus-shRNA, lentivirus-shRNA, adeno-associated virus-miRNA, or cholesterol-conjugated siRNA were successful in downregulating mutant HTT, reducing aggregates and improving motor functions and neuropathology [705–712]. Interestingly, chemically modified single-stranded siRNAs (ss-siRNAs) with mismatched bases have a 100-times higher mutant HTT targeting efficacy when compared to unmodified RNA, as tested in an HD mouse model expressing one mutant HTT copy with 150 CAG repeats and a normal HTT copy with 7 CAG repeats (HdhQ150/Q7 mice) after intraventricular infusion [697]. This increased potency likely stems from the ability of these ss-siRNAs to distinguish mutant from normal HTT optimally, in collaboration with RISC, in a similar fashion as miRNAs.

2.8. Discussion and future perspectives

Epigenetic dysregulation currently garners much attention as a potentially pivotal player in aging and age-related neurodegenerative disorders, mediating interactions between genetic and environmental risk factors, or directly interacting with disease-specific pathological factors. Despite the profound differences in the epigenetic aberrancies, some similar patters begin to emerge and key-player molecules arise and build bridges between the seemingly diverse psychopathophysiology of neurodegenerative diseases, such as AD, PD, and HD. For instance, careful consideration of the (de)methylation dysregulations reveals a differential methylation pattern in genes that contribute genetic predisposition to AD and PD; namely *APP*, *PS1*, *BACE* and *APOE* for AD and *SNCA* and *PARKIN16* for PD. Moreover, there is derailed histone acetylation in all three diseases discussed and, more specifically, in AD and PD, a genome wide deacetylation of histones is observed. The various modifications on H3 are another common factor of these diseases that cannot be overlooked and especially the upregulated tri-methylation of H3K9 in both AD and HD. Finally, the deviant expression of specific ncRNAs in all the three discussed diseases posits key-player roles in their pathophysiology. Briefly, the differential expression of miR-132 and miR-29 is a common observation not only among all three age-related neurodegenerative disorders but also normal aging. MiR-22, miR-26a and miR-125 also present a differential expression pattern that is common in these diseases.

Even though epigenetic research is expanding, covering more neurodegenerative disorders, the common points remain rather faint and sporadic, impeding the advancement towards innovative therapeutic strategies targeting neurodegeneration in general, instead of disease-specific processes. This notion stems from the fact that large, empirical and broad studies are rare, with most investigations using only small samples with low statistical power, focusing on very specific tissues, cell types, or genes, and looking only at one or a few epigenetic modifications [33]. This substantial heterogeneity in research makes it hard to draw concrete conclusions about the exact involvement of epigenetics in neurodegeneration, stressing the need for studies with larger sample sizes, longitudinal designs with repeated sampling schemes, study designs with tissue and cell-specific analyses – but not just one type at a time – the inclusion of multiple epigenetic markers and levels, and genome-wide approaches. Although epigenome-wide association studies are performed, it should be noted that the Illumina 450k Methylation Beadchip array, which is the most commonly used platform for such

studies, does not cover the complete methylome. Although this array covers most CpG-rich promoters, it may miss important phenotypically relevant variations in the methylome. Recent investigations have stressed the importance of DNA methylation at non-promoter and CpG-poor sites [713–715]. On a similar note, microarray-based transcriptome analyses are limited to known exons and transcripts [716]. For a whole transcriptome approach, including known and potentially novel ncRNAs, strategies based on next-generation sequencing should be employed, complemented with proper bioinformatic analyses. When compared to proteins, a much larger proportion of the human genome is transcribed into ncRNAs [117]. Nevertheless, due to their codon-bias, open reading frames and strong sequence conservation, protein genes can be detected more reliably than ncRNAs [717]. Raasch et al. [717] have therefore proposed a procedure combining multiple ncRNA identification strategies for increased sensitivity, but which is limited in its use for large genomes due to its high computational requirements.

An additional caveat of many published studies on epigenetics is the specificity of the detection techniques used. In the case of DNA modifications this is partly the result of the discovery of novel modifications. DNA methylation can be detected with techniques such as those based on sodium bisulfite sequencing or methylation-sensitive restriction enzyme cleavage. With the discovery of DNA hydroxymethylation, however, it was found that these methods cannot distinguish between methylated and hydroxymethylated DNA [49]. By a method of quantitative subtraction, oxidative bisulfate sequencing can be used to identify DNA methylation and hydroxymethylation in parallel. This procedure involves the oxidation of 5-hmC to 5-fC and subsequently to uracil. 5-fC, however, has recently been observed to play a role in epigenetic priming, and thus has an independent function from 5-mC and 5-hmC [57]. Epigenetic priming of 5-fC occurs mainly at poised enhancer sequences and is thought to activate these sites, possibly through the recruitment of transcriptional coactivator EP300. To specifically detect 5-fC, Song et al. [57] have described two methods, one of which has a single-base resolution and is also based on bisulfite sequencing. To detect 5-fC, this chemically assisted bisulfite sequencing method uses hydroxylamine protection of 5-fC to prevent it from bisulfite-mediated deamination and reduction to 5-hmC. The genomic location of 5-fC can then be determined by comparing hydroxylamine-treated bisulfite sequencing with traditional bisulfite sequencing. Sequencing of one of the various epigenetic DNA modifications should thus not be done without taking into account the other, functionally different, DNA modifications. Although epigenomic profiling provides valuable gene-specific information, the input material for profiling studies often consists of tissue homogenates. Investigations into the regional and cellular specific

effects of diseases illustrate that certain regions and cell-types are often differentially affected and using homogenates may thus prevent the proper detection of potentially crucial epigenetic changes that only occur in a limited number of cells [718]. Indeed, in the healthy brain region-specific differentially methylated regions can be distinguished [261, 713]. Even when using a homogenate of a specific brain region of interest, different cell types could still give interfering read-outs, for instance when considering the widely different levels of 5-mC and 5-hmC between cerebellar Purkinje and granule cells [54]. Although attempts are being made to investigate cell-specific epigenetic profiles these studies are few and are mostly limited to DNA methylation [12]. Interestingly, Guintivano et al. [719] have developed a model to correct DNA methylation patterns for cellular heterogeneity in the brain. Additionally, various methods to isolate cells of interest are nowadays available, including density gradients [720], laser capture microdissection [721], fluorescence-activated cell sorting [722] and magnetic affinity cell sorting [723]. These methods have only been sparingly used for epigenetic studies and need to be validated for this purpose. It has been suggested that the isolation processes themselves could already influence gene expression [33]. When looking at the potentially high variability of epigenetic markers across different tissue and cell types it may thus be worth investing in novel techniques such as CLARITY [724] and fluorescent *in situ* RNA sequencing [725] to determine the regional distribution of epigenetic markers and how this may result in regional differences in RNA and protein expression. To complicate matters further, there is increasing evidence that mitochondrial gene expression is also epigenetically regulated, the investigation of which presents a whole new set of challenges [628].

For molecular studies of the human brain, most investigations depend on postmortem tissue donated by patients. Apart from possible influences of cell isolation techniques on epigenetics markers, various peri- and postmortem factors, such as postmortem interval, are known to affect tissue components, including RNA, and which could thus potentially affect epigenetic analyses [726, 727]. Such factors are thus most likely to influence ncRNA quality, but are in addition likely to compromise chromatin structure and possibly some DNA modifications. DNA methylation, however, is thought to be relatively stable and thereby represents one of the more reliable epigenetic markers when analyzing postmortem tissue [728].

Although many epigenetic changes are associated with aging and neurodegeneration, it remains unclear whether they are integral to the aging and neurodegenerative processes, or are an epiphenomenon; the result of other factors such as increased oxidative stress. Investigating

causality with respect to epigenetic alterations is challenging in epidemiological studies and especially in studies relying on postmortem human tissue [728, 729]. Epigenetic alterations identified through the comparison of epigenetic profiles of post-mortem tissue between disease states and controls could be a combination of disease instigating alterations, but also epigenetic changes that are secondary to disease pathology [730], as well as changes that are an effect of medication [731]. Thus, when disease related epigenetic alterations are identified in epigenome-wide association studies, a major issue is to determine whether such changes actually played a role in the etiopathogenesis of the disease. An approach to overcome this hurdle would be to compare postmortem brain samples of subjects with varying stages of disease severity and including samples from preclinical, possibly prodromal stages of the disease [33]. Control samples should be very carefully selected, as for example amyloid plaques, a pathological hallmark of AD, also occur in subjects without any overt symptoms of the disease. Additionally, comparisons between familial and sporadic cases could help in the identification of causal epigenetic alternations and those that might be the secondary result of genetic mutations. Disease-specific epigenetic changes could in addition be identified by comparing patients with the target disease, with patients with similar diseases, such as frontotemporal lobar degeneration, and dementia with Lewy bodies when looking at AD, PD, and HD.

Alternatively, determining the exact role of epigenetic alterations in progressive, age-related neurodegenerative diseases could be achieved through the longitudinal assessment of the epigenome, starting with individuals in a preclinical stage of the disease. However, assessing the epigenome of living individuals is only achievable in easily accessible tissues, such as peripheral blood. Although robust disease associated epigenetic markers in the blood have great potential as diagnostic and prognostic markers, thorough comparisons between such markers in the blood and brain should be made before their relevance to the disease process can be established. Although many tissue-specific differentially methylated regions related to tissue-specific gene expression can be identified, an important study by Davies et al. [713] indicates that at least some inter-individual methylomic variation is represented in both brain and blood. Blood sampling could be used to investigate epigenetic markers in the brain in such cases. In addition to DNA methylation, chromatin status and ncRNAs in peripheral mononuclear cells have been identified as potential diagnostic markers for brain-related conditions [732, 733]. Currently, for AD, PD, and HD, it is largely unknown whether epigenetic alterations relevant to the disease process are present in blood. Nevertheless, in the case of AD, some changes in the blood transcriptome reflect disease-related changes in the brain [734].

Animal models could potentially be used to determine the relationships between disease-associated epigenetic markers in the brain and those in blood. Additionally, the epigenetic effects of specific environmental factors, such as medication, can be investigated in isolation from other possible confounding factors [33]. Presently, the most used models are transgenic mouse models that express mutated human genes associated with familial disease forms [735]. Overexpressing human mutant APP in mice may, however, result in unwanted side-effects as these models will likely also have elevated levels of APP-related products such as C-terminal fragment-β/α and amyloid precursor protein intracellular domain [736]. As Aβ plays an important role in AD, the increased presence of these additional APP-related products and APP itself may limited the usefulness of such models. Saito et al. [736] have recently circumvented these problems of APP overexpression by directly manipulating the mouse App gene, inducing fAD-related mutations that selectively enhance Aβ production and the Aβ42 to Aβ40 ratio, without affecting APP expression. Nevertheless, there are so far only few animal models of the more common late-onset sporadic forms of AD and PD. Some examples of sAD models are those based on APOE [737], or specific environmental/pharmacological interventions such as colchicine [738], cholesterol [739], or inhibition of the neuronal insulin receptor [740]. In case of sPD, models based on toxins are mainly used, such as those using the MPTP neurotoxin, which induces a permanent PD-like syndrome [741].

Using rodents to model diseases that occur mainly at the end of the life-span is attractive as they age relatively quickly. Rodent physiology, however, might prove to be too different to allow for the generation of a true model of sporadic late-onset neurodegenerative diseases. Moreover, as there are no natural counterparts of most of these diseases in rodents the successful generation of a true model depends on the available knowledge about the disease, which is in the case of sporadic late-onset neurodegenerative diseases very limited. Therefore, other model organisms may be more suitable, including non-human primates, which can naturally develop limited AD-like pathology [742], and *in vitro* models. Especially human primary cultures and induced pluripotent stem cells (iPSCs) represent highly promising alternatives to animal models [743, 744]. A number of methods have been described to generate iPSCs from easily accessible fibroblasts that can be differentiated into neurons, or induce neural progenitor-like cells (iNPCs) directly [745–748]. However, these methods have not been fully optimized yet and involve procedures that induce widespread epigenetic alterations [749].

To fully map the sequence of events leading to the development of complex diseases, epigenomic data should not be investigated in

isolation, but should be complemented with other modalities, including genomic, transcriptomic and proteomic data [750]. As such, through the integration of genetic and epigenetic approaches [334], non-coding genetic variation might be found to influence gene expression through epigenetic mechanisms. Such integrated data may also help in determining where in the etiopathogenesis of complex neurodegenerative conditions epigenetic players start to play a role. Integrated knowledge may additionally help to reveal whether therapeutic strategies targeting epigenetic mechanisms should have a general mode of action, aiming at, for example, DNA methylation at large [751], or a more targeted approach, for example changing the DNA methylation status of a specific DNA sequence [752].

Concluding, although it is clear that various levels of epigenetic regulation, including DNA and chromatin modifications, and ncRNAs, are affected during aging, AD, PD, and HD, it remains to be elucidated exactly how these epigenetic processes fit into the etiopathogenesis of these disorders and whether they play a causal role. Such knowledge is crucial for the exploration of novel therapeutic avenues, which are sorely needed to combat these devastating neurodegenerative diseases.

Acknowledgements

We thank T. Vaessen for helping with the figures. Funds have been provided by the Internationale Stichting Alzheimer Onderzoek (ISAO) grants 07551 and 11532 (D.L.A.vdH.), by the ISAO grants 09552 and 13515, and the Netherlands Organization for Scientific Research (NWO), grant 916.11.086 (Veni Award) (B.P.F.R.), the Maastricht University Medical Centre+ (Koostra Talent Fellowship) (R.L.), and the National Institutes of Health grant P50 AG005138 (P.R.H.). The authors declare that there are no conflicts of interest.

REFERENCES

[1] Choudhuri S. From Waddington's epigenetic landscape to small noncoding RNA: some important milestones in the history of epigenetics research. *Toxicol Mech Methods* 2011; 21: 252–274.

[2] Müller GB, Olsson L. Epigenesis and epigenetics. In: *Keywords and concepts in evolutionary developmental biology*. Amsterdam: Elsevier Science B.V., 2003, pp. 114–123.

[3] Handel AE, Ebers GC, Ramagopalan S V. Epigenetics: molecular mechanisms and implications for disease. *Trends Mol Med* 2010; 16: 7–16.

[4] Hsieh J, Eisch AJ. Epigenetics, hippocampal neurogenesis, and neuropsychiatric disorders: Unraveling the genome to understand the mind. *Neurobiol Dis* 2010; 39: 73–84.

[5] Hu X-L, Wang Y, Shen Q. Epigenetic control on cell fate choice in neural stem cells. *Protein Cell* 2012; 3: 278–290.

[6] Ma DK, Marchetto MC, Guo JU, et al. Epigenetic choreographers of neurogenesis in the adult mammalian brain. *Nat Neurosci* 2010; 13: 1338–1344.

[7] Henikoff S, Matzke MA, Mauro E Di. Exploring and explaining epigenetic effects. *Trends Genet* 1997; 13: 293–5.

[8] Liu L, Li Y, Tollefsbol TO. Gene-environment interactions and epigenetic basis of human diseases. *Curr Issues Mol Biol* 2008; 10: 25–36.

[9] Feinberg AP. Epigenetics at the epicenter of modern medicine. *JAMA* 2008; 299: 1345.

[10] Adwan L, Zawia NH. Epigenetics: A novel therapeutic approach for the treatment of Alzheimer's disease. *Pharmacol Ther* 2013; 139: 41–50.

[11] Razin A, Riggs AD. DNA methylation and gene function. *Science* 1980; 210: 604–10.

[12] Guo JU, Su Y, Shin JH, et al. Distribution, recognition and regulation of non-CpG methylation in the adult mammalian brain. *Nat Neurosci* 2013; 17: 215–222.

[13] Thomas B, Matson S, Chopra V, et al. A novel method for detecting 7-methyl guanine reveals aberrant methylation levels in Huntington disease. *Anal Biochem* 2013; 436: 112–120.

[14] Miller CA, Sweatt JD, Park A, et al. Covalent modification of DNA regulates memory formation. *Neuron* 2007; 53: 857–69.

[15] Silva PNO, Gigek CO, Leal MF, et al. Promoter methylation analysis of *SIRT3*, *SMARCA5*, *HTERT* and *CDH1* genes in aging and Alzheimer's disease. *J Alzheimers Dis* 2008; 13: 173–6.

[16] Flores K, Wolschin F, Corneveaux JJ, et al. Genome-wide association between DNA methylation and alternative splicing in an invertebrate. *BMC Genomics* 2012; 13: 480.

[17] Lyko F, Foret S, Kucharski R, et al. The Honey Bee Epigenomes: Differential Methylation of Brain DNA in Queens and Workers. *PLoS Biol* 2010; 8: e1000506.

[18] Ziller MJ, Gu H, Müller F, et al. Charting a dynamic DNA methylation landscape of the human genome. *Nature* 2013; 500: 477–81.

[19] Klose RJ, Bird AP. Genomic DNA methylation: the mark and its mediators. *Trends Biochem* Sci 2006; 31: 89–97.

[20] Portela A, Esteller M. Epigenetic modifications and human disease. *Nat Biotechnol* 2010; 28: 1057–1068.

[21] Bhattacharya SK, Ramchandani S, Cervoni N, et al. A mammalian protein with specific demethylase activity for mCpG DNA. *Nature* 1999; 397: 579–583.

[22] Levenson JM, Roth TL, Lubin FD, et al. Evidence that DNA (cytosine-5) methyltransferase regulates synaptic plasticity in the hippocampus. *J Biol Chem* 2006; 281: 15763–73.

[23] Weaver ICG, Cervoni N, Champagne FA, et al. Epigenetic programming by maternal behavior. *Nat Neurosci* 2004; 7: 847–854.

[24] Bergman Y, Cedar H. DNA methylation dynamics in health and disease. *Nat Struct Mol Biol* 2013; 20: 274–281.

[25] Guerrero-Bosagna C. Environmentally induced epigenetic transgenerational inheritance of phenotype and disease. *Mol Cell Endocrinol* 2012; 354: 3–8.

[26] Mastroeni D, Grover A, Delvaux E, et al. Epigenetic changes in Alzheimer's disease: Decrements in DNA methylation. *Neurobiol Aging* 2010; 31: 2025–2037.

[27] Jurkowski TP, Meusburger M, Phalke S, et al. Human DNMT2 methylates tRNA(Asp) molecules using a DNA methyltransferase-like catalytic mechanism. *RNA* 2008; 14: 1663–70.

[28] Ooi SKT, Qiu C, Bernstein E, et al. DNMT3L connects unmethylated lysine 4 of histone H3 to *de novo* methylation of DNA. *Nature* 2007; 448: 714–717.

[29] Gordon CA, Hartono SR, Chédin F, et al. Inactive DNMT3B splice variants modulate *de novo* DNA methylation. *PLoS One* 2013; 8: e69486.

[30] Okano M, Bell DW, Haber DA, et al. DNA methyltransferases Dnmt3a and Dnmt3b are essential for *de novo* methylation and mammalian development. *Cell* 1999; 99: 247–257.

[31] Mastroeni D, Grover A, Delvaux E, et al. Epigenetic mechanisms in Alzheimer's disease. *Neurobiol Aging* 2011; 32: 1161–1180.

[32] Wang J, Yu J-T, Tan M-S, et al. Epigenetic mechanisms in Alzheimer's disease: Implications for pathogenesis and therapy. *Ageing Res Rev* 2013; 12: 1024–1041.

[33] Lunnon K, Mill J. Epigenetic studies in Alzheimer's disease: current findings, caveats, and considerations for future studies. *Am J Med Genet B Neuropsychiatr Genet* 2013; 162B: 789–99.

[34] Mattson MP. Methylation and acetylation in nervous system development and neurodegenerative disorders. *Ageing Res Rev* 2003; 2: 329–342.

[35] Fan G, Beard C, Chen RZ, et al. DNA hypomethylation perturbs the function and survival of CNS neurons in postnatal animals. *J Neurosci*; http://www.jneurosci.org/content/21/3/788.short (2001, accessed 3 April 2017).

[36] Feng J, Zhou Y, Campbell SL, et al. Dnmt1 and Dnmt3a maintain DNA methylation and regulate synaptic function in adult forebrain neurons. *Nat Neurosci* 2010; 13: 423–430.

[37] Iskandar BJ, Rizk E, Meier B, et al. Folate regulation of axonal regeneration in the rodent central nervous system through DNA methylation. *J Clin Invest* 2010; 120: 1603–16.

[38] Chan MF, van Amerongen R, Nijjar T, et al. Reduced rates of gene loss, gene silencing, and gene mutation in Dnmt1-deficient embryonic stem cells. *Mol Cell Biol* 2001; 21:

7587–600.

[39] Espada J, Ballestar E, Santoro R, et al. Epigenetic disruption of ribosomal RNA genes and nucleolar architecture in DNA methyltransferase 1 (Dnmt1) deficient cells. *Nucleic Acids Res* 2007; 35: 2191–2198.

[40] Jackson M, Krassowska A, Gilbert N, et al. Severe global DNA hypomethylation blocks differentiation and induces histone hyperacetylation in embryonic stem cells. *Mol Cell Biol* 2004; 24: 8862–71.

[41] Milutinovic S, Brown SE, Zhuang Q, et al. DNA methyltransferase 1 knock down induces gene expression by a mechanism independent of DNA methylation and histone deacetylation. *J Biol Chem* 2004; 279: 27915–27.

[42] Ooi SKT, Bestor TH. The colorful history of active DNA demethylation. *Cell* 2008; 133: 1145–1148.

[43] Sharma RP, Tun N, Grayson DR. Depolarization induces downregulation of DNMT1 and DNMT3 in primary cortical cultures. *Epigenetics* 2008; 3: 74–80.

[44] Barreto G, Schäfer A, Marhold J, et al. Gadd45a promotes epigenetic gene activation by repair-mediated DNA demethylation. *Nature* 2007; 445: 671–675.

[45] Gavin DP, Chase KA, Sharma RP. Active DNA demethylation in post-mitotic neurons: A reason for optimism. *Neuropharmacology* 2013; 75: 233–245.

[46] Zhu B, Zheng Y, Angliker H, et al. 5-Methylcytosine DNA glycosylase activity is also present in the human MBD4 (G/T mismatch glycosylase) and in a related avian sequence. *Nucleic Acids Res* 2000; 28: 4157–4165.

[47] Zhu B, Zheng Y, Hess D, et al. 5-methylcytosine-DNA glycosylase activity is present in a cloned G/T mismatch DNA glycosylase associated with the chicken embryo DNA demethylation complex. *Proc Natl Acad Sci U S A* 2000; 97: 5135–9.

[48] Guo JU, Su Y, Zhong C, et al. Hydroxylation of 5-methylcytosine by TET1 promotes active DNA demethylation in the adult brain. *Cell* 2011; 145: 423–434.

[49] Ito S, Shen L, Dai Q, et al. Tet proteins can convert 5-methylcytosine to 5-formylcytosine and 5-carboxylcytosine. *Science*; http://science.sciencemag.org/content/333/6047/1300 (2011, accessed 3 April 2017).

[50] Delatte B, Fuks F. TET proteins: on the frenetic hunt for new cytosine modifications. *Brief Funct Genomics* 2013; 12: 191–204.

[51] van den Hove DLA, Chouliaras L, Rutten BPF. The role of 5-hydroxymethylcytosine in aging and Alzheimer's disease: current status and prospects for future studies. *Curr Alzheimer Res* 2012; 9: 545–9.

[52] Jin S-G, Wu X, Li AX, et al. Genomic mapping of 5-hydroxymethylcytosine in the human brain. *Nucleic Acids Res* 2011; 39: 5015–5024.

[53] Globisch D, Münzel M, Müller M, et al. Tissue distribution of 5-hydroxymethylcytosine and search for active demethylation intermediates. *PLoS One*; 5. Epub ahead of print 2010. DOI: 10.1371/journal.pone.0015367.

[54] Kriaucionis S, Heintz N. The nuclear DNA base 5-hydroxymethylcytosine is present in Purkinje neurons and the brain. *Science* (80-) 2009; 324: 929–30.

[55] Orr BA, Haffner MC, Nelson WG, et al. Decreased 5-hydroxymethylcytosine is associated with neural progenitor phenotype in normal brain and shorter survival in malignant glioma. *PLoS One* 2012; 7: e41036.

[56] Raiber E-A, Beraldi D, Ficz G, et al. Genome-wide distribution of 5-formylcytosine in embryonic stem cells is associated with transcription and depends on thymine DNA glycosylase. *Genome Biol* 2012; 13: R69.

[57] Song C-X, He C. Potential functional roles of DNA demethylation intermediates. *Trends Biochem Sci* 2013; 38: 480–484.

[58] Popp C, Dean W, Feng S, et al. Genome-wide erasure of DNA methylation in mouse primordial germ cells is affected by AID deficiency. *Nature* 2010; 463: 1101–1105.

[59] Cortellino S, Xu J, Sannai M, et al. Thymine DNA glycosylase is essential for active DNA demethylation by linked deamination-base excision repair. *Cell* 2011; 146: 67–79.

[60] He Y-F, Li B-Z, Li Z, et al. Tet-mediated formation of 5-carboxylcytosine and its excision by TDG in mammalian DNA. *Science*; http://science.sciencemag.org/content/333/6047/1303 (2011, accessed 3 April 2017).

[61] Matsubara M, Tanaka T, Terato H, et al. Mutational analysis of the damage-recognition and catalytic mechanism of human SMUG1 DNA glycosylase. *Nucleic Acids Res* 2004; 32: 5291–5302.

[62] Ma DK, Jang M-H, Guo JU, et al. Neuronal activity–induced Gadd45b promotes epigenetic DNA demethylation and adult neurogenesis. *Science*; http://science.sciencemag.org/content/323/5917/1074 (2009, accessed 3 April 2017).

[63] Rai K, Huggins IJ, James

SR, et al. DNA demethylation in zebrafish involves the coupling of a deaminase, a glycosylase, and Gadd45. *Cell* 2008; 135: 1201–1212.

[64] Schmitz K-M, Schmitt N, Hoffmann-Rohrer U, et al. TAF12 recruits Gadd45a and the nucleotide excision repair complex to the promoter of rRNA genes leading to active DNA demethylation. *Mol Cell* 2009; 33: 344–353.

[65] Richmond TJ, Luger K, Mäder AW, et al. Crystal structure of the nucleosome core particle at 2.8 A resolution. *Nature* 1997; 389: 251–260.

[66] Murray K. The occurrence of iε-N-methyl lysine in histones. *Biochemistry* 1964; 3: 10–15.

[67] Gershey EL, Vidali G, Allfrey VG. Chemical studies of histone acetylation. The occurrence of epsilon-N-acetyllysine in the f2a1 histone. *J Biol Chem* 1968; 243: 5018–22.

[68] Kleinsmith LJ, Allfrey VG, Mirsky AE. Phosphorylation of nuclear protein early in the course of gene activation in lymphocytes. *Science* 1966; 154: 780–1.

[69] Hunt LT, Dayhoff MO. Amino-terminal sequence identity of ubiquitin and the nonhistone component of nuclear protein A24. *Biochem Biophys Res Commun* 1977; 74: 650–655.

[70] Ueda K, Omachi A, Kawaichi M, et al. Natural occurrence of poly(ADP-ribosyl) histones in rat liver. *Proc Natl Acad Sci U S A* 1975; 72: 205–9.

[71] Tan M, Luo H, Lee S, et al. Identification of 67 histone marks and histone lysine crotonylation as a new type of histone modification. *Cell* 2011; 146: 1016–1028.

[72] Houston I, Peter CJ, Mitchell A, et al. Epigenetics in the human brain. *Neuropsychopharmacology* 2013; 38: 183–197.

[73] Kouzarides T. Chromatin modifications and their function. *Cell* 2007; 128: 693–705.

[74] Shiio Y, Eisenman RN. Histone sumoylation is associated with transcriptional repression. *Proc Natl Acad Sci U S A* 2003; 100: 13225–30.

[75] Jenuwein T, Allis CD. Translating the histone code. *Science*; http://science.sciencemag.org/content/293/5532/1074 (2001, accessed 3 April 2017).

[76] Day JJ, Sweatt JD. Epigenetic mechanisms in cognition. *Neuron* 2011; 70: 813–829.

[77] Allis CD, Berger SL, Cote J, et al. New nomenclature for chromatin-modifying enzymes. *Cell* 2007; 131: 633–636.

[78] Marmorstein R, Roth SY. Histone acetyltransferases: function, structure, and catalysis. *Curr Opin Genet Dev* 2001; 11: 155–161.

[79] Huynh JL, Casaccia P. Epigenetic mechanisms in multiple sclerosis: implications for pathogenesis and treatment. *Lancet Neurol* 2013; 12: 195–206.

[80] Dokmanovic M, Clarke C, Marks PA. Histone deacetylase inhibitors: overview and perspectives. *Mol Cancer Res*; http://mcr.aacrjournals.org/content/5/10/981 (2007, accessed 3 April 2017).

[81] Gregoretti I, Lee Y-M, Goodson H V. Molecular evolution of the histone deacetylase family: functional implications of phylogenetic analysis. *J Mol Biol* 2004; 338: 17–31.

[82] Marks PA, Breslow R. Dimethyl sulfoxide to vorinostat: development of this histone deacetylase inhibitor as an anticancer drug. *Nat Biotechnol* 2007; 25: 84–90.

[83] Minucci S, Pelicci PG. Histone deacetylase inhibitors and the promise of epigenetic (and more) treatments for cancer. *Nat Rev Cancer* 2006; 6: 38–51.

[84] Rosato RR, Grant S. Histone deacetylase inhibitors: insights into mechanisms of lethality. *Expert Opin Ther Targets* 2005; 9: 809–824.

[85] Xu WS, Parmigiani RB, Marks PA. Histone deacetylase inhibitors: molecular mechanisms of action. *Oncogene* 2007; 26: 5541–5552.

[86] Chang S, Young BD, Li S, et al. Histone deacetylase 7 maintains vascular integrity by repressing matrix metalloproteinase 10. *Cell* 2006; 126: 321–334.

[87] Harms KL, Chen X. Histone deacetylase 2 modulates p53 transcriptional activities through regulation of p53-DNA binding activity. *Cancer Res*; 67http://cancerres.aacrjournals.org/content/67/7/3145 (2007, accessed 3 April 2017).

[88] Kim S-H, Jeong J-W, Park JA, et al. Regulation of the HIF-1alpha stability by histone deacetylases. Oncol Rep 2007; 17: 647–51.

[89] Lagger G. Essential function of histone deacetylase 1 in proliferation control and CDK inhibitor repression. *EMBO J* 2002; 21: 2672–2681.

[90] Parra M, Mahmoudi T, Verdin E. Myosin phosphatase dephosphorylates HDAC7, controls its nucleocytoplasmic shuttling, and inhibits apoptosis in thymocytes. *Genes Dev* 2007; 21: 638–43.

[91] Vega RB, Matsuda K, Oh J, et al. Histone deacetylase 4 controls chondrocyte hypertrophy during skeletogenesis. *Cell* 2004; 119: 555–566.

[92] Zhang CL, McKinsey TA, Chang S, et al. Class II histone

deacetylases act as signal-responsive repressors of cardiac hypertrophy. *Cell* 2002; 110: 479–488.

[93] Hirschey MD. Old enzymes, new tricks: sirtuins are NAD+-dependent de-acylases. *Cell Metab* 2011; 14: 718–719.

[94] Michan S, Sinclair D. Sirtuins in mammals: insights into their biological function. *Biochem J*; http://www.biochemj.org/content/404/1/1 (2007, accessed 3 April 2017).

[95] Guan J-S, Haggarty SJ, Giacometti E, et al. HDAC2 negatively regulates memory formation and synaptic plasticity. *Nature* 2009; 459: 55–60.

[96] MacDonald JL, Roskams AJ. Histone deacetylases 1 and 2 are expressed at distinct stages of neuro-glial development. *Dev Dyn* 2008; 237: 2256–2267.

[97] Chang B, Chen Y, Zhao Y, et al. JMJD6 is a histone arginine demethylase. *Science*; http://science.sciencemag.org/content/318/5849/444 (2007, accessed 3 April 2017).

[98] Habibi E, Masoudi-Nejad A, Abdolmaleky HM, et al. Emerging roles of epigenetic mechanisms in Parkinson's disease. *Funct Integr Genomics* 2011; 11: 523–537.

[99] Brami-Cherrier K, Roze E, Girault J-A, et al. Role of the ERK/MSK1 signalling pathway in chromatin remodelling and brain responses to drugs of abuse. *J Neurochem* 2009; 108: 1323–1335.

[100] Koshibu K, Gräff J, Beullens M, et al. Protein phosphatase 1 regulates the histone code for long-term memory. *J Neurosci*; 29http://www.jneurosci.org/content/29/41/13079 (2009, accessed 3 April 2017).

[101] Sawicka A, Seiser C. Histone H3 phosphorylation – A versatile chromatin modification for different occasions. *Biochimie* 2012; 94: 2193–2201.

[102] Bernstein BE, Mikkelsen TS, Xie X, et al. A bivalent chromatin structure marks key developmental genes in embryonic stem cells. *Cell* 2006; 125: 315–326.

[103] Greer EL, Shi Y. Histone methylation: a dynamic mark in health, disease and inheritance. *Nat Rev Genet* 2012; 13: 343–357.

[104] Hwang J-Y, Aromolaran KA, Zukin RS. Epigenetic mechanisms in stroke and epilepsy. *Neuropsychopharmacology* 2013; 38: 167–182.

[105] Barski A, Cuddapah S, Cui K, et al. High-resolution profiling of histone methylations in the human genome. *Cell* 2007; 129: 823–837.

[106] Kondo Y, Issa J-PJ. Enrichment for histone H3 lysine 9 methylation at Alu repeats in human cells. *J Biol Chem* 2003; 278: 27658–62.

[107] Martens JHA, O'Sullivan RJ, Braunschweig U, et al. The profile of repeat-associated histone lysine methylation states in the mouse epigenome. *EMBO J* 2005; 24: 800–812.

[108] Pauler FM, Sloane MA, Huang R, et al. H3K27me3 forms BLOCs over silent genes and intergenic regions and specifies a histone banding pattern on a mouse autosomal chromosome. *Genome Res* 2008; 19: 221–233.

[109] Huda A, Jordan IK. Epigenetic regulation of mammalian genomes by transposable elements. *Ann N Y Acad Sci* 2009; 1178: 276–284.

[110] Clapier CR, Cairns BR. The biology of chromatin remodeling complexes. *Annu Rev Biochem* 2009; 78: 273–304.

[111] Hargreaves DC, Crabtree GR. ATP-dependent chromatin remodeling: genetics, genomics and mechanisms. *Cell Res* 2011; 21: 396–420.

[112] Vogel-Ciernia A, Wood MA. Neuron-specific chromatin remodeling: A missing link in epigenetic mechanisms underlying synaptic plasticity, memory, and intellectual disability disorders. *Neuropharmacology* 2014; 80: 18–27.

[113] Ho L, Crabtree GR. Chromatin remodelling during development. *Nature* 2010; 463: 474–484.

[114] Ronan JL, Wu W, Crabtree GR. From neural development to cognition: unexpected roles for chromatin. *Nat Rev Genet* 2013; 14: 347–59.

[115] Wang X, Nagl NG, Wilsker D, et al. Two related ARID family proteins are alternative subunits of human SWI/SNF complexes. *Biochem J*; http://www.biochemj.org/content/383/2/319 (2004, accessed 3 April 2017).

[116] Vogel-Ciernia A, Matheos DP, Barrett RM, et al. The neuron-specific chromatin regulatory subunit BAF53b is necessary for synaptic plasticity and memory. *Nat Neurosci* 2013; 16: 552–561.

[117] Amaral PP, Dinger ME, Mercer TR, et al. The eukaryotic genome as an RNA machine. *Science*; http://science.sciencemag.org/content/319/5871/1787 (2008, accessed 3 April 2017).

[118] Jády BE, Bertrand E, Kiss T. Human telomerase RNA and box H/ACA scaRNAs share a common Cajal body–specific localization signal. *J Cell Biol*; http://jcb.rupress.org/content/164/5/647 (2004, accessed 3 April 2017).

[119] Mattick JS. The central role of RNA in human development and cognition. *FEBS Lett* 2011; 585:

1600–1616.

[120] Preker P, Nielsen J, Kammler S, et al. RNA exosome depletion reveals transcription upstream of active human promoters. *Science*; http://science.sciencemag.org/content/322/5909/1851 (2008, accessed 3 April 2017).

[121] Schouten M, Buijink MR, Lucassen PJ, et al. New neurons in aging brains: molecular control by small non-coding RNAs. *Front Neurosci* 2012; 6: 25.

[122] Seila AC, Calabrese JM, Levine SS, et al. Divergent transcription from active promoters. *Science*; http://science.sciencemag.org/content/322/5909/1849 (2008, accessed 3 April 2017).

[123] Johnson R, Guigó R. The RIDL hypothesis: transposable elements as functional domains of long noncoding RNAs. *RNA* 2014; 20: 959–76.

[124] Kapranov P, Cheng J, Dike S, et al. RNA maps reveal new RNA classes and a possible function for pervasive transcription. *Science*; http://science.sciencemag.org/content/316/5830/1484 (2007, accessed 3 April 2017).

[125] Khalil AM, Guttman M, Huarte M, et al. Many human large intergenic noncoding RNAs associate with chromatin-modifying complexes and affect gene expression. *Proc Natl Acad Sci U S A* 2009; 106: 11667–72.

[126] Kim T-K, Hemberg M, Gray JM, et al. Widespread transcription at neuronal activity-regulated enhancers. *Nature* 2010; 465: 182–187.

[127] Nakamori M, Thornton C. Epigenetic changes and non-coding expanded repeats. *Neurobiol Dis* 2010; 39: 21–27.

[128] Werner A. Natural antisense transcripts. *RNA Biol* 2005; 2: 53–62.

[129] Cabili MN, Trapnell C, Goff L, et al. Integrative annotation of human large intergenic noncoding RNAs reveals global properties and specific subclasses. *Genes Dev* 2011; 25: 1915–27.

[130] Chooniedass-Kothari S, Emberley E, Hamedani MK, et al. The steroid receptor RNA activator is the first functional RNA encoding a protein. *FEBS Lett* 2004; 566: 43–47.

[131] Djebali S, Davis CA, Merkel A, et al. Landscape of transcription in human cells. *Nature* 2012; 489: 101–108.

[132] Johnsson P, Ackley A, Vidarsdottir L, et al. A pseudogene long-noncoding-RNA network regulates PTEN transcription and translation in human cells. *Nat Struct Mol Biol* 2013; 20: 440–446.

[133] Ashe HL, Monks J, Wijgerde M, et al. Intergenic transcription and transinduction of the human beta-globin locus. *Genes Dev* 1997; 11: 2494–509.

[134] Dinger ME, Gascoigne DK, Mattick JS. The evolution of RNAs with multiple functions. Epub ahead of print 2011. DOI: 10.1016/j.biochi.2011.07.018.

[135] Mercer TR, Wilhelm D, Dinger ME, et al. Expression of distinct RNAs from 3' untranslated regions. *Nucleic Acids Res* 2011; 39: 2393–2403.

[136] Jeon Y, Sarma K, Lee JT. New and Xisting regulatory mechanisms of X chromosome inactivation. *Curr Opin Genet Dev* 2012; 22: 62–71.

[137] Lisch D. Regulation of transposable elements in maize. *Curr Opin Plant Biol* 2012; 15: 511–516.

[138] Morrissy AS, Griffith M, Marra MA. Extensive relationship between antisense transcription and alternative splicing in the human genome. *Genome Res* 2011; 21: 1203–12.

[139] Koziol MJ, Rinn JL. RNA traffic control of chromatin complexes. *Curr Opin Genet Dev* 2010; 20: 142–148.

[140] Mercer TR, Mattick JS. Structure and function of long noncoding RNAs in epigenetic regulation. *Nat Struct Mol Biol* 2013; 20: 300–307.

[141] Di Ruscio A, Ebralidze AK, Benoukraf T, et al. DNMT1-interacting RNAs block gene-specific DNA methylation. *Nature* 2013; 503: 371–376.

[142] Han J, Pedersen JS, Kwon SC, et al. Posttranscriptional Crossregulation between Drosha and DGCR8. *Cell* 2009; 136: 75–84.

[143] Ambros V. The functions of animal microRNAs. Nature 2004; 431: 350–355.

[144] Han J, Lee Y, Yeom K-H, et al. The Drosha-DGCR8 complex in primary microRNA processing. *Genes Dev* 2004; 18: 3016–27.

[145] He L, Hannon GJ. MicroRNAs: small RNAs with a big role in gene regulation. *Nat Rev Genet* 2004; 5: 522–531.

[146] Lim LP, Lau NC, Garrett-Engele P, et al. Microarray analysis shows that some microRNAs downregulate large numbers of target mRNAs. *Nature* 2005; 433: 769–773.

[147] Zeng Y, Yi R, Cullen BR. MicroRNAs and small interfering RNAs can inhibit mRNA expression by similar mechanisms. *Proc Natl Acad Sci U S A* 2003; 100: 9779–84.

[148] Eulalio A, Huntzinger E, Izaurralde E. Getting to the root of miRNA-mediated gene silencing. *Cell* 2008; 132: 9–14.

[149] Fabian MR, Sonenberg N,

Filipowicz W. Regulation of mRNA translation and stability by microRNAs. *Annu Rev Biochem* 2010; 79: 351–379.

[150] The University of Manchester. miRBase; http://www.mirbase.org/ (2014).

[151] Gokey NG, Srinivasan R, Lopez-Anido C, et al. Developmental regulation of microRNA expression in Schwann cells. *Mol Cell Biol* 2012; 32: 558–68.

[152] Hu HY, Guo S, Xi J, et al. MicroRNA expression and regulation in human, chimpanzee, and macaque brains. *PLoS Genet* 2011; 7: e1002327.

[153] Qu Z, Adelson DL. Evolutionary conservation and functional roles of ncRNA. *Front Genet* 2012; 3: 205.

[154] Santosh B, Varshney A, Yadava PK. Non-coding RNAs: biological functions and applications. *Cell Biochem Funct* 2015; 33: 14–22.

[155] Bass BL. RNA editing by adenosine deaminases that act on RNA. *Annu Rev Biochem* 2002; 71: 817–846.

[156] Mattick JS. RNA as the substrate for epigenome-environment interactions. *BioEssays* 2010; 32: 548–552.

[157] Mattick JS, Mehler MF. RNA editing, DNA recoding and the evolution of human cognition. *Trends Neurosci* 2008; 31: 227–233.

[158] Athanasiadis A, Rich A, Maas S, et al. Widespread A-to-I RNA editing of *Alu*-containing mRNAs in the human transcriptome. *PLoS Biol* 2004; 2: e391.

[159] Kim DDY, Kim TTY, Walsh T, et al. Widespread RNA editing of embedded *Alu* elements in the human transcriptome. *Genome Res* 2004; 14: 1719–25.

[160] Lander ES, Linton LM, Birren B, et al. Initial sequencing and analysis of the human genome. *Nature* 2001; 409: 860–921.

[161] Levanon EY, Eisenberg E, Yelin R, et al. Systematic identification of abundant A-to-I editing sites in the human transcriptome. *Nat Biotechnol* 2004; 22: 1001–1005.

[162] Umylny B, Presting G, Efird JT, et al. Most human *Alu* and Murine B1 repeats are unique. *J Cell Biochem* 2007; 102: 110–121.

[163] Valente L, Nishikura K. ADAR gene family and A-to-I RNA editing: diverse roles in posttranscriptional gene regulation. *Prog Nucleic Acid Res Mol Biol* 2005; 79: 299–338.

[164] Conticello SG, Liang Y, Li L, et al. The AID/APOBEC family of nucleic acid mutators. *Genome Biol* 2008; 9: 229.

[165] Navaratnam N, Sarwar R. An overview of cytidine deaminases. *Int J Hematol* 2006; 83: 195–200.

[166] Muramatsu M, Sankaranand VS, Anant S, et al. Specific expression of activation-induced cytidine deaminase (AID), a novel member of the RNA-editing deaminase family in germinal center B cells. *J Biol Chem* 1999; 274: 18470–6.

[167] Blow M, Grocock R, van Dongen S, et al. RNA editing of human microRNAs. *Genome Biol* 2006; 7: R27.

[168] Kawahara Y, Megraw M, Kreider E, et al. Frequency and fate of microRNA editing in human brain. *Nucleic Acids Res* 2008; 36: 5270–5280.

[169] Nishikura K. Editor meets silencer: crosstalk between RNA editing and RNA interference. *Nat Rev Mol Cell Biol* 2006; 7: 919–931.

[170] Morse DP, Aruscavage PJ, Bass BL. RNA hairpins in noncoding regions of human brain and Caenorhabditis elegans mRNA are edited by adenosine deaminases that act on RNA. *Proc Natl Acad Sci U S A* 2002; 99: 7906–11.

[171] Conticello SG, Thomas CJF, Petersen-Mahrt SK, et al. Evolution of the AID/APOBEC family of polynucleotide (deoxy)cytidine deaminases. *Mol Biol Evol* 2004; 22: 367–377.

[172] Sawyer SL, Emerman M, Malik HS. Ancient adaptive evolution of the primate antiviral DNA-editing enzyme APOBEC3G. *PLoS Biol* 2004; 2: E275.

[173] Aguiar RS, Peterlin BM. APOBEC3 proteins and reverse transcription. *Virus Res* 2008; 134: 74–85.

[174] Schumann GG. APOBEC3 proteins: major players in intracellular defence against LINE-1-mediated retrotransposition. *Biochem Soc Trans*; http://www.biochemsoctrans.org/content/35/3/637 (2007, accessed 3 April 2017).

[175] Coufal NG, Garcia-Perez JL, Peng GE, et al. L1 retrotransposition in human neural progenitor cells. *Nature* 2009; 460: 1127–1131.

[176] Dunlap KA, Palmarini M, Varela M, et al. Endogenous retroviruses regulate periimplantation placental growth and differentiation. *Proc Natl Acad Sci U S A* 2006; 103: 14390–5.

[177] Faulkner GJ, Kimura Y, Daub CO, et al. The regulated retrotransposon transcriptome of mammalian cells. *Nat Genet* 2009; 41: 563–571.

[178] Sebastiani P, Montano M, Puca A, et al. RNA editing genes associated with extreme old age in humans and with lifespan in *C. elegans*. *PLoS One* 2009; 4: e8210.

[179] Holmes AP, Wood SH, Merry BJ, et al. A-to-I RNA editing does not change with age in the healthy

male rat brain. *Biogerontology* 2013; 14: 395–400.

[180] Nicholas A, de Magalhaes JP, Kraytsberg Y, et al. Age-related gene-specific changes of A-to-I mRNA editing in the human brain. Epub ahead of print 2010. DOI: 10.1016/j.mad.2010.06.001.

[181] Stilling RM, Benito E, Barth J, et al. De-regulation of gene expression and alternative splicing affects distinct cellular pathways in the aging hippocampus. *Front Cell Neurosci* 2014; 8: 373.

[182] Akbarian S, Smith MA, Jones EG. Editing for an AMPA receptor subunit RNA in prefrontal cortex and striatum in Alzheimer's disease, Huntington's disease and schizophrenia. *Brain Res* 1995; 699: 297–304.

[183] Gaisler-Salomon I, Kravitz E, Feiler Y, et al. Hippocampus-specific deficiency in RNA editing of GluA2 in Alzheimer's disease. *Neurobiol Aging* 2014; 35: 1785–1791.

[184] Desrosiers R, Friderici K, Rottman F. Identification of methylated nucleosides in messenger RNA from Novikoff hepatoma cells. *Proc Natl Acad Sci U S A* 1974; 71: 3971–5.

[185] Rottman F, Shatkin AJ, Perry RP. Sequences containing methylated nucleotides at the 5′ termini of messenger RNAs: Possible implications for processing. *Cell* 1974; 3: 197–199.

[186] Behm-Ansmant I, Helm M, Motorin Y. Use of specific chemical reagents for detection of modified nucleotides in RNA. *J Nucleic Acids* 2011; 2011: 408053.

[187] Kellner S, Burhenne J, Helm M. Detection of RNA modifications. *RNA Biol* 2010; 7: 237–247.

[188] Meyer KD, Saletore Y, Zumbo P, et al. Comprehensive analysis of mRNA methylation reveals enrichment in 3′ UTRs and near stop codons. *Cell* 2012; 149: 1635–1646.

[189] Fu L, Guerrero CR, Zhong N, et al. Tet-mediated formation of 5-hydroxymethylcytosine in RNA. *J Am Chem Soc* 2014; 136: 11582–11585.

[190] Bringmann P, Lührmann R. Antibodies specific for N 6 -methyladenosine react with intact snRNPs U2 and U4/U6. *FEBS Lett* 1987; 213: 309–315.

[191] Choi YC, Busch H. Modified nucleotides in T1 RNase oligonucleotides of 18S ribosomal RNA of the Novikoff hepatoma. *Biochemistry* 1978; 17: 2551–2560.

[192] Epstein P, Reddy R, Henning D, et al. The nucleotide sequence of nuclear U6 (4.7 S) RNA. *J Biol Chem* 1980; 255: 8901–6.

[193] Harada F, Kato N, Nishimura S. The nucleotide sequence of nuclear 4.8S RNA of mouse cells. *Biochem Biophys Res Commun* 1980; 95: 1332–40.

[194] Munns TW, Sims HF, Liszewski MK. Immunospecific retention of oligonucleotides possessing N6-methyladenosine and 7-methylguanosine. *J Biol Chem* 1977; 252: 3102–4.

[195] Perry RP, Kelley DE, Friderici K, et al. The methylated constituents of L cell messenger RNA: Evidence for an unusual cluster at the 5′ terminus. *Cell* 1975; 4: 387–394.

[196] Shimba S, Bokar JA, Rottman F, et al. Accurate and efficient N-6-adenosine methylation in spliceosomal U6 small nuclear RNA by HeLa cell extract *in vitro*. *Nucleic Acids Res* 1995; 23: 2421–6.

[197] Tanaka T, Weisblum B. Systematic difference in the methylation of ribosomal ribonucleic acid from gram-positive and gram-negative bacteria. *J Bacteriol* 1975; 123: 771–4.

[198] Dominissini D, Moshitch-Moshkovitz S, Schwartz S, et al. Topology of the human and mouse m6A RNA methylomes revealed by m6A-seq. *Nature* 2012; 485: 201–206.

[199] Bujnicki JM, Feder M, Radlinska M, et al. Structure prediction and phylogenetic analysis of a functionally diverse family of proteins homologous to the MT-A70 subunit of the human mRNA:m6A methyltransferase. *J Mol Evol* 2002; 55: 431–444.

[200] Ping X-L, Sun B-F, Wang L, et al. Mammalian WTAP is a regulatory subunit of the RNA N6-methyladenosine methyltransferase. *Cell Res* 2014; 24: 177–189.

[201] Wang Y, Li Y, Toth JI, et al. N6-methyladenosine modification destabilizes developmental regulators in embryonic stem cells. *Nat Cell Biol* 2014; 16: 191–198.

[202] Jia G, Fu Y, Zhao X, et al. N6-Methyladenosine in nuclear RNA is a major substrate of the obesity-associated FTO. *Nat Chem Biol* 2011; 7: 885–887.

[203] Zheng G, Dahl JA, Niu Y, et al. ALKBH5 is a mammalian RNA demethylase that Impacts RNA metabolism and mouse fertility. *Mol Cell* 2013; 49: 18–29.

[204] Fu Y, Jia G, Pang X, et al. FTO-mediated formation of N6-hydroxymethyladenosine and N6-formyladenosine in mammalian RNA. *Nat Commun* 2013; 4: 1798.

[205] Chandola U, Das R, Panda B. Role of the N6-methyladenosine RNA mark in gene regulation and its implications on development and disease. *Brief Funct Genomics* 2015; 14: 169–179.

[206] Wang X, Lu Z, Gomez A, et

al. N6-methyladenosine-dependent regulation of messenger RNA stability. *Nature* 2013; 505: 117–120.

[207] Bachellerie J-P, Cavaillé J, Hüttenhofer A. The expanding snoRNA world. *Biochimie* 2002; 84: 775–790.

[208] Maxwell E, Fournier M. The small nucleolar RNAs. *Annu Rev Biochem* 1995; 64: 897–934.

[209] Chen PY, Weinmann L, Gaidatzis D, et al. Strand-specific 5'-O-methylation of siRNA duplexes controls guide strand selection and targeting specificity. *RNA* 2008; 14: 263–74.

[210] Ender C, Krek A, Friedländer MR, et al. A Human snoRNA with MicroRNA-Like Functions. *Mol Cell* 2008; 32: 519–528.

[211] Ritland Politz JC, Hogan EM, Pederson T. MicroRNAs with a nucleolar location. *RNA* 2009; 15: 1705–1715.

[212] Saraiya AA, Wang CC, Nohynkova E, et al. snoRNA, a novel precursor of microRNA in *Giardia lamblia*. *PLoS Pathog* 2008; 4: e1000224.

[213] Taft RJ, Glazov EA, Lassmann T, et al. Small RNAs derived from snoRNAs. *RNA* 2009; 15: 1233–40.

[214] Schaefer M, Hagemann S, Hanna K, et al. Azacytidine inhibits RNA methylation at DNMT2 target sites in human cancer cell lines. *Cancer Res*; http://cancerres.aacrjournals.org/content/69/20/8127 (2009, accessed 3 April 2017).

[215] Phalke S, Nickel O, Walluscheck D, et al. Retrotransposon silencing and telomere integrity in somatic cells of Drosophila depends on the cytosine-5 methyltransferase DNMT2. *Nat Genet* 2009; 41: 696–702.

[216] Rai K, Chidester S, Zavala C V, et al. Dnmt2 functions in the cytoplasm to promote liver, brain, and retina development in zebrafish. *Genes Dev* 2007; 21: 261–6.

[217] Anderson J, Phan L, Hinnebusch AG. The Gcd10p/Gcd14p complex is the essential two-subunit tRNA(1-methyladenosine) methyltransferase of Saccharomyces cerevisiae. *Proc Natl Acad Sci U S A* 2000; 97: 5173–8.

[218] Björk GR, Wikström PM, Byström AS. Prevention of translational frameshifting by the modified nucleoside 1-methylguanosine. *Science* 1989; 244: 986–9.

[219] Jackman JE, Montange RK, Malik HS, et al. Identification of the yeast gene encoding the tRNA m1G methyltransferase responsible for modification at position 9. *RNA* 2003; 9: 574–85.

[220] Saikia M, Fu Y, Pavon-Eternod M, et al. Genome-wide analysis of N1-methyl-adenosine modification in human tRNAs. *RNA* 2010; 16: 1317–27.

[221] Giordano M, Cristiani C, Crocco P, et al. Methylation of the human mitochondrial 12S rRNA gene is correlated with aging. *12th Int FISV* 2012.

[222] Byun H-M, Baccarelli AA. Environmental exposure and mitochondrial epigenetics: study design and analytical challenges. *Hum Genet* 2014; 133: 247–257.

[223] Kudriashova IB, Kirnos MD, Vaniushin BF. [DNA-methylase activities from animal mitochondria and nuclei: different specificity of DNA methylation]. *Biokhimiia* 1976; 41: 1968–77.

[224] Nass MMK. Differential methylation of mitochondrial and nuclear DNA in cultured mouse, hamster and virus-transformed hamster cells In vivo and *in vitro* methylation. *J Mol Biol* 1973; 80: 155–175.

[225] Shmookler Reis RJ, Goldstein S. Mitochondrial DNA in mortal and immortal human cells. Genome number, integrity, and methylation. *J Biol Chem* 1983; 258: 9078–85.

[226] Shock LS, Thakkar P V, Peterson EJ, et al. DNA methyltransferase 1, cytosine methylation, and cytosine hydroxymethylation in mammalian mitochondria. *Proc Natl Acad Sci U S A 2011*; 108: 3630–5.

[227] Hong EE, Okitsu CY, Smith AD, et al. Regionally specific and genome-wide analyses conclusively demonstrate the absence of CpG methylation in human mitochondrial DNA. *Mol Cell Biol* 2013; 33: 2683–90.

[228] Choi Y-S, Hoon Jeong J, Min H-K, et al. Shot-gun proteomic analysis of mitochondrial D-loop DNA binding proteins: identification of mitochondrial histones. *Mol Biosyst* 2011; 7: 1523.

[229] Barrey E, Saint-Auret G, Bonnamy B, et al. Pre-microRNA and mature microRNA in human mitochondria. *PLoS One* 2011; 6: e20220.

[230] Chestnut BA, Chang Q, Price A, et al. Epigenetic regulation of motor neuron cell death through DNA methylation. *J Neurosci*; http://www.jneurosci.org/content/31/46/16619 (2011, accessed 3 April 2017).

[231] Dzitoyeva S, Chen H, Manev H, et al. Effect of aging on 5-hydroxymethylcytosine in brain mitochondria. *Neurobiol Aging* 2012; 33: 2881–2891.

[232] Iacobazzi V, Castegna A, Infantino V, et al. Mitochondrial DNA methylation as a next-generation biomarker and diagnostic tool. *Mol Genet Metab* 2013; 110: 25–34.

[233] Manev H, Dzitoyeva S,

Chen H. Mitochondrial DNA: a blind spot in neuroepigenetics. *Biomol Concepts* 2012; 3: 107–115.

[234] Bellizzi D, D'Aquila P, Scafone T, et al. The control region of mitochondrial DNA shows an unusual CpG and non-CpG methylation pattern. *DNA Res* 2013; 20: 537–547.

[235] Sun Z, Terragni J, Borgaro JG, et al. High-resolution enzymatic mapping of genomic 5-hydroxymethylcytosine in mouse embryonic stem cells. *Cell Rep* 2013; 3: 567–576.

[236] Feng S, Xiong L, Ji Z, et al. Correlation between increased ND2 expression and demethylated displacement loop of mtDNA in colorectal cancer. *Mol Med Rep* 2012; 6: 125–30.

[237] Pirola CJ, Gianotti TF, Burgueño AL, et al. Epigenetic modification of liver mitochondrial DNA is associated with histological severity of nonalcoholic fatty liver disease. *Gut* 2013; 62: 1356–1363.

[238] Grewal SIS, Jia S. Heterochromatin revisited. *Nat Rev Genet* 2007; 8: 35–46.

[239] Zhang Y, Reinberg D. Transcription regulation by histone methylation: interplay between different covalent modifications of the core histone tails. *Genes Dev* 2001; 15: 2343–60.

[240] Wu H, Coskun V, Tao J, et al. Dnmt3a-dependent nonpromoter DNA methylation facilitates transcription of neurogenic genes. *Science*; http://science.sciencemag.org/content/329/5990/444 (2010, accessed 4 April 2017).

[241] Liu C, Teng Z-Q, Santistevan NJ, et al. Epigenetic regulation of miR-184 by MBD1 governs neural stem cell proliferation and differentiation. *Cell Stem Cell* 2010; 6: 433–44.

[242] Detich N, Bovenzi V, Szyf M. Valproate induces replication-independent active DNA demethylation. *J Biol Chem* 2003; 278: 27586–92.

[243] Sun G, Yu RT, Evans RM, et al. Orphan nuclear receptor TLX recruits histone deacetylases to repress transcription and regulate neural stem cell proliferation. *Proc Natl Acad Sci U S A* 2007; 104: 15282–7.

[244] Saito Y, Jones PM. Epigenetic activation of tumor suppressor microRNAs in human cancer cells. *Cell Cycle* 2006; 5: 2220–2222.

[245] Bocklandt S, Lin W, Sehl ME, et al. Epigenetic predictor of age. *PLoS One* 2011; 6: e14821.

[246] Horvath S. DNA methylation age of human tissues and cell types. *Genome Biol* 2013; 14: R115.

[247] Beckman KB, Ames BN. The free radical theory of aging matures. *Physiol Rev* 1998; 78: 547–81.

[248] Cencioni C, Spallotta F, Martelli F, et al. Oxidative stress and epigenetic regulation in ageing and age-related diseases. *Int J Mol Sci* 2013; 14: 17643–17663.

[249] Obeid R, Schadt A, Dillmann U, et al. Methylation status and neurodegenerative markers in parkinson disease. *Clin Chem*; http://clinchem.aaccjnls.org/content/55/10/1852 (2009, accessed 4 April 2017).

[250] Siegmund KD, Connor CM, Campan M, et al. DNA methylation in the human cerebral cortex is dynamically regulated throughout the life span and involves differentiated neurons. *PLoS One* 2007; 2: e895.

[251] Tohgi H, Utsugisawa K, Nagane Y, et al. The methylation status of cytosines in a τ gene promoter region alters with age to downregulate transcriptional activity in human cerebral cortex. Epub ahead of print 1999. DOI: 10.1016/S0304-3940(99)00731-4.

[252] Chouliaras L, van den Hove DLA, Kenis G, et al. Caloric restriction attenuates age-related changes of DNA methyltransferase 3a in mouse hippocampus. Brain Behav Immun 2011; 25: 616–623.

[253] Chouliaras L, van den Hove DLA, Kenis G, et al. Prevention of age-related changes in hippocampal levels of 5-methylcytidine by caloric restriction. *Neurobiol Aging* 2012; 33: 1672–81.

[254] Lopatina N, Haskell JF, Andrews LG, et al. Differential maintenance and *de novo* methylating activity by three DNA methyltransferases in aging and immortalized fibroblasts. *J Cell Biochem* 2002; 84: 324–334.

[255] Oliveira AMM, Hemstedt TJ, Bading H. Rescue of aging-associated decline in Dnmt3a2 expression restores cognitive abilities. *Nat Neurosci* 2012; 15: 1111–1113.

[256] Hernandez DG, Nalls MA, Gibbs JR, et al. Distinct DNA methylation changes highly correlated with chronological age in the human brain. *Hum Mol Genet* 2011; 20: 1164–1172.

[257] Bollati V, Schwartz J, Wright R, et al. Decline in genomic DNA methylation through aging in a cohort of elderly subjects. *Mech Ageing Dev* 2009; 130: 234–239.

[258] Pan K, Chen Y, Roth M, et al. HBP1-mediated transcriptional regulation of DNA methyltransferase 1 and its impact on cell senescence. *Mol Cell Biol* 2013; 33: 887–903.

[259] Mazin AL. Suicidal function of DNA methylation in age-related genome disintegration. *Ageing Res Rev* 2009; 8: 314–327.

[260] Brown SE, Weaver ICG,

Meaney MJ, et al. Regional-specific global cytosine methylation and DNA methyltransferase expression in the adult rat hippocampus. Epub ahead of print 2008. DOI: 10.1016/j.neulet.2008.05.028.

[261] Ladd-Acosta C, Pevsner J, Sabunciyan S, et al. DNA methylation signatures within the human brain. *Am J Hum Genet* 2007; 81: 1304–15.

[262] Thompson RF, Atzmon G, Gheorghe C, et al. Tissue-specific dysregulation of DNA methylation in aging. *Aging Cell* 2010; 9: 506–518.

[263] Fraga MF, Ballestar E, Paz MF, et al. Epigenetic differences arise during the lifetime of monozygotic twins. *Proc Natl Acad Sci U S A* 2005; 102: 10604–9.

[264] Chouliaras L, van den Hove DLA, Kenis G, et al. Age-related increase in levels of 5-hydroxymethylcytosine in mouse hippocampus is prevented by caloric restriction. *Curr Alzheimer Res* 2012; 9: 536–44.

[265] Münzel M, Globisch D, Brückl T, et al. Quantification of the sixth DNA base hydroxymethylcytosine in the brain. *Angew Chemie Int Ed* 2010; 49: 5375–5377.

[266] Song C-X, Szulwach KE, Fu Y, et al. Selective chemical labeling reveals the genome-wide distribution of 5-hydroxymethylcytosine. *Nat Biotechnol* 2011; 29: 68–72.

[267] Madrigano J, Baccarelli AA, Mittleman MA, et al. Aging and epigenetics: Longitudinal changes in gene-specific DNA methylation. *Epigenetics* 2012; 7: 63–70.

[268] So K, Tamura G, Honda T, et al. Quantitative assessment of *RUNX3* methylation in neoplastic and non-neoplastic gastric epithelia using a DNA microarray. *Pathol Int* 2006; 56: 571–575.

[269] Westberry JM, Trout AL, Wilson ME. Epigenetic regulation of estrogen receptor beta expression in the rat cortex during aging. *Neuroreport* 2011; 22: 428–432.

[270] Ryan JM, Cristofalo VJ. Histone acetylation during aging of human cells in culture. *Biochem Biophys Res Commun* 1972; 48: 735–742.

[271] Thakur MK, Kanungo MS. Methylation of chromosomal proteins and DNA of rat brain and its modulation by estradiol and calcium during aging. *Exp Gerontol* 1981; 16: 331–336.

[272] Pina B, Martinez P, Suau P. Differential acetylation of core histones in rat cerebral cortex neurons during development and aging. *Eur J Biochem* 1988; 174: 311–315.

[273] Kawakami K, Nakamura A, Ishigami A, et al. Age-related difference of site-specific histone modifications in rat liver. *Biogerontology* 2009; 10: 415–421.

[274] Nakamura A, Kawakami K, Kametani F, et al. Biological significance of protein modifications in aging and calorie restriction. *Ann N Y Acad Sci* 2010; 1197: 33–39.

[275] Wang CM, Tsai SN, Yew TW, et al. Identification of histone methylation multiplicities patterns in the brain of senescence-accelerated prone mouse 8. *Biogerontology* 2010; 11: 87–102.

[276] Sarg B, Koutzamani E, Helliger W, et al. Postsynthetic trimethylation of histone H4 at lysine 20 in mammalian tissues is associated with aging. *J Biol Chem* 2002; 277: 39195–201.

[277] Agger K, Cloos PAC, Rudkjaer L, et al. The H3K27me3 demethylase JMJD3 contributes to the activation of the INK4A-ARF locus in response to oncogene- and stress-induced senescence. *Genes Dev* 2009; 23: 1171–6.

[278] Jung J-W, Lee S, Seo M-S, et al. Histone deacetylase controls adult stem cell aging by balancing the expression of polycomb genes and jumonji domain containing 3. *Cell Mol Life Sci* 2010; 67: 1165–1176.

[279] Chouliaras L, van den Hove DLA, Kenis G, et al. Histone deacetylase 2 in the mouse hippocampus: attenuation of age-related increase by caloric restriction. *Curr Alzheimer Res* 2013; 10: 868–76.

[280] Perry M, Chalkley R. Histone acetylation increases the solubility of chromatin and occurs sequentially over most of the chromatin. A novel model for the biological role of histone acetylation. *J Biol Chem* 1982; 257: 7336–47.

[281] Peleg S, Sananbenesi F, Zovoilis A, et al. Altered histone acetylation is associated with age-dependent memory impairment in mice. *Science* 2010; 328: 753–6.

[282] Fischer A, Sananbenesi F, Wang X, et al. Recovery of learning and memory is associated with chromatin remodelling. *Nature* 2007; 447: 178–182.

[283] Wellen KE, Hatzivassiliou G, Sachdeva UM, et al. ATP-citrate lyase links cellular metabolism to histone acetylation. *Science*; http://science.sciencemag.org/content/324/5930/1076 (2009, accessed 4 April 2017).

[284] Jiang N, Yan X, Zhou W, et al. NMR-based metabonomic investigations into the metabolic profile of the senescence-accelerated mouse. *J Proteome Res* 2008; 7: 3678–3686.

[285] Alarcón JM, Malleret G, Touzani K, et al. Chromatin acetylation, memory, and LTP are impaired

in CBP+/- mice: a model for the cognitive deficit in Rubinstein-Taybi syndrome and its amelioration. *Neuron* 2004; 42: 947–59.

[286] Korzus E, Rosenfeld MG, Mayford M, et al. CBP histone acetyltransferase activity is a critical component of memory consolidation. *Neuron* 2004; 42: 961–72.

[287] Gupta S, Kim SY, Artis S, et al. Histone methylation regulates memory formation. *J Neurosci*; http://www.jneurosci.org/content/30/10/3589 (2010, accessed 4 April 2017).

[288] Chwang WB, O'Riordan KJ, Levenson JM, et al. ERK/MAPK regulates hippocampal histone phosphorylation following contextual fear conditioning. *Learn Mem* 2006; 13: 322–8.

[289] Quintas A, de Solís AJ, Díez-Guerra FJ, et al. Age-associated decrease of SIRT1 expression in rat hippocampus: Prevention by late onset caloric restriction. Epub ahead of print 2012. DOI: 10.1016/j.exger.2011.11.010.

[290] Sommer M, Poliak N, Upadhyay S, et al. ΔNp63alpha overexpression induces downregulation of Sirt1 and an accelerated aging phenotype in the mouse. *Cell Cycle* 2006; 5: 2005–2011.

[291] Sasaki T, Maier B, Bartke A, et al. Progressive loss of SIRT1 with cell cycle withdrawal. *Aging Cell* 2006; 5: 413–422.

[292] Pruitt K, Zinn RL, Ohm JE, et al. Inhibition of SIRT1 reactivates silenced cancer genes without loss of promoter DNA hypermethylation. *PLoS Genet* 2006; 2: e40.

[293] Vaquero A, Scher M, Erdjument-Bromage H, et al. SIRT1 regulates the histone methyl-transferase SUV39H1 during heterochromatin formation. *Nature* 2007; 450: 440–444.

[294] Narita M, Nũnez S, Heard E, et al. Rb-mediated heterochromatin formation and silencing of E2F target genes during cellular senescence. *Cell* 2003; 113: 703–16.

[295] Ye X, Zerlanko B, Zhang R, et al. Definition of pRB- and p53-dependent and -independent steps in HIRA/ASF1a-mediated formation of senescence-associated heterochromatin foci. *Mol Cell Biol* 2007; 27: 2452–65.

[296] Schmeisser K, Mansfeld J, Kuhlow D, et al. Role of sirtuins in lifespan regulation is linked to methylation of nicotinamide. *Nat Chem Biol* 2013; 9: 693–700.

[297] Ristow M, Zarse K. How increased oxidative stress promotes longevity and metabolic health: The concept of mitochondrial hormesis (mitohormesis). *Exp Gerontol* 2010; 45: 410–418.

[298] Guarente L, Picard F, Ramsey CS, et al. Calorie restriction—the SIR2 connection. *Cell* 2005; 120: 473–482.

[299] Rutten BPF, Brasnjevic I, Steinbusch HWM, et al. Caloric restriction and aging but not overexpression of SOD1 affect hippocampal volumes in mice. *Mech Ageing Dev* 2010; 131: 574–579.

[300] Baur JA, Pearson KJ, Price NL, et al. Resveratrol improves health and survival of mice on a high-calorie diet. *Nature* 2006; 444: 337–342.

[301] Haigis MC, Sinclair DA. Mammalian sirtuins: biological insights and disease relevance. *Annu Rev Pathol Mech Dis* 2010; 5: 253–295.

[302] Lee RC, Feinbaum RL, Ambros V, et al. The C. elegans heterochronic gene lin-4 encodes small RNAs with antisense complementarity to lin-14. *Cell* 1993; 75: 843–54.

[303] Boulias K, Horvitz HR, Suchanek-Kavipurapu M, et al. The *C. elegans* microRNA mir-71 acts in neurons to promote germline-mediated longevity through regulation of DAF-16/FOXO. *Cell Metab* 2012; 15: 439–450.

[304] Maes OC, An J, Sarojini H, et al. Murine microRNAs implicated in liver functions and aging process. *Mech Ageing Dev* 2008; 129: 534–541.

[305] Noren Hooten N, Abdelmohsen K, Gorospe M, et al. microRNA expression patterns reveal differential expression of target genes with age. *PLoS One* 2010; 5: e10724.

[306] Boon RA, Iekushi K, Lechner S, et al. MicroRNA-34a regulates cardiac ageing and function. *Nature* 2013; 495: 107–110.

[307] Boon RA, Seeger T, Heydt S, et al. MicroRNA-29 in aortic dilation: implications for aneurysm formation novelty and significance. *Circ Res;* http://circres.ahajournals.org/content/109/10/1115 (2011, accessed 4 April 2017).

[308] Menghini R, Casagrande V, Cardellini M, et al. MicroRNA 217 modulates endothelial cell senescence via silent information regulator 1. *Circulation*; http://circ.ahajournals.org/content/120/15/1524 (2009, accessed 4 April 2017).

[309] Olivieri F, Lazzarini R, Recchioni R, et al. MiR-146a as marker of senescence-associated pro-inflammatory status in cells involved in vascular remodelling. *Age* (Omaha) 2013; 35: 1157–1172.

[310] Vasa-Nicotera M, Chen H, Tucci P, et al. miR-146a is modulated in human endothelial cell with aging. *Atherosclerosis* 2011; 217: 326–30.

[311] Hackl M, Brunner S, Fortschegger K, et al. miR-17, miR-19b, miR-20a, and miR-106a are down-regulated in human aging. *Aging Cell* 2010; 9: 291–296.

[312] Magenta A, Cencioni C, Fasanaro P, et al. miR-200c is upregulated by oxidative stress and induces endothelial cell apoptosis and senescence via ZEB1 inhibition. *Cell Death Differ* 2011; 18: 1628–1639.

[313] Hébert SS, De Strooper B. Alterations of the microRNA network cause neurodegenerative disease. *Trends Neurosci* 2009; 32: 199–206.

[314] Somel M, Guo S, Fu N, et al. MicroRNA, mRNA, and protein expression link development and aging in human and macaque brain. *Genome Res* 2010; 20: 1207–18.

[315] Persengiev S, Kondova I, Otting N, et al. Genome-wide analysis of miRNA expression reveals a potential role for miR-144 in brain aging and spinocerebellar ataxia pathogenesis. *Neurobiol Aging* 2011; 32: 2316.e17-2316.e27.

[316] Li N, Bates DJ, An J, et al. Up-regulation of key microRNAs, and inverse down-regulation of their predicted oxidative phosphorylation target genes, during aging in mouse brain. *Neurobiol Aging* 2011; 32: 944–55.

[317] Liu W, Liu C, Zhu J, et al. MicroRNA-16 targets amyloid precursor protein to potentially modulate Alzheimer's-associated pathogenesis in SAMP8 mice. *Neurobiol Aging* 2012; 33: 522–34.

[318] Coppedè F, Mancuso M, Siciliano G, et al. Genes and the environment in neurodegeneration. *Biosci Rep*; http://www.bioscirep.org/content/26/5/341 (2006, accessed 4 April 2017).

[319] Trapp BD, Nave K-A. Multiple sclerosis: an immune or neurodegenerative disorder? *Annu Rev Neurosci* 2008; 31: 247–269.

[320] Bates EA, Victor M, Jones AK, et al. Differential contributions of *Caenorhabditis elegans* histone deacetylases to huntingtin polyglutamine toxicity. *J Neurosci*; http://www.jneurosci.org/content/26/10/2830 (2006, accessed 4 April 2017).

[321] Chouliaras L, Rutten BPF, Kenis G, et al. Epigenetic regulation in the pathophysiology of Alzheimer's disease. *Prog Neurobiol* 2010; 90: 498–510.

[322] Chouliaras L, Sierksma ASR, Kenis G, et al. Gene-environment interaction research and transgenic mouse models of Alzheimer's disease. *Int J Alzheimers Dis*; 2010. Epub ahead of print January 2010. DOI: 10.4061/2010/859101.

[323] Migliore L, Coppedè F. Genetics, environmental factors and the emerging role of epigenetics in neurodegenerative diseases. *Mutat Res Mol Mech Mutagen* 2009; 667: 82–97.

[324] Babenko O, Kovalchuk I, Metz GA. Epigenetic programming of neurodegenerative diseases by an adverse environment. *Brain Res* 2012; 1444: 96–111.

[325] Jaenisch R, Bird A. Epigenetic regulation of gene expression: how the genome integrates intrinsic and environmental signals. *Nat Genet* 2003; 33: 245–254.

[326] Selkoe DJ. Preventing Alzheimer's Disease. Science (80-); 337http://science.sciencemag.org/content/337/6101/1488 (2012, accessed 4 April 2017).

[327] Bediou B, Ryff I, Mercier B, et al. Impaired social cognition in mild alzheimer disease. *J Geriatr Psychiatry Neurol* 2009; 22: 130–140.

[328] Budson AE, Solomon PR. New criteria for Alzheimer disease and mild cognitive impairment: implications for the practicing clinician. *Neurologist* 2012; 18: 356–363.

[329] Hardy J, Saura CA, Choi SY, et al. A hundred years of Alzheimer's disease research. *Neuron* 2006; 52: 3–13.

[330] Wenk GL. Neuropathologic changes in Alzheimer's disease. *J Clin Psychiatry* 2003; 64 Suppl 9: 7–10.

[331] Fukutani Y, Cairns NJ, Rossor MN, et al. Purkinje cell loss and astrocytosis in the cerebellum in familial and sporadic Alzheimer's disease. *Neurosci Lett* 1996; 214: 33–36.

[332] Alzheimer's Association. 2013 Alzheimer's disease facts and figures. *Alzheimer's Dement* 2013; 9: 208–245.

[333] Tiraboschi P, Hansen LA, Thal LJ, et al. The importance of neuritic plaques and tangles to the development and evolution of AD. *Neurology* 2004; 62: 1984–9.

[334] Mill J. Toward an integrated genetic and epigenetic approach to Alzheimer's disease. *Neurobiol Aging* 2011; 32: 1188–1191.

[335] Citron M, Teplow DB, Selkoe DJ, et al. Generation of amyloid beta protein from its precursor is sequence specific. *Neuron* 1995; 14: 661–70.

[336] Shoji M, Golde TE, Ghiso J, et al. Production of the Alzheimer amyloid beta protein by normal proteolytic processing. *Science* 1992; 258: 126–9.

[337] van Groen T. DNA methylation and Alzheimer's disease. In: *Epigenetics of Aging*. New York, NY: Springer New York, pp. 315–326.

[338] Hardy JA, Higgins GA. Alz-

heimer's disease: the amyloid cascade hypothesis. *Science* 1992; 256: 184–5.

[339] Mattson MP, Cheng B, Davis D, et al. beta-Amyloid peptides destabilize calcium homeostasis and render human cortical neurons vulnerable to excitotoxicity. *J Neurosci* 1992; 12: 376–89.

[340] Selkoe DJ. Physiological production of the β-amyloid protein and the mechanism of Alzheimer's disease. *Trends Neurosci* 1993; 16: 403–409.

[341] Tanzi RE. The genetics of Alzheimer disease. *Cold Spring Harb Perspect Med*; 2. Epub ahead of print 2012. DOI: 10.1101/cshperspect.a006296.

[342] Czech C, Tremp G, Pradier L. Presenilins and Alzheimer's disease: biological functions and pathogenic mechanisms. *Prog Neurobiol* 2000; 60: 363–384.

[343] De Strooper B, Saftig P, Craessaerts K, et al. Deficiency of presenilin-1 inhibits the normal cleavage of amyloid precursor protein. *Nature* 1998; 391: 387–390.

[344] Goate A, Chartier-Harlin M-C, Mullan M, et al. Segregation of a missense mutation in the amyloid precursor protein gene with familial Alzheimer's disease. *Nature* 1991; 349: 704–706.

[345] Sherrington R, Rogaev EI, Liang Y, et al. Cloning of a gene bearing missense mutations in early-onset familial Alzheimer's disease. *Nature* 1995; 375: 754–760.

[346] Tanzi RE, Kovacs DM, Kim T-W, et al. The gene defects responsible for familial Alzheimer's disease. *Neurobiol Dis* 1996; 3: 159–168.

[347] Lemere CA, Lopera F, Kosik KS, et al. The E280A presenilin 1 Alzheimer mutation produces increased A beta 42 deposition and severe cerebellar pathology. *Nat Med* 1996; 2: 1146–1150.

[348] van Goethem NP, Lardenoije R, Kompotis K, et al. Cognitive disorders: impairment, aging, and dementia. In: *In Vivo Models for Drug Discovery*. Wiley-VCH Verlag GmbH & Co. KGaA, pp. 349–366.

[349] Cacabelos R. Pharmacogenomics and therapeutic prospects in Alzheimer's disease. *Expert Opin Pharmacother* 2005; 6: 1967–1987.

[350] Cacabelos R. Pharmacogenetic basis for therapeutic optimization in Alzheimer's disease. *Mol Diagn Ther* 2007; 11: 385–405.

[351] Slooter AJC, Cruts M, Kalmijn S, et al. Risk estimates of dementia by apolipoprotein E genotypes from a population-based incidence study: The Rotterdam Study. *Arch Neurol* 1998; 55: 964.

[352] Harold D, Abraham R, Hollingworth P, et al. Genome-wide association study identifies variants at *CLU* and *PICALM* associated with Alzheimer's disease. *Nat Genet* 2009; 41: 1088–1093.

[353] Hollingworth P, Harold D, Sims R, et al. Common variants at *ABCA7, MS4A6A/MS4A4E, EPHA1, CD33* and *CD2AP* are associated with Alzheimer's disease. *Nat Genet* 2011; 43: 429–435.

[354] Naj AC, Jun G, Beecham GW, et al. Common variants at *MS4A4/MS4A6E, CD2AP, CD33* and *EPHA1* are associated with late-onset Alzheimer's disease. *Nat Genet* 2011; 43: 436–441.

[355] Sleegers K, Lambert J-C, Bertram L, et al. The pursuit of susceptibility genes for Alzheimer's disease: progress and prospects. *Trends Genet* 2010; 26: 84–93.

[356] Guerreiro R, Wojtas A, Bras J, et al. *TREM2* variants in Alzheimer's disease. *N Engl J Med* 2013; 368: 117–127.

[357] Jonsson T, Stefansson H, Steinberg S, et al. Variant of *TREM2* associated with the risk of Alzheimer's disease. *N Engl J Med* 2013; 368: 107–116.

[358] Neumann H, Daly MJ. Variant *TREM2* as risk factor for Alzheimer's disease. *N Engl J Med* 2013; 368: 182–184.

[359] Yamagata K, Urakami K, Ikeda K, et al. High expression of apolipoprotein E mRNA in the brains with sporadic Alzheimer's disease. *Dement Geriatr Cogn Disord*; 12: 57–62.

[360] Caesar I, Gandy S. Evidence that an APOE ε4 'double whammy' increases risk for Alzheimer's disease. *BMC Med* 2012; 10: 36.

[361] Castellano JM, Kim J, Stewart FR, et al. Human apoE isoforms differentially regulate brain amyloid-β peptide clearance. *Sci Transl Med*; http://stm.sciencemag.org/content/3/89/89ra57 (2011, accessed 4 April 2017).

[362] Mawuenyega KG, Sigurdson W, Ovod V, et al. Decreased clearance of CNS β-amyloid in Alzheimer's disease. *Science*; http://science.sciencemag.org/content/330/6012/1774 (2010, accessed 4 April 2017).

[363] Yu J-T, Tan L. The role of clusterin in Alzheimer's disease: pathways, pathogenesis, and therapy. *Mol Neurobiol* 2012; 45: 314–326.

[364] Schrijvers EMC, Koudstaal PJ, Hofman A, et al. Plasma clusterin and the risk of Alzheimer disease. *JAMA* 2011; 305: 1322.

[365] Thambisetty M, Simmons A, Velayudhan L, et al. Association of plasma clusterin concentration with

severity, pathology, and progression in Alzheimer disease. *Arch Gen Psychiatry* 2010; 67: 739.

[366] Weingarten MD, Lockwood AH, Hwo SY, et al. A protein factor essential for microtubule assembly. *Proc Natl Acad Sci U S A* 1975; 72: 1858–62.

[367] Lee VM-Y, Goedert M, Trojanowski JQ. Neurodegenerative tauopathies. *Annu Rev Neurosci* 2001; 24: 1121–1159.

[368] Lovestone S, Reynolds CH. The phosphorylation of tau: a critical stage in neurodevelopment and neurodegenerative processes. *Neuroscience* 1997; 78: 309–24.

[369] Alonso AD, Grundke-Iqbal I, Barra HS, et al. Abnormal phosphorylation of tau and the mechanism of Alzheimer neurofibrillary degeneration: sequestration of microtubule-associated proteins 1 and 2 and the disassembly of microtubules by the abnormal tau. *Proc Natl Acad Sci U S A* 1997; 94: 298–303.

[370] Iqbal K, Liu F, Gong C-X, et al. Mechanisms of tau-induced neurodegeneration. *Acta Neuropathol* 2009; 118: 53–69.

[371] Klafki H-W, Staufenbiel M, Kornhuber J, et al. Therapeutic approaches to Alzheimer's disease. *Brain* 2006; 129: 2840–2855.

[372] Khairallah MI, Kassem LAA. Alzheimer's disease: current status of etiopathogenesis and therapeutic strategies. *Pakistan J Biol Sci PJBS* 2011; 14: 257–72.

[373] Hardy J, Selkoe DJ. The amyloid hypothesis of Alzheimer's disease: progress and problems on the road to therapeutics. *Science*; http://science.sciencemag.org/content/297/5580/353 (2002, accessed 4 April 2017).

[374] Lahiri DK, Maloney B, Zawia NH. The LEARn model: an epigenetic explanation for idiopathic neurobiological diseases. *Mol Psychiatry* 2009; 14: 992–1003.

[375] Jankovic J. Parkinson's disease: clinical features and diagnosis. *J Neurol Neurosurg Psychiatry* 2008; 79: 368–376.

[376] Aarsland D, Larsen JP, Cummins JL, et al. Prevalence and clinical correlates of psychotic symptoms in Parkinson disease: a community-based study. *Arch Neurol* 1999; 56: 595–601.

[377] Naimark D, Jackson E, Rockwell E, et al. Psychotic symptoms in Parkinson's disease patients with dementia. *J Am Geriatr Soc* 1996; 44: 296–299.

[378] Riedel O, Klotsche J, Spottke A, et al. Cognitive impairment in 873 patients with idiopathic Parkinson's disease. *J Neurol* 2008; 255: 255–264.

[379] Francis PT, Perry EK. Cholinergic and other neurotransmitter mechanisms in Parkinson's disease, Parkinson's disease dementia, and dementia with Lewy bodies. *Mov Disord* 2007; 22: S351–S357.

[380] van de Berg WDJ, Hepp DH, Dijkstra AA, et al. Patterns of α-synuclein pathology in incidental cases and clinical subtypes of Parkinson's disease. *Parkinsonism Relat Disord* 2012; 18 Suppl 1: S28-30.

[381] Jellinger KA. Formation and development of Lewy pathology: a critical update. *J Neurol* 2009; 256: 270–279.

[382] Singleton AB, Farrer M, Johnson J, et al. α-Synuclein locus triplication causes Parkinson's disease. *Science*; http://science.sciencemag.org/content/302/5646/841 (2003, accessed 4 April 2017).

[383] Thomas B, Beal MF. Molecular insights into Parkinson's disease. *F1000 Med Rep* 2011; 3: 7.

[384] Edwards TL, Scott WK, Almonte C, et al. Genome-wide association study confirms SNPs in *SNCA* and the *MAPT* region as common risk factors for Parkinson disease. *Ann Hum Genet* 2010; 74: 97–109.

[385] Simón-Sánchez J, Schulte C, Bras JM, et al. Genome-wide association study reveals genetic risk underlying Parkinson's disease. *Nat Genet* 2009; 41: 1308–1312.

[386] Ammal Kaidery N, Tarannum S, Thomas B. Epigenetic landscape of Parkinson's disease: emerging role in disease mechanisms and therapeutic modalities. *Neurotherapeutics* 2013; 10: 698–708.

[387] Houlden H, Singleton AB. The genetics and neuropathology of Parkinson's disease. *Acta Neuropathol* 2012; 124: 325–338.

[388] Veldman BA, Wijn AM, Knoers N, et al. Genetic and environmental risk factors in Parkinson's disease. *Clin Neurol Neurosurg* 1998; 100: 15–26.

[389] de Lau LML, Breteler MMB, Louis E, et al. Epidemiology of Parkinson's disease. *Lancet Neurol* 2006; 5: 525–35.

[390] Fukuda T. Neurotoxicity of MPTP. *Neuropathology* 2001; 21: 323–332.

[391] Kopin IJ. Toxins and Parkinson's disease: MPTP parkinsonism in humans and animals. *Adv Neurol* 1987; 45: 137–44.

[392] Franco R, Li S, Rodriguez-Rocha H, et al. Molecular mechanisms of pesticide-induced neurotoxicity: Relevance to Parkinson's disease. *Chem Biol Interact* 2010; 188: 289–300.

[393] Kanthasamy A, Jin H, Anantharam V, et al. Emerging neurotoxic mechanisms in environmental factors-induced neurodegeneration. *Neurotoxicology* 2012; 33: 833–837.

[394] Ryu H, Rosas HD, Hersch SM, et al. The therapeutic role of creatine in Huntington's disease. *Pharmacol Ther* 2005; 108: 193–207.

[395] The Huntington's Disease Collaborative Research Group. A novel gene containing a trinucleotide repeat that is expanded and unstable on Huntington's disease chromosomes. *Cell* 1993; 72: 971–83.

[396] Kremer B, Goldberg P, Andrew SE, et al. A worldwide study of the Huntington's disease mutation: the sensitivity and specificity of measuring CAG repeats. *N Engl J Med* 1994; 330: 1401–1406.

[397] Myers RH, MacDonald ME, Koroshetz WJ, et al. *De novo* expansion of a (CAG)n repeat in sporadic Huntington's disease. *Nat Genet* 1993; *5*: 168–173.

[398] Okazawa H. Polyglutamine diseases: a transcription disorder? *Cell Mol Life Sci* 2003; 60: 1427–1439.

[399] Sugars KL, Rubinsztein DC. Transcriptional abnormalities in Huntington disease. *Trends Genet* 2003; 19: 233–8.

[400] Thomas EA. Striatal specificity of gene expression dysregulation in Huntington's disease. *J Neurosci Res* 2006; 84: 1151–1164.

[401] Ferrante RJ, Kowall NW, Beal MF, et al. Morphologic and histochemical characteristics of a spared subset of striatal neurons in Huntington's disease. *J Neuropathol Exp Neurol* 1987; 46: 12–27.

[402] Ferrante RJ, Kowall NW, Beal MF, et al. Selective sparing of a class of striatal neurons in Huntington's disease. *Science* 1985; 230: 561–3.

[403] Ferrante RJ, Kowall NW, Richardson EP, et al. Topography of enkephalin, substance P and acetylcholinesterase staining in Huntington's disease striatum. *Neurosci Lett* 1986; 71: 283–288.

[404] Ferrante RJ, Kowall NW, Richardson EP. Proliferative and degenerative changes in striatal spiny neurons in Huntington's disease: a combined study using the section-Golgi method and calbindin D28k immunocytochemistry. *J Neurosci* 1991; 11: 3877–87.

[405] Graveland GA, Williams RS, DiFiglia M. Evidence for degenerative and regenerative changes in neostriatal spiny neurons in Huntington's disease. *Science* 1985; 227: 770–3.

[406] Kowall NW, Ferrante RJ, Martin JB. Patterns of cell loss in Huntington's disease. *Trends Neurosci* 1987; 10: 24–29.

[407] Lee J, Hwang YJ, Kim KY, et al. Epigenetic Mechanisms of Neurodegeneration in Huntington's Disease. *Neurotherapeutics* 2013; 10: 664–676.

[408] Vonsattel J-P, Myers RH, Stevens TJ, et al. Neuropathological Classification of Huntington's Disease. *J Neuropathol Exp Neurol* 1985; 44: 559–577.

[409] Ross CA, Koshy BT, Cummings CJ, et al. Intranuclear neuronal inclusions: a common pathogenic mechanism for glutamine-repeat neurodegenerative diseases? *Neuron* 1997; 19: 1147–50.

[410] Cattaneo E. Dysfunction of wild-type huntingtin in Huntington disease. *Physiology*; http://physiologyonline.physiology.org/content/18/1/34 (2003, accessed 4 April 2017).

[411] Mangiarini L, Sathasivam K, Seller M, et al. Exon 1 of the HD gene with an expanded CAG repeat is sufficient to cause a progressive neurological phenotype in transgenic mice. *Cell* 1996; 87: 493–506.

[412] Nucifora Jr. FC, Sasaki M, Peters MF, et al. Interference by huntingtin and atrophin-1 with CBP-mediated transcription leading to cellular toxicity. *Science* 2001; 291: 2423–2428.

[413] Ross CA, Poirier MA. Protein aggregation and neurodegenerative disease. *Nat Med* 2004; 10: S10–S17.

[414] Zhang Y, Li M, Drozda M, et al. Depletion of wild-type huntingtin in mouse models of neurologic diseases. *J Neurochem* 2003; 87: 101–6.

[415] Beal MF, Ferrante RJ. Experimental therapeutics in transgenic mouse models of Huntington's disease. *Nat Rev Neurosci* 2004; *5*: 373–384.

[416] Szebenyi G, Morfini GA, Babcock A, et al. Neuropathogenic forms of huntingtin and androgen receptor inhibit fast axonal transport. *Neuron* 2003; 40: 41–52.

[417] Trushina E, Dyer RB, Badger JD, et al. Mutant huntingtin impairs axonal trafficking in mammalian neurons *in vivo* and *in vitro*. *Mol Cell Biol* 2004; 24: 8195–209.

[418] Li S-H, Cheng AL, Zhou H, et al. Interaction of Huntington disease protein with transcriptional activator Sp1. *Mol Cell Biol* 2002; 22: 1277–87.

[419] Thomas EA, Coppola G, Desplats PA, et al. The HDAC inhibitor 4b ameliorates the disease phenotype and transcriptional abnormalities in Huntington's disease transgenic mice. *Proc Natl Acad Sci* U S A 2008; 105: 15564–9.

[420] West RL, Lee JM, Maroun LE. Hypomethylation of the amyloid precursor protein gene in the brain of an Alzheimer's disease patient. *J Mol Neurosci* 1995; 6: 141–146.

[421] Barrachina M, Ferrer I. DNA methylation of Alzheimer disease and tauopathy-related genes in postmortem brain. *J Neuropathol Exp Neurol* 2009; 68: 880–891.

[422] Fuso A, Seminara L, Cavallaro RA, et al. S-adenosylmethionine/homocysteine cycle alterations modify DNA methylation status with consequent deregulation of PS1 and BACE and beta-amyloid production. *Mol Cell Neurosci* 2005; 28: 195–204.

[423] Brohede J, Rinde M, Winblad B, et al. A DNA methylation study of the amyloid precursor protein gene in several brain regions from patients with familial Alzheimer disease. *J Neurogenet* 2010; 24: 179–181.

[424] Wang S-C, Oelze B, Schumacher A, et al. Age-specific epigenetic drift in late-onset Alzheimer's disease. *PLoS One* 2008; 3: e2698.

[425] Morrison LD, Smith DD, Kish SJ. Brain S-adenosylmethionine levels are severely decreased in Alzheimer's disease. *J Neurochem* 1996; 67: 1328–31.

[426] Bottiglieri T, Godfrey P, Flynn T, et al. Cerebrospinal fluid S-adenosylmethionine in depression and dementia: effects of treatment with parenteral and oral S-adenosylmethionine. *J Neurol Neurosurg Psychiatry* 1990; 53: 1096–1098.

[427] Serot JM, Christmann D, Dubost T, et al. CSF-folate levels are decreased in late-onset AD patients. *J Neural Transm* 2001; 108: 93–99.

[428] Kennedy BP, Bottiglieri T, Arning E, et al. Elevated S-adenosylhomocysteine in Alzheimer brain: influence on methyltransferases and cognitive function. *J Neural Transm* 2004; 111: 547–567.

[429] Coppedè F, Tannorella P, Pezzini I, et al. Folate, homocysteine, vitamin B12, and polymorphisms of genes participating in one-carbon metabolism in late-onset Alzheimer's disease patients and healthy controls. *Antioxid Redox Signal* 2012; 17: 195–204.

[430] Sontag E, Nunbhakdi-Craig V, Sontag J-M, et al. Protein phosphatase 2A methyltransferase links homocysteine metabolism with tau and amyloid precursor protein regulation. *J Neurosci*; http://www.jneurosci.org/content/27/11/2751 (2007, accessed 4 April 2017).

[431] Zhou X-W, Gustafsson J-Å, Tanila H, et al. Tau hyperphosphorylation correlates with reduced methylation of protein phosphatase 2A. *Neurobiol Dis* 2008; 31: 386–394.

[432] Yoon SY, Choi HI, Choi JE, et al. Methotrexate decreases PP2A methylation and increases tau phosphorylation in neuron. *Biochem Biophys Res Commun* 2007; 363: 811–816.

[433] Zhang C-E, Tian Q, Wei W, et al. Homocysteine induces tau phosphorylation by inactivating protein phosphatase 2A in rat hippocampus. *Neurobiol Aging* 2008; 29: 1654–65.

[434] Cacciapuoti F. Lowering homocysteine levels with folic acid and B-vitamins do not reduce early atherosclerosis, but could interfere with cognitive decline and Alzheimer's disease. *J Thromb Thrombolysis* 2013; 36: 258–262.

[435] Fuso A, Nicolia V, Cavallaro RA, et al. B-vitamin deprivation induces hyperhomocysteinemia and brain S-adenosylhomocysteine, depletes brain S-adenosylmethionine, and enhances PS1 and BACE expression and amyloid-beta deposition in mice. *Mol Cell Neurosci* 2008; 37: 731–46.

[436] Fuso A, Nicolia V, Ricceri L, et al. S-adenosylmethionine reduces the progress of the Alzheimer-like features induced by B-vitamin deficiency in mice. *Neurobiol Aging* 2012; 33: 1482.e1-16.

[437] Fuso A, Nicolia V, Pasqualato A, et al. Changes in Presenilin 1 gene methylation pattern in diet-induced B vitamin deficiency. *Neurobiol Aging* 2011; 32: 187–199.

[438] Lee S, Lemere CA, Frost JL, et al. Dietary supplementation with S-adenosyl methionine delayed amyloid-β and tau pathology in 3xTg-AD mice. *J Alzheimers Dis* 2012; 28: 423–31.

[439] Chan A, Paskavitz J, Remington R, et al. Efficacy of a vitamin/nutriceutical formulation for early-stage Alzheimer's disease: a 1-year, open-label pilot study with an 16-month caregiver extension. *Am J Alzheimers Dis Other Demen* 2008; 23: 571–85.

[440] Remington R, Chan A, Paskavitz J, et al. Efficacy of a vitamin/nutriceutical formulation for moderate-stage to later-stage Alzheimer's disease: a placebo-controlled pilot study. *Am J Alzheimers Dis Other Demen* 2009; 24: 27–33.

[441] Chouliaras L, Mastroeni D, Delvaux E, et al. Consistent decrease in global DNA methylation and hydroxymethylation in the hippocampus of Alzheimer's disease patients. *Neurobiol Aging* 2013; 34: 2091–2099.

[442] Hoyaux D, Decaestecker C, Heizmann CW, et al. S100 proteins in Corpora Amylacea from normal human brain. *Brain Res* 2000; 867:

280–288.

[443] Urdinguio RG, Sanchez-Mut J V, Esteller M, et al. Epigenetic mechanisms in neurological diseases: genes, syndromes, and therapies. *Lancet Neurol* 2009; 8: 1056–72.

[444] De Jager PL, Srivastava G, Lunnon K, et al. Alzheimer's disease: early alterations in brain DNA methylation at *ANK1, BIN1, RHBDF2* and other loci. *Nat Neurosci* 2014; 17: 1156–1163.

[445] Lunnon K, Smith R, Hannon E, et al. Methylomic profiling implicates cortical deregulation of *ANK1* in Alzheimer's disease. *Nat Neurosci* 2014; 17: 1164–1170.

[446] Chen K-L, Wang SS-S, Yang Y-Y, et al. The epigenetic effects of amyloid-beta(1-40) on global DNA and neprilysin genes in murine cerebral endothelial cells. *Biochem Biophys Res Commun* 2009; 378: 57–61.

[447] Müerköster SS, Werbing V, Koch D, et al. Role of myofibroblasts in innate chemoresistance of pancreatic carcinoma-Epigenetic downregulation of caspases. *Int J Cancer* 2008; 123: 1751–1760.

[448] Sommer G, Kralisch S, Lipfert J, et al. Amyloid precursor protein expression is induced by tumor necrosis factor Ĩ± in 3T3-L1 adipocytes. *J Cell Biochem* 2009; 108: 1418–1422.

[449] Wilson AG. Epigenetic regulation of gene expression in the inflammatory response and relevance to common diseases. *J Periodontol* 2008; 79: 1514–1519.

[450] Xiong M, Zhang T, Zhang L-M, et al. Caspase inhibition attenuates accumulation of β-amyloid by reducing β-secretase production and activity in rat brains after stroke. *Neurobiol Dis* 2008; 32: 433–441.

[451] Mukaetova-Ladinska EB, Harrington CR, Roth M, et al. Alterations in tau protein metabolism during normal aging. *Dement Geriatr Cogn Disord* 1996; 7: 95–103.

[452] Rauhala HE, Porkka KP, Saramäki OR, et al. Clusterin is epigenetically regulated in prostate cancer. *Int J Cancer* 2008; 123: 1601–1609.

[453] Nuutinen T, Suuronen T, Kyrylenko S, et al. Induction of clusterin/apoJ expression by histone deacetylase inhibitors in neural cells. *Neurochem Int* 2005; 47: 528–538.

[454] Suuronen T, Nuutinen T, Ryhänen T, et al. Epigenetic regulation of clusterin/apolipoprotein J expression in retinal pigment epithelial cells. *Biochem Biophys Res Commun* 2007; 357: 397–401.

[455] Jee C Do, Lee HS, Bae SI, et al. *International journal of oncology*; https://www.spandidos-publications.com/10.3892/ijo.26.5.1265 (2005, accessed 4 April 2017).

[456] Moreira PR, Guimarães MM, Guimarães ALS, et al. Methylation of *P16, P21, P27, RB1* and *P53* genes in odontogenic keratocysts. *J Oral Pathol Med* 2008; 38: 99–103.

[457] Robertson KD, Jones PA. The human ARF cell cycle regulatory gene promoter is a CpG island which can be silenced by DNA methylation and down-regulated by wild-type p53. *Mol Cell Biol* 1998; 18: 6457–73.

[458] Tschöp K, Engeland K. Cell cycle-dependent transcription of cyclin B2 is influenced by DNA methylation but is independent of methylation in the CDE and CHR elements. *FEBS J* 2007; 274: 5235–5249.

[459] Rao JS, Keleshian VL, Klein S, et al. Epigenetic modifications in frontal cortex from Alzheimer's disease and bipolar disorder patients. *Transl Psychiatry* 2012; 2: e132.

[460] Bollati V, Galimberti D, Pergoli L, et al. DNA methylation in repetitive elements and Alzheimer disease. *Brain Behav Immun* 2011; 25: 1078–1083.

[461] Condliffe D, Wong A, Troakes C, et al. Cross-region reduction in 5-hydroxymethylcytosine in Alzheimer's disease brain. *Neurobiol Aging* 2014; 35: 1850–1854.

[462] Coppieters N, Dieriks B V, Lill C, et al. Global changes in DNA methylation and hydroxymethylation in Alzheimer's disease human brain. *Neurobiol Aging* 2014; 35: 1334–1344.

[463] Bradley-Whitman MA, Lovell MA. Epigenetic changes in the progression of Alzheimer's disease. *Mech Ageing Dev* 2013; 134: 486–95.

[464] Hutnick LK, Golshani P, Namihira M, et al. DNA hypomethylation restricted to the murine forebrain induces cortical degeneration and impairs postnatal neuronal maturation. *Hum Mol Genet* 2009; 18: 2875–2888.

[465] Morgan AR, Hamilton G, Turic D, et al. Association analysis of 528 intra-genic SNPs in a region of chromosome 10 linked to late onset Alzheimer's disease. *Am J Med Genet Part B Neuropsychiatr Genet* 2008; 147B: 727–731.

[466] Desplats P, Spencer B, Coffee E, et al. Alpha-synuclein sequesters Dnmt1 from the nucleus: a novel mechanism for epigenetic alterations in Lewy body diseases. *J Biol Chem* 2011; 286: 9031–7.

[467] Trojanowski JQ, Goedert M, Iwatsubo T, et al. Fatal attractions: abnormal protein aggregation and neuron death in Parkinson's disease and Lewy body dementia. *Cell Death Differ* 1998; 5: 832–837.

[468] Jowaed A, Schmitt I, Kaut O, et al. Methylation regulates

alpha-synuclein expression and is decreased in Parkinson's disease patients' brains. *J Neurosci*; http://www.jneurosci.org/content/30/18/6355 (2010, accessed 4 April 2017).

[469] Matsumoto L, Takuma H, Tamaoka A, et al. CpG demethylation enhances alpha-synuclein expression and affects the pathogenesis of Parkinson's disease. *PLoS One* 2010; 5: e15522.

[470] de Boni L, Tierling S, Roeber S, et al. Next-generation sequencing reveals regional differences of the α-synuclein methylation state independent of Lewy body disease. *NeuroMolecular Med* 2011; 13: 310–320.

[471] International Parkinson's Disease Genomics Consortium (IPDGC), Wellcome Trust Case Control Consortium 2 (WTCCC2). A two-stage meta-analysis identifies several new loci for Parkinson's disease. *PLoS Genet* 2011; 7: e1002142.

[472] Moore K, McKnight AJ, Craig D, et al. Epigenome-wide association study for Parkinson's disease. *NeuroMolecular Med* 2014; 16: 845–855.

[473] Agirre X, Román-Gómez J, Vázquez I, et al. Abnormal methylation of the common *PARK2* and *PACRG* promoter is associated with downregulation of gene expression in acute lymphoblastic leukemia and chronic myeloid leukemia. *Int J Cancer* 2006; 118: 1945–1953.

[474] Cai M, Tian J, Zhao G, et al. Study of methylation levels of parkin gene promoter in Parkinson's disease patients. *Int J Neurosci* 2011; 121: 497–502.

[475] Coppedè F. Genetics and epigenetics of Parkinson's disease. *Sci World J* 2012; 2012: 1–12.

[476] Ng CW, Yildirim F, Yap YS, et al. Extensive changes in DNA methylation are associated with expression of mutant huntingtin. *Proc Natl Acad Sci U S A* 2013; 110: 2354–9.

[477] Villar-Menéndez I, Blanch M, Tyebji S, et al. Increased 5-methylcytosine and decreased 5-hydroxymethylcytosine levels are associated with reduced striatal A2AR levels in Huntington's disease. *Neuro-Molecular Med* 2013; 15: 295–309.

[478] Wood H. Neurodegenerative disease: Altered DNA methylation and RNA splicing could be key mechanisms in Huntington disease. *Nat Rev Neurol* 2013; 9: 119–119.

[479] Zhang K, Schrag M, Crofton A, et al. Targeted proteomics for quantification of histone acetylation in Alzheimer's disease. *Proteomics* 2012; 12: 1261–1268.

[480] Gräff J, Kim D, Dobbin MM, et al. Epigenetic regulation of gene expression in physiological and pathological brain processes. *Physiol Rev*; http://physrev.physiology.org/content/91/2/603 (2011, accessed 4 April 2017).

[481] Marques SCF, Lemos R, Ferreiro E, et al. Epigenetic regulation of BACE1 in Alzheimer's disease patients and in transgenic mice. *Neuroscience* 2012; 220: 256–66.

[482] Kilgore M, Miller CA, Fass DM, et al. Inhibitors of class 1 histone deacetylases reverse contextual memory deficits in a mouse model of Alzheimer's disease. *Neuropsychopharmacology* 2010; 35: 870–80.

[483] Francis YI, Fà M, Ashraf H, et al. Dysregulation of histone acetylation in the APP/PS1 mouse model of Alzheimer's disease. *J Alzheimers Dis* 2009; 18: 131–9.

[484] Liu R, Lei JX, Luo C, et al. Increased EID1 nuclear translocation impairs synaptic plasticity and memory function associated with pathogenesis of Alzheimer's disease. *Neurobiol Dis* 2012; 45: 902–912.

[485] Caccamo A, Maldonado MA, Bokov AF, et al. CBP gene transfer increases BDNF levels and ameliorates learning and memory deficits in a mouse model of Alzheimer's disease. *Proc Natl Acad Sci U S A* 2010; 107: 22687–92.

[486] Oliveira AMM, Estévez MA, Hawk JD, et al. Subregion-specific p300 conditional knock-out mice exhibit long-term memory impairments. *Learn Mem* 2011; 18: 161–9.

[487] Oliveira AMM, Wood MA, McDonough CB, et al. Transgenic mice expressing an inhibitory truncated form of p300 exhibit long-term memory deficits. *Learn Mem* 2007; 14: 564–72.

[488] Maurice T, Duclot F, Meunier J, et al. Altered memory capacities and response to stress in p300/CBP-associated factor (PCAF) histone acetylase knockout mice. *Neuropsychopharmacology* 2008; 33: 1584–1602.

[489] Duclot F, Meffre J, Jacquet C, et al. Mice knock out for the histone acetyltransferase p300/CREB binding protein-associated factor develop a resistance to amyloid toxicity. *Neuroscience* 2010; 167: 850–863.

[490] Walker MP, LaFerla FM, Oddo SS, et al. Reversible epigenetic histone modifications and Bdnf expression in neurons with aging and from a mouse model of Alzheimer's disease. *Age* (Dordr) 2013; 35: 519–31.

[491] Ryu H, Barrup M, Kowall NW, et al. P3-260: Epigenetic modification in a monozygotic twin with Alzheimer's disease. *Alzheimer's Dement* 2008; 4: T598.

[492] Lithner CU, Hernandez CM, Nordberg A, et al. Epigenetic

changes related to beta-amyloid-implications for Alzheimer's disease. *Alzheimer's Dement J Alzheimer's Assoc* 2009; 5: P304.

[493] Gräff J, Rei D, Guan J-S, et al. An epigenetic blockade of cognitive functions in the neurodegenerating brain. *Nature* 2012; 483: 222–226.

[494] Zhang Z-Y, Schluesener HJ. Oral administration of histone deacetylase inhibitor MS-275 ameliorates neuroinflammation and cerebral amyloidosis and improves behavior in a mouse model. *J Neuropathol Exp Neurol* 2013; 72: 178–185.

[495] McQuown SC, Barrett RM, Matheos DP, et al. HDAC3 is a critical negative regulator of long-term memory formation. *J Neurosci*; http://www.jneurosci.org/content/31/2/764 (2011, accessed 4 April 2017).

[496] Ding H, Dolan PJ, Johnson GVW. Histone deacetylase 6 interacts with the microtubule-associated protein tau. *J Neurochem* 2008; 106: 2119–2130.

[497] Simões-Pires C, Zwick V, Nurisso A, et al. HDAC6 as a target for neurodegenerative diseases: what makes it different from the other HDACs? *Mol Neurodegener* 2013; 8: 7.

[498] Cook C, Carlomagno Y, Gendron TF, et al. Acetylation of the KXGS motifs in tau is a critical determinant in modulation of tau aggregation and clearance. *Hum Mol Genet* 2014; 23: 104–116.

[499] Cook C, Gendron TF, Scheffel K, et al. Loss of HDAC6, a novel CHIP substrate, alleviates abnormal tau accumulation. *Hum Mol Genet* 2012; 21: 2936–2945.

[500] Perez M, Santa-Maria I, de Barreda EG, et al. Tau - an inhibitor of deacetylase HDAC6 function. *J Neurochem* 2009; 109: 1756–1766.

[501] Govindarajan N, Rao P, Burkhardt S, et al. Reducing HDAC6 ameliorates cognitive deficits in a mouse model for Alzheimer's disease. *EMBO Mol Med* 2013; 5: 52–63.

[502] Xiong Y, Zhao K, Wu J, et al. HDAC6 mutations rescue human tau-induced microtubule defects in Drosophila. *Proc Natl Acad Sci U S A* 2013; 110: 4604–9.

[503] Fischer A. Targeting histone-modifications in Alzheimer's disease. What is the evidence that this is a promising therapeutic avenue? *Neuropharmacology* 2014; 80: 95–102.

[504] Sarthi J, Elefant F. dTip60 HAT activity controls synaptic bouton expansion at the *Drosophila* neuromuscular junction. *PLoS One* 2011; 6: e26202.

[505] Pirooznia SK, Sarthi J, Johnson AA, et al. Tip60 HAT activity mediates APP induced lethality and apoptotic cell death in the CNS of a *Drosophila* Alzheimer's disease model. *PLoS One* 2012; 7: e41776.

[506] Johnson AA, Sarthi J, Pirooznia SK, et al. Increasing Tip60 HAT levels rescues axonal transport defects and associated behavioral phenotypes in a *Drosophila* Alzheimer's disease model. *J Neurosci*; http://www.jneurosci.org/content/33/17/7535 (2013, accessed 4 April 2017).

[507] Kaidi A, Jackson SP. KAT5 tyrosine phosphorylation couples chromatin sensing to ATM signalling. *Nature* 2013; 498: 70–74.

[508] Müller T, Schrötter A, Loosse C, et al. A ternary complex consisting of AICD, FE65, and TIP60 down-regulates Stathmin1. *Biochim Biophys Acta - Proteins Proteomics* 2013; 1834: 387–394.

[509] Agis-Balboa RC, Pavelka Z, Kerimoglu C, et al. Loss of HDAC5 impairs memory function: implications for Alzheimer's disease. *J Alzheimers Dis* 2013; 33: 35–44.

[510] Kim M-S, Akhtar MW, Adachi M, et al. An essential role for histone deacetylase 4 in synaptic plasticity and memory formation. *J Neurosci*; 32http://www.jneurosci.org/content/32/32/10879 (2012, accessed 4 April 2017).

[511] Julien C, Tremblay C, Émond V, et al. Sirtuin 1 reduction parallels the accumulation of tau in Alzheimer disease. *J Neuropathol Exp Neurol* 2009; 68: 48–58.

[512] Morris BJ. Seven sirtuins for seven deadly diseases of aging. *Free Radic Biol Med* 2013; 56: 133–171.

[513] Kim D, Nguyen MD, Dobbin MM, et al. SIRT1 deacetylase protects against neurodegeneration in models for Alzheimer's disease and amyotrophic lateral sclerosis. *EMBO J* 2007; 26: 3169–3179.

[514] Donmez G, Wang D, Cohen DE, et al. SIRT1 suppresses beta-amyloid production by activating the alpha-secretase gene *ADAM10*. *Cell* 2010; 142: 320–32.

[515] Min S-W, Cho S-H, Zhou Y, et al. Acetylation of tau inhibits its degradation and contributes to tauopathy. *Neuron* 2010; 67: 953–66.

[516] Araki T, Sasaki Y, Milbrandt J. Increased nuclear NAD biosynthesis and SIRT1 activation prevent axonal degeneration. *Science*; http://science.sciencemag.org/content/305/5686/1010 (2004, accessed 4 April 2017).

[517] Chen J, Zhou Y, Mueller-Steiner S, et al. SIRT1 protects against microglia-dependent amyloid-toxicity through inhibiting NF- B signaling. *J Biol Chem* 2005; 280: 40364–40374.

[518] Myung N-H, Zhu X, Kruman II, et al. Evidence of DNA damage in Alzheimer disease: phosphorylation of histone H2AX in astrocytes. *Age* (Omaha) 2008; 30: 209–215.

[519] Ogawa O, Zhu X, Lee H-G, et al. Ectopic localization of phosphorylated histone H3 in Alzheimer's disease: a mitotic catastrophe? *Acta Neuropathol* 2003; 105: 524–8.

[520] Hyman BT, Elvhage TE, Reiter J. Extracellular signal regulated kinases. Localization of protein and mRNA in the human hippocampal formation in Alzheimer's disease. Am *J Pathol 1994*; 144: 565–72.

[521] Perry G, Roder H, Nunomura A, et al. Activation of neuronal extracellular receptor kinase (ERK) in Alzheimer disease links oxidative stress to abnormal phosphorylation. *Neuroreport* 1999; 10: 2411–5.

[522] Zhu X, Castellani RJ, Takeda A, et al. Differential activation of neuronal ERK, JNK/SAPK and p38 in Alzheimer disease: the 'two hit' hypothesis. *Mech Ageing Dev* 2001; 123: 39–46.

[523] Iqbal K, Tellez-Nagel I, Grunke-Iqbal I. Protein abnormalities in Huntington's chorea. Epub ahead of print 1974. DOI: 10.1016/0006-8993(74)90527-7.

[524] Mastroeni D, Chouliaras L, Grover A, et al. Reduced RAN expression and disrupted transport between cytoplasm and nucleus; a key event in Alzheimer's disease pathophysiology. *PLoS One*; 8. Epub ahead of print 2013. DOI: 10.1371/journal.pone.0053349.

[525] Fontán-Lozano Á, Suárez-Pereira I, Horrillo A, et al. Histone H1 poly[ADP]-ribosylation regulates the chromatin alterations required for learning consolidation. *J Neurosci*; http://www.jneurosci.org/content/30/40/13305 (2010, accessed 4 April 2017).

[526] Abeti R, Abramov AY, Duchen MR. Beta-amyloid activates PARP causing astrocytic metabolic failure and neuronal death. *Brain* 2011; 134: 1658–1672.

[527] Liu H-P, Lin W-Y, Wu B-T, et al. Evaluation of the poly(ADP-ribose) polymerase-1 gene variants in Alzheimer's disease. *J Clin Lab Anal* 2010; 24: 182–186.

[528] Strosznajder JB, Czapski GA, Adamczyk A, et al. Poly(ADP-ribose) polymerase-1 in amyloid beta toxicity and Alzheimer's disease. *Mol Neurobiol* 2012; 46: 78–84.

[529] Kontopoulos E, Parvin JD, Feany MB. Alpha-synuclein acts in the nucleus to inhibit histone acetylation and promote neurotoxicity. *Hum Mol Genet* 2006; 15: 3012–3023.

[530] Outeiro TF, Kontopoulos E, Altmann SM, et al. Sirtuin 2 inhibitors rescue α-synuclein-mediated toxicity in models of Parkinson's disease. *Science*; http://science.sciencemag.org/content/317/5837/516 (2007, accessed 4 April 2017).

[531] St. Laurent R, O'Brien LM, Ahmad ST. Sodium butyrate improves locomotor impairment and early mortality in a rotenone-induced *Drosophila* model of Parkinson's disease. *Neuroscience* 2013; 246: 382–390.

[532] Siddiqui A, Chinta SJ, Mallajosyula JK, et al. Selective binding of nuclear alpha-synuclein to the *PGC1alpha* promoter under conditions of oxidative stress may contribute to losses in mitochondrial function: Implications for Parkinson's disease. *Free Radic Biol Med* 2012; 53: 993–1003.

[533] Zheng B, Liao Z, Locascio JJ, et al. PGC-1 , A potential therapeutic target for early intervention in Parkinson's disease. *Sci Transl Med* 2010; 2: 52ra73-52ra73.

[534] Kirilyuk A, Shimoji M, Catania J, et al. An intrinsically disordered region of the acetyltransferase p300 with similarity to prion-like domains plays a role in aggregation. *PLoS One* 2012; 7: e48243.

[535] Jin H, Kanthasamy A, Ghosh A, et al. α-Synuclein negatively regulates protein kinase Cδ expression to suppress apoptosis in dopaminergic neurons by reducing p300 histone acetyltransferase activity. *J Neurosci*; http://www.jneurosci.org/content/31/6/2035 (2011, accessed 4 April 2017).

[536] Voutsinas GE, Stavrou EF, Karousos G, et al. Allelic imbalance of expression and epigenetic regulation within the alpha-synuclein wild-type and p.Ala53Thr alleles in Parkinson disease. *Hum Mutat* 2010; 31: 685–691.

[537] Nicholas AP, Lubin FD, Hallett PJ, et al. Striatal histone modifications in models of levodopa-induced dyskinesia. *J Neurochem* 2008; 106: 486–494.

[538] Song C, Kanthasamy A, Anantharam V, et al. Environmental neurotoxic pesticide increases histone acetylation to promote apoptosis in dopaminergic neuronal cells: relevance to epigenetic mechanisms of neurodegeneration. *Mol Pharmacol*; http://molpharm.aspetjournals.org/content/77/4/621 (2010, accessed 4 April 2017).

[539] Song C, Kanthasamy A, Jin H, et al. Paraquat induces epigenetic changes by promoting histone acetylation in cell culture models of dopaminergic degeneration. *Neurotoxicology* 2011; 32: 586–595.

[540] Ferrante RJ, Ryu H, Kubilus JK, et al. Chemotherapy for

the brain: the Antitumor antibiotic mithramycin prolongs survival in a mouse model of Huntington's disease. *J Neurosci*; http://www.jneurosci.org/content/24/46/10335 (2004, accessed 4 April 2017).

[541] Suzuki MM, Bird A. DNA methylation landscapes: provocative insights from epigenomics. *Nat Rev Genet* 2008; 9: 465–476.

[542] Gardian G, Browne SE, Choi D-K, et al. Neuroprotective effects of phenylbutyrate in the N171-82Q transgenic mouse model of Huntington's disease. *J Biol Chem* 2005; 280: 556–63.

[543] McFarland KN, Das S, Sun TT, et al. Genome-wide histone acetylation is altered in a transgenic mouse model of Huntington's disease. *PLoS One* 2012; 7: e41423.

[544] Ryu H, Lee J, Hagerty SW, et al. ESET/SETDB1 gene expression and histone H3 (K9) trimethylation in Huntington's disease. *Proc Natl Acad Sci U S A* 2006; 103: 19176–81.

[545] Sadri-Vakili G, Bouzou B, Benn CL, et al. Histones associated with downregulated genes are hypo-acetylated in Huntington's disease models. *Hum Mol Genet* 2007; 16: 1293–1306.

[546] Lee J, Hagerty S, Cormier KA, et al. Monoallele deletion of CBP leads to pericentromeric heterochromatin condensation through ESET expression and histone H3 (K9) methylation. *Hum Mol Genet* 2008; 17: 1774–1782.

[547] Stack EC, Del Signore SJ, Luthi-Carter R, et al. Modulation of nucleosome dynamics in Huntington's disease. *Hum Mol Genet* 2007; 16: 1164–1175.

[548] Lee J, Hwang YJ, Shin J-Y, et al. Epigenetic regulation of cholinergic receptor M1 (CHRM1) by histone H3K9me3 impairs Ca2+ signaling in Huntington's disease. *Acta Neuropathol* 2013; 125: 727–739.

[549] Calabresi P, Centonze D, Gubellini P, et al. Acetylcholine-mediated modulation of striatal function. *Trends Neurosci* 2000; 23: 120–6.

[550] Cha JH, Kosinski CM, Kerner JA, et al. Altered brain neurotransmitter receptors in transgenic mice expressing a portion of an abnormal human huntington disease gene. *Proc Natl Acad Sci U S A* 1998; 95: 6480–5.

[551] Wang Z, Kai L, Day M, et al. Dopaminergic control of corticostriatal long-term synaptic depression in medium spiny neurons is mediated by cholinergic interneurons. *Neuron* 2006; 50: 443–52.

[552] Sonntag K-C. MicroRNAs and deregulated gene expression networks in neurodegeneration. *Brain Res* 2010; 1338: 48–57.

[553] Schipper HM, Maes OC, Chertkow HM, et al. MicroRNA expression in Alzheimer blood mononuclear cells. *Gene Regul Syst Bio* 2007; 1: 263–74.

[554] Van den Hove DL, Kompotis K, Lardenoije R, et al. Epigenetically regulated microRNAs in Alzheimer's disease. *Neurobiol Aging* 2014; 35: 731–745.

[555] Bicchi I, Morena F, Montesano S, et al. MicroRNAs and molecular mechanisms of neurodegeneration. *Genes 2013*, Vol 4, Pages 244-263 2013; 4: 244–263.

[556] Delay C, Calon F, Mathews P, et al. Alzheimer-specific variants in the 3'UTR of Amyloid precursor protein affect microRNA function. *Mol Neurodegener* 2011 61 2011; 286: 241–251.

[557] Fan X, Liu Y, Jiang J, et al. Regulated intramembrane proteolysis of amyloid precursor protein and regulation of expression of putative target genes. *EMBO Rep* 2010; 7: 739–745.

[558] Liang C, Zhu H, Xu Y, et al. MicroRNA-153 negatively regulates the expression of amyloid precursor protein and amyloid precursor-like protein 2. *Brain Res* 2012; 1455: 103–13.

[559] Long JM, Lahiri DK. MicroRNA-101 downregulates Alzheimer's amyloid-β precursor protein levels in human cell cultures and is differentially expressed. Epub ahead of print 2011. DOI: 10.1016/j.bbrc.2010.12.053.

[560] Niwa R, Zhou F, Li C, et al. The expression of the Alzheimer's amyloid precursor protein-like gene is regulated by developmental timing microRNAs and their targets in *Caenorhabditis elegans*. *Dev Biol* 2008; 315: 418–425.

[561] Patel N, Hoang D, Miller N, et al. MicroRNAs can regulate human APP levels. *Mol Neurodegener* 2008 31 2008; 93: 1600–1608.

[562] Long JM, Ray B, Lahiri DK. MicroRNA-153 physiologically inhibits expression of amyloid-β precursor protein in cultured human fetal brain cells and is dysregulated in a subset of Alzheimer disease patients. *J Biol Chem* 2012; 287: 31298–310.

[563] Cheng L-C, Pastrana E, Tavazoie M, et al. miR-124 regulates adult neurogenesis in the subventricular zone stem cell niche. *Nat Neurosci* 2009; 12: 399–408.

[564] Smith P, Al Hashimi A, Girard J, et al. *In vivo* regulation of amyloid precursor protein neuronal splicing by microRNAs. *J Neurochem* 2011; 116: 240–247.

[565] Fang M, Wang J, Zhang X, et al. The miR-124 regulates the expression of BACE1/β-secretase correlated with cell death in Alzheimer's disease. *Toxicol Lett* 2012; 209: 94–105.

[566] Hébert SS, Horré K, Nicolaï L, et al. Loss of microRNA cluster miR-29a/b-1 in sporadic Alzheimer's disease correlates with increased BACE1/beta-secretase expression. *Proc Natl Acad Sci U S A* 2008; 105: 6415–20.

[567] Zhu H-C, Wang L-M, Wang M, et al. MicroRNA-195 downregulates Alzheimer's disease amyloid-β production by targeting BACE1. *Brain Res Bull* 2012; 88: 596–601.

[568] Zong Y, Wang H, Dong W, et al. miR-29c regulates BACE1 protein expression. *Brain Res* 2011; 1395: 108–115.

[569] Wang W-X, Rajeev BW, Stromberg AJ, et al. The expression of microRNA miR-107 decreases early in Alzheimer's disease and may accelerate disease progression through regulation of β-site amyloid precursor protein-cleaving enzyme 1. *J Neurosci*; http://www.jneurosci.org/content/28/5/1213 (2008, accessed 4 April 2017).

[570] Wang W-X, Huang Q, Hu Y, et al. Patterns of microRNA expression in normal and early Alzheimer's disease human temporal cortex: white matter versus gray matter. *Acta Neuropathol* 2011; 121: 193–205.

[571] Wang W-X, Wilfred BR, Madathil SK, et al. miR-107 regulates granulin/progranulin with implications for traumatic brain injury and neurodegenerative disease. *Am J Pathol* 2010; 177: 334–345.

[572] Boissonneault V, Plante I, Rivest S, et al. MicroRNA-298 and microRNA-328 regulate expression of mouse beta-amyloid precursor protein-converting enzyme 1. *J Biol Chem* 2009; 284: 1971–81.

[573] Faghihi MA, Zhang M, Huang J, et al. Evidence for natural antisense transcript-mediated inhibition of microRNA function. *Genome Biol* 2010; 11: R56.

[574] Geekiyanage H, Chan C. MicroRNA-137/181c regulates serine palmitoyltransferase and in turn amyloid β, novel targets in sporadic Alzheimer's disease. *J Neurosci*; http://www.jneurosci.org/content/31/41/14820 (2011, accessed 4 April 2017).

[575] Smrt RD, Szulwach KE, Pfeiffer RL, et al. MicroRNA miR-137 regulates neuronal maturation by targeting ubiquitin ligase mind bomb-1. *Stem Cells* 2010; 28: 1060–1070.

[576] Szulwach KE, Li X, Smrt RD, et al. Cross talk between microRNA and epigenetic regulation in adult neurogenesis. *J Cell Biol* 2010; 189: 127–141.

[577] Wang H, Liu J, Zong Y, et al. miR-106b aberrantly expressed in a double transgenic mouse model for Alzheimer's disease targets TGF-β type II receptor. *Brain Res* 2010; 1357: 166–174.

[578] Schonrock N, Humphreys DT, Preiss T, et al. Target gene repression mediated by miRNAs miR-181c and miR-9 both of which are down-regulated by amyloid-β. *J Mol Neurosci* 2012; 46: 324–335.

[579] Hébert SS, Horré K, Nicolaï L, et al. MicroRNA regulation of Alzheimer's Amyloid precursor protein expression. *Neurobiol Dis* 2009; 33: 422–428.

[580] Akram A, Schmeidler J, Katsel P, et al. Increased expression of cholesterol transporter ABCA1 is highly correlated with severity of dementia in AD hippocampus. *Brain Res* 2010; 1318: 167–177.

[581] Brett JO, Renault VM, Rafalski VA, et al. The microRNA cluster miR-106b-25 regulates adult neural stem/progenitor cell proliferation and neuronal differentiation. *Aging* (Albany NY) 2011; 3: 108–124.

[582] Delaloy C, Liu L, Lee J-A, et al. MicroRNA-9 coordinates proliferation and migration of human embryonic stem cell-derived neural progenitors. *Cell Stem Cell* 2010; 6: 323–35.

[583] Zhao C, Sun G, Li S, et al. A feedback regulatory loop involving microRNA-9 and nuclear receptor TLX in neural stem cell fate determination. *Nat Struct Mol Biol* 2009; 16: 365–371.

[584] Hébert SS, Sergeant N, Buée L. MicroRNAs and the regulation of tau metabolism. *Int J Alzheimers Dis* 2012; 2012: 1–6.

[585] Smith PY, Delay C, Girard J, et al. MicroRNA-132 loss is associated with tau exon 10 inclusion in progressive supranuclear palsy. *Hum Mol Genet* 2011; 20: 4016–4024.

[586] Liu F, Gong C-X. Tau exon 10 alternative splicing and tauopathies. *Mol Neurodegener* 2008; 3: 8.

[587] Caffrey TM, Joachim C, Paracchini S, et al. Haplotype-specific expression of exon 10 at the human *MAPT* locus. *Hum Mol Genet* 2006; 15: 3529–3537.

[588] Cogswell JP, Ward J, Taylor IA, et al. Identification of miRNA changes in Alzheimer's disease brain and CSF yields putative biomarkers and insights into disease pathways. *J Alzheimers Dis* 2008; 14: 27–41.

[589] Hébert SS, Wang W-X, Zhu Q, et al. A study of small RNAs from cerebral neocortex of pathology-ver-

ified Alzheimer's disease, dementia with lewy bodies, hippocampal sclerosis, frontotemporal lobar dementia, and non-demented human controls. *J Alzheimers Dis* 2013; 35: 335–48.

[590] Mohamed JS, Lopez MA, Boriek AM. Mechanical stretch up-regulates microRNA-26a and induces human airway smooth muscle hypertrophy by suppressing glycogen synthase kinase-3β. *J Biol Chem* 2010; 285: 29336–47.

[591] Zovoilis A, Agbemenyah HY, Agis-Balboa RC, et al. microRNA-34c is a novel target to treat dementias. EMBO J 2011; 30: 4299–4308.

[592] Carrettiero DC, Hernandez I, Neveu P, et al. The cochaperone BAG2 sweeps paired helical filament-insoluble tau from the microtubule. *J Neurosci*; http://www.jneurosci.org/content/29/7/2151 (2009, accessed 4 April 2017).

[593] Lukiw WJ. Micro-RNA speciation in fetal, adult and Alzheimer's disease hippocampus. *Neuroreport* 2007; 18: 297–300.

[594] Bilen J, Liu N, Burnett BG, et al. MicroRNA pathways modulate polyglutamine-induced neurodegeneration. *Mol Cell* 2006; 24: 157–63.

[595] Hébert SS, Papadopoulou AS, Smith P, et al. Alterations in glucose metabolism induce hypothermia leading to tau hyperphosphorylation through differential inhibition of kinase and phosphatase activities: implications for Alzheimer's disease. *J Neurosci* 2010; 24: 2401–2411.

[596] Cui JG, Li YY, Zhao Y, et al. Differential regulation of interleukin-1 receptor-associated kinase-1 (IRAK-1) and IRAK-2 by microRNA-146a and NF-kappaB in stressed human astroglial cells and in Alzheimer disease. *J Biol Chem* 2010; 285: 38951–60.

[597] Taganov KD, Boldin MP, Chang K-J, et al. NF-kappaB-dependent induction of microRNA miR-146, an inhibitor targeted to signaling proteins of innate immune responses. *Proc Natl Acad Sci U S A 2006*; 103: 12481–6.

[598] Lukiw WJ, Zhao Y, Cui JG. An NF-kappaB-sensitive micro RNA-146a-mediated inflammatory circuit in Alzheimer disease and in stressed human brain cells. *J Biol Chem* 2008; 283: 31315–22.

[599] Sethi P, Lukiw WJ. Micro-RNA abundance and stability in human brain: Specific alterations in Alzheimer's disease temporal lobe neocortex. Epub ahead of print 2009. DOI: 10.1016/j.neulet.2009.04.052.

[600] Lukiw WJ, Handley P, Wong L, et al. BC200 RNA in normal human neocortex, non-Alzheimer dementia (NAD), and senile dementia of the Alzheimer type (AD). *Neurochem Res* 1992; 17: 591–597.

[601] Mus E, Hof PR, Tiedge H. Dendritic BC200 RNA in aging and in Alzheimer's disease. *Proc Natl Acad Sci U S A* 2007; 104: 10679–84.

[602] Yao J, Hennessey T, Flynt A, et al. MicroRNA-related cofilin abnormality in Alzheimer's disease. *PLoS One* 2010; 5: e15546.

[603] Minamide LS, Striegl AM, Boyle JA, et al. Neurodegenerative stimuli induce persistent ADF/cofilin-actin rods that disrupt distal neurite function. *Nat Cell Biol* 2000; 2: 628–636.

[604] Massone S, Ciarlo E, Vella S, et al. NDM29, a RNA polymerase III-dependent non coding RNA, promotes amyloidogenic processing of APP and amyloid β secretion. *Biochim Biophys Acta - Mol Cell Res* 2012; 1823: 1170–1177.

[605] Faghihi MA, Modarresi F, Khalil AM, et al. Expression of a noncoding RNA is elevated in Alzheimer's disease and drives rapid feed-forward regulation of β-secretase. *Nat Med* 2008; 14: 723–730.

[606] Massone S, Vassallo I, Fiorino G, et al. 17A, a novel non-coding RNA, regulates GABA B alternative splicing and signaling in response to inflammatory stimuli and in Alzheimer disease. *Neurobiol Dis* 2011; 41: 308–317.

[607] Junn E, Lee K-W, Jeong BS, et al. Repression of alpha-synuclein expression and toxicity by microRNA-7. *Proc Natl Acad Sci U S A* 2009; 106: 13052–7.

[608] Doxakis E. Post-transcriptional regulation of alpha-synuclein expression by mir-7 and mir-153. *J Biol Chem* 2010; 285: 12726–34.

[609] Wang G, van der Walt JM, Mayhew G, et al. Variation in the miRNA-433 binding site of FGF20 confers risk for Parkinson disease by overexpression of alpha-synuclein. *Am J Hum Genet* 2008; 82: 283–9.

[610] Gillardon F, Mack M, Rist W, et al. MicroRNA and proteome expression profiling in early-symptomatic α-synuclein(A30P)-transgenic mice. *PROTEOMICS – Clin Appl* 2008; 2: 697–705.

[611] Asikainen S, Rudgalvyte M, Heikkinen L, et al. Global microRNA expression profiling of *Caenorhabditis elegans* Parkinson's disease models. *J Mol Neurosci 2010*; 41: 210–218.

[612] Cho HJ, Liu G, Jin SM, et al. MicroRNA-205 regulates the expression of Parkinson's disease-related leucine-rich repeat kinase 2 protein. *Hum Mol Genet* 2013; 22: 608–620.

[613] Gehrke S, Imai Y, Sokol N,

et al. Pathogenic LRRK2 negatively regulates microRNA-mediated translational repression. *Nature* 2010; 466: 637–41.

[614] Nishino J, Kim I, Chada K, et al. Hmga2 promotes neural stem cell self-renewal in young but not old mice by reducing p16Ink4a and p19Arf Expression. *Cell* 2008; 135: 227–39.

[615] Imai Y, Gehrke S, Wang H-Q, et al. Phosphorylation of 4E-BP by LRRK2 affects the maintenance of dopaminergic neurons in *Drosophila*. *EMBO J* 2008; 27: 2432–2443.

[616] Smith WW, Pei Z, Jiang H, et al. Kinase activity of mutant LRRK2 mediates neuronal toxicity. *Nat Neurosci* 2006; 9: 1231–1233.

[617] Minones-Moyano E, Porta S, Escaramis G, et al. MicroRNA profiling of Parkinson's disease brains identifies early downregulation of miR-34b/c which modulate mitochondrial function. *Hum Mol Genet* 2011; 20: 3067–3078.

[618] Margis R, Margis R, Rieder CRM. Identification of blood microRNAs associated to Parkinsoń s disease. *J Biotechnol* 2011; 152: 96–101.

[619] Johnson R, Zuccato C, Belyaev ND, et al. A microRNA-based gene dysregulation pathway in Huntington's disease. *Neurobiol Dis* 2008; 29: 438–445.

[620] Lee S-T, Chu K, Im W-S, et al. Altered microRNA regulation in Huntington's disease models. *Exp Neurol* 2011; 227: 172–179.

[621] Ghose J, Sinha M, Das E, et al. Regulation of miR-146a by RelA/NFkB and p53 in STHdhQ111/HdhQ111 cells, a cell model of Huntington's disease. *PLoS One* 2011; 6: e23837.

[622] Bae B-I, Xu H, Igarashi S, et al. p53 mediates cellular dysfunction and behavioral abnormalities in Huntington's disease. *Neuron* 2005; 47: 29–41.

[623] Xu Z, Li H, Jin P. Epigenetics-based therapeutics for neurodegenerative disorders. *Curr Transl Geriatr Exp Gerontol Rep* 2012; 1: 229–236.

[624] Coppedè F. The potential of epigenetic therapies in neurodegenerative diseases. *Front Genet* 2014; 5: 220.

[625] Durga J, van Boxtel MPJ, Schouten EG, et al. Effect of 3-year folic acid supplementation on cognitive function in older adults in the FACIT trial: a randomised, double blind, controlled trial. *Lancet* (London, England) 2007; 369: 208–16.

[626] Haan MN, Miller JW, Aiello AE, et al. Homocysteine, B vitamins, and the incidence of dementia and cognitive impairment: results from the Sacramento Area Latino Study on Aging. *Am J Clin Nutr* 2007; 85: 511–7.

[627] Scarpa S, Fuso A, D'Anselmi F, et al. Presenilin 1 gene silencing by S -adenosylmethionine: a treatment for Alzheimer disease? *FEBS Lett* 2003; 541: 145–148.

[628] Devall M, Mill J, Lunnon K. The mitochondrial epigenome: a role in Alzheimer's disease? *Epigenomics* 2014; 6: 665–675.

[629] How Kit A, Nielsen HM, Tost J. DNA methylation based biomarkers: Practical considerations and applications. *Biochimie* 2012; 94: 2314–2337.

[630] Malouf R, Grimley Evans J, Areosa Sastre A. Folic acid with or without vitamin B12 for cognition and dementia. In: Malouf R (ed) *The Cochrane Database of Systematic Reviews*. Chichester, UK: John Wiley & Sons, Ltd, p. CD004514.

[631] McMahon JA, Green TJ, Skeaff CM, et al. A controlled trial of homocysteine lowering and cognitive performance. *N Engl J Med* 2006; 354: 2764–2772.

[632] Campbell NRC. How safe are folic acid supplements? *Arch Intern Med* 1996; 156: 1638.

[633] Daniel P, Brazier M, Cerutti I, et al. Pharmacokinetic study of butyric acid administered in vivo as sodium and arginine butyrate salts. *Clin Chim Acta* 1989; 181: 255–263.

[634] Egorin MJ, Yuan Z-M, Sentz DL, et al. Plasma pharmacokinetics of butyrate after intravenous administration of sodium butyrate or oral administration of tributyrin or sodium butyrate to mice and rats. *Cancer Chemother Pharmacol* 1999; 43: 445–453.

[635] Miller AA, Kurschel E, Osieka R, et al. Clinical pharmacology of sodium butyrate in patients with acute leukemia. *Eur J Cancer Clin Oncol* 1987; 23: 1283–1287.

[636] Chen P-S, Peng G-S, Li G, et al. Valproate protects dopaminergic neurons in midbrain neuron/glia cultures by stimulating the release of neurotrophic factors from astrocytes. *Mol Psychiatry* 2006; 11: 1116–1125.

[637] Marinova Z, Ren M, Wendland JR, et al. Valproic acid induces functional heat-shock protein 70 via Class I histone deacetylase inhibition in cortical neurons: a potential role of Sp1 acetylation. *J Neurochem* 2009; 111: 976–987.

[638] Marinova Z, Leng Y, Leeds P, et al. Histone deacetylase inhibition alters histone methylation associated with heat shock protein 70 promoter modifications in astrocytes and neurons. *Neuropharmacology* 2011; 60: 1109–1115.

[639] Chen H, Dzitoyeva S,

Manev H. Effect of valproic acid on mitochondrial epigenetics. *Eur J Pharmacol* 2012; 690: 51–59.

[640] Kidd SK, Schneider JS. Protection of dopaminergic cells from MPP+-mediated toxicity by histone deacetylase inhibition. *Brain Res* 2010; 1354: 172–178.

[641] Leng Y, Marinova Z, Reis-Fernandes MA, et al. Potent neuroprotective effects of novel structural derivatives of valproic acid: Potential roles of HDAC inhibition and HSP70 induction. Epub ahead of print 2010. DOI: 10.1016/j.neulet.2010.04.013.

[642] Wu X, Chen PS, Dallas S, et al. Histone deacetylase inhibitors up-regulate astrocyte GDNF and BDNF gene transcription and protect dopaminergic neurons. *Int J Neuropsychopharmacol* 2008; 11: 1123.

[643] Zhou W, Bercury K, Cummiskey J, et al. Phenylbutyrate up-regulates the DJ-1 protein and protects neurons in cell culture and in animal models of Parkinson disease. *J Biol Chem* 2011; 286: 14941–51.

[644] Huang H-Y, Lin S-Z, Chen W-F, et al. Urocortin modulates dopaminergic neuronal survival via inhibition of glycogen synthase kinase-3β and histone deacetylase. *Neurobiol Aging* 2011; 32: 1662–77.

[645] Roy A, Ghosh A, Jana A, et al. Sodium phenylbutyrate controls neuroinflammatory and antioxidant activities and protects dopaminergic neurons in mouse models of Parkinson's disease. *PLoS One* 2012; 7: e38113.

[646] Brahe C, Vitali T, Tiziano FD, et al. Phenylbutyrate increases SMN gene expression in spinal muscular atrophy patients. *Eur J Hum Genet* 2005; 13: 256–259.

[647] Marks PA. The clinical development of histone deacetylase inhibitors as targeted anticancer drugs. *Expert Opin Investig Drugs* 2010; 19: 1049–1066.

[648] Marks PA, Xu W-S. Histone deacetylase inhibitors: Potential in cancer therapy. *J Cell Biochem* 2009; 107: 600–608.

[649] Salminen A, Tapiola T, Korhonen P, et al. Neuronal apoptosis induced by histone deacetylase inhibitors. *Mol Brain Res* 1998; 61: 203–206.

[650] Kelly-Sell MJ, Kim YH, Straus S, et al. The histone deacetylase inhibitor, romidepsin, suppresses cellular immune functions of cutaneous T-cell lymphoma patients. *Am J Hematol* 2012; 87: 354–360.

[651] Rossi LE, Avila DE, Spallanzani RG, et al. Histone deacetylase inhibitors impair NK cell viability and effector functions through inhibition of activation and receptor expression. *J Leukoc Biol* 2012; 91: 321–31.

[652] Haggarty SJ, Koeller KM, Wong JC, et al. Domain-selective small-molecule inhibitor of histone deacetylase 6 (HDAC6)-mediated tubulin deacetylation. *Proc Natl Acad Sci U S A* 2003; 100: 4389–94.

[653] Trapp J, Meier R, Hongwiset D, et al. Structure–activity studies on suramin analogues as inhibitors of NAD+-dependent histone deacetylases (sirtuins). *ChemMedChem* 2007; 2: 1419–1431.

[654] Yamada K, Mizuno M, Nabeshima T. Role for brain-derived neurotrophic factor in learning and memory. *Life Sci* 2002; 70: 735–744.

[655] Ishimaru N, Fukuchi M, Hirai A, et al. Differential epigenetic regulation of BDNF and NT-3 genes by trichostatin A and 5-aza-2′-deoxycytidine in Neuro-2a cells. Epub ahead of print 2010. DOI: 10.1016/j.bbrc.2010.02.139.

[656] Tian F, Marini AM, Lipsky RH. Effects of histone deacetylase inhibitor Trichostatin A on epigenetic changes and transcriptional activation of Bdnf promoter 1 by rat hippocampal neurons. *Ann N Y Acad Sci* 2010; 1199: 186–193.

[657] Yuan Su *,‡, John Ryder ‡,#, Baolin Li ‡, et al. Lithium, a common drug for bipolar disorder treatment, regulates amyloid-β precursor protein processing. Epub ahead of print 2004. DOI: 10.1021/BI035627J.

[658] Qing H, He G, Ly PTT, et al. Valproic acid inhibits Aβ production, neuritic plaque formation, and behavioral deficits in Alzheimer's disease mouse models. *J Exp Med*; http://jem.rupress.org/content/205/12/2781 (2008, accessed 4 April 2017).

[659] Ricobaraza A, Cuadrado-Tejedor M, Pérez-Mediavilla A, et al. Phenylbutyrate ameliorates cognitive deficit and reduces tau pathology in an Alzheimer's disease mouse model. *Neuropsychopharmacology* 2009; 34: 1721–1732.

[660] Ricobaraza A, Cuadrado-Tejedor M, Marco S, et al. Phenylbutyrate rescues dendritic spine loss associated with memory deficits in a mouse model of Alzheimer disease. *Hippocampus* 2012; 22: 1040–1050.

[661] Nuutinen T, Suuronen T, Kauppinen A, et al. Valproic acid stimulates clusterin expression in human astrocytes: Implications for Alzheimer's disease. Epub ahead of print 2010. DOI: 10.1016/j.neulet.2010.03.041.

[662] Vecsey CG, Hawk JD, Lattal KM, et al. Histone deacetylase inhibitors enhance memory and synaptic plasticity via CREB: CBP-dependent transcriptional activation. *J Neurosci*; http://www.jneurosci.org/con-

tent/27/23/6128 (2007, accessed 4 April 2017).

[663] Green KN, Steffan JS, Martinez-Coria H, et al. Nicotinamide restores cognition in Alzheimer's disease transgenic mice via a mechanism involving sirtuin inhibition and selective reduction of Thr231-phosphotau. *J Neurosci* 2008; 28: 11500–10.

[664] Arrowsmith CH, Bountra C, Fish P V., et al. Epigenetic protein families: a new frontier for drug discovery. *Nat Rev Drug Discov* 2012; 11: 384–400.

[665] Chatterjee S, Mizar P, Cassel R, et al. A novel activator of CBP/p300 acetyltransferases promotes neurogenesis and extends memory duration in adult mice. *J Neurosci*; http://www.jneurosci.org/content/33/26/10698 (2013, accessed 4 April 2017).

[666] Zhu M, Li W-W, Lu C-Z. Histone decacetylase inhibitors prevent mitochondrial fragmentation and elicit early neuroprotection against MPP+. *CNS Neurosci Ther* 2014; 20: 308–316.

[667] Kidd SK, Schneider JS. Protective effects of valproic acid on the nigrostriatal dopamine system in a 1-methyl-4-phenyl-1,2,3,6-tetrahydropyridine mouse model of Parkinson's disease. *Neuroscience* 2011; 194: 189–194.

[668] Chen PS, Wang C-C, Bortner CD, et al. Valproic acid and other histone deacetylase inhibitors induce microglial apoptosis and attenuate lipopolysaccharide-induced dopaminergic neurotoxicity. *Neuroscience* 2007; 149: 203–212.

[669] Peng G-S, Li G, Tzeng N-S, et al. Valproate pretreatment protects dopaminergic neurons from LPS-induced neurotoxicity in rat primary midbrain cultures: role of microglia. *Mol Brain Res* 2005; 134: 162–169.

[670] Darmopil S, Martín AB, De Diego IR, et al. Genetic inactivation of dopamine D1 but not D2 receptors inhibits L-DOPA–induced dyskinesia and histone activation. *Biol Psychiatry* 2009; 66: 603–613.

[671] Igarashi S, Morita H, Bennett KM, et al. Inducible PC12 cell model of Huntington's disease shows toxicity and decreased histone acetylation. *Neuroreport* 2003; 14: 565–8.

[672] Steffan JS, Bodai L, Pallos J, et al. Histone deacetylase inhibitors arrest polyglutamine-dependent neurodegeneration in Drosophila. *Nature* 2001; 413: 739–743.

[673] Sugai F, Yamamoto Y, Miyaguchi K, et al. Benefit of valproic acid in suppressing disease progression of ALS model mice. *Eur J Neurosci* 2004; 20: 3179–3183.

[674] Wood MA, Attner MA, Oliveira AMM, et al. A transcription factor-binding domain of the coactivator CBP is essential for long-term memory and the expression of specific target genes. *Learn Mem* 2006; 13: 609–17.

[675] McCampbell A, Taye AA, Whitty L, et al. Histone deacetylase inhibitors reduce polyglutamine toxicity. *Proc Natl Acad Sci U S A* 2001; 98: 15179–84.

[676] Hockly E, Richon VM, Woodman B, et al. Suberoylanilide hydroxamic acid, a histone deacetylase inhibitor, ameliorates motor deficits in a mouse model of Huntington's disease. *Proc Natl Acad Sci U S A* 2003; 100: 2041–6.

[677] Mielcarek M, Benn CL, Franklin SA, et al. SAHA decreases HDAC 2 and 4 levels *in vivo* and improves molecular phenotypes in the R6/2 mouse model of Huntington's disease. *PLoS One* 2011; 6: e27746.

[678] Ferrante RJ, Kubilus JK, Lee J, et al. Histone deacetylase inhibition by sodium butyrate chemotherapy ameliorates the neurodegenerative phenotype in Huntington's disease mice. *J Neurosci* 2003; 23: 9418–27.

[679] Dasgupta S, Zhou Y, Jana M, et al. Sodium phenylacetate inhibits adoptive transfer of experimental allergic encephalomyelitis in SJL/J mice at multiple steps. *J Immunol*; http://www.jimmunol.org/content/170/7/3874 (2003, accessed 4 April 2017).

[680] Ebbel EN, Leymarie N, Schiavo S, et al. Identification of phenylbutyrate-generated metabolites in Huntington disease patients using parallel liquid chromatography/electrochemical array/mass spectrometry and off-line tandem mass spectrometry. *Anal Biochem* 2010; 399: 152–161.

[681] Hogarth P, Lovrecic L, Krainc D. Sodium phenylbutyrate in Huntington's disease: A dose-finding study. *Mov Disord* 2007; 22: 1962–1964.

[682] Jia H, Kast RJ, Steffan JS, et al. Selective histone deacetylase (HDAC) inhibition imparts beneficial effects in Huntington's disease mice: implications for the ubiquitin-proteasomal and autophagy systems. *Hum Mol Genet* 2012; 21: 5280–5293.

[683] Jia H, Pallos J, Jacques V, et al. Histone deacetylase (HDAC) inhibitors targeting HDAC3 and HDAC1 ameliorate polyglutamine-elicited phenotypes in model systems of Huntington's disease. *Neurobiol Dis* 2012; 46: 351–361.

[684] Hu Y, Chopra V, Chopra R, et al. Transcriptional modulator H2A histone family, member Y (H2AFY) marks Huntington disease activity in

man and mouse. *Proc Natl Acad Sci U S A* 2011; 108: 17141–6.

[685] Blanco G, Fu H, Mendez C, et al. Deciphering the biosynthetic origin of the aglycone of the aureolic acid group of anti-tumor agents. Chem Biol 1996; 3: 193–6.

[686] Chakrabarti S, Bhattacharyya D, Dasgupta D. Structural basis of DNA recognition by anticancer antibiotics, chromomycin A3, and mithramycin: Roles of minor groove width and ligand flexibility. *Biopolymers* 2000; 56: 85–95.

[687] Prado L, Lombó F, Braña AF, et al. Analysis of two chromosomal regions adjacent to genes for a type II polyketide synthase involved in the biosynthesis of the antitumor polyketide mithramycin in *Streptomyces argillaceus*. *Mol Gen Genet MGG* 1999; 261: 216–225.

[688] Ralston SH. Pathogenesis and management of cancer associated hypercalcaemia. *Cancer Surv* 1994; 21: 179–96.

[689] Ryan WG. Treatment of Paget's disease of bone with mithramycin. *Clin Orthop Relat Res* 1977; 106–10.

[690] Kennedy BJ. Mithramycin therapy in testicular cancer. *J Urol* 1972; 107: 429–32.

[691] Hagen G, Dennig J, Preiss A, et al. Functional analyses of the transcription factor Sp4 reveal properties distinct from Sp1 and Sp3. *J Biol Chem* 1995; 270: 24989–94.

[692] Majello B, De Luca P, Suske G, et al. Differential transcriptional regulation of c-myc promoter through the same DNA binding sites targeted by Sp1-like proteins. *Oncogene* 1995; 10: 1841–8.

[693] Chatterjee S, Zaman K, Ryu H, et al. Sequence-selective DNA binding drugs mithramycin A and chromomycin A3 are potent inhibitors of neuronal apoptosis induced by oxidative stress and DNA damage in cortical neurons. *Ann Neurol* 2001; 49: 345–54.

[694] Junn E, Mouradian MM. MicroRNAs in neurodegenerative diseases and their therapeutic potential. *Pharmacol Ther* 2012; 133: 142–150.

[695] Krützfeldt J, Rajewsky N, Braich R, et al. Silencing of microRNAs *in vivo* with 'antagomirs'. *Nature* 2005; 438: 685–689.

[696] Kuhn DE, Nuovo GJ, Terry A V, et al. Chromosome 21-derived microRNAs provide an etiological basis for aberrant protein expression in human Down syndrome brains. *J Biol Chem* 2010; 285: 1529–43.

[697] Yu D, Pendergraff H, Liu J, et al. Single-stranded RNAs use RNAi to potently and allele-selectively inhibit mutant huntingtin expression. *Cell* 2012; 150: 895–908.

[698] Alvarez-Erviti L, Seow Y, Yin H, et al. Delivery of siRNA to the mouse brain by systemic injection of targeted exosomes. *Nat Biotechnol* 2011; 29: 341–345.

[699] Lakhal S, Andaloussi S El, O'Loughlin AJ, et al. RNAi therapeutic delivery by exosomes. *Springer US*, pp. 185–205.

[700] Xu T, Li L, Huang C, et al. MicroRNA-323-3p with clinical potential in rheumatoid arthritis, Alzheimer's disease and ectopic pregnancy. *Expert Opin Ther Targets* 2014; 18: 153–158.

[701] Hu J, Matsui M, Gagnon KT, et al. Allele-specific silencing of mutant huntingtin and ataxin-3 genes by targeting expanded CAG repeats in mRNAs. *Nat Biotechnol* 2009; 27: 478–484.

[702] Lombardi MS, Jaspers L, Spronkmans C, et al. A majority of Huntington's disease patients may be treatable by individualized allele-specific RNA interference. *Exp Neurol* 2009; 217: 312–319.

[703] Zhang Y, Friedlander RM. Using non-coding small RNAs to develop therapies for Huntington's disease. *Gene Ther* 2011; 18: 1139–1149.

[704] Harper SQ, Staber PD, He X, et al. RNA interference improves motor and neuropathological abnormalities in a Huntington's disease mouse model. *Proc Natl Acad Sci U S A* 2005; 102: 5820–5.

[705] Boudreau RL, McBride JL, Martins I, et al. Nonallele-specific silencing of mutant and wild-type huntingtin demonstrates therapeutic efficacy in Huntington's disease mice. *Mol Ther* 2009; 17: 1053–1063.

[706] DiFiglia M, Sena-Esteves M, Chase K, et al. Therapeutic silencing of mutant huntingtin with siRNA attenuates striatal and cortical neuropathology and behavioral deficits. *Proc Natl Acad Sci U S A* 2007; 104: 17204–9.

[707] Drouet V, Perrin V, Hassig R, et al. Sustained effects of nonallele-specific Huntingtin silencing. *Ann Neurol* 2009; 65: 276–285.

[708] Franich NR, Fitzsimons HL, Fong DM, et al. AAV vector–mediated RNAi of mutant huntingtin expression is neuroprotective in a novel genetic rat model of Huntington's disease. *Mol Ther* 2008; 16: 947–956.

[709] Huang B, Schiefer J, Sass C, et al. High-capacity adenoviral vector-mediated reduction of huntingtin aggregate load *in vitro* and *in vivo*. *Hum Gene Ther* 2007; 18: 303–311.

[710] Machida Y, Okada T, Kurosawa M, et al. rAAV-mediated shRNA ameliorated neuropathology

in Huntington disease model mouse. *Biochem Biophys Res Commun* 2006; 343: 190–197.

[711] McBride JL, Boudreau RL, Harper SQ, et al. Artificial miRNAs mitigate shRNA-mediated toxicity in the brain: implications for the therapeutic development of RNAi. *Proc Natl Acad Sci U S A* 2008; 105: 5868–73.

[712] Rodriguez-Lebron E, Denovan-Wright EM, Nash K, et al. Intrastriatal rAAV-mediated delivery of anti-huntingtin shRNAs induces partial reversal of disease progression in R6/1 Huntington's disease transgenic mice. *Mol Ther* 2005; 12: 618–633.

[713] Davies MN, Volta M, Pidsley R, et al. Functional annotation of the human brain methylome identifies tissue-specific epigenetic variation across brain and blood. *Genome Biol* 2012; 13: R43.

[714] Hansen KD, Timp W, Bravo HC, et al. Increased methylation variation in epigenetic domains across cancer types. *Nat Genet* 2011; 43: 768–775.

[715] Lister R, Pelizzola M, Dowen RH, et al. Human DNA methylomes at base resolution show widespread epigenomic differences. *Nature* 2009; 462: 315–322.

[716] Guffanti A, Simchovitz A, Soreq H. Emerging bioinformatics approaches for analysis of NGS-derived coding and non-coding RNAs in neurodegenerative diseases. *Front Cell Neurosci* 2014; 8: 89.

[717] Raasch P, Schmitz U, Patenge N, et al. Non-coding RNA detection methods combined to improve usability, reproducibility and precision. *BMC Bioinformatics* 2010; 11: 491.

[718] Blalock EM, Buechel HM, Popovic J, et al. Microarray analyses of laser-captured hippocampus reveal distinct gray and white matter signatures associated with incipient Alzheimer's disease. *J Chem Neuroanat* 2011; 42: 118–126.

[719] Guintivano J, Aryee MJ, Kaminsky ZA. A cell epigenotype specific model for the correction of brain cellular heterogeneity bias and its application to age, brain region and major depression. *Epigenetics* 2013; 8: 290–302.

[720] Whittemore SR, Sanon HR, Wood PM. Concurrent isolation and characterization of oligodendrocytes, microglia and astrocytes from adult human spinal cord. *Int J Dev Neurosci* 1993; 11: 755–764.

[721] Suarez-Quian CA, Goldstein SR, Pohida T, et al. Laser capture microdissection of single cells from complex tissues. *Biotechniques* 1999; 26: 328–35.

[722] Uchida N, Buck DW, He D, et al. Direct isolation of human central nervous system stem cells. *Proc Natl Acad Sci U S A* 2000; 97: 14720–5.

[723] Yu S, Zhang JZ, Zhao CL, et al. Isolation and characterization of the CD133 + precursors from the ventricular zone of human fetal brain by magnetic affinity cell sorting. *Biotechnol Lett* 2004; 26: 1131–1136.

[724] Chung K, Wallace J, Kim S-Y, et al. Structural and molecular interrogation of intact biological systems. *Nature* 2013; 497: 332–337.

[725] Lee JH, Daugharthy ER, Scheiman J, et al. Highly multiplexed subcellular RNA sequencing *in situ*. *Science*; http://science.sciencemag.org/content/343/6177/1360 (2014, accessed 5 April 2017).

[726] Barton AJL, Pearson RCA, Najlerahim A, et al. Pre-and Postmortem Influences on Brain RNA. *J Neurochem* 1993; 61: 1–11.

[727] Stan AD, Ghose S, Gao X-M, et al. Human postmortem tissue: What quality markers matter? *Brain Res* 2006; 1123: 1–11.

[728] Pidsley R, Mill J. Epigenetic studies of psychosis: current findings, methodological approaches, and implications for postmortem research. *Biol Psychiatry* 2011; 69: 146–156.

[729] Mill J, Heijmans BT. From promises to practical strategies in epigenetic epidemiology. *Nat Rev Genet* 2013; 14: 585–594.

[730] Relton CL, Davey Smith G. Two-step epigenetic Mendelian randomization: a strategy for establishing the causal role of epigenetic processes in pathways to disease. *Int J Epidemiol* 2012; 41: 161–176.

[731] Boks MP, de Jong NM, Kas MJH, et al. Current status and future prospects for epigenetic psychopharmacology. *Epigenetics* 2012; 7: 20–28.

[732] Pasinetti GM, Ho L, Dooley C, et al. Select non-coding RNA in blood components provide novel clinically accessible biological surrogates for improved identification of traumatic brain injury in OEF/OIF Veterans. *Am J Neurodegener Dis* 2012; 1: 88–98.

[733] Sharma RP. Blood chromatin as a biosensor of the epigenetic milieu: a tool for studies in living psychiatric patients. *Epigenomics* 2012; 4: 551–559.

[734] Lunnon K, Ibrahim Z, Proitsi P, et al. Mitochondrial dysfunction and immune activation are detectable in early Alzheimer's disease blood. *J Alzheimers Dis* 2012; 30: 685–710.

[735] German DC, Eisch AJ. Mouse models of Alzheimer's disease: insight into treatment. *Rev Neurosci*

2004; 15: 353–69.

[736] Saito T, Matsuba Y, Mihira N, et al. Single App knock-in mouse models of Alzheimer's disease. *Nat Neurosci* 2014; 17: 661–663.

[737] Raber J, Wong D, Buttini M, et al. Isoform-specific effects of human apolipoprotein E on brain function revealed in ApoE knockout mice: increased susceptibility of females. *Proc Natl Acad Sci U S A* 1998; 95: 10914–9.

[738] Kumar A, Seghal N, Naidu PS, et al. Colchicines-induced neurotoxicity as an animal model of sporadic dementia of Alzheimer's type. *Pharmacol Rep*; 59: 274–83.

[739] Sparks DL, Scheff SW, Hunsaker JC, et al. Induction of Alzheimer-like β-amyloid immunoreactivity in the brains of rabbits with dietary cholesterol. *Exp Neurol* 1994; 126: 88–94.

[740] Hoyer S, Lee SK, Löffler T, et al. Inhibition of the neuronal insulin receptor. An in vivo model for sporadic Alzheimer disease? *Ann N Y Acad Sci 2000*; 920: 256–8.

[741] Przedborski S, Vila M. The 1-methyl-4-phenyl-1,2,3,6-tetrahydropyridine mouse model: a tool to explore the pathogenesis of Parkinson's disease. *Ann N Y Acad Sci* 2003; 991: 189–98.

[742] Podlisny MB, Tolan DR, Selkoe DJ. Homology of the amyloid beta protein precursor in monkey and human supports a primate model for beta amyloidosis in Alzheimer's disease. *Am J Pathol* 1991; 138: 1423–35.

[743] Israel MA, Yuan SH, Bardy C, et al. Probing sporadic and familial Alzheimer's disease using induced pluripotent stem cells. *Nature* 2012; 482: 216–20.

[744] Wojda U, Kuznicki J. Alzheimer's disease modeling: ups, downs, and perspectives for human induced pluripotent stem cells. *J Alzheimers Dis* 2013; 34: 563–88.

[745] Qiang L, Fujita R, Yamashita T, et al. Directed conversion of Alzheimer's disease patient skin fibroblasts into functional neurons. *Cell* 2011; 146: 359–71.

[746] Takahashi K, Tanabe K, Ohnuki M, et al. Induction of pluripotent stem cells from adult human fibroblasts by defined factors. *Cell* 2007; 131: 861–872.

[747] Tian C, Liu Q, Ma K, et al. Characterization of induced neural progenitors from skin fibroblasts by a novel combination of defined factors. *Sci Rep* 2013; 3: 1345.

[748] Verma A, Verma N. Induced pluripotent stem cells and promises of neuroregenerative medicine. *Neurol India* 2011; 59: 555–7.

[749] Kim K, Doi A, Wen B, et al. Epigenetic memory in induced pluripotent stem cells. *Nature* 2010; 467: 285–90.

[750] Meaburn EL, Schalkwyk LC, Mill J. Allele-specific methylation in the human genome. *Epigenetics* 2010; 5: 578–582.

[751] Szyf M. Epigenetics, a key for unlocking complex CNS disorders? Therapeutic implications. *Eur Neuropsychopharmacol* 2015; 25: 682–702.

[752] de Groote ML, Verschure PJ, Rots MG. Epigenetic Editing: targeted rewriting of epigenetic marks to modulate expression of selected target genes. *Nucleic Acids Res* 2012; 40: 10596–10613.

RODENT MODELS OF COGNITIVE DISORDERS: IMPAIRMENT, AGING & DEMENTIA

ROY **LARDENOIJE**[A,*], NICK P. **VAN GOETHEM**[A,*], KONSTANTINOS **KOMPOTIS**[A], BART P.F. **RUTTEN**[A], JOS **PRICKAERTS**[A], HARRY W.M. **STEINBUSCH**[A]

[A]SCHOOL FOR MENTAL HEALTH AND NEUROSCIENCE (MHENS), DEPARTMENT OF PSYCHIATRY AND NEUROPSYCHOLOGY, MAASTRICHT UNIVERSITY, UNIVERSITEITSSINGEL 50, 6200 MD MAASTRICHT, THE NETHERLANDS
*THESE AUTHORS CONTRIBUTED EQUALLY TO THIS WORK.

Chapter in: *In Vivo* Models for Drug Discovery. Wiley-VCH Verlag GmbH & Co. KGaA. (2014)

3.1. Introduction

Cognitive dysfunction is a feature often encountered in a broad spectrum of neurological and psychiatric conditions. The property of animal models to study the development of a disease, and not just late-stage pathology, is crucial for disease models involving cognitive deficits, as such deficits are often the result of neurodegeneration. Considering the limited regenerative capacity of the brain, it is thus pivotal to treat neurodegenerative diseases as early as possible [1]. Since ameliorating these dysfunctions can dramatically improve the quality of life of patients, developing treatments, or “cognition enhancers,” is a major area of interest for the pharmaceutical industry. Accordingly, over the past few decades certain drugs have been approved for the treatment of cognitive impairments related to specific neurological and psychiatric conditions (for a recent review, see [2]). A diverse range of animal models are being used to identify potential cognition-enhancing drugs and such models can be based on pharmacological deficits, the naturally occurring aging process, and/or introduction of transgenic constructs in rodents. The first part of this chapter describes the most commonly used rodent pharmacological deficit models. Hereafter, animal models of aging and transgenic animal models will be discussed.

3.2. Pharmacological models

In pharmacological deficit models, specific drugs are administered to animals in order to induce cognitive deficits. The targets of these cognition-impairing drugs are hypothesis based and are often directed to alter distinct neurotransmitter systems, with different disorders showing specific dysregulation or impairments.

3.2.1. Inhibition of energy/ glucose metabolism

A variety of studies in both rodents and humans have shown that slight increases in circulating glucose concentrations exhibit beneficial effects in brain functions relating to learning and memory [3]. Administrating glucose has been shown to facilitate rodent performance and furthermore reverses both drug- and age-related cognitive deficits. The putative mechanism of action underlying these precognitive effects probably relates to altered neuronal metabolism, neuronal activity, or neurotransmitter synthesis [4].

The most straightforward way of inhibiting energy/glucose metabolism is glucose deprivation. *In vitro* studies often use oxygen–glucose deprivation to mimic ischemic injury and subsequently study acute stroke pathology [5]. *In vivo* studies, which use oxygen–glucose deprivation, mostly do this via middle cerebral artery occlusion [6]. *N*-methyl-D-aspartate (NMDA) receptor antagonists have been shown to be neuroprotective against excitotoxicity in both *in vitro* and *in vivo* models of ischemia or neurodegeneration [7, 8]. Another way of inhibiting energy/glucose metabolism is by treatment with the glycolytic inhibitor, 2-deoxyglucose. Although mostly used for glucose uptake measurement, 2-deoxyglucose has been shown to dose-dependently affect cognitive performance of rodents [9].

Another possible animal model for metabolic dysfunction (and/or generation of oxidative stress) is intracerebral ventricular (i.c.v.) administration of streptozotocin [10, 11]. Streptozotocin is a naturally occurring chemical that was discovered in the late 1950s and a little later identified as an antibacterial antibiotic [12]. Subsequently, it was discovered that i.c.v. administration of streptozotocin decreases the central metabolism of glucose and hence offers a useful animal/rodent model of neurodegeneration [13]. Furthermore, i.c.v. streptozotocin administration also reduces the concentrations of different neurotransmitters, including acetylcholine (ACh) [14, 15]. As will be described in the next section, this cholinergic reduction further contributes to the use of this animal model of neurodegeneration. Accordingly, middle-aged and old rats that have been treated with streptozotocin (i.c.v.) show cognitive deficits in tasks assessing learning and memory. These deficits can be reversed with specific cognition-enhancing drugs [13, 16].

3.2.2. Cholinergic interventions

3.2.2.1. Cholinergic toxins

The use of pharmacological deficit models targeting the cholinergic system became popular after the cholinergic hypothesis of geriatric memory dysfunction was postulated. This hypothesis states that the age-related decline in cognition is predominately caused by a decrement of cholinergic neurotransmission [17]. Nowadays, with the exception of one NMDA receptor antagonist (see also above), all approved drugs for the treatment of cognitive dysfunction in Alzheimer's disease (AD) aim at increasing cholinergic neurotransmission. Different approaches have

been used to induce cholinergic hypofunction in order to mimic AD-, and age-related cognitive decline. To achieve chronic dysregulation of the cholinergic system, cholinergic toxins have been used. The exact role of ACh in cognition is not fully understood, but ACh regulation has been associated with attention, learning, and memory processes [18].

Many of the early rat studies made use of excitotoxic lesions by means of central administrations of ibotenic acid or quisqualic acid. The excitotoxic lesions (especially with ibotenic acid) of cholinergic neurons revealed a vast range of cognitive impairments [19, 20]. However, a fundamental problem with this approach was the lack of a specific cholinergic toxin, introducing the possibility that such impairments may be due to damage to noncholinergic neurons. A more selective way to destruct cholinergic cells can be accomplished by locally injecting 192 IgG-saporin. 192 IgG-saporin is an antineuronal immunotoxin that consists of a monoclonal antibody (192 IgG) to the nerve growth factor (NGF) receptor that has been armed with saporin, a ribosome-inactivating protein [21, 22]. Injection of this 192 IgG-saporin complex produces long-lasting depletions in cholinergic markers throughout the forebrain of rats [23]. 192 IgG-saporin administration has been used to induce cognitive impairments in rodents to investigate the role of the cholinergic system in particular brain structures [24, 25].

3.2.2.2. Cholinergic antagonists

Induction of more transient or acute disruption of the cholinergic system can be induced with cholinergic antagonists. ACh has two types of receptors: the metabotropic muscarinic receptors (five subtypes in the central nervous system [CNS]) and the ionotropic nicotinic receptors (two major subtypes in the CNS). There are specific antagonists for each ACh receptor type. A further division can be made between selective and nonselective cholinergic antagonists. This applies to the selectivity/affinity of an antagonist to the isoforms of ACh receptor (sub)types.

The most widely used nonselective competitive cholinergic antagonists are the tropane alkaloids scopolamine hydrobromide and atropine. The nonselective muscarinic antagonist scopolamine is probably the most often used cognition deficit-inducing drug in (preclinical) rodent research. Since scopolamine induces amnesia that is caused by a blockade of cholinergic signaling, this drug is used to model cognitive deficits associated with aging and dementia [26]. In preclinical testing, scopolamine is often coadministered with putative cognition-enhancing drugs in order to test whether a new drug is effective in reversing a scopolamine induced cognitive deficit [27]. The rationale is that if a

new experimental drug can reverse such a deficit, it might also improve cognitive function in healthy participants or people diagnosed with a neuropsychiatric disorder [26].

Since scopolamine is a nonselective muscarinic antagonist, efforts have been made to promote the use of more selective muscarinic antagonists. Since muscarinic receptors are both centrally and peripherally present, it would be more “clean” to use a more centrally selective muscarinic antagonist. Of the five known muscarinic receptors (M1–M5), M1 might be a promising target since this receptor is predominantly located in the cortex and the hippocampus, brain regions known to be important for attention, learning, and memory. Peripheral presence of the M1 receptor is relatively limited [28]. The selective muscarinic M1 receptor antagonist biperiden is, therefore, an interesting drug candidate to more selectively induce cognitive, in particular memory, deficits in rodent models [29].

The other class of cholinergic receptors is the class of ionotropic nicotinic receptors (nAChRs). These receptors belong to a family of ligand-gated ion channel receptors that include type 3 serotonin (5HT3), gamma-aminobutyric acid A (GABAA) and strychnine-sensitive glycine receptors. nAChRs in the brain are composed of five subunits, which can be either α-subunits (nine identified subunits: α2–α10) or β-subunits (three identified subunits: β2–β4). These subunits can combine to result in different isoforms. In the CNS, the heteropentameric α4β2 and the homopentameric α7 nAChRs comprise >90% of the nAChR subtypes [30]. Since nAChRs have been shown to be involved in learning and memory [27] and postmortem research shows that nAChR densities are markedly decreased in the brains of both patients with AD and schizophrenia, the pharmaceutical industry has been developing different nAChR agonists in order to try to ameliorate the cognitive deficits that accompany these disorders [30]. Accordingly, antagonists of these nAChRs cause cognitive impairments in rodents, and hence certain drugs are used to mimic cognitive deficits seen in both AD and schizophrenia.

Mecamylamine is such a nonselective nAChR antagonist shown to induce learning and memory deficits (at high enough doses) in rodents [31]. In order to more specifically investigate the role of the different nAChR subtypes, selective nAChR antagonists are used. Methyllycaconitine (MLA) is a selective α7 nAChR competitive antagonist, and dihydro-beta-erythroidine (DHbE) is a selective α4β2 nAChR competitive antagonist. Both of these drugs have been shown to induce memory deficits in rodents [32], when administered at a high enough dose [33]. Besides inducing cognitive deficits on their own, these drugs are also used to counteract the procognitive effect of agonists at their corresponding nAChR subtype. This approach is used in order to confirm that the

procognitive effects of a selective nAChR agonist are indeed mediated via a specific nAChR [27, 33].

3.2.3. Glutamatergic antagonists

Another important neurotransmitter directly involved in cognitive processes is glutamate. Glutamate is an abundantly present excitatory neurotransmitter, which acts through the ionotropic NMDA receptor (besides the alpha-amino-3-hydroxy-5-methyl-4-isoxazolepropionic acid [AMPA] receptor). NMDA receptors have been implicated in cognitive processes, in particular memory formation [34].

Following this rationale, NMDA antagonists have been used to function as cognition-deficit models in rodents and of these the most widely used cognition impairers are noncompetitive NMDA receptor-channel blockers. The most frequently used NMDA receptor-channel blockers in rodent models are MK-801 (dizocilpine), phencyclidine (PCP), and ketamine. These receptor-channel blockers bind to specific sites within the NMDA receptor channel pore and subsequently block the channel, thereby inducing cognitive impairments.

MK-801 has been assessed in a broad range of rodent test paradigms and is considered a valid model to induce acute cognitive dysfunction provided the right dose is used (without inducing noncognitive side effects) [34]. PCP in rodents is mainly used in a (sub)chronic manner to mimic the impairments seen in schizophrenia patients. In contrast to MK-801, PCP was also tested in humans; hence, more direct comparisons between rodent and human behavior can be made [35]. PCP is believed to bind to a site within the NMDA receptor-channel pore (the PCP binding site) that is only accessible when the channel is open. Therefore, the antagonism is “use dependent.” PCP thus acts at the same site as other “open-channel” blockers such as MK-801 or ketamine [36]. Besides acting on the NMDA receptor channel, PCP also binds to the dopamine uptake site. MK-801 is considerably more potent than PCP in producing a noncompetitive blockade at the NMDA receptor. However, MK-801 lacks the direct action on dopamine uptake, which accounts for the argument that PCP might be a more suitable deficit model for schizophrenia specifically, since PCP intoxication is associated with more psychotic features. Ketamine also acts as a type 2 dopamine partial agonist, but is a weaker blocker of the NMDA ion channel. Therefore, for mimicking psychosis, PCP might represent a more (and ketamine a less) complete model. Although MK-801 is much less complex in its pharmacological

profile, it has proved to be valuable in animal studies because of its high selectivity for the NMDA receptor [35]. After scopolamine, MK-801 is probably the most widely used drug for the induction of cognitive impairments in rodents [34].

3.2.4. Serotonergic intervention

The serotonergic system has been implicated in cognitive processes as well. This system may have only minor effects on cognitive function on its own, but is assumed to interact with the cholinergic system. This serotonergic–cholinergic interaction probably plays an important role in the mediation of behavioral, including cognitive, performance [37].

A model used to decrease serotonin (5HT) entails the lowering of 5HT levels. Decreasing 5HT levels can be accomplished by manipulating the availability of the essential amino acid tryptophan via the food. Tryptophan has multiple functions, one of which is that it functions as a biochemical precursor for 5HT. Acute tryptophan depletion is used as a pharmacological deficit model to lower central 5HT levels. The acute tryptophan depletion method is widely used both preclinically and clinically as a model to investigate the implication of the 5HT system in affective disorders [38, 39]. This serotonergic-deficit model has been frequently used to study putative cognition enhancers in rats [39, 40].

3.3. Aging and transgenic models

Over the past few decades, ample transgenic rodent models modeling specific diseases and exhibiting cognitive deficits have been generated. It should, however, be noted that most of the diseases discussed below are not of simple genetic origin. Indeed, the exact etiology of most remains to be elucidated. This means that the specific mutations used to create a model may only have a small hand in the actual pathology. Single mutations might not even result in any detectable pathology and multiple mutations, or specific environmental interactions may be required to instigate disease pathology [41]. Described in this section is a selection of transgenic rodent models of some of the most common neurodegenerative diseases involving cognitive impairments, which are most widely used or have provided critical insights.

3.3.1. Normal aging

Of most cognitive disorders, aging is the top risk factor, while at the same time aging itself is also associated with cognitive decline [42]. Although aging is a natural process, it can result in quite severe functional limitations at the end of the life span, resulting inevitably in death. Rats and mice are useful laboratory species for studying the aging process, as they have relatively short life spans (up to 4 years for mice and up to 5 years for rats), are small and thus easy to keep, and reproduce fast [43]. For instance, nontransgenic mice can be used to study epigenetic, physiological, morphological, and behavioral changes as they occur during the aging process [44–46]. Importantly, interventions that may have a positive effect on age-related decline, such as caloric restriction, can be tested in these animals in a relatively short amount of time [46]. An even faster rodent model of aging is the senescence-accelerated mouse. This model consists of a collection of series created through the selective breeding of AKR/J mice, which already showed signs of accelerated aging, including multiple senescence-prone (P series) and senescence-resistant (R series) series [47, 48]. Of particular interest are the senescence-accelerated prone SAMP8 mice, which show ample age-related changes early in life, leading to a median survival time of only around 10 months. SAMP8 mice naturally present with neuropathological and neurochemical changes, including Aβ deposition, hyperphosphorylation of tau, and hampered dendritic spine development, as well as NMDA-, acetylcholine-, and noradrenaline-associated abnormalities [49]. This makes the SAMP8 model attractive for the study of, for example, age-related Parkinson's disease (PD) and AD. SAMP8 mice develop learning and memory impairments at a young age. Such deficits start at 2 months of age, as assessed with such tests as the water maze, T-maze, passive avoidance, and one-way active avoidance paradigms [49, 50].

The greatest advantage of mice and rats may, however, also be one of their greatest limitations as models of human aging. The large gap between the life spans of humans, and that of mice and rats, may be indicative of the latter being unable to fully elucidate the mechanisms influencing human aging [43]. For this reason, some investigators have chosen to use animal models that live longer, among which are also other rodent models. Some of these model organisms, including the naked mole rat, porcupines, and beavers, reach life spans of over 20 years. Comparing species of the same order of Rodentia with such diverging life spans may offer insights into the general mechanisms that increase a species age.

3.3.2. Alzheimer's disease

3.3.2.1. APP

Despite its relative rarity, familial AD (fAD) has garnered the most attention due to its large genetic component. It is thus not surprising that the first transgenic mouse model for AD, the PDAPP model made in 1995, is based on a mutation in the fAD-associated amyloid precursor protein (APP) gene [51, 52]. PDAPP mice express human APP cDNA with the Indiana mutation (V717F). In this model, plaque pathology arises between 6 and 9 months, paired with synapse, but no severe cell loss, or neurofibrillary tangle (NFT) deposition. Aged mice of this model display an impaired learning ability in the Morris water maze, the radial arm water maze, the cue task, and serial spatial reversal task [53].

Although some neuropathology occurs in this first model, it is the second transgenic model, Tg2576, implementing a double APP mutation (K670N and M671L), that successfully models an age-dependent buildup of amyloid plaques and related cognitive decline, as associated with AD [54]. The mutant APP expressed by Tg2576 mice is also referred to as APPswe, and is under control of the hamster prion promoter. Cognitive decline in these widely-used mice occurs progressively from 6 to 9 months of age. By the age of 12 months, this model shows an impaired performance on spatial and working memory tasks, including the Y-maze spontaneous alternation and visible platform recognition tasks, as well as amygdala-dependent fear conditioning tasks.

A more aggressive AD model, the TgCRND8 transgenic mouse model, combines the Swedish and Indiana mutations, expressing the human bAPP695 transgene under control of the Syrian hamster prion promoter, on a C3H/B6 background [55]. This combination results in rapid extracellular plaque formation in the hippocampus and frontal cortex, similar to human AD, paired with defunct spatial learning in the Morris water maze task at 3 months of age, and impaired nonspatial episodic memory, as determined with the object recognition task at 8 weeks of age.

3.3.2.2. PS1, PS2, and PS1 × APP

Apart from mutations in the APP gene, mutations in presenilin (PS) genes have also been used to generate transgenic mouse models. For instance, the PS1M146L, PS1M146V, and PS2N141I models were used to demonstrate *in vivo* that mutant PS1 and PS2 are able to selectively enhance Aβ42 levels [56]. This increased Aβ42 presence is, however,

without significant plaque pathology and cognitive deficits. It seems that the interaction between the PS and APP genes is of vital importance in the pathophysiology of AD and, therefore, PS mutations are usually combined with a mutated APP transgene. The biogenic PSAPP model, a crossing between APP and PS1 transgenic models (e.g., Tg2576 × PS1M146L, PS1-A246 + APPswe, and APPswe/PS1dE9), shows a grave acceleration in pathology, compared with mutant APP-only models [57]. This includes an earlier onset of cognitive impairments, as measured with the Morris water maze and radial arm water maze tests for working memory.

One of the most early-onset and aggressive amyloid models is the 5xFAD transgenic mouse model, sporting five fAD-associated mutations [58]. 5xFAD mice carry two transgenes under the mouse Thy-1 promoter: APPswe/Ind/fl and PS1M146L/L286V (on a B6/SJL background), resulting in a grossly exaggerated Aβ42 production. Consequently, amyloid deposits in the hippocampus start to form at the young age of 2 months. By the age of 6 months, massive amyloid pathology can be observed throughout the hippocampus and cortex of these mice, paired with impaired spatial working memory, as tested with the spontaneous alternation Y-maze. At this age 5xFAD mice also show impaired hippocampal-dependent contextual fear memory [59].

3.3.2.3. MAPT

APP, PS1, and PS2 transgenic models are able to capture some of the Aβ-associated pathology seen in AD. Most of these models, however, fail to recapitulate the widespread neurodegeneration and tangle pathology, which is critical for a suitable phenocopy of AD. A model that achieves just that is the TauP301S transgenic mouse model, based on the shortest isoform of 4R microtubule-associated protein tau (MAPT) with the P301S mutation, controlled by the mouse Thy-1 promoter on a C57BL/J background [60]. Around 5–6 months of age, widespread NFT pathology can be observed in the brain and spinal cord, as well as neuronal loss in the latter area, paired with severe paraparesis in mice of this model. Cognitive deficits at 5–6 months of age include decreased spontaneous alternation in the Y-maze test, impaired sociability and object recognition memory in Crawley's social interaction test, hampered spatial memory in the Morris water maze test, and slightly impaired contextual memory in the contextual and cued fear conditioning tests.

The peculiar TauV337M model, which expresses 4R MAPT with the V337M mutation controlled by the platelet-derived growth factor promoter (also exists with the mouse Thy-1 promoter) on a B6SJL background,

is characterized by a low-level synthesis of 4R MAPT, which is only 1/10 of endogenous mouse MAPT production [61]. The observation of neurofibrillary pathology in this model indicates that it may not be the absolute MAPT levels, but the nature of MAPT that instigates tangle pathology. At the age of 12 months, TauV337M mice seem to have defunct olfactory memory, as tested with the social transmission of food preferences task, and deficits in impulse control, as determined with the five-choice serial reaction time task, at 24 months of age and at 12 months of age when the intertrial intervals were increased. Note that in contrast to most other tau-based models, this model does not exhibit motor abnormalities until at least 24 months of age.

To investigate the reversibility of tangle pathology, the rTg4510 model was created [62]. These transgenic mice express MAPT with the P301L mutation under control of the TET-off system, making the transgene inducible. When the mutant MAPT is expressed, these mice show progressive NFT development and cell loss from 1 month of age, including severe hippocampal CA1 neuron death at the age of 5 months. From the age of 2.5 months, this model starts to display impaired spatial reference memory, as examined with the Morris water maze. Interestingly, turning off production of the mutant MAPT after 4 months of age leads to a recovery of cognitive performance, but a worsening of the tangle pathology, indicating that at this age tau pathology becomes independent of transgenic MAPT expression.

When considering the MAPT-based models discussed earlier as models for AD, it is important to realize that NFT pathology in AD arises in the absence of mutations in the MAPT gene; indeed, most of the mutations these models are based on are from other tauopathies such as frontotemporal dementia (FTD) [56]. Furthermore, most of the other transgenic models do not take into account endogenous gene expression of the model organism. For instance, all of the abovementioned transgenic mouse models that express a mutant form of MAPT also express mouse MAPT. The htau transgenic mouse model was created keeping the following point in mind; expressing nonmutant human genomic MAPT in a mouse MAPT knockout background (maintained on a Swiss Webster/129/SvJae/C57BL/6 background) [63]. This model presents with AD-like tau pathology, starting with pretangle-like hyperphosphorylated MAPT accumulation after 3 months, spreading at an age of 9 months through hippocampal and neocortical regions. At the age of 12 months, these htau mice start displaying cognitive impairments in the object recognition task and the Morris water maze, paired with disrupted long-term potentiation in the hippocampal CA1 region [64].

3.3.2.4. PS1 × APP × MAPT

One of the most used transgenic models for AD is the triple transgenic mouse model, which combines mutated PS1, APP, and MAPT genes into one model. This 3xTgAD model expresses mutant APPswe and MAPTP301L, under control of the mouse Thy-1 promoter, on a PSEN1M146V knock-in background (PSEN1-KI) [65]. Plaques develop from an age of 6 months in 3xTgAD mice, and tangle pathology arises by the age of 12 months. Although not completely mimicking AD, this is one of the best models available – developing progressive synaptic dysfunction, amyloid plaques, and neurofibrillary tangles in a temporal and spatial pattern that is similar to human AD. Around 4 months of age, 3xTgAD mice start to present with impaired spatial memory and long-term retention, as tested with the Morris water maze task, and at 6 months their short- and long-term retention for contextual fear also becomes significantly reduced [66]. Aged 3xTgAD mice show deficits in object discrimination memory in the object discrimination task, together with derailed long-term potentiation and paired-pulse facilitation.

3.3.2.5. APOE4

When looking at the genes used in the triple transgenic AD model, it can be argued that it is primarily a model of fAD and not of the far more common sporadic AD (sAD). Models employing the highest genetic risk factor for sAD, allele APOE4, have been constructed – expressing human APOE4 under control of the neuron-specific enolase (NSE) promoter in transgenic mice devoid of endogenous mouse APOE [67]. This NSE-APOE4 model exhibits a less severe phenotype than most other transgenic models of AD, failing to recapitulate most of the pathological hallmarks associated with the disease. Nevertheless, the NSE-APOE4 model displays impaired excitatory synaptic transmission, a decline in dendritic density and complexity, and cognitive impairments in a water maze task at the age of 6 months.

3.3.3. Parkinson's disease

3.3.3.1. α-Syn

α-Synuclein (α-Syn) transgenic mice overexpress human wild-type or mutant α-Syn usually under the regulatory control of the human *PDGF-β* promoter. α-Syn is expressed in high levels, resulting in an age-dependent increase of brain inclusions consisting of α-Syn, ubiquitin, and other proteins. Severity of the brain pathology correlates with increasing age. By 6 months of age, these transgenic mice exhibit deficits in cognition shown

by an increased time to find the platform in the water maze task [68]. Mice overexpressing wild-type α-Syn under regulation of the human *PDGF-β* promoter also display a progressive increase in α-Syn aggregation in multiple brain regions, a loss of dopaminergic terminals in the striatum, and mild changes in motor activity as shown by a decreased latency to fall on a rotarod. Another variation of these mice uses the human *Thy1* promoter for overexpressing α-Syn. Cognitive changes (Y-maze, novel object recognition, and operant reversal learning) are also evident in the *Thy1*-α-Syn mice beginning ~4–6 months of age [69].

Nuber et al. in 2008 [70] created a conditional mouse model for the overexpression of WT α-Syn under the *CAMK2A* promoter, using a tetracycline-regulated TET-off system. These mice displayed a progressive motor decline after 7 months (rotarod) of age, modest impairment in reference memory after 12 months (water maze), and α-Syn accumulation in the substantia nigra, hippocampus, and olfactory bulb.

3.3.3.2. DJ1(PARK7)KO

DJ1KO mice have a deficiency in expressing the Park7 protein, due to a knockout of the respective gene, namely, *DJ1*. *DJ1*-/- mice between 13 and 14 months of age show cognitive deficits, as characterized by reduced performance in an object recognition task [71].

3.3.3.3. Parkin(PARK2)KO

This PD mouse model is produced by a knockout in the *PARK2* gene, responsible for the expression of a protein called parkin. Parkin-/- mice display increased anxiety, as shown in the open-field and light/dark preference tests, and cognitive impairment exhibited as spatial memory deficits in the Morris water maze [72]. Mice that lack exon 3 in the parkin gene do not demonstrate loss of dopaminergic neurons; nevertheless, they show signs of altered synaptic transmission in the nigrostriatal circuit [73].

3.3.4. Huntington's disease

Various transgenic rodent models of Huntington's disease (HD) have been found to exhibit affective and cognitive abnormalities reflecting clinical data in HD patients. For example, R6/1 and R6/2 transgenic lines of HD mice have behavioral deficits that include impaired hippocampal-dependent spatial cognition [74, 75]. However, depression-like behavior also manifests in R6/1 HD mice prior to cognitive and motor symptoms [76].

3.3.4.1. R6/2

Of the transgenic chimeric models that express truncated forms of the human mutant HD allele, the R6/2 line is the most widely used. This line expresses an exon 1 fragment of *hHtt* with a range of 148–153 repeats, expressed from an unknown location in the mouse genome. R6/2 mice exhibit learning and memory tasks abnormalities as early as 3.5 weeks of age (water Morris maze), which follow them throughout their life span, as evaluated by various cognitive tests (T-maze, two-choice swim tank, and visual discriminate learning) [77–79]. Moreover, they show behavioral deficits by 5 weeks, neuroanatomic abnormalities including progressive reduction in brain and striatal volume, substantially reduced striatal neuron number by 12 weeks, and death by 12–15 weeks [79–81]. As the R6/2 model exhibits severe, early-onset and diffuse pathology, it is potentially a good model of juvenile-onset HD, displaying an aggressive phenotype and provides clear experimental endpoints.

3.3.4.2. YAC128

The YAC128 is a widely-used yeast-artificial-chromosome full-length human mutant HD transgenic model generated and characterized by the Hayden laboratory [82, 83]. Van Raamsdonk et al. in 2005 evaluated YAC128 mice with a variety of more cognitively oriented tests, demonstrating progressive cognitive deficits at 8 weeks (accelerated rotarod) and 32 weeks (water Morris maze, open-field habituation, and T-maze). Unlike the R6/2 mice, where there is probably a diffuse loss of brain volume, some regions of the YAC128 brain, such as the cerebellum and hippocampus, exhibit normal volume [84]. YAC128 mice also exhibit motor abnormalities as early as 3 months with increased open-field activity, followed by rotarod performance abnormalities at 6 months.

3.3.4.3. tgHD Rats

This transgenic rat model of HD, with a mutated huntingtin gene containing 51 CAG repeats, expresses adult-onset neurological phenotypes, cognitive impairments, progressive motor dysfunction, and neuronal nuclear inclusions in the brain [85]. The transgenic rat model exhibits a late-onset neurological phenotype, cognitive decline in spatial learning at 10 months (radial arm maze), and significantly impaired object recognition performance at 16 months [86], develops gradually progressive motor abnormalities, and dies between 15 and 24 months. However, according to a recent report by Fielding et al. in 2012 [87], the tgHD rat model does not show consistent, reliable, and progressive

impairment in a range of cognitive tests. The consistent failure to reveal impairments at any age on a range of tests of cognition and learning suggest that the tgHD rat is not a reliable model of the cognitive and behavioral impairments of human HD.

3.3.5. Frontotemporal dementia

3.3.5.1. TDP43

Transgenic murine models used in frontotemporal lobar degeneration (FTLD) research overexpress either wild-type or mutant human TAR DNA-binding protein (TDP) 43 knock-in (KI) via a human promoter. TDP43 is a multifunctional, nuclear protein that binds both DNA and RNA, as well as a member of the heterogeneous nuclear ribonuclear protein (hnRNP) family, and regulates several aspects of RNA processing, including alternative splicing, miRNA production, and mRNA trafficking and stabilization. Missense changes in the glycine-rich domain of TDP-43 lead to a shift in its localization from the nucleus to the cytoplasm, resulting in FTLD-TDP pathology [88]. This mouse model exhibits cognitive deficits at the age of 7 or 9 months, depending on the use of a mutated or a WT TDP43KI, respectively, as shown by passive avoidance test and Barns maze. Cognitive impairments for this murine model reach a peak at the age of 11–13 months [88, 89].

3.3.6. Down syndrome

3.3.6.1. TgDyrk1A

Apart from the trisomic mice used in Down syndrome research, transgenic models have also been constructed carrying human genes mapped in the repeated fragment of chromosome 21. One such model, namely, TgDyrk1a, overexpresses *DYRK1A*, a gene encoding a serine–threonine kinase, which is probably involved in neuroblast proliferation [90]. In the Morris water maze, TgDyrk1A mice show significant deficits in spatial learning and cognitive flexibility, due to hippocampal and prefrontal cortical dysfunction, a defect that was related specifically to reference memory. TgDyrk1A mice also exhibit delayed craniocaudal maturation, altered motor skill acquisition, and hyperactivity [91].

3.4. Translation to clinics: limitations and difficulties

To date, pharmacological, transgenic, and naturally aging rodent models have provided new insights into behavioral function. Although these models have given invaluable information, it is important to remember that they only provide approximations of the molecular and cellular mechanisms and cognitive impairments as seen in humans. In addition, whereas motor phenotypes can be readily assessed in rodent models, it is more challenging to characterize cognitive phenotypes. The frontal cortex of rodents is anatomically different from that of humans [92], and it is therefore difficult to model executive dysfunction, not to mention the existence of significant limitations in modeling complex behaviors in rats and mice, since they already differ in their own cognitive and social functions. Due to these obstacles, face validity gets compromised (Table 1). It has thus been suggested that the research community should take an “agnostic” approach as new models emerge and characterize their behavior as fully as possible. At present, face validity of the behavioral tests used is, in general, the same for pharmacological, aging, and transgenic rodent models (Table 2 and Table 3). This results from the fact that, independent of the manipulation used (pharmacological, age, or genetic), the same symptoms are being screened for. In addition, it is important to recognize that not all animal models currently in use or under development will be appropriate for mechanistic research, whereas other certain models exhibit phenotypes that are practical for therapy development. Compared with pharmacological models, transgenic models comprise more construct validity, and hence are more suited for mechanistic and fundamental research. On the other hand, pharmacological models comprise more predictive validity, and therefore contribute to more reliable testing of new (pharmacological) therapies (Table 2 and Table 3). Subjecting rodents to a comprehensive battery of tests provides a better framework not only for understanding the overall behavioral phenotype of the animal but also for more fully recognizing the limitations of the specific model. Nevertheless, it should be emphasized that the goal of animal research is to mimic as much as possible the human disease pathophysiology, and thus improving construct and face validity will provide greater insights into basic genetic and molecular mechanisms involved in expression of the behavior [93]. At the same time, once these mechanisms are better understood, predictive validity will improve and better efficacious therapeutic strategies can be explored and developed for treating cognitive deficits in human patients.

table 1.

Validities	Description:
Validity	The extent to which a test measures what it purports to measure. It is vital for a test to be valid in order for the results to be accurately applied and interpreted.
Construct validity	This is generally considered the most fundamental and all-inclusive validity concept, insofar as it specifies what the test measures. Construct validity holds that the model has a correct theoretical background compared to the human pathology. Therefore, it addresses the qualities contributing to the relation between X and Y. Overall, construct validity deals with the question: does the measure or observation in a test or model show behavior that corresponds to how the theory says a measure or observation of that construct should behave?
Face validity	The extent to which a test seems on its surface to be measuring what it purports to measure. Face validity refers not to what the test measures but only to how it looks. The concept of face validity is that the animal shows the same kind of behavior and has the same symptoms as humans have. In short; do the measures in a test or model appear to be relevant?
Predictive validity	The extent to which a test or model can predict future outcomes. Predictive validity implies that the manipulations and treatments that are beneficial in the appropriate animal model should also have the same effect in humans/patients, and vice versa.

table 2.

Pharmacological models	Construct validity	Face validity	Predictive validity
Inhibition of energy/glucose metabolism	+++	++	+
Cholinergic toxins	+++	++	+
Cholinergic antagonists	++	++	++
Glutamatergic antagonists	++	++	++
Serotonergic intervention	+	++	+

table 3.

Aging and transgenic models	Construct validity	Face validity	Predictive validity
Alzheimer's disease models	+++	++	++
Parkinson's disease models	+++	++	+
Huntinton's disease models	+++	++	+
Frontotemporal dementia TDP43 model	+++	++	+
Down syndrome TgDyrk model	+++	++	+

TABLE 1. Descriptions of construct, face, and, predictive validity.

TABLE 2. Validity of pharmacological models.
++++: meets validity perfectly, +++: meets validity good, ++: meets validity somewhat, +: meets validity poorly

TABLE 3. Validity of aging and transgenic models in general.
++++: meets validity perfectly, +++: meets validity good, ++: meets validity somewhat, +: meets validity poorly

REFERENCES

[1] Faigle R, Song H. Signaling mechanisms regulating adult neural stem cells and neurogenesis. *Biochim Biophys Acta - Gen Subj* 2013; 1830: 2435–2448.

[2] Froestl W, Muhs A, Pfeifer A. Cognitive enhancers (nootropics). Part 1: drugs interacting with receptors. *J Alzheimers Dis* 2012; 32: 793–887.

[3] Gold PE. Role of glucose in regulating the brain and cognition. *Am J Clin Nutr* 1995; 61: 987S–995S.

[4] Korol DL, Gold PE. Glucose, memory, and aging. *Am J Clin Nutr* 1998; 67: 764S–771S.

[5] Cho S, Wood A, Bowlby MR. Brain slices as models for neurodegenerative disease and screening platforms to identify novel therapeutics. *Curr Neuropharmacol* 2007; 5: 19–33.

[6] Bederson JB, Pitts LH, Tsuji M, et al. Rat middle cerebral artery occlusion: evaluation of the model and development of a neurologic examination. *Stroke*; 17: 472–6.

[7] Arias RL, Tasse JR, Bowlby MR. Neuroprotective interaction effects of NMDA and AMPA receptor antagonists in an *in vitro* model of cerebral ischemia. *Brain Res* 1999; 816: 299–308.

[8] Danysz W, Parsons CG. The NMDA receptor antagonist memantine as a symptomatological and neuroprotective treatment for Alzheimer's disease: preclinical evidence. *Int J Geriatr Psychiatry* 2003; 18: S23–S32.

[9] Ockuly JC, Gielissen JM, Levenick C V., et al. Behavioral, cognitive, and safety profile of 2-deoxy-2-glucose (2DG) in adult rats. *Epilepsy Res* 2012; 101: 246–252.

[10] Mayer G, Nitsch R, Hoyer S. Effects of changes in peripheral and cerebral glucose metabolism on locomotor activity, learning and memory in adult male rats. *Brain Res* 1990; 532: 95–100.

[11] Nitsch R, Mayer G, Hoyer S. The intracerebroventriculary streptozotocin-treated rat: Impairment of cerebral glucose metabolism resembles the alterations of carbohydrate metabolism of the brain in Alzheimer's disease. *J Neural Transm - Park Dis Dement Sect* 1989; 1: 109–110.

[12] Vavra JJ, Deboer C, Dietz A, et al. Streptozotocin, a new antibacterial antibiotic. *Antibiot Annu*; 7: 230–5.

[13] Prickaerts J, Blokland A, Honig W, et al. Spatial discrimination learning and choline acetyltransferase activity in streptozotocin-treated rats: effects of chronic treatment with acetyl-L-carnitine. *Brain Res* 1995; 674: 142–6.

[14] Ding A, Nitsch R, Hoyer S. Changes in brain monoaminergic neurotransmitter concentrations in rat after intracerebroventricular injection of streptozotocin. *J Cereb Blood Flow Metab* 1992; 12: 103–109.

[15] Hellweg R, Nitsch R, Hock C, et al. Nerve growth factor and choline acetyltransferase activity levels in the rat brain following experimental impairment of cerebral glucose and energy metabolism. *J Neurosci Res* 1992; 31: 479–486.

[16] Blokland A, Jolles J. Spatial learning deficit and reduced hippocampal ChAT activity in rats after an ICV injection of streptozotocin. *Pharmacol Biochem Behav* 1993; 44: 491–4.

[17] Bartus RT, Dean RL, Beer B, et al. The cholinergic hypothesis of geriatric memory dysfunction. *Science* 1982; 217: 408–14.

[18] Blokland A. Acetylcholine: a neurotransmitter for learning and memory? *Brain Res Brain Res Rev* 1995; 21: 285–300.

[19] Steckler T, Andrews JS, Marten P, et al. Effects of NBM lesions with two neurotoxins on spatial memory and autoshaping. *Pharmacol Biochem Behav* 1993; 44: 877–89.

[20] Peternel A, Hughey D, Wenk G, et al. Basal forebrain and memory: Neurotoxic lesions impair serial reversals of a spatial discrimination. *Psychobiology*; 16: 54–58.

[21] Wiley RG, Oeltmann TN, Lappi DA. Immunolesioning: selective destruction of neurons using immunotoxin to rat NGF receptor. *Brain Res* 1991; 562: 149–53.

[22] Wenk GL, Stoehr JD, Quintana G, et al. Behavioral, biochemical, histological, and electrophysiological effects of 192 IgG-saporin injections into the basal forebrain of rats. *J Neurosci* 1994; 14: 5986–95.

[23] Book AA, Wiley RG, Schweitzer JB. Specificity of 192 IgG-saporin for NGF receptor-positive cholinergic basal forebrain neurons in the rat. *Brain Res* 1992; 590: 350–5.

[24] Walsh TJ, Herzog CD, Gandhi C, et al. Injection of IgG 192-saporin into the medial septum produces cholinergic hypofunction and dose-dependent working memory deficits. *Brain Res* 1996; 726: 69–79.

[25] Lehmann O, Grottick AJ, Cassel J-C, et al. A double dissociation between serial reaction time and radial maze performance in rats subjected to 192 IgG-saporin lesions of the nucleus basalis and/or the septal region. *Eur J Neurosci* 2003; 18: 651–66.

[26] Klinkenberg I, Blokland A. The validity of scopolamine as a pharmacological model for cognitive impairment: A review of animal be-

havioral studies. *Neurosci Biobehav Rev* 2010; 34: 1307–1350.

[27] Prickaerts J, van Goethem NP, Chesworth R, et al. EVP-6124, a novel and selective α7 nicotinic acetylcholine receptor partial agonist, improves memory performance by potentiating the acetylcholine response of α7 nicotinic acetylcholine receptors. *Neuropharmacology* 2012; 62: 1099–1110.

[28] Caulfield MP. Muscarinic receptors--characterization, coupling and function. *Pharmacol Ther* 1993; 58: 319–79.

[29] Klinkenberg I, Blokland A. A comparison of scopolamine and biperiden as a rodent model for cholinergic cognitive impairment. *Psychopharmacology* (Berl) 2011; 215: 549–66.

[30] Toyohara J, Hashimoto K. α7 Nicotinic receptor agonists: potential therapeutic drugs for treatment of cognitive impairments in schizophrenia and Alzheimer's disease. *Open Med Chem J* 2010; 4: 37–56.

[31] Levin ED. Nicotinic systems and cognitive function. *Psychopharmacology* (Berl) 1992; 108: 417–31.

[32] Addy NA, Nakijama A, Levin ED. Nicotinic mechanisms of memory: effects of acute local DHbetaE and MLA infusions in the basolateral amygdala. *Brain Res Cogn Brain Res* 2003; 16: 51–7.

[33] Hahn B, Shoaib M, Stolerman IP. Selective nicotinic receptor antagonists: effects on attention and nicotine-induced attentional enhancement. *Psychopharmacology* (Berl) 2011; 217: 75–82.

[34] van der Staay FJ, Rutten K, Erb C, et al. Effects of the cognition impairer MK-801 on learning and memory in mice and rats. *Behav Brain Res* 2011; 220: 215–229.

[35] Ellison G. The *N*-methyl-D-aspartate antagonists phencyclidine, ketamine and dizocilpine as both behavioral and anatomical models of the dementias. *Brain Res Brain Res Rev* 1995; 20: 250–67.

[36] Morris BJ, Cochran SM, Pratt JA. PCP: from pharmacology to modelling schizophrenia. *Curr Opin Pharmacol* 2005; 5: 101–106.

[37] Steckler T, Sahgal A. The role of serotonergic-cholinergic interactions in the mediation of cognitive behaviour. *Behav Brain Res* 1995; 67: 165–99.

[38] Booij L, Van der Does AJW, Riedel WJ. Monoamine depletion in psychiatric and healthy populations: review. *Mol Psychiatry* 2003; 8: 951–973.

[39] van Donkelaar EL, Rutten K, Blokland A, et al. Phosphodiesterase 2 and 5 inhibition attenuates the object memory deficit induced by acute tryptophan depletion. *Eur J Pharmacol* 2008; 600: 98–104.

[40] Rutten K, Lieben C, Smits L, et al. The PDE4 inhibitor rolipram reverses object memory impairment induced by acute tryptophan depletion in the rat. *Psychopharmacology* (Berl) 2007; 192: 275–82.

[41] Chouliaras L, Sierksma ASR, Kenis G, et al. Gene-environment interaction research and transgenic mouse models of Alzheimer's disease. *Int J Alzheimers Dis*; 2010. Epub ahead of print January 2010. DOI: 10.4061/2010/859101.

[42] Gu Y, Huang C-S, Inoue T, et al. Drinking hydrogen water ameliorated cognitive impairment in senescence-accelerated mice. *J Clin Biochem Nutr* 2010; 46: 269–76.

[43] Gorbunova V, Bozzella MJ, Seluanov A. Rodents for comparative aging studies: from mice to beavers. *Age* (Dordr) 2008; 30: 111–9.

[44] Chouliaras L, van den Hove DLA, Kenis G, et al. Caloric restriction attenuates age-related changes of DNA methyltransferase 3a in mouse hippocampus. *Brain Behav Immun* 2011; 25: 616–623.

[45] Chouliaras L, van den Hove DLA, Kenis G, et al. Prevention of age-related changes in hippocampal levels of 5-methylcytidine by caloric restriction. *Neurobiol Aging* 2012; 33: 1672–81.

[46] Rutten BPF, Brasnjevic I, Steinbusch HWM, et al. Caloric restriction and aging but not overexpression of SOD1 affect hippocampal volumes in mice. *Mech Ageing Dev* 2010; 131: 574–579.

[47] Takeda T, Hosokawa M, Higuchi K. Senescence-accelerated mouse (SAM): a novel murine model of accelerated senescence. *J Am Geriatr Soc* 1991; 39: 911–9.

[48] Takeda T, Hosokawa M, Takeshita S, et al. A new murine model of accelerated senescence. *Mech Ageing Dev* 1981; 17: 183–94.

[49] Tomobe K, Nomura Y. Neurochemistry, neuropathology, and heredity in SAMP8: a mouse model of senescence. *Neurochem Res* 2009; 34: 660–669.

[50] Miyamoto M, Kiyota Y, Yamazaki N, et al. Age-related changes in learning and memory in the senescence-accelerated mouse (SAM). *Physiol Behav* 1986; 38: 399–406.

[51] Giuliani F, Vernay A, Leuba G, et al. Decreased behavioral impairments in an Alzheimer mice model by interfering with TNF-alpha metabolism. *Brain Res Bull* 2009; 80: 302–308.

[52] Nilsson LN., Arendash GW, Leighty RE, et al. Cognitive impairment in PDAPP mice depends on ApoE and ACT-catalyzed amyloid formation. *Neurobiol Aging* 2004; 25: 1153–1167.

[53] Chen G, Chen KS, Kobayashi D, et al. Active β-amyloid immunization restores spatial learning in PDAPP mice displaying very low levels of β-amyloid. *J Neurosci*; http://www.jneurosci.org/content/27/10/2654 (2007, accessed 6 April 2017).

[54] King DL, Arendash GW. Behavioral characterization of the Tg2576 transgenic model of Alzheimer's disease through 19 months. *Physiol Behav* 2002; 75: 627–42.

[55] Francis BM, Kim J, Barakat ME, et al. Object recognition memory and BDNF expression are reduced in young TgCRND8 mice. *Neurobiol Aging* 2012; 33: 555–563.

[56] McGowan E, Eriksen J, Hutton M. A decade of modeling Alzheimer's disease in transgenic mice. *Trends Genet* 2006; 22: 281–289.

[57] Arendash GW, King DL, Gordon MN, et al. Progressive, age-related behavioral impairments in transgenic mice carrying both mutant amyloid precursor protein and presenilin-1 transgenes. *Brain Res* 2001; 891: 42–53.

[58] Ohno M, Cole SL, Yasvoina M, et al. BACE1 gene deletion prevents neuron loss and memory deficits in 5XFAD APP/PS1 transgenic mice. *Neurobiol Dis* 2007; 26: 134–145.

[59] Kimura R, Ohno M. Impairments in remote memory stabilization precede hippocampal synaptic and cognitive failures in 5XFAD Alzheimer mouse model. *Neurobiol Dis* 2009; 33: 229–35.

[60] Takeuchi H, Iba M, Inoue H, et al. P301S mutant human tau transgenic mice manifest early symptoms of human tauopathies with dementia and altered sensorimotor gating. *PLoS One* 2011; 6: e21050.

[61] Lambourne SL, Sellers LA, Bush TG, et al. Increased tau phosphorylation on mitogen-activated protein kinase consensus sites and cognitive decline in transgenic models for Alzheimer's disease and FTDP-17: evidence for distinct molecular processes underlying tau abnormalities. *Mol Cell Biol* 2005; 25: 278–293.

[62] SantaCruz K, Lewis J, Spires T, et al. Tau suppression in a neurodegenerative mouse model improves memory function. *Science* 2005; 309: 476–481.

[63] Andorfer C, Kress Y, Espinoza M, et al. Hyperphosphorylation and aggregation of tau in mice expressing normal human tau isoforms. *J Neurochem* 2003; 86: 582–90.

[64] Polydoro M, Acker CM, Duff K, et al. Age-dependent impairment of cognitive and synaptic function in the htau mouse model of tau pathology. *J Neurosci* 2009; 29: 10741–10749.

[65] Oddo S, Caccamo A, Kitazawa M, et al. Amyloid deposition precedes tangle formation in a triple transgenic model of Alzheimer's disease. *Neurobiol Aging* 2003; 24: 1063–70.

[66] Billings LM, Oddo S, Green KN, et al. Intraneuronal Abeta causes the onset of early Alzheimer's disease-related cognitive deficits in transgenic mice. *Neuron* 2005; 45: 675–88.

[67] Raber J, Wong D, Buttini M, et al. Isoform-specific effects of human apolipoprotein E on brain function revealed in ApoE knockout mice: increased susceptibility of females. *Proc Natl Acad Sci U S A* 1998; 95: 10914–9.

[68] Masliah E, Rockenstein E, Mante M, et al. Passive immunization reduces behavioral and neuropathological deficits in an alpha-synuclein transgenic model of Lewy body disease. *PLoS One* 2011; 6: e19338.

[69] Magen I, Chesselet M-F. Genetic mouse models of Parkinson's disease. In: *Progress in brain research*, pp. 53–87.

[70] Nuber S, Petrasch-Parwez E, Winner B, et al. Neurodegeneration and motor dysfunction in a conditional model of Parkinson's disease. *J Neurosci* 2008; 28: 2471–2484.

[71] Pham TT, Giesert F, Röthig A, et al. DJ-1-deficient mice show less TH-positive neurons in the ventral tegmental area and exhibit non-motoric behavioural impairments. *Genes, Brain Behav* 2010; 9: 305–317.

[72] Zhu X-R, Maskri L, Herold C, et al. Non-motor behavioural impairments in parkin-deficient mice. *Eur J Neurosci* 2007; 26: 1902–1911.

[73] Goldberg MS, Fleming SM, Palacino JJ, et al. Parkin-deficient mice exhibit nigrostriatal deficits but not loss of dopaminergic neurons. *J Biol Chem* 2003; 278: 43628–43635.

[74] Nithianantharajah J, Barkus C, Murphy M, et al. Gene–environment interactions modulating cognitive function and molecular correlates of synaptic plasticity in Huntington's disease transgenic mice. *Neurobiol Dis* 2008; 29: 490–504.

[75] Pang TYC, Stam NC, Nithianantharajah J, et al. Differential effects of voluntary physical exercise on behavioral and brain-derived neurotrophic factor expression deficits in

huntington's disease transgenic mice. *Neuroscience* 2006; 141: 569–584.

[76] Pang TYC, Du X, Zajac MS, et al. Altered serotonin receptor expression is associated with depression-related behavior in the R6/1 transgenic mouse model of Huntington's disease. *Hum Mol Genet* 2009; 18: 753–766.

[77] Carter RJ, Lione LA, Humby T, et al. Characterization of progressive motor deficits in mice transgenic for the human Huntington's disease mutation. *J Neurosci* 1999; 19: 3248–57.

[78] Lione LA, Carter RJ, Hunt MJ, et al. Selective discrimination learning impairments in mice expressing the human Huntington's disease mutation. *J Neurosci* 1999; 19: 10428–37.

[79] Stack EC, Kubilus JK, Smith K, et al. Chronology of behavioral symptoms and neuropathological sequela in R6/2 Huntington's disease transgenic mice. *J Comp Neurol* 2005; 490: 354–370.

[80] Hickey M, Gallant K, Gross G, et al. Early behavioral deficits in R6/2 mice suitable for use in preclinical drug testing. *Neurobiol Dis* 2005; 20: 1–11.

[81] Morton AJ, Hunt MJ, Hodges AK, et al. A combination drug therapy improves cognition and reverses gene expression changes in a mouse model of Huntington's disease. *Eur J Neurosci* 2005; 21: 855–870.

[82] Slow EJ, van Raamsdonk J, Rogers D, et al. Selective striatal neuronal loss in a YAC128 mouse model of Huntington disease. *Hum Mol Genet* 2003; 12: 1555–67.

[83] Van Raamsdonk JM, Pearson J, Bailey CDC, et al. Cystamine treatment is neuroprotective in the YAC128 mouse model of Huntington disease. *J Neurochem* 2005; 95: 210–220.

[84] Van Raamsdonk JM, Pearson J, Slow EJ, et al. Cognitive dysfunction precedes neuropathology and motor abnormalities in the YAC128 mouse model of Huntington's disease. *J Neurosci* 2005; 25: 4169–4180.

[85] von Hörsten S, Schmitt I, Nguyen HP, et al. Transgenic rat model of Huntington's disease. *Hum Mol Genet* 2003; 12: 617–24.

[86] Zeef DH, van Goethem NP, Vlamings R, et al. Memory deficits in the transgenic rat model of Huntington's disease. *Behav Brain Res* 2012; 227: 194–198.

[87] Fielding SA, Brooks SP, Klein A, et al. Profiles of motor and cognitive impairment in the transgenic rat model of Huntington's disease. *Brain Res Bull* 2012; 88: 223–236.

[88] Swarup V, Phaneuf D, Bareil C, et al. Pathological hallmarks of amyotrophic lateral sclerosis/frontotemporal lobar degeneration in transgenic mice produced with TDP-43 genomic fragments. *Brain* 2011; 134: 2610–2626.

[89] Tsai K-J, Yang C-H, Fang Y-H, et al. Elevated expression of TDP-43 in the forebrain of mice is sufficient to cause neurological and pathological phenotypes mimicking FTLD-U. *J Exp Med* 2010; 207: 1661–1673.

[90] Altafaj X, Dierssen M, Baamonde C, et al. Neurodevelopmental delay, motor abnormalities and cognitive deficits in transgenic mice overexpressing Dyrk1A (minibrain), a murine model of Down's syndrome. *Hum Mol Genet* 2001; 10: 1915–23.

[91] Ahn K-J, Jeong HK, Choi H-S, et al. DYRK1A BAC transgenic mice show altered synaptic plasticity with learning and memory defects. *Neurobiol Dis* 2006; 22: 463–472.

[92] Uylings HBM, Groenewegen HJ, Kolb B. Do rats have a prefrontal cortex? *Behav Brain Res* 2003; 146: 3–17.

[93] D'Mello GD, Steckler T. Animal models in cognitive behavioural pharmacology: an overview. *Brain Res Cogn Brain Res* 1996; 3: 345–52.

EPIGENETIC MODIFICATIONS IN MOUSE CEREBELLAR PURKINJE CELLS: EFFECTS OF AGING, CALORIC RESTRICTION, AND OVEREXPRESSION OF SUPEROXIDE DISMUTASE 1 ON 5-METHYLCYTOSINE AND 5-HYDROXYMETHYLCYTOSINE

ROY **LARDENOIJE**[A], DANIËL L.A. V**AN DEN HOVE**[A,B,] THOMAS S.J. **VAESSEN**[A], ARTEMIS **IATROU**[A], KOEN P.V. **MEUWISSEN**[A], BRITT T.J. **VAN HAGEN**[A], GUNTER **KENIS**[A], HARRY W.M. **STEINBUSCH**[A], CHRISTOPH **SCHMITZ**[C], BART P.F. **RUTTEN**[A]

[A]SCHOOL FOR MENTAL HEALTH AND NEUROSCIENCE (MHENS), DEPARTMENT OF PSYCHIATRY AND NEUROPSYCHOLOGY, MAASTRICHT UNIVERSITY, UNIVERSITEITSSINGEL 50, 6200 MD MAASTRICHT, THE NETHERLANDS
[B]LABORATORY OF TRANSLATIONAL NEUROSCIENCE, DEPARTMENT OF PSYCHIATRY, PSYCHOSOMATICS AND PSYCHOTHERAPY, UNIVERSITY OF WUERZBURG, FUECHSLEINSTRASSE 15, 97080 WUERZBURG, GERMANY
[C]DEPARTMENT OF NEUROANATOMY, LUDWIG-MAXIMILIANS-UNIVERSITY OF MUNICH, MUNICH, GERMANY

Neurobiology of Aging 36:3079-3089
(2015)

Abstract

The aim of the present study was to assess alterations in DNA methylation and hydroxymethylation during aging in cerebellar Purkinje cells and to determine the effects of putatively preventative measures to such age-related changes. Employing immunohistochemical techniques, 5-methylcytosine (5-mC) and 5-hydroxymethylcytosine (5-hmC) immunoreactivity (IR) in cerebellar Purkinje cells of 12-month-, and 24-month-old mice was interrogated. Additionally, the modulatory effects of caloric restriction (CR) and normal human Cu/Zn super oxide dismutase (SOD) 1 overexpression on these changes were assessed. We show that aging is associated with an increase of 5-mC and 5-hmC IR in mouse cerebellar Purkinje cells. These age-related increases were mitigated by CR, but not SOD1 overexpression. Additionally, the ratio between 5-mC and 5-hmC decreased with age and CR treatment, suggesting that CR has a stronger effect on DNA methylation than DNA hydroxymethylation. These findings enforce the notion that aging is closely connected to marked epigenetic changes, affecting multiple brain regions, and that CR is an effective means to prevent or counteract deleterious age-related epigenetic alterations.

KEYWORDS: DNA methylation; DNA hydroxymethylation; Purkinje cells; aging; caloric restriction; anti-oxidant overexpression

4.1. Introduction

Preventing the global deterioration of the aging human body to extend the life span has been heavily researched and remains a lively field. The aging brain has been shown to undergo region-specific gene expression, morphological, and functional changes [1–8]. A downregulation of genes involved in synaptic plasticity, neurotropic support and an upregulation of immune-related genes, concomitant with progressive synaptic dysfunction, eventually leads to cognitive decline. Indeed, areas important for proper cognitive functioning, such as the neocortical and hippocampal networks, as well as the more recently identified cerebello-hippocampal network, seem to be particularly prone to deteriorate with age [9–13].

Dietary restriction of caloric intake and enhanced levels of endogenous and exogenous antioxidants are approaches that are potentially able to mitigate age-related deterioration of the brain [14–19]. While increasing exogenous antioxidants can simply be achieved through dietary supplementation, endogenous antioxidants can be experimentally upregulated in transgenic animal models [20]. This latter approach, applied to boost normal human Cu/Zn super oxide dismutase (SOD) 1 in mice, has been shown to attenuate age-related accumulation of oxidative damage to DNA and proteins in the brainstem [21] and neurodegeneration after various forms of trauma in the mammalian brain [20–26]. In addition, caloric restriction (CR), without undernutrition, appears to be a promising strategy to extend the lifespan and counteract detrimental age-related alterations in various species [14, 15, 27–34], although studies in humans are very limited and with mixed results [35].

Over the past few years, evidence has accumulated that epigenetic mechanisms may be critically involved in mediating age-related changes of the brain [36–40]. The epigenetic machinery comprises multiple pathways involved in the regulation of gene expression, including histone modifications, DNA methylation and DNA hydroxymethylation [41, 42]. These various epigenetic mechanisms work in concert to fine-tune gene expression at multiple levels, for instance to ensure that the correct genes are activated or deactivated during cell division and differentiation. Furthermore, these mechanisms are also thought to be critically involved in regulating synaptic plasticity and related memory functions [38, 43–45]. DNA methylation has been investigated intensively in relation to aging and age-related neurodegeneration [36, 37, 46–53], whereas DNA hydroxymethylation (i.e. the closely related, but functionally distinct DNA modification) has only recently received attention in this respect [42, 54–57]. DNA methylation is performed by DNA methyltransferases (DNMTs), which are able to covalently bind a methyl group to cytosine bases of the DNA, creating 5-methylcytosine

(5-mC) [58–61]. The ten-eleven translocation (TET) enzyme family is responsible for DNA hydroxymethylation [62]. TET enzymes convert 5-mC into 5-hydroxymethylcytosine (5-hmC) through the hydroxymethylation of methylated cytosines [63]. TET can further oxidize 5-hmC to 5-formylcytosine (5-fC) and 5-carboxylcytosine (5-caC), the exact functional roles of which, apart from being demethylation intermediates, remain to be determined [64–66]. As 5-hmC is created from pre-existing 5-mC, DNA methylation and DNA hydroxymethylation are closely related processes [67]. Nevertheless, as DNA methylation is generally associated with repression of gene expression through attraction of methyl-binding proteins (MBPs), thereby decreasing the accessibility of the DNA for the transcription apparatus, DNA hydroxymethylation has been reported to have a lower affinity for MBPs [68], and generally leads to an opening of the chromatin and promotion of transcription [69, 70]. Note, however, that recent findings suggest that the precise roles of 5-mC and 5-hmC in the regulation of gene transcription are likely much more complex than initially assumed [71–74].

DNA methylation and especially hydroxymethylation have been shown to be dynamic and are known to undergo widespread changes during development [71, 72, 75, 76]. The behavior of these epigenetic modifications in the aging brain, especially outside the hippocampus and frontal cortex, is largely unknown. Recently, our group has investigated how CR and SOD1 overexpression might affect age-related epigenetic changes in the hippocampus and reported striking age-related increases in hippocampal DNMT3A, 5-mC, 5-hmC and histone deacetylase (HDAC) 2 immunoreactivity (IR), and that these changes were attenuated by CR, but not by overexpression of SOD1 [47, 48, 54, 77]. Although the previous studies provided new insights into age-related epigenetic changes, they were limited to the hippocampus. The present study expands upon this previous work by focusing on cerebellar Purkinje cells. Purkinje cells, the output cells of the cerebellar cortex, represent an interesting target, as 5-hmC was discovered in these cells and they appear to exhibit some of the highest levels of 5-hmC [78]. Note that the first hint at the existence of 5-hmC was published much earlier by Penn et al. [79]. Purkinje cells are among the largest cells in the brain, whereas the other prominent class of neurons present in the cerebellum, the granule cells, which are several hundred times more abundant, are the smallest [80, 81]. Moreover, Purkinje cells have an unusually large nucleus, with a centrally located nucleolus, and are known to be highly heterogeneous in their production of neurotransmitters and other cell markers [81, 82]. Purkinje cells receive excitatory input from thousands of connections, resulting in huge surges of calcium, which results in a high metabolic rate to keep this in check and is thought to contribute to a selective vulnerability to various factors, including oxidative stress, hypoxia, metabolic insufficiencies and

many environmental toxins [83]. Additionally, their numbers are known to decrease with age [12]. Given previous observations of (i) age-related changes in 5-mC and 5-hmC in the mouse hippocampus [48, 54], (ii) the presence of high levels of 5-hmC in Purkinje cells [78], and (iii) major changes during development and aging in Purkinje cells [84–86], it is postulated that Purkinje cell 5-mC and 5-hmC levels increase with age and that this increase is attenuated by CR and SOD1 overexpression. To assess this hypothesis, 5-mC and 5-hmC IR was measured by employing design-based quantitative immunohistochemical techniques in 12- and 24-month-old wild-type (WT) and SOD1 transgenic mice kept on either CR or a control diet (CD).

4.2. Materials and methods

4.2.1. Animals

This study included brain sections of 12 12-month-old WT C57B16J mice, 12 24-month-old WT C57B16J mice, 12 12-month-old transgenic mice overexpressing SOD1 (SOD1 mice) and 12 24-month-old SOD1 mice. These mice stem from a large aging cohort of 240 male mice and are the same as those previously used to investigate epigenetic alterations in the hippocampus [47, 48, 54, 77]. The generation, diet, weight and survival curves of this cohort have been described previously [32, 34, 47]. In short, the transgenic mice were created by introducing 7 copies of the entire human SOD1 sequence into chromosome 3 of C57B16 mice, leading to enhanced SOD1 activity in the brain and other tissues [87]. Confirmation of human SOD1 expression specifically for the transgenic mice in the used cohort has been reported previously [32]. The cohort was initiated at the Central Animal Facilities (Maastricht University, Maastricht, the Netherlands), with 4 breeder pairs of female WT C57Bl6J mice and male transgenic mice hemizygous for the SOD1 transgene. After weaning at 21 days after birth, the mice were immediately assigned to different diet groups, which were maintained throughout the entire lifespan of the animals. Half of the mice of each genotype were provided with a CR diet of approximately 50% less calories than *ad libitum* consumption, while the other half received a CD of approximately 15% less calories [34]. This 15% reduction in calorie intake for the control group was chosen to have full control over calorie consumption, as *ad libitum* food consumption might introduce unwanted variation in the control diet groups. As reported previously, this CR paradigm resulted in a 46% reduction in body weights, as compared with the CD, and increased mean and maximum life span [32]. 6 mice per group were sacrificed at either 12, or 24-months of age for the current analyses. All animals were housed individually on a 12/12 hours light/dark cycle, under standard

temperature, humidity and specified pathogen free (SPF) conditions, and with *ad libitum* access to water. All the experimental procedures were approved by the Animal Ethics Board of Maastricht University.

This study had a 2 × 2 × 2 experimental design, based on genotype, age and diet. The 8 groups in total are thus (i) 12-months-old WT mice on the CD (12WT-CD), (ii) 24-months-old WT mice on the CD (24WT-CD), (iii) 12-months-old SOD1 mice on the CD (12SOD-CD), (iv) 24-months-old SOD1 mice on the CD (24SOD-CD), (v) 12-months-old WT mice on the CR diet (12WT-CR), (vi) 24-months-old WT mice on the CR diet (24WT-CR), (vii) 12-months-old SOD1 mice on the CR diet (12SOD-CR) and (viii) 24-months-old SOD1 mice on the CR diet (24SOD-CR).

4.2.2. Tissue processing

The brains were processed as described previously [32, 47]. Briefly, after deep anesthesia the animals underwent transcardial perfusion with 20 ml tyrode solution and 2 fixative solutions (20 ml of 4% paraformaldehyde, 0.9% NaCl, 1% acetic acid and 30 ml of 8% paraformaldehyde, 0.9% NaCl, 1% acetic acid). The heads were then removed and the opened skulls including the brain were postfixed for 24 hours in the 8% paraformaldehyde solution, but without acetic acid, at 4^{o}C. Following fixation, the brains were removed and hemisected along the midsaggital line, cryoprotected in sucrose solutions (consecutively, 10%, 20% and 30% sucrose, in Tris-HCl buffer, twice for 12 hours per solution, at 4^{o}C) and embedded in Tissue Tek® (Sakura Finetec Europe, Zoeterwoude, The Netherlands). For this study, only the left brain halves were used. They were frozen quickly and kept at -80^{o}C until being cut serially with a cryostat (type HM 500 OMV, Microm, Walldorf, Germany), in 30 µm-thick free-floating coronal sections. The brains were split into anterior (A), medial (B) and posterior (C) parts, each of which was again divided in 10 subseries of every 10th section. After cutting, the sections were stored at -80^{o}C until further use. The current study only used the C series, which included the cerebellum.

4.2.3. Immunohistochemical detection of 5-mC and 5-hmC

Two full series of free-floating sections containing the cerebellum were immunohistochemically stained, one for 5-mC and one for 5-hmC.

Sections first underwent antigen retrieval with 14 mM citric acid buffer (pH 6.0) in a water bath at 95°C for 20 minutes, quenching of endogenous peroxidase activity with 0.1% H_2O_2 for 1 hour at room temperature (RT), and blocking with 3% normal donkey serum for 30 minutes at RT. Sections were then incubated overnight at 4°C with either mouse monoclonal anti-5-mC antibody (dilution 1:500; GenWay Biotech Inc., San Diego, CA, USA), or rabbit polyclonal anti-5-hmC antiserum (dilution 1:25,000; Active Motif, Rixensart, Belgium) as a primary antibody. Subsequently, the sections were incubated with biotinylated donkey anti-mouse secondary antibody (dilution 1:200; Jackson, Westgrove, PA, USA) in case of 5-mC, or biotinylated donkey anti-rabbit (dilution 1:1,000; Jackson Westgrove, PA, USA) secondary antibody in case of 5-hmC, for 2 hours at RT, followed by an incubation with avidin-biotin-peroxidase complex (diluted 1:500; Vector laboratories, Burlingame, CA, USA) for 2 hours at RT. In order to visualize the horseradish peroxide reaction product, the sections were reacted with a 3,3'-diaminobenzidine tetrahydrochloride (DAB) solution (1:1 DAB:Tris-HCl, 0.01% H_2O_2; Sigma, Uithoorn, The Netherlands) at RT for 6 minutes. The sections were then mounted on gelatin-coated microscope slides, dehydrated, and coverslipped using Pertex (Histolab Products ab, Göteborg, Sweden). Sections from all 48 animals were stained at the same time, and handled in a randomized order.

For qualitative purposes, a 5-mC, 5-hmC and 4',6-diamidino-2-phenylindole dihydrochloride (DAPI; a fluorescent dye binding AT-rich regions of the DNA) triple immunofluorescent labeling was performed in a similar fashion. After antigen retrieval and blocking, the sections were first incubated overnight at 4°C with rabbit polyclonal anti-5-hmC antiserum (dilution 1:10,000), and then with donkey anti-rabbit Alexa 594 conjugated secondary antibody (dilution 1:1,000; Invitrogen, Eugene, OR, USA) for 2 hours at RT. After an additional blocking step, the sections were stained for 5-mC by first incubating them overnight at 4°C with mouse monoclonal anti-5-mC antibody (dilution 1:500), then with biotinylated donkey anti-mouse secondary antibody (dilution 1:1,000) for 2 hours at RT, followed by a 2 hour incubation at RT with streptavidin Alexa 488 conjugate (dilution 1:400; Invitrogen, Eugene, OR, USA). Finally, the sections were counterstained with DAPI (dilution 1:100,000; Sigma Aldrich, Zwijndrecht, The Netherlands). The sections were mounted on gelatin-coated microscope slides, shortly air-dried and coverslipped with 80% glycerol.

Of note, reversing the order of 5-mC and 5-hmC antibody incubation did not influence the fluorescent staining pattern (data not shown). For all staining procedures, negative controls, without primary antibody, were included and evaluated (data not shown). The specificity of the anti-5-mC and anti5-hmC primary antibodies has been shown previously [48, 54, 88].

4.2.4. Analysis of 5-mC and 5-hmC immunoreactivity

To quantify the level of 5-mC and 5-hmC immunoreactivity in cerebellar Purkinje cells, all sections of the cerebellum were selected (between Bregma levels -4.83 mm and -7.55 mm [89]) and, per animal, approximately 100 images of individual Purkinje cells within the Purkinje cell layer, spread across the different lobules of the cerebellum, were taken. Brightfield images were taken with a digital camera (F-view; Olympus, Tokyo, Japan) connected to an Olympus AX70 brightfield microscope (analysis; Imaging System, Münster, Germany), using the 100× objective and an IF550 filter. All slides were photographed in a randomized order.

Of the fluorescent 5-mC, 5-hmC and DAPI triple staining, 2-5 μm thick image stacks were taken, with an image spacing of 0.1 μm, using a Stereo Investigator Confocal Spinning Disk (SI-SD) system (MBF Bioscience, Williston, VT, USA), using the 100× objective. The SI-SD system consisted of a modified Olympus BX51 fluorescence microscope with a customized spinning disk unit (Olympus), computer-controlled excitation and emission filter wheels (Olympus), three axis high-accuracy computer controlled stepping motor 4 × 4 Grid Encoded Stage (Ludl Electronic Products, Hawthorne, NY, USA), linear z-axis position encoder (Ludl Electronic Products), ultra-high sensitivity electron multiplier charge-coupled device camera (1000 × 1000 pixels, C9100-02, Hamamatsu Photonics, Hamamatsu City, Japan) and Stereo Investigator controlling software (MBF Bioscience). Using the image stacks, three-dimensional section reconstructions were generated using the Imaris software (Bitplane AG, Zurich, Switzerland). The image stacks were also used for colocalization analyses of 5-mC, 5-hmC and DAPI in Purkinje cell nuclei, using the Coloc 2 plugin that comes with the Fiji software package [90].

A total of 4 mice were excluded from the 5-mC (1 of the 12WT-CD group, 1 of the 24SOD-CD group, and 2 of the 12SOD-CD group) image analysis, and 2 mice for the 5-hmC (1 of the 24SOD-CD group and 1 of the 12SOD-CD group) image analysis, because of insufficient numbers of sections per animal (due to histological processing). The mean IR of the photographed Purkinje cells was determined with the ImageJ software program (version 1.48v, Wayne Rasband, National Institutes of Health, Bethesda, Maryland, USA), by measuring the area of immunoreactivity in the nucleus and the mean grey value of this area. The grey value measurements were noise-corrected by subtracting the signal that was measured when the camera shutter was closed, and corrected for background variation by dividing the mean grey value of the Purkinje cell nucleus of each individual image

by the mean background grey value of areas of tissue without cells (in the molecular layer), of that same image. After analyzing all individual Purkinje cell images of a staining, the measured values were averaged for each animal. These animal means were used for further analyses. To get a complete picture of 5-mC and 5-hmC IR, the integrated density was calculated by multiplying the area and grey value measurements, and these values were then normalized to the data of the 12WT-CD group. Additionally, in order to compare the relative degree of DNA methylation and hydroxymethylation between groups, the ratio between the 5-mC and 5-hmC integrated densities was determined.

4.2.5. Statistical analysis

All data displayed below is presented as the mean and standard error of means. Comparisons between groups were made with the general linear model univariate analysis of variance (ANOVA), taking into account main and interactive effects of genotype, diet and age. In addition, pair-wise comparisons with a Bonferroni post-hoc test were done. Normality was inspected via a quantile-quantile plot of the ANOVA residuals and the Lilliefors adaptation of the Kolmogorov-Smirnov test. Heteroscedasticity was checked by plotting the ANOVA residuals versus the predicted values in addition to a Breusch-Pagan test. The correlation between 5-mC and 5-hmC IR was determined by calculating the Pearson's correlation coefficient (r). Statistical significance for all tests was set at $\alpha = 0.05$. All statistical calculations were performed using R (www.r-project.org) and RStudio (www.rstudio.com). Graphs were constructed in GraphPad Prism (Version 4, GraphPad Software, San Diego, USA).

4.3. Results

4.3.1. Qualitative analysis of 5-mC and 5-hmC immuno-reactivity

As can be seen in Figure 1 and Figure 2, most cells of the mouse cerebellum exhibited nuclear 5-mC and 5-hmC IR. In Purkinje cells, the expression patterns of 5-mC and 5-hmC were very different from the other cerebellar cell types. While 5-hmC appeared more diffusely throughout the nucleus, with darker spots, 5-mC was much more localized, mostly limited to one large site, with sporadically additional smaller sites of high IR. The nucleolus itself generally showed little to no 5-mC or 5-hmC IR.

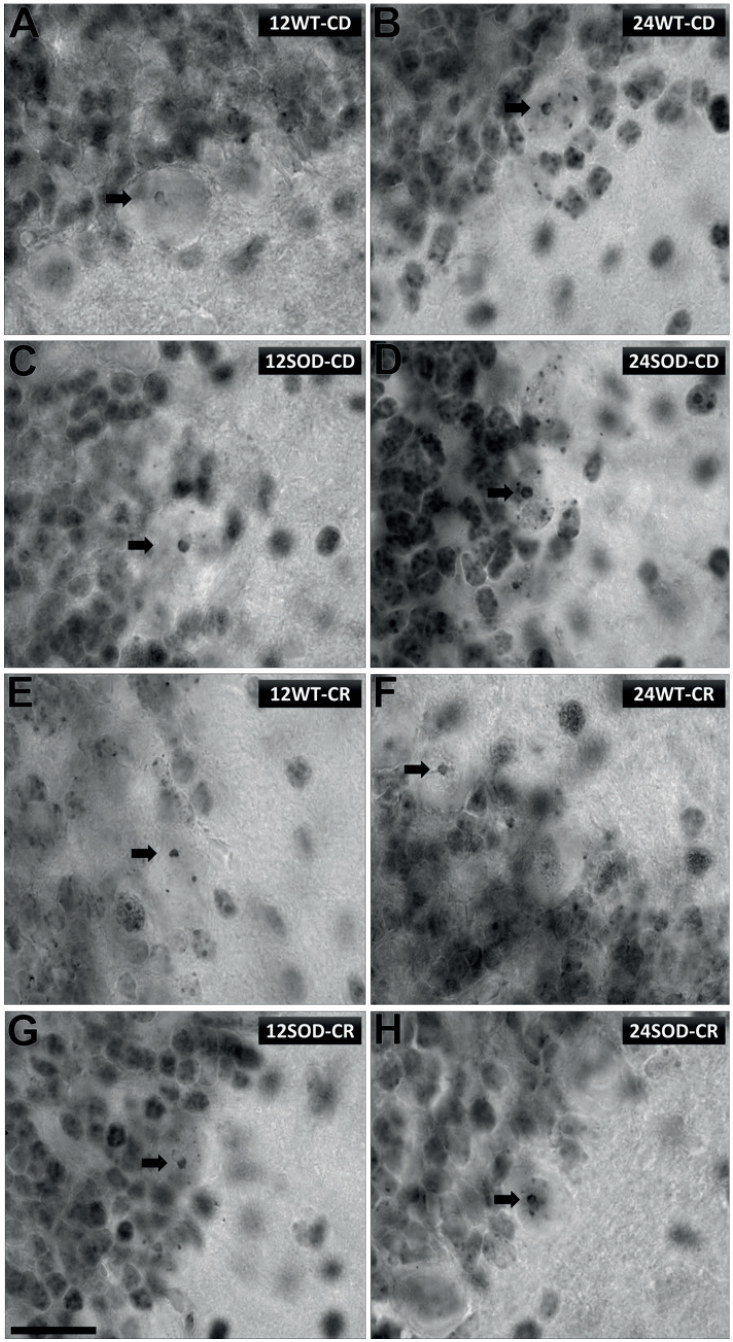

figure 1.

FIGURE 1. High magnification images of cerebellar 5-methylcytosine (5-mC) immunoreactivity (IR). Representative images of a wild-type (WT) mouse on control diet (CD) of 12 months (12WT-CD; A) and of 24 months (24WT-CD; B), of a transgenic Cu/Zn super oxide dismutase (SOD) 1 overexpressing mouse on CD of 12 months (12SOD-CD; C) and of 24 months (24SOD-CD; D), of a WT mouse on caloric restriction (CR) of 12 months (12WT-CR; E) and of 24 months (24WT-CR; F), and of a SOD1 mouse on CR of 12 months (12SOD-CR; G) and of 24 months (24SOD-CR; H). Arrows indicate Purkinje cell nuclei. Note the higher 5-mC IR, especially the increased amount of reactive boutons, in the 24WT-CD (B) and 24SOD-CD (D) groups, as compared to the other groups, indicating an age-related increase in 5-mC IR, which is not visible in the CR groups, as 24WT-CR (F) and 24SOD-CR (H) do not display a higher 5-mC IR as compared to their 12 months old counterparts (E and G, respectively). Scale bar represents 20 µm.

Figure 3 and the colocalization analyses showed that there is only limited overlap in Purkinje cell nuclear 5-mC and 5-hmC IR ($r = 0.19$), as well as

figure 2.

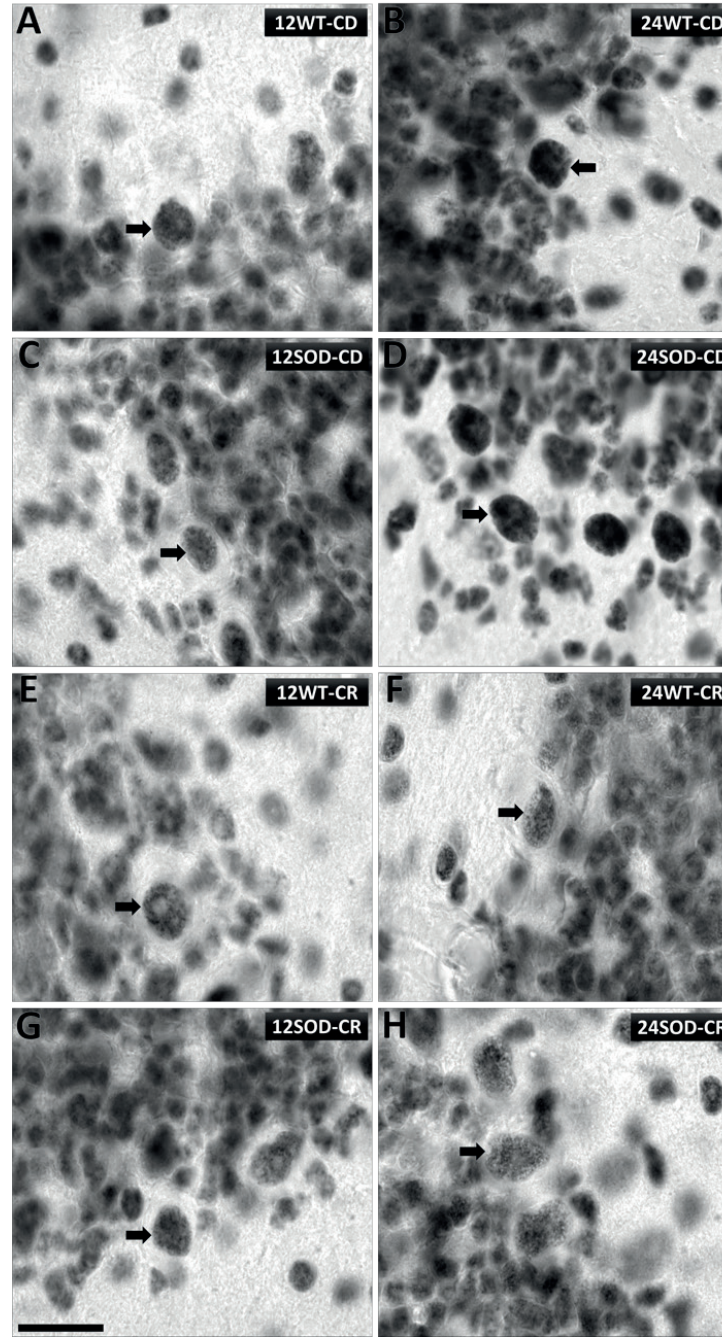

FIGURE 2. High magnification images of cerebellar 5-hydroxymethylcytosine (5-hmC) immunoreactivity (IR). Representative images of a wild-type (WT) mouse on control diet (CD) of 12 months (12WT-CD; A) and of 24 months (24WT-CD; B), of a transgenic Cu/Zn super oxide dismutase (SOD) 1 overexpressing mouse on CD of 12 months (12SOD-CD; C) and of 24 months (24SOD-CD; D), of a WT mouse on caloric restriction (CR) of 12 months (12WT-CR; E) and of 24 months (24WT-CR; F), and of a SOD1 mouse on CR of 12 months (12SOD-CR; G) and of 24 months (24SOD-CR; H). Arrows indicate Purkinje cell nuclei. Note the higher 5-hmC IR in the 24WT-CD (B) and 24SOD-CD (D) groups, as compared to the other groups, indicating an age-related increase in 5-hmC IR, which is not visible in the CR groups, as 24WT-CR (F) and 24SOD-CR (H) do not display a higher 5-mC IR as compared to their 12 months old counterparts (E and G, respectively). Scale bar represents 20 µm.

5-hmC and DAPI IR (r = 0.15), whereas 5-mC and DAPI IR had a high colocalization (r = 0.71).

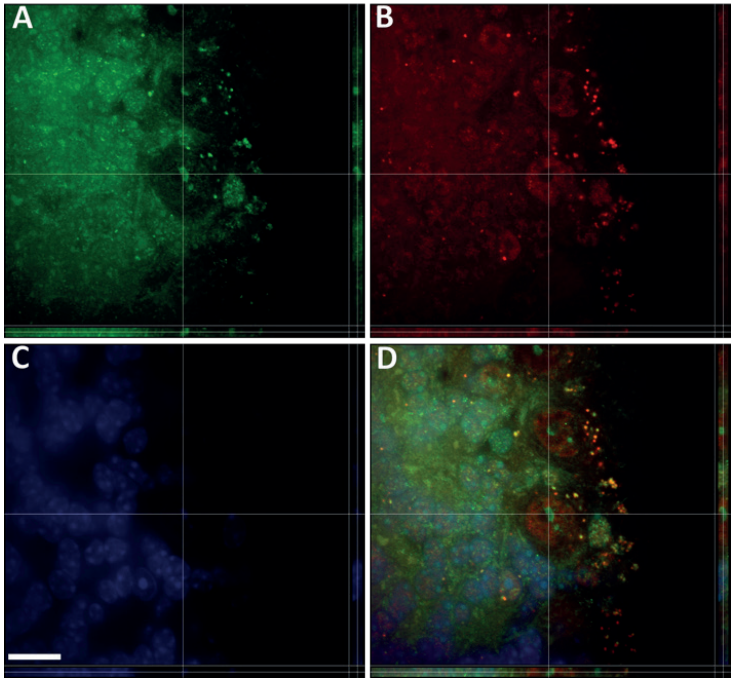

figure 3.

Further visual inspection of 5-mC and 5-hmC IR showed an age-related increase of 5-hmC IR intensity in the CD groups, as the Purkinje cells of the 24WT-CD and 24SOD-CD groups appeared to be strikingly darker than those of the other groups (Figure 1). While this increase in IR intensity was not as obvious in case of 5-mC, the number of 5-mC immunoreactive sites appeared to increase with age in the CD groups and not the CR groups (Figure 2). The intensity of the 5-mC and 5-hmC IR of the Purkinje cells was further quantitatively analyzed to corroborate these observations.

4.3.2. Semi-quantitative analysis of 5-mC and 5-hmC immunoreactivity

Results are summarized in Table 1 and Figure 4. Inspection of the quantile-quantile plots of the ANOVA residuals and the Lilliefors adaptation of the Kolmogorov-Smirnov tests ($p > 0.05$) indicated that the assumption of normality was met. No significant heteroscedasticity was detected in the residuals versus predicted values plots and the Breusch-Pagan tests ($p > 0.05$). The ANOVA showed statistically significant main effects of diet

FIGURE 3. Triple fluorescent staining of 5-methylcytosine (5-mC), 5-hydroxymethylcytosine (5-hmC) and 4',6-diamidino-2-phenylindole dihydrochloride (DAPI). Representative high magnification 3D reconstructions of image stacks of a 12 month wild-type mouse receiving the control diet. 5-mC visualization with Alexa 488 (A; green), 5-mC visualization with Alexa 594 (B; red), and DAPI counterstain (C; blue). The images are merged to show overlap between the 5-mC, 5-mC, and DAPI signals (D). See text for the results of the colocalization analysis. The most right and bottom parts of the images show a front and side view of the 3D reconstructions. Scale bar represents 20 µm.

on both 5-mC and 5-hmC IR (5-mC: $p < 0.001$; 5-hmC: $p < 0.01$), and of age on 5-hmC IR ($p < 0.001$). Significant interactions between diet and age were found for both 5-mC and 5-hmC IR (5-mC: $p < 0.001$; 5-hmC: $p < 0.01$). Stratified analyses showed statistically significant increases in 5-mC IR with age in the CD groups ($p < 0.05$) and a statistical significant decrease in the CR groups ($p < 0.05$) (Figure 4A). Pairwise comparisons furthermore indicated that 5-hmC IR increased statistically significantly with age in the CD groups ($p < 0.001$), but not in the CR groups ($p > 0.05$), and that these effects were independent of genotype (Figure 4B).

When looking at the ratio between 5-mC and 5-hmC, main effects of diet ($p < 0.01$) and age ($p < 0.001$) were observed, as well as interaction effects between genotype and diet ($p < 0.05$), and diet and age ($p < 0.001$). The Bonferroni corrected pairwise comparisons showed a statistically significant age-related decrease in 5-mC and 5-hmC ratio in the CR groups only ($p < 0.001$) (Figure 4C). At the same time, correlation analysis between 5-mC and 5-hmC IR indicates there is a positive correlation between 5-mC and 5-hmC IR (r = 0.484, $p < 0.001$).

table 1.

P-values	5-mC	5-hmC	Ratio
Age	0.806	< 0.001***	< 0.001***
Genotype	0.791	0.572	0.643
Diet	< 0.001***	0.001**	0.002**
Age x Genotype	0.604	0.687	0.819
Age x Diet	< 0.001***	0.001**	< 0.001***
Genotype x Diet	0.081	0.508	0.049*
Age x Genotype x Diet	0.877	0.849	0.867

TABLE 1. *P*-values of the general linear model univariate analysis of variance tests of the integrated density measurements.
ABBREVIATIONS: 5-mC, 5-methylcytosine; 5-hmC, 5-hydroxymethylcytosine; * $p < 0.05$; ** $p < 0.01$; *** $p < 0.001$.

4.4. Discussion

5-mC and 5-hmC IR in cerebellar Purkinje cells was immunohistochemically investigated in WT and transgenic SOD1 mice, fed with either a CR or CD, and divided in 12- and 24-month-old groups. Qualitative analysis revealed an age-related increase in 5-hmC IR in the CD groups only. A semi-quantitative analysis of 5-mC and 5-hmC IR corroborated these observations, indicating that IR significantly increased with age, CR seems to mitigate this epigenetic change, SOD1 overexpression does not affect this age-related increase, and that lifelong CR appears to favor DNA hydroxymethylation over methylation with age.

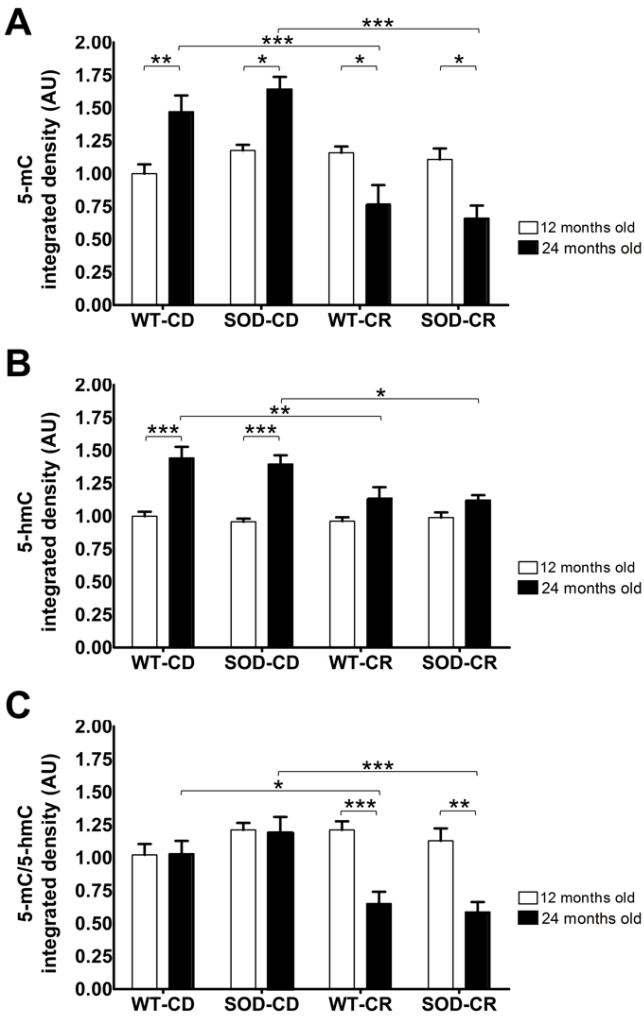

figure 4.

FIGURE 4. Integrated density of *5*-methylcytosine (*5*-mC) (A), *5*-hydroxymethylcytosine (*5*-hmC) (B), and the ratio between *5*-mC and *5*-hmC (C). Presented are the mean and standard error of means. Pooled data of the wild-type control diet (WT-CD), transgenic Cu/Zn super oxide dismutase 1 overexpressing control diet (SOD-CD), wild-type caloric restriction (WT-CR) and Cu/Zn super oxide dismutase 1 overexpressing caloric restriction (SOD-CR) groups are displayed separately at 12 months of age (white bars; WT-CD *5*-mC n = *5*, *5*-hmC n = 6, ratio n = *5*; SOD-CD *5*-mC n = 4, *5*-hmC n = *5*, ratio n = 4; WT-CR *5*-mC n = 6, *5*-hmC n = 6, ratio n = 6; SOD-CR *5*-mC n = 6, *5*-hmC n = 6, ratio n = 6) and at 24 months of age (black bars; WT-CD *5*-mC n = 6, *5*-hmC n = 6, ratio n = 6; SOD-CD *5*-mC n = *5*, *5*-hmC n = *5*, ratio n = *5*; WT-CR *5*-mC n = 6, *5*-hmC n = 6, ratio n = 6; SOD-CR *5*-mC n = 6, *5*-hmC n = 6, ratio n = 6). Indicated in the graph are the pairwise comparisons. AU: arbitrary units. * $p < 0.05$; ** $p < 0.01$; *** $p < 0.001$ (after Bonferroni correction).

4.4.1. Nuclear staining pattern of 5-mC and 5-hmC immunoreactivity

The immunohistochemical staining of 5-mC in mouse cerebellar Purkinje cells was limited to sites of high IR, while 5-hmC was located throughout the nucleus. 5-mC and 5-hmC staining showed only minor colocalization, while 5-mC and DAPI staining showed profound colocalization. This is in line with previous research on the localization of 5-mC and 5-hmC in the nuclei of hippocampal [48, 54] and embryonic stem cells [69] in

the mouse. These studies indicated that 5-mC co-localizes with DAPI, which is thought to primarily mark densely packed heterochromatin, whereas 5-hmC barely co-localizes with either, suggesting that 5-hmC favors the loosely packed euchromatin. This supports the suggested differential roles of 5-hmC and 5-mC in the regulation of gene expression [69, 70, 91]. The localization of 5-hmC to euchromatin, regions that are transcriptionally active, is in line with its suggested generally transcription-promoting function [62, 63], whereas the localization of 5-mC to heterochromatin, regions that are transcriptionally inactive, is in line with its suggested overall transcription-inhibiting function [91]. Note, however, that these suggested roles of 5-hmC and 5-mC are rather general and that how they exactly affect gene transcription is far from clear and appears to be much more complex than initially assumed [42, 67, 92–95]. For example, the effect on gene transcription seems to be gene-specific and highly dependent on the exact location of the DNA modification(s) in that particular gene (e.g. promoter region, intragenic) [73].

4.4.2. 5-mC and 5-hmC levels increase with age

Visual inspection and subsequent semi-quantitative analysis showed an age-related increase of Purkinje cell 5-mC and 5-hmC IR in the CD groups, similar to previous observations in the hippocampus by our group and by others [48, 54, 96]. It, however, remains to be elucidated what the functional impact of these age-related changes in 5-mC and 5-hmC are. For this reason, it is important to investigate which genes are affected by these DNA modifications and how these epigenetic changes impact upon gene expression. A good start would be to look at the genes whose expression is known to alter with age, in general, and more specifically in the cerebellum [1, 97, 98]. Additionally, it might be fruitful to explore the relation between 5-mC and 5-hmC levels and age-related changes in splicing in the cerebellum. Recently, it has been shown that more than a third of brain-specific genes undergo age-related changes in splicing in the cerebellum and other brain areas and that a portion of these changes are region-specific [99].

In order to successfully determine the exact role of 5-mC and 5-hmC in the aging cerebellum it is, however, crucial to further delve into the fundamental mechanisms underlying 5-mC and especially 5-hmC-mediated regulation of gene expression, as these are still far from clear. Studies have shown that in the body, 5-hmC is most abundant in the brain and that, in contrast to 5-mC, it specifically targets portions of the DNA

encoding genes [73]. As mentioned above, it has been suggested that the formation of 5-hmC from 5-mC is an intermediate stage in the process of active DNA demethylation and while 5-mC is thought to repress gene expression, it is argued that 5-hmC enhances gene expression [100, 101]. Observations from DNMT knock-out experiments in cell cultures indicate that 5-hmC can only be generated in the presence of 5-mC, supporting the notion that formation of 5-hmC is a step in DNA demethylation [67]. Evidence for a transcription-promoting role shows that 5-hmC has a relatively low affinity for MBPs 1, 2 and 4, as compared to 5-mC [68, 102]. These proteins can bind to 5-mC and play a pivotal role in its function as a transcriptional repressor. Although these findings seem to point towards an antagonistic role of 5-hmC in relation to 5-mC, recent studies have shown its function to be more complex. For instance, methyl-CpG binding protein (MeCP) 2 appears to have a higher affinity for 5-hmC in the brain [74], and only 5-hmC located in gene bodies, but not in promoter regions, seems to correlate positively with gene expression [73, 78, 96]. Furthermore, high levels of 5-hmC do not appear to be indicative of high levels of DNA demethylation [72]. These findings illustrate that the exact function of 5-hmC might be dependent on cell-type and location in the genome.

How changes in 5-mC and 5-hmC exactly relate to the aging process thus remains elusive. Nevertheless, levels of DNA damage, a factor that is thought to increase with age, do not appear to be related to 5-hmC levels in cerebellar and hippocampal cells, as observed in adult mice [78, 96]. Additionally, some of the genes found to exhibit increasing 5-hmC content with age in the cerebellum, such as those encoding secretases and presenilins, are associated with neurodegeneration [57], while the *APP* promoter region becomes hypomethylated with age [103] and several tumor-suppressor gene promoter regions become hypermethylated [104].

Previous research utilizing the same aging mice cohort as in the present study, focused on the hippocampus and found an age-related increase of 5-hmC, 5-mC and DNMT3A IR [47, 48, 54]. This brain structure is known for its importance for learning and memory, and DNA methylation and demethylation are thought to be critically involved in these processes, as well as synaptic plasticity and neurogenesis [105–107]. Additionally, age-related changes in the hippocampal methylation status of genes linked to memory have been observed [40, 108, 109]. The cerebellum is mostly associated with motor functions and its exact role in regulating cognition remains unclear. Purkinje cells are, however, cardinal for motor learning and recently have been implicated in the spatial navigation system, a cerebello-hippocampal network responsible for goal-directed navigation [10, 11]. Interestingly, spatial navigation is a cognitive process that has recently been shown to deteriorate with aging [110].

Since the age-related increases in cerebellar 5-mC and 5-hmC IR positively correlate, which was previously also found in the hippocampus, it could be that the observed increases in DNA methylation might reflect an increased methylation potential, which in turn could indicate an increased hydroxymethylation potential [54]. There are, however, reports that the methylation potential, which is critically dependent on the levels of the methyl-group donor S-adenosylmethionine (SAM) [111], actually decreases with age [112]. An alternative explanation of how changes in 5-mC and 5-hmC patterns might result in gene expression changes with age would be that an aberrant methylation-hydroxymethylation balance is responsible [54]. Clearly, additional efforts to unveil the precise role of 5-mC and 5-hmC in aging are warranted.

4.4.3. Diet affects age-related changes in 5-mC and 5-hmC

The detection of a significant interaction between diet and age signifies that the age-related increase of 5-mC and 5-hmC IR depended on the diet. This finding is in concert with observations in the hippocampus, where it was found that CR was able to attenuate age-related alterations in 5-mC and 5-hmC IR [48, 54]. Interestingly, the present results seem to suggest that 5-mC levels and the 5-mC:5-hmC ratio may actually decrease with age in the CR groups, whereas 5-hmC levels remain unchanged. This indicates that CR may differentially affect DNA methylation and hydroxymethylation in cerebellar Purkinje cells. The high decrease in 5-mC levels may be a result of either a decrease in DNA methylation, or an increase in active DNA demethylation. CR has been reported to affect DNA methyltransferases DNMT1 and DNMT3A [47, 113], but it remains to be established how CR may promote demethylation in cerebellar Purkinje cells. Although some demethylating agents, such as green tea polyphenols and soybean genistein, are thought to be beneficial in the treatment and prevention of cancer [114], more evidence in the case of aging is still needed.

Despite rigorous investigations into the life-prolonging effects of CR, it remains unknown exactly how CR modulates DNA methylation and hydroxymethylation. Current hypotheses mainly revolve around either a dietary impact of CR on the one-carbon metabolism, which determines the availability of methyl-groups necessary for DNA methylation and hydroxymethylation [115–117], or a chromatin remodeling process involving sirtuins, a class of HDACs that are known to influence life span [28, 118–123].

4.4.4. SOD1 does not affect age-related changes in 5-mC and 5-hmC levels

Despite previous reports on the neuroprotective effects of increased antioxidant levels [21–26], no effect of SOD1 overexpression on the age-related increase of 5-mC and 5-hmC IR was observed, nor was an additional or synergistic effect of combining CR and SOD1 overexpression detected. This finding complies with previous studies employing the same transgenic SOD1 overexpression model, which found that SOD1 overexpression did not affect lifespan and age-related changes in hippocampal volumes, and DNMT3A, 5-mC, 5-hmC and HDAC2 IR [32, 47, 48, 54, 77].

Despite these observations, it could be possible that SOD1 overexpression succeeds in reducing oxidative damage, but that this reduction is independent of epigenetic markers such as those previously investigated (i.e. DNMT3A, 5-mC, 5-hmC and HDAC2). This would, however, be in contrast of previous reports stating that oxidative stress is able to induce epigenetic changes [124, 125]. Alternatively, as suggested previously [48, 54], it might be that the effects of SOD1 overexpression are only observable in other brain regions than hippocampus or cerebellum. The observation that SOD1 overexpression does not appear to have an effect in both the hippocampus and the cerebellum points towards another option, i.e. that the level of SOD1 overexpression was insufficient to incite any detectable alterations, despite the observation that apart from SOD1, these mice also present with increased levels of other antioxidants, including catalase and Mn-SOD [32, 87, 126]. In light of previously reported beneficial results of increasing antioxidant levels, it would be interesting to investigate the effects of other antioxidants, such as glutathione, which have been shown to be pivotally involved in the aging process [126–128].

Curiously, although the genotype may not affect age-related changes in 5-mC and 5-hmC, the significant genotype and diet interaction observed for the ratio between 5-mC and 5-hmC suggests that 5-mC levels are increased in the SOD mice, but only in those that received the CD. This effect should, however, be confirmed in additional studies.

4.4.5. Strengths, limitations, and future perspectives

Strengths of the current study include the strictly controlled conditions the mouse cohort was maintained under, the implementation of established histological techniques that allowed for the qualitative and quantitative analyses of 5-mC and 5-hmC IR at a cellular level and the availability of 12 and 24 months old mice to allow for the detection of age-related alterations. The discovery of 5-hmC as an epigenetic marker very similar to, but functionally distinct from 5-mC spawned a controversy concerning 5-mC detection methods. Apparently, many techniques commonly used to measure 5-mC are unable to distinguish 5-mC from 5-hmC, meaning that reports on 5-mC relying on these techniques should be interpreted with caution [42]. The present study, however, uses highly specific antibodies for the selective detection of 5-hmC, without non-specific interference of 5-mC [54, 69]. Indeed, detection methods involving antibodies have been shown to be specific, while alternative methods, such as classical bisulfite conversion, are unable to distinguish 5-hmC from 5-mC [102, 129–131].

A limitation of the study is that the strictly monitored dietary intake necessitated individual housing [34], and as a consequence confounding effects of social isolation cannot be excluded [132]. The choice to refrain from behavioral and cognitive testing might be pointed out as another limitation. However, since it is known that stress, learning, or other factors connected to testing are able to induce epigenetic changes by themselves, testing was not performed to prevent the introduction of unwanted bias into the dependent variables. Furthermore, a trade-off was made by choosing for an immunohistochemical approach that allows for a cell-type specific semi-quantitative analysis, but is unable to determine absolute 5-mC and 5-hmC levels. Although a cell-type specific analysis was performed, the different cerebellar subregions were grouped together, as not all animals had sections of all the subregions. As it has been reported that the total numbers of Purkinje cells show age related decreases [12], it is possible that the loss of a specific subset of Purkinje cells in the older animals may have influenced the average 5-mC and 5-hmC IR levels as determined in this study. Finally, interpreting age-related alterations in 5-mC and 5-hmC, or other epigenetic markers, should be done with caution, as causal relationships remain elusive. Changes in epigenetic DNA modifications could either contribute to the aging process or be a consequence of it, or both. Future studies, possibly investigating whether the induction of age-related epigenetic changes results in an age-related phenotype, are required to establish such a causal relationship. Additionally, future studies should not only elucidate which genes are regulated by 5-mC and 5-hmC, and how this regulation

is influenced by age, but should do so in a region- and cell-type-specific manner. Furthermore, 5-mC and 5-hmC should preferably not be viewed and investigated as isolated epigenetic mechanisms, but rather as two out of numerous connected components in the complex epigenetic machinery that regulates gene expression. Apart from studies on a molecular, cellular and genetic level, it is also crucial to relate changes on these various levels with behavioral outcomes, such as alterations in cognition and motor skills.

4.5. Conclusion

The findings presented here indicate that mouse cerebellar Purkinje cells display an age-related increase in levels of DNA methylation and hydroxymethylation. It was furthermore shown that these age-related alterations could be mitigated through CR, but that SOD1 overexpression failed to exert any effect on the observed changes during aging. These results are mostly in agreement with previous investigations in the hippocampus, but in addition indicate that CR has a stronger effect on DNA methylation than DNA hydroxymethylation with age, leading to a decreased methylated DNA to hydroxymethylated DNA ratio. This corroborates the notion that widespread epigenetic changes occur during the aging process and that CR is able to strongly impact on these epigenetic mechanisms.

Acknowledgments

Funds have been provided by the Internationale Stichting Alzheimer Onderzoek (ISAO) grants 07551 and 11532 (D.L.A.vdH.), by the ISAO grants 09552 and 13515, and the Netherlands Organization for Scientific Research (NWO), grant 916.11.086 (Veni Award) (B.P.F.R.), by the NWO grant 911.06.086 (C.S.), by a fellowship as part of the NWO grant 022.005.019 and the Maastricht University Medical Centre+ (Koostra Talent Fellowship) (R.L.). We thank H. P. J. Steinbusch and D. Mastroeni for expert technical advice, and K. Kompotis and J. Dela Cruz for assistance during the laboratory experiments. The authors declare that there are no conflicts of interest.

REFERENCES

[1] Berchtold NC, Cribbs DH, Coleman PD, et al. Gene expression changes in the course of normal brain aging are sexually dimorphic. *Proc Natl Acad Sci* 2008; 105: 15605–15610.

[2] Dickstein DL, Kabaso D, Rocher AB, et al. Changes in the structural complexity of the aged brain. *Aging Cell* 2007; 6: 275–84.

[3] Hegde ML, Mantha AK, Hazra TK, et al. Oxidative genome damage and its repair: Implications in aging and neurodegenerative diseases. *Mech Ageing Dev* 2012; 133: 157–168.

[4] Hof PR, Morrison JH. The aging brain: morphomolecular senescence of cortical circuits. *Trends Neurosci* 2004; 27: 607–613.

[5] Lee C-K, Weindruch R, Prolla TA. Gene-expression profile of the ageing brain in mice. *Nat Genet* 2000; 25: 294–297.

[6] Lu T, Pan Y, Kao S-Y, et al. Gene regulation and DNA damage in the ageing human brain. *Nature* 2004; 429: 883–891.

[7] Morrison JH, Hof PR. Life and death of neurons in the aging brain. Science 1997; 278: 412–9.

[8] Rutten BPF, Korr H, Steinbusch HWM, et al. The aging brain: less neurons could be better. *Mech Ageing Dev* 2003; 124: 349–55.

[9] Luebke JI, Weaver CM, Rocher AB, et al. Dendritic vulnerability in neurodegenerative disease: insights from analyses of cortical pyramidal neurons in transgenic mouse models. *Brain Struct Funct* 2010; 214: 181–199.

[10] Rochefort C, Arabo A, André M, et al. Cerebellum shapes hippocampal spatial code. *Science*; http://science.sciencemag.org/content/334/6054/385 (2011, accessed 7

April 2017).

[11] Rochefort C, Lefort J, Rondi-Reig L. The cerebellum: a new key structure in the navigation system. *Front Neural Circuits* 2013; 7: 35.

[12] Rutten BPF, Schmitz C, Gerlach OHH, et al. The aging brain: Accumulation of DNA damage or neuron loss? *Neurobiol Aging* 2007; 28: 91–98.

[13] Wu W, Brickman AM, Luchsinger J, et al. The brain in the age of old: The hippocampal formation is targeted differentially by diseases of late life. *Ann Neurol* 2008; 64: 698–706.

[14] Anderson RM, Shanmuganayagam D, Weindruch R. Caloric restriction and aging: studies in mice and monkeys. *Toxicol Pathol* 2009; 37: 47–51.

[15] Colman RJ, Anderson RM, Johnson SC, et al. Caloric restriction delays disease onset and mortality in rhesus monkeys. *Science* 2009; 325: 201–4.

[16] Devore EE, Grodstein F, van Rooij FJA, et al. Dietary antioxidants and long-term risk of dementia. *Arch Neurol* 2010; 67: 819–25.

[17] Fontana L, Partridge L, Longo VD. Extending healthy life span--from yeast to humans. *Science* 2010; 328: 321–326.

[18] Joseph J, Cole G, Head E, et al. Nutrition, Brain aging, and neurodegeneration. *J Neurosci*; http://www.jneurosci.org/content/29/41/12795 (2009, accessed 7 April 2017).

[19] Llewellyn DJ, Lang IA, Langa KM, et al. Vitamin D and risk of cognitive decline in elderly persons. *Arch Intern Med* 2010; 170: 1135.

[20] Rutten BPF, Steinbusch HWM, Korr H, et al. Antioxidants and Alzheimer's disease: from bench to bedside (and back again). *Curr Opin Clin Nutr Metab Care* 2002; 5: 645–51.

[21] Cardozo-Pelaez F, Song S, Parthasarathy A, et al. Attenuation of age-dependent oxidative damage to DNA and protein in brainstem of Tg Cu/Zn SOD mice. *Neurobiol Aging* 1998; 19: 311–6.

[22] Borg J, Chereul E. Differential MRI patterns of brain atrophy in double or single transgenic mice for APP and/or SOD. *J Neurosci Res* 2008; 86: 3275–3284.

[23] Borg J, London J. Copper/zinc superoxide dismutase overexpression promotes survival of cortical neurons exposed to neurotoxins *in vitro*. *J Neurosci Res* 2002; 70: 180–189.

[24] Cadet JL, Sheng P, Ali S, et al. Attenuation of methamphetamine-induced neurotoxicity in copper/zinc superoxide dismutase transgenic mice. *J Neurochem* 1994; 62: 380–3.

[25] Chan PH, Epstein CJ, Kinouchi H, et al. SOD-1 transgenic mice as a model for studies of neuroprotection in stroke and brain trauma. Ann N Y Acad Sci 1994; 738: 93–103.

[26] Sha SH, Zajic G, Epstein CJ, et al. Overexpression of copper/zinc-superoxide dismutase protects from kanamycin-induced hearing loss. *Audiol Neurootol* 2001; 6: 117–23.

[27] Adams MM, Shi L, Linville MC, et al. Caloric restriction and age affect synaptic proteins in hippocampal CA3 and spatial learning ability. *Exp Neurol* 2008; 211: 141–149.

[28] Bordone L, Guarente L. Calorie restriction, SIRT1 and metabolism: understanding longevity. *Nat Rev Mol Cell Biol* 2005; 6: 298–305.

[29] Levenson CW, Rich NJ. Eat less, live longer? New insights into the role of caloric restriction in the brain. *Nutr Rev* 2007; 65: 412–5.

[30] Mattson MP, Chan SL, Duan W. Modification of brain aging and neurodegenerative disorders by genes, diet, and behavior. *Physiol Rev* 2002; 82: 637–672.

[31] Mattson MP, Duan W, Chan SL, et al. Neuroprotective and neurorestorative signal transduction mechanisms in brain aging: modification by genes, diet and behavior. *Neurobiol Aging* 2002; 23: 695–705.

[32] Rutten BPF, Brasnjevic I, Steinbusch HWM, et al. Caloric restriction and aging but not overexpression of SOD1 affect hippocampal volumes in mice. *Mech Ageing Dev* 2010; 131: 574–579.

[33] Sohal RS, Weindruch R. Oxidative stress, caloric restriction, and aging. Science 1996; 273: 59–63.

[34] Weindruch R, Walford RL, Fligiel S, et al. The retardation of aging in mice by dietary restriction: longevity, cancer, immunity and lifetime energy intake. *J Nutr* 1986; 116: 641–54.

[35] Lee S-H, Min K-J. Caloric restriction and its mimetics. *BMB Rep* 2013; 46: 181–7.

[36] Calvanese V, Lara E, Kahn A, et al. The role of epigenetics in aging and age-related diseases. *Ageing Res Rev* 2009; 8: 268–276.

[37] Chouliaras L, Rutten BPF, Kenis G, et al. Epigenetic regulation in the pathophysiology of Alzheimer's disease. *Prog Neurobiol* 2010; 90: 498–510.

[38] Day JJ, Sweatt JD. DNA methylation and memory formation. *Nat Neurosci* 2010; 13: 1319–1323.

[39] Peleg S, Sananbenesi F, Zovoilis A, et al. Altered histone acetylation is associated with age-dependent memory impairment in mice.

Science 2010; 328: 753–6.

[40] Penner MR, Roth TL, Barnes CA, et al. An epigenetic hypothesis of aging-related cognitive dysfunction. *Front Aging Neurosci* 2010; 2: 9.

[41] Goldberg AD, Allis CD, Bernstein E. Epigenetics: a landscape takes shape. *Cell* 2007; 128: 635–638.

[42] van den Hove DLA, Chouliaras L, Rutten BPF. The role of 5-hydroxymethylcytosine in aging and Alzheimer's disease: current status and prospects for future studies. *Curr Alzheimer Res* 2012; 9: 545–9.

[43] Day JJ, Sweatt JD. Cognitive neuroepigenetics: A role for epigenetic mechanisms in learning and memory. *Neurobiol Learn Mem* 2011; 96: 2–12.

[44] Fitzsimons CP, van Bodegraven E, Schouten M, et al. Epigenetic regulation of adult neural stem cells: implications for Alzheimer's disease. *Mol Neurodegener* 2014; 9: 25.

[45] Serrano L, Vazquez BN, Tischfield J. Chromatin structure, pluripotency and differentiation. *Exp Biol Med* 2013; 238: 259–270.

[46] Ben-Avraham D, Muzumdar RH, Atzmon G. Epigenetic genome-wide association methylation in aging and longevity. *Epigenomics* 2012; 4: 503–509.

[47] Chouliaras L, van den Hove DLA, Kenis G, et al. Caloric restriction attenuates age-related changes of DNA methyltransferase 3a in mouse hippocampus. *Brain Behav Immun* 2011; 25: 616–623.

[48] Chouliaras L, van den Hove DLA, Kenis G, et al. Prevention of age-related changes in hippocampal levels of 5-methylcytidine by caloric restriction. *Neurobiol Aging* 2012; 33: 1672–81.

[49] Fraga MF, Esteller M. Epigenetics and aging: the targets and the marks. *Trends Genet* 2007; 23: 413–418.

[50] Hernandez DG, Nalls MA, Gibbs JR, et al. Distinct DNA methylation changes highly correlated with chronological age in the human brain. *Hum Mol Genet* 2011; 20: 1164–1172.

[51] Lunnon K, Smith R, Hannon E, et al. Methylomic profiling implicates cortical deregulation of *ANK1* in Alzheimer's disease. *Nat Neurosci* 2014; 17: 1164–1170.

[52] Mastroeni D, Grover A, Delvaux E, et al. Epigenetic changes in Alzheimer's disease: Decrements in DNA methylation. *Neurobiol Aging* 2010; 31: 2025–2037.

[53] Thompson RF, Atzmon G, Gheorghe C, et al. Tissue-specific dysregulation of DNA methylation in aging. *Aging Cell* 2010; 9: 506–518.

[54] Chouliaras L, van den Hove DLA, Kenis G, et al. Age-related increase in levels of 5-hydroxymethylcytosine in mouse hippocampus is prevented by caloric restriction. *Curr Alzheimer Res* 2012; 9: 536–44.

[55] Condliffe D, Wong A, Troakes C, et al. Cross-region reduction in 5-hydroxymethylcytosine in Alzheimer's disease brain. *Neurobiol Aging* 2014; 35: 1850–1854.

[56] Coppieters N, Dieriks B V, Lill C, et al. Global changes in DNA methylation and hydroxymethylation in Alzheimer's disease human brain. *Neurobiol Aging* 2014; 35: 1334–1344.

[57] Song C-X, Szulwach KE, Fu Y, et al. Selective chemical labeling reveals the genome-wide distribution of 5-hydroxymethylcytosine. *Nat Biotechnol* 2011; 29: 68–72.

[58] Bestor TH. The DNA methyltransferases of mammals. *Hum Mol Genet* 2000; 9: 2395–402.

[59] Handel AE, Ebers GC, Ramagopalan S V. Epigenetics: molecular mechanisms and implications for disease. *Trends Mol Med* 2010; 16: 7–16.

[60] Lan J, Hua S, He X, et al. DNA methyltransferases and methyl-binding proteins of mammals. *Acta Biochim Biophys Sin* (Shanghai) 2010; 42: 243–52.

[61] Razin A, Riggs AD. DNA methylation and gene function. *Science* 1980; 210: 604–10.

[62] Tahiliani M, Koh KP, Shen Y, et al. Conversion of 5-methylcytosine to 5-hydroxymethylcytosine in mammalian DNA by MLL partner TET1. *Science* 2009; 324: 930–935.

[63] Ito S, D'Alessio AC, Taranova O V., et al. Role of Tet proteins in 5-mC to 5-hmC conversion, ES-cell self-renewal and inner cell mass specification. *Nature* 2010; 466: 1129–1133.

[64] Ito S, Shen L, Dai Q, et al. Tet proteins can convert 5-methylcytosine to 5-formylcytosine and 5-carboxylcytosine. *Science*; http://science.sciencemag.org/content/333/6047/1300 (2011, accessed 3 April 2017).

[65] Raiber E-A, Beraldi D, Ficz G, et al. Genome-wide distribution of 5-formylcytosine in embryonic stem cells is associated with transcription and depends on thymine DNA glycosylase. *Genome Biol* 2012; 13: R69.

[66] Song C-X, He C. Potential functional roles of DNA demethylation intermediates. *Trends Biochem Sci* 2013; 38: 480–484.

[67] Williams K, Christensen J, Pedersen MT, et al. TET1 and hydroxymethylcytosine in transcription and DNA methylation fidelity. *Nature* 2011; 473: 343–348.

[68] Valinluck V, Tsai H-H, Rogstad DK, et al. Oxidative damage to methyl-CpG sequences inhibits the

binding of the methyl-CpG binding domain (MBD) of methyl-CpG binding protein 2 (MeCP2). *Nucleic Acids Res* 2004; 32: 4100–4108.

[69] Ficz G, Branco MR, Seisenberger S, et al. Dynamic regulation of 5-hydroxymethylcytosine in mouse ES cells and during differentiation. *Nature* 2011; 473: 398–402.

[70] Münzel M, Globisch D, Carell T. 5-Hydroxymethylcytosine, the sixth base of the genome. *Angew Chemie Int Ed* 2011; 50: 6460–6468.

[71] Guo JU, Su Y, Shin JH, et al. Distribution, recognition and regulation of non-CpG methylation in the adult mammalian brain. *Nat Neurosci* 2013; 17: 215–222.

[72] Hahn MA, Qiu R, Wu X, et al. Dynamics of 5-hydroxymethylcytosine and chromatin marks in mammalian neurogenesis. *Cell Rep* 2013; 3: 291–300.

[73] Jin S-G, Wu X, Li AX, et al. Genomic mapping of 5-hydroxymethylcytosine in the human brain. *Nucleic Acids Res* 2011; 39: 5015–5024.

[74] Mellén M, Ayata P, Dewell S, et al. MeCP2 binds to 5-hmC enriched within active genes and accessible chromatin in the nervous system. *Cell* 2012; 151: 1417–1430.

[75] Siegmund KD, Connor CM, Campan M, et al. DNA methylation in the human cerebral cortex is dynamically regulated throughout the life span and involves differentiated neurons. *PLoS One* 2007; 2: e895.

[76] Tan L, Shi YG. Tet family proteins and 5-hydroxymethylcytosine in development and disease. *Development* 2012; 139: 1895–1902.

[77] Chouliaras L, van den Hove DLA, Kenis G, et al. Histone deacetylase 2 in the mouse hippocampus: attenuation of age-related increase by caloric restriction. *Curr Alzheimer Res* 2013; 10: 868–76.

[78] Kriaucionis S, Heintz N. The nuclear DNA base 5-hydroxymethylcytosine is present in Purkinje neurons and the brain. *Science* 2009; 324: 929–30.

[79] Penn NW, Suwalski R, O'Riley C, et al. The presence of 5-hydroxymethylcytosine in animal deoxyribonucleic acid. *Biochem J* 1972; 126: 781–90.

[80] Lange W. Cell number and cell density in the cerebellar cortex of man and some other mammals. *Cell Tissue Res* 1975; 157: 115–24.

[81] Palay SL, Chan-Palay V. Cerebellar cortex: cytology and organization. https://books.google.nl/books?id=ZVTmCAAAQBAJ&dq=Cerebellar+cortex:+cytology+and+organization&lr=&source=gbs_navlinks_s (1974, accessed 7 April 2017).

[82] Chan-Palay V, Nilaver G, Palay SL, et al. Chemical heterogeneity in cerebellar Purkinje cells: existence and coexistence of glutamic acid decarboxylase-like and motilin-like immunoreactivities. *Proc Natl Acad Sci U S A* 1981; 78: 7787–91.

[83] Kern JK, Jones AM. Evidence of toxicity, oxidative stress, and neuronal insult in autism. *J Toxicol Environ Heal Part B* 2006; 9: 485–499.

[84] Brock B, Basha R, DiPalma K, et al. Co-localization and distribution of cerebral APP and SP1 and its relationship to amyloidogenesis. *J Alzheimers Dis* 2008; 13: 71–80.

[85] Fukutani Y, Cairns NJ, Rossor MN, et al. Purkinje cell loss and astrocytosis in the cerebellum in familial and sporadic Alzheimer's disease. *Neurosci Lett* 1996; 214: 33–36.

[86] Zhang C, Zhu Q, Hua T. Aging of cerebellar Purkinje cells. *Cell Tissue Res* 2010; 341: 341–7.

[87] Epstein CJ, Avraham KB, Lovett M, et al. Transgenic mice with increased Cu/Zn-superoxide dismutase activity: animal model of dosage effects in Down syndrome. *Proc Natl Acad Sci U S A* 1987; 84: 8044–8.

[88] Globisch D, Münzel M, Müller M, et al. Tissue distribution of 5-hydroxymethylcytosine and search for active demethylation intermediates. *PLoS One*; 5. Epub ahead of print 2010. DOI: 10.1371/journal.pone.0015367.

[89] Franklin KBJ, Paxinos G. Paxinos and Franklin's The mouse brain in stereotaxic coordinates. 2012.

[90] Schindelin J, Arganda-Carreras I, Frise E, et al. Fiji: an open-source platform for biological-image analysis. *Nat Methods* 2012; 9: 676–682.

[91] Miller CA, Sweatt JD, Park A, et al. Covalent modification of DNA regulates memory formation. *Neuron* 2007; 53: 857–69.

[92] Bhutani N, Burns DM, Blau HM. DNA demethylation dynamics. *Cell* 2011; 146: 866–872.

[93] Pastor WA, Pape UJ, Huang Y, et al. Genome-wide mapping of 5-hydroxymethylcytosine in embryonic stem cells. *Nature* 2011; 473: 394–397.

[94] Wu H, D'Alessio AC, Ito S, et al. Dual functions of Tet1 in transcriptional regulation in mouse embryonic stem cells. *Nature* 2011; 473: 389–393.

[95] Xu Y, Wu F, Tan L, et al. Genome-wide Regulation of 5-hmC, 5-mC, and Gene Expression by Tet1 Hydroxylase in Mouse Embryonic Stem Cells. *Mol Cell* 2011; 42: 451–464.

[96] Münzel M, Globisch D, Brückl T, et al. Quantification of the sixth DNA base hydroxymethylcyto-

sine in the brain. *Angew Chemie Int Ed* 2010; 49: 5375–5377.

[97] Fraser HB, Khaitovich P, Plotkin JB, et al. Aging and gene expression in the primate brain. *PLoS Biol* 2005; 3: e274.

[98] Park S-K, Kim K, Page GP, et al. Gene expression profiling of aging in multiple mouse strains: identification of aging biomarkers and impact of dietary antioxidants. *Aging Cell* 2009; 8: 484–495.

[99] Mazin P, Xiong J, Liu X, et al. Widespread splicing changes in human brain development and aging. *Mol Syst Biol* 2014; 9: 633–633.

[100] Guo JU, Su Y, Zhong C, et al. Hydroxylation of 5-methylcytosine by TET1 promotes active DNA demethylation in the adult brain. *Cell* 2011; 145: 423–434.

[101] Valinluck V, Sowers LC. Endogenous cytosine damage products alter the site selectivity of human DNA maintenance methyltransferase DNMT1. *Cancer Res* 2007; 67: 946–950.

[102] Jin S-G, Kadam S, Pfeifer GP. Examination of the specificity of DNA methylation profiling techniques towards 5-methylcytosine and 5-hydroxymethylcytosine. *Nucleic Acids Res* 2010; 38: e125–e125.

[103] Tohgi H, Utsugisawa K, Nagane Y, et al. The methylation status of cytosines in a tau gene promoter region alters with age to downregulate transcriptional activity in human cerebral cortex. Epub ahead of print 1999. DOI: 10.1016/S0304-3940(99)00731-4.

[104] Madrigano J, Baccarelli AA, Mittleman MA, et al. Aging and epigenetics: Longitudinal changes in gene-specific DNA methylation. *Epigenetics* 2012; 7: 63–70.

[105] Feng J, Chang H, Li E, et al. Dynamic expression of *de novo* DNA methyltransferases Dnmt3a and Dnmt3b in the central nervous system. *J Neurosci Res* 2005; 79: 734–746.

[106] Feng J, Zhou Y, Campbell SL, et al. Dnmt1 and Dnmt3a maintain DNA methylation and regulate synaptic function in adult forebrain neurons. *Nat Neurosci* 2010; 13: 423–430.

[107] Wu H, Coskun V, Tao J, et al. Dnmt3a-dependent nonpromoter DNA methylation facilitates transcription of neurogenic genes. *Science*; http://science.sciencemag.org/content/329/5990/444 (2010, accessed 4 April 2017).

[108] Mugatroyd C, Wu Y, Bockmühl Y, et al. The Janus face of DNA methylation in aging. *Aging* (Albany NY) 2010; 2: 107–110.

[109] Penner MR, Roth TL, Chawla MK, et al. Age-related changes in Arc transcription and DNA methylation within the hippocampus. *Neurobiol Aging* 2011; 32: 2198–2210.

[110] Gazova I, Vlcek K, Laczó J, et al. Spatial navigation—a unique window into physiological and pathological aging. *Front Aging Neurosci* 2012; 4: 16.

[111] Obeid R, Schadt A, Dillmann U, et al. Methylation status and neurodegenerative markers in Parkinson disease. *Clin Chem*; http://clinchem.aaccjnls.org/content/55/10/1852 (2009, accessed 4 April 2017).

[112] Hooijmans CR, Blom HJ, Oppenraaij-Emmerzaal D, et al. S-adenosylmethionine and S-adenosylhomocysteine levels in the aging brain of APP/PS1 Alzheimer mice. *Neurol Sci* 2009; 30: 439–445.

[113] Li Y, Liu L, Tollefsbol TO. Glucose restriction can extend normal cell lifespan and impair precancerous cell growth through epigenetic control of hTERT and p16 expression. *FASEB J* 2010; 24: 1442–1453.

[114] Li Y, Tollefsbol TO. Impact on DNA methylation in cancer prevention and therapy by bioactive dietary components. *Curr Med Chem* 2010; 17: 2141–51.

[115] Fuso A, Nicolia V, Cavallaro RA, et al. DNA methylase and demethylase activities are modulated by one-carbon metabolism in Alzheimer's disease models. *J Nutr Biochem* 2011; 22: 242–251.

[116] Fuso A, Seminara L, Cavallaro RA, et al. S-adenosylmethionine/homocysteine cycle alterations modify DNA methylation status with consequent deregulation of PS1 and BACE and beta-amyloid production. *Mol Cell Neurosci* 2005; 28: 195–204.

[117] Sugden C. One-carbon metabolism in psychiatric illness. *Nutr Res Rev* 2006; 19: 117.

[118] Blander G, Guarente L. The Sir2 Family of Protein Deacetylases. *Annu Rev Biochem* 2004; 73: 417–435.

[119] Cantó C, Auwerx J. Caloric restriction, SIRT1 and longevity. *Trends Endocrinol Metab* 2009; 20: 325–331.

[120] Chen D, Bruno J, Easlon E, et al. Tissue-specific regulation of SIRT1 by calorie restriction. *Genes Dev* 2008; 22: 1753–1757.

[121] Chen D, Guarente L. SIR2: a potential target for calorie restriction mimetics. *Trends Mol Med* 2007; 13: 64–71.

[122] Chen D, Steele AD, Lindquist S, et al. Increase in activity during calorie restriction requires Sirt1. *Science*; http://science.sciencemag.org/content/310/5754/1641 (2005, accessed 7 April 2017).

[123] Dillin A, Kelly JW.

The Yin-Yang of Sirtuins. *Science*; http://science.sciencemag.org/content/317/5837/461 (2007, accessed 7 April 2017).

[124] Bhusari SS, Dobosy JR, Fu V, et al. Superoxide dismutase 1 knockdown induces oxidative stress and DNA methylation loss in the prostate. *Epigenetics* 2010; 5: 402–9.

[125] Davis CD, Uthus EO. DNA methylation, cancer susceptibility, and nutrient interactions. *Exp Biol Med* (Maywood) 2004; 229: 988–95.

[126] Przedborski S, Jackson-Lewis V, Kostic V, et al. Superoxide dismutase, catalase, and glutathione peroxidase activities in copper/zinc-superoxide dismutase transgenic mice. *J Neurochem* 1992; 58: 1760–7.

[127] Cerutti P, Ghosh R, Oya Y, et al. The role of the cellular antioxidant defense in oxidant carcinogenesis. *Environ Health Perspect* 1994; 123–9.

[128] Rebrin I, Sohal RS. Pro-oxidant shift in glutathione redox state during aging. *Adv Drug Deliv Rev* 2008; 60: 1545–1552.

[129] Hayatsu H, Shiragami M. Reaction of bisulfite with the 5-hydroxymethyl group in pyrimidines and in phage DNAs. *Biochemistry* 1979; 18: 632–7.

[130] Huang Y, Pastor WA, Shen Y, et al. The behaviour of 5-hydroxymethylcytosine in bisulfite sequencing. *PLoS One* 2010; 5: e8888.

[131] Nestor C, Ruzov A, Meehan R, et al. Enzymatic approaches and bisulfite sequencing cannot distinguish between 5-methylcytosine and 5-hydroxymethylcytosine in DNA. *Biotechniques* 2010; 48: 317–319.

[132] Miura H, Qiao H, Ohta T. Influence of aging and social isolation on changes in brain monoamine turnover and biosynthesis of rats elicited by novelty stress. *Synapse* 2002; 46: 116–124.

AGE-RELATED EPIGENETIC CHANGES IN HIPPOCAMPAL SUBREGIONS OF FOUR ANIMAL MODELS OF ALZHEIMER'S DISEASE

ROY **LARDENOIJE**[A,B], DANIËL L.A. **VAN DEN HOVE**[B,C], MONIQUE **HAVERMANS**[B], ANNE VAN **CASTEREN**[B], KEVIN X. **LE**[A], ROBERTA **PALMOUR**[D,E], CYNTHIA A. **LEMERE**[A,*], BART P.F. **RUTTEN**[B,*]

[A]ANN ROMNEY CENTER FOR NEUROLOGIC DISEASES, DEPARTMENT OF NEUROLOGY, BRIGHAM AND WOMEN'S HOSPITAL, HARVARD MEDICAL SCHOOL, USA
[B]SCHOOL FOR MENTAL HEALTH AND NEUROSCIENCE (MHENS), DEPARTMENT OF PSYCHIATRY AND NEUROPSYCHOLOGY, MAASTRICHT UNIVERSITY, THE NETHERLANDS
[C]LABORATORY OF TRANSLATIONAL NEUROSCIENCE, DEPARTMENT OF PSYCHIATRY, PSYCHOSOMATICS AND PSYCHOTHERAPY, UNIVERSITY OF WUERZBURG, GERMANY
[D]BEHAVIORAL SCIENCE FOUNDATION, ST. KITTS AND NEVIS, EASTERN CARIBBEAN
[E]MCGILL UNIVERSITY FACULTY OF MEDICINE, MONTREAL, QUEBEC, CANADA
*THESE AUTHORS CONTRIBUTED EQUALLY TO THIS WORK.

Abstract

Both aging and Alzheimer's disease (AD) are associated with widespread epigenetic changes, with most evidence suggesting global hypomethylation in AD. It is, however, unclear how these age-related epigenetic changes are linked to molecular aberrations as expressed in animal models of AD. Here, we investigated age-related changes of epigenetic markers of DNA methylation and hydroxymethylation in a range of animal models of AD, and their correlations with amyloid plaque load. Three transgenic mouse models, including the J20, APP/PS1dE9 and 3xTg-AD models, as well as Caribbean vervets (a non-transgenic non-human primate model of AD) were investigated. In the J20 mouse model, an age-related decrease in DNA methylation was found in the dentate gyrus (DG) and a decrease in the ratio between DNA methylation and hydroxymethylation was found in the DG and cornu ammonis (CA) 3. In the 3xTg-AD mice, an age-related increase in DNA methylation was found in the DG and CA1-2. No significant age-related alterations were found in the APP/PS1dE9 mice and non-human primate model. Hippocampal plaque load showed a negative correlation with DNA methylation in the J20 model, and a positive correlation with DNA methylation in the 3xTg-AD model. Thus, only the J20 model showed an age-related reduction in global DNA methylation, while DNA hypermethylation was observed in the 3xTg-AD model. Given these differences between animal models, future studies are needed to further elucidate the contribution of different AD-related genetic variation to age-related epigenetic changes.

KEYWORDS: Alzheimer's disease; aging; hippocampus; DNA methylation; DNA hydroxymethylation; DNA methyltransferase; animal models

5.1. Introduction

Alzheimer's disease (AD) is a complex age-related neurodegenerative disorder and the most common form of dementia [1], for which presently no effective treatment exists [2, 3]. Although recent studies indicate that the widespread neurodegeneration in the AD brain may be initiated in brainstem regions [4], the development of cognitive impairment is associated with degeneration of the entorhinal cortex and hippocampus [5]. The exact molecular mechanisms underlying the neurodegeneration in AD remain unclear. Nevertheless, there are two pathological hallmarks; extracellular neuritic plaques and intracellular neurofibrillary tangles, which are thought to play a pivotal role in the progression of AD and that are currently the basis of a definitive postmortem diagnosis [6, 7]. These protein aggregates mainly consist of amyloid-β (Aβ) and hyperphosphorylated tau, respectively. Genetic studies have offered important insights and have confirmed the importance of Aβ, especially in the development of familial forms of AD, by identifying mutations in the amyloid precursor protein (APP) and presenilin (PS) genes that are associated with familial AD [8].

A growing body of evidence indicates that epigenetics may play a crucial role in complex age-related neurodegenerative diseases such as AD [9–11]. Epigenetic processes dynamically regulate gene expression at both the transcriptional and translational level [12]. They are thought to be able to translate environmental exposures into alterations in gene expression [13]. In particular, DNA methylation has received attention in the context of AD, and DNA hydroxymethylation has more recently also been increasingly studied [9, 14, 15]. Our group and others have found that with normal aging, region-specific DNA methylation and hydroxymethylation, as well as DNA methyltransferase (DNMT) 3A levels rise [16–22]. In AD, however, overall DNA methylation and hydroxymethylation levels appear to be lowered [23–25]. Depending on the brain region, and likely also methodological differences (e.g. concerning tissue processing), there are, however, also conflicting reports, showing no changes in DNA methylation levels between AD patients and controls [25], or increased DNA methylation and hydroxymethylation levels [26]. Recent studies employing techniques such as Illumina's HumanMethylation450 BeadChip assay have provided further insights beyond global changes in epigenetic markers [27, 28]. These epigenome-wide association studies on homogenates of brain samples can help to identify important new candidate genes that, through altered epigenetic regulation, may play a role in the pathogenesis of AD.

Many studies investigating epigenetic changes related to AD have studied differences between postmortem brain tissue from diseased and control

cases. To go beyond associations and elucidate the exact functional and potentially causal role of epigenetic dysregulation in the course of AD, live model systems are required. To this end, a plethora of AD animal models have been established, including many transgenic rodent models that overexpress mutated human genes that have been associated with rare forms of familial AD [29], but also non-human primate models that naturally develop Aβ plaque pathology have been used [30, 31]. While these animal models capture some of the molecular, physiological, or behavioral aspects of AD, none of the animal models display the full complexity of AD [32]. Most animal models have been characterized based on classical hallmarks of AD, such as plaque development and cognitive impairment, but there are currently no reports comparing different animal models of AD on an epigenetic level. The aim of the present study was therefore to investigate age-related changes in epigenetic markers related to DNA methylation (5-methylcytosine [5-mC] and DNMT3A) and DNA hydroxymethylation (5-hydroxymethylcytosine [5-hmC]), in three genetically different transgenic mouse models of AD and a non-human primate model that naturally develops Aβ plaque pathology [30, 33]. In addition, correlations between 5-mC, 5-hmC, and DNMT3A immunoreactivity (IR) and amyloid plaque load were assessed, and compared with findings in humans and other studies related to epigenetic dysregulation in AD.

5.2. Materials and methods

5.2.1. Animal models

For this study, 3 transgenic mouse models of AD were used, including J20 mice on a C57BL6 background [34], APP/PS1dE9 mice on a C57BL6J background [35, 36], and 3xTg-AD mice on a C57BL6 background [37]. J20 mice harbor the mutated human APP gene (APPK670N/M671L, V717F), APP/PS1dE9 mice express both mutated humanized APP and human PS1 (APPK595N/M596LPS1 deletion of exon 9), and 3xTg-AD mice express 3 mutated human genes, APP, PS1, and tau (APPK670N/M671L, PS1M146V, TauP301L). In addition to these transgenic mouse models, archived fixed brain tissue from 12 Caribbean vervets (*Chlorocebus sabaeuss*; 12.2 – 32 years of age) was used (Behavioral Science Foundation, St. Kitts) [33]. See Table 1 for additional information about the used animal models. The Harvard Medical Area Standing Committee approved of the use of mice at Brigham and Women's Hospital, which is in line with all state and federal regulations. Vervet brain tissue was retrieved following protocols approved by the Behavioral Science Foundation Animal Care Committee acting under the auspices of the Canadian Council on Animal Care.

table 1.

Animal model	Mutations	Promotor	Start plaque deposition (region)	Start cognitive deficits	Age	References
J20	APPK670N/ M671L, V717F	*PDGF*	5-7 months (hippocampus, neocortex)	1-2 months	4 months (n = 4) 8 months (n = 4) 16 months (n = 3) 24 months (n = 2)	[34, 38]
APP/PS1dE9	APPK595N/ M596LPS1 deletion of exon 9	*mPrP*	6 months (hippocampus, cortex)	4 months	6 months (n = 4) 16 months (n = 1) 17 months (n = 1) 18 months (n = 1) 23 months (n = 1) 27 months (n = 1)	[36, 39, 40]
3xTg-AD	APPK670N/ M671L, PS1M146V, TauP301L	*mThy-1*	6 months (frontal cortex)*	4 months*	5 months (n = 4) 14 months (n = 2) 17 months (n = 1) 27 months (n = 3)	[37, 41]
Caribbean vervet	NA	NA	15 years (hippocampus) †	15 years †	12.2 years (n = 1) 14 years (n = 1) 14.9 years (n = 1) 15 years (n = 2) 16.4 years (n = 1) 17 years (n = 2) 19 years (n = 1) 24 years (n = 1) 27.4 years (n = 1) 32 years (n = 1)	This article (Supplementary Figure 9)

TABLE 1. Overview of investigated animal models.

*The 3xTg-AD mice used in this paper appeared to have a 2-3 month delay in Alzheimer's disease pathology compared to previously published reports, possibly due to a loss of transgene copies with successive breeding (see https://www.jax.org/strain/004807).

†This was the youngest vervet with plaques and cognitive impairment, but note that while generally plaque deposition increases with age, there is no clear relationship between age, onset of plaque pathology, and cognitive decline (see Supplementary Figure 9).

NA, not applicable.

5.2.2. Tissue preparation

After anesthetization via CO_2 inhalation, mice were perfused with 20 mL ice-cold saline. The brains were then removed and hemisected, fixed in 10% formalin or 4% paraformaldehyde for 2 to 24 hours, paraffin-embedded, and further sectioned into 10 μm-thick slices. The archived non-human primate brain tissue was formalin-fixed for months to several years and was divided into nine rostrocaudal regions, paraffin-embedded and further cut into 10 μm-thick coronal sections.

5.2.3. Immunohisto-chemistry

10 micron-thick serial sagittal mouse brain sections or coronal vervet brain sections were used for immunohistochemistry. All steps were performed at room temperature unless specified otherwise. Sections were first deparaffinized in Histo-Clear (National Diagnostics, Atlanta, GA) and rehydrated in a series of decreasing ethanol solutions, ending with deionized water. Hydrogen peroxide (0.3%) diluted in methanol was used to quench endogenous peroxidase for 10 minutes. To unmask antigen-binding sites, antigen retrieval was performed with BioGenex citrate buffer (BioGenex, San Ramon, CA), keeping the solution around boiling temperature for 5 minutes in the microwave. Aβ42 staining on the vervet tissue required incubating the sections in 88% formic acid

for 10 minutes. The sections were washed with deionized water for 10 minutes and incubated in blocking solution for 20 minutes. The blocking solution consisted of 10% serum dissolved in Tris-buffered saline, with serum from the same species as the secondary antibody host. The sections were subsequently incubated overnight with primary antibody, at 4°C. The following antibodies were used: a mouse monoclonal anti-5-mC antibody (1:1000 dilution for mouse sections and 1:500 for vervet sections; GenWay Biotech Inc., San Diego, CA), a rabbit polyclonal anti-5-hmC antiserum (1:10,000 dilution; Active Motif, Carlsbad, CA), a rabbit polyclonal anti-DNMT3A antibody (1:200 dilution; Santa Cruz Biotechnology, Dallas, TX), a general monoclonal IgG1 anti-Aβ antibody for staining mouse sections (3A1; 1:1000 dilution, kindly provided by Dr. Brian O`Naullain at the Ann Romney Center for Neurologic Diseases, Boston, MA), and a mouse monoclonal IgG1 anti-Aβ42 antibody for staining vervet sections (1:500 dilution; BioLegend, San Diego, CA). After another wash with deionized water, the slides were incubated with biotinylated secondary antibodies for 30 minutes. Secondary antibodies included a horse anti-mouse secondary antibody (Vector Laboratories, Burlingame, CA) for the 5-mC antibody, a goat anti-rabbit secondary antibody (Vector Laboratories) for the 5-hmC and DNMT3A antibodies, a goat anti-mouse secondary antibody (Vector Laboratories) for 3A1, and a goat anti-mouse antibody (SouthernBiotech, Birmingham, AL) for Aβ42. The VectorElite horseradish peroxidase ABC kit (Vector Laboratories), with 3,3'-diaminobenzidine tetrahydrochloride (DAB; Sigma-Aldrich, St. Louis, MO) as chromogen, was used to visualize IR. For each staining run, omission of the primary antibody was included as a negative control, which consistently showed no staining (data not shown).

5.2.4. Analysis of 5-mC, 5-hmC and DNMT3A immunoreactivity, and plaque load

For each staining, 3 sagittal hippocampal sections per mouse and 2 coronal hippocampal sections per vervet were examined at approximately equidistant planes. For the IR analysis of 5-mC, 5-hmC, and DNMT3A stainings, images were captured from hippocampal subregions, including 4 images of the dentate gyrus (DG), 2 of the cornu ammonis (CA) 3, and 2 of the CA1-2 (Supplementary Figure 1), using the 20X objective of a BX50 brightfield microscope (Olympus, Tokyo, Japan) in conjunction with a QIcam digital camera (QImaging, Surrey, BC, Canada). The IR

in the regions of interest (DG, CA3, and CA1-2) was analyzed in the images of the hippocampal subregions using ImageJ (version 1.48v, Wayne Rasband, National Institutes of Health, Bethesda, Maryland, USA). For each image, the mean grey value of the region of interest (ROI) was measured after delineating the ROI in the image and setting a fixed threshold for background correction. Additionally, the total ROI area and ROI area above the background threshold was determined. The grey value and area measures were then combined by multiplying the background-corrected mean grey values of the ROI with the fraction of the ROI area with values above the background threshold (i.e. the specifically stained area of the ROI), to get the integrated density. This combined measurement is a more robust representation of protein levels than intensity or area alone, as for instance a decrease in area may lead to the detection of a higher mean intensity while the actual protein levels remained unchanged.

The fraction of the hippocampal area containing plaques was determined in the sections stained for 3A1 with a BIOQUANT image analysis setup (Nashville, TN, USA), and using a fixed threshold of detection. For this analysis, the hippocampus was manually delineated using the 4X objective, after which plaques where automatically detected based on the fixed threshold. Before performing the final measurements, artifacts were manually removed. The sections of the vervet brains varied in plane-cut and often only a part of the hippocampus could be assessed on a single section, which made them unsuited for a BIOQUANT analysis. The plaque load in the vervets was therefore semi-quantitatively scored, with 0 for no plaques, 1 for plaques in the temporal cortex but not inside the hippocampus, 2 for 1 to 5 plaques in the hippocampus, 3 for 6 to 10 plaques in hippocampus, 4 for 11 to 100 plaques in hippocampus, and 5 for more than 100 plaques in hippocampus. All slides and images were processed blinded and in a randomized order.

5.2.5. Statistical analysis

To compare the relative degree of DNA methylation and hydroxymethylation between ages, the ratio of the integrated density of 5-mC and 5-hmC was calculated (i.e. 5-mC IR / 5-hmC IR). Values deviating more than two times the standard deviation from the mean were replaced by the mean plus or minus two times the standard deviation (of the uncorrected dataset). Before performing the analyses and generating plots, the data was scaled through division by the root mean square of the data per region, to allow for a better comparison between the different stainings. For each animal model, hippocampal subregion, and epigenetic marker, including the 5-mC:5-hmC ratio, a linear regression

model was fitted with integrated density as the outcome and age as the predictor. The data was visually inspected for abnormalities and quantile-quantile plots of the regression model residuals were analyzed to check for severe deviations from normality. The correlation between the epigenetic markers and plaque load was determined by calculating Pearson's *r*. For all significance tests, the alpha was set at 0.05. The ImageJ measurements were collected in Microsoft Excel 2013 (Microsoft, Redmond, WA) and processed, normalized, and analyzed in R (version 3.2.2; The R Foundation, Vienna, Austria) and RStudio (version 0.99.486; The Foundation for Open Access Statistics, Boston, MA). In addition to standard R functions, the *dplyr* package was used for data handling [42], the 'rcorr' function of the *Hmisc* package was used to determine correlation coefficients with *p*-values [43], and the *ggplot2* package was used for generating graphs [44].

5.3. Results

5.3.1. Qualitative analysis of 5-mC, 5-hmC, and DNMT3A IR

Three main hippocampal subregions (dentate gyrus, DG; cornu ammonis 3, CA3; and CA1-2) were examined by immunohistochemical analysis as shown in Supplementary Figure 1. A few (7%) images were excluded from the analysis due to artifacts. Visual inspection of the analyzed images indicated most cells show nuclear 5-mC, 5-hmC, and DNMT3A IR (Supplementary Figures 2-5). DNMT3A, however, also appeared to be expressed outside the nucleus, especially in the CA3. The vervet tissue also exhibited some extranuclear 5-mC and 5-hmC IR. Upon closer observation, the 5-hmC and DNMT3A signals appeared diffusely throughout the nucleus, whereas the 5-mC signal was limited to a small number of distinct punctuae. Again, the staining pattern in the vervet tissue deviated from this general pattern and appeared diffusely throughout the nucleus for 5-mC, 5-hmC, and DNMT3A.

A conservative visual comparison of the stainings at the different ages did not reveal obvious age-related changes in IR of the epigenetic markers in the J20 (Supplementary Figure 2) and APP/PS1dE9 models (Supplementary Figure 3). In the 3xTg-AD model an age-related increase of 5-mC signal can be observed mainly in the DG, but also the CA3 and CA1-2 (Supplementary Figure 4). The vervet images did not show any consistent age-related alterations in IR (Supplementary Figure 5).

The hippocampal DNMT3A signal was generally too variable to draw any conclusions based on visual inspection alone. Some of these observations were confirmed through a semiquantitative analysis.

5.3.2. Semiquantitative analysis of 5-mC, 5-hmC, and DNMT3A IR

Quantile-quantile plots of the residuals of the regression models were inspected, and although the residuals of some individual models showed deviations from normality, there were no overall indications for either right- or left-skewness of the residuals. Linear regression showed a statistically significant age-related decrease of 5-mC IR (β = -0.034, p = 0.036) and the 5-mC:5-hmC ratio (β = -0.037, p = 0.018) in the DG, and of the 5-mC:5-hmC ratio in the CA3 (β = -0.038, p = 0.034), in the J20 transgenic mouse model (Figure 1). No statistically significant age-related changes of 5-mC IR were observed in APP/PS1dE9 mice (Figure 2). In contrast to the J20 mice, a statistically significant age-related increase of 5-mC IR was found in the DG (β = 0.021, p = 0.034) and CA1-2 (β = 0.019, p = 0.045) of the 3xTg-AD model (Figure 3). Also, no statistically significant age-related changes of 5-mC IR were observed in vervets (Figure 4), and no changes in 5-hmC or DNMT3A were detected in any of the tested animal models (Figures 1-4).

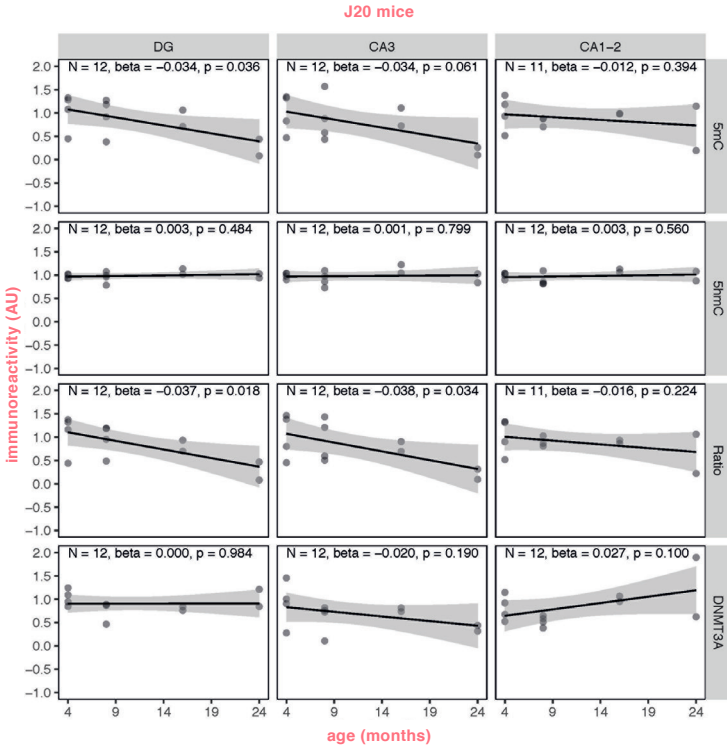

figure 1.

FIGURE 1. Semi-quantitative analysis results of age-related alterations in 5-methylcytosine (5-mC), 5-hydroxymethylcytosine (5-hmC) and DNA methyltransferase (DNMT) 3A immunoreactivity (IR), and the 5-mC:5-hmC ratio in J20 mice. Shown are the background-corrected and scaled integrated density data plotted against the age of the animals, the fitted linear regression lines and the standard error (SE) of the regression lines, for the dentate gyrus (DG), cornu ammonis (CA) 3, and CA1-2 subregions of the hippocampus. A statistically significant effect of age on 5-mC IR was found in the DG (p = 0.036), and on the 5-mC:5-hmC ratio in the DG (p = 0.018) and CA3 (p = 0.034). AU, arbitrary units.

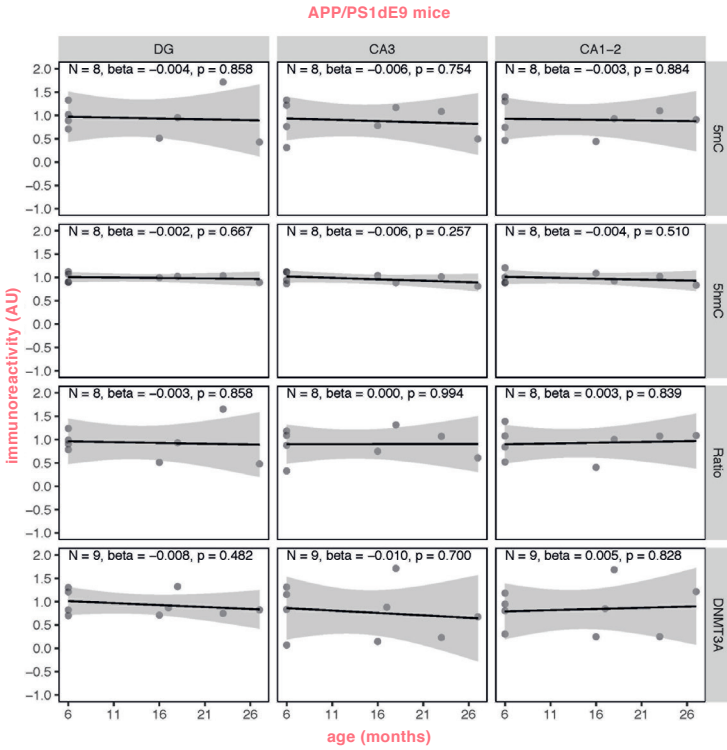

figure 2.

FIGURE 2. Semi-quantitative analysis results of age-related alterations in 5-methylcytosine (5-mC), 5-hydroxymethylcytosine (5-hmC) and DNA methyltransferase (DNMT) 3A immunoreactivity (IR), and the 5-mC:5-hmC ratio in APP/PS1dE9 mice. Shown are the background-corrected and scaled integrated density data plotted against the age of the animals, the fitted linear regression lines and the standard error (SE) of the regression lines, for the dentate gyrus (DG), cornu ammonis (CA) 3, and CA1-2 subregions of the hippocampus. No statistically significant effect of age on any of the investigated epigenetic markers was found. AU, arbitrary units.

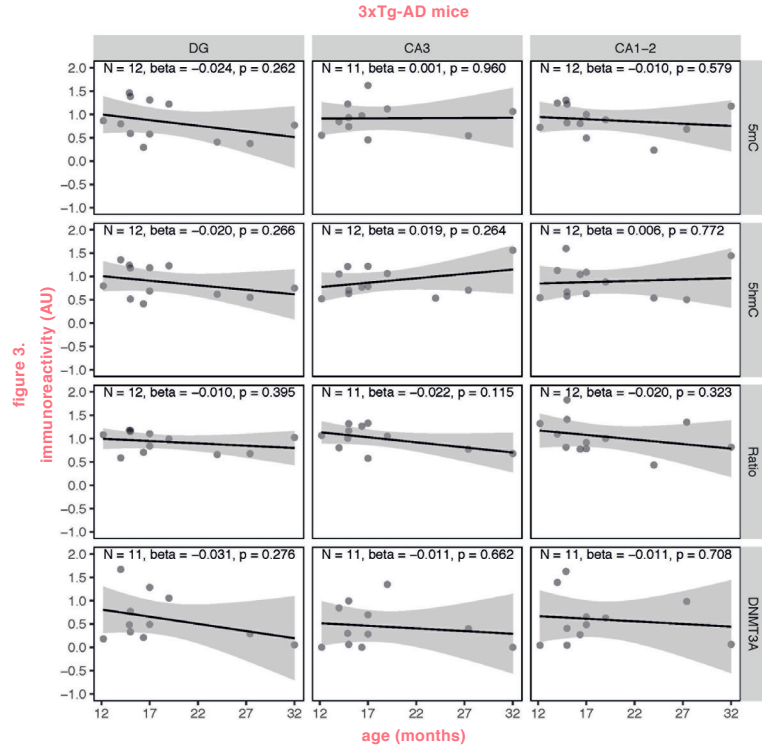

figure 3.

FIGURE 3. Semi-quantitative analysis results of age-related alterations in 5-methylcytosine (5-mC), 5-hydroxymethylcytosine (5-hmC) and DNA methyltransferase (DNMT) 3A immunoreactivity (IR), and the 5-mC:5-hmC ratio in 3xTg-AD mice. Shown are the background-corrected and scaled integrated density data plotted against the age of the animals, the fitted linear regression lines and the standard error (SE) of the regression lines, for the dentate gyrus (DG), cornu ammonis (CA) 3, and CA1-2 subregions of the hippocampus. A statistically significant effect of age on 5-mC IR was found in the DG (p = 0.034) and CA1-2 (p = 0.045). AU, arbitrary units.

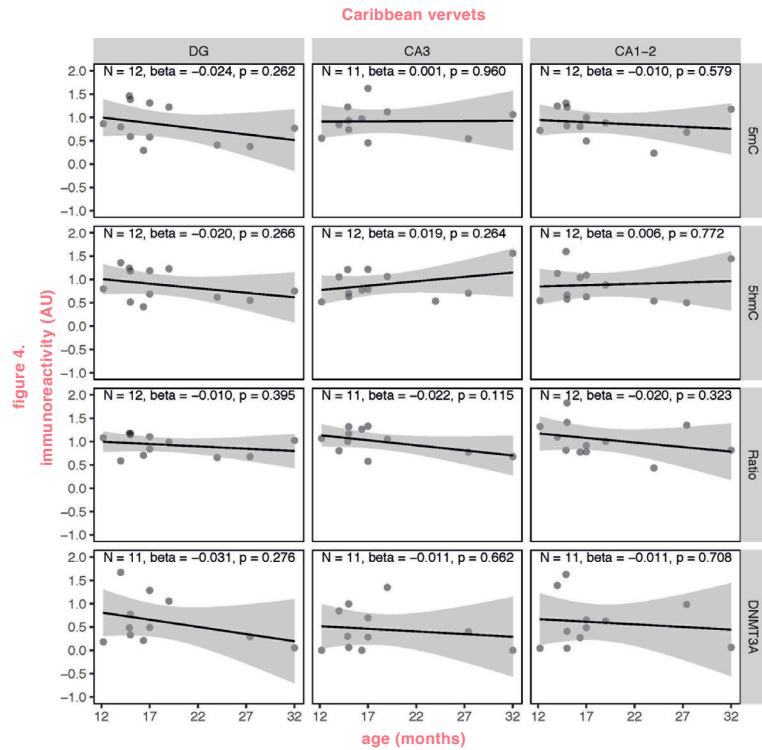

figure 4.

FIGURE 4. Semi-quantitative analysis results of age-related alterations in 5-methylcytosine (5-mC), 5-hydroxymethylcytosine (5-hmC) and DNA methyltransferase (DNMT) 3A immunoreactivity (IR), and the 5-mC:5-hmC ratio in Caribbean vervets. Shown are the background-corrected and scaled integrated density data plotted against the age of the animals, the fitted linear regression lines and the standard error (SE) of the regression lines, for the dentate gyrus (DG), cornu ammonis (CA) 3, and CA1-2 subregions of the hippocampus. No statistically significant effect of age on any of the investigated epigenetic markers was found. AU, arbitrary units.

5.3.3. Plaque load correlates with age-related changes in 5-mC IR

As expected, all of the oldest animals of the transgenic mouse models exhibited Aβ plaques (Supplementary Figures 6-8), varying between 17% and 63% of the hippocampus being covered in plaques. The regional distribution of the plaques in the different hippocampal subregions was, however, highly variable between the different mouse models. Hippocampal plaque density was the highest in the J20 model and plaques were observed within (and in vicinity of) the investigated subregions (Supplementary Figure 6). In the APP/PS1dE9 model, Aβ plaques were present throughout the hippocampus, but the load was lower than that seen in the J20 model (Supplementary Figure 7). In the 3xTg-AD model, however, plaques were mainly located in the dorsal subiculum and deeper layers (oriens and alveus) of the hippocampus, with a generally low plaque load close to the investigated regions (Supplementary Figure 8). In the vervets, six animals (of 15, 16.4, 19, 24, 27.4 and 32 years old) had plaque pathology in temporal cortex and/or hippocampus, although not all had hippocampal plaques. Plaques were not seen in these brain regions in the other six vervets (of 12.2, 14, 14.9, 15, 17 and 17 years old). The oldest animals did not necessarily have the most severe pathology (Supplementary Figure 9).

Correlation analysis between plaque load and 5-mC, 5-hmC, or DNMT3A IR revealed statistically significant inverse correlations in the J20 model between plaque load and 5-mC IR in the DG (r = -0.60, p = 0.039) and between plaque load and the 5-mC:5-hmC ratio in the DG (r = -0.66, p = 0.020) and CA3 (r = -0.60, p = 0.038) (Figure 5). No statistically significant correlations between plaque load and epigenetic markers were observed in the APP/PS1dE9 model (Figure 6). In the 3xTg-AD model statistically significant positive correlations were found between plaque load and 5-mC IR in the DG (r = 0.70, p = 0.026) and CA1-2 (r = 0.69, p = 0.027), as well as between plaque load and the 5-mC:5-hmC ratio in the DG (r = 0.67, p = 0.034) (Figure 7). No statistically significant correlations between plaque load and epigenetic markers were observed in the vervets (Figure 8).

5.4. Discussion

Age-related alterations of 5-mC, 5-hmC, and DNMT3A, three epigenetic markers previously associated with aging, age-related cognitive decline,

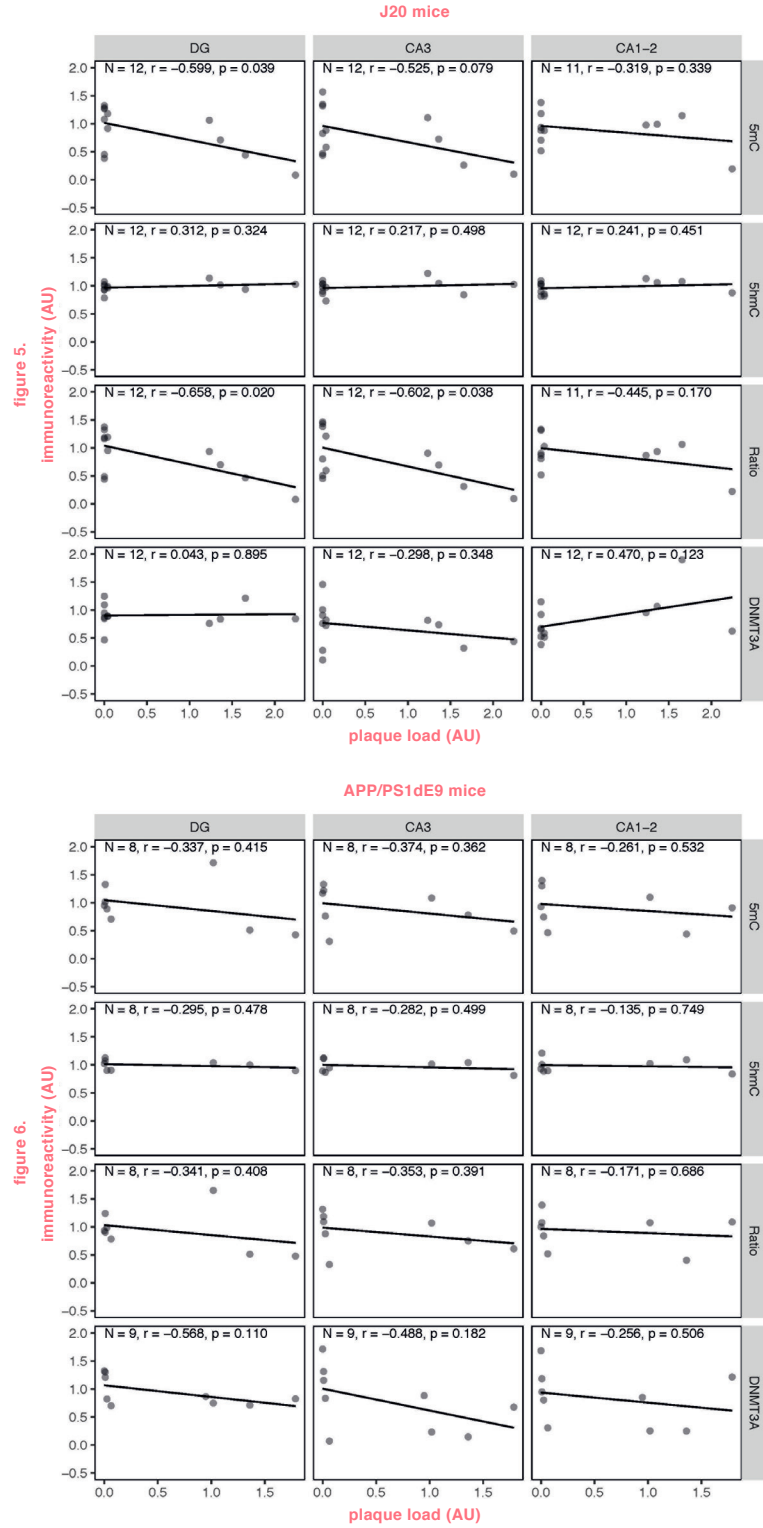

figure 5.

FIGURE 5. Correlation analysis results between epigenetic markers 5-methylcytosine (5-mC), 5-hydroxymethylcytosine (5-hmC) and DNA methyltransferase (DNMT) 3A immunoreactivity (IR), and the 5-mC:5-hmC ratio, and plaque load in J20 mice. Shown are the background-corrected and scaled integrated density data plotted against the scaled fraction of hippocampal area covered by plaques, for the dentate gyrus (DG), cornu ammonis (CA) 3, and CA1-2 subregions of the hippocampus. Fitted linear regression lines are shown for clarity. A statistically significant correlation with plaque load was found for 5-mC IR in the DG (r = -0.60, p = 0.039), and for the 5-mC:5-hmC ratio in the DG (r = -0.66, p = 0.020) and CA3 (r = -0.60, p = 0.038). AU, arbitrary units.

figure 6.

FIGURE 6. Correlation analysis results between epigenetic markers 5-methylcytosine (5-mC), 5-hydroxymethylcytosine (5-hmC) and DNA methyltransferase (DNMT) 3A immunoreactivity (IR), and the 5-mC:5-hmC ratio, and plaque load in APP/PS1dE9 mice. Shown are the background-corrected and scaled integrated density data plotted against the scaled fraction of hippocampal area covered by plaques, for the dentate gyrus (DG), cornu ammonis (CA) 3, and CA1-2 subregions of the hippocampus. Fitted linear regression lines are shown for clarity. No statistically significant correlation was found between plaque load and any of the investigated epigenetic markers. AU, arbitrary units.

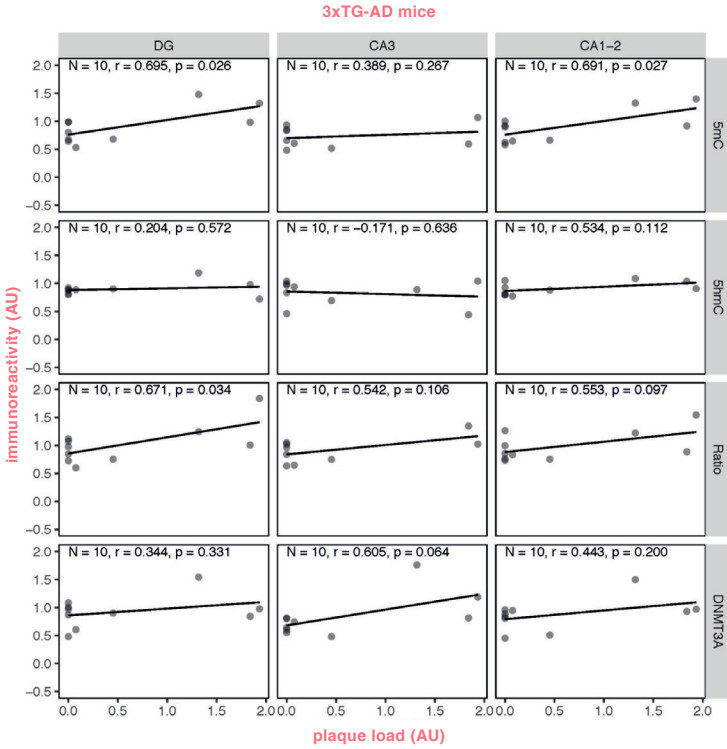

figure 7.

FIGURE 7. Correlation analysis results between epigenetic markers 5-methylcytosine (5-mC), 5-hydroxymethylcytosine (5-hmC) and DNA methyltransferase (DNMT) 3A immunoreactivity (IR), and the 5-mC:5-hmC ratio, and plaque load in 3xTg-AD mice. Shown are the background-corrected and scaled integrated density data plotted against the scaled fraction of hippocampal area covered by plaques, for the dentate gyrus (DG), cornu ammonis (CA) 3, and CA1-2 subregions of the hippocampus. Fitted linear regression lines are shown for clarity. A statistically significant correlation with plaque load was found for 5-mC IR in the DG (r = 0.70, p = 0.026) and CA1-2 (r = 0.69, p = 0.027), and for the 5-mC:5-hmC ratio in the DG (r = 0.67, p = 0.034). AU, arbitrary units.

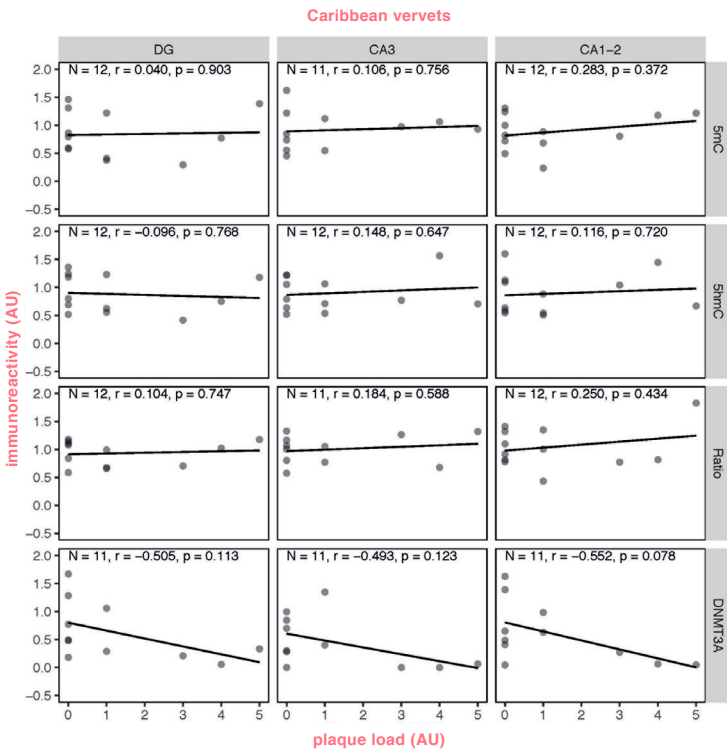

figure 8.

FIGURE 8. Correlation analysis results between epigenetic markers 5-methylcytosine (5-mC), 5-hydroxymethylcytosine (5-hmC) and DNA methyltransferase (DNMT) 3A immunoreactivity (IR), and the 5-mC:5-hmC ratio, and plaque load in Caribbean vervets. Shown are the background-corrected and scaled integrated density data plotted against the scores of hippocampal plaque load, for the dentate gyrus (DG), cornu ammonis (CA) 3, and CA1-2 subregions of the hippocampus. Fitted linear regression lines are shown for clarity. No statistically significant correlation was found between plaque load and any of the investigated epigenetic markers. AU, arbitrary units.

and/or AD, were investigated in 3 transgenic mouse models of AD and a non-human primate model that is known to develop Aβ plaque pathology with age. Semi-quantitative analysis of 5-mC, 5-hmC, and DNMT3A IR indicated striking differences in age-related DNA methylation patterns between the different models, while none of the models showed age-related differences in levels of DNA hydroxymethylation and DNMT3A. Generally, plaque load correlated with DNA methylation, but only in the J20 and 3xTg-AD models where age-related DNA methylation changes were detected, although in opposite directions.

5.4.1. Age-related decrease of DNA methylation levels in the DG and CA3 of J20 mice

In the present study, aging was associated with a decrease in 5-mC IR in the DG and a decrease of the 5-mC:5-hmC ratio in the DG and CA3. Since 5-hmC seems to remain stable with age, this decrease in the 5-mC:5-hmC ratio is likely due to a decrease in 5-mC, even though 5-mC IR alone was not significantly decreased in the CA3. Furthermore, correlation analysis between hippocampal plaque load and the investigated epigenetic markers only showed a statistically significant correlation between plaque load and 5-mC in the DG and the 5-mC:5-hmC ratio in the DG and CA3 region; the same areas that showed age-related alterations.

Transgenic J20 mice express human APP with both the Swedish and Indiana mutations associated with the development of familial AD [34]. It has previously been reported that these mice already show cognitive deficits starting at 1-2 months of age, but that these impairments do not seem to progress with age up to the development of plaque pathology, which starts around 6 months of age, but ramps up around 10 months of age [34, 38].

It is most likely that in these models based on mutations seen in familial AD, epigenetic alterations play a role in the progression of the disease and are instigated through other pathological processes directly related to these mutated genes. For instance, Aβ has been reported to influence DNA methylation, inducing global hypomethylation [45], which is in line with the observations in the J20 model in the present study. Interestingly, the observation that the promoter of the *MAPT* gene, which

has been implicated in AD, was hypomethylated in J20 mice already at 5 months of age indicates that epigenetic processes may be involved in the development of AD before the occurrence of senile plaques [46]. Note, however, that the global changes in DNA methylation observed in the present study occur after the development of extracellular plaque formation.

Another study reports increased levels of histone deacetylase (HDAC) activity in J20 mice 19-20 months of age [47]. Although an increase in HDAC activity is generally linked to an increase in DNA methylation [48], this is not consistently observed in AD [9]. This inconsistency is also reflected in the present study and may implicate possible methodological differences or the existence of different pathological mechanisms with alternative effects on epigenetic profiles.

5.4.2. Epigenetic markers remain stable with age in APP/PS1dE9 mice

In the present study, extensive plaque deposition was observed in the hippocampus of APP/PS1dE9, but no age-related epigenetic changes were detected. The APP/PS1dE9 transgenic mouse model expresses human PS1 with the deletion of exon 9 and humanized APP with the Swedish mutation [36, 49]. This mouse model is widely used and cognitive impairments have been reported for spatial working memory as early as 4 months of age, with additional impairments in reference memory, associative learning, and passive avoidance with increasing age [38, 40, 50].

Another study in the APP/PS1dE9 mice revealed that treatment with HDAC inhibitors can ameliorate cognitive impairments, but that there are no global differences in hippocampal histone (H) 3 and H4 acetylation levels [51]. Interestingly, studies in similar models with the same AD-related genes, but different mutations, have reported different results. A study using an APP/PS1 model expressing human PS1 with the M146V mutation, found hippocampal decreases in H4 acetylation after fear conditioning, compared to wild-type mice [52]. Treatment with an HDAC inhibitor was able to both rescue the acetylation levels and behavioral responses in the APP/PS1 mice. Similar findings were obtained in APP/PS1 mice with the APP KM670/671NL and PS1 L166P mutations [53], and in APP/PS1 mice with chimeric APP with the K670N/M671L mutation and the PS1 A246E mutation [54].

A genome-wide analysis of DNA methylation has also been performed in cortex of the APP/PS1dE9 model [55]. In this study, sites that were observed to be differentially methylated in the APP/PS1dE9 model, as compared to wild-type controls, were mainly hypermethylated. Additionally, they identified transforming growth factor β1 and its associated signaling pathway to be mainly dysregulated. However, due to the differences in approach and brain area, these results cannot be reliably compared with the present findings.

5.4.3. DNA methylation levels increase in the DG and CA1-2 of 3xTg-AD mice

In contrast to the J20 and APP/PS1 models, the 3xTg-AD model, expressing mutated APP, PS1, and tau, not only develops plaques, but also neurofibrillary tangles [37]. Contrary to the J20 model, the 3xTg-AD model shows an increase in DNA methylation in the DG and CA1-2 subregions. A possible explanation for this disparity between the models would be the addition of the mutated *MAPT* transgene, although there is evidence that tau does not cause global hypermethylation, but hypomethylation through oxidative stress and DNA damage [56]. The 3xTg-AD mice are reported to develop extracellular amyloid deposits in frontal cortex by 6 months, which progressively spread throughout the brain by 12 months of age [37], and tau pathology which appears later, after about 12 to 15 months [41]. We observed a 2-3 month delay in AD pathology within our 3xTg-AD colony, possibly due to reduced transgene copies with successive breeding (see https://www.jax.org/strain/004807).

However, our findings confirm that hippocampal plaque formation occurs mainly in the deeper layers of the hippocampus and subiculum, and fewer plaques were seen in the DG, CA3, and CA1-2 subregions when compared to the J20 and APP/PS1 models. Importantly, cognitive impairments occur before the development of plaques and tangles, starting around 4 months, and correlate with intraneuronal Aβ [41].

The direction of the DNA methylation changes may appear contra intuitive, but it appears that other studies investigating epigenetic changes in this triple transgenic model have made similar observations. For instance, Sanchez-Mut et al. [57] found an increase in *TBXA2R*, *F2RL2*, *SPNB4*, and *SORBS3* methylation, with a decrease in the corresponding mRNA levels in the cortex of 3xTg-AD mice. Walker et al. [58] investigated age-related histone modification changes in neurons

from wild-type and 3xTg-AD mice. They found that the repressive H3 lysine (K) 9 methylation marker increased with age in 3xTg-AD neurons, more so than in wild-type neurons. This finding of increased epigenetic repression of gene expression is confirmed by the detection of lower BDNF gene expression. Importantly, increases in H3K9 methylation were already observed at 4 months, the same age at which cognitive deficits start to emerge [58]. Another study focusing on the hippocampus of 3xTg-AD mice reported an age-related loss of H3K4 trimethylation, an epigenetic marker that is associated with decreased gene expression [59]. These observations of increased epigenetic repression are in line with the present study, as DNA methylation is also generally associated with suppression of gene expression [60].

Interestingly, however, in neurons isolated from 3xTg-AD mice, Walker et al. [58] also observed increases in H3 and H4 acetylation levels with age; epigenetic markers which are associated with enhanced gene expression. As stated previously, these markers decreased in the J20 and APP/PS1 models. A gene-specific analysis showed that the promoter region of the AD-associated *BACE1* gene exhibited increased H3 acetylation, concomitant with increased mRNA levels, in the cortex of 3xTg-AD mice [61]. H4K12 acetylation has also been investigated as a potential biomarker in blood monocytes of 3xTg-AD mice and it was found that this marker was elevated at 10 months of age, during the development of plaque pathology, but not anymore at 20 months of age when plaque pathology is already widespread [62].

Nevertheless, treatment with HDAC inhibitors is also able to improve cognition in the 3xTg-AD mice [63, 64]. It is therefore necessary for future studies to elucidate which genes are affected by these global changes in histone acetylation, as treatment with HDAC inhibitors may have a beneficial effect independent of AD-related alterations in histone acetylation. This is exemplified by studies showing beneficial effects of HDAC inhibitors during normal aging [65].

In the present study, we do not detect any significant age-related changes in 5-hmC IR. Another immunohistochemical study, however, comparing wild-type and 3xTg-AD mice at 17 months detected an increase in cortical 5-hmC levels [66]. These differences may be due to differences in methodology, brain area investigated, and age of the studied animals, and stress the sensitive and complex nature of epigenetic processes and investigations thereof.

5.4.4. No age-related alterations of global epigenetic marks are detected in the hippocampus of Caribbean vervets

We observed no age-related changes in the level of epigenetic marks in the hippocampus of vervets. As opposed to the transgenic mouse models, the vervets serve as a more natural model of AD as some of these non-human primates develop AD-like pathology as they age, without the introduction of mutated transgenes. Interestingly, as AD in humans generally develops at advanced ages, vervets exhibit plaque pathology as early as 15 years. While their lifespan is only 15 to 20 years in the wild, it is 20 to 30 years in captivity [33]. In general, plaque deposition in vervets starts in the frontal cortex and spreads with age (C. Lemere, personal communication), sometimes approaching, by 30 years of age, Aβ pathology as seen in human AD. In the J20 and 3xTg-AD models, the most drastic changes in the levels of the studied epigenetic marks were seen in the extremely old age groups. Thus, it may thus be the case that AD-pathology in the vervets was not advanced enough, especially in the hippocampus, to induce detectable changes. As the pathology in the vervets was much more variable than in the transgenic mice, the sample size may have been too small to detect significant correlations between age, Aβ pathology, and epigenetic markers. Alternatively, the long-term fixation of the archived vervet brain tissue may have limited the accessibility of antigens for accurate immunohistochemical detection.

Other studies focusing on age-related epigenetic alterations in vervets are scarce, although a study investigating blood DNA methylation in relation to a high fat diet also found no significant association between age and DNA methylation levels (ages between 9.7 and 23.7 years) [67].

5.4.5. Translational validity

Given the discrepancy in observations regarding DNA methylation across the different animal models, it is essential to compare the results from the animal models with observations from human and related studies in order to elucidate how the genetically different models may be able to reflect the epigenetic alterations associated with AD. However, as noted previously, differences in brain regions and methodology already hamper

comparisons between studies performed on human tissue, let alone comparisons with other species. Additionally, whereas animal models have the advantage to facilitate the study of the temporal sequence of events, human studies focusing on brain markers generally need to rely on postmortem tissue. Therefore, instead of comparing changes over time, they compare diseased with control brains. It is also important to consider that non-human primates and humans have greater genetic heterozygosity and environmental diversity than homogenous transgenic mouse models.

Targeted approaches aside, there are several studies that investigated AD-related global changes in DNA methylation and hydroxymethylation markers using human brain material. Initial studies, also by our group, have shown an AD-associated global DNA hypomethylation and hypohydroxymethylation in the entorhinal cortex and hippocampus [23, 24]. These studies also found an AD-associated decrease in DNA methylation and hydroxymethylation in a monozygotic twin pair of which only one developed AD. Other groups, however, either did not find significant changes in global DNA methylation in the entorhinal cortex [68], or even increases in DNA methylation and hydroxymethylation in the hippocampus, middle frontal gyrus and middle temporal gyrus [26, 69]. Although these studies do not all show the same direction of change, they observe similar alterations in DNA methylation and hydroxymethylation, whereas Condliffe et al. [25] found a decrease of only DNA hydroxymethylation in the entorhinal cortex and cerebellum. Rao et al. [70] only investigated DNA methylation and found an increase in the frontal cortex of AD patients. Using the HumanMethylation450 BeadChip assay on tissue from the dorsolateral prefrontal cortex De Jager et al. [27] reported a modest increase of the methylation value of differentially methylated loci in AD.

Since findings in the same brain region also disagree, it is unlikely that the discrepancies can be explained solely by differences in brain areas. As has been noted previously [9, 26, 68], the most likely explanation would be differences in methodology, such as tissue processing and quantification methods. To elucidate how differences in methodology can influence detected DNA methylation and hydroxymethylation levels, different procedures should be systemically tested on the same tissue, and vice versa, the same approach should be used on various tissues. For the present study, however, similar methodology was used to process all of the mouse tissues and to quantify the epigenetic markers. The different observations for the various mouse models would thus point to a genotype effect, possibly due to the expression of different transgenes and/or the use of different promoters. A genotype effect, in turn, is unlikely to explain the differences between the human studies as they generally

study mixed samples of, based on the average age, mainly late-onset AD, although due to the large age-range and lack of (reported) genetic tests also familial cases may be included [26].

To get a better idea of the direction of the epigenetic changes in AD it may help to look at related studies. Observations from *in vitro* work related to the effect of Aβ and APP mutations on DNA methylation, are more consistent and indicate there is global hypomethylation [45, 71, 72]. Additionally, work on tau indicates that it induces global heterochromatin loss, which may lead to aberrant gene expression patterns in AD [56]. A loss of heterochromatin also points towards a hypomethylated state of the DNA.

DNMTs depend on S-adenosylmethionine (SAM) as methyl donor and some studies have found striking deficiencies of SAM and S-adenosylhomocysteine (SAH), the demethylated metabolite of SAM, throughout the AD-afflicted brain and cerebrospinal fluid [73–75]. *In vitro* work investigating the relationship between folate, SAM, and DNA methylation indicates a SAM deficiency leads to global hypomethylation [76]. Another study found increased levels of brain SAH in AD patients and showed that SAH inhibits methyltransferases, suggesting that increased levels of SAH would also lead to DNA hypomethylation [77]. Others have indeed shown decreased methyltransferase activity in the brain of AD patients [78]. Inhibition of DNMTs could also explain alterations in DNA methylation, without changes in the levels of DNMT3A, as seen in the present study.

The direct and indirect evidence mainly points towards a hypomethylated state in AD. Of the investigated models, only the J20 mice exhibit an age-related global DNA hypomethylation in the hippocampus and therefore seems to best capture this view. Of note, in light of previous observations that DNA methylation increases with age [17, 19], the lack of an increase in global DNA methylation in the old mice of the APP/PS1dE9 model could be interpreted as hypomethylation when compared to normal aging. Similarly, DNA hydroxymethylation and DNMT3A levels have been observed to increase with age [16, 18, 20, 21], therefore, the lack of an age-related change in these markers could be seen as a decrease in comparison to wild-type aged animals. This, however, should be confirmed through a direct comparison of transgenic and non-transgenic litter-mates.

5.4.6. Strengths, limitations, and future perspectives

A strength of the present study is the inclusion of multiple animal models, which has provided crucial insights in how the different mouse models capture AD on an epigenetic level. The inclusion of a non-transgenic non-human primate model provides an additional angle more related to sporadic AD, in contrast to the transgenic mouse models, which are limited to familial forms of AD. Additionally, the use of established immunohistochemistry-based techniques allows the subregion-specific qualitative and semi-quantitative analysis of epigenetic markers. Importantly, by using highly specific antibodies 5-mC and 5-hmC can be reliably distinguished [18, 79], which is not possible with most other commonly used techniques for 5-mC detection [14].

The study also has its limitations, which thus should be taken into account when interpreting the results. First, although the staining and image-analysis procedures were identical for all the models and performed at the same time, the breeding, sacrificing and tissue processing were not done at the same time, which may have resulted in slight differences between the mouse models. The vervet tissue was differently processed and fixed for a longer time, which may affect immunoreactivity. Additionally, the vervets did not live under strict experimentally controlled conditions such as the mouse models, which may result in more variation. The exclusion of an aging wild-type mouse group may be seen as a limitation, but our group has previously reported extensive epigenetic investigations in normally aging mice [16–18, 22], which were done in a similar manner and can therefore be used to compare the current findings in relation to AD with.

The borderline significance often observed in the present study suggests that it could have benefitted from larger sample sizes to increase power. However, since this explorative study depended on the availability of animals from other studies, it was not possible to increase the sample sizes. It remains an important point, which has been previously raised [80, 81], that most current epigenetic studies are relatively small, which may result in the large differences in results. Therefore, there is a need for large, high-powered studies that may provide more conclusive results. Nevertheless, the present study serves as an important foundation to guide future AD-related epigenetics research in animal models.

REFERENCES

[1] Sosa-Ortiz AL, Acosta-Castillo I, Prince MJ. Epidemiology of dementias and Alzheimer's disease. *Arch Med Res* 2012; 43: 600–608.

[2] Raina P, Santaguida P, Ismaila A, et al. Effectiveness of cholinesterase inhibitors and memantine for treating dementia: evidence review for a clinical practice guideline. *Ann Intern Med* 2008; 148: 379–397.

[3] Lansdall CJ. An effective treatment for Alzheimer's disease must consider both amyloid and tau. *Biosci Horizons* 2014; 7: hzu002.

[4] Stratmann K, Heinsen H, Korf HW, et al. Precortical phase of Alzheimer's disease (AD)-related tau cytoskeletal pathology. *Brain Pathol*. Epub ahead of print 2015. DOI: 10.1111/bpa.12289.

[5] Bartsch T, Wulff P. The hippocampus in aging and disease: From plasticity to vulnerability. *Neuroscience*. Epub ahead of print 2015. DOI: 10.1016/j.neuroscience.2015.07.084.

[6] Kurz A, Perneczky R. Novel insights for the treatment of Alzheimer's disease. *Prog Neuropsychopharmacol Biol Psychiatry* 2011; 35: 373–379.

[7] Defina PA, Moser RS, Glenn M, et al. Alzheimer's disease clinical and research update for health care practitioners. *J Aging Res* 2013; 2013: 207178.

[8] Price DL, Sisodia SS. Mutant genes in familial Alzheimer's disease and transgenic models. *Annu Rev Neurosci* 1998; 21: 479–505.

[9] Lardenoije R, Iatrou A, Kenis G, et al. The epigenetics of aging and neurodegeneration. *Prog Neurobiol* 2015; 131: 21–64.

[10] Van den Hove DL, Kompotis K, Lardenoije R, et al. Epigenetically regulated microRNAs in Alzhei-

5.5. Conclusion

This study set out to determine age-related changes in immunohistochemically detectable markers related to DNA methylation in several widely used and genetically different animal models of AD, and to determine how these models reflect the epigenetic changes observed in AD. In the J20 model global DNA hypomethylation was observed in the hippocampus, while in the 3xTg-AD model global hypermethylation was observed. No alterations in DNA hydroxymethylation or DNMT3A levels were detected in these models. In APP/PS1dE9 and Caribbean vervets, no age-related global epigenetic changes were observed. Plaque load correlated with DNA methylation in those cases where age-related changes were detected, with a negative correlation in the J20 model and a positive correlation in the 3xTg-AD model. The main differences between the investigated models were thus in the age-related changes in DNA methylation. Other studies looking at DNA methylation or the effects of Aβ, tau, and SAM/SAH on DNA methylation report mixed results, but appear to lean towards global hypomethylation in AD. Although this would suggest the J20 model best captures the global epigenetic changes related to AD, it appears the different genotypes of the models differentially affect the course of age-related epigenetic changes. Exactly how mutations in the *APP*, *PS1*, and *MAPT* genes interact with the epigenome remains to be elucidated in future studies.

Acknowledgements

We kindly thank H Crehan, Q Shi, and S Chowdhury for technical assistance. Funds have been provided by the Internationale Stichting Alzheimer Onderzoek (ISAO) grants 07551 and 11532 (D.L.A.vdH.), by the ISAO grants 09552 and 13515, and the Netherlands Organization for Scientific Research (NWO), grant 916.11.086 (Veni Award) (B.P.F.R.), by an ISAO fellowship and a fellowship as part of NWO grant 022.005.019, (R.L.), and by an Anonymous Foundation and NIH/NIA R01 AG040092 (C.A.L.). Additional funds have been provided by the Joint Programme—Neurodegenerative Disease Research (JPND) for the EPI-AD consortium (http://www.neurodegenerationresearch.eu/wp-content/uploads/2015/10/Factsheet_EPI-AD.pdf). The funding agencies were not involved in the study design, data collection, analysis and interpretation, writing of the report, and the decision to submit the article for publication. The authors declare no conflicts of interest.

mer's disease. *Neurobiol Aging* 2014; 35: 731–745.

[11] Iatrou A, Kenis G, Rutten BPF, et al. Epigenetic dysregulation of brainstem nuclei in the pathogenesis of Alzheimer's disease: looking in the correct place at the right time? *Cellular and Molecular Life Sciences*, 2016, pp. 1–15.

[12] Choudhuri S. From Waddington's epigenetic landscape to small noncoding RNA: some important milestones in the history of epigenetics research. *Toxicol Mech Methods* 2011; 21: 252–274.

[13] Liu L, Li Y, Tollefsbol TO. Gene-environment interactions and epigenetic basis of human diseases. *Curr Issues Mol Biol* 2008; 10: 25–36.

[14] van den Hove DLA, Chouliaras L, Rutten BPF. The role of 5-hydroxymethylcytosine in aging and Alzheimer's disease: current status and prospects for future studies. *Curr Alzheimer Res* 2012; 9: 545–9.

[15] Chouliaras L, Rutten BPF, Kenis G, et al. Epigenetic regulation in the pathophysiology of Alzheimer's disease. *Prog Neurobiol* 2010; 90: 498–510.

[16] Chouliaras L, van den Hove DLA, Kenis G, et al. Caloric restriction attenuates age-related changes of DNA methyltransferase 3a in mouse hippocampus. *Brain Behav Immun* 2011; 25: 616–623.

[17] Chouliaras L, van den Hove DLA, Kenis G, et al. Prevention of age-related changes in hippocampal levels of 5-methylcytidine by caloric restriction. *Neurobiol Aging* 2012; 33: 1672–81.

[18] Chouliaras L, van den Hove DLA, Kenis G, et al. Age-related increase in levels of 5-hydroxymethylcytosine in mouse hippocampus is prevented by caloric restriction. *Curr Alzheimer Res* 2012; 9: 536–44.

[19] Hernandez DG, Nalls MA, Gibbs JR, et al. Distinct DNA methylation changes highly correlated with chronological age in the human brain. *Hum Mol Genet* 2011; 20: 1164–1172.

[20] Münzel M, Globisch D, Brückl T, et al. Quantification of the sixth DNA base hydroxymethylcytosine in the brain. *Angew Chemie Int Ed* 2010; 49: 5375–5377.

[21] Song C-X, Szulwach KE, Fu Y, et al. Selective chemical labeling reveals the genome-wide distribution of 5-hydroxymethylcytosine. *Nat Biotechnol* 2011; 29: 68–72.

[22] Lardenoije R, van den Hove DA, Vaessen TSJ, et al. Epigenetic modifications in mouse cerebellar Purkinje cells: effects of aging, caloric restriction, and overexpression of superoxide dismutase 1 on 5-methylcytosine and 5-hydroxymethylcytosine. *Neurobiol Aging* 2015; 36: 3079–3089.

[23] Mastroeni D, Grover A, Delvaux E, et al. Epigenetic changes in Alzheimer's disease: Decrements in DNA methylation. *Neurobiol Aging* 2010; 31: 2025–2037.

[24] Chouliaras L, Mastroeni D, Delvaux E, et al. Consistent decrease in global DNA methylation and hydroxymethylation in the hippocampus of Alzheimer's disease patients. *Neurobiol Aging* 2013; 34: 2091–2099.

[25] Condliffe D, Wong A, Troakes C, et al. Cross-region reduction in 5-hydroxymethylcytosine in Alzheimer's disease brain. *Neurobiol Aging* 2014; 35: 1850–1854.

[26] Coppieters N, Dieriks B V, Lill C, et al. Global changes in DNA methylation and hydroxymethylation in Alzheimer's disease human brain. *Neurobiol Aging* 2014; 35: 1334–1344.

[27] De Jager PL, Srivastava G, Lunnon K, et al. Alzheimer's disease: early alterations in brain DNA methylation at *ANK1*, *BIN1*, *RHBDF2* and other loci. *Nat Neurosci* 2014; 17: 1156–1163.

[28] Lunnon K, Smith R, Hannon E, et al. Methylomic profiling implicates cortical deregulation of *ANK1* in Alzheimer's disease. *Nat Neurosci* 2014; 17: 1164–1170.

[29] van Goethem NP, Lardenoije R, Kompotis K, et al. Cognitive disorders: impairment, aging, and dementia. In: In Vivo *Models for Drug Discovery*. Wiley-VCH Verlag GmbH & Co. KGaA, pp. 349–366.

[30] Frost JL, Le KX, Cynis H, et al. Pyroglutamate-3 amyloid-beta deposition in the brains of humans, non-human primates, canines, and Alzheimer disease-like transgenic mouse models. *Am J Pathol* 2013; 183: 369–381.

[31] Woodruff-Pak DS. Animal models of Alzheimer's disease: therapeutic implications. *J Alzheimers Dis* 2008; 15: 507–521.

[32] Cavanaugh SE, Pippin JJ, Barnard ND. Animal models of Alzheimer disease: historical pitfalls and a path forward. *ALTEX* 2014; 31: 279–302.

[33] Lemere CA, Beierschmitt A, Iglesias M, et al. Alzheimer's disease abeta vaccine reduces central nervous system abeta levels in a non-human primate, the Caribbean vervet. *Am J Pathol* 2004; 165: 283–297.

[34] Mucke L, Masliah E, Yu G-Q, et al. High-level neuronal expression of abeta 1-42 in wild-type human amyloid protein precursor transgenic mice: synaptotoxicity without plaque formation. *J Neurosci* 2000; 20: 4050–4058.

[35] Garcia-Alloza M, Robbins EM, Zhang-Nunes SX, et al. Characterization of amyloid deposition in the APPswe/PS1dE9 mouse model of Alzheimer disease. *Neurobiol Dis* 2006; 24: 516–524.

[36] Jankowsky JL, Slunt HH, Ratovitski T, et al. Co-expression of multiple transgenes in mouse CNS: a comparison of strategies. *Biomol Eng* 2001; 17: 157–165.

[37] Oddo S, Caccamo A, Shepherd JD, et al. Triple-transgenic model of Alzheimer's disease with plaques and tangles: intracellular Abeta and synaptic dysfunction. *Neuron* 2003; 39: 409–421.

[38] Webster SJ, Bachstetter AD, Nelson PT, et al. Using mice to model Alzheimer's dementia: an overview of the clinical disease and the preclinical behavioral changes in 10 mouse models. *Front Genet* 2014; 5: 88.

[39] Jankowsky JL, Fadale DJ, Anderson J, et al. Mutant presenilins specifically elevate the levels of the 42 residue beta-amyloid peptide in vivo: evidence for augmentation of a 42-specific gamma secretase. *Hum Mol Genet* 2004; 13: 159–70.

[40] Park JH, Widi GA, Gimbel DA, et al. Subcutaneous Nogo receptor removes brain amyloid-beta and improves spatial memory in Alzheimer's transgenic mice. *J Neurosci* 2006; 26: 13279–86.

[41] Billings LM, Oddo S, Green KN, et al. Intraneuronal Abeta causes the onset of early Alzheimer's disease-related cognitive deficits in transgenic mice. *Neuron* 2005; 45: 675–88.

[42] Wickham H, Francois R. dplyr: A grammar of data manipulation. R package version 0.4.3. http://CRANR-project.org/package=dplyr.

[43] Harrell FE. *Hmisc: Harrell Miscellaneous*. R package version 3.17-0. http://CRANR-project.org/package=Hmisc.

[44] Wickham H. *ggplot2 - Elegant Graphics for Data Analysis*. New York: Springer-Verlag. Epub ahead of print 2009. DOI: 10.1007/978-0-387-98141-3.

[45] Chen K-L, Wang SS-S, Yang Y-Y, et al. The epigenetic effects of amyloid-beta(1-40) on global DNA and neprilysin genes in murine cerebral endothelial cells. *Biochem Biophys Res Commun* 2009; 378: 57–61.

[46] Coupland K, Kim WS, Halliday G, et al. *MAPT* methylation in Alzheimer's disease. *Alzheimer's Dement* 2014; 10: P317–P318.

[47] Kuo J-W, Su K-H, Wu C-Y, et al. 18F-FAHA PET signatures of histone deacetylase activity in the transgenic mouse model of Alzheimer's disease. *J Nucl Med* 2012; 53: 1902-.

[48] Cedar H, Bergman Y. Linking DNA methylation and histone modification: patterns and paradigms. *Nat Rev Genet* 2009; 10: 295–304.

[49] Jankowsky JL, Fadale DJ, Anderson J, et al. Mutant presenilins specifically elevate the levels of the 42 residue -amyloid peptide *in vivo*: evidence for augmentation of a 42-specific secretase. *Hum Mol Genet* 2003; 13: 159–170.

[50] Frost JL, Liu B, Rahfeld J-U, et al. An anti-pyroglutamate-3 Aβ vaccine reduces plaques and improves cognition in APPswe/PS1ΔE9 mice. *Neurobiol Aging* 2015; 36: 3187–99.

[51] Kilgore M, Miller CA, Fass DM, et al. Inhibitors of class 1 histone deacetylases reverse contextual memory deficits in a mouse model of Alzheimer's disease. *Neuropsychopharmacology* 2010; 35: 870–80.

[52] Francis YI, Fà M, Ashraf H, et al. Dysregulation of histone acetylation in the APP/PS1 mouse model of Alzheimer's disease. *J Alzheimers Dis* 2009; 18: 131–9.

[53] Govindarajan N, Agis-Balboa RC, Walter J, et al. Sodium butyrate improves memory function in an Alzheimer's disease mouse model when administered at an advanced stage of disease progression. *J Alzheimers Dis* 2011; 26: 187–97.

[54] Wang Z, Zhang X-J, Li T, et al. Valproic acid reduces neuritic plaque formation and improves learning deficits in APP(Swe) /PS1(A246E) transgenic mice via preventing the prenatal hypoxia-induced down-regulation of neprilysin. *CNS Neurosci Ther* 2014; 20: 209–17.

[55] Cong L, Jia J, Qin W, et al. Genome-wide analysis of DNA methylation in an APP/PS1 mouse model of Alzheimer's disease. *Acta Neurol Belg* 2014; 114: 195–206.

[56] Frost B, Hemberg M, Lewis J, et al. Tau promotes neurodegeneration through global chromatin relaxation. *Nat Neurosci* 2014; 17: 357–66.

[57] Sanchez-Mut J V., Aso E, Panayotis N, et al. DNA methylation map of mouse and human brain identifies target genes in Alzheimer's disease. *Brain* 2013; 136: 3018–3027.

[58] Walker MP, LaFerla FM, Oddo SS, et al. Reversible epigenetic histone modifications and Bdnf expression in neurons with aging and from a mouse model of Alzheimer's disease. *Age* (Dordr) 2013; 35: 519–31.

[59] Mastroeni D, Delvaux E, Nolz J, et al. Aberrant intracellular localization of H3k4me3 demonstrates an early epigenetic phenomenon in Alzheimer's disease. *Neurobiol Aging*

2015; 36: 3121–9.

[60] Bird AP, Wolffe AP. Methylation-induced repression— belts, braces, and chromatin. *Cell* 1999; 99: 451–454.

[61] Marques SCF, Lemos R, Ferreiro E, et al. Epigenetic regulation of *BACE1* in Alzheimer's disease patients and in transgenic mice. *Neuroscience* 2012; 220: 256–66.

[62] Plagg B, Ehrlich D, Kniewallner KM, et al. Increased acetylation of histone H4 at lysine 12 (H4K12) in monocytes of transgenic Alzheimer's mice and in human patients. *Curr Alzheimer Res* 2015; 12: 752–60.

[63] Green KN, Steffan JS, Martinez-Coria H, et al. Nicotinamide restores cognition in Alzheimer's disease transgenic mice via a mechanism involving sirtuin inhibition and selective reduction of Thr231-phosphotau. *J Neurosci* 2008; 28: 11500–10.

[64] Sung YM, Lee T, Yoon H, et al. Mercaptoacetamide-based class II HDAC inhibitor lowers Aβ levels and improves learning and memory in a mouse model of Alzheimer's disease. Exp Neurol 2013; 239: 192–201.

[65] Peleg S, Sananbenesi F, Zovoilis A, et al. Altered histone acetylation is associated with age-dependent memory impairment in mice. *Science* 2010; 328: 753–6.

[66] Cadena-del-Castillo C, Valdes-Quezada C, Carmona-Aldana F, et al. Age-dependent increment of hydroxymethylation in the brain cortex in the triple-transgenic mouse model of Alzheimer's disease. *J Alzheimers Dis* 2014; 41: 845–54.

[67] Pheiffer C, Dias S, Muller C, et al. Decreased global DNA methylation in the white blood cells of high fat diet fed vervet monkeys (*Chlorocebus aethiops*). *J Physiol Biochem* 2014; 70: 725–733.

[68] Lashley T, Gami P, Valizadeh N, et al. Alterations in global DNA methylation and hydroxymethylation are not detected in Alzheimer's disease. *Neuropathol Appl Neurobiol* 2015; 41: 497–506.

[69] Bradley-Whitman MA, Lovell MA. Epigenetic changes in the progression of Alzheimer's disease. *Mech Ageing Dev* 2013; 134: 486–95.

[70] Rao JS, Keleshian VL, Klein S, et al. Epigenetic modifications in frontal cortex from Alzheimer's disease and bipolar disorder patients. *Transl Psychiatry* 2012; 2: e132.

[71] Sung HY, Choi EN, Ahn Jo S, et al. Amyloid protein-mediated differential DNA methylation status regulates gene expression in Alzheimer's disease model cell line. *Biochem Biophys Res Commun* 2011; 414: 700–5.

[72] Hodgson N, Trivedi M, Muratore C, et al. Soluble oligomers of amyloid-β cause changes in redox state, DNA methylation, and gene transcription by inhibiting EAAT3 mediated cysteine uptake. *J Alzheimers Dis* 2013; 36: 197–209.

[73] Morrison LD, Smith DD, Kish SJ. Brain S-adenosylmethionine levels are severely decreased in Alzheimer's disease. *J Neurochem* 1996; 67: 1328–31.

[74] Bottiglieri T, Godfrey P, Flynn T, et al. Cerebrospinal fluid S-adenosylmethionine in depression and dementia: effects of treatment with parenteral and oral S-adenosylmethionine. *J Neurol Neurosurg Psychiatry* 1990; 53: 1096–1098.

[75] Eto K, Asada T, Arima K, et al. Brain hydrogen sulfide is severely decreased in Alzheimer's disease. *Biochem Biophys Res Commun* 2002; 293: 1485–8.

[76] Fuso A, Seminara L, Cavallaro RA, et al. S-adenosylmethionine/homocysteine cycle alterations modify DNA methylation status with consequent deregulation of PS1 and BACE and beta-amyloid production. *Mol Cell Neurosci* 2005; 28: 195–204.

[77] Kennedy BP, Bottiglieri T, Arning E, et al. Elevated S-adenosylhomocysteine in Alzheimer brain: influence on methyltransferases and cognitive function. *J Neural Transm* 2004; 111: 547–567.

[78] Goggins M, Scott JM, Weir DG. Methylation of cortical brain proteins from patients with HIV infection. *Acta Neurol Scand* 1999; 100: 326–31.

[79] Ficz G, Branco MR, Seisenberger S, et al. Dynamic regulation of 5-hydroxymethylcytosine in mouse ES cells and during differentiation. *Nature* 2011; 473: 398–402.

[80] Sanchez-Mut J V, Gräff J. Epigenetic alterations in Alzheimer's disease. *Front Behav Neurosci* 2015; 9: 347.

[81] Lunnon K, Mill J. Epigenetic studies in Alzheimer's disease: current findings, caveats, and considerations for future studies. *Am J Med Genet B Neuropsychiatr Genet* 2013; 162B: 789–99.

SUPPLEMENTARY DATA

SUPPLEMENTARY FIGURE 1. Overview of analyzed hippocampal subregions. Shown is a representative image of the 5-hydroxymethylcytosine staining in a 6 months old APP/PS1dE9 mouse, to illustrate the relative location of the analyzed dentate gyrus (DG), cornu ammonis (CA) 3, and CA1-2 subregions in the hippocampus (A). Also shown are high magnification images of these subregions (B-D, respectively), representative of those that were analyzed for the semiquantitative analysis. Scale bar represents 200 µm in A and 75 µm in B-D.

supplementary figure 1.

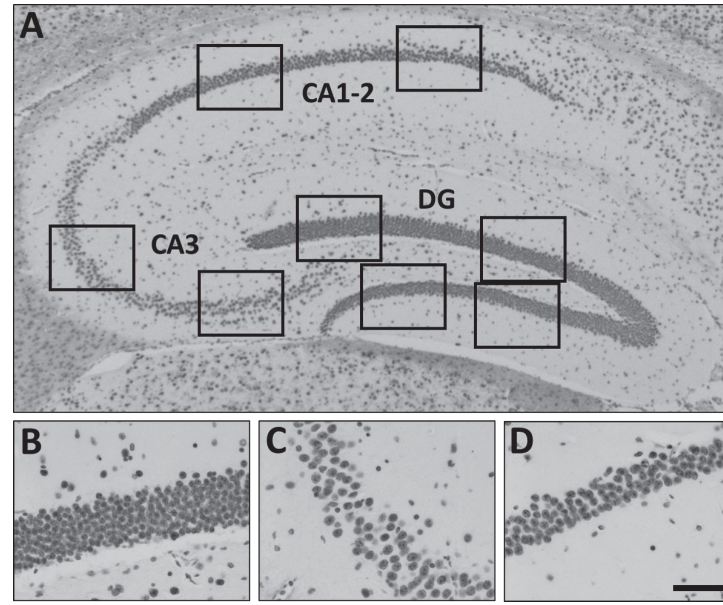

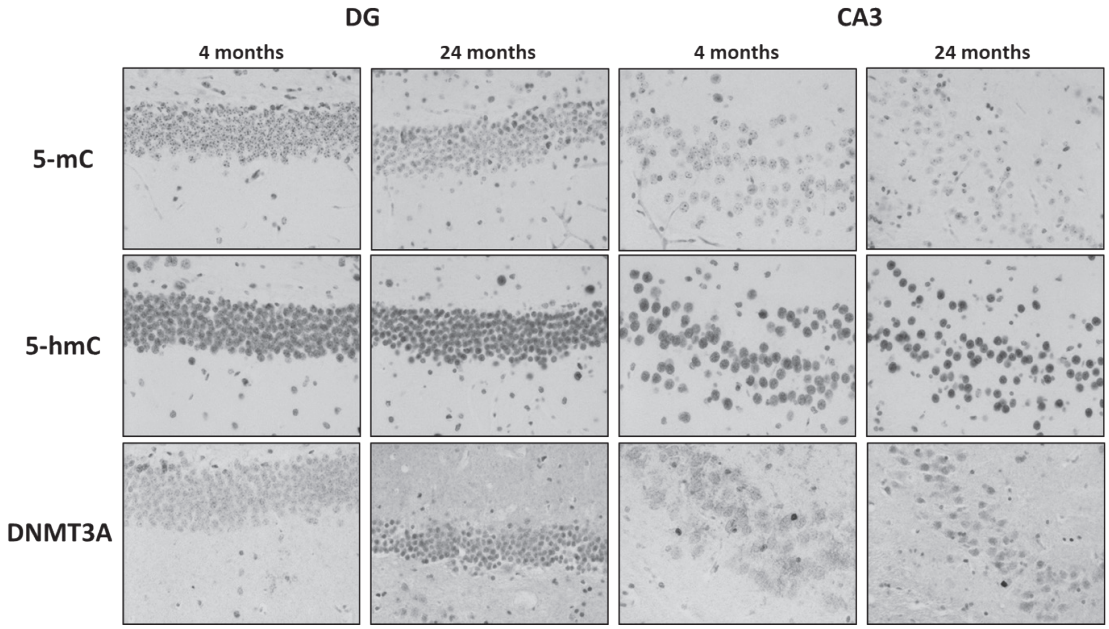

supplementary figure 2.

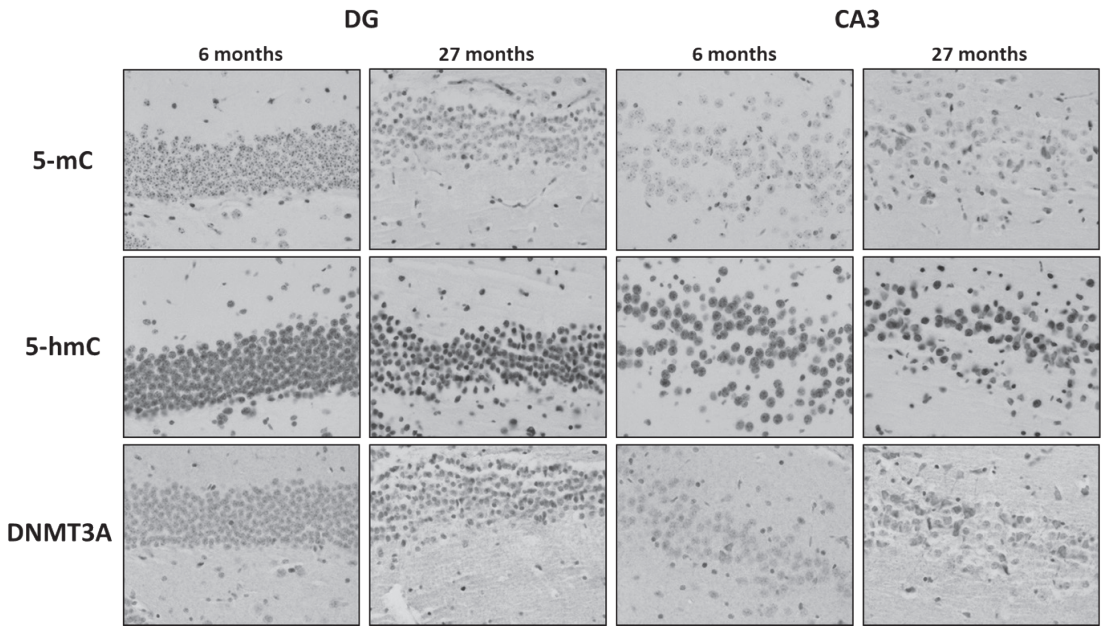

supplementary figure 3.

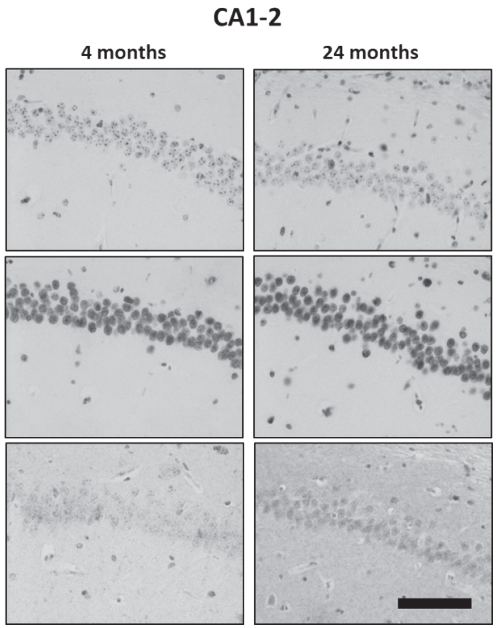

supplementary figure 2.

SUPPLEMENTARY FIGURE 2. Overview of the analyzed immunohistochemical stainings of epigenetic markers in the J20 transgenic mouse model. Shown are representative examples of analyzed images of the 5-methylcytosine (5-mC), 5-hydroxymethylcytosine (5-hmC), and DNA methyltransferase (DNMT) 3A stainings, in the dentate gyrus (DG), cornu ammonis (CA) 3, and CA1-2 subregions in the hippocampus, from the youngest (4 months old) and oldest (24 months) animals studied. A statistically significant age-related decrease in DG 5-mC immunoreactivity was detected after a semiquantitative analysis of the images. Scale bar represents 100 µm.

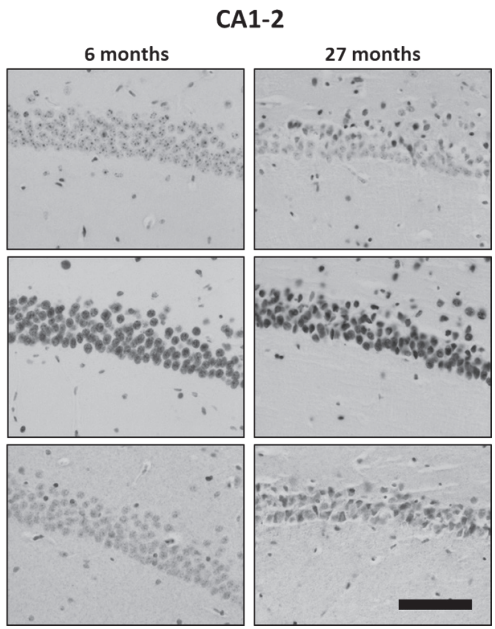

supplementary figure 3.

SUPPLEMENTARY FIGURE 3. Overview of the analyzed immunohistochemical stainings of epigenetic markers in the APP/PS1dE9 transgenic mouse model. Shown are representative examples of analyzed images of the 5-methylcytosine (5-mC), 5-hydroxymethylcytosine (5-hmC), and DNA methyltransferase (DNMT) 3A stainings, in the dentate gyrus (DG), cornu ammonis (CA) 3, and CA1-2 subregions in the hippocampus, from the youngest (6 months old) and oldest (27 months) animals studied. Apart from some structural changes, no clear age-related alterations in immunoreactivity can be observed, which is in line with observations from the semiquantitative analysis. Scale bar represents 100 µm.

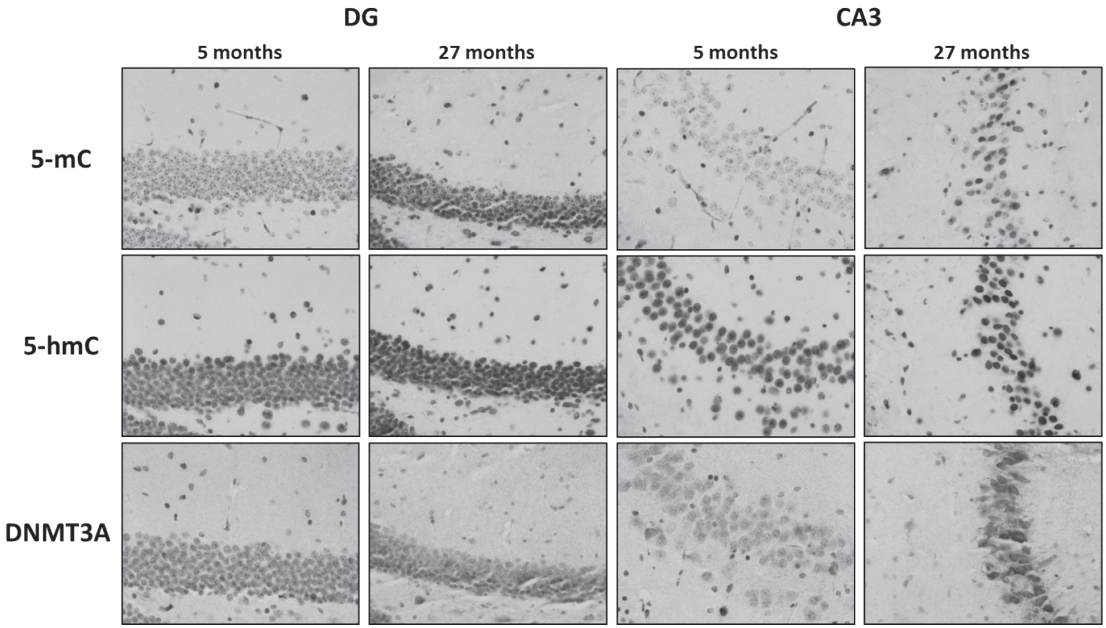

supplementary figure 4.

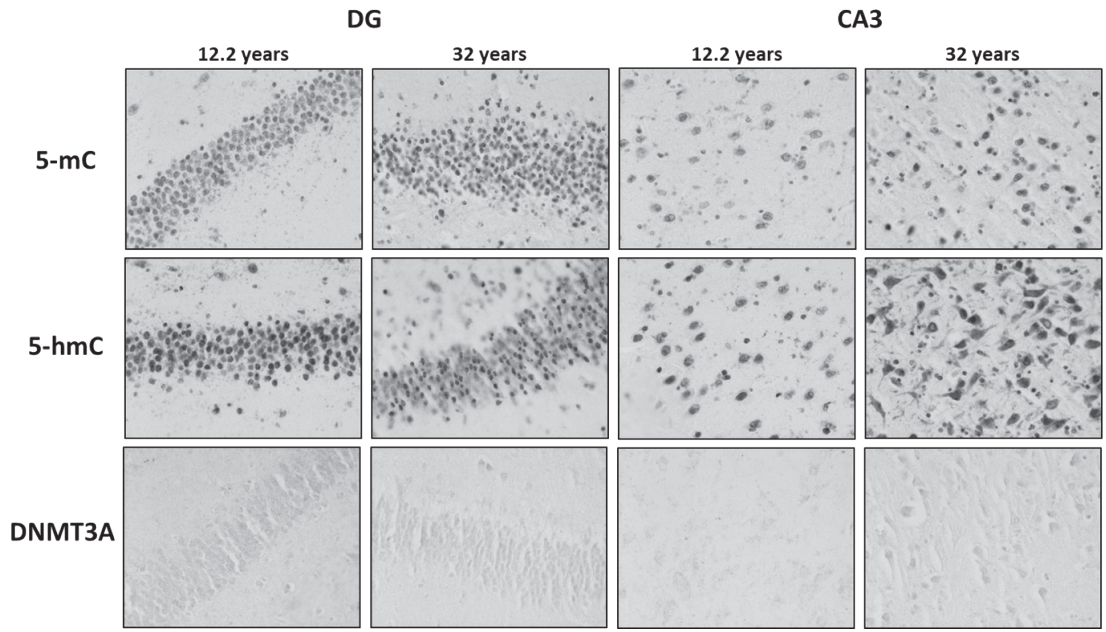

supplementary figure 5.

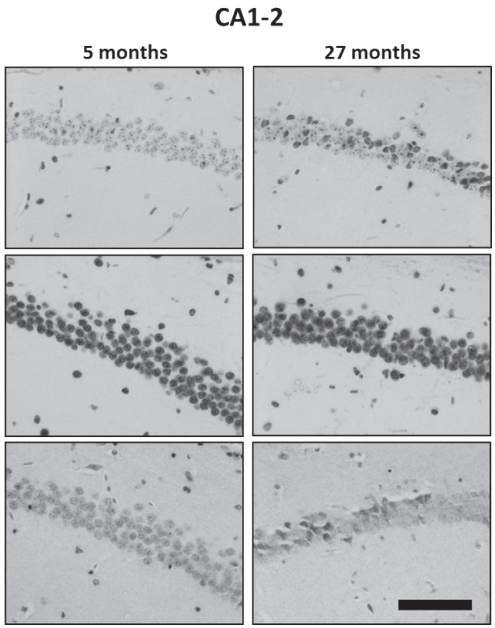

supplementary figure 4.

SUPPLEMENTARY FIGURE 4. Overview of the analyzed immunohistochemical stainings of epigenetic markers in the 3xTg-AD transgenic mouse model. Shown are representative examples of analyzed images of the 5-methylcytosine (5-mC), 5-hydroxymethylcytosine (5-hmC), and DNA methyltransferase (DNMT) 3A stainings, in the dentate gyrus (DG), cornu ammonis (CA) 3, and CA1-2 subregions in the hippocampus, from the youngest (5 months old) and oldest (27 months) animals studied. An age-related increase in 5-mC immunoreactivity can be observed in the DG, CA3, and CA1-2 regions of this mouse model. A semiquantitative analysis, however, shows this increase is only statistically significant in the DG and CA1-2 regions. Scale bar represents 100 µm.

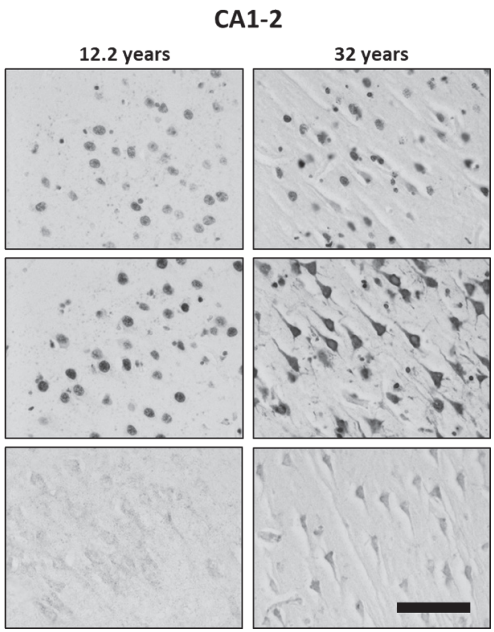

supplementary figure 5.

SUPPLEMENTARY FIGURE 5. Overview of the analyzed immunohistochemical stainings of epigenetic markers in the Caribbean vervets. Shown are representative examples of analyzed images of the 5-methylcytosine (5-mC), 5-hydroxymethylcytosine (5-hmC), and DNA methyltransferase (DNMT) 3A stainings, in the dentate gyrus (DG), cornu ammonis (CA) 3, and CA1-2 subregions in the hippocampus, from the youngest (12.2 years old) and oldest (32 years old) animals studied. From the images shown there may appear to be some age-related differences, mainly in the DG, but these did not appear consistently, as signified by a semiquantitative analysis which did not reveal any statistically significant age-related alterations in immunoreactivity of any of the tested epigenetic markers. Scale bar represents 100 µm.

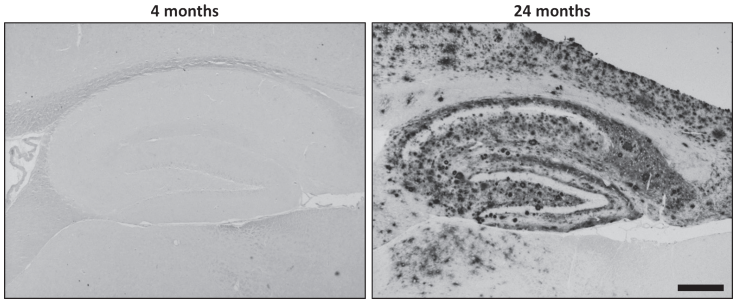

supplementary figure 6.

SUPPLEMENTARY FIGURE 6. Hippocampal 3A1 plaque staining in transgenic J20 mice. Shown are representative images of the youngest (4 months) and oldest (24 months) animals. Note the high plaque load throughout the whole hippocampus in the oldest animals. Scale bar represents 400 µm.

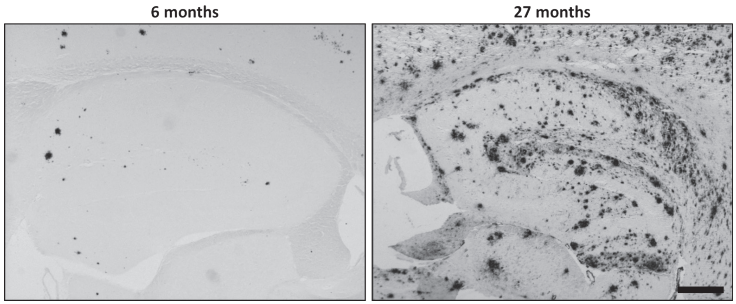

supplementary figure 7.

SUPPLEMENTARY FIGURE 7. Hippocampal 3A1 plaque staining in transgenic APP/PS1dE9 mice. Shown are representative images of the youngest (6 months) and oldest (27 months) animals. Note the distribution of plaques throughout the whole hippocampus in the oldest animals. Amyloid deposition seems to be lower than in the J20 mice (Supplementary Figure 6). Scale bar represents 400 µm.

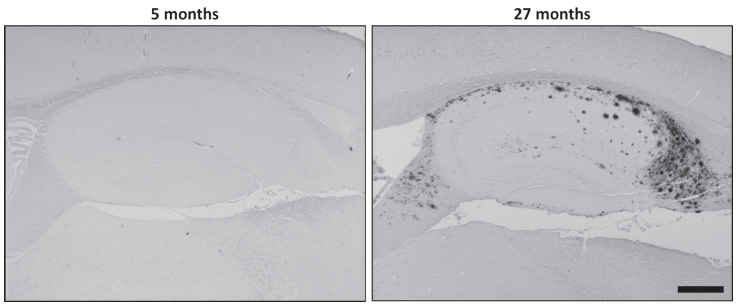

supplementary figure 8.

SUPPLEMENTARY FIGURE 8. Hippocampal 3A1 plaque staining in transgenic 3xTg-AD mice. Shown are representative images of the youngest (5 months) and oldest (27 months) animals. Note the uneven distribution of plaques throughout the hippocampus in the oldest animals, with the highest amyloid beta immunoreactivity in the dorsal subiculum and deeper layers of the hippocampus (oriens and alveus). Scale bar represents 400 µm.

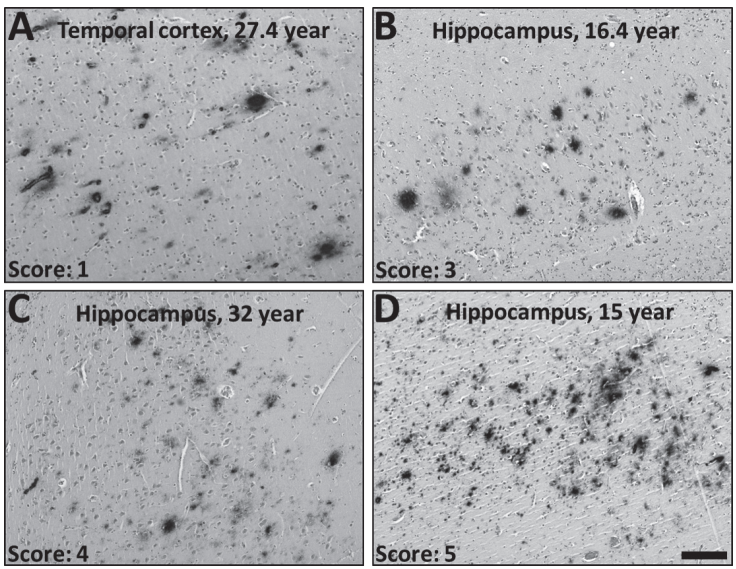

supplementary figure 9.

SUPPLEMENTARY FIGURE 9. Amyloid beta 42 plaque staining in Caribbean vervets. The images were scored according to their plaque load; 0 for no plaques, 1 for plaques in the temporal cortex but not yet inside the hippocampus, 2 for 1 to 5 plaques in the hippocampus, 3 for 6 to 10 plaques, 4 for 11 to 100 plaques, and 5 for more than 100 plaques. Shown are representative images of the scores observed. Not all of the older vervets developed plaques

in the hippocampus, although all vervets over 18 years of age developed plaques in the frontal cortex, prefrontal cortex and/or temporal cortex. A is from a 27.4 years old vervet, B from a 16.4 years old, C from a 32 years old, and D from a 15 years old. Note that A is an image of the temporal cortex outside the hippocampus, while B-D are images taken inside the hippocampus. Scale bar represents 200 µm.

ACTIVE AMYLOID-β IMMUNOTHERAPY RESULTS IN EPIGENETIC CHANGES IN THE HIPPOCAMPUS OF AN ALZHEIMER'S DISEASE MOUSE MODEL

ROY **LARDENOIJE**[A,B], DANIËL L.A. **VAN DEN HOVE**[B,C], SOPHIE E. **JUNG**[B], MONIQUE **HAVERMANS**[B], BIN **LIU**[A], BART P.F. **RUTTEN**[B,*], CYNTHIA A. **LEMERE**[A,*]

[A]ANN ROMNEY CENTER FOR NEUROLOGIC DISEASES, DEPARTMENT OF NEUROLOGY, BRIGHAM AND WOMEN'S HOSPITAL, HARVARD MEDICAL SCHOOL, USA
[B]SCHOOL FOR MENTAL HEALTH AND NEUROSCIENCE (MHENS), DEPARTMENT OF PSYCHIATRY AND NEUROPSYCHOLOGY, MAASTRICHT UNIVERSITY, THE NETHERLANDS
[C]LABORATORY OF TRANSLATIONAL NEUROSCIENCE, DEPARTMENT OF PSYCHIATRY, PSYCHOSOMATICS AND PSYCHOTHERAPY, UNIVERSITY OF WUERZBURG, GERMANY
*THESE AUTHORS CONTRIBUTED EQUALLY TO THIS WORK.

Abstract

While evidence accumulates for a role of epigenetic modifications in the pathophysiological cascade of Alzheimer's disease (AD), amyloid-β (Aβ)-targeted active immunotherapy approaches are employed to prevent the progression of AD. The impact of active immunotherapy on epigenetic markers has not been studied thus far. The current study aims to establish the relation between active immunotherapy with a MER5101-based vaccine and epigenetic DNA modifications, using semi-quantitative immunohistochemistry in the hippocampus of APPswe/PS1dE9 mice. Immunotherapy started when the mice were 10 months of age, behavioral testing occurred at 14 months of age, after which the mice were sacrificed for further analysis of their brains. Global levels of DNA methylation and hydroxymethylation were compared to previously established immunization-induced changes in AD-related neuropathology and cognition. It was found that active immunization did not affect global DNA methylation levels, but resulted in decreased DNA hydroxymethylation and DNA methyltransferase (DNMT) 3A levels. In addition, correlations with behavioral outcomes were observed for levels of DNA methylation and hydroxymethylation, but not DNMT3A, while Aβ pathology and synaptic markers did not correlate with DNA methylation levels, but did correlate with DNA hydroxymethylation and levels of DNMT3A. These findings indicate that active Aβ immunization has significant effects on the epigenome in APPswe/PS1dE9 mice, and that DNA methylation and hydroxymethylation may be involved in cognitive functioning.

KEYWORDS: Alzheimer's disease; amyloid-β; active immunization; epigenetics; DNA methylation; mouse model

6.1. Introduction

Although the exact role of neuritic plaques and amyloid-β (Aβ) in the pathogenesis of Alzheimer's disease (AD) remains to be elucidated, studies have shown beneficial effects of Aβ immunization in various animal models [1]. The first reported study of Aβ immunization involved injecting transgenic PDAPP mice intraperitoneally (i.p.) with human Aβ1-42 peptide in conjunction with Freund's adjuvant [2]. When immunized before plaque development, the PDAPP mice barely developed any plaques at all. Interestingly, even after the initial development of plaques, Aβ immunization resulted in striking decreases in brain Aβ levels. Later studies have corroborated these findings and found similar effects when immunizing intranasally (i.n.) with Aβ1-40 [3, 4] and were able to enhance antibody titers using the *Escherichia coli* heat-labile enterotoxin mucosal adjuvant (LT) [5].

The beneficial effects of Aβ immunization are not limited to a reduction of plaques and Aβ levels, but, importantly, also include reports of ameliorated behavioral and cognitive impairments in animal models of AD [6, 7] and limited evidence for cognitive stabilization in humans [8]. The mechanisms, however, linking Aβ-reduction by immunization to beneficial effects on cognitive performance remain to be determined. Indeed, the relationship between soluble and aggregated forms of Aβ and cognitive deficits in AD remains a hotly debated topic [9]. A possible explanation for how Aβ is able to affect so many systems, including those involved in cognition, would be an interaction with the epigenetic machinery. Epigenetic mechanisms dynamically govern gene expression at both transcriptional and translational levels [10], and are thought to mediate interactions between genetic aberrations and environmental influences [11]. In particular, DNA methylation appears to be dysregulated in AD [12, 13], and the closely related epigenetic process of DNA hydroxymethylation has been implicated as well [14]. Long-term DNA methylation is maintained by maintenance DNA methyltransferases, whereas novel methylation modifications are imparted by *de novo* DNA methyltransferases [13]. DNA hydroxymethylation arises through the oxidation of DNA methylation groups by ten-eleven translocation (TET) enzymes and is particularly enriched in the brain [15, 16].

It has been suggested that the epigenetic alterations observed in relation to AD are, at least in part, induced by Aβ [17]. The exact role of Aβ in the epigenetic dysregulation observed in AD is, however, not well understood, nor is the impact of Aβ vaccination on the epigenome. In order to explore these questions, the present study was undertaken to establish the epigenetic impact of active Aβ immunization, using brain tissues from a previously published, well-characterized cohort of Aβ immunized

mice [18], and examining the relationship between several epigenetic markers (5-methylcytosine [5-mC], a marker of DNA methylation, 5-hydroxymethylcytosine [5-hmC], a marker of DNA hydroxymethylation, and *de novo* DNA methyltransferase [DNMT] 3A) and indicators of AD-related pathology.

6.2. Materials and methods
6.2.1. Animals and treatment

For this study, the APPswe/PS1dE9 model [18] was used. APPswe/PS1dE9 mice carry a human amyloid precursor protein (APP) transgene with the Swedish mutation (K594N/M595L) and a human presenilin (PS) 1 transgene with deletion of exon 9 (PS1dE9), co-expressed under the mouse prion protein promoter [19]. APPswe/PS1dE9 breeders (on a C57BL/6 background) were obtained from The Jackson Laboratory (Bar Harbor, ME) and crossed with DBA/2 wild-type mice to generate the APPswe/PS1dE9 mice on a B6D2F1 background that were used for the immunization experiment. Animal use was approved by the Harvard Standing Committee for Animal Use and was in line with state and federal regulations. See Table 1 for an overview of the studied animals.

table 1.

Model	Mutations	Age	Gender	Treatment	N
APPswe/PS1dE9	APP K594N,M595L, deletion of exon 9	10 months	Female	Vaccine	2
				Vehicle	2
			Male	Vaccine	3
				Vehicle	4

The mice in this study were previously immunized with MER5101 as described [18]. Eleven 10-month-old male (n = 7) and female (n = 4) APPswe/PS1dE9 mice were randomly distributed between MER5101 immunized (n = 5) and vehicle treated control (n = 6) groups. The MER5101 vaccine was formulated in Mercia's Th2-biased adjuvant (MAS-1; Mercia Pharma, Scarsdale, NY) and consisted of multiple Aβ1-15 copies, conjugated with a 7 aa spacer to the diphtheria toxoid (DT) carrier protein. MER5101 vaccine was prepared as described previously [18]. The vehicle formulation for the control group contained sterile phosphate-buffered saline (PBS) mixed with MAS-1. Treatment consisted of five subcutaneous injections of 0.1 ml of MER5101, containing 100 μg Aβ1-15:DT conjugate, or PBS instead of antigen in case of the vehicle controls. The first two injections were administered 2 weeks apart, and the following three were given 4 weeks apart. After treatment, at 14 months old, the mice were cognitively assessed and sacrificed by CO_2 inhalation and transcardial perfusion with 20 ml PBS. Tail plasma was

TABLE 1. Overview of the animals from each treatment group available for the current study.

sampled as previously indicated [20]. After sacrificing the animals, one brain hemisphere was processed for paraffin sectioning after a 2-hours fixation in 10% neutral-buffered formalin. The other half was snap frozen and kept at -80°C for biochemical analysis. The archived tissue from these animals was used for the current study.

6.2.2. Immunohistochemistry

The paraffin embedded brains were cut in 10 μm-thick serial sagittal sections for immunohistochemistry (IHC). The staining procedure was performed at room temperature unless specified otherwise. After deparaffinization in Histo-Clear (National Diagnostics, Atlanta, GA), the sections were rehydrated in a graded ethanol series through to demineralized water. Endogenous peroxidase activity was quenched through submersion in a methanol solution containing 0.3% H_2O_2 for 10 minutes. BioGenex citrate buffer (BioGenex, San Ramon, CA) was used for antigen retrieval, keeping it around the boiling point in the microwave for 5 minutes. The sections were cooled and then washed for 10 minutes in demineralized water before being placed in blocking solution for 20 minutes. Blocking solution contained 10% serum from the secondary antibody host species, dissolved in Tris-buffered saline. Primary antibody incubation took place overnight at 4°C. Primary antibodies used included a mouse monoclonal anti-5-mC antibody (1:1000 dilution; GenWay Biotech Inc., San Diego, CA) for 5-mC detection, rabbit polyclonal anti-5-hmC anti-serum (1:10,000 dilution; Active Motif, Carlsbad, CA) for 5-hmC, a rabbit polyclonal anti-DNMT3A antibody (1:200 dilution; Santa Cruz Biotechnology, Dallas, TX) for DNMT3A, and 3A1, a general monoclonal IgG1 anti-Aβ antibody (1:1000 dilution, provided by Dr. Brian O`Naullain at the Ann Romney Center for Neurologic Diseases, Boston, MA), for plaques. The specificity of the 3A1 antibody has previously been established [21]. After washing off the primary antibody solution, the slides were covered in secondary antibody solution for 30 minutes. Biotinylated secondary antibodies were used; horse anti-mouse (Vector Laboratories, Burlingame, CA) for 5-mC, goat anti-rabbit (Vector Laboratories) for 5-hmC and DNMT3A, and goat anti-mouse (Vector Laboratories) for the 3A1 Aβ antibody. For visualization, the VectorElite horseradish peroxidase ABC kit (Vector Laboratories), with 3,3'-diaminobenzidine tetrahydrochloride (DAB; Sigma-Aldrich, St. Louis, MO) as chromogen, was used. A negative control, leaving out the primary antibody, was added to each of the staining runs, and which, in all cases, displayed no signal (data not shown).

6.2.3. Immunoreactivity of epigenetic markers and plaque load

Three sagittal sections at varying hippocampal planes were selected for each immunohistochemical staining. A BX50 brightfield microscope (Olympus, Tokyo, Japan) coupled to a QIcam digital camera (QImaging, Surrey, Canada) was used to take photographic images of hippocampal subregions. For the immunoreactivity (IR) analysis of 5-mC, 5-hmC and DNMT3A, 4 pictures of the dentate gyrus (DG), 2 of the cornu ammonis (CA) 3 and 2 of the CA1-2 regions were taken with the 20X objective (see Figure 1 for representative images). ImageJ (version 1.48v, Wayne Rasband, National Institutes of Health, Bethesda, Maryland, USA) was used to delineate the region of interest (ROI; DG, CA3 or CA1-2) in each image, set a fixed threshold for background correction, and measure the mean grey value, the area of the ROI, and the area of the ROI with grey value above threshold. From these measurements the integrated density was determined by multiplying the background-corrected mean grey values with the fraction of the ROI area with values above the background threshold (as also described in [22]). In addition, the ratio of 5-mC to 5-hmC integrated density values was calculated. Hippocampal plaque load was determined in 3 sagittal sections per mouse that were stained using the 3A1 antibody (see Figure 2 for representative images). A BIOQUANT image analysis setup (Nashville, TN, USA) was used to measure the fraction of the hippocampal area covered by plaques. After manual delineation of the hippocampus and artifact removal, a fixed threshold was used to detect plaques and determine the area fraction of interest.

6.2.4. Additional characterizations

The effects of MER5101 vaccination on AD-related markers and cognition have previously been reported for the APPswe/PS1dE9 mice [18]. Some of these measurements were included in the current study to evaluate the correlation with the measured epigenetic markers. The included data concerns brain levels of Aβx-40 and Aβx-42 protein, as determined through enzyme-linked immunosorbent assays (ELISA), and optical density measurements of postsynaptic density protein (PSD)-95 and synaptophysin (SYP) in the CA3 and CA1 [18]. PSD-95 and SYP are markers of post- and presynaptic integrity, respectively. Moreover, behavioral data from the contextual fear conditioning (CFC) and Morris

water maze (MWM) tests was included [18]. The MWM test data included the escape latency as a measure for spatial learning, and the annulus crossing index (ACI), determined 2 and 24 hours after the last hidden platform trial, as a measure for spatial memory. The ACI is calculated as the number of crosses over the platform location in the correct quadrant, adjusted for crosses of the same location in the other quadrants [18].

6.2.5. Data analysis

Data were analyzed with SPSS Statistics 21 (IBM; Armonk, NY). Data were checked for normality and homoscedasticity. Due to non-normal data, the Mann-Whitney U test was performed. These tests were performed to examine differences between vaccinated and control mice on the following variables: 1) fraction of the hippocampal area covered by plaques, 2) integrated density measures of the epigenetic markers 5-mC, 5-hmC, their ratio (5-mC:5-hmC), and DNMT3A. In addition, Pearson's correlation was used to correlate AD markers (i.e. Aβx-40, Aβx-42, plaque covered hippocampal area fraction, SYN, and PSD-95) with epigenetic markers (5-mC, 5-hmC, 5-mC:5-hmC, and DNMT3A). All analyses were two-tailed, with alpha set at 0.05.

6.3. Results

As reported previously [18], brain Aβx-40 protein levels were not significantly altered in vaccinated mice, while Aβx-42 protein levels were significantly reduced in vaccinated mice. Furthermore, MER5101-immunized mice displayed enhanced densities of pre-synaptic SYP and post-synaptic PSD-95 in the hippocampal regions CA1 and CA3, when compared to vehicle-treated APPswe/PS1dE9 mice. Behaviorally, vaccinated animals showed an increase in freezing frequency during the CFC test and better spatial learning and memory in the MWM, when compared to the vehicle-treated mice. The following section contains a summary of the novel findings. For the full results, see Supplementary Tables 1-4.

6.3.1. Fraction of hippocampal area covered by plaques

We found a statistically significant difference between groups in the fraction of the hippocampal area covered by plaques ($U = 3$, $p = 0.028$). Coverage by plaques in the hippocampus was greater in the control group

(M = 0.19, SD = 0.03) than in the treatment group (M = 0.14, SD = 0.02) (Figure 2).

6.3.2. Integrated density measures of epigenetic markers

Staining and quantification of epigenetic markers in hippocampal subregions was performed (Figure 1). No differences in 5-mC levels were found between the groups (Figure 3). The 5-hmC values were higher in the control group than in the vaccinated group across the whole hippocampus (U = 0.00, p = 0.006), as well as in each hippocampal subregion, i.e. the DG (U = 3.00, p = 0.028), CA3 (U = 3.00, p = 0.028), and CA1-2 (U = 0.00, p = 0.006; Figure 4). Moreover, the DNMT3A integrated density measures were observed to be higher in the CA3 (U = 2.00, p = 0.018) and in the hippocampus as a whole (U = 4.00, p = 0.045) of control compared to vaccinated mice (Figure 5). Also, no difference in the 5-mC:5-hmC ratio was found between the groups (Figure 6).

6.3.3. Correlation analysis of AD markers, epigenetic markers, and behavior

Whereas 5-mC and the 5-mC:5-hmC ratio did not correlate statistically significantly with any of the AD markers, 5-hmC values correlated positively with hippocampal area fraction containing plaques (r = 0.643, p = 0.033), as well as with SYP in the CA1 (r = 0.831, p = 0.002), SYP in the CA3 (r = 0.823, p = 0.002), PSD-95 in the CA1 (r = 0.692, p = 0.018), and PSD-95 in the CA3 (r = 0.702, p = 0.016). Note that for the densitometric analysis of SYP and PSD-95 a lower value indicates a higher density [18]. Further, DNMT3A values correlated significantly with hippocampal area fraction containing plaques (r = 0.629, p = 0.038).

Of the behavioral outcomes, average escape latency on day 5 of the MWM correlated best with markers associated with AD pathology, showing a positive correlation with brain Aβx-40 (r = 0.694, p = 0.018) and Aβx-42 (r = 0.703, p = 0.016), as well as with hippocampal Aβ load (r = 0.676, p = 0.022). CFC freezing behavior, while not correlating well with Aβ directly, correlated negatively with PSD95 in the CA3 (r = -0.709, p = 0.015).

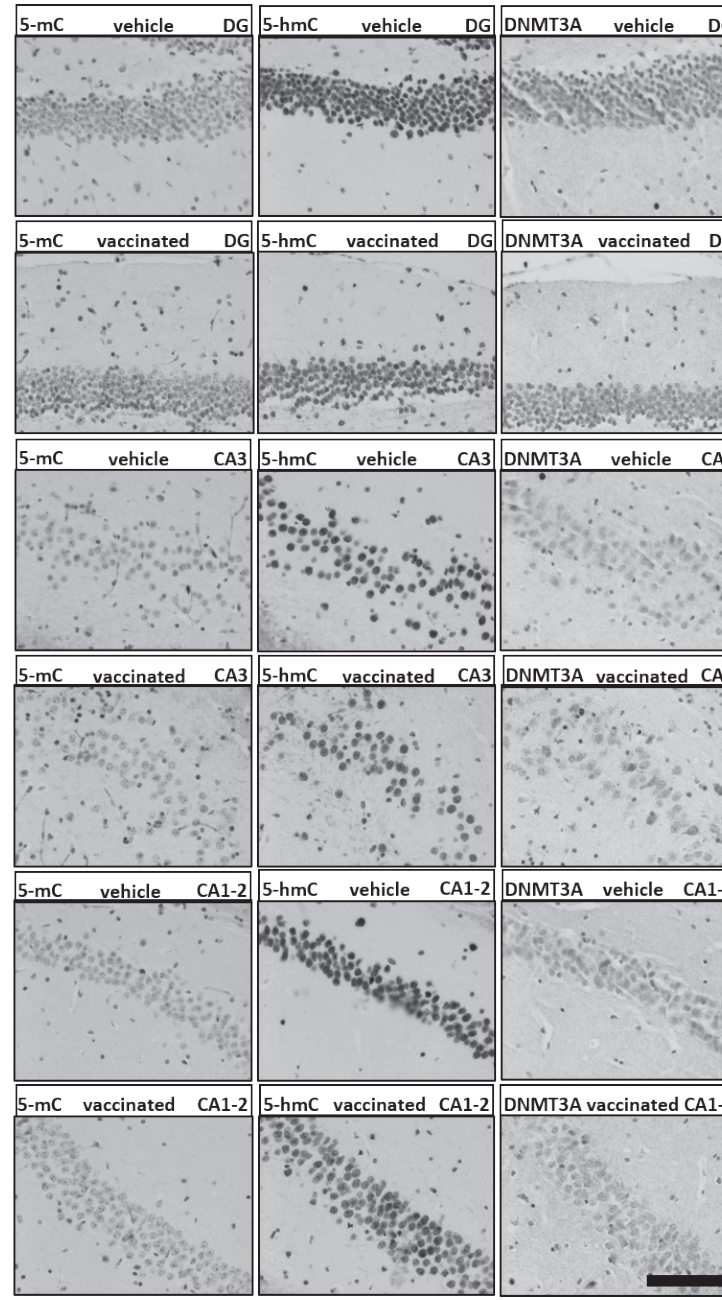

figure 1.

FIGURE 1. Overview of the immunohistochemically stained epigenetic markers analyzed in the APP/PS1dE9 transgenic mouse model.
Shown are representative examples of analyzed images of the 5-methylcytosine (5-mC), 5-hydroxymethylcytosine (5-hmC), and DNA methyltransferase (DNMT) 3A staining, in the dentate gyrus (DG), cornu ammonis (CA) 3, and CA1-2 hippocampal subregions, from the vehicle-treated and vaccinated groups. Integrated density measurements showed a decrease in 5-hmC across all regions, and a decrease in DNMT3A in the CA3. Scale bar represents 100 µm.

DNA methylation correlated inversely with MWM outcomes ACI after 2 (r = -0.805, p = 0.003) and 24 hours (r = -0.670, p = 0.024), as well as with time in the target quadrant after 2 (r = -0.608, p = 0.047) and 24 hours (r = -0.730, p = 0.011). For DNA hydroxymethylation only a statistically significant

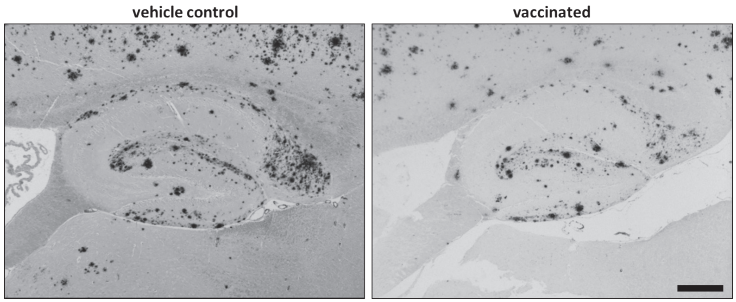

figure 2.

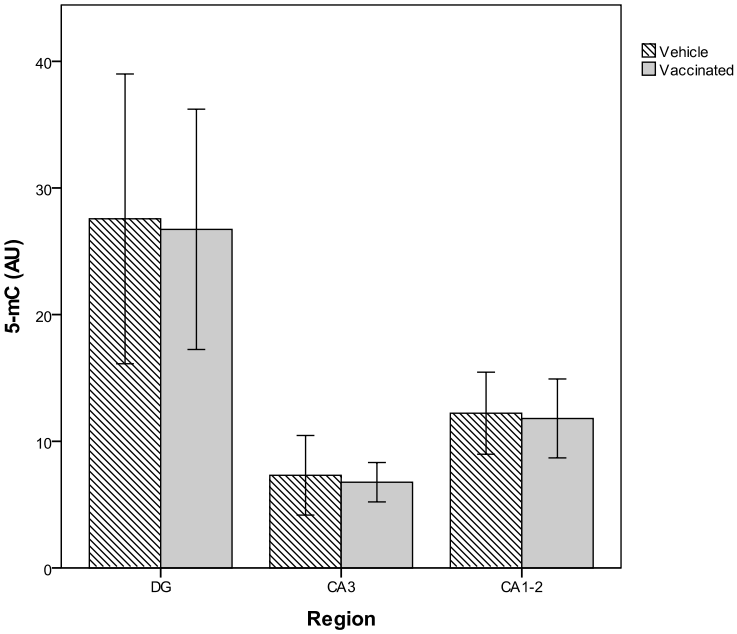

figure 3.

inverse correlation with ACI after 24 hours was found ($r = -0.656$, $p = 0.028$). DNMT3A negatively correlated with ACI after 24 hours ($r = -0.619$, $p = 0.042$), and positively with the average escape latency in the MWM task ($r = 0.679$, $p = 0.022$). The 5-mC:5-hmC ratio only inversely correlated with ACI after 2 hours ($r = -0.817$, $p = 0.002$). The 5-mC:5-hmC ratio showed a strong correlation with 5-mC ($r = 0.903$, $p < 0.001$), but not with 5-hmC ($r = -0.159$, $p = 0.640$). Additionally, DNMT3A showed a statistically significant correlation with 5-hmC ($r = 0.714$, $p = 0.014$), but only a trend towards a statistically significant correlation with 5-mC ($r = 0.594$, $p = 0.054$). 5-mC and 5-hmC also did not correlate with each other ($r = 0.258$, $p = 0.445$).

FIGURE 2. Hippocampal 3A1 plaque staining in transgenic APP/PS1dE9 mice.
Shown are representative images of vehicle-treated and vaccinated animals. Note the marked decrease in amyloid-β immunoreactivity in the vaccinated animal. Scale bar represents 400 µm.

FIGURE 3. Integrated density of 5-methylcytosine (5-mC) for the vaccinated and vehicle-treated groups in the dentate gyrus (DG), cornu ammonis (CA) 3, and CA1-2 subregions of the hippocampus.
Shown are the mean and 95% confidence interval. No differences between the groups were detected with a Mann-Whitney U test. AU, arbitrary units.

figure 4.

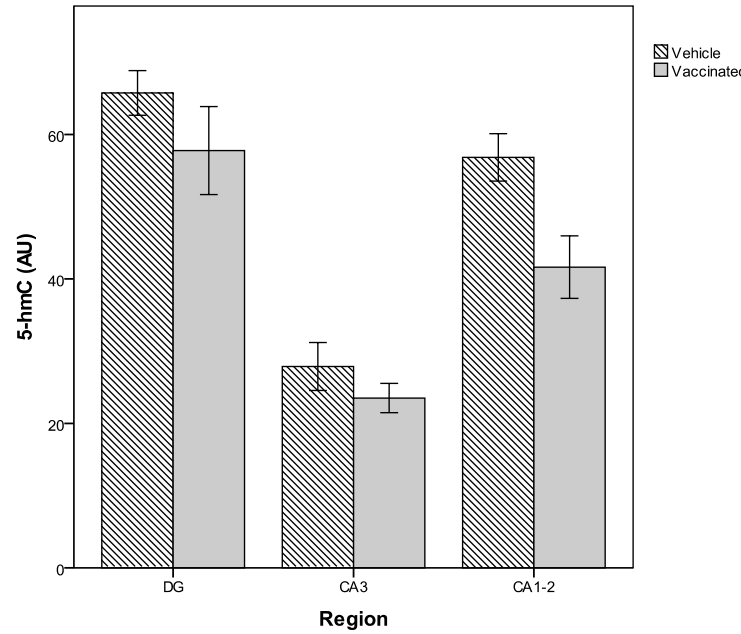

FIGURE 4. Integrated density of 5-hydroxymethylcytosine (5-hmC) for the vaccinated and vehicle-treated groups in the dentate gyrus (DG), cornu ammonis (CA) 3, and CA1-2 subregions of the hippocampus. Shown are the mean and 95% confidence interval. Mann-Whitney U tests showed that 5-hmC levels were lowered in the vaccinated group, in all subregions. AU, arbitrary units; * $p < 0.05$; ** $p < 0.01$.

figure 5.

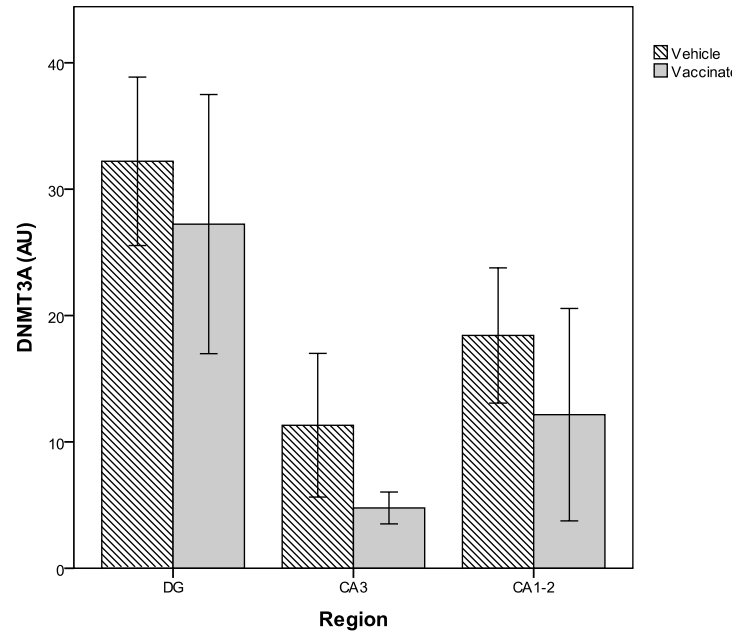

FIGURE 5. Integrated density of DNA methyltransferase (DNMT) 3A for the vaccinated and vehicle-treated groups in the dentate gyrus (DG), cornu ammonis (CA) 3, and CA1-2 subregions of the hippocampus. Shown are the mean and 95% confidence interval. Mann-Whitney U tests showed that DNMT3A levels were lowered in the CA3 region of the vaccinated group. AU, arbitrary units; * $p < 0.05$.

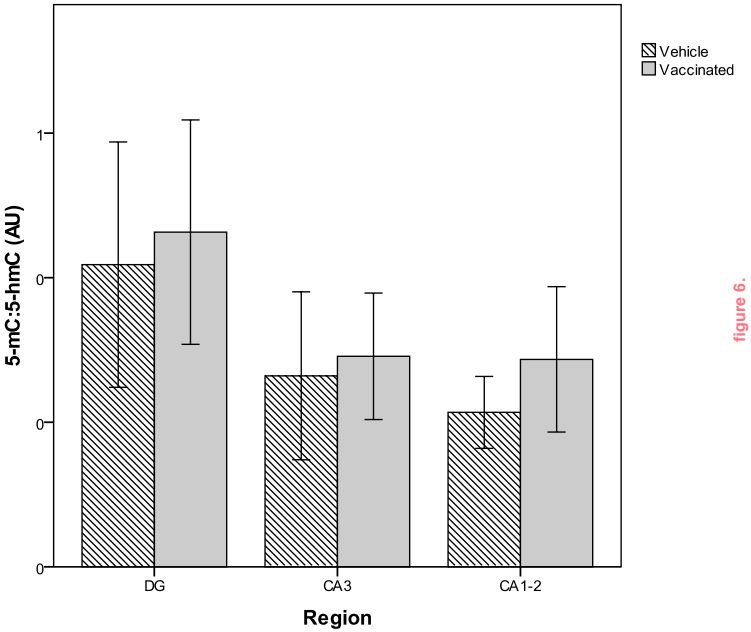

figure 6.

6.4. Discussion

Although there are many studies showing that AD involves profound epigenetic changes and studies that indicate immunotherapy may be an effective means to combat this disease, this is, to our knowledge, the first study to investigate the epigenetic impact of immunotherapy in a relevant mouse model.

As previously reported [18], following chronic, active Aβ immunization, APPswe/PS1dE9 mice showed decreased plaque pathology in the hippocampus. The present study indicates that these same mice show an additional decrease in general DNA hydroxymethylation and DNMT3A levels. Moreover, a positive correlation was found between 5-hmC and DNMT3A levels, and Aβ pathology. However, only 5-hmC correlated with SYP and PSD-95, thus indicating that higher levels of 5-hmC are associated with reduced synaptic integrity. On a behavioral level, escape latency in the MWM correlated best with Aβ pathology, with (as expected) greater pathology associated with poorer performance, while freezing in the CFC task was the only behavioral outcome correlating with synaptic density. Interestingly, higher 5-mC, and to a lesser extent 5-hmC and DNMT3A, levels were associated with a decreased performance in the MWM test.

These observations corroborate that there is a relationship between epigenetic mechanisms and plaque pathology, and suggest that Aβ may

FIGURE 6. Ratio of the 5-methylcytosine (5-mC) and 5-hydroxymethylcytosine (5-hmC) integrated densities for the vaccinated and vehicle-treated groups in the dentate gyrus (DG), cornu ammonis (CA) 3, and CA1-2 subregions of the hippocampus. Shown are the mean and 95% confidence interval. No differences between the groups were detected with a Mann-Whitney U test. AU, arbitrary units.

not only be involved in inducing epigenetic changes, but may play a role in maintaining these alterations. However, the differential observations for DNA methylation and hydroxymethylation suggest that these mechanisms may play separate roles in AD. Previous studies in humans and mice show DNA methylation is involved in AD [12, 13, 23]. Our findings, however, indicate this dysregulated DNA methylation may not be directly related to Aβ pathology, or is not readily reversible, as global DNA methylation was not affected after lowering plaque levels. In contrast, DNA hydroxymethylation, which has previously also been implicated in AD, may be more directly affected by the presence of Aβ, as a global decrease in 5-hmC was observed after lowering Aβ levels. It is thus possible that Aβ is able to increase DNA hydroxymethylation, possibly through a decrease in 5-hmC oxidation and downstream demethylation, which may result in changes in gene expression. The observation that Aβ can induce global demethylation [17] is partly in line with our findings, but further investigations should elucidate whether Aβ induces complete demethylation (back to cytosine), or conversion of 5-mC to 5-hmC.

Interesting in this respect is the potential role of DNMT3A, which was observed to decrease with 5-hmC levels after lowering Aβ levels, and which showed a strong correlation with 5-hmC levels. 5-hmC is generated through the oxidation of 5-mC by TET enzymes, but ultimately, novel methylated cytosines are required to create more hydroxymethylated cytosines. A possible mechanism driving *de novo* DNA hydroxymethylation is through the combined actions of DNMT3A and TET3, but for which there is still limited evidence in zygotes [24], and much remains to be elucidated in this respect. Note that while the *de novo* DNA methyltransferase DNMT3A has also been attributed demethylation activity, this is proposed to involve a direct 5-mC to C conversion, without a hydroxymethylated intermediate [25].

The findings of this study should be viewed in light of some limitations. Only a limited amount of animals was available for the current investigation, limiting its power. Additionally, while the mice used in this study develop Aβ plaque pathology, they do not develop tau pathology or robust loss of neurons. Therefore, it is possible that the epigenetic changes we observed here may differ from those seen in mouse models with both plaques and tau pathologies and/or in humans with AD.

In summary, we confirm that active Aβ immunotherapy effectively lowered Aβ plaque levels, and that epigenetic markers 5-mC, 5-hmC, and DNM3A correlated with behavioral outcomes, but that mainly 5-hmC and DNMT3A were associated with AD-related pathology. Accordingly, active immunotherapy only appeared to affect 5-hmC and DNMT3A levels. These preliminary findings raise important questions about the possibly (partially)

independent roles of DNA methylation and hydroxymethylation in AD, the involvement of DNMT3A in enhancing 5-hmC levels, and the interplay between immunotherapy and epigenetic regulation, which should be addressed in future studies.

Acknowledgments

We kindly thank K Le, H Crehan, Q Shi, and S Chowdhury for technical assistance. Funds have been provided by the Internationale Stichting Alzheimer Onderzoek (ISAO) grants 07551 and 11532 (D.L.A.vdH.), by the ISAO grants 09552 and 13515, and the Netherlands Organization for Scientific Research (NWO), grant 916.11.086 (Veni Award) (B.P.F.R.), and by an ISAO fellowship and a fellowship as part of NWO grant 022.005.019, (R.L.), and by an Anonymous Foundation and NIH/NIA R01 AG040092 (C.A.L.). Additional funds have been provided by the Joint Programme—Neurodegenerative Disease Research (JPND) for the EPI-AD consortium (http://www.neurodegenerationresearch.eu/wp-content/uploads/2015/10/Factsheet_EPI-AD.pdf). The funding agencies were not involved in the study design, data collection, analysis and interpretation, writing of the report, and the decision to submit the article for publication. The authors declare no conflicts of interest.

REFERENCES

[1] Agadjanyan MG, Petrovsky N, Ghochikyan A. A fresh perspective from immunologists and vaccine researchers: Active vaccination strategies to prevent and reverse Alzheimer's disease. *Alzheimer's Dement* 2015; 11: 1246–1259.

[2] Schenk D, Barbour R, Dunn W, et al. Immunization with amyloid-b attenuates Alzheimer disease-like pathology in the PDAPP mouse. *Nature* 1999; 400: 173–177.

[3] Weiner HL, Lemere CA, Maron R, et al. Nasal administration of amyloid-beta peptide decreases cerebral amyloid burden in a mouse model of Alzheimer's disease. *Ann Neurol* 2000; 48: 567–79.

[4] Lemere CA, Maron R, Spooner ET, et al. Nasal A.beta. treatment induces anti-A.beta. antibody production and decreases cerebral amyloid burden in PD-APP mice. *Ann NY Acad Sci* 2000; 920: 328–331.

[5] Lemere CA, Spooner ET, Leverone JF, et al. Intranasal immunotherapy for the treatment of Alzheimer's disease: Escherichia coli LT and LT(R192G) as mucosal adjuvants. *Neurobiol Aging* 2002; 23: 991–1000.

[6] Janus C, Pearson J, McLaurin J, et al. A beta peptide immunization reduces behavioural impairment and plaques in a model of Alzheimer's disease. *Nature* 2000; 408: 979–982.

[7] Morgan D, Diamond DM, Gottschall PE, et al. A beta peptide vaccination prevents memory loss in an animal model of Alzheimer's disease. *Nature* 2000; 408: 982–985.

[8] Bayer AJ, Bullock R, Jones RW, et al. Evaluation of the safety and immunogenicity of synthetic A beta 42 (AN1792) in patients with AD. *Neurology* 2005; 64: 94–101.

[9] Cerasoli E, Ryadnov MG, Austen BM. The elusive nature and diagnostics of misfolded Aβ oligomers. *Front Chem* 2015; 3: 17.

[10] Choudhuri S. From Waddington's epigenetic landscape to small noncoding RNA: some important milestones in the history of epigenetics research. *Toxicol Mech Methods* 2011; 21: 252–274.

[11] Liu L, Li Y, Tollefsbol TO. Gene-environment interactions and epigenetic basis of human diseases. *Curr Issues Mol Biol* 2008; 10: 25–36.

[12] Chouliaras L, Mastroeni D, Delvaux E, et al. Consistent decrease in global DNA methylation and hydroxymethylation in the hippocampus of Alzheimer's disease patients. *Neurobiol Aging* 2013; 34: 2091–2099.

[13] Lardenoije R, Iatrou A, Kenis G, et al. The epigenetics of aging and neurodegeneration. *Prog Neurobiol* 2015; 131: 21–64.

[14] Condliffe D, Wong A, Troakes C, et al. Cross-region reduction in 5-hydroxymethylcytosine in Alzheimer's disease brain. *Neurobiol Aging* 2014; 35: 1850–1854.

[15] Globisch D, Münzel M, Müller M, et al. Tissue distribution of 5-hydroxymethylcytosine and search for active demethylation intermediates. *PLoS One*; 5. Epub ahead of print 2010. DOI: 10.1371/journal.pone.0015367.

[16] Kriaucionis S, Heintz N. The nuclear DNA base 5-hydroxymethylcytosine is present in Purkinje neurons and the brain. *Science* 2009; 324: 929–30.

[17] Chen K-L, Wang SS-S, Yang Y-Y, et al. The epigenetic effects of amyloid-beta(1-40) on global DNA and neprilysin genes in murine cerebral endothelial cells. *Biochem Biophys Res Commun* 2009; 378: 57–61.

[18] Liu B, Frost JL, Sun J, et al. MER5101, a novel Aβ1-15:DT conjugate vaccine, generates a robust anti-Aβ antibody response and attenuates Aβ pathology and cognitive deficits in APPswe/PS1dE9 transgenic mice. *J Neurosci* 2013; 33: 7027–7037.

[19] Jankowsky JL, Fadale DJ, Anderson J, et al. Mutant presenilins specifically elevate the levels of the 42 residue β-amyloid peptide in vivo: Evidence for augmentation of a 42-specific γ secretase. *Human Molecular Genetics* 2004; 13: 159–170.

[20] Maier M, Seabrook TJ, Lemere CA. Modulation of the humoral and cellular immune response in Aβ immunotherapy by the adjuvants monophosphoryl lipid A (MPL), cholera toxin B subunit (CTB) and *E. coli* enterotoxin LT(R192G). *Vaccine* 2005; 23: 5149–5159.

[21] Frost JL, Liu B, Rahfeld J-U, et al. An anti-pyroglutamate-3 Aβ vaccine reduces plaques and improves cognition in APPswe/PS1ΔE9 mice. *Neurobiol Aging* 2015; 36: 3187–99.

[22] Lardenoije R, van den Hove DA, Vaessen TSJ, et al. Epigenetic modifications in mouse cerebellar Purkinje cells: effects of aging, caloric restriction, and overexpression of superoxide dismutase 1 on 5-methylcytosine and 5-hydroxymethylcytosine. *Neurobiol Aging* 2015; 36: 3079–3089.

[23] Coppieters N, Dieriks B V, Lill C, et al. Global changes in DNA methylation and hydroxymethylation in Alzheimer's disease human brain. *Neurobiol Aging* 2014; 35: 1334–1344.

[24] Amouroux R, Nashun B, Shirane K, et al. *De novo* DNA methylation drives 5-hmC accumulation in mouse zygotes. *Nat Cell Biol* 2016; 18: 225–233.

[25] Chen C-C, Wang K-Y, Shen C-KJ. DNA 5-methylcytosine demethylation activities of the mammalian DNA methyltransferases. *J Biol Chem* 2013; 288: 9084–91.

supplementary table 1.

	Variables	Vaccinated (mean ± SD)	Control (mean ± SD)	Mann-Whitney U
AD marker	Fraction of hippocampal area covered by plaques	0.1447 ± 0.0225	0.1939 ± 0.0254	$U = 3.00$, $p = 0.028$*
Epigenetic markers	5-mC	Hip: 15.10 ± 3.05	Hip: 15.70 ± 5.50	Hip: $U = 14.00$, $p = 0.855$
		DG: 26.73 ± 7.64	DG: 27.56 ± 10.90	DG: $U = 14.00$, $p = 0.855$
		CA3: 6.77 ± 1.25	CA3: 7.32 ± 2.99	CA3: $U = 15.00$, $p = 1.00$
		CA1-2: 11.80 ± 2.51	CA1-2: 12.22 ± 3.09	CA1-2: $U = 14.00$, $p = 0.855$
	5-hmC	Hip: 40.97 ± 2.12	Hip: 50.15 ± 2.13	Hip: $U = 0.00$, P = 0.006**
		DG: 57.77 ± 4.90	DG: 65.75 ± 2.95	DG: $U = 3.00$, $p = 0.028$*
		CA3: 23.51 ± 1.63	CA3: 27.88 ± 3.17	CA3: $U = 3.00$, $p = 0.028$*
		CA1-2: 41.63 ± 3.49	CA1-2: 56.82 ± 3.12	CA1-2: $U = 0.00$, $p = 0.006$**
	DNMT3A	Hip: 14.73 ± 1.40	Hip: 20.65 ± 5.37	Hip: $U = 4.00$, $p = 0.045$*
		DG: 27.24 ± 8.26	DG: 32.21 ± 6.35	DG: $U = 9.00$, $p = 0.273$
		CA3: 4.78 ± 1.01	CA3: 11.32 ± 5.41	CA3: $U = 2.00$, $p = 0.018$*
		CA1-2: 12.16 ± 6.77	CA1-2: 18.43 ± 5.10	CA1-2: $U = 6.00$, $p = 0.100$
	5-mC:5-hmC	Hip: 0.35 ± 0.06	Hip: 0.30 ± 0.10	Hip: $U = 10.00$, $p = 0.361$
		DG: 0.46 ± 0.13	DG: 0.42 ± 0.16	DG: $U = 10.00$, $p = 0.361$
		CA3: 0.29 ± 0.07	CA3: 0.26 ± 0.11	CA3: $U = 11.00$, $p = 0.465$
		CA1-2: 0.29 ± 0.08	CA1-2: 0.21 ± 0.05	CA1-2: $U = 5.00$, $p = 0.068$

supplementary table 2.

	Aβx-40	Aβx-42	Fraction of hippocampal area covered by plaques	SYP CA1	SYP CA3	PSD-95 CA1	PSD-95 CA3
5-mC	$r = 0.574$	$r = 0.173$	$r = 0.221$	$r = -0.087$	$r = 0.036$	$r = 0.091$	$r = 0.023$
	$p = 0.065$	$p = 0.610$	$p = 0.514$	$p = 0.799$	$p = 0.915$	$p = 0.790$	$p = 0.946$
5-hmC	$r = 0.305$	$r = 0.600$	$r = 0.643$	$r = 0.831$	$r = 0.823$	$r = 0.692$	$r = 0.702$
	p =0.361	$p = 0.051$	$p = 0.033$*	$p = 0.002$**	$p = 0.002$**	$p = 0.018$*	$p = 0.016$*
5-mC:5-hmC	$r = 0.409$	$r = -0.093$	$r = -0.032$	$r = -0.455$	$r = -0.297$	$r = -0.155$	$r = -0.246$
	$p = 0.212$	$p = 0.785$	$p = 0.925$	$p = 0.160$	$p = 0.376$	$p = 0.648$	$p = 0.466$
DNMT3A	$r = 0.594$	$r = 0.443$	$r = 0.629$	$r = 0.499$	$r = 0.439$	$r = 0.456$	$r = 0.440$
	$p = 0.054$	$p = 0.172$	$p = 0.038$*	$p = 0.118$	$p = 0.177$	$p = 0.158$	$p = 0.176$

supplementary table 3.

	Aβx-40	Aβx-42	Fraction of hippocampal area covered by plaques	SYP CA1	SYP CA3	PSD-95 CA1	PSD-95 CA3
CFC	$r = -0.296$,	$r = -0.539$,	$r = -0.427$,	$r = -0.198$,	$r = -0.267$,	$r = -0.599$,	$r = -0.709$,
	$p = 0.376$	$p = 0.087$	$p = 0.190$	$p = 0.559$	$p = 0.428$	$p = 0.052$	$p = 0.015$*
MWM escape latency	$r = 0.694$,	$r = 0.703$,	$r = 0.586$,	$r = 0.144$,	$r = 0.230$,	$r = 0.300$,	$r = 0.403$,
	p =0.018*	$p = 0.016$*	$p = 0.058$	$p = 0.672$	p =0.496	p =0.370	$p = 0.220$
MWM quadrant 2h	$r = -0.279$,	$r = -0.297$,	$r = -0.152$,	$r = -0.423$,	$r = -0.335$,	$r = 0.019$,	$r = -0.067$,
	$p = 0.406$	$p = 0.374$	$p = 0.655$	$p = 0.194$	$p = 0.314$	$p = 0.995$	$p = 0.845$
MWM quadrant 24h	$r = -0.250$,	$r = -0.255$,	$r = -0.113$,	$r = -0.318$,	$r = -0.245$,	$r = -0.083$,	$r = -0.144$,
	$p = 0.459$	$p = 0.449$	$p = 0.740$	p =0.340	$p = 0.468$	$p = 0.809$	$p = 0.674$
MWM ACI 2h	$r = -0.271$,	$r = 0.019$,	$r = -0.060$,	$r = 0.315$,	$r = 0.162$,	$r = -0.065$,	$r = -0.025$,
	$p = 0.420$	$p = 0.956$	$p = 0.860$	$p = 0.346$	$p = 0.634$	$p = 0.849$	$p = 0.942$
MWM ACI 24h	$r = -0.278$,	$r = -0.352$,	$r = -0.232$,	$r = -0.430$,	$r = -0.439$,	$r = -0.377$,	$r = -0.321$,
	$p = 0.409$	$p = 0.288$	$p = 0.493$	$p = 0.187$	$p = 0.177$	$p = 0.253$	$p = 0.336$

supplementary table 4.

	CFC	MWM escape latency	MWM quadrant 2h	MWM quadrant 24h	MWM ACI 2h	MWM ACI 24h
5-mC	*r* = -0.149	*r* = 0.455	*r* = -0.608	*r* = -0.730	*r* = -0.805	*r* = -0.670
	p = 0.662	*p* = 0.160	*p* = 0.047*	*p* = 0.011*	*p* = 0.003**	*p* = 0.024*
5-hmC	*r* = -0.496	*r* = 0.460	*r* = -0.582	*r* = -0.561	*r* = -0.063	*r* = -0.656
	p =0.121	*p* = 0.154	*p* = 0.061	*p* = 0.072	*p* = 0.854	*p* = 0.028*
5-mC:5-hmC	*r* = 0.032	*r* = 0.234	*r* = -0.342	*r* = -0.509	*r* = -0.817	*r* = -0.365
	p = 0.926	*p* = 0.488	*p* = 0.304	*p* = 0.110	*p* = 0.002**	*p* = 0.270
DNMT3A	*r* = -0.464	*r* = 0.679	*r* = -0.423	*r* = -0.538	*r* = -0.292	*r* = -0.619
	p = 0.151	*p* = 0.022*	*p* = 0.195	*p* = 0.088	*p* = 0.383	*p* = 0.042*

SUPPLEMENTARY DATA

SUPPLEMENTARY TABLE 1. Overview of main results.

ABBREVIATIONS: *5*-mC, *5*-methylcytosine; *5*-hmC, *5*-hydroxymethylcytosine; AD, Alzheimer's disease; CA, cornu ammonis; DG, dentate gyrus; DNMT, DNA methyltransferase; Hip, hippocampus; SD, standard deviation; * $p < 0.05$; ** $p < 0.01$.

SUPPLEMENTARY TABLE 2. Correlation Alzheimer's disease markers with epigenetic markers.

ABBREVIATIONS: *5*-mC, *5*-methylcytosine; *5*-hmC, *5*-hydroxymethylcytosine; Aβ, amyloid-β; CA, cornu ammonis; DNMT, DNA methyltransferase; PSD-95, postsynaptic density protein 95; *r*, Pearson's r; SYP, synaptophysin; * $p < 0.05$; ** $p < 0.01$.

SUPPLEMENTARY TABLE 3. Correlation behavior with Alzheimer's disease markers.

ABBREVIATIONS: Aβ, amyloid-β; ACI, annulus crossing index; CA, cornu ammonis; CFC, contextual fear conditioning; MWM, Morris water maze; PSD-95, postsynaptic density protein 95; *r*, Pearson's r; SYP, synaptophysin; * $p < 0.05$.

SUPPLEMENTARY TABLE 4. Correlation epigenetic markers with behavior.

ABBREVIATIONS: *5*-mC, *5*-methylcytosine; *5*-hmC, *5*-hydroxymethylcytosine; ACI, annulus crossing index; CFC, contextual fear conditioning; DNMT, DNA methyltransferase; MWM, Morris water maze; *r*, Pearson's r; * $p < 0.05$; ** $p < 0.01$.

THE DNA METHYLOME AND HYDROXYMETHYLOME IN ALZHEIMER'S DISEASE; CORTICAL DYSREGULATION OF *OXT*, *C3*, *ANK1* AND *RHBDF2*

ROY **LARDENOIJE**[A,*], JANOU A.Y. **ROUBROEKS**[A,B,*], EHSAN **PISHVA**[A,B,*], ARTEMIS **IATROU**[A], ADAM R. **SMITH**[B], REBECCA G. **SMITH**[B], LARS M.T. **EIJSSEN**[A,C], GUNTER **KENIS**[A], DIEGO **MASTROENI**[A,D,E], ELAINE **DELVAUX**[D,E], PAUL D. **COLEMAN**[D,E], JONATHAN **MILL**[B,F], BART P. **RUTTEN**[A], KATIE **LUNNON**[B], DANIËL L.A. **VAN DEN HOVE**[A,G]

[A]SCHOOL FOR MENTAL HEALTH AND NEUROSCIENCE (MHENS), DEPARTMENT OF PSYCHIATRY AND NEUROPSYCHOLOGY, MAASTRICHT UNIVERSITY, UNIVERSITEITSSINGEL 50, 6200 MD MAASTRICHT, THE NETHERLANDS
[B]UNIVERSITY OF EXETER MEDICAL SCHOOL, UNIVERSITY OF EXETER, EXETER, UK.
[C]DEPARTMENT OF BIOINFORMATICS—BIGCAT, MAASTRICHT UNIVERSITY, PO BOX 616, 6200 MD MAASTRICHT, THE NETHERLANDS.
[D]L.J. ROBERTS ALZHEIMER'S DISEASE CENTER, BANNER SUN HEALTH RESEARCH INSTITUTE, 10515 W. SANTA FE DRIVE, SUN CITY, AZ 85351, USA
[E]BIODESIGN INSTITUTE, NEURODEGENERATIVE DISEASE RESEARCH CENTER, ARIZONA STATE UNIVERSITY, TEMPE, AZ, 85287, US.
[F]INSTITUTE OF PSYCHIATRY, KING'S COLLEGE LONDON, LONDON, UK.
[G]LABORATORY OF TRANSLATIONAL NEUROSCIENCE, DEPARTMENT OF PSYCHIATRY, PSYCHOSOMATICS AND PSYCHOTHERAPY, UNIVERSITY OF WUERZBURG, FUECHSLEINSTRASSE 15, 97080 WUERZBURG, GERMANY
*THESE AUTHORS CONTRIBUTED EQUALLY TO THIS WORK.

Abstract

In the present study, we identified methylomic and hydroxymethylomic differences in middle temporal gyrus tissue from Alzheimer's disease (AD) patients and age-matched controls. Using genome-wide arrays, AD-specific cytosine, 5-methylcytosine and 5-hydroxymethylcytosine profiles were identified in numerous genes, including *ANK1*, *RHBDF2* and *C3*, all of which have previously been implicated in AD. Moreover, the present study, which is the first of its kind examining the methylome and hydroxymethylome in AD, suggests that *OXT* harbors Braak stage-dependent *OXT* DNA hyperhydroxymethylation, concomitant with DNA hypomethylation.

KEYWORDS: Alzheimer's disease; DNA methylation; DNA hydroxymethylation; epigenetics; *OXT*; *C3*; *ANK1*; *RHBDF2*

7.1. Introduction

The world's leading cause of dementia, Alzheimer's disease (AD), is characterized by a progressive development of amyloid plaques and intracellular neurofibrillary tangles, followed by neuronal cell death [1, 2]. Large-scale genome-wide association studies (GWAS) have identified high effect size risk variants of genes such as *APOE*, as well as a number of common variants with a low effect size [3]. In addition, recent studies have suggested an important role for epigenetic mechanisms in the etiology of AD [4], with reports of both global and gene-specific alterations in epigenetic modifications [5–8]. 5-Methylcytosine (5-mC), reflecting DNA methylation, is the most abundant and best understood epigenetic DNA modification, but regular bisulfite (BS) conversion, a widely used procedure for quantifying DNA methylation, cannot distinguish between 5-mC and the more recently identified 5-hydroxymethylcytosine (5-hmC), reflecting DNA hydroxymethylation. As 5-hmC is particularly enriched in the brain [9, 10], where it may be involved in learning and memory [11], it is crucial to investigate 5-mC and 5-hmC separately in the context of AD.

7.2. Methods

In the present study, we quantified both 5-mC and 5-hmC in middle temporal gyrus (MTG) tissue obtained from 46 AD patients and 36 age-matched, non-demented controls (see Supplementary Table 1 for cohort demographics). The MTG shows early AD pathology [12], and differences in global levels of MTG DNA methylation and hydroxymethylation have been previously observed in association with AD progression [13]. In order to quantify the genome-wide levels of 5-mC and 5-hmC at a single base resolution, oxidative bisulfite (oxBS) and regular BS conversion of genomic DNA was performed using the TrueMethyl™ 24 Kit version 2.0 of CEGX™ (Cambridge Epigenetix Limited, Cambridge, UK). OxBS- and BS-converted DNA was amplified and hybridized on the Illumina HumanMethylation450 BeadChip (450K BeadChip) [14]. Although readings from the oxBS-converted DNA are directly representative of 5-mC levels, 5-hmC levels were determined by subtracting the oxBS signal from the BS signal (Figure 1), the latter of which represents the combined fraction of 5-mC and 5-hmC modified cytosines. See the Supplementary methods section for a more detailed overview of the used methods.

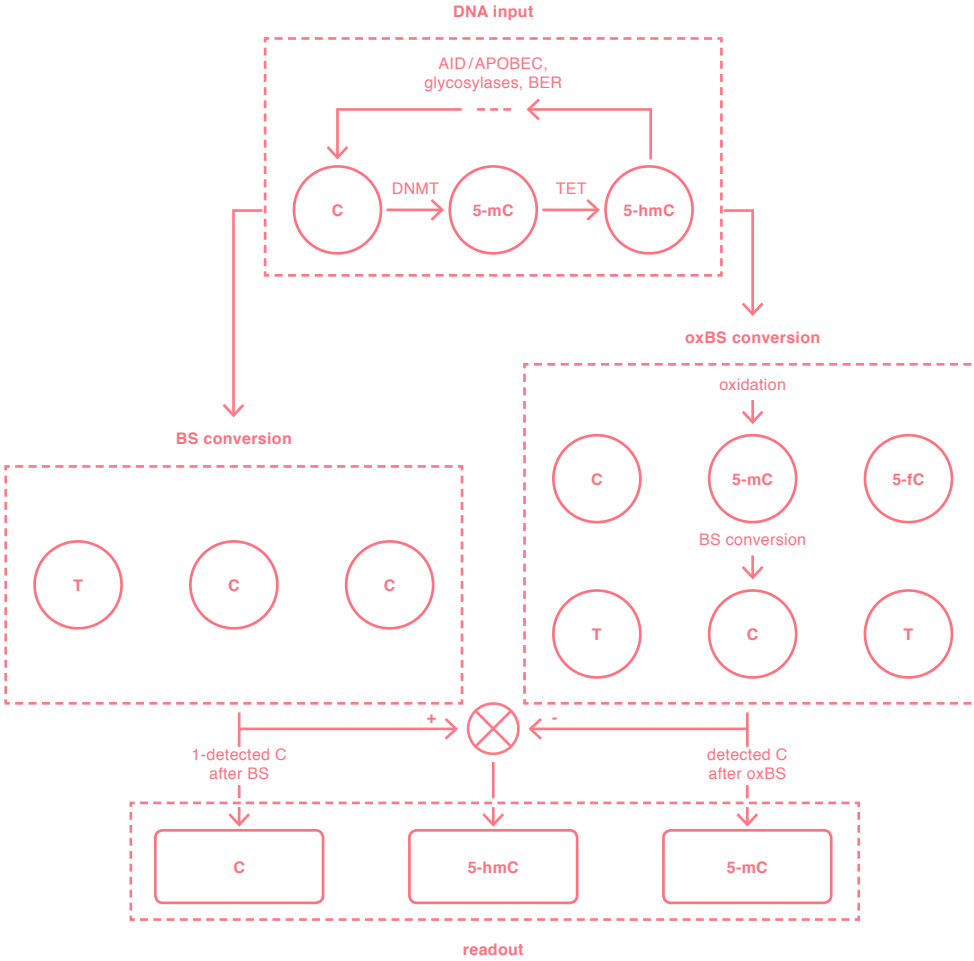

figure 1.

7.3. Results and discussion

Differentially methylated, hydroxymethylated, and unmodified cytosine positions (DMPs, DHPs, and DUPs, respectively) associated with disease diagnosis were identified (Supplementary Tables 2-4). At the nominal significance threshold (p = 0.05), 24,673 DMPs and 21,264 DUPs were identified among the 396,600 probes analyzed, while 9,261 DHPs out of a total of 178,951 probes passing the 5-hmC detection criteria were identified (see Supplementary Methods). Several genes annotated to the 25 highest ranked DMPs, including *SYNJ2* (cg05270236; β = 0.04, p = 1.07x10-4, Δ = 4.35%), *ANK1* (cg11823178; β = 0.05, p = 3.04x10-4, Δ = 5.08%) and *RHBDF2* (cg12163800; β = 0.04, p = 1.88x10-4, Δ = 4.32%), have been associated with AD or cognitive ability in previous DNA methylation studies [6, 15] (Supplementary Table 2). *ANK1* (cg05066959;

FIGURE 1. Overview of the procedure to detect unmodified cytosines (C), 5-methylcytosine (5-mC), and 5-hydroxymethylcytosine (5-hmC). Naturally, C can be converted to 5-mC by DNA methyltransferases (DNMTs) and 5-mC can be oxidized by ten-eleven translocation (TET) enzymes, resulting in 5-hmC. There are several proposed demethylation pathways through which 5-mC and 5-hmC can be converted back to C. DNA samples were split in two, one half was only treated with bisulfite (BS), which converts C into thymine (T). 5-mC and 5-hmC are protected against this conversion, and will be read as a C on the array. The detected C signal after BS conversion is thus actually the combined 5-mC and 5-hmC signal. As the signals are converted to fractions, with C + 5-mC + 5-hmC = 1, the fraction of C in the input DNA can be determined by subtracting the C signal after BS conversion (representing the combined 5-mC and 5-hmC fraction in the input DNA) from 1. The other half of the DNA sample was first oxidized, which converts 5-hmC into 5-formylcytosine (5-fC), and then treated with BS. 5-fC is not protected against the BS conversion, so it also turns into T. C detected on the array after this oxidative BS (oxBS) conversion thus represents the fraction of 5-mC in the input DNA. The 5-hmC fraction in the input DNA can be determined by subtracting the fraction of 5-mC (detected C after oxBS) from the combined 5-mC and 5-hmC fraction (detected C after BS). This procedure results in three readout signals: unmodified C, 5-mC, and 5-hmC. Note that 5-fC, and probably also 5-carboxylcytosine (5-caC), are included in the unmodified C fraction.

β = -0.05, p = 9.98x10-4, Δ = -4.94%) and *RHBDF2* (cg13076843; β = -0.05, p = 2.62x10-5, Δ = -4.57%, cg05810363; β = -0.04, p = 9.19x10-5, Δ = -4.07%, cg12163800; β = -0.04, p = 5.12x10-5, Δ = -3.54%) were also found among the 25 highest-ranked DUPs (Supplementary Table 4). Notably, the gene *OXT* is annotated to the highest-ranked DMP (cg13285174; β = -0.07, p = 6.52x10-5, Δ = -6.95%), as well as the fifteenth-ranked DHP (cg19592472; β = 0.04, p = 6.35x10-5, Δ = 4.39%). The third highest-ranked disease-associated DHP is located in the gene *DDR2* (cg00457087; β = -0.05, p = 2.63x10-5, Δ = -4.65%), of which total DNA modifications have previously been linked to the pathogenesis of AD [16] (Supplementary Table 3). Note that no loci reached statistical significance after a false discovery rate (FDR) correction. Therefore, in addition to positions, differentially modified regions of DNA were identified, by determining spatial correlations between DMPs, DHPs or DUPs within a 500 bp window, using *comb-p* [17]. After Šidák correction, we identified six significant differentially methylated regions (DMRs) in *OXT*, *ADIRF*, *RHBDF2*, *CDX1*, *RAP1GAP2*, and *FAM198B*, two significant differentially hydroxymethylated regions (DHRs) in *OXT* and *SLC12A4*, and six regions with significant differential levels of unmodified cytosine (DURs) in *RHBDF2*, *LOC100190940*, *CDX1*, *TNK2*, *C3*, and *ANK1* (Table 1).

Using neuropathological Braak staging of the subjects, significant Braak stage-associations were observed for the majority of probes located within the DMRs, DHRs, and DURs (Supplementary Tables 5-7), demonstrating the relevance of our findings in relation to AD.

Studies using standard BS conversion only, and thus looking at the combined 5-mC and 5-hmC levels, have found strong associations between AD and *RHBDF2* in the prefrontal cortex (PFC) [6] and EC, as well as between AD and *ANK1* in the PFC and superior temporal gyrus [5]. *ANK1* and *RHBDF2* are involved in axonal compartmentalization and tumor necrosis factor signaling, respectively [18, 19] Distinguishing between 5-mC and 5-hmC signals in the current study indicates that these two genes are mainly affected by differential DNA methylation. In contrast, a region in *C3* only showed AD-related differences in total DNA modifications, but not 5-mC and 5-hmC separately. *C3* encodes a central component of the complement system and mediates developmental synapse elimination by phagocytic microglia, and has been implicated in mediating synaptic loss during aging [20] and in the early stages of AD [21]. That there are no significant AD-related changes in *C3* 5-mC and 5-hmC levels when analyzed separately, and that the combined fraction of modified cytosines (BS signal) at the same time indirectly reflects the fraction of unmodified cytosine, suggests that differential levels of unmodified cytosine may be primarily relevant for the dysregulation of *C3* in AD.

Position	n	*p*-value	Šidák-*p*	Gene	Gene feature	Change in AD
DMR (5-mC)						
chr 20: 3052115 - 3052346	8	3.25E-13	5.57E-10	*OXT*	TSS + utr5 + cds	↓
chr 10: 88728073 - 88728236	4	1.88E-07	4.58E-04	*C10orf116*	TSS + exon + utr5	↓
chr 17: 74475240 - 74475403	5	5.23E-07	1.27E-03	*RHBDF2*	intron + cds	↑
chr 5: 149546331 - 149546472	5	5.18E-07	1.46E-03	*CDX1*	TSS + utr5 + cds	↑
chr 17: 2951666 - 2951720	3	2.07E-06	1.51E-02	*RAP1GAP2*	intergenic	↑
chr 4: 159092536 - 159092554	2	1.68E-06	3.63E-02	*FAM198B*	exon + utr5	↓
DHR (5-hmC)						
chr 20: 3052115 - 3052275	7	4.05E-08	4.52E-05	*OXT*	TSS + exon + utr5	↑
chr 16: 67978445 - 67978451	2	1.18E-06	3.45E-02	*SLC12A4*	exon + utr3	↓
DUR (1 – (5-mC + 5-hmC))						
chr 17: 74475240 - 74475403	5	1.23E-11	2.99E-08	*RHBDF2*	intron + cds	↑
chr 12: 130554977 - 130555092	3	1.97E-08	6.80E-05	*LOC100190940*	intergenic	↓
chr 5: 149546331 - 149546472	5	3.93E-07	1.10E-03	*CDX1*	TSS + utr5 + cds	↑
chr 3: 195610084 - 195610232	3	6.45E-07	1.73E-03	*TNK2*	intron + cds	↑
chr 19: 6712321 - 6712407	5	1.10E-06	5.05E-03	*C3*	cds	↑
chr 8: 41519308 - 41519400	2	2.66E-06	1.14E-02	*ANK1*	intron + cds	↑

table 1.

TABLE 1. Differentially methylated, hydroxymethylated, and unmodified regions in the middle temporal gyrus associated with Alzheimer's disease. Displayed for each region is the chromosomal position, number of probes in the region (n), *p*-value and multiple testing-corrected *p* (Šidák-*p*), UCSC gene name, gene feature, and directionality of modification changes in AD (up or down).

ABBREVIATIONS: *5*-hmC, *5*-hydroxymethylcytosine; *5*-mC, *5*-methylcytosine; AD, Alzheimer's disease; chr, chromosome; DHR, differentially hydroxymethylated region; DMR, differentially methylated region; DUR, differentially unmodified region; TSS, transcription start site; utr*5*, *5*' untranslated region; cds, coding sequence).

A novel finding in relation to AD is *OXT*, the gene encoding oxytocin, a neuropeptide involved in the neuromodulation of social behavior, stress regulation, and associative learning [22]. *OXT* contained the fifteenth highest ranked DHP, and the highest ranked DMP, DMR and DHR. The DMR spans 231 bp, starts 223 bp upstream from the *OXT* transcription start site (TSS), and overlaps with the 160 bp long DHR that starts at the same position. All eight DMPs within the *OXT* DMR showed decreased levels of methylation in the MTG of AD cases, whereas four significant DHPs in the DHR showed higher levels of hydroxymethylation. Additionally, several probes within the DMR (4 probes) and DHR (3 probes; all in DMR as well) showed significant associations with Braak stages (Supplementary Tables 5 and 6). Moreover, while the 5-mC levels of all probes within the DMR were negatively correlated with *OXT* mRNA expression (most significant probe cg07747220; r = -0.292, p = 0.01), the 5-hmC levels of the probes in the DHR showed a positive correlation with mRNA expression (most significant probe cg01644611; r = -0.283, p = 0.01; Figure 2, Supplementary Table 8). Taken together, this data suggests *OXT* is hyperhydroxymethylated and hypomethylated. Of note,

previous EWAS utilizing only BS-treated DNA could not have revealed this gene as a strong candidate for an epigenetic signature of AD, as the combined level of DNA modifications in *OXT* is not altered between AD cases and controls, and remains stable over Braak stages.

Although *OXT* has been linked to several forms of cognitive function, evidence implicating it in AD is very limited. A recent study did not find an association between AD and *OXT* mRNA levels in the paraventricular nucleus and supraoptic nucleus, two hypothalamic nuclei that are considered to be the sole source of central oxytocin production [23]. Nevertheless, we found correlations between *OXT* mRNA expression and DNA (hydroxy)methylation levels. Possibly, MTG DNA (hydroxy) methylation signatures reflect those in hypothalamic oxytocin-expressing neurons, regulating *OXT* mRNA levels in their nerve endings that innervate the MTG. Evidently, the exact site-specific role of oxytocin, oxytocin receptors and their epigenetic regulation in AD await further research. On a behavioral level, both oxytocin and the MTG have been implicated in facial recognition, which is impaired in AD [24–26]. However, there is currently no evidence directly linking alterations in oxytocin levels to diminished facial recognition in AD.

Concluding, the present study is the first of its kind, exploring the methylome and hydroxymethylome in parallel, shedding more light on previous observations made in relation to AD, but also providing compelling evidence for a role of dysregulated *OXT* in AD.

FIGURE 2. Methylation, hydroxymethylation, and expression of oxytocin (OXT) across Braak staging. Regressed OXT expression values and average regressed 5-methylcytosine (5-mC) and 5-hydroxymethylcytosine (5-hmC) values of 8 and 7 overlapping probes within the OXT differentially methylated region and differentially hydroxymethylated region, respectively, are shown. AU, arbitrary units.

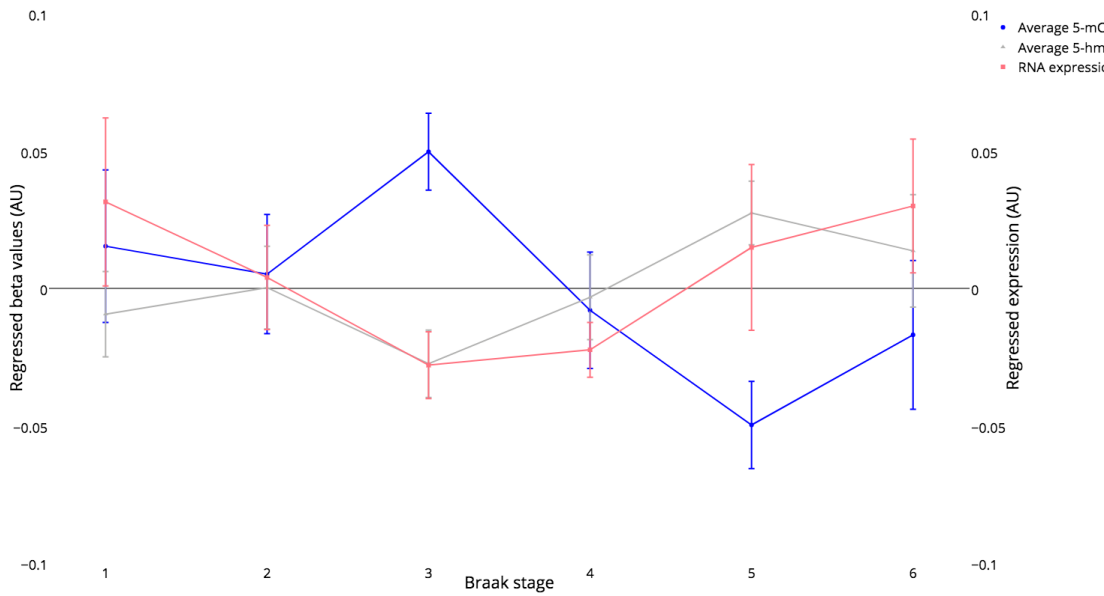

figure 2.

REFERENCES

[1] Yates D, McLoughlin DM. The molecular pathology of Alzheimer's disease. *Psychiatry* 2008; 7: 1–5.

[2] World Health Organization. Dementia: Fact Sheet. http://www.who.int/mediacentre/factsheets/fs362/en/ (2016, accessed 15 April 2017)

[3] Lambert J-C, Ibrahim-Verbaas CA, Harold D, et al. Meta-analysis of 74,046 individuals identifies 11 new susceptibility loci for Alzheimer's disease. *Nat Genet* 2013; 45: 1452–1458.

[4] Lardenoije R, Iatrou A, Kenis G, et al. The epigenetics of aging and neurodegeneration. *Prog Neurobiol* 2015; 131: 21–64.

[5] Lunnon K, Smith R, Hannon E, et al. Methylomic profiling implicates cortical deregulation of ANK1 in Alzheimer's disease. *Nat Neurosci* 2014; 17: 1164–1170.

[6] De Jager PL, Srivastava G, Lunnon K, et al. Alzheimer's disease: early alterations in brain DNA methylation at *ANK1, BIN1, RHBDF2* and other loci. *Nat Neurosci* 2014; 17: 1156–1163.

[7] Chouliaras L, Mastroeni D, Delvaux E, et al. Consistent decrease in global DNA methylation and hydroxymethylation in the hippocampus of Alzheimer's disease patients. *Neurobiol Aging* 2013; 34: 2091–2099.

[8] Zhao J, Zhu Y, Yang J, et al. A genome-wide profiling of brain DNA hydroxymethylation in Alzheimer's disease. *Alzheimer's Dement*. Epub ahead of print 2017. DOI: 10.1016/j.jalz.2016.10.004.

[9] Kriaucionis S, Heintz N. The nuclear DNA base 5-hydroxymethylcytosine is present in Purkinje neurons and the brain. *Science* 2009; 324: 929–30.

[10] Globisch D, Münzel M, Müller M, et al. Tissue distribution of 5-hydroxymethylcytosine and search for active demethylation intermediates. *PLoS One*; 5. Epub ahead of print 2010. DOI: 10.1371/journal.pone.0015367.

[11] Zhang RR, Cui QY, Murai K, et al. Tet1 regulates adult hippocampal neurogenesis and cognition. *Cell Stem Cell* 2013; 13: 237–245.

[12] Ray M, Zhang W, Liang W, et al. Analysis of Alzheimer's disease severity across brain regions by topological analysis of gene co-expression networks. *BMC Syst Biol* 2010; 4: 136.

[13] Coppieters N, Dragunow M. Epigenetics in Alzheimers disease: a focus on DNA modifications. *Curr Pharm Des* 2011; 17: 3398–3412.

[14] Lunnon K, Hannon E, Smith RG, et al. Variation in 5-hydroxymethylcytosine across human cortex and cerebellum. *Genome Biol* 2016; 17: 27.

[15] Lopez LM, Harris SE, Luciano M, et al. Evolutionary conserved longevity genes and human cognitive abilities in elderly cohorts. *Eur J Hum Genet* 2012; 20: 341–347.

[16] Sung HY, Choi EN, Ahn Jo S, et al. Amyloid protein-mediated differential DNA methylation status regulates gene expression in Alzheimer's disease model cell line. *Biochem Biophys Res Commun* 2011; 414: 700–5.

[17] Pedersen BS, Schwartz DA, Yang I V, et al. *Comb-p*: software for combining, analyzing, grouping and correcting spatially correlated P-values. *Bioinformatics* 2012; 28: 2986–8.

[18] Boiko T, Vakulenko M, Ewers H, et al. Ankyrin-dependent and -independent mechanisms orchestrate axonal compartmentalization of L1 family members neurofascin and L1/neuron-glia cell adhesion molecule. *J Neurosci* 2007; 27: 590–603.

[19] Adrain C, Zettl M, Christova Y, et al. Tumor necrosis factor signaling requires iRhom2 to promote trafficking and activation of TACE. *Sci Reports* 2012; 335: 225–228.

[20] Shi Q, Colodner KJ, Matousek SB, et al. Complement C3-deficient mice fail to display age-related hippocampal decline. *J Neurosci* 2015; 35: 13029–13042.

[21] Hong S, Beja-Glasser VF, Nfonoyim BM, et al. Complement and microglia mediate early synapse loss in Alzheimer mouse models. *Science* 2016. DOI: 10.1126/science.aad8373.

[22] Olff M, Frijling JL, Kubzansky LD, et al. The role of oxytocin in social bonding, stress regulation and mental health: An update on the moderating effects of context and interindividual differences. *Psychoneuroendocrinology* 2013; 38: 1883–1894.

[23] Swaab DF. Chapter II Neurobiology and neuropathology of the human hypothalamus. *Handb Chem Neuroanat* 1997; 13: 39–137.

[24] Gorno-Tempini M-L. Category differences in brain activation studies: where do they come from? *Proc Biol Sci*; 267: 1253-8.

[25] Haas BW, Filkowski MM, Cochran RN, et al. Epigenetic modification of *OXT* and human sociability. *Proc Natl Acad Sci U S A* 2016; 113: E3816-23.

[26] Hargrave R, Maddock RJ, Stone V. Impaired recognition of facial expressions of emotion in Alzheimer's disease. *J Neuropsychiatry Clin Neurosci* 2002; 14: 64–71.

[27] Beach TG, Sue LI, Walker DG, et al. The Sun Health Research Institute Brain Donation Program: Description and experience, 1987–2007. *Cell Tissue Bank* 2008; 9: 229–245.

[28] Davis S, Du P, Bilke S, et al. *methylumi*: Handle Illumina methylation data. 2016.

[29] Schalkwyk LC, Pidsley R, Wong CCY. *wateRmelon*: Illumina 450 methylation array normalization and metrics. R package version 1.2.2 2013.

[30] Aryee MJ, Jaffe AE, Corrada-Bravo H, et al. *Minfi*: a flexible and comprehensive Bioconductor package for the analysis of Infinium DNA methylation microarrays. *Bioinformatics* 2014; 30: 1363–1369.

[31] Pidsley R, CC YW, Volta M, et al. A data-driven approach to preprocessing Illumina 450K methylation array data. *BMC Genomics* 2013; 14: 293.

[32] Chen Y, Lemire M, Choufani S, et al. Discovery of cross-reactive probes and polymorphic CpGs in the Illumina Infinium HumanMethylation450 microarray. *Epigenetics* 2013; 8: 203–209.

[33] Fukuzawa S, Takahashi S, Tachibana K, et al. Simple and accurate single base resolution analysis of 5-hydroxymethylcytosine by catalytic oxidative bisulfite sequencing using micelle incarcerated oxidants. *Bioorg Med Chem* 2016; 24: 4254–4262.

[34] Song C-X, He C. Potential functional roles of DNA demethylation intermediates. *Trends Biochem Sci* 2013; 38: 480–484.

[35] Slieker RC, Bos SD, Goeman JJ, et al. Identification and systematic annotation of tissue-specific differentially methylated regions using the Illumina 450k array. *Epigenetics Chromatin* 2013; 6: 26.

[36] Phipson B, Maksimovic J, Oshlack A. missMethyl: an R package for analyzing data from Illumina's HumanMethylation450 platform. *Bioinformatics* 2015; 32: btv560.

Supplementary methods

Subjects and tissue preparation

MTG tissue samples were obtained from 82 postmortem brains from both AD patients and neurologically normal controls provided by the Brain and Tissue Bank of the Banner Sun Health Research Institute (Sun City, Arizona, USA). Brain samples were frozen and stored at -80°C after autopsy, with an average postmortem interval of 2.8 hours. Braak staging was carried out for AD neurofibrillary pathology. A consensus diagnosis of AD or non-demented control was reached by following National Institutes of Health (NIH) AD Center criteria [27]. Comorbidity with any other type of dementia, cerebrovascular disorders, mild cognitive impairment (MCI), and presence of non-microscopic infarcts were applied as exclusion criteria. Further information about the samples is provided in Supplementary Table 1.

DNA samples were isolated at the Banner Sun Health Research Institute. Approximately 76 mg of frozen tissue was obtained from each of the 82 samples. The tissue was placed in a microfuge tube containing 0.5 ml fresh lysis buffer (100 mM Tris HCl pH 8.5, 200 mM NaCl, 5 mM EDTA, 100 μg/ml Proteinase K [Sigma-Aldrich, St. Louis, Missouri, USA], and 0.2% SDS), and then kept overnight on a heat block at 55°C. To break up the tissue, samples were incubated for 1-2 hours in a hand-held pellet pestle mixer (Kontes), and were further homogenized the next day if needed. Next, 4 μL of RNase (Qiagen, Valencia, California, USA) was added, and the samples were then kept at room temperature (RT) for 30 minutes. After incubation, phenol/chloroform/isoamyl alcohol (Sigma) was added in equal volumes and each tube was vortexed and placed on a rocking platform for 5 minutes. Samples were then centrifuged for 10 minutes at RT, at a speed of 10,000 RPM, and the aqueous phase was transferred to a new tube. Ethanol-precipitation took place overnight at -20°C, and pellets were resuspended in 50 μL TE buffer (pH 8.0). Before storing the samples at -20°C, they were quantified and checked for purity using spectrophotometry.

Methylomic and hydroxymethylomic profiling

The TrueMethyl™ 24 Kit version 2.0 by CEGX™ (Cambridge Epigenetix Limited, Cambridge, UK) was used for BS and oxBS conversion of genomic DNA (gDNA). All laboratory procedures were performed at

ServiceXS (ServiceXS B.V., Leiden, the Netherlands), according to the manufacturer's instructions. Prior to the conversion, high molecular weight (HMW) gDNA was quantified using a PicoGreen assay (Invitrogen, Carlsbad, California, USA), and gel-electrophoresis was performed to assess gDNA quality. All samples were of sufficient quantity and quality. A volume of 1 μg HMW gDNA was used per sample, which, after purification and denaturation, was split into two samples which underwent either DNA oxidation (oxBS samples) or mock DNA oxidation (BS samples). Subsequently, all samples were BS treated, and the yield of the samples was assessed by a Qubit single-stranded DNA assay (Invitrogen). An additional restriction quality control was performed for a qualitative assessment of 5-hmC oxidation and BS conversion.

From each BS/oxBS-treated DNA sample, 8 μL was amplified and hybridized on the HumanMethylation450 BeadChip (Illumina, Inc., San Diego, CA, U.S.A.), and the Illumina iScan was used for imaging of the array. Sample preparation, hybridization, and washing steps for the Illumina Infinium II Methylation Assay of the BeadChip arrays were performed according to the manufacturer's protocol.

Quality control and data normalization

GenomeStudio (version 2011.1, Illumina) reports were generated using the raw data imported from Illumina iScanner. Further computational and statistical analyses were performed using the statistical programming language R (version 3.3.1; https://www.r-project.org) and RStudio (version 0.99.902). The *methylumi* package (version 2.20.0) [28] was used in order to import the GenomeStudio reports into the R statistical environment. The QC analysis and normalization have been conducted using the *methylumi*, *wateRmelon* (version 1.18.0) [29] and *minfi* (version 1.20.0) [30] packages, according to the method described by Pidsley et al. [31]. Initial tests using non-CpG single nucleotide polymorphism (SNP) probes and sex chromosome probes were performed to assess whether corresponding BS and oxBS samples were genetically identical, and whether reported sample gender was identical to predicted gender, respectively. Next, cross-hybridizing probes, probes containing a common SNP in the sequence or within 10bp of the sequence, and probes on the X and Y chromosomes were removed [32]. Lastly, a test to estimate the efficiency of the BS conversions was performed by calculating signal intensity percentages on control probes known to show 100% signal in BS samples (5-mC + 5-hmC signal). All 82 samples showed BS conversion percentages above the 80% threshold (average: 93%).

Prior to normalization, a *p*-filter was applied which removed samples having more than 1% of probes with a detection *p*-value greater than 0.05, in addition to removing probes with a beadcount lower than 3 in more than 5% of samples, and probes having more than 1% of samples with a detection *p*-value greater than 0.05. Although all samples passed the *p*-filter, 6,969 probes were removed due to a low beadcount or large detection *p*-value, leaving 396,600 probes for analysis.

From the *wateRmelon* package, thirteen different normalization strategies were tested and ranked based on three performance metrics, as described in Lunnon et al. [14] (Supplementary Table 9). Of these strategies, *dasen* performed consistently well, and was therefore chosen for data normalization. Following *dasen* normalization, two samples were dropped from the 5-mC dataset due to a skewed distribution of the global values in a density plot. The remaining 80 cases in the oxBS dataset and 82 cases in the BS dataset were used for further analyses.

Data analysis

Following normalization, two sets of beta values, from the standard BS arrays (5-mC + 5-hmC) and from the oxBS arrays (5-mC), were generated. By subtracting oxBS beta values from the BS beta values ($\Delta\beta_{BS\text{-}oxBS}$) for each probe in each sample, 5-hmC levels were calculated. Unmodified cytosine (UC) values were determined as 1-BS ($1\text{-}\beta_{BS}$). It should be noted that other DNA demethylation intermediates, such as 5-formylcytosine (5-fC) and 5-carboxylcytosine (5-caC) may be represented in the BS or unmodified cytosine levels, as it is currently unclear how these intermediates respond to oxBS conversion [33]. However, these intermediates are present at very low levels, and are not enriched in brain tissue [34]. Due to technical variation, some 5-hmC values were negative. Therefore, outliers deviating more than ± 2SD from the probe mean in the 5-hmC dataset were determined and set to the mean ± 2SD, and subsequently a threshold of zero was applied to the mean of individual probes. Application of the threshold above zero left 178,591 probes in the 5-hmC dataset. See Supplementary Figure 1 for the UC, 5-mC, and 5-hmC beta value distributions. Given the well-described influence of age and sex on methylation levels, these factors were regressed out from the normalized methylation and hydroxymethylation beta values. Subsequently, a linear regression analysis was performed, with DNA methylation, hydroxymethylation or the UC signal as outcome, and AD diagnosis as predictor (coded as a two-level factor; see Supplementary Figure 2 for Manhattan and QQ plots). Probes were then ordered based on a combined *p*-value and regression estimate ranking (i.e. probes with low *p*-values and high estimates ranked highest), and *p*-values were adjusted

for multiple testing using the Benjamini-Hochberg FDR procedure. To examine the distribution of 5-mC and 5-hmC across genomic regions, we annotated probes using the ENCODE annotation data, as described by Slieker et al. [35]. A Fisher's exact test was used to assess enrichment of 5-mC and 5-hmC in specific genomic regions (Supplementary Figure 3 and Supplementary Table 10).

Individual probes were annotated using the Illumina UCSC gene annotation. For identification of differentially (hydroxy)methylated and unmodified regions (DHRs/DMRs/DURs) containing spatially correlated DMPs, DHPs and DUPs (respectively), *comb-p* was used [17]. This software examined probes above a significance threshold of 0.05, and within 500 base pairs of each other. Obtained *p*-values are Stouffer-Liptak-Kechris (SLK) corrected for adjacent *p*-values, and are subsequently corrected for multiple testing using the Šidák correction.

Gene ontology (GO)-term enrichment analysis was conducted using the *missMethyl* package (version 1.8.0) [36], which takes into account the potential bias due to differing number of probes for each gene. Analyses were performed on the top 1000 probes, based on the combined *p*-value and estimate ranking from the 5-mC, 5-hmC and UC regression analyses that compared AD patients and controls, while the probes included in the regression analyses were used as background lists. The top 25 GO terms for each analysis are presented in Supplementary Tables 11-13.

Expression data generation and analysis

Raw expression data was obtained by the Banner Sun Health Research Institute (Sun City, Arizona, U.S.A.) from the same MTG samples as used for the epigenetic analyses, using the HumanHT-12 v4 BeadChip (Illumina). Total RNA extracted from frozen MTG was isolated with RNEasy Mini Kit (Qiagen) starting with at least 60 mg of tissue. The raw data was exported from Illumina's GenomeStudio (version 2011.1) with the Expression Module (v1.9.0) for further analysis in R. Of the 82 subjects used for the epigenetic analyses, 1 case was not included on the expression array, and 3 additional cases were excluded after quality control of the data, due to extreme outlying values or failed reads, leaving 78 subjects for further analyses. Data was quantile-quantile normalized and outlier corrected. Based on the genomic position (MAPINFO), probes were matched to the DMRs, DHRs and DURs, and correlation between gene expression and corresponding probes was tested. Regions were annotated using UCSC gene annotation. Ranking is done by gene name and *p*-value (Supplementary Table 8).

Cross-region validation of DMRs

To test the robustness of our D(h)MR and Braak association analysis, we performed a cross-regional validation using a similar dataset in an independent cohort of 96 samples from the MRC London Neurodegenerative Disease Brain Bank (http://www.kcl.ac.uk/iop/depts/cn/research/MRC-London-Neurodegenerative-Diseases-Brain-Bank/MRC-London-Neurodegenerative-Diseases-Brain-Bank.aspx), including both entorhinal cortex (EC) and cerebellum (CER) tissue from AD patients and neurologically normal controls (Supplementary Table 14). Standard UC, 5-mC and 5-hmC levels were measured using the 450K BeadChip and processed with a similar methodology as described above. Braak stage pathology within all samples ranged from 0-VI, and all AD patients were aged 65 and over at the time of diagnosis. Cross-region validation was performed by running a Braak association analysis on MTG data on a total of 396 probes for UC and 5-mC and 217 5-hmC probes related to 11 DMR genes previously identified in our UC, 5-mC and 5-hmC AD association analyses. Subsequently, the regression coefficients available from the MTG, EC and CER Braak association were correlated (Supplementary Table 15 and Supplementary Figure 4).

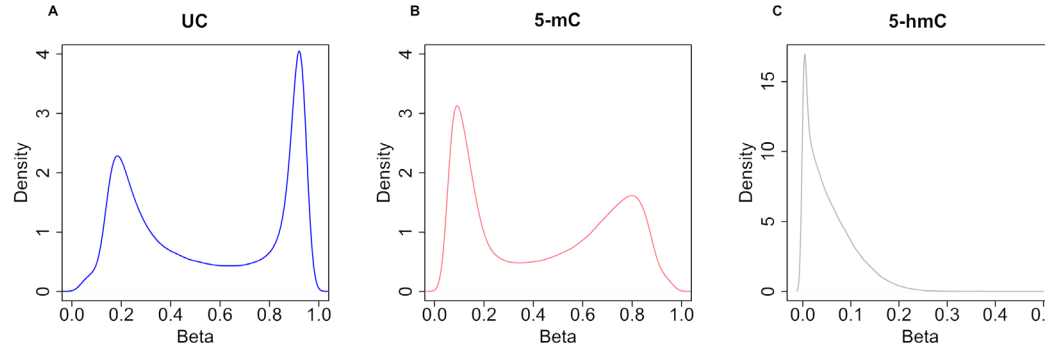

supplementary figure 1.

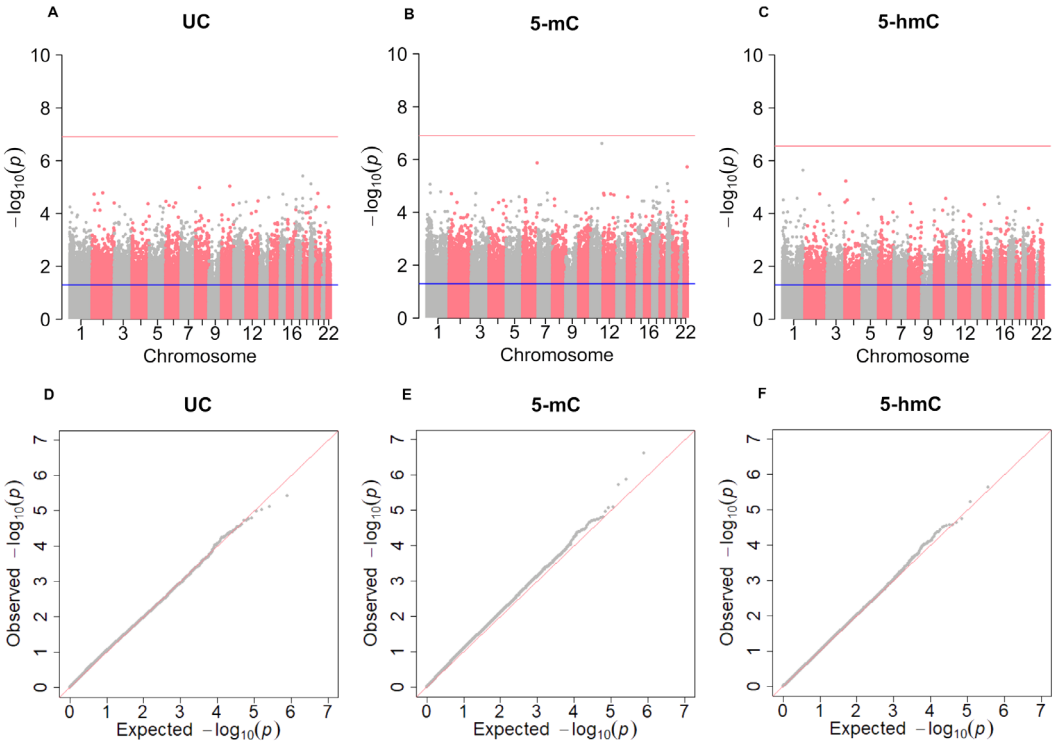

supplementary figure 2.

SUPPLEMENTARY DATA

SUPPLEMENTARY FIGURE 1. Density plots of normalized beta values for unmodified cytosines (UC; A), 5-methylcytosine (5-mC; B), and 5-hydroxymethylcytosine (5-hmC; C). Plots include all probes used for the analysis. The UC beta values are computed by subtracting the normalized beta values obtained from bisulfite converted DNA (BS; containing signals from both 5-mC and 5-hmC), from 1. The 5-mC beta values directly correspond to the normalized beta values from oxidative bisulfite converted DNA (oxBS). 5-hmC beta values are determined by subtracting the normalized oxBS beta values from the BS beta values, applying outlier correction (± 2SD) and a threshold for probe means of > 0.

SUPPLEMENTARY FIGURE 2. Manhattan and QQ plots of the unmodified cytosine (UC; A and D, respectively), 5-methylcytosine (5-mC; B and E, respectively), and 5-hydroxymethylcytosine (5-hmC; C and F, respectively) regression analyses. The blue line in the Manhattan plots indicates the nominal significance threshold of 0.05 and the pink line indicates the genome-wide significance threshold based on the amount of probes included in the analysis (1.261e-7 in case of UC and 5-mC, and 2.800e-7 in case of 5-hmC).

SUPPLEMENTARY FIGURE 3.A. Distribution of probes across genomic regions. Shown are all 5-methylcytosine (5-mC) and unmodified cytosine (UC) probes, all 5-hydroxymethylcytosine (5-hmC) probes passing threshold, and the top 1000 Alzheimer's disease (AD)-associated 5-mC, 5-hmC and UC probes. IG, intergenic region; DP, distal promoter; PP, proximal promoter; GB, gene body; DS, downstream region; CGI, CpG island; SHO, shore; SHE, shelf; NC, non-CGI.

SUPPLEMENTARY FIGURE 3.B. Distribution of probes across functional genomic regions. Displayed are the distributions of all 5-mC and UC probes, all 5-hmC probes passing threshold, and the top 1000 AD-associated 5-mC, 5-hmC and UC probes. A3SS, alternative 3' splice site; A5SS, alternative 5' splice site; AFE, alternative first exon; ALE, alternative last exon; CE, cassette exon; CNE, constitutive exon; EI, exon isoforms; II, intron isoforms; IR, intron retention; MXE, mutually exclusive exon.

supplementary figure 3.A.

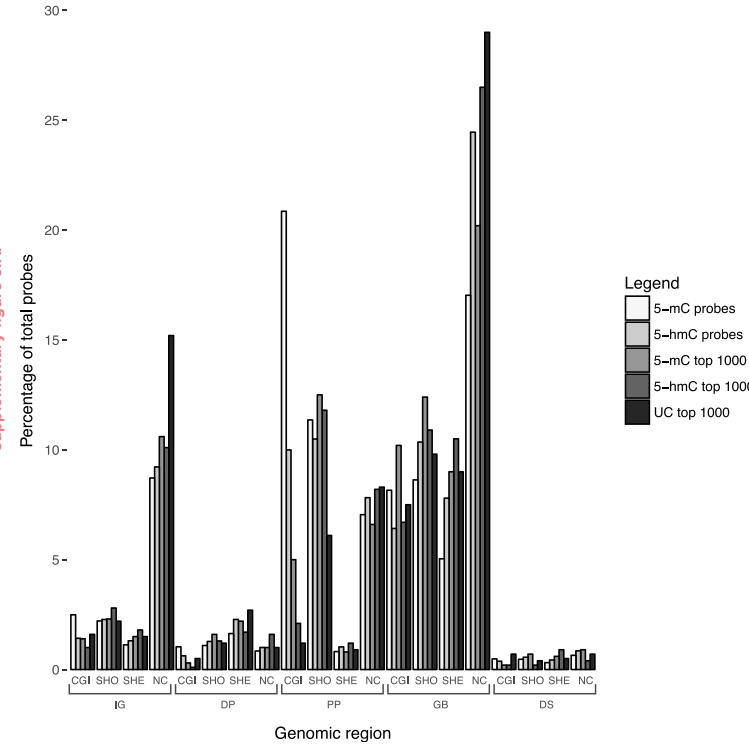

supplementary figure 3.B.

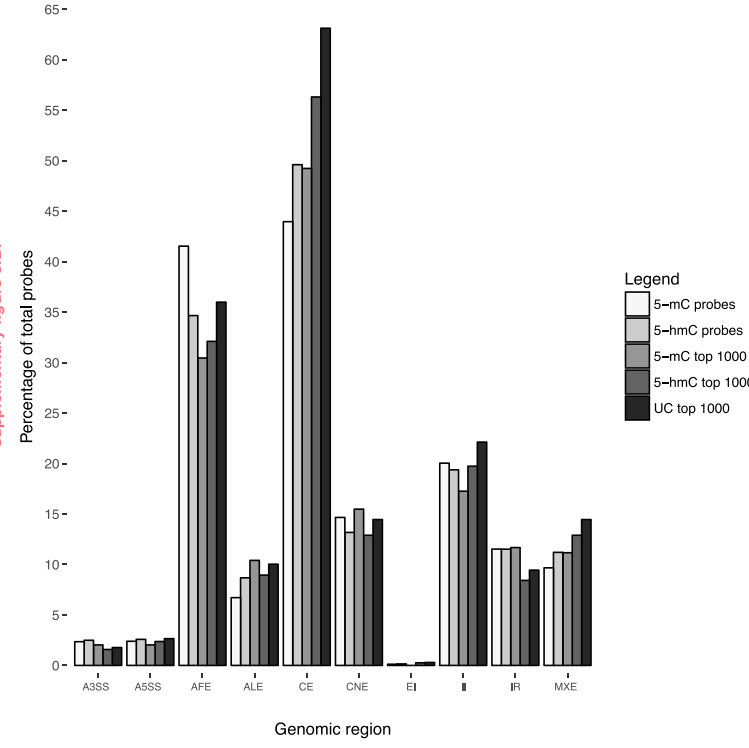

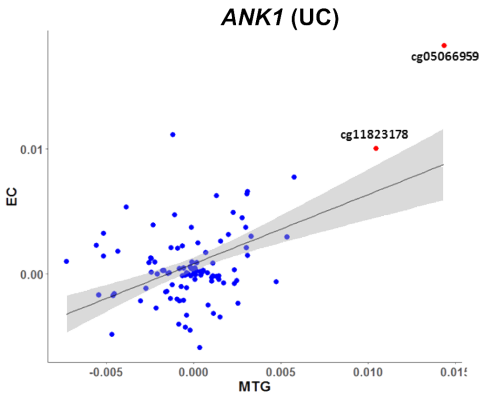

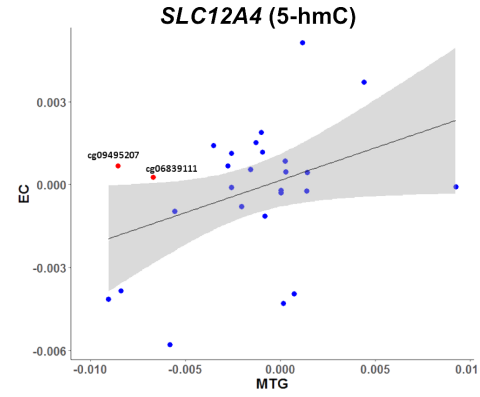

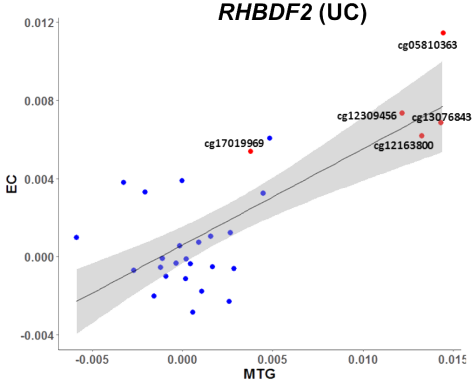

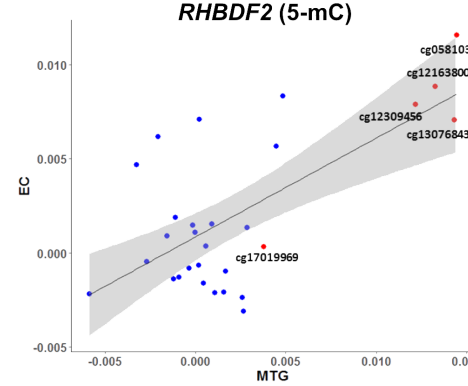

supplementary figure 4.

SUPPLEMENTARY FIGURE 4. The regression coefficients derived from Braak-association analysis of the middle temporal gyrus (MTG), entorhinal cortex (EC) and cerebellum (CER) showed significant correlations between (A) MTG and EC for *ANK1* unmodified cytosine (UC) analysis (r = 0.490, p = 2.68E-07), (B) MTG and EC for *SLC12A4* 5-hydroxymethylcytosine (5-hmC) analysis (r = 0.384, p = 0.048), and (C and D) MTG and EC for *RHBDF2* UC and 5-methylcytosine (5-mC) analysis (r = 0.759, p = 1.78E-06) and (r = 0. 662, p = 9.12E-05), respectively.

supplementary table 1.

	AD patients	Non-demented controls
N	46	36
Gender (male / female)	22 / 24	17 / 19
Age of death (mean ± SD)	85.1 ± 6.1	84.6 ± 5.5
PMI (mean ± SD)	2.8 ± 0.7	2.8 ± 1.0
Plaque total (mean ± SD)	13.01 ± 2.24	4.81 ± 4.35
Tangle total (mean ± SD)	11.10 ± 4.15	4.03 ± 2.11
Braak stage (range (median))	II – VI (V)	I – IV (III)

SUPPLEMENTARY TABLE 1. Cohort demographics.
Middle temporal gyrus tissue obtained from the Banner Sun Health Research Institute (Sun City, Arizona, US) of Alzheimer's disease (AD patients and non-demented controls. Displayed is the number of samples in each group, and the distributions of gender, age, postmortem interval (PMI; hours), Braak stage, and total plaque and tangle load, i.e. the sum of average amyloid-β plaque and tangle densities, respectively, in the entorhinal cortex, hippocampus, parietal lobe, temporal lobe and frontal lobe cortex).

SUPPLEMENTARY TABLE 2. Top 50 differentially methylated positions (DMPs).
Displayed for each probe is chromosomal position (genome build 37), regression estimate for the Alzheimer's disease (AD) case-control analysis (Diagnosis est.), accompanying *p*-values and Benjamini-Hochberg false discovery rate (FDR) adjusted values (*q*-value), Illumina UCSC gene annotation and gene region feature category, GREAT annotation (distance to closest transcription start site [TSS] shown in parentheses), and average 5-methylcytosine (5-mC) percentage and standard deviation per sample group. Probes are ranked based on a combined *p*-value and regression estimate score. UTR, untranslated region.

SUPPLEMENTARY TABLE 3. Top 50 differentially hydroxymethylated positions (DHPs).
Displayed for each probe is chromosomal position (genome build 37), regression estimate for the Alzheimer's disease (AD) case-control analysis (Diagnosis est.), accompanying *p*-values and Benjamini-Hochberg false discovery rate (FDR) adjusted values (*q*-value), Illumina UCSC gene annotation and gene region feature category, GREAT annotation (distance to closest transcription start site shown in parentheses), and average 5-hydroxymethylcytosine (5-hmC) percentage and standard deviation per sample group. Probes are ranked based on a combined *p*-value and regression estimate score.

SUPPLEMENTARY TABLE 4. Top 50 differentially unmodified cytosine positions (DUPs).
Displayed for each probe is chromosomal position (genome build 37), regression estimate for the Alzheimer's disease (AD) case-control analysis (Diagnosis est.), accompanying *p*-values and Benjamini-Hochberg false discovery rate (FDR) adjusted values (*q*-value), Illumina UCSC gene annotation and gene region feature category, GREAT annotation (distance to closest transcription start site shown in parentheses), and average unmodified cytosine (UC) percentage and standard deviation per sample group. Probes are ranked based on a combined *p*-value and regression estimate score.

Rank	Probe ID	Position	Diagnosis est.	*p*-value	*q*-value	Illumina annotation (UCSC)	Gene feature (UCSC)
1	cg13285174	chr 20: 3052221	-0.066611928	6.52E-05	0.613096979	*OXT*	TSS200
2	cg05417607	chr 17: 1373605	0.056371791	3.69E-05	0.503975885	*MYO1C*	Body
3	cg00539564	chr 22: 43254081	0.072180813	1.37E-04	0.683679545	*ARFGAP3*	TSS1500
4	cg04819081	chr 2: 24026544	0.046852736	1.98E-05	0.503975885	*ATAD2B*	Body
5	cg22122808	chr 17: 61511683	-0.050218021	2.38E-04	0.683679545	*CYB561*	3'UTR
6	cg05749855	chr 16: 89472771	0.054927341	3.26E-04	0.683679545	*ANKRD11*	5'UTR
7	cg00857907	chr 2: 202896898	-0.044749354	1.26E-04	0.683679545		
8	cg08597839	chr 1: 29461008	0.059264985	3.77E-04	0.683679545		
9	cg24616382	chr 7: 99767035	0.042200295	1.84E-05	0.503975885	*GAL3ST4*	TSS1500
10	cg06463221	chr 17: 75212862	0.04265807	4.35E-05	0.507974086	*SEC14L1*	3'UTR
11	cg11823178	chr 8: 41519399	0.049548502	3.04E-04	0.683679545	*ANK1; MIR486*	Body; TSS1500
12	cg11239720	chr 4: 152967415	-0.049160769	2.99E-04	0.683679545		
13	cg07871971	chr 17: 40839766	0.041574964	1.10E-05	0.503975885	*CNTNAP1*	Body
14	cg23184226	chr 7: 97880563	0.044935867	1.90E-04	0.683679545	*TECPR1*	5'UTR
15	cg14730223	chr 19: 18232604	0.044646058	1.85E-04	0.683679545	*MAST3*	Body
16	cg25775386	chr 19: 17932001	0.044521783	1.82E-04	0.683679545	*INSL3*	Body
17	cg05270236	chr 6: 158269807	0.042941651	1.07E-04	0.683679545	*SNX9*	Body
18	cg11684897	chr 17: 2951666	0.046484459	2.39E-04	0.683679545		
19	cg14951497	chr 2: 191875807	0.043417747	1.48E-04	0.683679545	*STAT1*	5'UTR
20	cg18419358	chr 6: 158384009	-0.040522539	1.35E-06	0.251170502		
21	cg12163800	chr 17: 74475355	0.043215319	1.88E-04	0.683679545	*RHBDF2*	Body
22	cg03131724	chr 11: 58731433	0.051079548	3.99E-04	0.683679545		
23	cg26733846	chr 6: 112824384	0.044549814	2.66E-04	0.683679545		
24	cg21597025	chr 3: 142837564	0.04427415	2.55E-04	0.683679545	*CHST2*	TSS1500
25	cg18235088	chr 6: 32120623	0.044162472	2.72E-04	0.683679545	*PPT2; PRRT1*	TSS1500
26	cg16908552	chr 1: 231174153	0.040553923	9.30E-05	0.683679545	*FAM89A*	Body
27	cg13523576	chr 8: 21909636	0.040390561	5.63E-05	0.561982879	*EPB49*	TSS1500
28	cg08752433	chr 12: 111016566	0.040773375	1.59E-04	0.683679545	*PPTC7*	Body
29	cg19592472	chr 20: 3052274	-0.057753516	5.96E-04	0.707540795	*OXT*	1stExon; 5'UTR
30	cg20580578	chr 7: 75189143	0.040671812	2.02E-04	0.683679545	*HIP1*	Body
31	cg23238119	chr 6: 74009041	0.043743752	3.78E-04	0.683679545	*C6orf147*	Body
32	cg26033513	chr 3: 195595933	0.044605126	4.11E-04	0.683679545	*TNK2*	Body
33	cg10433043	chr 6: 152432725	-0.039675137	1.50E-04	0.683679545		
34	cg26565893	chr 17: 73501109	0.05019307	5.92E-04	0.707540795	*CASKIN2*	Body
35	cg06439547	chr 1: 230779251	0.040185254	2.13E-04	0.683679545	*COG2*	Body
36	cg21179912	chr 9: 2024387	0.038816208	9.70E-05	0.683679545	*SMARCA2*	5'UTR
37	cg14871225	chr 5: 139040820	-0.03870046	8.75E-05	0.683679545	*CXXC5*	5'UTR
38	cg10082647	chr 12: 107348855	0.060028988	7.43E-04	0.707540795	*C12orf23*	TSS1500
39	cg06345462	chr 16: 13263104	0.038537598	1.43E-04	0.683679545	*SHISA9*	Body
40	cg24859236	chr 1: 9750213	0.037944609	1.21E-04	0.683679545	*PIK3CD*	5'UTR
41	cg01644611	chr 20: 3052253	-0.047108887	6.32E-04	0.707540795	*OXT*	TSS200
42	cg00422578	chr 11: 119968331	0.036593553	2.47E-07	0.098096921		
43	cg13725599	chr 20: 3052262	-0.041713301	4.93E-04	0.701395427	*OXT*	TSS200
44	cg06389574	chr 2: 133834998	0.039731155	3.76E-04	0.683679545	*NCKAP5*	Body
45	cg16803678	chr 3: 133941748	0.039281733	3.39E-04	0.683679545	*RYK*	Body
46	cg07881210	chr 17: 398090	-0.040709357	4.57E-04	0.698683046		
47	cg09375205	chr 11: 63885665	0.038821644	3.26E-04	0.683679545	*FLRT1; MACROD1*	Body
48	cg03783110	chr 17: 1463739	0.037571181	2.62E-04	0.683679545	*PITPNA*	Body
49	cg01025302	chr 5: 3213214	0.036681752	2.09E-04	0.683679545		
50	cg02481714	chr 22: 40439396	-0.03649075	1.79E-04	0.683679545	*TNRC6B*	TSS1500

supplementary table 2.

supplementary table 2.

GREAT annotation		Control		AD	
		Average 5-mC (%)	Standard deviation (%)	Average 5-mC (%)	Standard deviation (%)
OXT (-44)		74.61	6.16	67.66	9.08
CRK (-14045)	*MYO1C* (+22395)	71.35	5.69	76.98	6.41
ARFGAP3 (-674)		59.68	8.12	67.03	8.08
ATAD2B (+123391)		59.05	5.03	63.83	4.31
CYB561 (+11861)	*TANC2* (+424786)	30.66	6.37	25.58	5.59
ANKRD11 (+84197)	*ZNF778* (+188661)	69.46	7.86	75.16	5.97
FZD7 (-2411)		60.53	4.74	56.04	5.61
TMEM200B (-10588)	*SRSF4* (+47628)	44.65	6.49	50.65	7.91
GAL3ST4 (-663)		56.29	4.12	60.57	4.14
SEPT9 (-64629)	*SEC14L1* (+75858)	41.00	3.78	45.34	4.83
NKX6-3 (-14525)	*ANK1* (+234880)	78.23	5.69	83.31	6.06
PET112 (-285241)	*FBXW7* (+488769)	51.07	5.14	46.21	6.32
CNTNAP1 (+5135)	*EZH1* (+57304)	74.07	4.57	78.31	3.47
TECPR1 (+904)		30.03	4.36	34.43	5.80
PIK3R2 (-31411)	*MAST3* (+24002)	69.91	4.77	74.39	5.38
INSL3 (+318)		70.16	4.67	74.53	5.41
SYNJ2 (-133080)	*SNX9* (+25514)	58.65	4.78	63.00	4.61
OR1D5 (+15234)	*RAP1GAP2* (+251935)	33.52	4.75	38.22	5.88
STAT1 (+3168)	*GLS* (+130261)	54.62	6.00	59.10	4.07
SYNJ2 (-18878)	*SNX9* (+139716)	57.17	2.80	53.01	4.07
RHBDF2 (+8635)	*AANAT* (+11726)	79.05	5.52	83.37	4.37
FAM111B (-143224)	*GLYATL1* (+20712)	40.38	6.08	45.59	6.26
RFPL4B (+155853)		32.90	5.13	37.41	5.27
CHST2 (-1053)		62.39	5.70	66.86	4.83
PRRT1 (-904)	*PPT2* (-605)	50.45	5.48	55.01	5.27
TRIM67 (-124520)	*ARV1* (+59331)	46.12	5.41	50.31	3.81
EPB49 (-2691)		55.78	4.54	59.83	3.93
PPTC7 (+4497)	*RAD9B* (+76562)	59.16	4.66	63.23	4.54
OXT (+9)		61.96	6.06	55.93	8.94
POM121C (-73576)	*HIP1* (+179139)	59.57	3.79	63.68	5.31
KHDC1 (-36135)	*DPPA5* (+54957)	20.92	5.50	25.40	5.15
MUC4 (-57090)	*TNK2* (+26498)	71.94	6.51	76.51	4.48
ESR1 (+304272)	*SYNE1* (+525808)	47.89	4.79	44.04	4.51
CASKIN2 (+10517)	*KIAA0195* (+48446)	68.36	7.36	73.53	5.52
COG2 (+1050)	*AGT* (+71084)	66.23	5.40	70.29	3.92
VLDLR (-597405)	*SMARCA2* (+9046)	68.11	4.74	72.06	3.80
PSD2 (-134585)	*CXXC5* (+12520)	18.91	4.82	15.01	3.62
C12orf23 (-688)		24.48	7.34	30.54	7.78
ERCC4 (-750909)	*SHISA9* (+267628)	65.80	4.36	69.69	4.21
PIK3CD (+38424)	*CLSTN1* (+134336)	28.00	4.41	31.83	4.09
OXT (-12)		84.15	3.88	79.27	7.61
PVRL1 (-368897)	*TRIM29* (+40531)	68.76	3.45	72.33	2.77
OXT (-3)		86.27	3.28	81.92	6.65
LYPD1 (-406518)	*NCKAP5* (+491032)	44.78	5.08	48.72	4.51
SLCO2A1 (-192829)	*RYK* (+27837)	44.79	4.57	48.75	4.71
RPH3AL (-195458)	*VPS53* (+220005)	50.14	4.86	45.90	5.57
FLRT1 (+14304)	*MACROD1* (+47919)	78.40	4.92	82.29	4.47
INPP5K (-43558)	*PITPNA* (+2370)	26.04	4.87	29.85	3.96
IRX1 (-382953)	*C5orf38* (+460953)	72.06	4.70	75.73	3.76
TNRC6B (-134532)	*GRAP2* (+142311)	39.13	4.48	35.45	3.85

Rank	Probe ID	Position	Diagnosis est.	*p*-value	*q*-value	Illumina annotation (UCSC)	Gene feature (UCSC)
1	cg10857341	chr 2: 161952702	0.060721423	1.82E-05	0.612604396		
2	cg01024962	chr 14: 31389792	0.053715414	4.49E-05	0.614686985	*STRN3*	Body
3	cg00457087	chr 1: 162602295	-0.045664223	2.63E-05	0.612604396	*DDR2*	1stExon; 5'UTR
4	cg10310119	chr 12: 129276152	-0.053614088	1.25E-04	0.677914758		
5	cg14962509	chr 1: 36039655	-0.073302356	1.92E-04	0.742185585	*TFAP2E*	Body
6	cg05270236	chr 6: 158269807	-0.048035626	8.99E-05	0.614686985	*SNX9*	Body
7	cg26565893	chr 17: 73501109	-0.047161946	8.24E-05	0.614686985	*CASKIN2*	Body
8	cg15418423	chr 3: 23225524	-0.044713764	4.98E-05	0.614686985		
9	cg08117728	chr 6: 32179567	-0.048833262	1.36E-04	0.692660621	*NOTCH4*	Body
10	cg24859236	chr 1: 9750213	-0.042085566	3.03E-05	0.612604396	*PIK3CD*	5'UTR
11	cg04197347	chr 3: 66022776	-0.046419228	1.91E-04	0.742185585	*MAGI1*	Body
12	cg20703928	chr 2: 106364229	-0.056359478	3.19E-04	0.828359319	*NCK2*	5'UTR
13	cg07719898	chr 1: 200274728	-0.04422518	1.22E-04	0.677914758		
14	cg08752433	chr 12: 111016566	-0.043912438	1.11E-04	0.641340409	*PPTC7*	Body
15	cg19592472	chr 20: 3052274	0.042227248	6.35E-05	0.614686985	*OXT*	1stExon; 5'UTR
16	cg10287485	chr 11: 69473145	-0.042090888	5.76E-05	0.614686985		
17	cg18804147	chr 7: 882010	-0.044346638	1.82E-04	0.742185585	*UNC84A*	Body
18	cg04580750	chr 1: 244199781	-0.041448388	7.14E-05	0.614686985		
19	cg24158936	chr 1: 177177623	-0.043067269	1.89E-04	0.742185585	*FAM5B*	5'UTR
20	cg13829089	chr 17: 7460690	-0.043681654	2.51E-04	0.744217143	*TNFSF13; TNFSF12*	TSS1500; 3'UTR; Body
21	cg16908552	chr 1: 231174153	-0.046104182	3.51E-04	0.839277644	*FAM89A*	Body
22	cg22211672	chr 15: 74610366	-0.039776338	2.34E-05	0.612604396	*CCDC33*	Body; TSS1500
23	cg08410533	chr 10: 375830	-0.041469539	1.94E-04	0.742185585	*DIP2C*	Body
24	cg10082647	chr 12: 107348855	-0.049976039	5.60E-04	0.849211551	*C12orf23*	TSS1500
25	cg25449950	chr 4: 24797174	-0.039420471	3.09E-05	0.612604396	*SOD3*	5'UTR; 1stExon
26	cg23987137	chr 5: 58653624	-0.0407906	2.87E-04	0.776384934	*PDE4D*	Body
27	cg04889800	chr 1: 16163555	0.050313798	7.22E-04	0.873057029	*FLJ37453*	Body
28	cg27365991	chr 5: 123036376	-0.0380364	2.86E-05	0.612604396		
29	cg14525270	chr 1: 43766647	0.039702108	2.15E-04	0.743364204	*TIE1*	TSS200
30	cg00937742	chr 2: 133429299	-0.039427167	1.99E-04	0.742185585	*LYPD1*	TSS1500
31	cg10249224	chr 1: 32828191	-0.040004587	3.46E-04	0.839277644	*TSSK3*	1stExon; 5'UTR; TSS1500
32	cg13594542	chr 9: 138850547	0.037747194	7.17E-05	0.614686985	*UBAC1*	Body
33	cg01779732	chr 15: 90015521	-0.037431465	4.17E-05	0.614686985	*RHCG*	3'UTR
34	cg07655487	chr 11: 66849820	-0.037710951	1.03E-04	0.635609177		
35	cg00682103	chr 8: 141554380	0.038203375	2.15E-04	0.743364204	*EIF2C2*	Body
36	cg00539564	chr 22: 43254081	-0.059919292	1.06E-03	0.899315199	*ARFGAP3*	TSS1500
37	cg03503988	chr 20: 52827774	-0.048685182	9.63E-04	0.899315199	*PFDN4*	Body
38	cg13613245	chr 9: 139390036	-0.052895981	9.98E-04	0.899315199	*NOTCH1*	3'UTR
39	cg26827533	chr 8: 22458122	-0.038430688	2.85E-04	0.776384934	*C8orf58*	Body
40	cg23369670	chr 14: 104171944	-0.037854307	1.98E-04	0.742185585	*XRCC3*	Body
41	cg22023879	chr 6: 31767600	-0.041759014	6.60E-04	0.873057029	*LSM2*	Body
42	cg02071305	chr 15: 41185973	-0.038885457	3.71E-04	0.839277644	*VPS18*	TSS1500
43	cg24601055	chr 1: 87372153	-0.037782265	2.14E-04	0.743364204	*SEP15*	Body
44	cg06853339	chr 17: 76117687	0.05693702	1.13E-03	0.899315199	*TMC6*	Body
45	cg27094173	chr 11: 73371753	-0.037025022	9.27E-05	0.614686985	*PLEKHB1*	Body
46	cg03402235	chr 15: 42749336	-0.041794305	8.95E-04	0.899315199	*ZFP106*	1stExon
47	cg24697460	chr 12: 124908653	-0.048955399	1.20E-03	0.899315199	*NCOR2*	Body
48	cg26319169	chr 15: 65870540	-0.037601875	3.76E-04	0.839277644	*PTPLAD1*	3'UTR
49	cg01783195	chr 16: 53524545	0.039006548	6.06E-04	0.857358768	*RBL2*	3'UTR
50	cg08371947	chr 4: 8477793	0.035581593	5.92E-06	0.52858505	*C4orf23*	3'UTR

supplementary table 3.

supplementary table 3.

GREAT annotation		Control		AD	
		Average 5-hmC (%)	Standard deviation (%)	Average 5-hmC (%)	Standard deviation (%)
RBMS1 (-602385)	*TANK* (-40763)	1.90	6.49	8.12	5.65
AP4S1 (-104519)	*COCH* (+46052)	2.69	5.03	8.08	5.94
DDR2 (+68)		3.55	4.28	-1.10	4.80
SLC15A4 (+32388)	*TMEM132C* (+524205)	13.00	6.64	7.38	6.09
TFAP2E (+685)		10.35	7.96	2.82	8.96
SYNJ2 (-133080)	*SNX9* (+25514)	21.86	5.70	17.02	4.72
CASKIN2 (+10517)	*KIAA0195* (+48446)	11.78	5.47	6.91	5.01
UBE2E2 (-19259)		7.49	3.86	2.92	5.25
GPSM3 (-16268)	*NOTCH4* (+12276)	10.80	5.87	5.85	5.12
PIK3CD (+38424)	*CLSTN1* (+134336)	2.69	3.76	-1.50	4.63
MAGI1 (+1732)		17.14	5.27	12.42	5.31
FHL2 (-348549)	*NCK2* (-103974)	15.06	6.21	9.53	7.42
FAM58BP (+92073)	*ZNF281* (+104437)	3.27	4.26	-1.12	5.42
PPTC7 (+4497)	*RAD9B* (+76562)	21.12	4.91	16.71	4.88
OXT (+9)		12.99	4.10	17.38	5.25
ORAOV1 (+17019)	*CCND1* (+17273)	9.76	4.39	5.48	4.46
GET4 (-34180)	*SUN1* (+9869)	7.88	4.18	3.31	5.97
AKT3 (-193198)	*ZNF238* (-14779)	4.16	4.09	-0.09	4.74
FAM5B (+36991)	*SEC16B* (+761426)	10.92	5.46	6.77	4.88
SENP3 (-4618)		5.25	4.84	0.95	5.31
TRIM67 (-124520)	*ARV1* (+59331)	7.78	4.94	3.09	5.90
CYP11A1 (+49714)	*CCDC33* (+81700)	8.89	3.84	4.93	4.04
ZMYND11 (+149897)	*DIP2C* (+359777)	10.46	4.52	6.34	4.86
C12orf23 (-688)		15.85	5.85	10.85	6.95
SOD3 (+90)		3.97	4.19	0.01	3.76
PDE4D (+535996)	*RAB3C* (+774686)	8.20	5.20	4.01	4.62
UQCRHL (-29362)	*SPEN* (-10803)	24.24	6.20	29.21	6.51
CSNK1G3 (+188584)		6.12	3.79	2.15	4.28
TIE1 (+82)		8.10	5.22	11.90	4.50
LYPD1 (-819)		13.08	5.17	9.08	3.91
TSSK3 (+330)		9.00	4.65	4.96	4.83
CAMSAP1 (-51543)	*UBAC1* (+2678)	10.32	3.76	14.15	4.20
POLG (-137496)	*RHCG* (+24277)	4.70	3.76	0.91	3.92
KDM2A (-36919)	*RHOD* (+25532)	4.12	4.04	0.36	4.13
CHRAC1 (+32984)	*EIF2C2* (+91265)	8.95	3.30	12.83	5.09
ARFGAP3 (-674)		18.99	7.23	12.89	8.38
DOK5 (-264491)	*PFDN4* (+3273)	22.86	6.57	17.94	6.23
SEC16A (-12530)	*NOTCH1* (+50201)	10.99	7.00	5.59	6.86
KIAA1967 (-4416)		12.47	4.52	8.70	4.60
XRCC3 (+9878)	*KLC1* (+76420)	15.99	4.09	12.14	5.05
VARS (-3889)		8.73	5.95	4.52	4.72
VPS18 (-654)		4.50	4.29	0.62	4.89
SEP15 (+7953)	*SH3GLB1* (+201901)	14.62	4.30	10.81	4.34
TMC6 (+7173)	*TNRC6C* (+117370)	4.66	7.75	10.40	7.30
PLEKHB1 (+13160)	*RAB6A* (+100447)	10.27	3.93	6.58	4.03
ZFP106 (+393)		6.25	4.88	2.04	5.73
NCOR2 (+143356)	*ZNF664* (+450892)	18.12	7.16	13.17	5.99
C15orf44 (+33086)	*PTPLAD1* (+47714)	15.53	4.11	11.65	4.95
AKTIP (+12624)	*RBL2* (+56195)	8.18	5.17	12.19	4.73
GPR78 (-104423)	*METTL19* (+35262)	1.05	3.16	4.65	3.48

Rank	Probe ID	Position	Diagnosis est.	*p*-value	*q*-value	Illumina annotation (UCSC)	Gene feature (UCSC)
1	cg13076843	chr 17: 74475294	-0.045204925	2.62E-05	0.729466165	*RHBDF2*	Body
2	cg22090150	chr 17: 4098227	-0.046966411	5.68E-05	0.729466165	*ANKFY1*	Body
3	cg10676327	chr 4: 6659735	-0.05946734	2.28E-04	0.894099205		
4	cg09288218	chr 12: 130554977	0.03948029	3.33E-05	0.729466165		
5	cg05810363	chr 17: 74475270	-0.040155937	9.19E-05	0.81747108	*RHBDF2*	Body
6	cg15363134	chr 18: 77161214	0.040840506	1.46E-04	0.894099205	*NFATC1*	Body; 5'UTR
7	cg03183215	chr 10: 1252341	0.039967737	1.14E-04	0.894099205	*ADARB2*	Body
8	cg23689722	chr 1: 3100956	0.038762272	5.64E-05	0.729466165	*PRDM16*	Body
9	cg14150252	chr 2: 64069583	0.03824478	4.14E-05	0.729466165	*UGP2*	Body; 5'UTR
10	cg23449541	chr 21: 47855893	-0.040487636	2.20E-04	0.894099205	*PCNT*	Body
11	cg11491537	chr 2: 132511720	-0.04461105	3.94E-04	0.894099205	*C2orf27A*	Body
12	cg25898192	chr 15: 33418895	0.04452749	4.97E-04	0.894099205		
13	cg06674932	chr 11: 110299342	0.040780155	4.14E-04	0.894099205	*FDX1*	TSS1500
14	cg18102633	chr 19: 17487776	-0.044204533	5.38E-04	0.894099205	*PLVAP*	1stExon
15	cg12163800	chr 17: 74475355	-0.03505837	5.12E-05	0.729466165	*RHBDF2*	Body
16	cg12362517	chr 11: 133800685	0.034839834	3.60E-05	0.729466165	*IGSF9B*	Body
17	cg07799395	chr 5: 125577565	-0.040752803	5.00E-04	0.894099205		
18	cg19457506	chr 17: 43099559	0.038902462	3.98E-04	0.894099205		
19	cg12141052	chr 12: 66349603	-0.039391985	4.40E-04	0.894099205	*HMGA2*	Body
20	cg14464361	chr 2: 237029101	0.036664939	3.55E-04	0.894099205	*AGAP1*	Body
21	cg09169779	chr 13: 20751710	0.04098168	6.92E-04	0.894099205		
22	cg14761019	chr 1: 3028485	0.039329024	6.01E-04	0.894099205	*PRDM16*	Body
23	cg05121497	chr 18: 60186078	-0.033337125	9.22E-05	0.81747108		
24	cg23441248	chr 15: 50140549	-0.041251947	8.03E-04	0.894099205		
25	cg05066959	chr 8: 41519308	-0.04860746	9.98E-04	0.894099205	*ANK1; MIR486*	Body; TSS1500
26	cg23434815	chr 10: 75839302	-0.041809422	8.36E-04	0.894099205	*VCL*	Body
27	cg05417607	chr 17: 1373605	-0.032566779	2.85E-05	0.729466165	*MYO1C*	Body
28	cg27583010	chr 16: 30198505	-0.042414	8.91E-04	0.894099205	*CORO1A*	Body; TSS1500
29	cg27630153	chr 16: 88845038	-0.036347746	6.62E-04	0.894099205	*FAM38A*	Body
30	cg03717755	chr 6: 16136539	-0.034894835	4.83E-04	0.894099205	*MYLIP*	Body
31	cg10688297	chr 7: 2606824	0.035274842	5.84E-04	0.894099205	*IQCE*	Body
32	cg11823178	chr 8: 41519399	-0.032817675	1.90E-04	0.894099205	*ANK1; MIR486*	Body; TSS1500
33	cg25588787	chr 5: 154027256	0.032358662	6.19E-05	0.767470651		
34	cg26844804	chr 15: 102267900	-0.03982849	9.42E-04	0.894099205		
35	cg21686171	chr 1: 9504429	-0.037272429	8.23E-04	0.894099205		
36	cg12309456	chr 17: 74475402	-0.03225529	1.55E-04	0.894099205	*RHBDF2*	Body
37	cg01434302	chr 8: 3267208	-0.035820147	7.36E-04	0.894099205	*CSMD1*	Body
38	cg01513307	chr 6: 108479557	0.031561305	3.95E-05	0.729466165		
39	cg07318609	chr 10: 128585354	0.032460468	2.58E-04	0.894099205		
40	cg01892689	chr 8: 97657072	0.032411115	2.90E-04	0.894099205	*PGCP*	TSS1500
41	cg00542992	chr 5: 141595654	0.033403906	5.88E-04	0.894099205		
42	cg02920514	chr 3: 195610120	-0.037030653	1.07E-03	0.894099205	*TNK2*	Body
43	cg22705835	chr 10: 65332833	0.049158901	1.43E-03	0.894099205	*REEP3*	Body
44	cg17145559	chr 2: 114866027	-0.034973236	9.24E-04	0.894099205		
45	cg01064286	chr 1: 212777218	-0.032117679	4.52E-04	0.894099205	*ATF3*	5'UTR
46	cg04329433	chr 8: 55365596	-0.041449813	1.37E-03	0.894099205		
47	cg04972348	chr 1: 1100035	-0.032278297	5.00E-04	0.894099205		
48	cg19137748	chr 11: 69466054	-0.031730838	4.01E-04	0.894099205	*CCND1*	3'UTR
49	cg05802560	chr 22: 24381773	-0.045715242	1.50E-03	0.894099205	*GSTT1*	Body
50	cg20488756	chr 6: 30131586	-0.032945715	7.25E-04	0.894099205	*TRIM15*	1stExon

supplementary table 4.

supplementary table 4.

GREAT annotation		Control		AD	
		Average UC (%)	Standard deviation (%)	Average UC (%)	Standard deviation (%)
RHBDF2 (+8696)	*AANAT* (+11665)	19.98	5.34	15.41	3.94
CYB5D2 (+51766)	*ANKFY1* (+69046)	20.55	5.11	15.82	4.92
S100P (-35830)	*MRFAP1* (+17291)	34.46	6.97	28.50	6.92
TMEM132D (-166766)	*FZD10* (-92026)	59.15	3.56	63.05	4.55
RHBDF2 (+8720)	*AANAT* (+11641)	11.88	5.46	7.81	3.41
NFATC1 (+889)		29.04	3.68	33.05	5.52
IDI1 (-157281)	*ADARB2* (+527328)	9.79	2.23	13.78	5.57
ARHGEF16 (-270190)	*PRDM16* (+115215)	39.60	3.65	43.53	4.50
UGP2 (+570)		74.54	3.77	78.36	4.22
DIP2A (-22968)	*PCNT* (+111858)	27.68	5.00	23.58	4.54
GPR39 (-662426)	*LOC150776* (+261335)	27.69	5.95	23.26	5.11
RYR3 (-184281)	*FMN1* (-58811)	73.62	5.96	78.07	5.30
FDX1 (-1318)		28.94	5.63	32.99	4.45
PLVAP (+360)		23.94	5.64	19.47	5.51
RHBDF2 (+8635)	*AANAT* (+11726)	16.19	4.59	12.65	2.89
SPATA19 (-85294)	*IGSF9B* (+26194)	30.35	2.94	33.80	4.21
ALDH7A1 (+353516)		44.26	6.06	40.14	4.19
C1QL1 (-53916)	*DCAKD* (+29418)	79.91	5.69	83.79	3.97
HMGA2 (+131364)	*LLPH* (+174929)	52.43	5.31	48.53	4.59
GBX2 (+47550)	*AGAP1* (+626369)	19.25	3.84	22.82	5.28
GJA3 (-16528)	*GJB2* (+15403)	57.60	4.63	61.68	5.75
ARHGEF16 (-342661)	*PRDM16* (+42744)	32.35	5.15	36.32	4.89
ZCCHC2 (-4579)		24.99	3.56	21.68	3.76
ATP8B4 (+270869)	*FGF7* (+425175)	36.18	6.54	32.05	4.14
NKX6-3 (-14434)	*ANK1* (+234971)	24.51	6.52	19.57	6.45
AP3M1 (+71523)	*VCL* (+81431)	33.09	6.07	28.84	5.00
CRK (-14045)	*MYO1C* (+22395)	13.96	3.60	10.68	3.07
SLX1B (-6658)	*CORO1A* (+3775)	47.50	4.16	43.24	6.39
PIEZO1 (+6333)	*CTU2* (+72148)	24.53	5.48	20.84	3.89
GMPR (-102271)	*MYLIP* (+7223)	30.15	5.04	26.68	3.83
TTYH3 (-64778)	*IQCE* (+8193)	58.17	4.16	61.64	4.75
NKX6-3 (-14525)	*ANK1* (+234880)	15.80	4.19	12.45	3.64
HAND1 (-169433)	*LARP1* (-65205)	64.60	3.66	67.85	3.27
TARSL2 (-3256)		18.79	7.71	14.89	2.21
SLC25A33 (-95098)	*SPSB1* (+151489)	27.80	5.31	24.04	4.44
RHBDF2 (+8588)	*AANAT* (+11773)	13.63	4.30	10.36	3.16
NONE		38.86	4.43	35.30	4.73
OSTM1 (-83617)	*NR2E1* (-7657)	73.07	3.24	76.23	3.29
C10orf90 (-375345)	*DOCK1* (-8668)	63.68	3.97	66.93	3.70
PGCP (-426)		49.92	3.40	53.17	4.17
NDFIP1 (+107331)	*SPRY4* (+108965)	57.33	3.73	60.67	4.52
MUC4 (-71277)	*TNK2* (+12311)	33.04	4.48	29.31	5.54
REEP3 (+51711)		53.78	5.81	58.67	7.45
ACTR3 (+218491)		24.59	5.45	21.09	3.84
ATF3 (-4751)		27.37	3.91	24.13	4.04
SOX17 (-4898)		42.50	5.90	38.34	5.45
C1orf159 (-48300)	*TTLL10* (-9250)	49.33	4.52	46.12	3.57
CCND1 (+10182)	*ORAOV1* (+24110)	22.02	4.15	18.87	3.66
GSTT1 (+2510)	*GSTT2* (+59460)	23.00	8.41	18.44	3.85
TRIM10 (-2876)		34.63	4.57	31.37	4.02

Probe ID	Position	Braak est.	*p*-value	Illumina annotation (UCSC)	GREAT annotation	
cg09573585	chr 10: 88728128	-0.006016595	0.028384459	*C10orf116*	*AGAP11* (-2369)	*C10orf116* (-59)
cg11805311	chr 10: 88728073	-0.007035095	0.048298223	*C10orf116*	*AGAP11* (-2424)	*C10orf116* (-114)
cg26395382	chr 10: 88728235	-0.005149	0.145609597	*C10orf116*	*AGAP11* (-2262)	*C10orf116* (+48)
cg01754756	chr 10: 88728078	-0.006316606	0.067157772	*C10orf116*	*AGAP11* (-2419)	*C10orf116* (-109)
cg05066959	chr 8: 41519308	0.012616633	0.017133805	*ANK1*; *MIR486*	*NKX6-3* (-14434)	*ANK1* (+234971)
cg11823178	chr 8: 41519399	0.013034543	0.005944986	*ANK1*; *MIR486*	*NKX6-3* (-14525)	*ANK1* (+234880)
cg15481294	chr 19: 6712406	0.002846515	0.141314636	*C3*	*TNFSF14* (-41808)	*C3* (+8255)
cg26861457	chr 19: 6712380	0.003943492	0.082611145	*C3*	*TNFSF14* (-41782)	*C3* (+8281)
cg10628785	chr 19: 6712321	0.001278944	0.49652103	*C3*	*TNFSF14* (-41723)	*C3* (+8340)
cg25406665	chr 19: 6712357	0.004362112	0.006920004	*C3*	*TNFSF14* (-41759)	*C3* (+8304)
cg15755240	chr 19: 6712372	0.002804723	0.175757492	*C3*	*TNFSF14* (-41774)	*C3* (+8289)
cg24811290	chr 4: 159092553	-0.006856254	0.019508101	*FAM198B*	*FAM198B* (+1648)	*GRIA2* (+950818)
cg03304437	chr 4: 159092536	-0.009786048	0.003876177	*FAM198B*	*FAM198B* (+1665)	*GRIA2* (+950801)
cg06370094	chr 12: 130555091	-0.00659553	0.141338936		*TMEM132D* (-166880)	*FZD10* (-91912)
cg09288218	chr 12: 130554977	-0.006743524	0.153451358		*TMEM132D* (-166766)	*FZD10* (-92026)
cg07070348	chr 12: 130555007	-0.002413988	0.561815254		*TMEM132D* (-166796)	*FZD10* (-91996)
cg07747220	chr 20: 3052115	-0.008173965	0.069260258	*OXT*	*OXT* (-150)	
cg01644611	chr 20: 3052253	-0.011736189	0.013759205	*OXT*	*OXT* (-12)	
cg13725599	chr 20: 3052262	-0.009424932	0.023323502	*OXT*	*OXT* (-3)	
cg26267561	chr 20: 3052224	-0.007403822	0.055313901	*OXT*	*OXT* (-41)	
cg13285174	chr 20: 3052221	-0.015282407	0.008729542	*OXT*	*OXT* (-44)	
cg19592472	chr 20: 3052274	-0.010865231	0.063920724	*OXT*	*OXT* (+9)	
cg16887334	chr 20: 3052151	-0.010386509	0.022978398	*OXT*	*OXT* (-114)	
cg26955850	chr 20: 3052345	-0.001848332	0.565728654	*OXT*	*OXT* (+80)	
cg02046423	chr 17: 2951689	0.006873988	0.037249269		*OR1D5* (+15211)	*RAP1GAP2* (+251958)
cg11684897	chr 17: 2951666	0.010822722	0.013858777		*OR1D5* (+15234)	*RAP1GAP2* (+251935)
cg24015889	chr 17: 2951719	0.002697856	0.481274149		*OR1D5* (+15181)	*RAP1GAP2* (+251988)
cg12163800	chr 17: 74475355	0.013257607	0.00082286	*RHBDF2*	*RHBDF2* (+8635)	*AANAT* (+11726)
cg12309456	chr 17: 74475402	0.012145479	1.56E-06	*RHBDF2*	*RHBDF2* (+8588)	*AANAT* (+11773)
cg05810363	chr 17: 74475270	0.01445045	0.000161102	*RHBDF2*	*RHBDF2* (+8720)	*AANAT* (+11641)
cg13076843	chr 17: 74475294	0.01431989	0.000597182	*RHBDF2*	*RHBDF2* (+8696)	*AANAT* (+11665)
cg17019969	chr 17: 74475240	0.003757517	0.286766652	*RHBDF2*	*RHBDF2* (+8750)	*AANAT* (+11611)
cg06839111	chr 16: 67978450	0.005045647	0.033641168	*SLC12A4*; *LCAT*	*LCAT* (-436)	
cg09495207	chr 16: 67978445	0.004184379	0.059896273	*SLC12A4*; *LCAT*	*LCAT* (-431)	
cg20697427	chr 3: 195610231	0.002414777	0.498219531	*TNK2*	*MUC4* (-71388)	*TNK2* (+12200)
cg02920514	chr 3: 195610120	0.003748243	0.480665527	*TNK2*	*MUC4* (-71277)	*TNK2* (+12311)
cg16047223	chr 3: 195610084	0.005125395	0.126645191	*TNK2*	*MUC4* (-71241)	*TNK2* (+12347)

supplementary table 5.

SUPPLEMENTARY TABLE 5. Association of probes in differentially methylated regions (DMRs) with Braak stage. Braak stage-association analysis of probes located in Alzheimer's disease (AD)-associated DMRs. Displayed for each probe is chromosomal position (genome build 37), regression estimate for the Braak-associated analysis (Braak est.), accompanying *p*-values, Illumina gene annotation, GREAT annotation (distance to closest tran-

supplementary table 5.

Braak stage I		Braak stage II		Braak stage III		Braak stage IV		Braak stage V		Braak stage VI	
Average 5-mC (%)	Standard deviation (%)	Average 5-mC (%)	Standard deviation (%)	Average 5-mC (%)	Standard deviation (%)	Average 5-mC (%)	Standard deviation (%)	Average 5-mC (%)	Standard deviation (%)	Average 5-mC (%)	Standard deviation (%)
33.69	3.00	32.00	3.56	33.72	3.15	31.86	3.38	29.03	4.17	32.64	1.95
30.21	3.09	30.07	4.40	30.95	4.54	28.89	4.38	27.32	4.84	28.97	5.99
13.94	2.90	12.45	2.89	16.45	5.30	13.21	4.95	11.89	4.13	13.06	4.44
26.60	2.35	25.12	4.54	27.63	4.71	26.03	5.22	24.30	4.14	24.11	3.92
71.71	5.30	78.93	5.94	74.86	7.14	77.20	6.84	81.29	7.42	79.43	6.87
76.08	5.22	81.39	7.13	78.49	5.54	80.15	5.50	84.79	5.68	83.16	6.90
77.03	2.45	78.25	2.53	79.46	2.46	79.28	2.13	79.73	2.70	79.21	3.01
71.14	3.93	73.07	2.44	72.61	2.51	72.84	4.15	73.27	3.04	74.12	2.18
65.18	0.91	67.30	3.66	67.31	2.79	66.61	2.14	66.74	1.56	67.58	2.36
81.51	2.57	83.26	2.17	82.35	1.87	83.61	2.01	84.32	1.89	83.79	2.20
79.41	2.29	78.82	2.77	79.38	2.97	80.14	3.05	79.81	2.41	80.53	2.82
20.34	3.25	20.44	3.79	19.43	3.84	19.18	4.57	17.39	4.00	17.34	3.84
26.50	5.18	21.18	5.21	24.89	5.01	22.96	3.44	21.56	3.20	19.38	2.54
41.26	4.59	39.41	6.68	38.46	6.63	39.29	3.76	37.25	6.13	37.07	6.41
44.95	4.63	42.92	4.35	42.30	6.26	41.22	7.52	39.25	5.74	41.85	7.08
31.78	4.69	30.40	6.53	27.58	5.44	30.47	7.02	27.60	4.67	29.88	4.37
79.29	4.71	78.35	6.21	80.78	4.78	77.83	6.99	76.29	6.98	77.13	7.13
84.37	2.82	81.03	5.38	84.68	3.95	81.51	7.19	77.34	8.34	80.70	6.91
86.58	2.59	84.16	5.04	86.12	3.32	83.84	6.34	79.97	7.06	84.00	6.27
67.42	4.07	65.87	6.00	66.92	3.63	64.26	4.80	63.14	5.41	65.56	7.44
73.42	7.48	71.80	8.01	74.36	5.90	70.45	9.68	65.53	8.04	70.11	10.53
61.07	4.38	58.90	8.21	61.66	6.53	58.27	9.33	53.75	8.37	59.28	9.32
81.38	7.44	77.09	6.64	82.22	4.40	77.67	6.00	75.31	6.13	77.71	7.76
50.63	4.72	51.62	4.21	51.49	3.41	49.22	3.43	47.92	3.44	53.30	5.54
22.42	4.65	24.67	4.83	23.23	4.35	24.38	2.86	26.18	5.93	26.77	3.63
29.45	7.09	33.72	5.68	35.92	4.57	37.45	5.62	39.19	6.18	35.71	5.04
30.17	5.09	32.57	6.08	33.91	4.58	34.60	5.79	34.35	5.56	33.43	5.52
76.09	5.59	82.70	4.29	78.32	4.97	81.04	5.79	84.50	4.17	84.14	3.23
85.16	5.41	89.18	3.50	88.51	3.21	89.81	4.03	92.28	1.38	92.13	1.39
80.38	6.64	86.15	3.76	85.05	5.41	87.34	6.66	89.93	3.26	89.23	3.15
75.15	6.35	82.78	3.84	80.08	5.48	79.26	6.92	85.75	2.87	84.54	3.77
76.72	2.34	77.10	3.70	76.24	4.81	76.29	6.11	77.70	4.41	78.24	4.26
36.23	3.32	38.53	3.72	38.06	3.28	38.96	3.64	38.89	2.24	39.90	2.34
32.27	1.33	34.90	3.04	34.05	3.10	35.61	3.13	34.73	2.72	35.73	2.49
62.90	3.36	63.45	5.30	63.08	4.22	61.44	4.89	65.28	4.64	62.64	5.65
65.67	6.08	68.11	8.89	65.01	6.75	65.38	5.83	70.11	8.62	64.85	8.73
78.13	3.80	80.27	5.90	78.87	5.65	78.22	3.62	81.81	4.63	79.98	3.85

scription start site shown in parentheses), and average 5-methylcytosine (5-mC) signal and standard deviation per sample group.

Probe ID	Position	Braak est.	*p*-value	Illumina annotation (UCSC)	GREAT annotation	
cg09573585	chr 10: 88728128	0.002993664	0.195490293	*C10orf116*	*AGAP11* (-2369)	*C10orf116* (-59)
cg11805311	chr 10: 88728073	0.000351648	0.918297434	*C10orf116*	*AGAP11* (-2424)	*C10orf116* (-114)
cg26395382	chr 10: 88728235	-0.00254397	0.554518377	*C10orf116*	*AGAP11* (-2262)	*C10orf116* (+48)
cg01754756	chr 10: 88728078	-0.000124756	0.97226127	*C10orf116*	*AGAP11* (-2419)	*C10orf116* (-109)
cg05066959	chr 8: 41519308	0.001590789	0.633584577	*ANK1*; *MIR486*	*NKX6-3* (-14434)	*ANK1* (+234971)
cg11823178	chr 8: 41519399	-0.002706607	0.342571371	*ANK1*; *MIR486*	*NKX6-3* (-14525)	*ANK1* (+234880)
cg15481294	chr 19: 6712406	0.001097194	0.668522069	*C3*	*TNFSF14* (-41808)	*C3* (+8255)
cg26861457	chr 19: 6712380	0.001560152	0.550822267	*C3*	*TNFSF14* (-41782)	*C3* (+8281)
cg10628785	chr 19: 6712321	0.001777699	0.355525449	*C3*	*TNFSF14* (-41723)	*C3* (+8340)
cg15755240	chr 19: 6712372	-0.002177933	0.307227836	*C3*	*TNFSF14* (-41774)	*C3* (+8289)
cg24811290	chr 4: 159092553	0.001450316	0.676894745	*FAM198B*	*FAM198B* (+1648)	*GRIA2* (+950818)
cg03304437	chr 4: 159092536	0.002938581	0.424369174	*FAM198B*	*FAM198B* (+1665)	*GRIA2* (+950801)
cg07070348	chr 12: 130555007	-0.005354324	0.209154879		*TMEM132D* (-166796)	*FZD10* (-91996)
cg07747220	chr 20: 3052115	0.002986068	0.395279658	*OXT*	*OXT* (-150)	
cg01644611	chr 20: 3052253	0.006354246	0.06460808	*OXT*	*OXT* (-12)	
cg13725599	chr 20: 3052262	0.006387303	0.024953675	*OXT*	*OXT* (-3)	
cg26267561	chr 20: 3052224	0.00265964	0.409742344	*OXT*	*OXT* (-41)	
cg13285174	chr 20: 3052221	0.008335871	0.046156832	*OXT*	*OXT* (-44)	
cg19592472	chr 20: 3052274	0.009599409	0.009292317	*OXT*	*OXT* (+9)	
cg16887334	chr 20: 3052151	0.003805097	0.323232339	*OXT*	*OXT* (-114)	
cg02046423	chr 17: 2951689	-0.005535107	0.099080805		*OR1D5* (+15211)	*RAP1GAP2* (+251958)
cg24015889	chr 17: 2951719	0.002035964	0.526532833		*OR1D5* (+15181)	*RAP1GAP2* (+251988)
cg12163800	chr 17: 74475355	0.000165722	0.951440963	*RHBDF2*	*RHBDF2* (+8635)	*AANAT* (+11726)
cg05810363	chr 17: 74475270	0.000790935	0.730915416	*RHBDF2*	*RHBDF2* (+8720)	*AANAT* (+11641)
cg13076843	chr 17: 74475294	0.004644871	0.104219756	*RHBDF2*	*RHBDF2* (+8696)	*AANAT* (+11665)
cg17019969	chr 17: 74475240	-0.000446842	0.909127934	*RHBDF2*	*RHBDF2* (+8750)	*AANAT* (+11611)
cg06839111	chr 16: 67978450	-0.006720141	0.002478319	*SLC12A4*; *LCAT*	*LCAT* (-436)	
cg09495207	chr 16: 67978445	-0.008556322	9.93E-05	*SLC12A4*; *LCAT*	*LCAT* (-431)	
cg20697427	chr 3: 195610231	0.002684102	0.426144824	*TNK2*	*MUC4* (-71388)	*TNK2* (+12200)
cg02920514	chr 3: 195610120	0.005771686	0.273051915	*TNK2*	*MUC4* (-71277)	*TNK2* (+12311)
cg16047223	chr 3: 195610084	0.001484324	0.60624638	*TNK2*	*MUC4* (-71241)	*TNK2* (+12347)

supplementary table 6.

SUPPLEMENTARY TABLE 6. Association of probes in differentially hydroxymethylated regions (DHRs) with Braak stage.
Braak stage-association analysis of probes located in Alzheimer's disease (AD)-associated DHRs. Displayed for each probe is chromosomal position (genome build 37), regression estimate for the Braak-associated analysis (Braak est.), accompanying *p*-values, Illumina gene annotation, GREAT annotation (distance to closest transcription start site shown in parentheses), and average 5-hydroxymethylcytosine (5-hmC) signal and standard deviation per sample group.

supplementary table 6.

Braak stage I		Braak stage II		Braak stage III		Braak stage IV		Braak stage V		Braak stage VI	
Average 5-hmC (%)	Standard deviation (%)	Average 5-hmC (%)	Standard deviation (%)	Average 5-hmC (%)	Standard deviation (%)	Average 5-hmC (%)	Standard deviation (%)	Average 5-hmC (%)	Standard deviation (%)	Average 5-hmC (%)	Standard deviation (%)
5.71	1.51	8.07	3.38	7.06	3.05	7.68	2.73	8.91	3.35	7.63	2.69
6.98	4.22	7.75	5.43	7.45	4.39	8.43	3.70	7.09	4.80	7.97	4.75
16.02	5.28	19.97	5.44	16.88	6.31	17.72	5.12	15.92	5.41	17.59	5.62
11.07	4.87	11.28	4.75	10.65	5.08	10.26	5.34	9.45	4.19	12.33	3.85
-0.75	2.38	1.19	2.91	-0.33	5.48	-0.07	3.71	1.81	4.53	-0.05	4.77
5.76	3.85	4.01	3.97	6.02	3.32	5.92	3.24	3.33	3.61	4.70	4.34
1.67	2.99	0.10	3.75	-0.76	3.28	0.13	2.48	0.83	3.56	0.44	3.89
7.72	3.76	7.23	3.79	6.15	2.79	8.00	3.71	8.27	3.85	6.95	2.97
8.71	0.17	8.41	3.13	7.55	2.81	8.41	2.38	9.35	2.31	8.55	2.38
5.57	3.32	7.93	3.76	6.20	2.81	6.42	3.34	6.39	1.80	5.49	1.93
17.22	3.28	14.75	3.78	16.78	4.67	15.83	4.35	17.58	5.38	16.47	5.17
12.23	3.66	14.49	5.95	11.68	4.81	12.54	5.13	15.20	4.56	13.52	3.64
0.69	6.60	-0.39	6.44	4.38	5.90	-0.29	6.32	-0.31	4.97	-0.22	4.14
2.30	3.79	2.33	4.64	0.18	4.03	2.01	5.43	2.41	5.77	2.94	3.50
4.53	1.83	8.15	4.56	4.17	2.68	5.63	5.02	9.07	5.44	7.12	5.20
3.40	2.06	5.88	3.69	4.09	2.68	5.46	3.93	8.64	4.40	5.52	3.74
9.41	3.76	9.63	5.19	9.37	3.70	11.06	4.08	11.05	4.35	9.38	5.15
7.14	3.43	8.89	4.39	7.24	4.79	8.48	6.84	11.91	5.76	9.84	8.02
12.78	2.18	15.03	4.75	13.47	5.04	14.76	5.04	19.31	5.03	15.73	5.23
4.05	6.87	5.30	5.64	1.45	4.46	4.53	5.65	5.12	4.65	4.73	4.75
3.80	4.56	7.14	4.63	5.42	4.29	4.10	3.05	4.64	5.21	2.48	4.48
4.90	4.51	6.59	4.34	3.90	3.31	4.37	5.23	6.17	4.22	5.28	4.67
2.86	1.79	3.21	2.78	5.01	4.00	5.48	4.14	4.04	3.86	3.15	2.92
3.63	1.14	3.93	2.97	2.88	3.70	2.59	3.11	3.79	3.04	3.59	2.74
-0.46	2.08	-1.09	2.78	-0.48	3.42	2.77	4.87	-0.02	3.73	1.45	2.95
2.24	4.78	4.14	5.66	4.29	4.32	4.28	6.53	4.82	5.68	3.14	4.64
2.47	1.66	2.19	3.48	2.53	2.11	2.52	3.27	-0.97	2.67	0.75	2.32
3.69	3.45	2.16	2.52	2.32	2.29	0.92	2.64	-0.80	3.33	-0.04	2.45
3.20	2.20	2.06	4.19	2.91	4.08	5.49	5.16	2.67	4.19	4.13	4.74
2.82	4.84	0.58	4.25	1.59	7.08	2.75	6.88	0.82	8.78	6.15	7.47
6.25	4.24	4.32	2.96	4.62	4.39	6.18	4.36	4.95	3.06	6.10	4.09

supplementary table 7.

Probe ID	Position	Braak est.	*p*-value	Illumina annotation (UCSC)	GREAT annotation	
cg09573585	chr 10: 88728128	0.002955329	0.175284782	*C10orf116*	*AGAP11* (-2369)	*C10orf116* (-59)
cg11805311	chr 10: 88728073	0.006461492	0.037608595	*C10orf116*	*AGAP11* (-2424)	*C10orf116* (-114)
cg26395382	chr 10: 88728235	0.007835025	0.023230722	*C10orf116*	*AGAP11* (-2262)	*C10orf116* (+48)
cg01754756	chr 10: 88728078	0.006116733	0.054790161	*C10orf116*	*AGAP11* (-2419)	*C10orf116* (-109)
cg05066959	chr 8: 41519308	-0.014326128	0.004492258	*ANK1*; *MIR486*	*NKX6-3* (-14434)	*ANK1* (+234971)
cg11823178	chr 8: 41519399	-0.010445652	0.000482155	*ANK1*; *MIR486*	*NKX6-3* (-14525)	*ANK1* (+234880)
cg15481294	chr 19: 6712406	-0.004136299	0.043201185	*C3*	*TNFSF14* (-41808)	*C3* (+8255)
cg26861457	chr 19: 6712380	-0.006152461	0.000628683	*C3*	*TNFSF14* (-41782)	*C3* (+8281)
cg10628785	chr 19: 6712321	-0.00363932	0.029086896	*C3*	*TNFSF14* (-41723)	*C3* (+8340)
cg25406665	chr 19: 6712357	-0.003830795	0.019017945	*C3*	*TNFSF14* (-41759)	*C3* (+8304)
cg15755240	chr 19: 6712372	-0.000475072	0.724170054	*C3*	*TNFSF14* (-41774)	*C3* (+8289)
cg24811290	chr 4: 159092553	0.006148823	0.028865291	*FAM198B*	*FAM198B* (+1648)	*GRIA2* (+950818)
cg03304437	chr 4: 159092536	0.007125833	0.023797972	*FAM198B*	*FAM198B* (+1665)	*GRIA2* (+950801)
cg06370094	chr 12: 130555091	0.010645547	0.00069916		*TMEM132D* (-166880)	*FZD10* (-91912)
cg09288218	chr 12: 130554977	0.010566119	0.001316707		*TMEM132D* (-166766)	*FZD10* (-92026)
cg07070348	chr 12: 130555007	0.007600781	0.017910978		*TMEM132D* (-166796)	*FZD10* (-91996)
cg07747220	chr 20: 3052115	0.00433216	0.177233877	*OXT*	*OXT* (-150)	
cg01644611	chr 20: 3052253	0.004740962	0.025082208	*OXT*	*OXT* (-12)	
cg13725599	chr 20: 3052262	0.002084246	0.291146331	*OXT*	*OXT* (-3)	
cg26267561	chr 20: 3052224	0.004746563	0.054074549	*OXT*	*OXT* (-41)	
cg13285174	chr 20: 3052221	0.006144414	0.057850503	*OXT*	*OXT* (-44)	
cg19592472	chr 20: 3052274	0.000478175	0.892360099	*OXT*	*OXT* (+9)	
cg16887334	chr 20: 3052151	0.005530593	0.070362053	*OXT*	*OXT* (-114)	
cg26955850	chr 20: 3052345	-0.00256852	0.335887208	*OXT*	*OXT* (+80)	
cg02046423	chr 17: 2951689	-0.000626478	0.82804506		*OR1D5* (+15211)	*RAP1GAP2* (+251958)
cg11684897	chr 17: 2951666	-0.003618111	0.29502693		*OR1D5* (+15234)	*RAP1GAP2* (+251935)
cg24015889	chr 17: 2951719	-0.003588238	0.247758184		*OR1D5* (+15181)	*RAP1GAP2* (+251988)
cg12163800	chr 17: 74475355	-0.013370883	3.59E-06	*RHBDF2*	*RHBDF2* (+8635)	*AANAT* (+11726)
cg12309456	chr 17: 74475402	-0.012716619	7.33E-06	*RHBDF2*	*RHBDF2* (+8588)	*AANAT* (+11773)
cg05810363	chr 17: 74475270	-0.015211785	9.19E-06	*RHBDF2*	*RHBDF2* (+8720)	*AANAT* (+11641)
cg13076843	chr 17: 74475294	-0.019003194	6.50E-08	*RHBDF2*	*RHBDF2* (+8696)	*AANAT* (+11665)
cg17019969	chr 17: 74475240	-0.002638742	0.219478874	*RHBDF2*	*RHBDF2* (+8750)	*AANAT* (+11611)
cg06839111	chr 16: 67978450	0.001968227	0.440743522	*SLC12A4*; *LCAT*	*LCAT* (-436)	
cg09495207	chr 16: 67978445	0.004566565	0.059860794	*SLC12A4*; *LCAT*	*LCAT* (-431)	
cg20697427	chr 3: 195610231	-0.005242366	0.029006958	*TNK2*	*MUC4* (-71388)	*TNK2* (+12200)
cg02920514	chr 3: 195610120	-0.010537855	0.006467596	*TNK2*	*MUC4* (-71277)	*TNK2* (+12311)
cg16047223	chr 3: 195610084	-0.006897202	0.009572732	*TNK2*	*MUC4* (-71241)	*TNK2* (+12347)

SUPPLEMENTARY TABLE 7. Association of probes in differentially unmodified regions (DURs) with Braak stage. Braak stage-association analysis of probes located in Alzheimer's disease (AD)-associated DURs. Displayed for each probe is chromosomal position (genome build 37), regression estimate for the Braak-associated analysis (Braak est.), accompanying *p*-values, Illumina gene annotation, GREAT annotation (distance to closest tran-

supplementary table 7.

Braak stage I		Braak stage II		Braak stage III		Braak stage IV		Braak stage V		Braak stage VI	
Average UC (%)	Standard deviation (%)	Average UC (%)	Standard deviation (%)	Average UC (%)	Standard deviation (%)	Average UC (%)	Standard deviation (%)	Average UC (%)	Standard deviation (%)	Average UC (%)	Standard deviation (%)
60.60	2.16	59.77	2.74	59.47	2.71	60.51	2.26	62.02	3.92	59.82	2.70
62.81	4.27	62.54	6.00	61.98	2.96	62.68	2.92	65.63	5.84	63.50	2.34
70.04	5.16	67.58	4.69	66.84	3.37	69.07	3.71	72.56	5.73	69.26	3.30
62.34	5.23	63.75	5.50	61.98	3.71	63.72	3.43	66.36	4.62	63.63	2.82
29.04	6.42	19.88	6.87	25.02	5.13	22.87	6.21	16.90	5.54	20.22	7.54
18.16	2.82	14.60	5.22	15.35	3.62	13.93	3.33	11.95	3.70	11.94	4.49
21.31	2.26	21.65	3.93	21.31	2.39	20.58	2.74	19.29	2.74	20.37	1.80
21.14	2.25	19.70	2.63	21.26	1.91	19.07	1.88	18.21	2.66	18.73	1.99
26.11	0.86	24.67	2.41	24.90	2.84	24.78	1.87	23.82	2.16	23.60	1.75
18.58	1.52	17.47	2.71	17.88	2.01	17.19	2.69	16.12	1.67	16.79	1.75
15.11	1.94	13.15	2.26	14.16	1.65	13.43	2.01	13.81	1.44	13.86	1.51
62.44	4.31	64.84	4.96	63.57	2.92	65.20	3.07	64.96	3.85	66.42	4.05
61.26	4.30	64.51	5.16	63.76	3.75	64.50	3.12	63.11	3.87	67.61	4.47
60.57	3.66	64.23	4.2	63.32	3.44	62.96	2.78	67.22	4.82	66.57	4.23
58.01	1.87	61.81	4.41	58.62	3.97	61.23	3.03	64.03	4.58	63.24	5.10
67.54	2.28	70.05	4.56	68.26	4.57	69.79	2.02	72.71	4.32	70.59	4.79
18.41	5.41	19.33	3.97	19.42	2.99	20.22	5.41	21.17	4.93	19.80	4.87
11.10	2.57	10.47	1.97	11.31	2.57	12.82	3.26	13.15	3.31	12.05	2.77
10.02	3.20	9.77	2.55	9.96	2.23	10.59	3.22	10.64	2.57	10.52	3.38
23.16	4.14	24.17	3.52	23.90	2.95	24.64	3.48	25.73	3.72	25.02	2.93
19.44	5.17	19.31	4.96	18.55	3.32	21.01	4.78	22.30	4.57	19.93	5.05
26.15	6.10	26.07	5.87	25.60	3.16	27.03	5.61	26.61	4.95	25.29	5.15
14.99	1.78	17.45	3.10	16.76	3.89	17.80	5.25	19.50	4.11	17.41	4.61
52.00	5.22	50.14	5.22	50.65	2.42	51.32	3.83	51.76	2.76	48.03	3.57
73.78	5.78	68.04	4.96	71.30	2.66	71.52	3.57	69.31	2.98	71.03	3.93
67.25	6.66	63.29	5.34	65.40	2.94	65.18	4.59	63.42	4.95	63.60	4.99
64.93	5.24	60.71	4.00	62.29	3.34	61.05	4.52	59.47	4.05	62.05	4.27
21.05	5.03	14.09	2.87	16.48	3.98	13.41	3.97	11.25	1.77	12.77	2.40
17.58	5.58	12.06	3.61	13.64	3.73	11.60	3.92	9.34	2.88	9.79	1.74
15.99	6.02	9.92	5.42	11.85	4.69	10.03	4.84	6.31	1.86	7.01	2.10
25.31	7.33	18.31	3.70	19.94	4.46	17.35	4.94	14.27	2.81	13.74	2.97
21.04	3.76	18.77	3.70	19.16	3.58	19.47	2.39	17.67	2.70	18.68	2.43
61.30	2.93	59.12	2.86	59.46	2.56	58.52	3.87	62.26	3.63	59.37	2.93
63.99	3.86	62.94	2.89	63.77	2.51	63.46	3.64	66.39	3.47	64.36	2.67
33.90	2.09	34.57	4.68	33.65	3.23	32.65	2.52	32.06	3.75	32.90	2.83
31.51	3.22	31.31	7.33	33.23	4.53	31.69	4.21	29.07	6.51	28.35	3.87
15.62	2.55	15.42	5.17	16.05	2.90	15.53	3.84	13.24	4.05	13.45	2.39

scription start site shown in parentheses), and average unmodified cytosine (UC) signal and standard deviation per sample group.

Gene	Probe ID	5-mC			5-hmC			UC		
		Pearson's *r*	*p*-value	*q*-value	Pearson's *r*	*p*-value	*q*-value	Pearson's *r*	*p*-value	*q*-value
FAM198B	cg24811290	-0.067	0.567	0.682	-0.070	0.548	0.680	0.125	0.276	0.464
	cg03304437	-0.066	0.572	0.682	-0.132	0.254	0.394	0.187	0.102	0.221
ADIRF (C10orf116)	cg09573585	-0.157	0.175	0.340	-0.082	0.483	0.623	0.260	0.022	0.089
	cg01754756	-0.084	0.471	0.646	-0.133	0.252	0.394	0.232	0.041	0.123
	cg11805311	-0.151	0.192	0.356	-0.126	0.279	0.411	0.320	0.004	0.053
	cg26395382	-0.116	0.317	0.498	-0.134	0.249	0.394	0.292	0.009	0.066
OXT	cg13285174	-0.246	0.033	0.111	0.230	0.045	0.169	0.087	0.451	0.599
	cg13725599	-0.266	0.020	0.111	0.227	0.049	0.169	0.144	0.209	0.368
	cg19592472	-0.245	0.033	0.111	0.229	0.046	0.169	0.109	0.343	0.512
	cg01644611	-0.291	0.011	0.111	0.283	0.013	0.136	0.163	0.153	0.297
	cg16887334	-0.219	0.058	0.164	0.193	0.095	0.268	0.080	0.486	0.599
	cg26267561	-0.258	0.024	0.111	0.240	0.037	0.169	0.058	0.615	0.734
	cg07747220	-0.292	0.010	0.111	0.179	0.122	0.291	0.173	0.129	0.266
	cg26955850	-0.168	0.147	0.320	-	-	-	0.051	0.660	0.740
RAP1GAP2	cg11684897	-0.263	0.022	0.111	-	-	-	0.280	0.013	0.066
	cg02046423	-0.347	0.002	0.078	0.157	0.177	0.361	0.222	0.050	0.133
	cg24015889	-0.190	0.100	0.246	-0.034	0.768	0.833	0.276	0.014	0.066
RHBDF2	cg12163800	0.287	0.012	0.111	-0.089	0.442	0.596	-0.280	0.013	0.066
	cg12309456	0.270	0.019	0.111	-	-	-	-0.250	0.028	0.102
	cg13076843	0.138	0.233	0.401	0.228	0.048	0.169	-0.303	0.007	0.064
	cg05810363	0.215	0.063	0.166	0.029	0.806	0.833	-0.229	0.043	0.123
	cg17019969	0.071	0.543	0.682	-0.015	0.895	0.895	-0.042	0.717	0.769
SLC12A4	cg06839111	0.105	0.368	0.545	-0.560	1.41E-07	4.38E-06	0.450	3.52E-05	6.51E-04
	cg09495207	0.007	0.952	0.952	-0.485	8.91E-06	1.38E-04	0.474	1.18E-05	4.35E-04
TNK2	cg02920514	-0.031	0.790	0.846	0.100	0.388	0.547	-0.082	0.476	0.599
	cg16047223	0.029	0.801	0.846	0.042	0.716	0.822	-0.095	0.410	0.583
	cg20697427	-0.137	0.239	0.401	0.237	0.039	0.169	-0.116	0.310	0.499
ANK1	cg11823178	-0.044	0.708	0.794	0.033	0.779	0.833	0.040	0.727	0.769
	cg05066959	-0.160	0.169	0.340	0.169	0.143	0.317	0.054	0.642	0.740
LOC100190940	cg09288218	0.066	0.570	0.682	-	-	-	-0.144	0.208	0.368
	cg06370094	0.170	0.143	0.320	-	-	-	-0.193	0.091	0.210
	cg07070348	0.022	0.853	0.877	0.151	0.194	0.361	-0.232	0.041	0.123
C3	cg25406665	-0.088	0.448	0.637	-	-	-	-0.085	0.457	0.599
	cg26861457	-0.236	0.040	0.124	0.192	0.096	0.268	0.028	0.806	0.806
	cg15481294	-0.249	0.030	0.111	0.149	0.198	0.361	0.034	0.767	0.788
	cg10628785	-0.115	0.323	0.498	0.063	0.588	0.700	0.108	0.346	0.512
	cg15755240	-0.056	0.632	0.731	0.188	0.104	0.268	-0.216	0.058	0.143

supplementary table 8.

SUPPLEMENTARY TABLE 8. Correlation of DNA (hydroxy)methylation with expression.
5-methylcytosine (5-mC), 5-hydroxymethylcytosine (5-hmC), and unmodified cytosine (UC) levels of probes within Alzheimer's disease (AD)-associated differentially methylated regions (DMRs), differentially hydroxymethylated regions (DHRs), and differentially unmodified regions (DURs) were correlated with gene expression levels. Displayed per dataset

supplementary table 9.

	All processed and metrics together			All processed together then metrics on BS only			All processed together then metrics on oxBS only		
	Type I	Type II	Combined	Type I	Type II	Combined	Type I	Type II	Combined
raw	5.333	9.333	9.333	8.333	10.667	8.667	5.333	12	9
dasen	7.667	7.667	4.667	6.667	6.667	5.333	4	4	2.667
betaqn	10.667	12.667	11.667	8.667	7	8	8.333	10.333	11
naten	7	5.667	8	6	4.667	7	7.333	3	7
nanet	7	3	6.333	6.667	4	5.333	9.333	5	10.333
nanes	8	8	9.333	8.333	5	6.333	9	5.667	6.667
danes	8	9	7	9	7.667	5.667	7.333	7	4
danet	4.333	6.333	6	6.667	6	8	8.333	10.667	6.333
danen	6	5	8.333	10	7.667	10.667	8.667	8.333	8.333
daten1	7.333	7.667	4.333	9.333	7.667	8	8.667	5.667	6.333
daten2	7	7.333	5	8.667	8.333	6.333	7.667	6.667	5
nasen	9.667	6.667	6.667	5	8	5.333	7.333	4.333	6
fuks	10	9.667	10	9	13	13	5.667	13.667	13.667
tost	7	7	8.333	2.667	8.667	7.333	8	8.667	8.667
best	*danet*	*nanet*	*daten1*	*tost*	*nanet*	*dasen/ nanet/ nasen*	*dasen*	*naten*	*dasen*

	Processed and metrics on BS only			Processed and metrics on oxBS only		
	Type I	Type II	Combined	Type I	Type II	Combined
raw	8	10.667	8.667	5.333	12	9
dasen	6	6.667	4	4	6	3.667
betaqn	9.333	9.333	9	10.333	6.667	10.667
naten	8.333	7.667	8	7.333	4.667	7.667
nanet	7.333	4.667	6	7	6	10
nanes	10.333	5.333	7	7.667	6	6
danes	4.667	4	6	7	4.667	5
danet	8.333	8	6.333	8	11	6.667
danen	8	7.667	9.333	7.667	9.333	8
daten1	7.667	7	7.667	9.667	6.667	6
daten2	6.667	5.667	6.333	7	5.333	4.667
nasen	7	7	5.333	9	4.333	5.333
fuks	9	13	13	5.667	13.333	13.667
tost	4.333	8.333	8.333	9.333	9	8.667
best	*tost*	*danes*	*dasen*	*dasen*	*nasen*	*dasen*

is Pearson's r, p-value and Benjamini-Hochberg false discovery rate (FDR)-corrected q-value.

SUPPLEMENTARY TABLE 9. Performance of *wateRmelon* normalization methods.
Comparison of raw data from raw bisulfite converted (BS) and oxidative BS (oxBS) converted DNA and 13 normalization and processing methods based on the *wateRmelon* R package. Ranking is based on the three performance metrics described in [31]. Type I and Type II refer to the probe types included on Illumina's HumanMethylation450 BeadChip.

	5-mC/UC probes (%)	Number of sites (%)	Top 1000 5-mC probes		
			Enrichment (95% CI)	*p*-value	Number of sites (%)
All probes	396600	1000	-	-	1000
CpG island feature					
Island	130971 (33.0)	171 (17.1)	0.52 (0.44 - 0.61)	**< 2.2E-16**	115 (11.5)
Shore	94237 (23.8)	295 (29.5)	1.24 (1.09 - 1.42)	**1.46E-03**	197 (19.7)
Shelf	35409 (8.9)	141 (14.1)	1.58 (1.31 - 1.89)	**1.41E-06**	146 (14.6)
NonCGI	135983 (34.3)	393 (39.3)	1.15 (1.02 - 1.29)	**2.28E-02**	542 (54.2)
Gene feature					
Intergenic	57664 (14.5)	158 (15.8)	1.09 (0.91 - 1.29)	3.31E-01	205 (20.5)
Distal promoter	18269 (4.6)	51 (5.1)	1.11 (0.82 - 1.47)	4.52E-01	54 (5.4)
Proximal promoter	158959 (40.1)	249 (24.9)	0.62 (0.54 - 0.71)	**2.85E-12**	165 (16.5)
Gene body	154140 (38.9)	518 (51.8)	1.33 (1.20 - 1.48)	**1.82E-07**	553 (55.3)
Downstream	7568 (1.9)	24 (2.4)	1.26 (0.80 - 1.88)	2.48E-01	23 (2.3)
Transcription factor binding site	33468 (48.8)	385 (38.5)	0.79 (0.70 - 0.89)	**6.70E-05**	300 (30.0)
DNase 1 hypersensitivity site	189731 (47.8)	449 (44.9)	0.94 (0.84 - 1.05)	2.73E-01	369 (36.9)
Alternative transcription events					
All probes	146785	394	-	-	339
A3SS	3450 (2.4)	8 (2.0)	0.96 (0.41 – 1.90)	1.00E+00	8 (2.4)
A5SS	3512 (2.4)	8 (2.0)	0.94 (0.40 – 1.86)	1.00E+00	8 (2.4)
AFE	60973 (41.5)	120 (30.5)	0.81 (0.66 – 0.99)	**3.53E-02**	85 (25.1)
ALE	9857 (6.7)	41 (10.4)	1.71 (1.22 – 2.36)	**1.84E-03**	43 (12.7)
CE	64532 (44.0)	194 (49.2)	1.24 (1.05 – 1.46)	**1.10E-02**	194 (57.2)
CNE	21520 (14.7)	61 (15.5)	1.17 (0.88 – 1.52)	2.51E-01	47 (13.9)
EI	176 (0.1)	0 (0.0)	0.00 (0.00 – 8.76)	1.00E+00	0 (0.0)
II	29413 (20.0)	68 (17.3)	0.95 (0.73 – 1.23)	7.54E-01	63 (18.6)
IR	16918 (11.5)	46 (11.7)	1.12 (0.81 – 1.51)	4.68E-01	39 (11.5)
MXE	14192 (9.7)	44 (11.2)	1.28 (0.92 – 1.74)	1.17E-01	50 (14.7)

supplementary table 10.

SUPPLEMENTARY TABLE 10. Structural and functional genomic annotation and enrichment analysis. Enrichment of the 1000 highest ranked 5-methylcytosine (5-mC), 5-hydroxymethylcytosine (5-hmC), and unmodified cytosine (UC) positions in specific structural and functional genomic features, calculated using Fisher's exact test. NG, non-CpG island; A3SS, alternative 3' splice site; A5SS, alternative 5' splice site; AFE, alternative first exon; ALE, alternative last exon; CE, cassette exon; CI, confidence interval; CNE, constitutive exon; EI, exon isoforms; II, intron isoforms; IR, intron retention; MXE, mutually exclusive exon.

supplementary table 10.

Top 1000 UC probes			Top 1000 5-hmC probes		
Enrichment (95% CI)	*p*-value	5-hmC probes (%)	Number of sites (%)	Enrichment (95% CI)	*p*-value
-	-	178591	1000	-	-
CpG island feature					
0.35 (0.28 - 0.42)	**< 2.2E-16**	33644 (18.8)	101 (10.1)	0.54 (0.43 – 0.66)	**1.15E-10**
0.83 (0.71 - 0.97)	**1.53E-02**	44575 (25.0)	270 (27.0)	1.08 (0.94 – 1.24)	2.60E-01
1.64 (1.36 - 1.95)	**1.97E-07**	22956 (12.9)	161 (16.1)	1.25 (1.05 – 1.48)	**9.47E-03**
1.58 (1.42 - 1.76)	**< 2.2E-16**	77416 (43.3)	468 (46.8)	1.08 (0.96 – 1.21)	1.72E-01
Gene feature					
1.41 (1.21 - 1.64)	**1.72E-05**	25409 (14.2)	157 (15.7)	1.10 (0.93 - 1.31)	2.46E-01
1.17 (0.87 - 1.54)	0.2589	9258 (5.2)	47 (4.7)	0.91 (0.66 - 1.22)	5.67E-01
0.41 (0.35 - 0.49)	**< 2.2E-16**	52396 (29.3)	233 (23.3)	0.79 (0.69 - 0.92)	**1.34E-03**
1.42 (1.28 - 1.58)	**6.86E-11**	87560 (49.0)	546 (54.6)	1.11 (1.00 - 1.24)	**4.46E-02**
1.21 (0.76 - 1.82)	0.3548	3968 (2.2)	17 (1.7)	0.77 (0.44 - 1.23)	3.30E-01
0.61 (0.54 - 0.70)	**1.847E-14**	68710 (38.5)	360 (36)	0.94 (0.83 - 1.06)	0.2881
0.77 (0.68 - 0.87)	**1.603E-05**	72283 (40.8)	425 (42.5)	1.05 (0.93 - 1.18)	0.4115
Alternative transcription events					
-	-	66205	380	-	-
0.88 (0.38 – 1.74)	0.8673	1649 (2.5)	6 (1.6)	0.66 (0.24 – 1.45)	3.99E-01
0.86 (0.37 – 1.71)	0.8677	1709 (2.6)	9 (2.4)	0.95 (0.43 – 1.83)	1.00E+00
0.53 (0.42 – 0.66)	**2.16E-09**	22945 (34.7)	122 (32.1)	0.96 (0.79 – 1.17)	7.69E-01
1.65 (1.18 – 2.25)	**0.002862**	5746 (8.7)	34 (8.9)	1.07 (0.74 – 1.52)	6.49E-01
1.14 (0.96 – 1.34)	0.1269	32843 (49.6)	214 (56.3)	1.18 (1.01 – 1.38)	**3.80E-02**
0.83 (0.60 – 1.11)	0.2358	8724 (13.2)	49 (12.9)	1.02 (0.74 – 1.36)	8.81E-01
0.00 (0.00 – 8.03)	1.00	98 (0.1)	1 (0.3)	1.85 (0.05 – 10.58)	4.20E-01
0.81 (0.61 – 1.05)	0.1147	12828 (19.4)	75 (19.7)	1.06 (0.82 – 1.35)	6.16E-01
0.87 (0.61 – 1.20)	0.4379	7624 (11.5)	32 (8.4)	0.76 (0.52 – 1.09)	1.47E-01
1.33 (0.98 – 1.78)	0.05523	7416 (11.2)	49 (12.9)	1.20 (0.88 – 1.61)	2.27E-01

Significant results are displayed in bold.

Rank	ID	Name	Type	Genes in term	Genes in test list and term	*p*-value	OR
1	GO:0001776	leukocyte homeostasis	biological process	56	9	2.04E-06	5.856837735
2	GO:0005089	Rho guanyl-nucleotide exchange factor activity	molecular function	66	12	1.05E-05	4.366362966
3	GO:0001782	B cell homeostasis	biological process	19	5	1.42E-05	10.10052838
4	GO:0048541	Peyer`s patch development	biological process	11	4	2.05E-05	15.14263875
5	GO:0002260	lymphocyte homeostasis	biological process	45	7	2.19E-05	5.846940236
6	GO:0005088	Ras guanyl-nucleotide exchange factor activity	molecular function	111	16	2.24E-05	3.327644456
7	GO:0016137	glycoside metabolic process	biological process	15	3	2.88E-05	15.45419598
8	GO:0048537	mucosal-associated lymphoid tissue development	biological process	12	4	3.13E-05	13.40151995
9	GO:0008093	cytoskeletal adaptor activity	molecular function	17	5	4.59E-05	8.891298139
10	GO:0051923	sulfation	biological process	15	3	8.15E-05	12.79767839
11	GO:0045669	positive regulation of osteoblast differentiation	biological process	62	9	0.000154719	3.909317115
12	GO:0016782	transferase activity, transferring sulfur-containing groups	molecular function	62	8	0.000161209	4.192740378
13	GO:0008146	sulfotransferase activity	molecular function	50	7	0.000162915	4.6709011
14	GO:0042975	peroxisome proliferator activated receptor binding	molecular function	10	3	0.000179133	13.56004287
15	GO:0030647	aminoglycoside antibiotic metabolic process	biological process	10	2	0.000187903	20.08216287
16	GO:0050727	regulation of inflammatory response	biological process	225	17	0.000196101	2.544112361
17	GO:0004033	aldo-keto reductase (NADP) activity	molecular function	18	3	0.000207595	10.25016515
18	GO:0060457	negative regulation of digestive system process	biological process	10	3	0.000212253	13.13860491
19	GO:0046683	response to organophosphorus	biological process	117	13	0.000232085	2.949037581
20	GO:0042730	fibrinolysis	biological process	19	3	0.000240734	9.847792817
21	GO:0050829	defense response to Gram-negative bacterium	biological process	21	3	0.000241259	9.646249054
22	GO:0051000	positive regulation of nitric-oxide synthase activity	biological process	16	4	0.000243565	8.317115164
23	GO:0031904	endosome lumen	cellular component	12	3	0.000264042	11.43265297
24	GO:0050729	positive regulation of inflammatory response	biological process	75	8	0.000274534	3.846610095
25	GO:0050671	positive regulation of lymphocyte proliferation	biological process	101	10	0.000306663	3.296160951

supplementary table 11.

SUPPLEMENTARY TABLE 11. Gene Ontology (GO) enrichment analysis results for the top 1000 differentially methylated positions (DMPs). Displayed for each GO term is the ID, name, type, the number of genes in the pathway and the top 1000 (test list), *p*-value, odds ratio (OR) and genes in both the test list and GO term. Terms are ranked based on *p*-value.

supplementary table 11.

Gene names in GO term and test list
SH2B2;IL6;SPNS2;PIK3CD;STAT5A;MEF2A;BCL2;JAM3;CHST3
ABR;MCF2L;FARP1;ARHGEF10L;KALRN;PLEKHG5;ALS2CL;TRIO;SGEF;TIAM2;NGEF;ECT2L
SH2B2;SPNS2;PIK3CD;MEF2A;BCL2
CACNB4;ID2;FOXL1;STAT5A
SH2B2;SPNS2;PIK3CD;STAT5A;MEF2A;BCL2;CHST3
ABR;MCF2L;FARP1;ARHGEF10L;KALRN;PLEKHG5;DENND1A;ALS2CL;RAB3IP;TRIO;RAPGEF4;SGEF;TIAM2;RGL1;NGEF;ECT2L
TH;AKR1C4;AKR1C3
CACNB4;ID2;FOXL1;STAT5A
BAIAP2;MTSS1;GAS2L1;ANK1;NCK2
CHST4;TPST1;UST
IL6;CD276;FAM20C;DDR2;LTF;MSX2;MEF2A;CYR61;BMPR1B
WSCD1;CHST4;GAL3ST4;TPST1;UST;CHST2;TRMU;CHST3
WSCD1;CHST4;GAL3ST4;TPST1;UST;CHST2;CHST3
EP300;NFATC4;ASXL2
AKR1C4;AKR1C3
ABR;IL6;SBNO2;CD276;NLRP12;CD47;IER3;STAT5A;PDE2A;CNR1;CD28;CD59;BRD4;F12;TLR4;PTGIS;TBC1D23
ALDH3A1;AKR1C4;AKR1C3
ABCG5;ABCG8;OXT
KCNQ1;TRPV1;STAT1;SREBF1;ALDH3A1;EPB49;P2RX4;BSG;PDE2A;SLC6A4;BRAF;OXT;SLC5A5
ANXA2;F12;PLAUR
IL6;AZU1;TLR4
FCER2;NPR3;ESR1;SCARB1
CTSB;PRF1;CTSK
IL6;NLRP12;CD47;STAT5A;PDE2A;CNR1;CD28;TLR4
IL6;CD276;STAT5A;NCK2;ICOSLG;MEF2A;BCL2;CD28;CD59;TLR4

Rank	ID	Name	Type	Genes in term	Genes in test list and term	*p*-value	OR
1	GO:0004714	transmembrane receptor protein tyrosine kinase activity	molecular function	67	14	2.59E-07	5.122981614
2	GO:0019199	transmembrane receptor protein kinase activity	molecular function	84	15	1.94E-06	4.18507835
3	GO:0018108	peptidyl-tyrosine phosphorylation	biological process	118	18	3.32E-06	3.513449487
4	GO:0018212	peptidyl-tyrosine modification	biological process	120	18	4.83E-06	3.432993693
5	GO:0005925	focal adhesion	cellular component	123	18	1.99E-05	3.180778045
6	GO:0030055	cell-substrate junction	cellular component	134	19	2.37E-05	3.049805048
7	GO:0070848	response to growth factor	biological process	542	51	2.57E-05	1.965162042
8	GO:0071363	cellular response to growth factor stimulus	biological process	527	50	3.00E-05	1.968324786
9	GO:0005924	cell-substrate adherens junction	cellular component	128	18	3.83E-05	3.035139208
10	GO:0016310	phosphorylation	biological process	753	61	3.93E-05	1.805512553
11	GO:0007173	epidermal growth factor receptor signaling pathway	biological process	190	22	4.02E-05	2.641330765
12	GO:0038127	ERBB signaling pathway	biological process	191	22	4.64E-05	2.619521312
13	GO:0005154	epidermal growth factor receptor binding	molecular function	21	5	7.29E-05	7.935357156
14	GO:0031122	cytoplasmic microtubule organization	biological process	20	5	0.000106065	7.570852389
15	GO:0007167	enzyme linked receptor protein signaling pathway	biological process	733	64	0.000107325	1.748759123
16	GO:0002381	immunoglobulin production involved in immunoglobulin mediated immune response	biological process	21	4	0.00012466	8.499630695
17	GO:0008093	cytoskeletal adaptor activity	molecular function	17	5	0.000144563	7.896468269
18	GO:0006468	protein phosphorylation	biological process	505	45	0.000156254	1.881144509
19	GO:0007169	transmembrane receptor protein tyrosine kinase signaling pathway	biological process	548	50	0.000181425	1.830552043
20	GO:2001222	regulation of neuron migration	biological process	13	4	0.00018842	9.508650146
21	GO:0007264	small GTPase mediated signal transduction	biological process	393	37	0.000225578	1.969856232
22	GO:0002204	somatic recombination of immunoglobulin genes involved in immune response	biological process	16	3	0.000292117	10.01031101
23	GO:0002208	somatic diversification of immunoglobulins involved in immune response	biological process	16	3	0.000292117	10.01031101
24	GO:0045190	isotype switching	biological process	16	3	0.000292117	10.01031101
25	GO:0060396	growth hormone receptor signaling pathway	biological process	24	5	0.000367005	6.040651405

supplementary table 12.

SUPPLEMENTARY TABLE 12. Gene Ontology (GO) enrichment analysis results for the top 1000 differentially hydroxymethylated positions (DHPs). Displayed for each GO term is the

supplementary table 12.

Gene names in GO term and test list
CRIM1;EPHA8;ROR1;INSR;DDR2;IGF2R;NRP2;ERBB4;EPHB3;TIE1;RYK;ERBB3;MET;PDGFRL
CRIM1;EPHA8;ROR1;INSR;DDR2;IGF2R;NRP2;ERBB4;EPHB3;BMPR1A;TIE1;RYK;ERBB3;MET;PDGFRL
CRIM1;SHC1;EPHA8;MAPK3;ROR1;INSR;DDR2;CSK;IGF2R;PXN;NRP2;ERBB4;EPHB3;RELN;TIE1;RYK;MET;PDGFRL
CRIM1;SHC1;EPHA8;MAPK3;ROR1;INSR;DDR2;CSK;IGF2R;PXN;NRP2;ERBB4;EPHB3;RELN;TIE1;RYK;MET;PDGFRL
MAPK1;LPP;MAPK3;LIMD1;GAK;DLC1;ITGB5;IRF2;PDLIM2;ARHGAP26;PXN;SORBS3;FLNB;PARVA;ARHGEF7;TRPV4;NOX4;ADAM17
MAPK1;LPP;DST;MAPK3;LIMD1;GAK;DLC1;ITGB5;IRF2;PDLIM2;ARHGAP26;PXN;SORBS3;FLNB;PARVA;ARHGEF7;TRPV4;NOX4;ADAM17
MAPK1;ABR;MCF2L;PMEPA1;SHC1;WNT10A;MYC;NCOR2;EIF2C2;MAPK3;PRKAR1B;VAV2;PARD3;NOTCH1;TFDP1;PRKCE;INSR;PRKCA;TRIO;SKI;AKAP13;KALRN;TRIM71;GDF15;FGF1;PDE3A;ERBB4;PIK3CD;TNRC6B;BMPR1A;TH;KLB;PLK5P;ARHGEF7;AP2A2;NDST1;RAPGEF2;LTBP2;NOX4;ITPR1;PCSK6;ADAM17;STAT3;MAP3K1;RELA;ERBB3;NET1;TGIF1;CDC34;PDGFRL;IBSP
MAPK1;ABR;MCF2L;PMEPA1;SHC1;WNT10A;MYC;NCOR2;EIF2C2;MAPK3;PRKAR1B;VAV2;PARD3;NOTCH1;TFDP1;PRKCE;INSR;PRKCA;TRIO;SKI;AKAP13;KALRN;TRIM71;GDF15;FGF1;PDE3A;ERBB4;PIK3CD;TNRC6B;BMPR1A;TH;KLB;PLK5P;ARHGEF7;AP2A2;NDST1;RAPGEF2;LTBP2;NOX4;ITPR1;PCSK6;ADAM17;STAT3;MAP3K1;RELA;ERBB3;NET1;TGIF1;PDGFRL;IBSP
MAPK1;LPP;MAPK3;LIMD1;GAK;DLC1;ITGB5;IRF2;PDLIM2;ARHGAP26;PXN;SORBS3;FLNB;PARVA;ARHGEF7;TRPV4;NOX4;ADAM17
MAPK1;CRIM1;CTBP1;SHC1;MYC;EPHA8;MAPK3;PRKAR1B;LIMD1;DAPK2;ROR1;PFKFB3;PRKCE;INSR;MKNK2;DDR2;PRKCA;CSK;IGF2R;MAP4K4;NDUFS6;MINK1;SPTBN1;GRK7;AKAP13;ADAM10;TSSK3;TOLLIP;KALRN;PXN;SIK3;NRP2;ERBB4;DLG2;PTPLAD1;PIK3CD;TNF;EPHB3;BMPR1A;SPHK2;ZAK;FASTK;RBM4;NDST1;MAST2;CDC42EP5;RAPGEF2;RELN;CDS1;TIE1;ULK2;NEK7;STAT3;CDC25B;MAP3K1;RYK;CCNE1;NDUFS8;MET;NDUFAF1;PDGFRL
MAPK1;SHC1;EIF2C2;MAPK3;PRKAR1B;PRKCE;PRKCA;CSK;NCK2;ADAM10;PXN;FGF1;ERBB4;PIK3CD;TNRC6B;KLB;ARHGEF7;AP2A2;ADAM12;ITPR1;ADAM17;ERBB3
MAPK1;SHC1;EIF2C2;MAPK3;PRKAR1B;PRKCE;PRKCA;CSK;NCK2;ADAM10;PXN;FGF1;ERBB4;PIK3CD;TNRC6B;KLB;ARHGEF7;AP2A2;ADAM12;ITPR1;ADAM17;ERBB3
SHC1;VAV2;ERBB4;PLSCR1;ATXN2
DST;DVL1;CHP;TRPV4;TACC2
MAPK1;ABR;MTSS1;CRIM1;MCF2L;PMEPA1;RPTOR;SHC1;MYC;NCOR2;EIF2C2;EPHA8;MAPK3;PRKAR1B;PTPRE;VAV2;PARD3;ROR1;TFDP1;PRKCE;INSR;DDR2;PLAT;PRKCA;CSK;IGF2R;TRIO;SKI;SPTBN1;AKAP13;NCK2;ADAM10;KALRN;TRIM71;PXN;GDF15;FGF1;NRP2;ERBB4;GNG7;PIK3CD;EPHB3;TNRC6B;BMPR1A;KLB;ARHGEF7;AP2A2;ADAM12;NDST1;RAPGEF2;EIF4G1;ZFP106;LTBP2;ITPR1;PCSK6;ADAM17;STAT3;MAP3K1;RELA;ERBB3;NET1;TGIF1;RHOQ;PDGFRL
SWAP70;TNFSF13;AICDA;XRCC4
MTSS1;NCK2;BICD1;ARHGAP26;SORBS2
MAPK1;CRIM1;CTBP1;SHC1;EPHA8;MAPK3;PRKAR1B;DAPK2;ROR1;PRKCE;INSR;MKNK2;DDR2;PRKCA;CSK;IGF2R;MAP4K4;MINK1;SPTBN1;GRK7;AKAP13;ADAM10;TSSK3;KALRN;PXN;SIK3;NRP2;ERBB4;PIK3CD;EPHB3;BMPR1A;ZAK;FASTK;MAST2;RELN;CDS1;TIE1;ULK2;NEK7;CDC25B;MAP3K1;RYK;CCNE1;MET;PDGFRL
MAPK1;ABR;MTSS1;CRIM1;MCF2L;RPTOR;SHC1;EIF2C2;EPHA8;MAPK3;PRKAR1B;VAV2;ROR1;PRKCE;INSR;DDR2;PLAT;PRKCA;CSK;IGF2R;TRIO;AKAP13;NCK2;ADAM10;KALRN;TRIM71;PXN;FGF1;NRP2;ERBB4;PIK3CD;EPHB3;TNRC6B;KLB;ARHGEF7;AP2A2;ADAM12;NDST1;RAPGEF2;EIF4G1;ZFP106;ITPR1;PCSK6;ADAM17;STAT3;RELA;ERBB3;NET1;RHOQ;PDGFRL
PLXNB2;RAPGEF2;RELN;STAT3
MAPK1;ARHGAP15;ABR;AGAP1;VANGL2;MCF2L;SHC1;DOCK7;MAPK3;VAV2;IQGAP2;DLC1;RASGEF1C;TRIO;AKAP13;CHP;GNA12;RASL11B;ARHGAP26;KALRN;ARHGAP23;PTPLAD1;RASGRP2;RGL1;ARL4C;ARHGEF7;DNAJC27;RAB40B;CDC42EP1;CDC42EP5;RAPGEF2;C1orf89;RAB7L1;ARF1;RHOV;NET1;RHOQ
SWAP70;AICDA;XRCC4
SWAP70;AICDA;XRCC4
SWAP70;AICDA;XRCC4
MAPK1;MAPK3;PXN;ADAM17;STAT3

ID, name, type, the number of genes in the pathway and the top 1000 (test list), *p*-value, odds ratio (OR) and genes in both the test list and GO term. Terms are ranked based on *p*-value.

Rank	ID	Name	Type	Genes in term	Genes in test list and term	*p*-value	OR
1	GO:0042730	fibrinolysis	biological process	19	4	1.98E-06	14.24957707
2	GO:0005938	cell cortex	cellular component	204	21	1.47E-05	2.801758255
3	GO:0051963	regulation of synapse assembly	biological process	35	7	3.22E-05	5.955198998
4	GO:0007259	JAK-STAT cascade	biological process	52	7	4.30E-05	5.331965552
5	GO:0051015	actin filament binding	molecular function	81	11	5.69E-05	3.776980208
6	GO:0061351	neural precursor cell proliferation	biological process	61	9	6.43E-05	4.289995618
7	GO:0032421	stereocilium bundle	cellular component	32	6	6.70E-05	6.125801749
8	GO:0008092	cytoskeletal protein binding	molecular function	696	50	0.000112678	1.820492951
9	GO:0051962	positive regulation of nervous system development	biological process	21	5	0.000114217	7.335784516
10	GO:0051965	positive regulation of synapse assembly	biological process	21	5	0.000114217	7.335784516
11	GO:0032420	stereocilium	cellular component	23	5	0.00011531	6.999602648
12	GO:0001776	leukocyte homeostasis	biological process	56	7	0.000119626	4.747572229
13	GO:0017048	Rho GTPase binding	molecular function	54	8	0.000137865	4.328550938
14	GO:0044087	regulation of cellular component biogenesis	biological process	393	31	0.000145058	2.081034444
15	GO:0003014	renal system process	biological process	73	9	0.000152347	3.874264306
16	GO:0071715	icosanoid transport	biological process	16	3	0.000194661	10.38716022
17	GO:1901571	fatty acid derivative transport	biological process	16	3	0.000194661	10.38716022
18	GO:0015631	tubulin binding	molecular function	212	19	0.000200735	2.468580873
19	GO:0006928	cellular component movement	biological process	1199	76	0.000224954	1.601565508
20	GO:2000725	regulation of cardiac muscle cell differentiation	biological process	17	4	0.00025007	7.974004154
21	GO:0008236	serine-type peptidase activity	molecular function	159	11	0.000288542	3.031572068
22	GO:0050795	regulation of behavior	biological process	161	14	0.000300286	2.751896245
23	GO:0030866	cortical actin cytoskeleton organization	biological process	19	4	0.000333383	7.598867402
24	GO:0015629	actin cytoskeleton	cellular component	380	30	0.000346647	2.01591256
25	GO:0044089	positive regulation of cellular component biogenesis	biological process	24	5	0.000384951	6.029902321

supplementary table 13.

SUPPLEMENTARY TABLE 13. Gene Ontology (GO) enrichment analysis results for the top 1000 differentially unmodified positions (DUPs). Displayed for each GO term is the ID, name, type, the number of genes in the pathway and the top 1000 (test list), *p*-value, odds ratio (OR) and genes in both the test list and GO term. Terms are ranked based on *p*-value.

supplementary table 13.

Gene names in GO term and test list
ANXA2;TMPRSS6;PLAT;KLK3
EPS8;EXOC4;CLIC5;PRKCZ;HMCN1;EPB41L2;ANXA2;ANK1;PKD1;MLPH;MYO7A;CAPZA2;NEDD9;DLG4;FMNL1;MYO10;FGF1;STIM1;AKAP12;CORO1A;SEPT14
CHRNB2;PVRL1;NRXN2;NRXN3;ACCN1;EPHB1;OXT
PKD1;F2R;STAT3;LYN;CLCF1;PIAS1;PAR1
MYO1C;CYFIP1;MYO7A;MACF1;ADD2;FMNL1;MYO10;CORO2B;CORO1A;HTT;MAP1S
WNT3A;PCNT;FZD6;NCOR2;DAGLB;FGFR1;HMGA2;EPHB1;SIP1
EPS8;MYO1C;CLIC5;CDH23;MYO7A;TMC2
BAIAP2;EPS8;KIF26B;GAS2L1;MYO1C;SGIP1;CYFIP1;EPB41L2;TBCD;ANXA2;ENAH;CCDC64;ANK1;WIPF3;ARL8B;MLPH;MYO7A;CAPZA2;CAPN2;MACF1;KIF17;TNNI3K;CCDC88A;STMN1;SDC3;TPM1;SHROOM3;PALLD;KIAA1543;CACNA1C;ADD2;PEX14;FMNL1;KIF1B;VCL;MYO10;FRMD5;CORO2B;STIM1;CORO1A;MYLIP;KIF21B;HTT;FXYD5;TNS1;MAP1S;KLHL3;VPS41;CAV3;CAPN3
NRXN2;NRXN3;ACCN1;EPHB1;OXT
NRXN2;NRXN3;ACCN1;EPHB1;OXT
EPS8;MYO1C;CLIC5;CDH23;MYO7A
SPNS2;RIPK3;CORO1A;LYN;NKX2-3;JAM3;SKIL
EPS8;CYFIP1;CDC42EP4;CIT;AKAP13;FMNL1;CDC42BPB;DOCK9
FAM38A;EPS8;MYO1C;DNM1L;PRKCZ;TBCD;CHRNB2;ARHGEF10L;CDC42EP4;CAPZA2;MACF1;SMAD3;STMN1;RAF1;PVRL1;TPM1;NRXN2;NRXN3;ACCN1;ADD2;PEX14;MYO10;RHOQ;CORO1A;EPHB1;OXT;TACR1;NOX4;HYAL1;CAV3;CNOT6
MYO1C;CHRNB2;PTGER3;CACNA1C;F2R;OXT;TACR1;KLHL3;PAR1
ABCC2;SLCO2B1;PLA2G5
ABCC2;SLCO2B1;PLA2G5
KIF26B;GAS2L1;SGIP1;TBCD;ARL8B;MLPH;MACF1;KIF17;CCDC88A;STMN1;KIAA1543;PEX14;KIF1B;STIM1;KIF21B;HTT;MAP1S;VPS41;CAV3
TNFSF12;EPS8;KIF26B;UNC5A;FOXP1;MYO1C;SLC7A5;WNT3A;SNX29;PCNT;PRKCZ;SPG7;SPNS2;ENAH;ANK1;NR4A2;ANKS1A;LIMD1;EFNB2;MATN2;SEMA6A;MYO7A;CAPZA2;VCAN;PDE4D;MACF1;SLC7A11;KIF17;SKI;FGFR1;TNS3;CCDC88A;KCNQ3;PLAT;RAF1;PVRL1;TPM1;KRAS;SCN3B;BOC;DLG4;NRXN3;B3GNT6;SEMA3C;CACNA1C;PEX14;MDGA1;FMNL1;KIF1B;PIK3CA;VCL;MYO10;FAT1;CDC42BPB;CORO1A;MYLIP;AP2A2;STAT3;EPHB1;NFASC;PLXNC1;KIF21B;HTT;LYN;SLC16A3;SIP1;FN1;NKX2-3;ST8SIA2;JAM3;TNS1;MAP1S;MET;CNTNAP1;KIAA0319;BH
FOXP1;WNT3A;EFNB2;CAV3
DPP10;TMPRSS6;IMMP2L;PLAT;RHBDF2;PRSS22;MBTPS1;KLK10;CTSA;TMPRSS11E;KLK3
STRA6;WNT3A;SGIP1;CAMK1D;CHRNB2;EFNB2;PKD1;PRKD2;SMAD3;DSCAM;DLG4;LYN;JAM3;MET
EPB41L2;DLG4;FMNL1;RHOQ
BAIAP2;GAS2L1;MYO1C;CLIC5;HDAC4;SH3PXD2A;EPB41L2;DDX58;ENAH;CDC42EP4;MLPH;MYO7A;CAPZA2;MYOM2;MACF1;TPM1;PALLD;DLG4;CIT;MRPL38;ADD2;VCL;MYO10;CORO2B;RHOQ;CDC42BPB;CORO1A;DENND2A;SLC16A3;HIST4H4
NRXN2;NRXN3;ACCN1;EPHB1;OXT

supplementary table 14.

		Entorhinal cortex			Cerebellum		
Demographics		UC	5-mC	5-hmC	UC	5-mC	5-hmC
N		91	85	85	95	94	94
Gender (%) M / F (%)		(56.0) 51 / 40 (44.0)	(56.5) 48 / 37 (43.5)	(56.5) 48 / 37 (43.5)	(56.8) 54 / 41 (43.2)	(57.4) 54 / 40 (42.6)	(57.4) 54 / 40 (42.6)
Age (mean ± SD)		81.2 ± 9.5	81.3 ± 9.5	81.2 ± 9.5	81.2 ± 9.3	81.2 ± 9.3	81.2 ± 9.3
Diagnosis (%) AD / control (%)		(70.3) 64 / 27 (29.7)	(70.6) 60 / 25 (29.4)	(70.6) 60 / 25 (29.4)	(70.5) 67 / 28 (29.5)	(70.2) 66 / 28 (29.8)	(70.2) 66 / 28 (29.8)
Braak stage	0	8	7	7	8	8	8
	I	3	3	3	3	3	3
	II	11	10	10	12	12	12
	III	6	6	6	6	6	6
	IV	8	7	7	10	10	10
	V	18	17	17	19	18	18
	VI	37	35	35	37	37	37
Postmortem interval (mean ± SD)		2539.5 (1288.1)	2490.7 (1288.5)	2490.7 (1288.5)	2576.5 (1315.2)	2581.6 (1321.3)	2581.6 (1321.3)

SUPPLEMENTARY TABLE 14. Validation cohort demographics.
Entorhinal cortex and cerebellum samples from the MRC London Neurodegenerative Disease Brain Bank (London, UK). Displayed is the number of samples for each brain region and unmodified cytosine (UC), 5-methylcytosine (5-mC), and 5-hydroxymethylcytosine (5-hmC) dataset, and the distributions of gender, age, Alzheimer's disease (AD) diagnosis, Braak stage, and postmortem interval (minutes). SD, standard deviation.

supplementary table 15.

			UC		5-mC		5-hmC	
			ECest	CERest	ECest	CERest	ECest	CERest
ANK1	**UC**	Pearson correlation	0.490**	0.123				
		p-value	2.682E-07	0.227				
		# probes	99	99				
C10orf116	**5-mC**	Pearson correlation			0.259	-0.172		
		p-value			0.393	0.574		
		# probes			13	13		
C3	**UC**	Pearson correlation	-0.379	0.209				
		p-value	0.068	0.328				
		# probes	24	24				
CDX1	**UC**	Pearson correlation	-0.269	-0.330				
		p-value	0.331	0.229				
		# probes	15	15				
FAM198B	**5-mC**	Pearson correlation			-0.653*	0.293		
		p-value			0.029	0.381		
		# probes			11	11		
LOC100190940	**UC**	Pearson correlation	-0.226	0.432				
		p-value	0.667	0.393				
		# probes	6	6				
OXT	**5-mC & 5-hmC**	Pearson correlation			-0.259	-0.346	-0.159	-0.169
		p-value			0.470	0.327	0.707	0.689
		# probes			10	10	8	8
RAP1GAP2	**5-mC**	Pearson correlation			-0.278*	0.169		
		p-value			0.044	0.226		
		# probes			53	53		
RHBDF2	**UC & 5-mC**	Pearson correlation	0.759**	-0.215	0.662**	-0.062		
		p-value	1.778E-06	0.262	9.119E-05	0.748		
		# probes	29	29	29	29		
SLC12A4	**5-hmC**	Pearson correlation					0.384*	-0.054
		p-value					0.048	0.788
		# probes					27	27
TNK2	**UC**	Pearson correlation	0.249	0.141				
		p-value	0.067	0.306				
		# probes	55	55				

SUPPLEMENTARY TABLE 15. Cross-regional validation results. Pearson correlations for middle temporal gyrus (MTG) regression coefficients of probes in the 11 genes with a differentially methylated region (DMR), differentially hydroxymethylated region (DHR) and/or differentially unmodified region (DUR) genes and the regression coefficients of the same probes from the entorhinal cortex (ECest) and cerebellum (CERest). Displayed for each gene is the data (5-methylcytosine [5-mC], 5-hydroxymethylcytosine [5-hmC] or unmodified cytosine [UC]) in which a differentially modified region was found in the current study (indicated in bold), the corresponding Pearson correlation with the EC and CER data, the *p*-value and number of probes in the comparison. * $p < 0.05$; ** $p < 0.001$.

DETECTION OF BLOOD METHYLOMIC MARKERS ASSOCIATED WITH CLINICAL FEATURES OF ALZHEIMER'S DISEASE; AN EXPLORATORY APPROACH

ROY **LARDENOIJE**[A], EHSAN **PISHVA**[A,B], HEIDI **JACOBS**[A], INEZ **RAMAKERS**[A], PIETER J. **VISSER**[A], HARRY W. M. **STEINBUSCH**[A], DANIËL L.A. **VAN DEN HOVE**[A,C], BART P.F. **RUTTEN**[A]

[A]SCHOOL FOR MENTAL HEALTH AND NEUROSCIENCE (MHENS), DEPARTMENT OF PSYCHIATRY AND NEUROPSYCHOLOGY, MAASTRICHT UNIVERSITY, UNIVERSITEITSSINGEL 50, 6200 MD MAASTRICHT, THE NETHERLANDS
[B]UNIVERSITY OF EXETER MEDICAL SCHOOL, UNIVERSITY OF EXETER, EXETER, UK.
[C]LABORATORY OF TRANSLATIONAL NEUROSCIENCE, DEPARTMENT OF PSYCHIATRY, PSYCHOSOMATICS AND PSYCHOTHERAPY, UNIVERSITY OF WUERZBURG, FUECHSLEINSTRASSE 15, 97080 WUERZBURG, GERMANY

Abstract

Alzheimer's disease (AD), the foremost cause of dementia in the elderly, is associated with an epigenetic disarray. Most previous studies have focused on the brain, which is the primary site of pathology, but has strictly limited accessibility for diagnostic purposes. The present exploratory study therefore assessed the blood methylome associated with the diagnosis of AD, as well as with AD-related phenotypes, i.e. the mini-mental state examination (MMSE) score, cerebrospinal fluid levels of amyloid-β and phosphorylated tau, and hippocampal volume. The findings corroborate an epigenetic component in AD and find the previously reported altered DNA methylation in the AD brain of *HLA-DRB5* to be reflected in the blood. Additional promising candidate genes that may be investigated as epigenetic blood biomarkers of AD dementia are put forward, including *PCDHA1*, *CDH13*, *CLSTN2*, *NEFL*, and *MAD1L1*.

KEYWORDS

Alzheimer's disease; epigenetics; DNA methylation; cognition; hippocampal volume; cerebrospinal fluid

8.1. Introduction

Alzheimer's disease (AD) is the primary cause of dementia and it is associated with the progressive development of protein aggregates in the brain; the extracellular amyloid plaques and the intracellular neurofibrillary tangles [1, 2]. The main constituents of these protein aggregates are amyloid-β (Aβ) and tau, respectively. Aβ and tau aggregates have been the center of focus of AD research for years, especially Aβ 1-42 (Aβ42) and phosphorylated tau (ptau), generally thought to be the most toxic forms [2]. However, it remains unclear exactly how these proteins drive the progressive neurodegeneration and subsequent cognitive decline seen in AD [3]. Recent years have seen a great expansion of research on biological processes that are affected in AD, including the immune system [4], fat and glucose homeostasis [5, 6], and protein quality control [7]. At the center, connecting all these systems, acting as a molecular mediator or inciter, resides the epigenetic apparatus [8, 9].

Indeed, recent studies have uncovered widespread epigenetic alterations in association with AD, including DNA and chromatin modifications as well as non-coding RNAs [8]. Especially DNA and chromatin modifications have strong intrinsic relationships with each other [10], while the stability of DNA modifications has made them a prime target for a first wave epigenetic inquiries in postmortem tissue [11]. Understandably, most of these studies focus on the brain as the primary site of analysis. However, this limits their use for the identification of biomarkers assessible in living patients. Although the epigenome has a high variability between tissues [12], exploring the AD methylomic profile of more assessible tissues, like blood, may be more fruitful for diagnostic and prognostic purposes. Being a stable marker and with many tools available for its investigation, the methylome represents a logical first target [11].

A definite diagnosis of AD depends on the postmortem identification of plaques and tangles in the brain [13]. Several diagnostic markers can be assessed in living patients and allow for the diagnosis dementia of the Alzheimer type with a certain level of certainty. Among these are levels of ptau and Aβ42 in cerebrospinal fluid (CSF) [14], hippocampal atrophy [15], and measures of cognitive performance, such as the mini-mental state examination (MMSE) [16, 17]. These markers have furthermore been shown to predict development of cognitive impairments and conversion to dementia [18].

In order to explore the feasibility of performing genome-wide analyses of DNA methylation profiles using blood samples in relation to AD and AD-related phenotypes, the present study examined the blood methylomic profile associated with the clinical diagnosis of AD, and explored within

this profile, which genes present with altered DNA methylation levels in relation to AD-related cognitive, CSF, and imaging phenotypes.

8.2. Methods

8.2.1. Subjects

Blood was collected from 6 AD patients, 11 subjects with mild cognitive impairment (MCI), and 8 healthy controls from the EDAR cohort (Early Diagnosis of AD and as marker for treatment Response, http://www.edarstudy.eu/). These subjects were selected based on the availability of blood and CSF samples and availability of magnetic resonance imaging (MRI) data, and on an equal distribution of gender. MMSE scores were also obtained for all subjects [16], CSF from most cases, but not all controls (3), and MRI scans (3 Tesla, Philips, Amsterdam, the Netherlands) only from MCI and AD subjects (Table 1). All procedures were approved by the Medical Ethics Committee of Maastricht University Medical Centre, in accordance with the declaration of Helsinki.

8.2.2. CSF tau and amyloid beta

CSF was obtained through a lumbar puncture and collected in 10 mL polypropylene tubes. Tubes were centrifuged at 2000 g at 4°C, and stored within one hour after collection at -80°C. Ptau and Aβ42 levels were determined in the CSF samples using the INNO-BIA AlzBio3 Luminex assay (Fujirebio, Gent, Belgium). The ptau:Aβ42 ratio was calculated and used for subsequent analyses, as this was previously found to be a good predictor of dementia [19].

8.2.3. Hippocampal volume

Left and right hippocampal volumes, as well as the total intracranial volume, were determined from T1-weighted MRI scans using FreeSurfer 5.3 software [20]. Analyses were performed on the mean of the left and right hippocampal volumes, expressed as percentage of the total intracranial volume.

table 1.

	N	Gender (female / male)	Age (mean ± SD)	MMSE (mean ± SD)	CSF (mean ± SD)	HV (mean ± SD)
Control	8	4 / 4	67.63 ± 5.78	28.75 ± 1.49	0.058 ± 0.017	NA
MCI	11	4 / 7	62.64 ± 10.06	28.45 ± 1.51	0.107 ± 0.087	0.239 ± 0.039
AD	6	3 / 3	68.83 ± 14.34	23.33 ± 5.09	0.161 ± 0.111	0.199 ± 0.026
Total	25	11 / 14	65.72 ± 10.14	27.32 ± 3.50	0.116 ± 0.092	0.226 ± 0.039

TABLE 1. Sample overview. AD, Alzheimer's disease; CSF, ratio of phosphorylated tau and amyloid-β levels in the cerebrospinal fluid; HV, mean hippocampal volume as percentage of the total intracranial volume; MCI, mild cognitive impairment; MMSE, mini-mental state examination scores.

8.2.4. Methylomic profiling

Whole blood was used for genomic DNA extraction with the AutoGen Flex Star DNA isolation system (Autogen, Holliston, MA, USA), following the manufacturer's protocol. 500 ng genomic DNA was bisulfite (BS) treated with the EZ-96 DNA Methylation-Gold™ Kit (Zymo Research, Irvine, CA, USA). To limit possible bias due to variable conversion efficiency, the BS conversion reaction was performed twice for each sample, after which the duplicates were pooled. Genome-wide DNA methylation levels were determined with Illumina's HumanMethylation450 BeadChip (Illumina, San Diego, CA, USA). The BS-treated DNA was amplified, fragmented, and hybridized according to the instructions of the manufacturer. The Illumina iScan was used for reading the chip.

8.2.5. Processing of array data

All data processing and analysis was done with the statistical programming environment R (version 3.3.2) [21] and RStudio (version 1.0.136) [22], running on a 64-bit Windows 10 pro (Microsoft, Redmond, WA, USA) machine. Raw IDAT data from the scanner was inspected for outlying samples with the *MethylAid* package (version 1.8.0) [23], using the default settings, and loaded into the R environment for further analysis with the *minfi* package (version 1.20.2) [24]. Background and dye bias correction was performed according to the *noob* method [25], followed by functional normalization [26], as implemented in the *DNAmArray* package (version 0.0.1) [27]. Probes with a mean of exactly 0, or with intensity measurements from less than 3 beads, were removed. Additionally, probes with a detection *p*-value above 0.01 (as compared to background control probes) were removed, as well as probes with a success rate below 95%. After filtering, samples with more than 5% of their probes removed were excluded.
As a simple check for sample mix-ups, the gender of the samples was determined based on X chromosome methylation (using the *DNAmArray* package), and compared with the assumed gender. Cross-hybridizing probes and probes binding polymorphic sites, as identified by Chen et al. [28], were also removed, as well as probes on the X and Y chromosomes.

8.2.6. Data analysis

M-values were used for all analyses [29]. Data was analyzed following a two-step approach; first, probes associated with AD status were selected, followed by three separate analyses looking at the association between the AD-related probes and clinical features of AD, as captured by MMSE scores, CSF ptau:Aβ42 and hippocampal volume. Associations were tested using linear models, as implemented in the *limma* package (version 3.30.11) [30], using AD diagnosis, MMSE scores, CSF ptau:Aβ42 or hippocampal volume as predictors, and normalized M-values as outcome. Potential confounding sources of variation were investigated using the *sva* package [31] and were captured in surrogate variables to be included in the *limma* model. After fitting the model, empirical Bayes moderated test statistics were determined [32]. Bias and inflation corrected *p*-values were then calculated using the empirical null distribution, as implemented in the *bacon* package (version 1.2.0) [33]. All probes passing the probe filtering steps were included in the AD diagnosis-based analysis, and the probes from that analysis with a bias and inflation corrected *p*-values < 0.05 were used as input for the analyses based on MMSE scores, CSF ptau:Aβ42 and hippocampal volume. Differentially methylated positions (DMPs) were identified as probes with a Benjamini-Hochberg false discovery rate (FDR) corrected *p*-value < 0.05. Probes were annotated to genes based on proximity, using the UCSC human genome build 19, with the *DNAmArray* package. In addition to DMPs, differentially methylated regions (DMRs) were determined with *comb-p* [34], using a seeding *p*-value of 0.05 and an extension distance of 200 base pairs. The software corrects for multiple testing according to the Šidák procedure. *Comb-p* analyses were done in a 64-bit virtual Kali Linux 2016.2 distribution (Offensive Security Ltd.), running in VirtualBox 5.1.18 (Oracle Corporation, Redwood City, CA, USA). DMRs were identified as regions with a corrected *p*-value below 0.05 and containing at least two probes. The presence of the AD-associated DMPs and DMRs was also investigated in the MCI cases, using the same approach, but using MCI status as predictor instead of AD.

For a subsequent Gene Ontology (GO) and Kyoto Encyclopedia of Genes and Genomes (KEGG) gene set analysis, probes were ordered based on a combined *p*-value and effect size ranking (i.e. from lowest *p*-value and highest effect size to highest *p*-value and lowest effect size). Unique gene names annotated to the top 1000 probes were used as test list and the unique gene names annotated to the complete set of probes included in the *limma* analysis were used as background list. The *missMethyl* R package (version 1.8.0) was used for the GO term (using the ‘gometh’ function) and KEGG pathway (using the ‘gsameth’ function) enrichment analysis, as it takes into account there are varying numbers of probes

per gene on the array, which may lead to bias [35, 36]. Only GO terms containing between 10 and 2000 genes, and KEGG pathways with more than 10 genes (the maximum number of genes in a KEGG pathway is 1272) were considered in the gene set enrichment analysis.

8.3. Results

All samples passed the quality control steps and for all samples the assumed gender matched the predicted gender. See Supplementary Figure 1 for a density plot of the raw beta values. 3 principal components were used for functional normalization (see Supplementary Figure 2 for a screeplot and Supplementary Figure 3 for a density plot of the normalized beta values). After removal of cross-reacting and polymorphic site-associated probes, probes on the X and Y chromosomes, and probes not passing the performance thresholds, 396,333 probes remained. There were no global DNA methylation level differences in de MCI and AD groups when compared to the controls (controls = 48.75%; MCI = 48.66%, p = 5.970E-01; AD = 48.61%, p = 4.640E-01).

8.3.1. Alzheimer's disease

Using processed M-values from the control and AD subjects, a surrogate variable analysis indicated the presence of 5 significant surrogate variables, which were included in the *limma* analysis. When applying the Gibbs sampler algorithm of the *bacon* package to the coefficients and standard errors from the *limma* analysis, a bias of -0.098 was detected and an inflation of 1.1 (Supplementary Figure 4). After FDR correction, 171 DMPs were detected ($p_{FDR} < 0.05$; Table 2; Supplementary Figure 5), some of which were also associated with MCI (Table 3). *Comb-p* detected a total 12 DMRs that survived the Šidák p-value adjustment and contained more than 1 probe (Table 4; Supplementary Figure 5). The DMR in *PRRT2* was also associated with MCI ($p_{Šidák}$ = 3.21E-04). 896 unique genes were annotated to the top 1000 probes with the highest effect sizes and lowest p-values (all $p < 0.05$). None of the terms or pathways remained statistically significantly enriched after FDR correction for the GO and KEGG gene set enrichment analysis (Supplementary Table 1 and Supplementary Table 2, respectively). There were 25,186 probes with a p-value below 0.05, which were used for the subsequent MMSE, CSF marker, and hippocampal volume association analyses.

table 2.

Probe	Gene	Region	ES	SE	*P*	FDR
cg22508626	*HLA-DRB5*	Body	-0.86	0.00	2.03E-16	8.03E-11
cg19611616	*STK38L*	5'UTR	5.62	1.00	1.68E-14	3.32E-09
cg01963573	*BEND3*	3'UTR	0.80	0.00	1.18E-10	1.35E-05
cg08435945	*CERS6*	Body	0.58	0.00	1.36E-10	1.35E-05
cg13876921	*LOC390705*		1.91	0.00	3.38E-10	2.68E-05
cg21926612	*PACRG*	5'UTR; 1st Exon; TSS1500	1.12	0.00	6.87E-10	4.54E-05
cg15068079	*BTNL9*	Body	1.25	0.00	1.31E-09	7.43E-05
cg16502980	*NEDD4L*	TSS1500	-2.35	0.00	9.57E-09	4.74E-04
cg13047596	*C2orf82*	5'UTR; 1st Exon	0.74	0.00	1.46E-08	6.43E-04
cg23192683	*LINC00884*		1.01	0.00	1.93E-08	7.01E-04
ch.6.8638596F	*LOC100506207*		-0.57	0.00	1.95E-08	7.01E-04
cg23919678	*TIAM2*	Body	0.58	0.00	4.34E-08	1.43E-03
cg17712928	*MAD1L1*	Body	0.78	0.00	5.01E-08	1.53E-03
cg09868354	*CDK1*		0.55	0.00	7.15E-08	1.92E-03
cg08698856	*RAB2A*	Body	0.56	0.00	7.26E-08	1.92E-03
cg14903685	*TLE3*	TSS1500	-0.92	0.00	8.37E-08	2.07E-03
cg11021661	*B3GNT6*	3'UTR	0.68	0.00	9.45E-08	2.20E-03
cg03130180	*GPX6*	TSS200	-0.88	0.00	1.29E-07	2.75E-03
cg18052984	*ATF1*	5'UTR	-0.59	0.00	1.44E-07	2.75E-03
cg16554516	*RASSF5*	TSS200	-0.92	0.00	1.49E-07	2.75E-03
cg07687332	*GPR63*	TSS1500	-0.75	0.00	1.50E-07	2.75E-03
cg03352657	*POLDIP2*	1st Exon; 5'UTR; TSS200	-0.51	0.10	1.59E-07	2.75E-03
cg04270085	*MIR4262*		0.41	0.08	1.60E-07	2.75E-03
cg02611675	*IGLL1*		-0.43	0.08	2.51E-07	4.04E-03
cg20054157	*SFTA1P*	TSS1500	0.71	0.14	2.55E-07	4.04E-03
cg17548431	*C4orf45*		-0.66	0.13	2.80E-07	4.11E-03
cg13421247	*CDK2AP1*	TSS1500	0.72	0.14	2.92E-07	4.11E-03
cg03361810	*AP3M2*	TSS1500	-0.54	0.10	2.92E-07	4.11E-03
cg09238162	*CREB3L2*	Body	-0.41	0.08	3.01E-07	4.11E-03
cg24513433	*LIPG*	TSS200	-0.83	0.16	3.30E-07	4.32E-03
cg12833168	*FBXO33*		0.66	0.13	3.41E-07	4.32E-03
cg03999372	*IRX3*	TSS1500	1.03	0.20	3.49E-07	4.32E-03
cg13406003	*RSPO3*		0.59	0.12	3.84E-07	4.58E-03
cg22273042	*TPD52*	5'UTR; 1st Exon	-0.64	0.13	3.95E-07	4.58E-03
cg08639523	*HIST3H2A*	TSS1500; 1st Exon; 3'UTR	-0.56	0.11	4.21E-07	4.58E-03
cg07638589	*CBFA2T3*		0.61	0.12	4.26E-07	4.58E-03
cg27657525	*URI1*	TSS1500	-0.69	0.14	4.38E-07	4.58E-03
cg12518535	*ANKRD20A19P*		-0.69	0.14	4.39E-07	4.58E-03
cg01922613	*ABCA4*	Body	0.58	0.11	4.90E-07	4.98E-03
cg11228480	*FBRSL1*	TSS1500	-0.66	0.13	5.45E-07	5.40E-03
cg25533943	*MAP3K14-AS1*	Body	-0.68	0.14	5.66E-07	5.47E-03
cg08524474	*ARHGAP22*	TSS200	-0.41	0.08	6.19E-07	5.84E-03
cg20546782	*TRPV1*	5'UTR	0.78	0.16	6.92E-07	6.35E-03
cg04571941	*TNRC18*	TSS200	-0.50	0.10	7.19E-07	6.35E-03
cg00546448	*SNAI3-AS1*	Body; 3'UTR	0.67	0.13	7.26E-07	6.35E-03
cg09306214	*TACR1*	TSS1500	-0.70	0.14	7.41E-07	6.35E-03
cg17504306	*PHLDA2*	TSS1500	-0.56	0.11	7.53E-07	6.35E-03
cg17720554	*SMOC2*		0.98	0.20	8.39E-07	6.93E-03

TABLE 2. DMPs from the Alzheimer's disease methylome-wide association analysis.

ABBREVIATIONS: DMPs, differentially methylated positions; ES, effect size; FDR, false discovery rate adjusted *p*-values; SE, standard error; TSS, transcription start site; UTR, untranslated region.

table 2. (continued)

Probe	Gene	Region	ES	SE	*P*	FDR
cg11228717	*DERA*	TSS1500	0.94	0.19	9.99E-07	8.08E-03
cg02131513	*UBE2I*	TSS1500	-0.72	0.15	1.16E-06	9.23E-03
cg26817121	*GPX6*	TSS1500	0.43	0.09	1.25E-06	9.70E-03
cg11164618	*RHBDF2*	5'UTR	0.58	0.12	1.63E-06	1.25E-02
cg03524116	*PREP*		-0.37	0.08	1.71E-06	1.28E-02
cg12030690	*SNCA*	TSS1500; 5'UTR	0.64	0.14	1.85E-06	1.34E-02
cg16323293	*PACRG*	Body	-0.41	0.09	1.89E-06	1.34E-02
cg05577437	*DLGAP2*	Body	0.57	0.12	1.90E-06	1.34E-02
cg07244268	*SLITRK3*		0.64	0.14	2.05E-06	1.43E-02
cg01220469	*RNF26*	TSS1500	0.54	0.11	2.13E-06	1.45E-02
cg13688765	*GALP*	TSS1500	-0.84	0.18	2.16E-06	1.45E-02
cg22784047	*SMG1P2*	Body	0.56	0.12	2.33E-06	1.53E-02
cg01849466	*ZFYVE21*	Body	1.82	0.39	2.37E-06	1.53E-02
cg12424548	*KCNQ1*	Body	0.52	0.11	2.42E-06	1.53E-02
cg05985988	*JARID2*	Body	0.58	0.12	2.43E-06	1.53E-02
cg15815375	*RRBP1*	3'UTR	0.51	0.11	2.50E-06	1.55E-02
cg22174623	*RPL22*	Body	0.50	0.11	2.55E-06	1.56E-02
cg07538944	*C7orf50*	Body	0.57	0.12	2.62E-06	1.56E-02
cg22077894	*TAF5L*	Body	0.60	0.13	2.64E-06	1.56E-02
cg05131623	*PEX5L*	TSS1500	0.77	0.16	2.78E-06	1.62E-02
cg04200362	*RAB11FIP5*	TSS1500	0.39	0.08	2.93E-06	1.68E-02
cg02869486	*FANCC*		-0.63	0.13	3.08E-06	1.72E-02
cg10213762	*SMOC2*		1.55	0.33	3.09E-06	1.72E-02
cg22312275	*NAALADL2*		0.66	0.14	3.21E-06	1.73E-02
cg25104727	*ASTN1*	Body	-0.88	0.19	3.21E-06	1.73E-02
cg09596260	*ADCY7*	Body	0.78	0.17	3.22E-06	1.73E-02
cg06582575	*PACRG*	5'UTR; 1st Exon; TSS1500	1.07	0.23	3.43E-06	1.81E-02
cg12762799	*CLEC4E*	1st Exon; 5'UTR	0.90	0.19	3.73E-06	1.93E-02
cg08045063	*POMGNT2*	TSS200	-0.98	0.21	3.76E-06	1.93E-02
cg24524451	*ADCK2*	TSS1500	-0.90	0.2	3.80E-06	1.93E-02
cg20022862	*GPR152*	1st Exon	0.75	0.16	3.98E-06	1.98E-02
cg17096191	*NOS1AP*	TSS1500	1.15	0.25	4.00E-06	1.98E-02
cg10441013	*KCNJ10*	TSS200	-0.72	0.16	4.24E-06	2.07E-02
cg00324693	*PCED1A*	TSS200	-0.42	0.09	4.51E-06	2.16E-02
cg10256121	*SP9*		-0.77	0.17	4.52E-06	2.16E-02
cg05588757	*ZNF514*	TSS1500	-0.54	0.12	4.61E-06	2.18E-02
cg11855759	*USP43*	TSS200	-0.42	0.09	4.73E-06	2.20E-02
cg04587220	*ARHGAP45*	Body	0.88	0.19	4.99E-06	2.28E-02
cg05423688	*FMNL1*	TSS200	-0.43	0.09	5.03E-06	2.28E-02
cg13722651	*ZNF507*	5'UTR	-0.59	0.13	5.10E-06	2.28E-02
cg24434232	*CLIP2*		0.56	0.12	5.16E-06	2.28E-02
cg13446235	*CENPBD1*	Body; TSS1500	-0.44	0.10	5.18E-06	2.28E-02
cg11586124	*CTDSP2*		-0.87	0.19	5.47E-06	2.38E-02
cg02856606	*IFFO2*	1st Exon	-0.38	0.08	6.03E-06	2.60E-02
cg25433267	*ZNF503-AS2*	Body; TSS200	-0.85	0.19	6.16E-06	2.62E-02
cg08180070	*EDAR*		0.64	0.14	6.24E-06	2.62E-02
cg12598048	*CYFIP1*	5'UTR; 1st Exon	-0.65	0.14	6.28E-06	2.62E-02
cg13008094	*FABP6*	3'UTR	0.61	0.14	6.41E-06	2.64E-02
cg08805662	*C2orf42*		-0.54	0.12	6.55E-06	2.68E-02

Probe	Gene	Region	ES	SE	*P*	FDR
cg17245135	*MEF2C*	Body	0.60	0.13	6.75E-06	2.71E-02
cg26204328	*C1QTNF9B-AS1*	Body; 5'UTR	0.63	0.14	6.76E-06	2.71E-02
cg09414557	*AGXT2*	TSS200	0.49	0.11	6.98E-06	2.76E-02
cg02862748	*TBX15*	3'UTR	0.61	0.13	7.08E-06	2.76E-02
cg04510639	*JMJD6*	1st Exon; TSS200; 5'UTR	-0.56	0.13	7.11E-06	2.76E-02
cg18103836	*SERPINB9P1*		0.43	0.10	7.19E-06	2.77E-02
cg24877558	*FOXJ3*	TSS1500	-0.70	0.16	7.40E-06	2.82E-02
cg20863949	*TEX261*	3'UTR	-0.61	0.14	7.47E-06	2.82E-02
cg12531601	*HLA-DRB5*	TSS1500; 5'UTR	-0.38	0.08	7.67E-06	2.87E-02
cg22603628	*DLGAP2*	Body	0.33	0.07	7.77E-06	2.88E-02
cg10318313	*NAP1L4*	TSS1500	0.57	0.13	8.07E-06	2.94E-02
cg16457196	*DDX41*	TSS1500	-0.69	0.15	8.09E-06	2.94E-02
cg19865375	*KIAA1324L*	Body	0.56	0.13	8.24E-06	2.97E-02
cg03321231	*RPH3AL*	Body	0.64	0.14	8.68E-06	3.09E-02
cg04546186	*FOXF1*		-0.70	0.16	8.75E-06	3.09E-02
cg23230176	*GTF2I*	TSS1500	-0.48	0.11	8.83E-06	3.10E-02
cg01471259	*PDPK1*	Body	0.64	0.14	9.17E-06	3.14E-02
cg15787377	*ITIH1*	TSS1500	0.69	0.16	9.27E-06	3.14E-02
cg01383268	*SLC39A11*	TSS200	-0.59	0.13	9.33E-06	3.14E-02
cg18268492	*PGAM1*	TSS200	-0.51	0.12	9.37E-06	3.14E-02
cg06521562	*JRK*	3'UTR	0.72	0.16	9.41E-06	3.14E-02
cg14276515	*IFITM3*		0.54	0.12	9.42E-06	3.14E-02
cg15814898	*JAK2*	1st Exon; 5'UTR	-0.42	0.10	9.52E-06	3.14E-02
cg04607442	*MIPEPP3*		-0.43	0.10	9.96E-06	3.25E-02
cg14034968	*ZIC1*		-0.65	0.15	1.00E-05	3.25E-02
cg12344004	*POLG*	5'UTR; 1st Exon	-0.48	0.11	1.07E-05	3.46E-02
cg21786289	*LOC100130417*	TSS200	0.99	0.23	1.11E-05	3.56E-02
cg07078467	*RPTOR*	Body	0.47	0.11	1.13E-05	3.59E-02
cg00656410	*SDF4*	Body	0.60	0.14	1.15E-05	3.61E-02
cg03143697	*LOC202181*	TSS200	-0.48	0.11	1.16E-05	3.61E-02
cg01453052	*TRIM65*	Body	-0.79	0.18	1.23E-05	3.79E-02
cg25289803	*AEBP1*	TSS200	-0.79	0.18	1.23E-05	3.79E-02
cg16234986	*ATP10D*	3'UTR	-0.40	0.09	1.25E-05	3.81E-02
cg21857846	*C8orf37-AS1*		-0.66	0.15	1.27E-05	3.86E-02
cg06557630	*ZNF423*		-0.68	0.16	1.31E-05	3.94E-02
cg25418508	*CDR2L*		-0.59	0.14	1.32E-05	3.95E-02
cg03187713	*COBL*	Body	0.61	0.14	1.35E-05	3.98E-02
cg08379212	*ENTPD1-AS1*	TSS200	-0.34	0.08	1.36E-05	3.99E-02
cg27045062	*EFNA3*	Body	-0.69	0.16	1.38E-05	4.03E-02
cg27514286	*AP2M1*	5'UTR; 1st Exon	-0.56	0.13	1.40E-05	4.04E-02
cg11993118	*NFATC2*	TSS200; Body	-0.67	0.15	1.41E-05	4.04E-02
cg09610084	*LOC286083*		-0.81	0.19	1.45E-05	4.11E-02
cg08985029	*TBX5*	5'UTR	1.15	0.26	1.46E-05	4.11E-02
cg19465737	*SDHAP1*		0.63	0.14	1.47E-05	4.11E-02
cg12828819	*FAT4*	TSS1500	-0.65	0.15	1.47E-05	4.11E-02
cg00278494	*CPZ*		0.69	0.16	1.49E-05	4.12E-02
cg03180953	*IGFALS*	Body	0.47	0.11	1.54E-05	4.17E-02

table 2. (continued)

table 2. (continued)

Probe	Gene	Region	ES	SE	*P*	FDR
cg04634493	*ZMIZ1-AS1*	TSS1500; TSS200	-0.61	0.14	1.54E-05	4.17E-02
cg09829176	*PPARA*	TSS1500	0.59	0.14	1.54E-05	4.17E-02
cg14495729	*PTPRN2*	Body	0.71	0.16	1.58E-05	4.26E-02
cg21918513	*GDNF*	5'UTR	-0.48	0.11	1.62E-05	4.35E-02
cg06486593	*PMPCA*		0.54	0.12	1.69E-05	4.48E-02
cg18132228	*PRTG*	TSS1500	-0.81	0.19	1.70E-05	4.48E-02
cg13944219	*SREK1*	TSS200; Body	-0.44	0.10	1.71E-05	4.49E-02
cg25736626	*MGLL*	Body	-0.51	0.12	1.74E-05	4.53E-02
cg21271026	*SLC9A3*	Body	-0.49	0.12	1.75E-05	4.53E-02
cg00597087	*MFSD12*	1st Exon; 5'UTR	-0.56	0.13	1.77E-05	4.55E-02
cg21777154	*C1orf21*	5'UTR	0.70	0.16	1.79E-05	4.55E-02
cg13028789	*ANKS1A*	TSS200; TSS1500	-0.40	0.09	1.79E-05	4.55E-02
cg07802917	*MYLK*	TSS200	0.66	0.15	1.82E-05	4.59E-02
cg10927461	*TSN*		-0.40	0.09	1.84E-05	4.61E-02
cg24032666	*NEFL*	5'UTR; 1st Exon	1.18	0.28	1.85E-05	4.61E-02
cg04678713	*BDH1*	3'UTR	-0.99	0.23	1.92E-05	4.72E-02
cg13852536	*NDUFB6*	Body	0.97	0.23	1.94E-05	4.72E-02
cg13808325	*SMIM20*	5'UTR; 1st Exon	-0.46	0.11	1.94E-05	4.72E-02
cg24309739	*NAF1*	TSS1500	-1.04	0.24	1.94E-05	4.72E-02
cg13701768	*PAX5*	Body	0.55	0.13	1.99E-05	4.82E-02
cg07835232	*DENND2A*	TSS1500	0.43	0.10	2.01E-05	4.82E-02
cg27165920	*SYT7*	3'UTR	0.64	0.15	2.03E-05	4.83E-02
cg07684809	*CAPS2*	TSS1500	0.54	0.13	2.04E-05	4.83E-02
cg17864206	*SZT2*	Body; TSS1500	-0.43	0.10	2.05E-05	4.83E-02
cg08894891	*HOMER3*	Body	0.64	0.15	2.08E-05	4.87E-02
cg23710594	*PHC2*	TSS200	0.60	0.14	2.12E-05	4.93E-02
cg07719172	*KCTD10*	Body	1.06	0.25	2.13E-05	4.93E-02

table 3.

Probe	Gene	Region	ES	SE	*P*	FDR
cg02856606	IFFO2	1st Exon	-0.42	7.00E-02	1.96E-08	4.04E-03
cg27657525	URI1	TSS1500	-0.61	1.20E-01	4.60E-07	1.40E-02
cg17712928	MAD1L1	Body	0.60	1.30E-01	1.55E-06	2.93E-02
cg08805662	C2orf42		-0.50	1.10E-01	2.11E-06	3.34E-02
cg22784047	SMG1P2	Body	0.47	1.00E-01	5.85E-06	4.54E-02
cg12518535	ANKRD20A19P		-0.54	1.20E-01	6.43E-06	4.54E-02
cg00324693	PCED1A	TSS200	-0.36	8.00E-02	6.76E-06	4.54E-02
cg04510639	JMJD6	1st Exon; TSS200; 5'UTR	-0.50	1.10E-01	6.96E-06	4.54E-02
cg01963573	BEND3	3'UTR	0.49	1.10E-01	8.18E-06	4.94E-02

TABLE 3. DMPs from the Alzheimer's disease methylome-wide association analysis also associated with MCI.

ABBREVIATIONS: DMPs, differentially methylated positions; ES, effect size; FDR, false discovery rate adjusted *p*-values; MCI, mild cognitive impairment; SE, standard error; TSS, transcription start site; UTR, untranslated region.

Position	Gene	Region	# probes	*P*	Šidák
chr5:180479586-180479623	*BTNL9*	Intron	2	2.20E-08	2.36E-04
chr16:29824542-29824600	*PRRT2*	CDS	2	3.54E-08	2.42E-04
chr3:123603306-123603312	*MYLK*	Intergenic	3	1.01E-07	6.64E-03
chr1:75139347-75139365	*ERICH3*	Exon; 5'UTR	2	1.33E-07	2.93E-03
chr15:89877906-89877926	*POLG*	Exon; 5'UTR; Intron	2	1.97E-07	3.89E-03
chr18:55710779-55710830	*NEDD4L*	Intergenic	2	2.11E-07	1.63E-03
chr15:101419479-101419519	*ALDH1A3*	Intergenic	4	3.14E-07	3.11E-03
chr1:5907446-5907509	*MIR4689*	Intergenic	2	4.26E-07	2.68E-03
chr16:54320670-54320675	*IRX3*	Intergenic	3	5.13E-07	3.98E-02
chr4:54966187-54966248	*GSX2*	TSS; Exon; 5'UTR	2	1.41E-06	9.09E-03
chr18:48405353-48405388	*ME2*	Intergenic	3	4.27E-06	4.73E-02
chr14:91853682-91853729	*CCDC88C*	Intron	2	5.16E-06	4.26E-02

table 4.

8.3.2. Mini-mental state examination scores

As expected, there was a significant difference between AD patient and control MMSE scores (Δ = -5.42, p = 2.36E-02), which was not observed between the MCI cases and controls (Δ = -0.30, p = 3.38E-01) (Supplementary Figure 6). For the MMSE association analysis of the AD-associated probes 6 surrogate variables were included in the *limma* analysis. A bias of -0.11 and an inflation of 1 was detected after the 'bacon' function was applied to the test statistics (Supplementary Figure 7). After bias, inflation, and FDR adjustment, 110 MMSE-associated DMPs were identified (Table 5; Supplementary Figure 8), of which cg03999372 (*IRX3*) and cg24032666 (*NEFL*) were also AD-associated DMPs, whereas *HLA-DRB5* contained 3 different DMPs than those found in relation to AD. 5 MMSE-associated DMRs were found (Table 6; Supplementary Figure 8), and the region in *IRX3* exactly matches the *IRX3* DMR found in relation to AD. A total of 883 unique genes were annotated to the top 1000 ranked CpG sites. GO enrichment analysis identified 1 significantly enriched biological processes after FDR correction (GO:0007156, "homophilic cell adhesion via plasma membrane adhesion molecules", Table 7; Supplementary Table 3). There was some overlap between the genes in the enriched term, the genes associated with the top 1000 altered CpGs, and genes with DMPs; *CDH13*, *PCDHA1*, and *CLSTN2*.

TABLE 4. DMRs associated with Alzheimer's disease.
ABBREVIATIONS: CDS, coding DNA sequence; chr, chromosome; DMRs, differentially methylated regions; Šidák, Šidák-corrected *p*-values; TSS, transcription start site; UTR, untranslated region.

Of note, a DMP in *PCDHA1* was also detected in association with MCI (ES = -0.58, p_{FDR} = 4.54E-02). The top 10 enriched KEGG pathways are shown in Supplementary Table 4, although none of them reached statistical significance after the FDR adjustment.

table 5.

Probe	Gene	Region	ES	SE	*P*	FDR
cg27228168	*IRX3*	TSS1500	-0.15	0.02	3.01E-12	7.58E-08
cg03998835	*TBX18*		-0.14	0.02	3.41E-10	4.29E-06
cg20188282	*GTF3C5*	5'UTR; 1st Exon	-0.10	0.02	7.96E-10	4.81E-06
cg03999372	*IRX3*	TSS1500	-0.09	0.02	8.50E-10	4.81E-06
cg00767058	*ADPRHL1*	Body; TSS1500	0.14	0.02	9.55E-10	4.81E-06
cg09973375	*PPID*	TSS1500	0.15	0.03	2.69E-09	1.13E-05
cg15125763	*SPAG16*	TSS1500	-0.13	0.02	6.84E-09	2.46E-05
cg24032666	*NEFL*	5'UTR; 1st Exon	-0.14	0.02	1.11E-08	3.48E-05
cg19073576	*F10*		-0.24	0.04	1.27E-08	3.56E-05
cg23303311	*ZNF728*		-0.06	0.01	2.23E-08	5.24E-05
cg08143038	*GPR78*		0.12	0.02	2.29E-08	5.24E-05
cg14942906	*DOC2GP*		0.16	0.03	2.50E-08	5.24E-05
cg02350039	*NHSL1*	Body	-0.09	0.02	3.26E-08	6.32E-05
cg04704193	*HIST1H3G*	TSS1500	0.15	0.03	3.83E-08	6.89E-05
cg20992181	*FGF3*		0.07	0.01	5.59E-08	9.39E-05
cg14930075	*KCNK9*	1st Exon	-0.19	0.04	6.89E-08	1.08E-04
cg01849212	*MYOF*	TSS1500	0.25	0.05	1.05E-07	1.51E-04
cg20138055	*BIN3*	Body	-0.12	0.02	1.08E-07	1.51E-04
cg16588852	*FAM86EP*		0.14	0.03	1.21E-07	1.60E-04
cg25772658	*HLA-DRB5*	Body	0.07	0.01	1.46E-07	1.83E-04
cg06323727	*EXD3*	5'UTR	-0.07	0.01	1.84E-07	2.21E-04
cg10485752	*MAN1C1*	Body	-0.13	0.02	2.19E-07	2.51E-04
cg04229851	*SORCS2*	3'UTR; 1st Exon; Body	0.08	0.01	2.63E-07	2.77E-04
cg02833117	*ERMN*	TSS1500; Body	-0.08	0.02	2.75E-07	2.77E-04
cg00103448	*HOXB1*		0.07	0.01	2.85E-07	2.77E-04
cg05163330	*ADPRHL1*	Body; TSS1500	0.16	0.03	2.94E-07	2.77E-04
cg26112170	*ADPRHL1*	Body; TSS1500	0.12	0.02	2.97E-07	2.77E-04
cg22830844	*TOPAZ1*	TSS200	0.07	0.01	3.33E-07	2.99E-04
cg04108615	*SLC39A1*	TSS1500	0.11	0.02	3.84E-07	3.34E-04
cg14656245	*GPX6*	Body	0.06	0.01	4.22E-07	3.55E-04
cg23161492	*ANPEP*	5'UTR	0.10	0.02	5.77E-07	4.69E-04
cg01000236	*CACNA1H*	Body	-0.07	0.01	6.26E-07	4.84E-04
cg16119483	*ERGIC1*	Body	0.09	0.02	6.34E-07	4.84E-04
cg01056174	*ANAPC1*	1st Exon; 5'UTR	0.10	0.02	6.60E-07	4.87E-04
cg09608383	*FAM189A1*	Body	-0.12	0.02	6.77E-07	4.87E-04
cg07829001	*NPHP4*	Body	-0.10	0.02	8.31E-07	5.81E-04
cg08705329	*VPS25*	3'UTR; TSS1500	0.08	0.02	1.43E-06	9.75E-04
cg13424608	*PLXNA1*	Body	-0.09	0.02	1.55E-06	1.00E-03

TABLE 5. DMPs from the MMSE score association analysis.

ABBREVIATIONS: DMPs, differentially methylated positions; ES, effect size; FDR, false discovery rate adjusted *p*-values; MMSE, mini-mental state examination; SE, standard error; TSS, transcription start site; UTR, untranslated region.

Probe	Gene	Region	ES	SE	*P*	FDR
cg00035847	*MECR*	Body; 5'UTR	-0.15	0.03	1.55E-06	1.00E-03
cg24735129	*SHANK2*		0.10	0.02	1.62E-06	1.02E-03
cg20971147	*KAZN*		-0.09	0.02	2.09E-06	1.28E-03
cg02755131	*CDH13*	Body	0.08	0.02	2.49E-06	1.49E-03
cg10089963	*NR4A2*	Body	-0.09	0.02	3.86E-06	2.26E-03
cg00089091	*DPP10*	Body	-0.08	0.02	5.08E-06	2.91E-03
cg25319337	*HUS1*	Body	-0.10	0.02	6.81E-06	3.81E-03
cg03432817	*TFAP2B*		0.08	0.02	7.54E-06	4.13E-03
cg17393016	*LINC00482*	TSS1500	0.10	0.02	8.00E-06	4.20E-03
cg10342447	*TMEM97*	TSS1500	0.09	0.02	8.01E-06	4.20E-03
cg08463297	*SPECC1*		-0.11	0.02	8.57E-06	4.41E-03
cg19711879	*FAM193A*		-0.07	0.02	1.03E-05	5.19E-03
cg14624329	*BRINP1*		0.08	0.02	1.05E-05	5.21E-03
cg10905495	*PPP2R2A*	Body	-0.11	0.03	1.20E-05	5.84E-03
cg12751354	*CYP24A1*	3'UTR	-0.08	0.02	1.26E-05	6.00E-03
cg01807426	*C7orf50*	Body	0.06	0.01	1.42E-05	6.63E-03
cg04524088	*MIR129-1*	TSS200	0.09	0.02	1.74E-05	7.96E-03
cg03043296	*CPEB1-AS1*	Body	0.06	0.01	1.77E-05	7.96E-03
cg10624914	*ADPRHL1*	Body; TSS200	0.11	0.03	1.84E-05	8.11E-03
cg26282566	*PCDHA1*	Body; TSS200	-0.09	0.02	1.87E-05	8.11E-03
cg11386080	*COL21A1*	TSS200	0.06	0.01	1.94E-05	8.29E-03
cg07384357	*TPD52L2*	Body	0.09	0.02	2.13E-05	8.94E-03
cg08687052	*SYN3*	Body; TSS1500	-0.08	0.02	2.30E-05	9.42E-03
cg18220087	*LOC283177*		-0.06	0.01	2.33E-05	9.42E-03
cg20594961	*ADRA2C*		0.16	0.04	2.36E-05	9.42E-03
cg07684809	*CAPS2*	TSS1500	-0.05	0.01	2.98E-05	1.17E-02
cg24073777	*CASZ1*	5'UTR	0.09	0.02	3.16E-05	1.22E-02
cg01029685	*PCDHA1*	Body; TSS1500	-0.10	0.02	3.22E-05	1.23E-02
cg13826105	*FBXW5*		0.05	0.01	3.69E-05	1.39E-02
cg25487047	*PCDHA1*	3'UTR	0.09	0.02	3.84E-05	1.40E-02
cg13267298	*C14orf180*		-0.17	0.04	3.85E-05	1.40E-02
cg06609489	*NOL4*	TSS1500	-0.10	0.02	4.82E-05	1.72E-02
cg04689720	*VLDLR*	TSS1500; Body	-0.05	0.01	4.83E-05	1.72E-02
cg05733554	*C14orf37*	5'UTR	-0.06	0.02	4.94E-05	1.73E-02
cg13921570	*LBX2-AS1*	Body; TSS200	-0.04	0.01	5.36E-05	1.85E-02
cg11726572	*TYMS*	Body; TSS1500	-0.06	0.01	6.01E-05	2.04E-02
cg05726756	*HOXB1*	TSS200	0.07	0.02	6.16E-05	2.04E-02
cg21577260	*SLC25A19*	TSS200	0.06	0.01	6.19E-05	2.04E-02
cg08966155	*IQCG*	5'UTR; TSS1500	0.10	0.03	6.25E-05	2.04E-02
cg23795893	*LOC101054525*	TSS200	-0.10	0.03	6.75E-05	2.18E-02
cg04936970	*EXO5*	TSS1500	-0.05	0.01	7.74E-05	2.47E-02
cg09322349	*GRHL3*	TSS1500	-0.12	0.03	7.86E-05	2.47E-02
cg15975598	*CREB3L2*	Body	0.04	0.01	8.69E-05	2.70E-02
cg15557878	*TSLP*	TSS1500	-0.07	0.02	9.62E-05	2.96E-02
cg17589866	*ALK*	Body	0.15	0.04	9.95E-05	3.02E-02
cg06866655	*SLC9A3*	Body	0.05	0.01	1.02E-04	3.06E-02
cg05918002	*ZNF232*	5'UTR	0.19	0.05	1.06E-04	3.15E-02

table 5. (continued)

table 5. (continued)

Probe	Gene	Region	ES	SE	*P*	FDR
cg25858232	*PTPRN2*	Body	0.06	0.02	1.12E-04	3.29E-02
cg05936555	*HLA-DRB5*	Body	-0.05	0.01	1.30E-04	3.73E-02
cg25559849	*STK32C*	TSS200	0.10	0.03	1.32E-04	3.73E-02
cg25671428	*CLSTN2*	Body	-0.06	0.02	1.32E-04	3.73E-02
cg13957827	*TMA16*	TSS1500	-0.04	0.01	1.35E-04	3.74E-02
cg15447775	*NEDD1*	TSS200; TSS1500	0.05	0.01	1.35E-04	3.74E-02
cg13230208	*WDTC1*		0.09	0.02	1.47E-04	4.01E-02
cg04314247	*SLC44A3*	5'UTR; 1st Exon; Body	-0.06	0.02	1.54E-04	4.14E-02
cg16736080	*FAM181A*	Body; TSS1500	0.07	0.02	1.55E-04	4.14E-02
cg01150044	*MIR124-1*		0.06	0.01	1.63E-04	4.31E-02
cg12382153	*ALDH1A2*	Body	-0.09	0.03	1.70E-04	4.44E-02
cg09139451	*TRAF5*	TSS200; TSS1500	-0.04	0.01	1.71E-04	4.44E-02
cg10801102	*DUS1L*	TSS1500	-0.05	0.01	1.74E-04	4.48E-02
cg20370505	*CARS2*	TSS200	-0.05	0.01	1.77E-04	4.51E-02
cg11212451	*CPEB4*		0.06	0.02	1.87E-04	4.69E-02
cg00986580	*DAD1*		-0.05	0.01	1.89E-04	4.69E-02
cg20440187	*HLA-DRB5*	Body	0.04	0.01	1.90E-04	4.69E-02
cg22700328	*MIR193A*	TSS1500	-0.05	0.01	1.96E-04	4.79E-02
cg10935723	*KCNK10*	TSS1500	0.12	0.03	2.00E-04	4.84E-02
cg22448433	*UCHL3*	TSS1500	0.05	0.01	2.03E-04	4.86E-02
cg24973289	*TPT1*		-0.06	0.02	2.05E-04	4.86E-02
cg22520791	*ADAMTS2*		-0.04	0.01	2.06E-04	4.86E-02
cg23191380	*FZD1*	TSS200	-0.04	0.01	2.11E-04	4.93E-02
cg26874163	*FLJ33360*	TSS200	0.08	0.02	2.18E-04	5.00E-02
cg11519760	*DLL1*	Body	0.08	0.02	2.18E-04	5.00E-02

table 6.

Position	Gene	Region	# probes	*P*	Šidák
chr16:54320672-54320675	*IRX3*	Intergenic	2	1.52E-18	1.28E-14
chr13:114103713-114103797	*ADPRHL1*	Intron	2	2.26E-14	6.79E-12
chr13:45885542-45885565	*TPT1*	Intergenic	2	2.96E-06	3.23E-03
chr2:10184444-10184458	*KLF11*	Exon; 5'UTR; Intron	2	7.39E-06	1.32E-02
chr19:48774586-48774653	*ZNF114*	Exon; 5'UTR	2	1.88E-05	7.03E-03

TABLE 6. DMRs associated with MMSE score.

ABBREVIATIONS: chr, chromosome; DMRs, differentially methylated regions; MMSE, mini-mental state examination; Šidák, Šidák-corrected *p*-values; UTR, untranslated region.

ID	Description	Ontology	Genes in term	Genes altered	Gene names	*P*	FDR
GO:0007156	homophilic cell adhesion via plasma membrane adhesion molecules	BP	105	27	*CDH11; CDH13; CELSR3; SDK1; PCDHB1; PCDHB18; PCDHGA3; PCDHGA2; PCDHGA1; PCDHB10; PCDHB7; PCDHAC2; PCDHAC1; PCDHA13; PCDHA12; PCDHA11; PCDHA10; PCDHA8; PCDHA7; PCDHA6; PCDHA5; PCDHA4; PCDHA3; PCDHA2; PCDHA1; CLSTN2; PCDHA9*	6.74E-06	4.27E-02

table 7.

8.3.3. Cerebrospinal fluid phosphorylated tau amyloid-β ratio

The CSF ptau:Aβ42 ratio (Supplementary Figure 9), was increased in AD patients when compared to controls (Δ = 0.10, p = 3.58E-02), as expected, whereas the ratio was not statistically significantly increased in the MCI group, although a tendency towards an increase can be observed (Δ = 0.05, p = 5.16E-02). With the ptau:Aβ42 ratio as predictor, 5 significant surrogate variables were detected with the 'sva' function, and which were included in the *limma* analysis to correct for unobserved covariates. The 'bacon' function estimated the bias and inflation of the limma test results to be 0.036 and 0.96, respectively (Supplementary Figure 10). CSF ptau:Aβ42 was associated with 12 DMPs that passed the FDR correction (Table 8; Supplementary Figure 11), including cg14930075 and cg01849212 in *KCNK9* and *MYOF*, respectively, that were also associated with MMSE scores. There was 1 DMR associated with the ptau:Aβ42 ratio (Table 9; Supplementary Figure 11). The top GO terms and KEGG pathways from the gene set (including 898 unique genes) enrichment analysis are shown in Supplementary Table 5 and Supplementary Table 6, respectively, but none of them reached statistical significance after FDR adjustment.

TABLE 7. GO term enriched by genes with altered DNA methylation in relation to MMSE score.
ABBREVIATIONS: BP, biological process; FDR, false discovery rate adjusted p-values; GO, Gene Ontology; MMSE, mini-mental state examination.

table 8.

Probe	Gene	Region	ES	SE	*P*	FDR
cg11217960	*IQSEC3*	Body; 5'UTR	-4.83	0.93	2.10E-07	5.28E-03
ch.5.1134768F	*PDE4D*	Body	-3.63	0.73	6.54E-07	8.24E-03
cg14930075	*KCNK9*	1st Exon	7.21	1.48	1.15E-06	8.70E-03
cg23248424	*GFPT2*	Body	11.94	2.47	1.38E-06	8.70E-03
cg02401454	*HBQ1*	1st Exon; 5'UTR	3.70	0.78	1.82E-06	9.17E-03
cg08262378	*AGRN*		-2.52	0.56	7.26E-06	2.87E-02
cg14092045	*RGS3*		3.71	0.83	8.50E-06	2.87E-02
cg25099892	*ATP11AUN*	5'UTR	-3.51	0.79	9.11E-06	2.87E-02
cg01978237	*SIM1*	Body	4.44	1.01	1.08E-05	3.02E-02
cg01849212	*MYOF*	TSS1500	-9.45	2.19	1.62E-05	4.08E-02
cg08553437	*PP12613*	TSS200; Body	3.23	0.76	2.18E-05	4.86E-02
cg02330494	*ITPKA*	1st Exon	2.37	0.56	2.31E-05	4.86E-02

TABLE 8. DMPs from the CSF ptau:Aβ42 association analysis.
ABBREVIATIONS: Aβ42, amyloid-β 1-42; CSF, cerebrospinal fluid; DMPs, differentially methylated positions; ES, effect size; FDR, false discovery rate adjusted *p*-values; ptau, phosphorylated tau; SE, standard error; TSS, transcription start site; UTR, untranslated region.

table 9.

Position	Gene	Region	# probes	*P*	Šidák
chr4:103998289-103998292	*SLC9B2*	Intron; 5'UTR	2	2.25E-07	1.88E-03

TABLE 9. DMRs associated with CSF ptau:Aβ42.
ABBREVIATIONS: Aβ42, amyloid-β 1-42; chr, chromosome; CSF, cerebrospinal fluid; DMRs, differentially methylated regions; ptau, phosphorylated tau; Šidák, Šidák-corrected *p*-values; UTR, untranslated region.

8.3.4. Hippocampal volume

The final association analysis focused on mean hippocampal volume (Supplementary Figure 12), which was decreased in AD patients when compared to the MCI group (Δ = -0.04, p = 1.63E-02). The surrogate variable analysis detected 4 significant variables. After running the *limma* association analysis with these variables, *bacon* detected a bias of -0.12 and an inflation of 1.1 in the test statistics (Supplementary Figure 13). After adjustment of the test statistics, 14 DMPs were detected (Table 10; Supplementary Figure 14), including one in the *TMEM232* gene that also contained one of the 2 DMRs associated with hippocampal volume (Table 11; Supplementary Figure 14). For the gene set (including 896 unique genes) enrichment analysis none of the GO terms or KEGG pathways were statistically significantly enriched after FDR correction (Supplementary Table 7 and Supplementary Table 8, respectively).

Probe	Gene	Region	ES	SE	*P*	FDR
cg01590699	*PRLH*	1st Exon	10.89	2.05	1.17E-07	2.94E-03
cg03704673	*GLTPD2*	5'UTR; 1st Exon	-11.19	2.18	2.70E-07	3.25E-03
cg02388865	*LIN28A*	1st Exon; 5'UTR	-7.67	1.54	5.83E-07	3.25E-03
cg15472170	*PLOD1*	Body	9.52	1.91	6.34E-07	3.25E-03
cg06583576	*ZIC4*		-7.67	1.54	6.46E-07	3.25E-03
cg11543397	*MAL2*	TSS1500	-8.29	1.77	2.69E-06	9.14E-03
cg04101934	*SORBS2*		7.32	1.56	2.80E-06	9.14E-03
cg03030994	*KCNQ1*	Body	-5.66	1.21	2.90E-06	9.14E-03
cg14549976	*CTDP1*		-6.21	1.40	9.60E-06	2.69E-02
cg02371040	*ZNF558*		5.28	1.20	1.07E-05	2.70E-02
cg20478120	*BAK1*	Body; TSS1500	-6.54	1.53	1.82E-05	3.89E-02
cg15535683	*CADPS2*		-6.73	1.58	1.91E-05	3.89E-02
cg23217512	*UACA*		-8.82	2.07	2.01E-05	3.89E-02
cg11641395	*TMEM232*	TSS200	-14.57	3.43	2.17E-05	3.90E-02

table 10.

Position	Gene	Region	# probes	*P*	Šidák
chr5:110062384-110062399	*TMEM232*	Exon; 5'UTR	2	2.02E-07	3.39E-04
chr6:31148370-31148525	*PSORS1C3*	Intergenic	8	7.83E-06	1.27E-03

table 11.

8.4. Discussion

The present study investigated the blood methylomic profile of AD and established sub-profiles related to cognitive performance, CSF ptau:Aβ42, and hippocampal volume. Unlike previous reports focusing on the brain [37, 38], but also blood [39], no global changes in DNA methylation were detected, although this is likely because the used array to assess gene-specific DNA methylation levels covers less than 2% of all CpGs within the human genome, with an especially low coverage of the large intergenic regions of DNA that are likely heavily methylated [40].

Previous methylome-wide association studies investigating AD-related changes in DNA methylation focusing on the brain identified various genes with altered methylation patterns related to AD pathology, including the AD-susceptibility gene *HLA-DRB5* [41, 42]. In blood, the current study identifies 2 DMPs in *HLA-DRB5* associated with AD, including the top DMP, and an additional 3 DMPs related to MMSE score. *HLA-DRB5* encodes a major histocompatibility complex class II protein, the altered regulation of which supports a role for the immune system in AD [41].

TABLE 10. DMPs from the hippocampal volume association analysis. **ABBREVIATIONS:** DMPs, differentially methylated positions; ES, effect size; FDR, false discovery rate adjusted *p*-values; SE, standard error; TSS, transcription start site; UTR, untranslated region.

TABLE 11. DMRs associated with hippocampal volume. **ABBREVIATIONS:** chr, chromosome; DMRs, differentially methylated regions; Šidák, Šidák-corrected *p*-values; UTR, untranslated region.

An AD-associated DMR was detected in the *ALDH1A3* gene, part of the gene family encoding aldehyde dehydrogenases (ALDHs). Aldehydes may be exogenous, or internally produced during various metabolic processes, and can have cytotoxic effects [43]. ALDHs play an important role in detoxifying aldehydes and their dysregulation has been implicated in AD [43, 44]. The observed hypermethylation of probes near the *ALDH1A3* transcription start site (TSS) in AD cases would support a lowered expression of aldehyde dehydrogenase family 1 member A3, which could result in the increased levels of aldehydes observed in AD [45]. 3 DMPs associated with AD were identified near the promotor of *PACRG*, a gene linked to Parkinsonism, also a neurodegenerative condition, and which was previously reported to be abnormally methylated in relation to leukemia [46]. *NEDD4L*, containing a DMP and DMR associated with AD, encodes an E3 ubiquitin ligase, crucial for targeted lysosomal degradation, and was found to be differentially expressed in the hippocampus of AD patients [47]. E3 ubiquitin ligases are thought to be important for the clearance of toxic proteins in AD [48].

POLG, encoding DNA polymerase gamma (POLG), presented with a DMP and DMR in relation to AD. POLG is crucial for the maintenance of mitochondrial DNA (mtDNA) and decreased CSF levels of POLG have been found in AD patients [14], as well as low levels of cell-free mtDNA [49]. Notably, low levels of CSF mtDNA has been proposed as a biomarker for preclinical AD [49], and as POLG is responsible for the synthesis of mtDNA, it may be fruitful to investigate the potential of the POLG DMR as an even earlier biomarker for the development of AD. Additionally, it may be interesting to note that altered methylation patterns in relation to AD have also been observed for mitochondrial DNA itself [50].

Neurofilament light (NEFL), encoded by the *NEFL* gene, has also been investigated as a biomarker for AD progression [51], with higher levels in the CSF being associated with AD, hippocampal atrophy, and lower MMSE scores. In the current study a DMP in *NEFL* was found in relation to AD and MMSE scores. If a relationship between *NEFL* methylation status and NEFL CSF levels can be established, the epigenetic marker may serve as an even earlier marker of AD development than changes in NEFL levels in the CSF. As NEFL CSF levels have also been proposed as a biomarker for other neurodegenerative diseases (e.g. [52–54]), its specificity for detecting prodromal AD may be limited, and should be combined with other biomarkers. Another potential early risk factor for AD may be methylation of *MAD1L1*, a regulator of leukocyte telomere length [55]. Shorter leukocyte telomeres is a risk factor for age-related diseases, including AD [56]. Epigenetic dysregulation of *MAD1L1* appeared to already exist in MCI cases, as the *MAD1L1* DMP (cg17712928) was

found to be hypermethylated in both MCI and AD cases, but more so in the AD cases. Interestingly, differential methylation of the *MAD1L1* gene has previously been reported in association with schizophrenia, along with the suggestion there may be overlap in the epigenetic dysregulation seen AD and schizophrenia [57].

The *IRX3* gene was associated with a DMP and DMR in relation to AD, as well as 2 DMPs and a DMR associated with MMSE score, with AD and a lower MMSE score resulting in hypermethylation. *IRX3* regulation is connected to the obesity- and type 2 diabetes- associated gene *FTO* [58, 59]. Both obesity and diabetes are risk factors for AD, which may be explained by a possible interaction between *FTO* and *APOE* [60], the latter of which represents a major genetic risk factor for sporadic AD [61]. *GFPT2*, containing a DMP associated with CSF ptau:Aβ42, encodes glutamine-fructose-6-phosphate transaminase (GFPT) 2, that is important for glucose energy metabolism and has been linked to diabetes mellitus [62, 63], and may therefore play a role in the suggested link between AD and diabetes mellitus [64–66]. Additionally, GFPT22-mediated glutamate metabolism may be disturbed in AD [67]. For other genes, such as *EXO5*, with an MMSE-associated DMP, *TMEM232*, with a DMP and DMR associated with hippocampal volume, and *SLC9B2*, with a DMR related to CSF ptau:Aβ42, no clear relationships with AD have yet been reported.

The performed GO and KEGG analyses were an attempt to identify functionally linked genes affected by altered methylation levels. Although many terms and pathways relevant for neurodegeneration could be observed amongst those that were most enriched, only one term survived FDR correction, GO:0007156 (“homophilic cell adhesion via plasma membrane adhesion molecules”), related to MMSE score. Looking at the genes associated with the top 1000 most altered CpGs in this pathway reveals a high representation of protocadherin (PCDH) genes, including *PCDHA1*, which contained 3 MMSE-associated DMPs and a DMP associated with MCI. PCDH proteins are cell-adhesion proteins located in the plasma membrane, critical for neuronal cell-cell interactions, including synaptogenesis [68, 69]. Other genes in the enriched GO term and including a MMSE-associated DMP are *CDH13* and *CLSTN2*. *CDH13* also belongs to the cadherin family of membrane proteins, this variant being implicated in regulating neurite growth and prevention of cell death in response to oxidative stress [70, 71]. Although not previously implicated in AD, *CDH13* hypermethylation has been observed in a multitude of cancer types (e.g. [72, 73]), and specific gene variants are associated with diabetes type 2 [74] and metabolic syndrome [75], but also with schizophrenia [76], attention deficit hyperactivity disorder [77], particularly in relation to working memory performance [78], and violent behavior [79], and even chronic obstructive pulmonary disease [80] and atherosclerosis

[81]. However, its implication in such diverse pathologies may limit the usefulness of *CDH13* as a specific biomarker for AD, although its related disorders may be investigated as possible comorbidities of AD to identify disease subtypes. Interestingly, genetic variation in *CLSTN2*, encoding calsyntenin 2, a component of the postsynaptic membrane [82], has been linked to episodic memory performance [83, 84], which is strongly affected in AD [85]. All in all, methylation of *PCDHA1*, *CDH13*, and *CLSTN2* may be investigated as early markers of dementia.

The findings of the present study should be viewed in light of some limitations. One of the limitations is the relatively small sample size, which limited the power of the study, as well as the covariates that could be included. To accommodate the latter limitation, the effects of age and gender, which may influence AD diagnosis [86, 87], were individually tested and no effect was found on AD diagnosis (data not shown). Additionally, it has been suggested differences in blood cell type composition may affect the outcome of epigenetic studies in blood [88, 89]. Components of CD4+ and CD8+ T cells, B cells, monocytes, granulocytes, and natural killer cells were estimated with the 'estimateCellCounts' function of *minfi* [88, 89] and the effects on AD status were investigated (data not shown). Although no significant effects were found, this may also be attributed to the low sample size, and therefore surrogate variables were included to account for potential confounders, as described in the methods section. Lastly, it should be noted that the used method to quantify DNA methylation levels cannot distinguish between DNA methylation and hydroxymethylation, a related, but functionally different epigenetic marker [90]. However, it is expected this has less impact on studies focusing on the blood methylome than those focusing on the brain, as DNA hydroxymethylation is much less prevalent than DNA methylation and is not enriched in the blood like it is in the brain [91].

Summarizing, this small exploratory study corroborates an epigenetic component in AD and associated measures, and shows some of the epigenetic dysregulation observed in the brain, mainly concerning *HLA-DRB5*, is reflected in the blood methylome, in addition to some novel potential blood biomarkers of AD. Especially methylation of the plasma membrane triad *PCDHA1*, *CDH13*, and *CLSTN2* may be further explored as early markers of AD dementia, possibly complemented by the methylation status of *HLA-DRB5*, *NEFL*, and *MAD1L1*.

Acknowledgments

Funds have been provided by the Internationale Stichting Alzheimer Onderzoek (ISAO) grant 11532 (D.L.A.vdH.), by the ISAO grants 09552 and 13515, and the Netherlands Organization for Scientific Research (NWO), grant 916.11.086 (Veni Award) (B.P.F.R.), and by a fellowship as part of NWO grant 022.005.019, (R.L.). The funding agencies were not involved in the study design, data collection, analysis and interpretation, writing of the report, and the decision to submit the article for publication. The authors declare no conflicts of interest.

REFERENCES

[1] Yates D, McLoughlin DM. The molecular pathology of Alzheimer's disease. *Psychiatry* 2008; 7: 1–5.

[2] Godyń J, Jończyk J, Panek D, et al. Therapeutic strategies for Alzheimer's disease in clinical trials. *Pharmacol Reports* 2015; 68: 127–138.

[3] Castellani RJ, Perry G. The complexities of the pathology–pathogenesis relationship in Alzheimer disease. *Biochem Pharmacol* 2014; 88: 671–676.

[4] Heppner FL, Ransohoff RM, Becher B. Immune attack: the role of inflammation in Alzheimer disease. *Nat Rev Neurosci* 2015; 16: 358–372.

[5] Yadav RS, Tiwari NK. Lipid integration in neurodegeneration: an overview of Alzheimer's disease. *Mol Neurobiol* 2014; 50: 168–176.

[6] Chen Z, Zhong C. Decoding Alzheimer's disease from perturbed cerebral glucose metabolism: Implications for diagnostic and therapeutic strategies. *Prog Neurobiol* 2013; 108: 21–43.

[7] Ciechanover A, Kwon YT. Degradation of misfolded proteins in neurodegenerative diseases: therapeutic targets and strategies. *Exp Mol Med* 2015; 47: e147.

[8] Lardenoije R, Iatrou A, Kenis G, et al. The epigenetics of aging and neurodegeneration. *Prog Neurobiol* 2015; 131: 21–64.

[9] Iatrou A, Kenis G, Rutten BPF, et al. Epigenetic dysregulation of brainstem nuclei in the pathogenesis of Alzheimer's disease: looking in the correct place at the right time? *Cellular and Molecular Life Sciences*, 2016, pp. 1–15.

[10] Hashimoto H, Vertino PM, Cheng X. Molecular coupling of DNA

methylation and histone methylation. *Epigenomics* 2010; 2: 657–669.

[11] Lunnon K, Mill J. Epigenetic studies in Alzheimer's disease: current findings, caveats, and considerations for future studies. *Am J Med Genet B Neuropsychiatr Genet* 2013; 162B: 789–99.

[12] Slieker RC, Bos SD, Goeman JJ, et al. Identification and systematic annotation of tissue-specific differentially methylated regions using the Illumina 450k array. *Epigenetics Chromatin* 2013; 6: 26.

[13] Defina PA, Moser RS, Glenn M, et al. Alzheimer's disease clinical and research update for health care practitioners. *J Aging Res* 2013; 2013: 207178.

[14] Oláh Z, Kálmán J, Tóth ME, et al. Proteomic analysis of cerebrospinal fluid in Alzheimer's disease: wanted dead or alive. *J Alzheimer's Dis* 2015; 44: 1303–1312.

[15] Peng G-P, Feng Z, He F-P, et al. Correlation of hippocampal volume and cognitive performances in patients with either mild cognitive impairment or Alzheimer's disease. *CNS Neurosci Ther* 2015; 21: 15–22.

[16] Folstein MF, Folstein SE, McHugh PR. 'Mini-mental state'. A practical method for grading the cognitive state of patients for the clinician. *J Psychiatr Res* 1975; 12: 189–98.

[17] Pradier C, Sakarovitch C, Le Duff F, et al. The mini mental state examination at the time of Alzheimer's disease and related disorders diagnosis, according to age, education, gender and place of residence: a cross-sectional study among the French National Alzheimer database. *PLoS One* 2014; 9: e103630.

[18] van Rossum IA, Visser PJ, van der Flier WM, et al. Predictors of time to AD diagnosis in subjects with MCI. *Alzheimer's Dement* 2010; 6: S99.

[19] Fagan AM, Roe CM, Xiong C, et al. Cerebrospinal fluid tau/β-amyloid42 ratio as a prediction of cognitive decline in nondemented older adults. *Arch Neurol* 2007; 64: 343.

[20] Fischl B. FreeSurfer. *Neuroimage* 2012; 62: 774–781.

[21] R Core Team. R: A language and environment for statistical computing. https://www.r-project.org/ (2016).

[22] RStudio Team. RStudio: Integrated Development for Rhttp://www.rstudio.com/ (2016).

[23] van Iterson M, Tobi EW, Slieker RC, et al. *MethylAid*: visual and interactive quality control of large Illumina 450k datasets. *Bioinformatics* 2014; 30: 3435–3437.

[24] Aryee MJ, Jaffe AE, Corrada-Bravo H, et al. *Minfi*: a flexible and comprehensive Bioconductor package for the analysis of Infinium DNA methylation microarrays. *Bioinformatics* 2014; 30: 1363–1369.

[25] Triche TJ, Weisenberger DJ, Van Den Berg D, et al. Low-level processing of Illumina Infinium DNA Methylation BeadArrays. *Nucleic Acids Res* 2013; 41: e90–e90.

[26] Fortin J-P, Labbe A, Lemire M, et al. Functional normalization of 450k methylation array data improves replication in large cancer studies. *Genome Biol* 2014; 15: 503.

[27] van Iterson M, Tobi E, Slieker R, et al. *DNAmArray*. Epub ahead of print 2017. DOI: https://doi.org/10.5281/zenodo.158908.

[28] Chen Y, Lemire M, Choufani S, et al. Discovery of cross-reactive probes and polymorphic CpGs in the Illumina Infinium HumanMethylation450 microarray. *Epigenetics* 2013; 8: 203–209.

[29] Du P, Zhang X, Huang C-C, et al. Comparison of Beta-value and M-value methods for quantifying methylation levels by microarray analysis. *BMC Bioinformatics* 2010; 11: 587.

[30] Ritchie ME, Phipson B, Wu D, et al. *limma* powers differential expression analyses for RNA-sequencing and microarray studies. *Nucleic Acids Res* 2015; 43: e47.

[31] Leek JT, Johnson WE, Parker HS, et al. The *sva* package for removing batch effects and other unwanted variation in high-throughput experiments. *Bioinformatics* 2012; 28: 882–3.

[32] Smyth GK. Linear models and empirical Bayes methods for assessing differential expression in microarray experiments. *Stat Appl Genet Mol Biol* 2004; 3: 1–25.

[33] van Iterson M, van Zwet EW, BIOS Consortium BT, et al. Controlling bias and inflation in epigenome- and transcriptome-wide association studies using the empirical null distribution. *Genome Biol* 2017; 18: 19.

[34] Pedersen BS, Schwartz DA, Yang I V, et al. *Comb-p*: software for combining, analyzing, grouping and correcting spatially correlated *P*-values. *Bioinformatics* 2012; 28: 2986–8.

[35] Phipson B, Maksimovic J, Oshlack A. *missMethyl*: an R package for analyzing data from Illumina's HumanMethylation450 platform. *Bioinformatics* 2015; 32: btv560.

[36] Geeleher P, Hartnett L, Egan LJ, et al. Gene-set analysis is severely biased when applied to genome-wide methylation data. *Bioinformatics* 2013; 29: 1851–1857.

[37] Chouliaras L, Mastroeni D,

Delvaux E, et al. Consistent decrease in global DNA methylation and hydroxymethylation in the hippocampus of Alzheimer's disease patients. *Neurobiol Aging* 2013; 34: 2091–2099.

[38] Coppieters N, Dieriks B V, Lill C, et al. Global changes in DNA methylation and hydroxymethylation in Alzheimer's disease human brain. *Neurobiol Aging* 2014; 35: 1334–1344.

[39] Di Francesco A, Arosio B, Falconi A, et al. Global changes in DNA methylation in Alzheimer's disease peripheral blood mononuclear cells. *Brain Behav Immun* 2015; 45: 139–144.

[40] Weber M, Schübeler D. Genomic patterns of DNA methylation: targets and function of an epigenetic mark. *Curr Opin Cell Biol* 2007; 19: 273–280.

[41] Lambert J-C, Ibrahim-Verbaas CA, Harold D, et al. Meta-analysis of 74,046 individuals identifies 11 new susceptibility loci for Alzheimer's disease. *Nat Genet* 2013; 45: 1452–1458.

[42] Yu L, Chibnik LB, Srivastava GP, et al. Association of brain DNA methylation in *SORL1* , *ABCA7* , *HLA-DRB5*, *SLC24A4*, and *BIN1* with pathological diagnosis of Alzheimer disease. *JAMA Neurol* 2015; 72: 15.

[43] Vasiliou V, Nebert DW. Analysis and update of the human aldehyde dehydrogenase (ALDH) gene family. *Hum Genomics* 2005; 2: 138–43.

[44] Kamino K, Nagasaka K, Imagawa M, et al. Deficiency in mitochondrial aldehyde dehydrogenase increases the risk for late-onset Alzheimer's disease in the Japanese population. *Biochem Biophys Res Commun* 2000; 273: 192–196.

[45] Chen K, Maley J, Yu PH. Potential implications of endogenous aldehydes in beta-amyloid misfolding, oligomerization and fibrillogenesis. *J Neurochem* 2006; 99: 1413–1424.

[46] Agirre X, Román-Gómez J, Vázquez I, et al. Abnormal methylation of the common *PARK2* and *PACRG* promoter is associated with downregulation of gene expression in acute lymphoblastic leukemia and chronic myeloid leukemia. *Int J Cancer* 2006; 118: 1945–1953.

[47] Hokama M, Oka S, Leon J, et al. Altered expression of diabetes-related genes in Alzheimer's disease brains: The Hisayama Study. *Cereb Cortex* 2014; 24: 2476–2488.

[48] Kumar P, Jha NK, Jha SK, et al. Tau phosphorylation, molecular chaperones, and ubiquitin E3 ligase: clinical relevance in Alzheimer's disease. *J Alzheimer's Dis* 2015; 43: 341–361.

[49] Podlesniy P, Figueiro-Silva J, Llado A, et al. Low cerebrospinal fluid concentration of mitochondrial DNA in preclinical Alzheimer disease. *Ann Neurol* 2013; 74: 655–668.

[50] Blanch M, Mosquera JL, Ansoleaga B, et al. Altered mitochondrial DNA methylation pattern in Alzheimer disease–related pathology and in Parkinson disease. *Am J Pathol* 2016; 186: 385–397.

[51] Zetterberg H, Skillbäck T, Mattsson N, et al. Association of cerebrospinal fluid neurofilament light concentration with Alzheimer disease progression. *JAMA Neurol* 2016; 73: 60.

[52] Lu C-H, Macdonald-Wallis C, Gray E, et al. Neurofilament light chain: A prognostic biomarker in amyotrophic lateral sclerosis. *Neurology* 2015; 84: 2247–2257.

[53] Skillback T, Farahmand B, Bartlett JW, et al. CSF neurofilament light differs in neurodegenerative diseases and predicts severity and survival. *Neurology* 2014; 83: 1945–1953.

[54] Abdulle S, Mellgren Å, Brew BJ, et al. CSF neurofilament protein (NFL) — a marker of active HIV-related neurodegeneration. *J Neurol* 2007; 254: 1026–1032.

[55] Buxton JL, Suderman M, Pappas JJ, et al. Human leukocyte telomere length is associated with DNA methylation levels in multiple subtelomeric and imprinted loci. *Sci Rep* 2014; 4: 1496–1505.

[56] Guan J-Z, Guan W-P, Maeda T, et al. The subtelomere of short telomeres is hypermethylated in Alzheimer's disease. *Aging Dis* 2012; 3: 164–70.

[57] Montano C, Taub MA, Jaffe A, et al. Association of DNA methylation differences with schizophrenia in an epigenome-wide association study. *JAMA Psychiatry* 2016; 73: 506.

[58] Smemo S, Tena JJ, Kim K-H, et al. Obesity-associated variants within *FTO* form long-range functional connections with *IRX3*. *Nature* 2014; 507: 371–375.

[59] Cedernaes J, Benedict C. Human obesity: *FTO*, *IRX3*, or both? *Mol Metab* 2014; 3: 505–6.

[60] Keller L, Xu W, Wang H-X, et al. The obesity related gene, *FTO*, interacts with *APOE*, and is associated with Alzheimer's disease risk: a prospective cohort study. *J Alzheimers Dis* 2011; 23: 461–9.

[61] Liu C-C, Kanekiyo T, Xu H, et al. Apolipoprotein E and Alzheimer disease: risk, mechanisms and therapy. *Nat Rev Neurol* 2013; 9: 106–118.

[62] Zhang H, Jia Y, Cooper JJ, et al. Common variants in glutamine:-fructose-6-phosphate amidotransferase 2 (GFPT2) gene are associated with type 2 diabetes, diabetic nephropathy, and increased GFPT2 mRNA levels.

J Clin Endocrinol Metab 2004; 89: 748–755.

[63] Coomer M, Essop MF. Differential hexosamine biosynthetic pathway gene expression with type 2 diabetes. *Mol Genet Metab Reports* 2014; 1: 158–169.

[64] Aliev G, Shahida K, Hua Gan S, et al. Alzheimer disease and type 2 diabetes mellitus: the link to tyrosine hydroxylase and probable nutritional strategies. http://www.ingentaconnect.com/content/ben/cnsnddt/2014/00000013/00000003/art00013 (accessed 19 April 2017).

[65] de la Monte SM. Brain insulin resistance and deficiency as therapeutic targets in Alzheimer's disease. *Curr Alzheimer Res* 2012; 9: 35–66.

[66] Yu R, Deochand C, Krotow A, et al. Tobacco smoke-induced brain white matter myelin dysfunction: potential co-factor role of smoking in neurodegeneration. *J Alzheimer's Dis* 2015; 50: 133–148.

[67] Zhang M, Schmitt-Ulms G, Sato C, et al. Drug repositioning for Alzheimer's disease based on systematic 'omics' data mining. *PLoS One* 2016; 11: e0168812.

[68] Hirayama T, Yagi T. The role and expression of the protocadherin-alpha clusters in the CNS. *Curr Opin Neurobiol* 2006; 16: 336–342.

[69] Lachman HM, Petruolo OA, Pedrosa E, et al. Analysis of protocadherin alpha gene deletion variant in bipolar disorder and schizophrenia. *Psychiatr Genet* 2008; 18: 110–115.

[70] Rivero O, Selten MM, Sich S, et al. Cadherin-13, a risk gene for ADHD and comorbid disorders, impacts GABAergic function in hippocampus and cognition. *Transl Psychiatry* 2015; 5: e655.

[71] Joshi MB, Philippova M, Ivanov D, et al. T-cadherin protects endothelial cells from oxidative stress-induced apoptosis. *FASEB J* 2005; 19: 1737–9.

[72] Yang J, Niu H, Huang Y, et al. A systematic analysis of the relationship of *CDH13* promoter methylation and breast cancer risk and prognosis. *PLoS One* 2016; 11: e0149185.

[73] Ye M, Huang T, Li J, et al. Role of CDH13 promoter methylation in the carcinogenesis, progression, and prognosis of colorectal cancer. *Medicine* (Baltimore) 2017; 96: e5956.

[74] Nicolas A, Aubert R, Bellili-Muñoz N, et al. T-cadherin gene variants are associated with type 2 diabetes and the Fatty Liver Index in the French population. *Diabetes Metab* 2017; 43: 33–39.

[75] Kitamoto A, Kitamoto T, Nakamura T, et al. *CDH13* polymorphisms are associated with adiponectin levels and metabolic syndrome traits independently of visceral fat mass. *J Atheroscler Thromb* 2016; 23: 309–319.

[76] Børglum AD, Demontis D, Grove J, et al. Genome-wide study of association and interaction with maternal cytomegalovirus infection suggests new schizophrenia loci. *Mol Psychiatry* 2014; 19: 325–333.

[77] Salatino-Oliveira A, Genro JP, Polanczyk G, et al. Cadherin-13 gene is associated with hyperactive/impulsive symptoms in attention/deficit hyperactivity disorder. *Am J Med Genet Part B Neuropsychiatr Genet* 2015; 168: 162–169.

[78] Arias-Vásquez A, Altink ME, Rommelse NNJ, et al. *CDH13* is associated with working memory performance in attention deficit/hyperactivity disorder. *Genes, Brain Behav* 2011; 10: 844–851.

[79] Tiihonen J, Rautiainen M-R, Ollila HM, et al. Genetic background of extreme violent behavior. *Mol Psychiatry* 2015; 20: 786–792.

[80] Yuan Y, Zhang J, Xu S, et al. Genetic variants of *CDH13* determine the susceptibility to chronic obstructive pulmonary disease in a Chinese population. *Acta Pharmacol Sin* 2016; 37: 390–397.

[81] Kostopoulos CG, Spiroglou SG, Varakis JN, et al. Adiponectin/T-cadherin and apelin/APJ expression in human arteries and periadventitial fat: implication of local adipokine signaling in atherosclerosis? *Cardiovasc Pathol* 2014; 23: 131–138.

[82] Hintsch G, Zurlinden A, Meskenaite V, et al. The calsyntenins--a family of postsynaptic membrane proteins with distinct neuronal expression patterns. *Mol Cell Neurosci* 2002; 21: 393–409.

[83] Pantzar A, Laukka EJ, Atti AR, et al. Interactive effects of *KIBRA* and *CLSTN2* polymorphisms on episodic memory in old-age unipolar depression. *Neuropsychologia* 2014; 62: 137–142.

[84] Preuschhof C, Heekeren HR, Li S-C, et al. *KIBRA* and *CLSTN2* polymorphisms exert interactive effects on human episodic memory. *Neuropsychologia* 2010; 48: 402–408.

[85] Tromp D, Dufour A, Lithfous S, et al. Episodic memory in normal aging and Alzheimer disease: Insights from imaging and behavioral studies. *Ageing Res Rev* 2015; 24: 232–262.

[86] Kawas C, Gray S, Brookmeyer R, et al. Age-specific incidence rates of Alzheimer's disease: the Baltimore Longitudinal Study of Aging.

Neurology 2000; 54: 2072–7.

[87] Podcasy JL, Epperson CN. Considering sex and gender in Alzheimer disease and other dementias. *Dialogues Clin Neurosci* 2016; 18: 437–446.

[88] Jaffe AE, Irizarry RA. Accounting for cellular heterogeneity is critical in epigenome-wide association studies. *Genome Biol* 2014; 15: R31.

[89] Houseman E, Accomando WP, Koestler DC, et al. DNA methylation arrays as surrogate measures of cell mixture distribution. *BMC Bioinformatics* 2012; 13: 86.

[90] van den Hove DLA, Chouliaras L, Rutten BPF. The role of 5-hydroxymethylcytosine in aging and Alzheimer's disease: current status and prospects for future studies. *Curr Alzheimer Res* 2012; 9: 545–9.

[91] Skvortsova K, Zotenko E, Luu P-L, et al. Comprehensive evaluation of genome-wide 5-hydroxymethylcytosine profiling approaches in human DNA. *Epigenetics Chromatin* 2017; 10: 16.

SUPPLEMENTARY DATA

SUPPLEMENTARY FIGURE 1. Density plot of raw beta values.
Plot includes all DNA methylation probes on the Illumina HumanMethylation450 BeadChip, plotted for each sample separately.

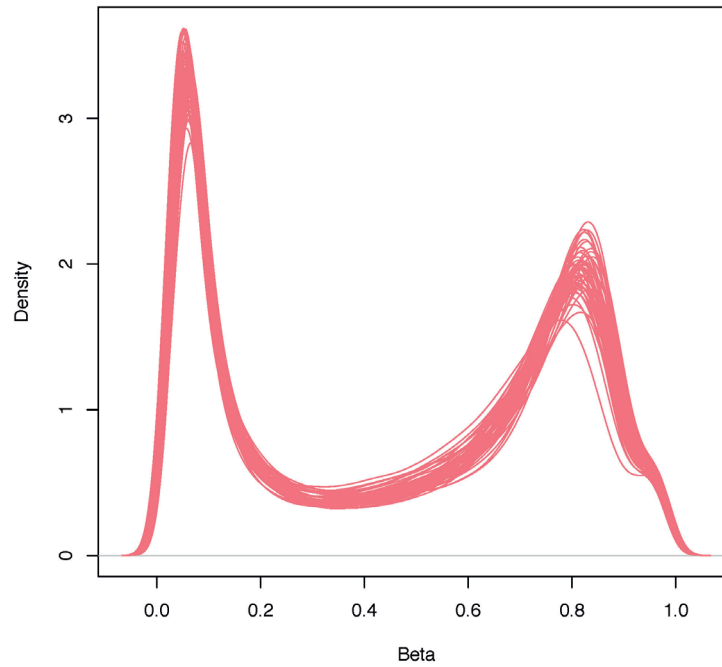

supplementary figure 1.

SUPPLEMENTARY FIGURE 2. Screeplot for the Illumina HumanMethylation450 BeadChip assay data.
Most variance is captured by the first 3 principal components (PCs), thus 3 principal components were selected for functional normalization of the data.

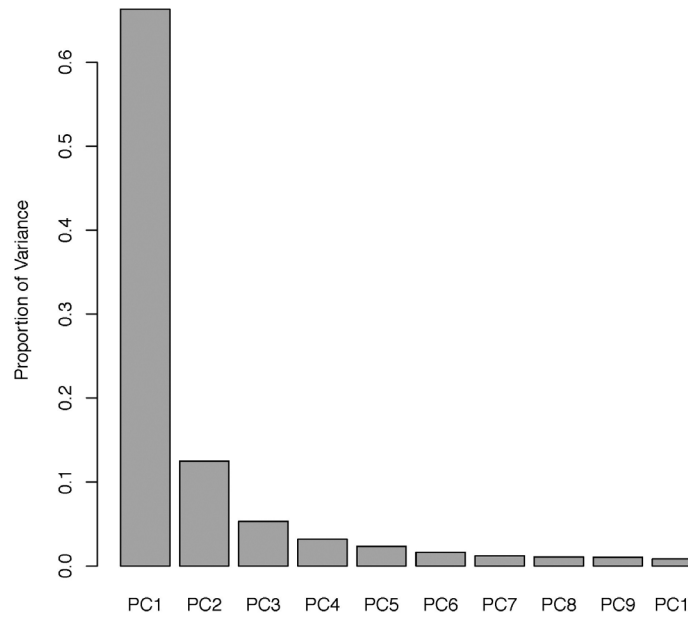

supplementary figure 2.

SUPPLEMENTARY FIGURE 3. Density plot of normalized beta values. Plot includes all DNA methylation probes on the Illumina HumanMethylation450 BeadChip, plotted for each sample separately.

SUPPLEMENTARY FIGURE 4. Histogram of test-statistics showing potential bias (A) and quantile-quantile (QQ) plot showing potential inflation (B) of the Alzheimer's disease methylome-wide association study results. The pink line in A represents the fit of the empirical null distribution and the black line the fit of the mixture of the empirical null distribution, the proportion of positively associated features, and the proportion of negatively associated features, both estimated as described in [33]. The estimated bias and inflation was -0.098 and 1.1, respectively.

supplementary figure 3.

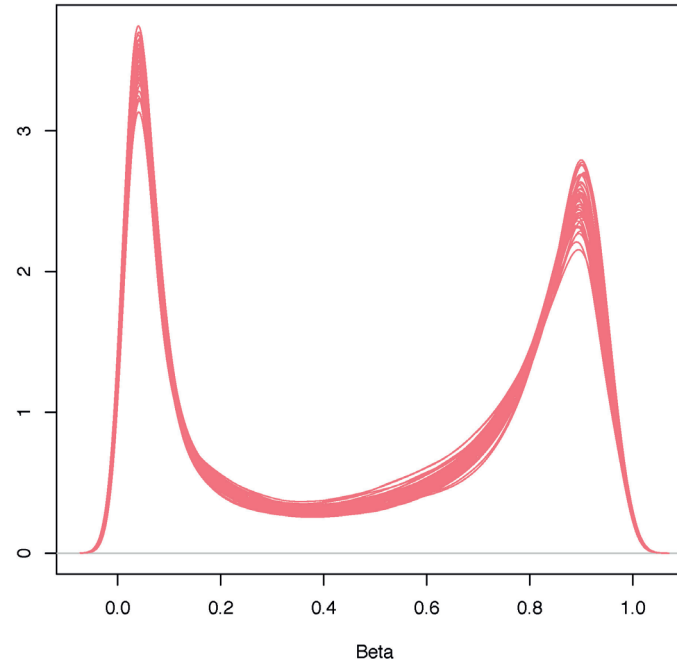

supplementary figure 4.

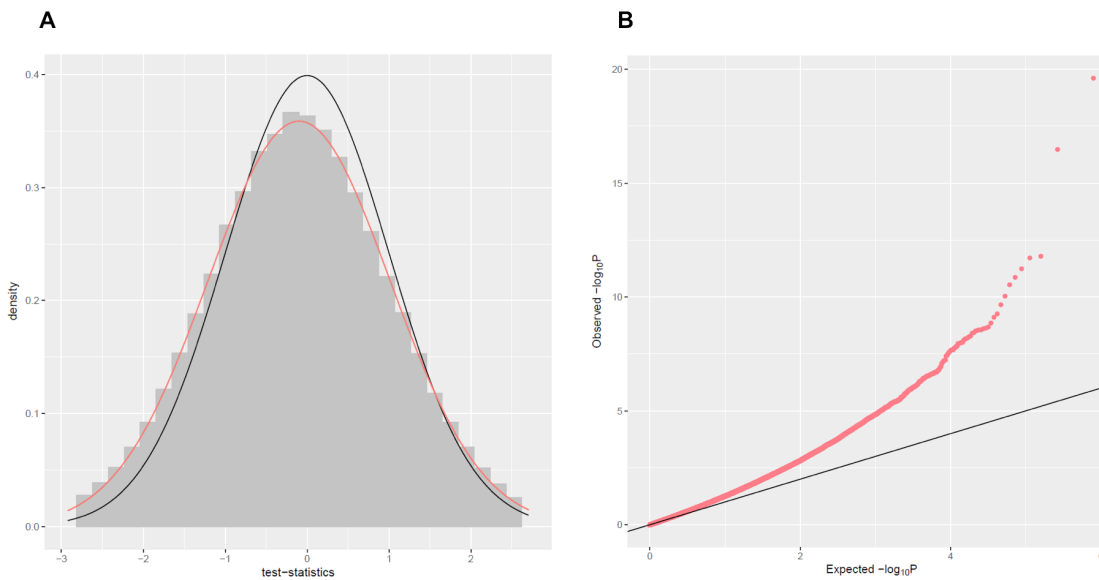

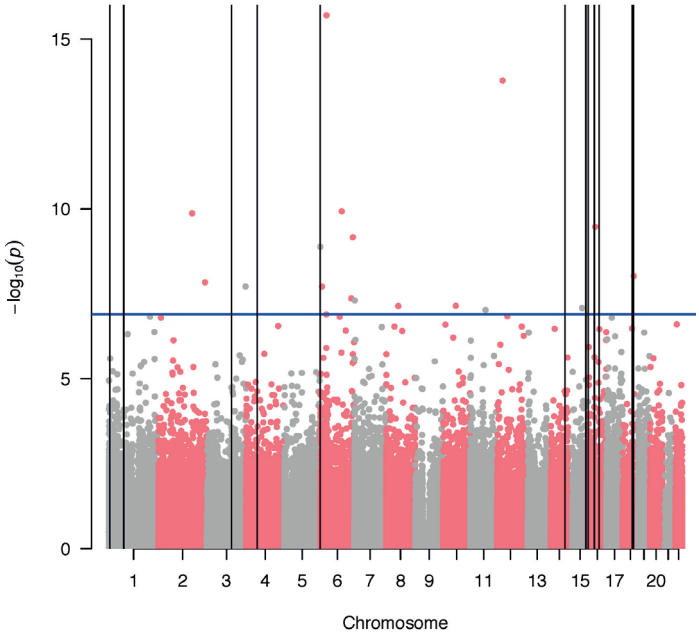

supplementary figure 5.

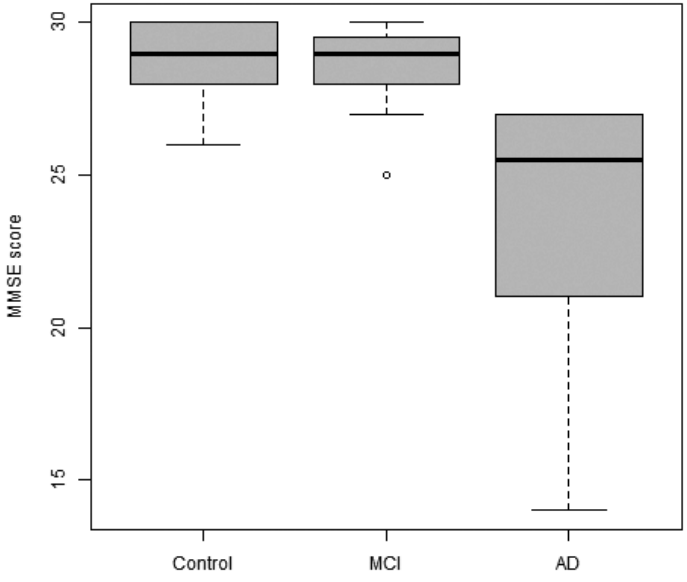

supplementary figure 6.

SUPPLEMENTARY FIGURE 5. Manhattan plot of the Alzheimer's disease methylome-wide association study. The blue horizontal line indicates the genome-wide significance threshold (0.05 / # probes in analysis). Vertical black lines indicate differentially methylated regions as determined with *comb-p*, using a seeding p-value threshold of 0.05 and an extension window of 200 base pairs, and with more than two probes and a Šidák-adjusted p-value below 0.05.

SUPPLEMENTARY FIGURE 6. Boxplot of mini-mental state examination (MMSE) scores for the control, mild cognitive impairment (MCI), and Alzheimer's disease (AD) groups.

SUPPLEMENTARY FIGURE 7. Histogram of test-statistics showing potential bias (A) and quantile-quantile (QQ) plot showing potential inflation (B) of the mini-mental state examination (MMSE) score association analysis in the Alzheimer's disease methylomic profile. The pink line in A represents the fit of the empirical null distribution and the black line the fit of the mixture of the empirical null distribution, the proportion of positively associated features, and the proportion of negatively associated features, both estimated as described in [33]. The estimated bias and inflation was -0.11 and 1, respectively.

supplementary figure 7.

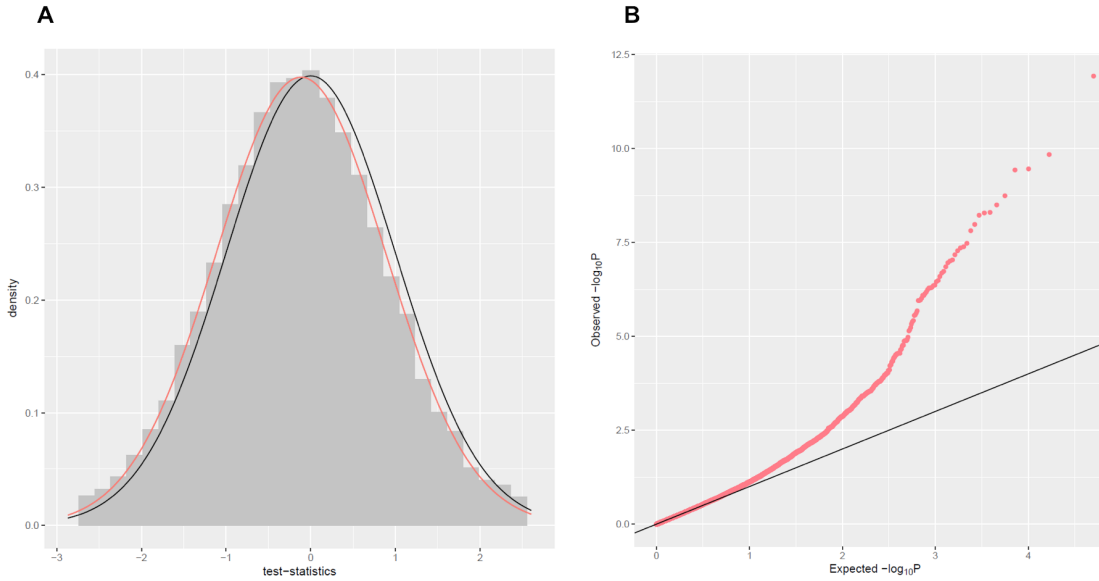

supplementary figure 8.

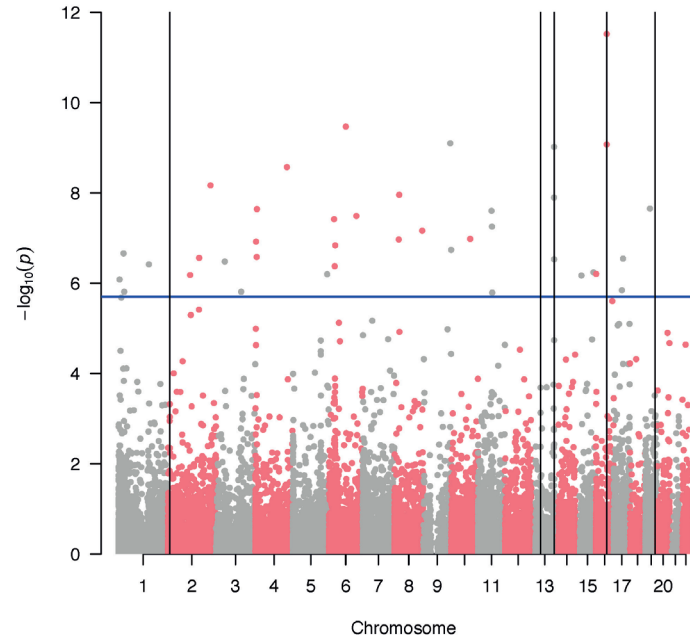

SUPPLEMENTARY FIGURE 8. Manhattan plot of the mini-mental state examination (MMSE) score association analysis in the Alzheimer's disease methylomic profile. The blue horizontal line indicates the genome-wide significance threshold (0.05 / # probes in analysis). Vertical black lines indicate differentially methylated regions as determined with *comb-p*, using a seeding *p*-value threshold of 0.05 and an extension window of 200 base pairs, and with more than two probes and a Šidák-adjusted *p*-value below 0.05.

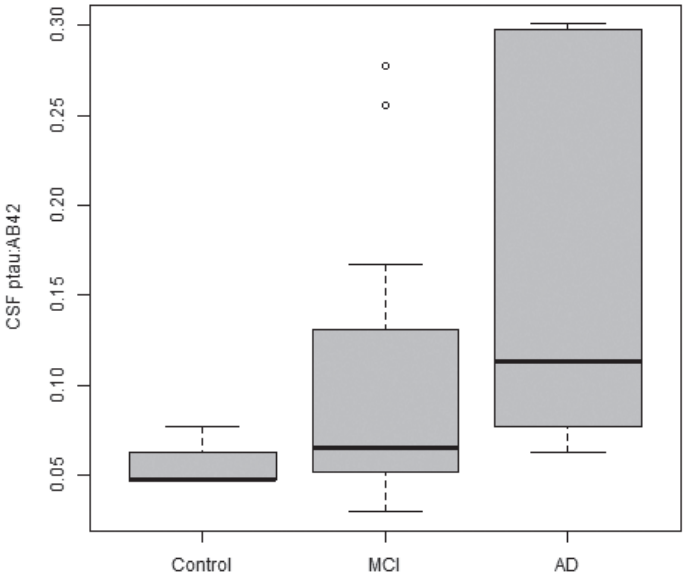

supplementary figure 9.

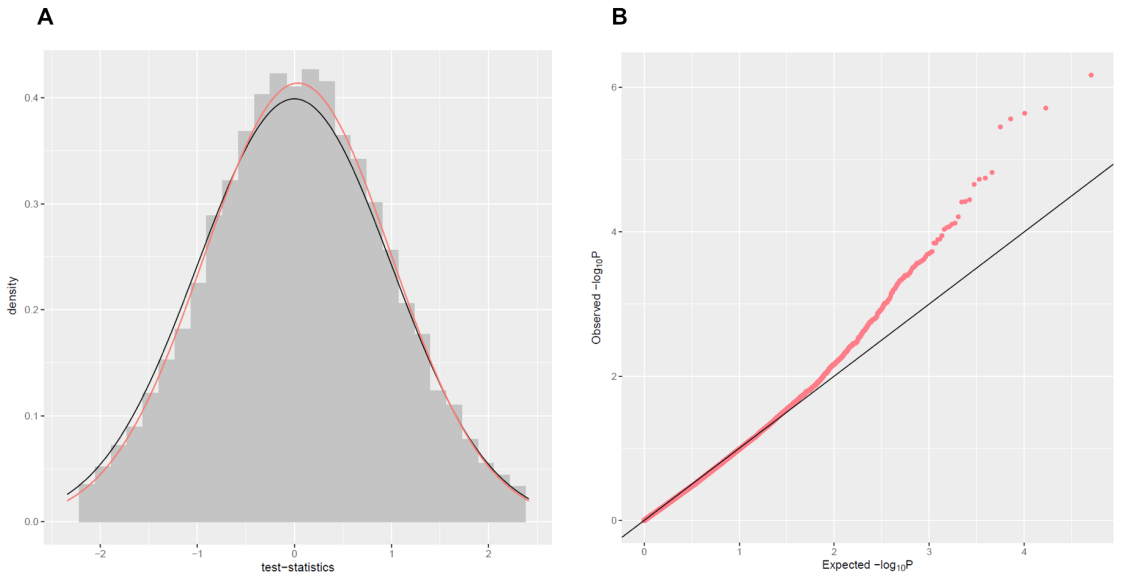

supplementary figure 10.

SUPPLEMENTARY FIGURE 9. Boxplot of the cerebrospinal fluid (CSF) phosphorylated tau (ptau) and amyloid-β 1-42 (Aβ41) ratio for the control, mild cognitive impairment (MCI), and Alzheimer's disease (AD) groups.

SUPPLEMENTARY FIGURE 10. Histogram of test-statistics showing potential bias (A) and quantile-quantile (QQ) plot showing potential inflation (B) of the cerebrospinal fluid phosphorylated tau and amyloid-β ratio association analysis in the Alzheimer's disease methylomic profile. The pink line in A represents the fit of the empirical null distribution and the black line the fit of the mixture of the empirical null distribution, the proportion of positively associated features, and the proportion negatively associated features, both estimated as described in [33]. The estimated bias and inflation was 0.036 and 0.96, respectively.

supplementary figure 11.

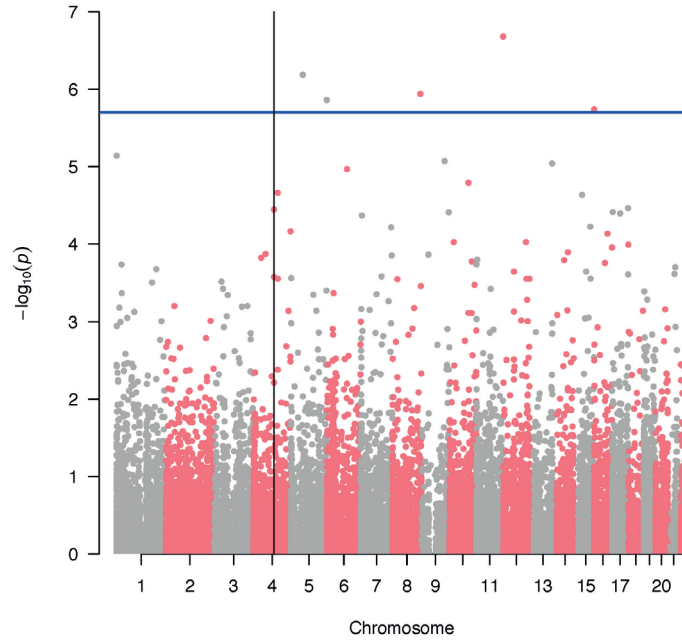

supplementary figure 12.

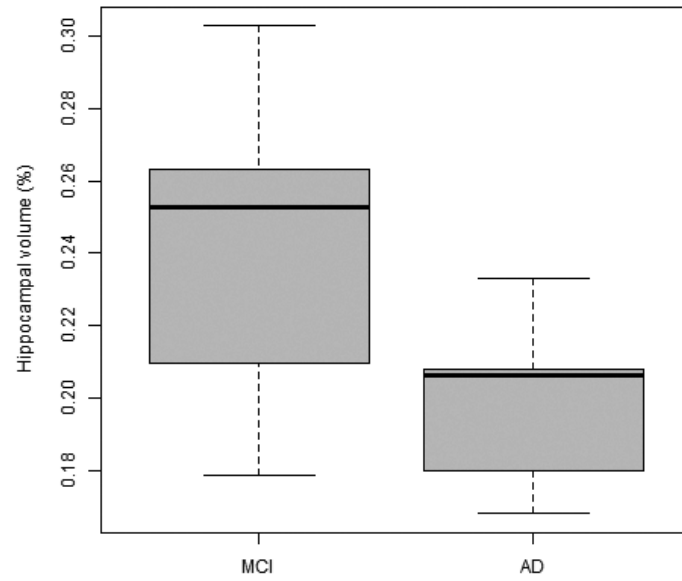

SUPPLEMENTARY FIGURE 11. Manhattan plot of the cerebrospinal fluid phosphorylated tau and amyloid-β ratio association analysis in the Alzheimer's disease methylomic profile. The blue horizontal line indicates the genome-wide significance threshold (0.05 / # probes in analysis). Vertical black lines indicate differentially methylated regions as determined with *comb-p*, using a seeding *p*-value threshold of 0.05 and an extension window of 200 base pairs, and with more than two probes and a Šidák-adjusted *p*-value below 0.05.

SUPPLEMENTARY FIGURE 12. Boxplot of the mean hippocampal volume as percentage of the total intracranial volume for the mild cognitive impairment (MCI) and Alzheimer's disease (AD) groups.

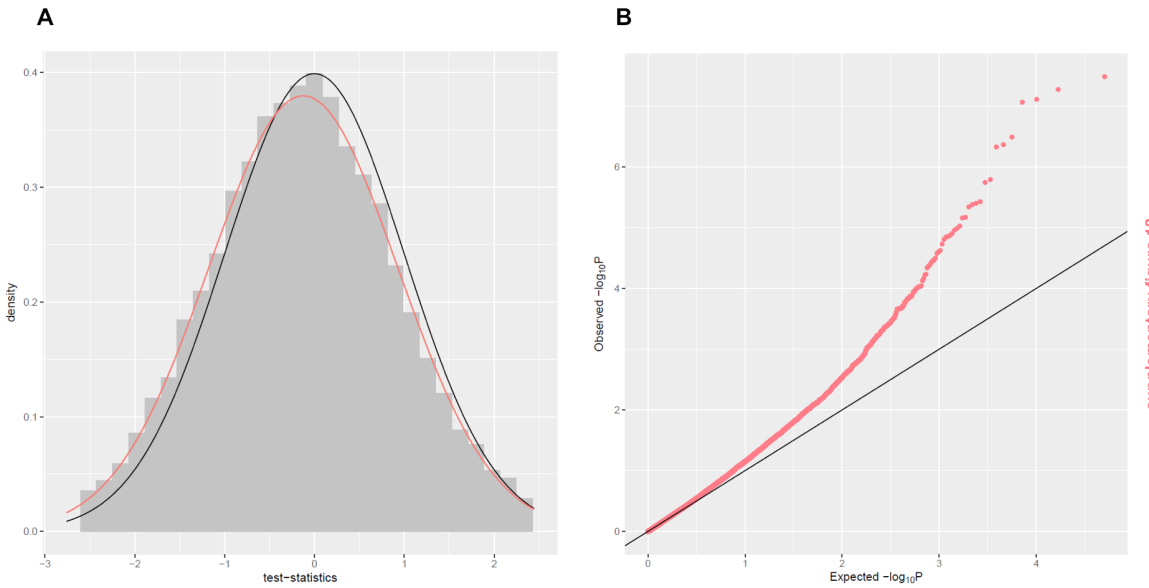

supplementary figure 13.

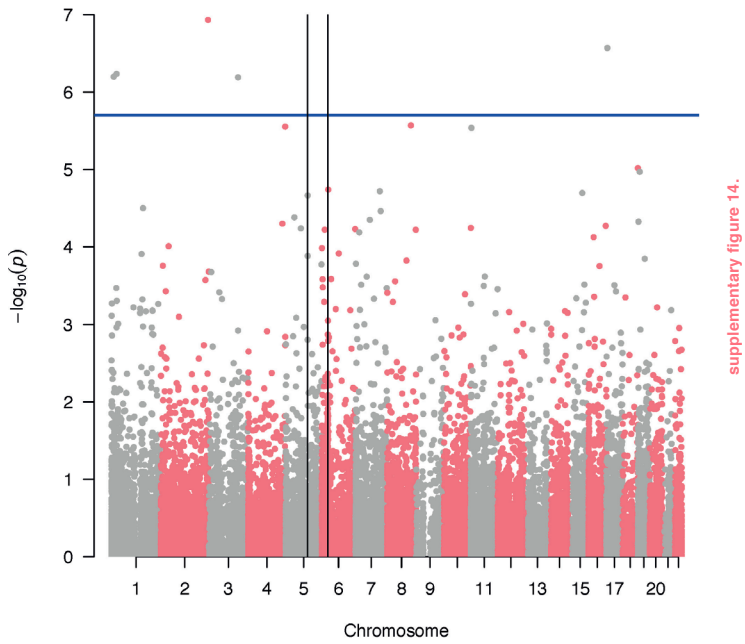

supplementary figure 14.

SUPPLEMENTARY FIGURE 13. Histogram of test-statistics showing potential bias (A) and quantile-quantile (QQ) plot showing potential inflation (B) of the mean hippocampal volume association analysis in the Alzheimer's disease methylomic profile. The pink line in A represents the fit of the empirical null distribution and the black line the fit of the mixture of the empirical null distribution, the proportion of positively associated features, and the proportion negatively associated features, both estimated as described in [33]. The estimated bias and inflation was -0.12 and 1.1, respectively.

SUPPLEMENTARY FIGURE 14. Manhattan plot of the mean hippocampal volume association analysis in the Alzheimer's disease methylomic profile. The blue horizontal line indicates the genome-wide significance threshold (0.05 / # probes in analysis). Vertical black lines indicate differentially methylated regions as determined with *comb-p*, using a seeding *p*-value threshold of 0.05 and an extension window of 200 base pairs, and with more than two probes and a Šidák-adjusted *p*-value below 0.05.

supplementary table 1.

ID	Description	Genes in term	Genes altered	*P*	FDR
Biological processes					
GO:0009887	animal organ morphogenesis	936	76	6.79E-04	9.86E-01
GO:0007417	central nervous system development	838	71	7.79E-04	9.86E-01
GO:0035883	enteroendocrine cell differentiation	27	7	8.83E-04	9.86E-01
GO:0007399	nervous system development	1994	143	1.20E-03	9.86E-01
GO:0060560	developmental growth involved in morphogenesis	191	24	1.50E-03	9.86E-01
GO:0048589	developmental growth	525	47	1.55E-03	9.86E-01
GO:0048812	neuron projection morphogenesis	503	50	1.69E-03	9.86E-01
GO:0007409	axonogenesis	379	40	1.72E-03	9.86E-01
GO:0001845	phagolysosome assembly	10	4	1.83E-03	9.86E-01
GO:0060191	regulation of lipase activity	77	10	2.10E-03	9.86E-01
Cellular components					
GO:0032153	cell division site	52	9	2.17E-03	9.86E-01
GO:0032155	cell division site part	52	9	2.17E-03	9.86E-01
GO:0005887	integral component of plasma membrane	1490	87	5.49E-03	1.00E+00
GO:0031226	intrinsic component of plasma membrane	1548	88	1.20E-02	1.00E+00
GO:0031519	PcG protein complex	41	6	1.92E-02	1.00E+00
GO:0031430	M band	21	4	2.67E-02	1.00E+00
GO:0032154	cleavage furrow	43	6	2.96E-02	1.00E+00
GO:0097610	cell surface furrow	43	6	2.96E-02	1.00E+00
GO:0030667	secretory granule membrane	80	8	3.08E-02	1.00E+00
GO:0005732	small nucleolar ribonucleoprotein complex	18	3	3.16E-02	1.00E+00
Molecular functions					
GO:0001223	transcription coactivator binding	10	4	2.17E-03	9.86E-01
GO:0043274	phospholipase binding	16	4	6.43E-03	1.00E+00
GO:1990837	sequence-specific double-stranded DNA binding	668	51	6.61E-03	1.00E+00
GO:0043565	sequence-specific DNA binding	988	70	8.48E-03	1.00E+00
GO:0001158	enhancer sequence-specific DNA binding	77	10	9.84E-03	1.00E+00
GO:0043014	alpha-tubulin binding	21	4	9.97E-03	1.00E+00
GO:0001221	transcription cofactor binding	22	5	1.00E-02	1.00E+00
GO:0000977	RNA polymerase II regulatory region sequence-specific DNA binding	558	43	1.08E-02	1.00E+00
GO:0001012	RNA polymerase II regulatory region DNA binding	559	43	1.10E-02	1.00E+00
GO:0003690	double-stranded DNA binding	739	54	1.11E-02	1.00E+00

SUPPLEMENTARY TABLE 1. Top 10 GO terms for each ontology, enriched by genes with altered DNA methylation in relation to Alzheimer's disease. **ABBREVIATIONS:** FDR, false discovery rate adjusted *p*-values; GO, Gene Ontology.

supplementary table 2.

ID	Description	Genes in term	Genes altered	Gene names	*P*	FDR
hsa04950	maturity onset diabetes of the young	26	4	*NEUROD1*; *NKX2-2*; *NKX6-1*; *PAX6*	1.00E-02	9.13E-01
hsa00512	mucin type O-glycan biosynthesis	31	4	*B3GNT6*; *GALNT1*; *GALNTL6*; *GALNT9*	1.31E-02	9.13E-01
hsa05034	alcoholism	180	12	*HIST3H2BB*; *GNG4*; *NPY*; *NTRK2*; *H2AFY2*; *PRKACA*; *BDNF*; *SLC6A3*; *HIST1H2AJ*; *HIST1H2BM*; *HDAC10*; *HIST3H2A*	2.02E-02	9.13E-01
hsa00130	ubiquinone and other terpenoid-quinone biosynthesis	11	1	*VKORC1*	2.85E-02	9.13E-01
hsa03018	RNA degradation	77	6	*DCP1B*; *ENO3*; *PABPC3*; *PFKL*; *PABPC4*; *RQCD1*	3.07E-02	9.13E-01
hsa04921	oxytocin signaling pathway	153	13	*MYL9*; *ADCY3*; *ADCY7*; *EGFR*; *GUCY1A2*; *KCNJ12*; *MEF2C*; *MYLK*; *NFATC1*; *NFATC2*; *PRKACA*; *TRPM2*; *CAMK2B*	3.94E-02	9.13E-01
hsa00600	sphingolipid metabolism	47	4	*LASS1*; *LASS6*; *UGT8*; *LASS4*	4.10E-02	9.13E-01
hsa05012	Parkinson's disease	142	8	*NDUFB6*; *NDUFS3*; *PARK2*; *PRKACA*; *NDUFA4L2*; *SLC6A3*; *SNCA*; *UBE2G2*	4.42E-02	9.13E-01
hsa04810	regulation of actin cytoskeleton	212	16	*MYL9*; *NCKAP1*; *DIAPH1*; *EGFR*; *FGFR3*; *FGFR2*; *CYFIP1*; *FGF20*; *MYH10*; *MYLK*; *PDGFRA*; *PTK2*; *VAV2*; *PIP5K1B*; *ITGA8*; *BCAR1*	4.43E-02	9.13E-01
hsa04350	TGF-beta signaling pathway	84	7	*E2F5*; *ID3*; *NBL1*; *SMURF2*; *TFDP1*; *TGFBR1*; *GDF5*	4.80E-02	9.13E-01

SUPPLEMENTARY TABLE 2. Top 10 KEGG pathways, enriched by genes with altered DNA methylation in relation to Alzheimer's disease.
ABBREVIATIONS: FDR, false discovery rate adjusted *p*-values; KEGG, Kyoto Encyclopedia of Genes and Genomes.

supplementary table 3.

ID	Description	Genes in term	Genes altered	*P*	FDR
Biological processes					
GO:0007156	homophilic cell adhesion via plasma membrane adhesion molecules	105	27	6.74E-06	4.27E-02
GO:0098742	cell-cell adhesion via plasma-membrane adhesion molecules	143	30	3.46E-05	1.10E-01
GO:0072073	kidney epithelium development	98	21	6.05E-05	1.25E-01
GO:0072009	nephron epithelium development	72	17	7.92E-05	1.25E-01
GO:0035136	forelimb morphogenesis	32	10	1.91E-04	2.26E-01
GO:0001822	kidney development	179	29	2.15E-04	2.26E-01
GO:0048704	embryonic skeletal system morphogenesis	69	15	3.14E-04	2.39E-01
GO:0072006	nephron development	89	18	3.63E-04	2.39E-01
GO:0009954	proximal/distal pattern formation	24	8	3.83E-04	2.39E-01
GO:0030182	neuron differentiation	804	92	3.99E-04	2.39E-01
Cellular components					
GO:0005887	integral component of plasma membrane	908	89	1.10E-03	3.01E-01
GO:0031226	intrinsic component of plasma membrane	941	91	1.69E-03	3.70E-01
GO:0005578	proteinaceous extracellular matrix	215	29	2.66E-03	5.27E-01
GO:0044304	main axon	44	9	7.66E-03	7.94E-01
GO:0033267	axon part	140	19	8.23E-03	8.01E-01
GO:0034702	ion channel complex	177	21	1.54E-02	9.43E-01
GO:0005615	extracellular space	639	57	2.02E-02	1.00E+00
GO:0044420	extracellular matrix component	86	13	2.45E-02	1.00E+00
GO:0043596	nuclear replication fork	20	4	2.64E-02	1.00E+00
GO:0005743	mitochondrial inner membrane	255	23	3.02E-02	1.00E+00
Molecular functions					
GO:0022843	voltage-gated cation channel activity	88	16	9.51E-04	2.74E-01
GO:0005509	calcium ion binding	412	51	1.21E-03	3.20E-01
GO:0005244	voltage-gated ion channel activity	123	19	1.59E-03	3.70E-01
GO:0022832	voltage-gated channel activity	123	19	1.59E-03	3.70E-01
GO:0022892	substrate-specific transporter activity	646	64	1.70E-03	3.70E-01
GO:0022891	substrate-specific transmembrane transporter activity	548	55	3.28E-03	6.11E-01
GO:0008528	G-protein coupled peptide receptor activity	75	12	3.46E-03	6.11E-01
GO:0005215	transporter activity	744	70	3.63E-03	6.11E-01
GO:0001653	peptide receptor activity	76	12	3.71E-03	6.11E-01
GO:0022836	gated channel activity	208	26	4.67E-03	6.87E-01

SUPPLEMENTARY TABLE 3. Top 10 GO terms for each ontology, enriched by genes with altered DNA methylation in relation to MMSE score.
ABBREVIATIONS: FDR, false discovery rate adjusted *p*-values; GO, Gene Ontology; MMSE, mini-mental state examination.

supplementary table 4.

ID	Description	Genes in term	Genes altered	Gene names	*P*	FDR
hsa04722	neurotrophin signaling pathway	119	12	*SH2B2*; *SHC2*; *HRAS*; *MATK*; *MAP3K3*; *NTRK2*; *PDPK1*; *PIK3R2*; *BAX*; *RPS6KA2*; *BDNF*; *TP73*	2.48E-03	7.51E-01
hsa05016	Huntington's disease	193	14	*AP2S1*; *COX6C*; *UQCRQ*; *HIP1*; *TBPL2*; *NDUFB5*; *NDUFS3*; *BAX*; *BDNF*; *CREB3L2*; *VDAC2*; *DNAL1*; *CASP8*; *DNAH17*	8.74E-03	7.51E-01
hsa05033	nicotine addiction	40	5	*CHRNA7*; *GABRA2*; *GABRD*; *SLC17A6*; *CACNA1B*	1.02E-02	7.51E-01
hsa04931	insulin resistance	107	10	*CRTC2*; *FOXO1*; *SLC27A1*; *PDPK1*; *PIK3R2*; *PRKCZ*; *RPS6KA2*; *CREB3L2*; *NR1H2*; *GFPT2*	1.23E-02	7.51E-01
hsa04974	protein digestion and absorption	90	8	*COL1A2*; *COL11A2*; *COL12A1*; *SLC1A1*; *SLC9A3*; *COL14A1*; *COL18A1*; *COL21A1*	1.82E-02	7.51E-01
hsa00072	synthesis and degradation of ketone bodies	10	1	*OXCT2*	2.16E-02	7.51E-01
hsa04320	dorso-ventral axis formation	28	4	*NOTCH3*; *NOTCH4*; *ETV7*; *PIWIL2*	2.38E-02	7.51E-01
hsa00730	thiamine metabolism	16	2	*AK3L1*; *ALPI*	2.43E-02	7.51E-01
hsa00563	glycosylphos-phatidylinositol (GPI)-anchor biosynthesis	25	3	*PIGV*; *PIGY*; *PIGL*	2.69E-02	7.51E-01
hsa00062	fatty acid elongation	25	3	*MECR*; *ELOVL6*; *ELOVL7*	3.31E-02	7.51E-01

SUPPLEMENTARY TABLE 4. Top 10 KEGG pathways, enriched by genes with altered DNA methylation in relation to MMSE score.
ABBREVIATIONS: FDR, false discovery rate adjusted *p*-values; KEGG, Kyoto Encyclopedia of Genes and Genomes; MMSE, mini-mental state examination.

supplementary table 5.

ID	Description	Genes in term	Genes altered	*P*	FDR
Biological processes					
GO:0048665	neuron fate specification	24	8	4.98E-04	1.00E+00
GO:0001709	cell fate determination	29	9	7.71E-04	1.00E+00
GO:2000463	positive regulation of excitatory postsynaptic potential	18	7	9.51E-04	1.00E+00
GO:0021517	ventral spinal cord development	33	9	1.38E-03	1.00E+00
GO:0021515	cell differentiation in spinal cord	41	10	2.35E-03	1.00E+00
GO:0042733	embryonic digit morphogenesis	45	11	2.49E-03	1.00E+00
GO:0060579	ventral spinal cord interneuron fate commitment	11	5	2.53E-03	1.00E+00

SUPPLEMENTARY TABLE 5. Top 10 GO terms for each ontology, enriched by genes with altered DNA methylation in relation to CSF ptau:Aβ42.
ABBREVIATIONS: Aβ42, amyloid-β 1-42; CSF, cerebrospinal fluid; FDR, false discovery rate adjusted *p*-values; GO, Gene Ontology; ptau, phosphorylated tau.

supplementary table 5. (continued)

ID	Description	Genes in term	Genes altered	*P*	FDR
GO:0060581	cell fate commitment involved in pattern specification	11	5	2.53E-03	1.00E+00
GO:0050961	detection of temperature stimulus involved in sensory perception	11	5	3.19E-03	1.00E+00
GO:0050965	detection of temperature stimulus involved in sensory perception of pain	11	5	3.19E-03	1.00E+00
Cellular components					
GO:0005887	integral component of plasma membrane	908	86	4.32E-03	1.00E+00
GO:0031226	intrinsic component of plasma membrane	941	88	6.23E-03	1.00E+00
GO:0044445	cytosolic part	131	16	1.52E-02	1.00E+00
GO:0005581	collagen trimer	52	9	1.86E-02	1.00E+00
GO:0043197	dendritic spine	81	12	3.58E-02	1.00E+00
GO:0044309	neuron spine	81	12	3.58E-02	1.00E+00
GO:0043209	myelin sheath	99	12	3.68E-02	1.00E+00
GO:0097542	ciliary tip	29	5	4.64E-02	1.00E+00
GO:0044459	plasma membrane part	1464	123	5.66E-02	1.00E+00
GO:0043235	receptor complex	198	22	5.86E-02	1.00E+00
Molecular functions					
GO:0005085	guanyl-nucleotide exchange factor activity	201	31	7.07E-04	1.00E+00
GO:0030674	protein binding, bridging	100	16	2.96E-03	1.00E+00
GO:0005088	Ras guanyl-nucleotide exchange factor activity	153	23	5.89E-03	1.00E+00
GO:0060090	binding, bridging	110	16	9.48E-03	1.00E+00
GO:0008528	G-protein coupled peptide receptor activity	75	11	1.01E-02	1.00E+00
GO:0001653	peptide receptor activity	76	11	1.06E-02	1.00E+00
GO:0005198	structural molecule activity	375	39	1.32E-02	1.00E+00
GO:0030159	receptor signaling complex scaffold activity	19	5	1.99E-02	1.00E+00
GO:0016763	transferase activity, transferring pentosyl groups	30	5	3.40E-02	1.00E+00
GO:0001637	G-protein coupled chemoattractant receptor activity	12	3	3.59E-02	1.00E+00

supplementary table 6.

ID	Description	Genes in term	Genes altered	Gene names	*P*	FDR
hsa04910	insulin signaling pathway	138	13	*EIF4E1B*; *SHC2*; *MKNK2*; *HK3*; *HRAS*; *PDPK1*; *PIK3R2*; *PRKAA1*; *PRKCZ*; *RPTOR*; *SOCS2*; *PPP1R3E*; *TRIP10*	5.06E-03	5.26E-01
hsa03320	PPAR signaling pathway	72	6	*CPT1A*; *DBI*; *ACSL1*; *ACAA1*; *PDPK1*; *RXRA*	1.12E-02	5.26E-01
hsa04510	focal adhesion	199	18	*MYL9*; *COL9A1*; *ITGA11*; *FLT1*; *PIP5K1C*; *SHC2*; *LAMA1*; *PARVB*; *HRAS*; *MYLK4*; *MYLK*; *PDGFA*; *PDPK1*; *PIK3R2*; *RELN*; *TNXB*; *VAV2*; *ITGA8*	1.50E-02	5.26E-01
hsa04150	mTOR signaling pathway	151	14	*RNF152*; *LPIN1*; *EIF4E1B*; *GRB10*; *HRAS*; *PDPK1*; *ATP6V1B1*; *PIK3R2*; *PRKAA1*; *RPTOR*; *WNT6*; *WNT7A*; *MAPKAP1*; *FZD4*	1.70E-02	5.26E-01
hsa00072	synthesis and degradation of ketone bodies	10	1	*BDH1*	2.02E-02	5.26E-01
hsa00071	Fatty acid degradation	44	4	*CPT1A*; *ACSL1*; *ACAA1*; *ACADS*	2.35E-02	5.26E-01
hsa04022	cGMP-PKG signaling pathway	163	14	*MEF2B*; *MRVI1*; *MYL9*; *ADCY3*; *ADRB1*; *GNA12*; *MYLK4*; *LOC729991-MEF2B*; *MYLK*; *FXYD2*; *NPR1*; *BDKRB2*; *SLC8A3*; *CACNA1C*	2.40E-02	5.26E-01
hsa04930	type II diabetes mellitus	46	6	*HK3*; *PDX1*; *PIK3R2*; *PRKCZ*; *CACNA1C*; *SOCS2*	2.40E-02	5.26E-01
hsa00520	amino sugar and nucleotide sugar metabolism	48	4	*GMDS*; *HK3*; *UGDH*; *GFPT2*	2.46E-02	5.26E-01
hsa00360	phenylalanine metabolism	17	2	*ALDH3B1*; *IL4I1*	2.63E-02	5.26E-01

SUPPLEMENTARY TABLE 6. Top 10 KEGG pathways, enriched by genes with altered DNA methylation in relation to CSF ptau:Aβ42.
ABBREVIATIONS: Aβ42, amyloid-β 1-42; CSF, cerebrospinal fluid; FDR, false discovery rate adjusted *p*-values; KEGG, Kyoto Encyclopedia of Genes and Genomes; ptau, phosphorylated tau.

supplementary table 7.

ID	Description	Genes in term	Genes altered	*P*	FDR
Biological processes					
GO:0071875	adrenergic receptor signaling pathway	13	6	4.35E-04	8.29E-01
GO:0050954	sensory perception of mechanical stimulus	99	18	4.54E-04	8.29E-01
GO:0097435	fibril organization	15	6	5.62E-04	8.29E-01
GO:0002456	T cell mediated immunity	34	9	6.84E-04	8.29E-01
GO:0032098	regulation of appetite	12	5	7.62E-04	8.29E-01
GO:0007605	sensory perception of sound	88	16	7.86E-04	8.29E-01
GO:0021545	cranial nerve development	33	9	1.75E-03	1.00E+00
GO:1903037	regulation of leukocyte cell-cell adhesion	154	22	2.30E-03	1.00E+00
GO:0008306	associative learning	52	10	2.38E-03	1.00E+00
GO:0014850	response to muscle activity	14	5	2.45E-03	1.00E+00
Cellular components					
GO:0005578	proteinaceous extracellular matrix	215	28	3.76E-03	1.00E+00
GO:0005615	extracellular space	639	56	1.27E-02	1.00E+00
GO:0031082	BLOC complex	12	3	1.71E-02	1.00E+00
GO:0005871	kinesin complex	34	6	1.84E-02	1.00E+00
GO:0005884	actin filament	49	9	2.02E-02	1.00E+00
GO:0008076	voltage-gated potassium channel complex	64	10	2.46E-02	1.00E+00
GO:0034705	potassium channel complex	65	10	2.58E-02	1.00E+00
GO:0031226	intrinsic component of plasma membrane	941	80	2.81E-02	1.00E+00
GO:0005887	integral component of plasma membrane	908	77	2.90E-02	1.00E+00
GO:0030864	cortical actin cytoskeleton	37	6	3.15E-02	1.00E+00
Molecular functions					
GO:0005179	hormone activity	54	10	1.46E-03	1.00E+00
GO:0004888	transmembrane signaling receptor activity	503	50	4.23E-03	1.00E+00
GO:0043236	laminin binding	17	5	4.51E-03	1.00E+00
GO:0005001	transmembrane receptor protein tyrosine phosphatase activity	14	5	8.08E-03	1.00E+00
GO:0019198	transmembrane receptor protein phosphatase activity	14	5	8.08E-03	1.00E+00
GO:0035064	methylated histone binding	31	7	9.83E-03	1.00E+00
GO:0099600	transmembrane receptor activity	535	51	9.97E-03	1.00E+00
GO:0038023	signaling receptor activity	575	54	1.01E-02	1.00E+00
GO:0043394	proteoglycan binding	18	5	1.21E-02	1.00E+00
GO:0008066	glutamate receptor activity	21	5	1.34E-02	1.00E+00

SUPPLEMENTARY TABLE 7. Top 10 GO terms for each ontology, enriched by genes with altered DNA methylation in relation to hippocampal volume.
ABBREVIATIONS: FDR, false discovery rate adjusted *p*-values; GO, Gene Ontology.

supplementary table 8.

ID	Description	Genes in term	Genes altered	Gene names	*P*	FDR
hsa05033	nicotine addiction	40	6	*SLC17A8*; *GABRA1*; *GABRA5*; *GRIN1*; *GRIN2A*; *SLC17A6*	1.96E-03	5.97E-01
hsa04024	cAMP signaling pathway	198	16	*ADCY3*; *ADRB2*; *GLI3*; *GRIN1*; *GRIN2A*; *NFATC1*; *ATP1B2*; *NPR1*; *ATP2B4*; *PDE4D*; *GHRL*; *FXYD1*; *BRAF*; *VAV2*; *VIPR2*; *CREB5*	8.00E-03	8.70E-01
hsa04610	complement and coagulation cascades	79	5	*CD55*; *F2RL2*; *CD46*; *THBD*; *C1QC*	1.23E-02	8.70E-01
hsa00760	nicotinate and nicotinamide metabolism	29	4	*NT5C2*; *NT5C3*; *NADSYN1*; *NAPRT1*	1.64E-02	8.70E-01
hsa04672	intestinal immune network for IgA production	49	4	*HLA-DMB*; *CCL25*; *CXCL12*; *TNFSF13*	1.65E-02	8.70E-01
hsa04974	protein digestion and absorption	90	8	*COL1A1*; *COL5A1*; *COL9A1*; *SLC6A19*; *KCNQ1*; *ATP1B2*; *SLC8A3*; *SLC9A3*	1.88E-02	8.70E-01
hsa04080	neuroactive ligand-receptor interaction	278	16	*ADRB2*; *F2RL2*; *GABRA1*; *GABRA5*; *GRIK3*; *GRIN1*; *GRIN2A*; *GRM7*; *GRM8*; *MTNR1A*; *NMBR*; *AVPR1A*; *PTGFR*; *TACR2*; *TBXA2R*; *VIPR2*	2.93E-02	8.70E-01
hsa04970	salivary secretion	90	7	*ADCY3*; *CST3*; *ADRB2*; *KCNMA1*; *ATP1B2*; *ATP2B4*; *SLC4A2*	3.38E-02	8.70E-01
hsa04940	type I diabetes mellitus	43	4	*HLA-DMB*; *HLA-E*; *ICA1*; *PTPRN2*	3.78E-02	8.70E-01
hsa04120	ubiquitin mediated proteolysis	137	10	*RHOBTB2*; *NEDD4L*; *RCHY1*; *PARK2*; *UBR5*; *UBE2D2*; *CUL3*; *TRIP12*; *UBE3C*; *CDC20*	4.29E-02	8.70E-01

SUPPLEMENTARY TABLE 8. Top 10 KEGG pathways, enriched by genes with altered DNA methylation in relation to hippocampal volume.
ABBREVIATIONS: FDR, false discovery rate adjusted *p*-values; KEGG, Kyoto Encyclopedia of Genes and Genomes.

IDENTIFICATION OF PRE-CLINICAL METHYLOMIC BLOOD MARKERS ASSOCIATED WITH CONVERSION TO ALZHEIMER'S DISEASE

ROY **LARDENOIJE**[A], MARKUS **LEBER**[B], EHSAN **PISHVA**[A,C], BART P.F. **RUTTEN**[A], DANIËL L.A. **VAN DEN HOVE**[A,D], ALFREDO **RAMIREZ**[B]

[A]SCHOOL FOR MENTAL HEALTH AND NEUROSCIENCE (MHENS), DEPARTMENT OF PSYCHIATRY AND NEUROPSYCHOLOGY, MAASTRICHT UNIVERSITY, UNIVERSITEITSSINGEL 50, 6200 MD MAASTRICHT, THE NETHERLANDS
[B]GERMAN CENTER FOR NEURODEGENERATIVE DISEASES (DZNE), BONN, GERMANY
[C]UNIVERSITY OF EXETER MEDICAL SCHOOL, UNIVERSITY OF EXETER, EXETER, UK.
[D]LABORATORY OF TRANSLATIONAL NEUROSCIENCE, DEPARTMENT OF PSYCHIATRY, PSYCHOSOMATICS AND PSYCHOTHERAPY, UNIVERSITY OF WUERZBURG, FUECHSLEINSTRASSE 15, 97080 WUERZBURG, GERMANY

Abstract

Previous studies have made a solid case for the entanglement of epigenetic processes in the etiopathogenesis of Alzheimer's disease (AD). However, these investigations have mainly focused on the direct comparison of AD cases and healthy controls. The present study employs a longitudinal design, including only healthy aged individuals without signs of dementia at baseline, subdivided into converters to AD dementia (n = 55) and non-converters (n = 44) at follow-up ~4.5 years later. In this sample, blood methylomic profiles of converters and non-converters were compared at baseline to identify differences in DNA methylation associated with subsequent conversion to AD, before the presence of clinical symptoms. Additionally, time-related methylomic changes were compared between converters and non-converters in a group by time interaction analysis, to reveal differences in methylomic changes that may dynamically signify conversion to dementia or, alternatively, protective mechanisms preventing such a conversion. The comparison between converters and non-converters at baseline led to the identification of 35 differentially methylated positions (DMPs), including one in the AD-susceptibility gene *HLA-DRB5*, 43 differentially methylated regions (DMRs), including one located in *OXT*, which was recently shown to exhibit altered DNA methylation in postmortem brain samples of patients with AD. Additionally, 113 DMPs and 3 DMRs showed different time-related methylation patterns between converters and controls, also including a DMP in *HLA-DRB5* and one in another human leukocyte antigen gene, *HLA-DQA1*. Whilst these findings provide important evidence for epigenetic involvement in the etiopathogenesis of AD, they furthermore are a solid basis for further investigations into the diagnostic and prognostic value of blood methylomic markers, and give preliminary insight into which genes may be involved in the stages before the development of clinical dementia, or, alternatively, resilience to conversion.

KEYWORDS: Alzheimer's disease; preclinical; epigenetics; DNA methylation; blood

9.1. Introduction

Alzheimer's disease (AD) is a progressive neurodegenerative disorder with a complex, as of yet not well understood, etiology [1, 2]. A distinction can be made between early-onset familial AD and the far more common late-onset sporadic variant of AD [3]. While both variants have a strong genetic origin, the relationship between genetic risk factors and disease development remains elusive, particularly for the sporadic variant [4]. It is therefore thought that a combination of genetic and environmental factors is responsible not only for triggering, but also for determining the pace of disease pathogenesis. In recent years, epigenetics has risen as an important player in AD, although it remains to be unveiled whether its role is that of an innocent bystander or one of the main kingpins [5–7]. Nevertheless, where genetic factors can identify persons at risk for developing AD, epigenetic markers may offer more dynamic views on trajectories of (biological) change and therefore a more timely insight into the very early stages of AD, perhaps even before any clinical symptoms arise. Identifying disease-predicting biological profiles before the appearance of clinical manifestations may give potential treatments a better timeframe to successfully impede, or even halt disease progression [8, 9]. Additionally, due the dynamic nature of epigenetics, identification of epigenetic profiles associated with the pathogenesis of the disease may also open novel therapeutic avenues [10, 11].

Previous studies implicating epigenetic dysregulation on various levels in AD have laid important groundwork, but focus mainly on directly comparing AD patients and healthy controls, or the association of epigenetic markers with mainstay hallmarks such as amyloid beta and phosphorylated tau [5, 6, 12]. The current study uses blood samples from the AgeCoDe study, comprising a large aging cohort of elderly (>75 years, n = 3,327) who had no signs of dementia at baseline and were monitored across the conversion to AD over time [13]. This allowed for the post-hoc selection of a group of controls that did not develop dementia over the course of ~4,5 years and a group of converters that had developed clinical AD at follow-up. Using this design, converters and non-converting controls could be compared at a stage before the development of clinical dementia, to gain insight into the blood methylomic profile associated with this preclinical stage. Additionally, time-related methylomic changes could be compared between converters and controls, to identify rapidly changing sites of DNA methylation that reflect the latest stages in the development of clinical AD.

9.2. Methods

9.2.1. Subjects

A subsample of 99 individuals aged above 75 years was selected from the German Study on Ageing, Cognition and Dementia in Primary Care Patients (AgeCoDe) cohort, based on the criteria outlined below (Table 1) [13]. Of these, 55 were converters, who showed no signs of dementia at baseline, had DNA samples available at baseline and follow-up (after 4.5 years), and were diagnosed with AD dementia at follow-up. The remaining 44 subjects constitute the control group and had to adhere to the same criteria, except that they should have no signs of dementia both at baseline and follow-up. The groups were matched for age, gender, and *APOE* genotype. The presence of dementia was assessed in all subjects with the Structured Interview for Diagnosis of Dementia of Alzheimer Type, Multi-infarct Dementia, and Dementia of Other Etiology (SIDAM) [14], and the diagnosis of AD was based on the criteria of the National Institute of Neurological and Communicative Disorders and Stroke and the Alzheimer's Disease and Related Disorders Association (NINCDS-ADRDA) [15], a score of 4 or higher on the Global Deterioration Scale (GDS) [16], and a Clinical Dementia Rating (CDR) of 1 [17]. DNA samples from whole blood were used to determine the methylomic profile at baseline and follow-up with the HumanMethylation450 BeadChip (450K BeadChip; Illumina, San Diego, CA, USA).

table 1.

	N	Gender (female / male)	Age at baseline (mean ± SD)
Converters	55	17 / 38	82.33 ± 3.52
Controls	44	12 / 32	81.14 ± 3.10
Total	99	29 / 70	81.80 ± 3.38

TABLE 1. Sample overview.
ABBREVIATIONS: SD, standard deviation.

9.2.2. Processing of array data

All data processing and analysis was performed in the statistical programming environment R (version 3.3.2) [18], running on SUSE Linux Enterprise Server 11 (SUSE LINUX GmbH, Nürnberg, Germany). The *MethylAid* package (version 1.6.2) [19] was used to detect outlying samples based on control probes on the array. Raw IDAT files were loaded into R using the *minfi* package (version 1.18.6) [20]. The 'pfilter' function of the *wateRmelon* package (version 1.17.0) [21] was used for probe filtering; probes with readings from less than 3 beads in 5% or

more of the samples, and probes with a detection *p*-value above 0.05 in at least 1% of the samples were removed. Additionally, samples with more than 1% probes with a detection *p*-value greater than 0.05 were excluded. After removal of probes based on technical performance, probes overlapping SNPs (common in Europe) and repeats, cross-reacting probes, and probes with mapping issues as recommended by Zhou et al. [22] were also removed. The removed set of probes ('MASK.general.EUR') was included in the *DNAmArray* package ('hm450.manifest.pop.GoNL'; version 0.0.2) [23]. Normalization was done according to the dasen method [24], as incorporated in the *wateRmelon* package. Additional quality control was performed by comparing the reported with the predicted gender (using the 'getSex.DNAmArray' function) and by visual inspection of a dendrogram after clustering the samples. For clustering, hierarchical clustering was performed with the 'hclust' function from the *fastcluster* package (version 1.1.22) [25]. Probes were annotated using the 'TxDb.Hsapiens.UCSC.hg19.knownGene' database, retrieved with the 'cpgInfo' function from *DNAmArray* and gene, with additional gene feature information added manually, as described by Price et al. [26].

9.2.3. Data analysis

To account for the heterogeneity of cell types in whole blood, cellular components were estimated for CD4+ and CD8+ T cells, B cells, monocytes, granulocytes, and natural killer cells using the 'estimateCellCounts' function of *minfi* [27, 28].

M-values were used for all subsequent analyses [29], calculated with the 'beta2m' function of *lumi* (version 2.27.3) [30], and probes targeting the X and Y chromosomes were excluded. Beta values are reported as percentages. Mean DNA methylation levels were determined for each individual by averaging the values of all probes, after which the converters and controls were compared at baseline and follow-up using linear regression.

Association analyses were performed with the *limma* package (version 3.28.21) [31]. To find methylation sites that (i) distinguish converters from controls at baseline and (ii) sites that show alternative time-related changes for converters and controls, a model was constructed with M-values as outcome and a factor variable with four levels (control at baseline, converter at baseline, control at follow-up, and converter at follow-up), as main outcome. As covariates were included age, gender, chip barcode, position on the chip, and the blood cell type estimates. Correlation between samples from the same individual were determined

with ‘duplicateCorrelation’ from *limma* and added to the ‘lmFit’ *limma* function, used for fitting the model, to account for the within-subject comparisons between baseline and follow-up. After fitting the model, contrasts were determined (i) between converters and controls at baseline, and (ii) between the differences between converters and controls at baseline and at follow-up, and empirical Bayes moderation of the test statistics was applied [39]. Results were then adjusted for bias and inflation using the empirical null distribution with the *bacon* package (version 1.3.5) [32]. Probes with a Benjamini-Hochberg false discovery rate (FDR) corrected *p*-value below 0.05 signified differentially methylated positions (DMPs). The changes over time of the DMPs identified in the group by time interaction analysis were also investigated with *limma* for the converters and non-converters separately to identify sites that only change in one group (as opposed to differences in the magnitude of change) and which may therefore signify sites particularly involved in the progression of dementia, or resilience against such progression.

The results of the association analysis were subsequently used to determine differentially methylated regions (DMRs) with *comb-p* [41], with a seeding *p*-value of 0.05 and an extension distance of 200 base pairs. Only regions with a corrected *p*-value below 0.05 and comprising at least two probes were termed DMRs. *Comb-p* corrects for multiple testing with the Šidák method. As for the DMPs from the group by time interaction analysis, the DMRs were also investigated separately for converters and non-converters.

To investigate the potential biological impact of the altered methylomic profiles, probes were ranked based on a combined *p*-value and effect size score, and used for a Gene Ontology (GO) and Kyoto Encyclopedia of Genes and Genomes (KEGG) gene set enrichment analysis. The top 1000 probes, based on the combined ranking, were used as input for the enrichment analysis, which was performed with the *missMethyl* package (version 1.6.2), using modified versions of the ‘gometh’ function for the GO analysis and ‘gsameth’ function for the KEGG analysis. This package was chosen because it takes into account that genes are not covered by the same amount of probes, possibly leading to bias [42, 43]. All probes included in the *limma* analysis were used as background list for the enrichment analyses. The results were filtered to only include GO terms with between 10 and 2000 genes, and KEGG pathways consisting of more than 10 genes (the largest KEGG pathway contains 1272 genes).

9.3. Results

Out of the 198 samples (99 baseline and 99 follow-up), 28 did not pass the stringent quality control (13 converters and 15 controls) and due to the longitudinal design, the matching samples from the same individuals also had to be excluded, leaving a total of 142 samples. Supplementary Figure 1 shows a density and boxplot of the raw beta values, and Supplementary Figure 2 shows these for the normalized beta values. After processing, 430,904 probes remained for the analyses. No differences in global DNA methylation were found between converters and controls at both timepoints (controls baseline = 51.19%, converters baseline = 51.25%, p = 8.97E-01; controls follow-up = 51.22%, converters follow-up = 51.22%, p = 9.55E-01).

9.3.1. Methylomic differences before the development of dementia

After determination of the contrast between converters to AD dementia and controls at baseline, *bacon* detected and adjusted for a bias of -0.042 and inflation of 0.96 (Supplementary Figure 3). Following FDR correction, 35 DMPs were identified, the top 3 of which were annotated to *HLA-DRB5*, *TBX2*, and *PCDHB5*, and *ADGRD1* and *HLA-DRB5* were associated with multiple DMPs (2 and 4, respectively) (Table 2; Supplementary Figure 4). In addition to the DMPs, 43 DMRs were detected, with the top 3 DMRs located in *PRRT1*, *OXT*, and *CACNA2D2* (Table 3; Supplementary Figure 4).

The top 1000 probes for the gene set enrichment analyses were annotated to 760 unique genes. After FDR correction, 68 enriched GO terms were found, with a strong representation of plasma membrane components and related processes such as transmembrane transport, but also terms related to synaptic functioning (Table 4). As for KEGG, 12 pathways were enriched, many relating to the immune system or related diseases, including diabetes mellitus type I, but also a pathway related to the glutamatergic synapse (Table 5).

table 2.

Probe	Gene	Region	ES	SE	*P*	FDR
cg14531663	*HLA-DRB5*	3'UTR	1.14	0.20	7.48E-09	2.08E-03
cg04304333	*TBX2*		0.46	0.08	1.14E-08	2.08E-03
cg13601275	*PCDHB5*	1st Exon	1,00	0.18	1.45E-08	2.08E-03
cg06493930	*GAS2*	5'UTR; 1st Exon	-1.16	0.21	2.32E-08	2.12E-03
cg05871254	*HS3ST3B1*	Body	-0.83	0.15	2.46E-08	2.12E-03
cg19746397	*LHX3*	Body	0.89	0.16	3.43E-08	2.34E-03
cg22670759	*CACNA2D2*	Body	0.58	0.11	3.80E-08	2.34E-03
cg21191810	*CEP85L*	TSS1500	1.24	0.23	6.69E-08	3.41E-03
cg13782301	*HLA-DRB5*	3'UTR	0.73	0.14	7.12E-08	3.41E-03
cg18114294	*KIAA1614*		0.51	0.10	9.34E-08	4.03E-03
cg17272563	*HLA-DRB5*	3'UTR	0.61	0.11	1.16E-07	4.48E-03
cg26827033	*ADGRD1*	Body	0.40	0.07	1.25E-07	4.48E-03
cg00386456	*PTH2*	Body	0.95	0.18	2.56E-07	8.49E-03
cg26270027	*TECTA*	Body	-0.92	0.18	3.14E-07	9.11E-03
cg08182160	*PDE2A*	1st Exon; 5'UTR	-0.87	0.17	3.27E-07	9.11E-03
cg11051095	*ADGRD1*	Body	-0.58	0.11	3.38E-07	9.11E-03
cg08549605	*ADGRA1*		-0.52	0.10	4.59E-07	1.16E-02
cg23264547	*EXT2*	Body	-0.55	0.11	5.37E-07	1.29E-02
cg10664768	*ZBTB46*	Body	-1.04	0.21	6.65E-07	1.51E-02
cg00223593	*ALG10*		0.65	0.13	8.37E-07	1.80E-02
cg09415485	*CDH13*	Body	-0.83	0.17	1.23E-06	2.53E-02
cg14915854	*ARHGAP1*	TSS200	-0.77	0.16	1.39E-06	2.73E-02
cg25203916	*TRIM63*	Body	-0.33	0.07	1.55E-06	2.91E-02
cg07482373	*MAPK12*	TSS200	-0.41	0.09	1.64E-06	2.93E-02
cg08530537	*DPEP3*	1st Exon; 5'UTR	1.07	0.22	1.70E-06	2.93E-02
cg21232671	*NKX2-8*		1.12	0.24	2.02E-06	3.26E-02
cg12275981	*TLR5*	5'UTR	0.48	0.10	2.04E-06	3.26E-02
cg27545611	*GNG12-AS1*	TSS1500	0.72	0.15	2.18E-06	3.36E-02
cg03654598	*SHANK1*	Body	-0.67	0.14	2.45E-06	3.63E-02
cg04200224	*SCGN*	TSS200	0.45	0.09	2.58E-06	3.71E-02
cg24029819	*PTPRN2*	Body	0.85	0.18	2.82E-06	3.91E-02
cg18243760	*HLA-DRB5*	3'UTR	0.58	0.12	3.07E-06	3.96E-02
cg17100218	*SMAD2*		0.41	0.09	3.09E-06	3.96E-02
cg06247406	*GRIK2*	TSS200	0.53	0.11	3.13E-06	3.96E-02
cg21571166	*ZIC1*	3'UTR	0.99	0.21	3.92E-06	4.82E-02

TABLE 2. DMPs of the baseline methylome-wide association analysis.
ABBREVIATIONS: DMPs, differentially methylated positions; ES, effect size; FDR, false discovery rate adjusted *p*-values; SE, standard error; TSS, transcription start site; UTR, untranslated region.

table 3.

Position	Gene	Region	# probes	*P*	Šidák
chr6:32116538-32116995	*PRRT1*	Exon; 3'UTR	15	5.81E-31	5.48E-28
chr20:3052115-3052346	*OXT*	TSS; 5'UTR; CDS	8	7.55E-16	1.45E-12
chr3:50487955-50488231	*CACNA2D2*	Intron	4	1.14E-15	1.73E-12
chr6:72130539-72130800	*LINC01626*	Exon	9	1.18E-15	2.02E-12
chr12:75785089-75785296	*GLIPR1L2*	Intron; CDS; Exon	5	4.63E-13	9.64E-10
chr6:118973309-118973354	*CEP85L*	Intron	3	1.47E-12	1.41E-08

TABLE 3. DMRs of the baseline methylome-wide association analysis.
ABBREVIATIONS: CDS, coding DNA sequence; chr, chromosome; DMRs, differentially methylated regions; Šidák, Šidák-corrected *p*-values; TSS, transcription start site; UTR, untranslated region.

table 3. (continued)

Position	Gene	Region	# probes	*P*	Šidák
chr6:31846769-31847029	*SLC44A4*	TSS; Exon; 5'UTR	8	2.30E-12	3.81E-09
chr1:68517177-68517274	*GNG12-AS1*; *DIRAS3*	Intron; Exon; 5'UTR	4	1.49E-11	6.63E-08
chr6:25652381-25652408	*SCGN*	Intergenic	6	1.97E-11	3.14E-07
chr5:140700449-140700639	*TAF7*	Intergenic	7	2.75E-10	6.24E-07
chr18:45275452-45275568	*SMAD2*	Intergenic	2	3.64E-10	1.35E-06
chr12:75784855-75784885	*GLIPR1L2*	Exon; 5'UTR	4	8.55E-10	1.23E-05
chr6:32053600-32053749	*TNXB*	CDS	5	1.51E-09	4.36E-06
chr19:44324856-44324952	*LYPD5*	Intergenic	6	9.76E-09	4.38E-05
chr10:29698447-29698471	*SVIL-AS1*	Exon	5	1.24E-08	2.22E-04
chr15:90039794-90039823	*RHCG*	Exon; 5'UTR; TSS	5	1.63E-08	2.43E-04
chr3:170304031-170304046	*LOC101928583*	Intron	2	3.07E-08	8.81E-04
chr6:32223076-32223115	*LOC101929163*	Exon	4	4.86E-08	5.36E-04
chr1:223316219-223316273	*TLR5*	Intron; 5'UTR	3	5.97E-08	4.76E-04
chr2:177503592-177503640	*LINC01117*	Intron	3	8.44E-08	7.57E-04
chr18:13611370-13611490	*LDLRAD4*	TSS; Exon; 5'UTR; Intron	5	8.81E-08	3.16E-04
chr5:68710808-68710832	*MARVELD2*	Intergenic	4	8.83E-08	1.58E-03
chr17:37123669-37123910	*FBXO47*	Intergenic	5	9.77E-08	1.75E-04
chr10:90343166-90343286	*RNLS*	Intergenic	6	1.15E-07	4.11E-04
chr3:10806047-10806176	*LINC00606*	Intergenic	4	1.19E-07	3.98E-04
chr1:212688916-212688998	*LINC01740*	Intergenic	3	2.15E-07	1.13E-03
chr6:101846767-101846806	*GRIK2*	Intergenic	5	2.54E-07	2.80E-03
chr17:14201680-14201745	*HS3ST3B1*	Intergenic	2	2.91E-07	1.93E-03
chr8:57360586-57360614	*LOC101929415*	Intron	2	3.89E-07	5.97E-03
chr8:110656096-110656167	*SYBU*	Intron; 5'UTR	2	3.98E-07	2.42E-03
chr17:29297380-29297459	*RNF135*	Intergenic	5	4.39E-07	2.39E-03
chr20:30073521-30073577	*LINC00028*	Intergenic	4	5.93E-07	4.55E-03
chr2:177004975-177004999	*HOXD-AS2*	Intergenic	2	6.99E-07	1.25E-02
chr20:36148954-36149122	*BLCAP*	Intron; 5'UTR; TSS; Exon	10	8.58E-07	2.20E-03
chr2:242904738-242904794	*LINC01237*	Intron	3	9.19E-07	7.04E-03
chr7:93205237-93205296	*CALCR*	Intergenic	4	9.75E-07	7.09E-03
chr14:102990211-102990252	*ANKRD9*	Intergenic	2	1.75E-06	1.82E-02
chr20:61668419-61668470	*LINC01749*	Intron	2	2.23E-06	1.87E-02

table 3. (continued)

Position	Gene	Region	# probes	*P*	Šidák
chr16:68014338-68014375	*DPEP3*	5'UTR; CDS	2	2.30E-06	2.64E-02
chr14:65239327-65239358	*SPTB*	CDS	2	3.23E-06	4.39E-02
chr17:8905741-8905776	*NTN1*	Intergenic	2	3.56E-06	4.29E-02
chr12:132293656-132293703	*SFSWAP*	Intergenic	2	4.67E-06	4.19E-02
chr7:102553369-102553438	*FBXL13*; *LRRC17*	Intron; Exon; 5'UTR	3	8.06E-06	4.91E-02

table 4.

ID	Description	Ontology	Genes in term	Genes altered	Genes in term with DMP / DMR	*P*	FDR
GO:0007156	homophilic cell adhesion via plasma membrane adhesion molecules	BP	149	42	*PCDHB5*; *CDH13*	1.91E-21	1.50E-17
GO:0098742	cell-cell adhesion via plasma-membrane adhesion molecules	BP	214	43	*PCDHB5*; *CDH13*	1.42E-17	5.60E-14
GO:0031226	intrinsic component of plasma membrane	CC	1557	98	*HS3ST3B1*; *TLR5*; *SHANK1*; *PTPRN2*; *GRIK2*; *RHCG*; *CALCR*; *SPTB*	2.32E-11	4.80E-08
GO:0005887	integral component of plasma membrane	CC	1498	95	*HS3ST3B1*; *TLR5*; *SHANK1*; *PTPRN2*; *GRIK2*; *RHCG*; *CALCR*	2.44E-11	4.80E-08
GO:0005509	calcium ion binding	MF	663	61	*PCDHB5*; *CDH13*; *SCGN*	3.05E-11	4.80E-08
GO:0007268	chemical synaptic transmission	BP	564	47	*PCDHB5*; *CACNA2D2*; *SHANK1*; *PTPRN2*; *GRIK2*; *OXT*	5.25E-07	0.00046
GO:0098916	anterograde trans-synaptic signaling	BP	564	47	*PCDHB5*; *CACNA2D2*; *SHANK1*; *PTPRN2*; *GRIK2*; *OXT*	5.25E-07	0.00046
GO:0099536	synaptic signaling	BP	564	47	*PCDHB5*; *CACNA2D2*; *SHANK1*; *PTPRN2*; *GRIK2*; *OXT*	5.25E-07	0.00046
GO:0099537	trans-synaptic signaling	BP	564	47	*PCDHB5*; *CACNA2D2*; *SHANK1*; *PTPRN2*; *GRIK2*; *OXT*	5.25E-07	0.00046

TABLE 4. Enriched GO terms by genes displaying altered DNA methylation at baseline.

ABBREVIATIONS: DMP, differentially methylated position; DMR, differentially methylated region; FDR, false discovery rate adjusted *p*-values; GO, Gene Ontology.

table 4. (continued)

ID	Description	Ontology	Genes in term	Genes altered	Genes in term with DMP / DMR	*P*	FDR
GO:0034220	ion transmembrane transport	BP	890	59	*CACNA2D2*; *PDE2A*; *SHANK1*; *GRIK2*; *RHCG*	7.04E-07	0.000555
GO:0098609	cell-cell adhesion	BP	1090	71	*PCDHB5*; *CDH13*; *ARHGAP1*	1.29E-06	0.000927
GO:0006811	ion transport	BP	1336	76	*CACNA2D2*; *PDE2A*; *SHANK1*; *GRIK2*; *OXT*; *SLC44A4*; *RHCG*	1.61E-06	0.000998
GO:0007267	cell-cell signaling	BP	1418	86	*PCDHB5*; *CACNA2D2*; *SHANK1*; *PTPRN2*; *GRIK2*; *OXT*	1.64E-06	0.000998
GO:0055085	transmembrane transport	BP	1225	70	*CACNA2D2*; *PDE2A*; *SHANK1*; *GRIK2*; *SLC44A4*; *RHCG*	4.87E-06	0.00274
GO:0071556	integral component of lumenal side of endoplasmic reticulum membrane	CC	26	8		8.29E-06	0.00408
GO:0098553	lumenal side of endoplasmic reticulum membrane	CC	26	8		8.29E-06	0.00408
GO:0006812	cation transport	BP	901	55	*CACNA2D2*; *PDE2A*; *SLC44A4*; *RHCG*	9.22E-06	0.00428
GO:0008324	cation transmembrane transporter activity	MF	574	40	*CACNA2D2*; *PDE2A*; *SLC44A4*; *RHCG*	1.07E-05	0.00467
GO:0050877	neurological system process	BP	1129	57	*TECTA*; *SHANK1*; *GRIK2*; *OXT*; *MARVELD2*	1.13E-05	0.00469
GO:0042613	MHC class II protein complex	CC	14	6		2.05E-05	0.00809
GO:0098655	cation transmembrane transport	BP	655	43	*CACNA2D2*; *PDE2A*; *RHCG*	3.13E-05	0.0118
GO:0045202	synapse	CC	678	51	*PDE2A*; *SHANK1*; *SCGN*; *PTPRN2*; *GRIK2*; *PRRT1*; *OXT*	3.39E-05	0.0121
GO:0015075	ion transmembrane transporter activity	MF	759	47	*CACNA2D2*; *PDE2A*; *GRIK2*; *SLC44A4*; *RHCG*	3.61E-05	0.0124
GO:0006140	regulation of nucleotide metabolic process	BP	201	19	*PDE2A*; *CALCR*	4.48E-05	0.0146
GO:0042611	MHC protein complex	CC	23	7		4.62E-05	0.0146

ID	Description	Onto-logy	Genes in term	Genes altered	Genes in term with DMP / DMR	*P*	FDR
GO:0007610	behavior	BP	518	39	*SHANK1*; *GRIK2*; *ZIC1*; *OXT*	5.73E-05	0.0174
GO:0030658	transport vesicle membrane	CC	150	16	*SCGN*; *PTPRN2*	6.32E-05	0.0185
GO:0007155	cell adhesion	BP	1606	88	*PCDHB5*; *TECTA*; *CDH13*; *ARHGAP1*; *TNXB*; *LYPD5*	7.02E-05	0.0194
GO:0005261	cation channel activity	MF	288	25	*CACNA2D2*; *PDE2A*	7.12E-05	0.0194
GO:0003008	system process	BP	1799	83	*CACNA2D2*; *TECTA*; *PDE2A*; *SHANK1*; *GRIK2*; *OXT*; *MARVELD2*	7.47E-05	0.0196
GO:0022610	biological adhesion	BP	1611	88	*PCDHB5*; *TECTA*; *CDH13*; *ARHGAP1*; *TNXB*; *LYPD5*	8.00E-05	0.0203
GO:0022891	substrate-specific transmembrane transporter activity	MF	884	50	*CACNA2D2*; *PDE2A*; *GRIK2*; *SLC44A4*; *RHCG*	9.68E-05	0.0238
GO:0031644	regulation of neurological system process	BP	62	10	*OXT*	9.98E-05	0.0238
GO:0034702	ion channel complex	CC	263	24	*CACNA2D2*; *SHANK1*; *GRIK2*	1.04E-04	0.0241
GO:1900542	regulation of purine nucleotide metabolic process	BP	195	18	*PDE2A*; *CALCR*	1.14E-04	0.0256
GO:0022836	gated channel activity	MF	307	26	*CACNA2D2*; *GRIK2*	1.25E-04	0.0267
GO:0030001	metal ion transport	BP	753	46	*CACNA2D2*; *PDE2A*	1.28E-04	0.0267
GO:0099600	transmembrane receptor activity	MF	1171	51	*TLR5*; *PTPRN2*; *GRIK2*; *CALCR*	1.29E-04	0.0267
GO:0046873	metal ion transmembrane transporter activity	MF	399	30	*CACNA2D2*; *PDE2A*	1.41E-04	0.0281
GO:0030669	clathrin-coated endocytic vesicle membrane	CC	44	8		1.42E-04	0.0281
GO:0007193	adenylate cyclase-inhibiting G-protein coupled receptor signaling pathway	BP	69	10		1.48E-04	0.0284
GO:0022890	inorganic cation transmembrane transporter activity	MF	482	33	*CACNA2D2*; *PDE2A*	1.61E-04	0.0302
GO:0044057	regulation of system process	BP	474	34	*CACNA2D2*; *OXT*	1.72E-04	0.0311

table 4. (continued)

table 4. (continued)

ID	Description	Ontology	Genes in term	Genes altered	Genes in term with DMP / DMR	*P*	FDR
GO:0045334	clathrin-coated endocytic vesicle	CC	59	9		1.73E-04	0.0311
GO:0022838	substrate-specific channel activity	MF	412	30	*CACNA2D2*; *PDE2A*; *GRIK2*	1.85E-04	0.0324
GO:0098797	plasma membrane protein complex	CC	486	35	*CACNA2D2*; *SHANK1*; *GRIK2*	1.91E-04	0.0326
GO:0015267	channel activity	MF	441	31	*CACNA2D2*; *PDE2A*; *GRIK2*	1.94E-04	0.0326
GO:0022803	passive transmembrane transporter activity	MF	442	31	*CACNA2D2*; *PDE2A*; *GRIK2*	2.00E-04	0.0328
GO:0007416	synapse assembly	BP	126	16	*PCDHB5*; *OXT*	2.13E-04	0.0342
GO:0004888	transmembrane signaling receptor activity	MF	1120	48	*TLR5*; *PTPRN2*; *GRIK2*; *CALCR*	2.17E-04	0.0342
GO:0019233	sensory perception of pain	BP	90	11	*OXT*	2.60E-04	0.0392
GO:0022892	substrate-specific transporter activity	MF	1059	55	*CACNA2D2*; *PDE2A*; *GRIK2*; *SLC44A4*; *RHCG*; *CALCR*	2.63E-04	0.0392
GO:0098662	inorganic cation transmembrane transport	BP	595	38	*CACNA2D2*; *PDE2A*	2.64E-04	0.0392
GO:0044306	neuron projection terminus	CC	113	13	*PTPRN2*; *GRIK2*; *OXT*	2.74E-04	0.0401
GO:0051349	positive regulation of lyase activity	BP	58	9	*CALCR*	3.01E-04	0.0427
GO:0044708	single-organism behavior	BP	372	29	*SHANK1*; *GRIK2*; *ZIC1*; *OXT*	3.05E-04	0.0427
GO:1903522	regulation of blood circulation	BP	277	23	*CACNA2D2*; *OXT*	3.09E-04	0.0427
GO:0031281	positive regulation of cyclase activity	BP	58	9	*CALCR*	3.21E-04	0.0429
GO:0005216	ion channel activity	MF	398	29	*CACNA2D2*; *PDE2A*; *GRIK2*	3.21E-04	0.0429
GO:0012507	ER to Golgi transport vesicle membrane	CC	52	8		3.58E-04	0.0468
GO:0016339	calcium-dependent cell-cell adhesion via plasma membrane cell adhesion molecules	BP	28	6	*PCDHB5*; *CDH13*	3.64E-04	0.0468
GO:0022857	transmembrane transporter activity	MF	956	51	*CACNA2D2*; *PDE2A*; *GRIK2*; *SLC44A4*; *RHCG*	3.68E-04	0.0468
GO:0042391	regulation of membrane potential	BP	331	26	*SHANK1*; *GRIK2*	3.78E-04	0.0471

table 4. (continued)

ID	Description	Onto-logy	Genes in term	Genes altered	Genes in term with DMP / DMR	*P*	FDR
GO:0007188	adenylate cyclase-modulating G-protein coupled receptor signaling pathway	BP	157	14	*CALCR*	3.87E-04	0.0471
GO:0086019	cell-cell signaling involved in cardiac conduction	BP	22	6		3.93E-04	0.0471
GO:1902495	transmembrane transporter complex	CC	294	24	*CACNA2D2*; *SHANK1*; *GRIK2*	4.05E-04	0.0471
GO:0043679	axon terminus	CC	103	12	*PTPRN2*; *GRIK2*; *OXT*	4.06E-04	0.0471
GO:0045762	positive regulation of adenylate cyclase activity	BP	45	8	*CALCR*	4.07E-04	0.0471

table 5.

ID	Description	Genes in term	Genes altered	Genes in pathway with DMP / DMR	*P*	FDR
hsa05150	*Staphylococcus aureus* infection	56	7		3.50E-05	7.24E-03
hsa05320	autoimmune thyroid disease	53	7		4.76E-05	7.24E-03
hsa05310	asthma	31	5		1.19E-04	8.06E-03
hsa05330	allograft rejection	38	6		1.44E-04	8.06E-03
hsa04940	type I diabetes mellitus	43	7	*PTPRN2*	1.50E-04	8.06E-03
hsa05332	graft-versus-host disease	41	6		1.59E-04	8.06E-03
hsa05416	viral myocarditis	59	8		2.34E-04	1.02E-02
hsa04724	glutamatergic synapse	114	13	*SHANK1*; *GRIK2*	2.91E-04	1.10E-02
hsa05321	inflammatory bowel disease	65	7	*TLR5*	5.58E-04	1.80E-02
hsa05323	rheumatoid arthritis	90	8		5.94E-04	1.80E-02
hsa04672	intestinal immune network for IgA production	49	5		1.20E-03	3.16E-02
hsa00565	ether lipid metabolism	45	5		1.25E-03	3.16E-02

9.3.2. Methylomic differences during conversion to dementia

Test statistics from the timepoint by group interaction analysis had an estimated bias of 0.16 and an estimated inflation of 0.89 (Supplementary

TABLE 5. KEGG pathways enriched by genes displaying altered DNA methylation at baseline.
ABBREVIATIONS: FDR, false discovery rate adjusted *p*-values; KEGG, Kyoto Encyclopedia of Genes and Genomes.

Figure 5). 113 DMPs were identified, with one in *ATP11B*, one in *DGKD*, and one in *ATG2B* comprising the top 3 (Table 6; Supplementary Figure 6), and 3 DMRs, in *GLB1L3*, *TAF3*, and *DOC2GP* (Table 7; Supplementary Figure 6). Of the positions showing different longitudinal methylation patterns for converters and controls, 3 in *ADGRD1*, *ZBTB46*, and *ARHGAP1* also showed up as DMPs at baseline. Additionally, *HLA-DRB5* contained 4 DMPs at the baseline comparison and an additional, different DMP was detected in the group by time interaction analysis. The 113 DMPs from the group by time interaction analysis were analyzed for methylation differences between baseline and follow-up for the converters and non-converters separately. For the converters, 4 out of the 113 positions showed significant changes in methylation, interestingly all of which were hypermethylated at follow-up (Table 8). Additionally, the DMR in *DOC2GP* from the group by time interaction analysis was also detected for the converters separately ($p_{Šidák}$ = 4.80E-03). The non-converters presented with significantly altered methylation at 35 out of the 113 positions (Table 9). There was no overlap between the DMPs observed for the converters and non-converters.

None of the GO terms or KEGG pathways were significantly enriched after FDR correction for the group by time interaction analysis (Supplementary Table 1; Supplementary Table 2). However, it is interesting to note that there was overlap between the GO terms significantly enriched at baseline and those enriched with an uncorrected *p*-value < 0.05 in the interaction analysis; GO:0007267 ('cell-cell signaling'), GO:0007416 ('synapse assembly'), and GO:0045202 ('synapse').

table 6.

Probe	Gene	Region	ES	SE	*P*	FDR
cg19820921	*ATP11B*	Body	-0.77	0.13	9.15E-09	3.94E-03
cg26215113	*DGKD*	Body	0.44	0.08	3.70E-08	7.63E-03
cg04173048	*ATG2B*		0.43	0.08	5.83E-08	7.63E-03
cg26827033	*ADGRD1*	Body	-0.42	0.08	7.08E-08	7.63E-03
cg07934604	*LINC00616*		0.37	0.07	1.81E-07	1.26E-02
cg10540754	*FAM49A*	5'UTR	0.42	0.08	2.06E-07	1.26E-02
cg03049303	*C10orf76*	TSS1500	0.43	0.08	2.40E-07	1.26E-02
cg21984711	*BCL2*	3'UTR	-0.64	0.12	2.49E-07	1.26E-02
cg19282889	*KLHL25*	TSS1500	-0.43	0.08	2.64E-07	1.26E-02
cg10664768	*ZBTB46*	Body	1.10	0.22	3.80E-07	1.56E-02
ch.11.720675R	*NAT10*	Body	-0.57	0.11	4.22E-07	1.56E-02
cg26854588	*WIPF2*		0.43	0.08	4.34E-07	1.56E-02
ch.11.2495959R	*ARHGEF12*	Body	-1.00	0.20	6.65E-07	1.79E-02
cg11642909	*TRIM59*		-0.34	0.07	7.37E-07	1.79E-02
cg26577348	*NCOA3*	TSS1500	0.32	0.06	7.89E-07	1.79E-02
cg00087005	*CTBP2*	5'UTR	0.36	0.07	7.96E-07	1.79E-02
cg20576094	*ADAM21P1*	TSS1500	0.47	0.09	8.05E-07	1.79E-02
cg13126206	*LOC286059*		0.95	0.19	8.40E-07	1.79E-02
cg19536127	*C2orf61*	TSS1500	-0.44	0.09	8.66E-07	1.79E-02

TABLE 6. DMPs of the group by time interaction methylome-wide association analysis.

ABBREVIATIONS: DMPs, differentially methylated positions; ES, effect size; FDR, false discovery rate adjusted *p*-values; SE, standard error; TSS, transcription start site; UTR, untranslated region.

Probe	Gene	Region	ES	SE	*P*	FDR
cg16838132	*MIEF1*	3'UTR	-0.84	0.17	9.02E-07	1.79E-02
cg03101580	*TOLLIP*	Body	0.41	0.08	9.23E-07	1.79E-02
cg24628076	*ARAP3*	Body	-0.38	0.08	9.44E-07	1.79E-02
cg04337538	*MYCN*		-0.52	0.11	9.69E-07	1.79E-02
cg03047400	*ZFYVE1*		-0.81	0.17	9.99E-07	1.79E-02
cg27487704	*CYLD*		0.32	0.07	1.25E-06	2.15E-02
cg26207102	*TEAD1*	5'UTR	-0.67	0.14	1.38E-06	2.27E-02
cg25554183	*COBL*	Body	-0.57	0.12	1.42E-06	2.27E-02
cg04905421	*IFT140*	Body	-0.38	0.08	1.55E-06	2.36E-02
cg00005861	*SMNDC1*		-0.45	0.09	1.63E-06	2.36E-02
cg12501870	*ZNF704*		0.54	0.11	1.64E-06	2.36E-02
cg18575438	*CCDC170*		0.51	0.11	2.13E-06	2.89E-02
cg25750404	*VAMP1*	Body	-0.27	0.06	2.19E-06	2.89E-02
cg07937999	*LINC00645*		-0.51	0.11	2.26E-06	2.89E-02
cg06111454	*NFATC4*	Body	0.85	0.18	2.29E-06	2.89E-02
cg14088090	*TMEM125*	Body	-0.35	0.07	2.39E-06	2.89E-02
cg05194545	*ARHGAP12*	3'UTR	0.64	0.14	2.42E-06	2.89E-02
cg09510874	*WNK1*	1st Exon	-0.42	0.09	2.59E-06	3.01E-02
cg09506183	*ASB3*	Body; TSS1500	-0.35	0.08	2.91E-06	3.26E-02
cg10960920	*CPQ*	Body	-0.51	0.11	2.95E-06	3.26E-02
cg14337324	*PACRG*	Body	-0.33	0.07	3.09E-06	3.31E-02
cg07794500	*EMBP1*	Body	0.36	0.08	3.37E-06	3.31E-02
cg16475558	*GNAO1*	Body	-0.44	0.09	3.44E-06	3.31E-02
cg14915854	*ARHGAP1*	TSS200	0.77	0.17	3.53E-06	3.31E-02
cg01768433	*ADGRV1*	Body	0.61	0.13	3.59E-06	3.31E-02
cg13654276	*GRAMD1C*	TSS1500	-0.43	0.09	3.60E-06	3.31E-02
cg18388802	*ARVCF*	TSS200	0.43	0.09	3.66E-06	3.31E-02
cg21104351	*GLB1L3*	Body	-0.29	0.06	3.75E-06	3.31E-02
cg24251448	*AGO2*	Body	0.56	0.12	3.83E-06	3.31E-02
cg22703724	*ETS2*	TSS1500	0.72	0.16	3.95E-06	3.31E-02
cg23817292	*CCT8*	Body	-0.83	0.18	4.04E-06	3.31E-02
cg27614376	*PLCL2*		-0.69	0.15	4.05E-06	3.31E-02
cg15946545	*MRPS31*	1st Exon	1.30	0.28	4.12E-06	3.31E-02
cg10456710	*SNAP23*	5'UTR; 1st Exon	-0.74	0.16	4.18E-06	3.31E-02
cg05289055	*SOST*		0.36	0.08	4.22E-06	3.31E-02
cg26554699	*WFIKKN2*	Body	0.28	0.06	4.22E-06	3.31E-02
cg15582126	*BTBD3*		-0.56	0.12	4.37E-06	3.36E-02
cg10981736	*CTBP1*	TSS1500; 5'UTR; 1st Exon	-0.39	0.09	4.52E-06	3.42E-02
cg10527300	*COL4A1*	Body	-0.44	0.10	4.65E-06	3.44E-02
cg07608496	*MCM3AP-AS1*	Body; TSS1500	-0.50	0.11	4.71E-06	3.44E-02
cg26414731	*PSMF1*	TSS200	-0.61	0.13	5.32E-06	3.75E-02
cg11631610	*DOCK6*	Body	0.37	0.08	5.43E-06	3.75E-02
cg05879527	*DLGAP3*	Body	0.41	0.09	5.54E-06	3.75E-02
cg06151171	*NCOA1*		-0.83	0.18	5.67E-06	3.75E-02
cg23844090	*TMEM42*	Body	1.47	0.32	5.74E-06	3.75E-02
cg26824807	*GPX6*	5'UTR; 1st Exon	-0.31	0.07	5.78E-06	3.75E-02
cg08124722	*CCL7*	Body	-0.40	0.09	6.00E-06	3.75E-02
cg12764704	*PCNX2*		-0.27	0.06	6.03E-06	3.75E-02
cg00734760	*RCC1L*	TSS200	0.36	0.08	6.05E-06	3.75E-02
ch.16.1667936F	*PSMD7*		-0.50	0.11	6.12E-06	3.75E-02
cg05794244	*RNH1*	TSS1500; TSS200	-0.28	0.06	6.12E-06	3.75E-02
cg09027493	*TCP11*	TSS1500	0.28	0.06	6.21E-06	3.75E-02
cg00875096	*SLC39A10*	5'UTR	0.35	0.08	6.26E-06	3.75E-02
cg05028306	*LAP3*	TSS1500	0.37	0.08	6.84E-06	4.04E-02

table 6. (continued)

table 6. (continued)

Probe	Gene	Region	ES	SE	*P*	FDR
cg13477253	*MIR548G*	Body; TSS1500	0.33	0.07	7.17E-06	4.12E-02
cg08241225	*ATP4A*	3'UTR	-0.56	0.12	7.18E-06	4.12E-02
cg00483886	*HLA-DRB5*	5'UTR; 1st Exon; Body	0.45	0.10	7.76E-06	4.38E-02
cg17037924	*DUT*	TSS1500	-0.69	0.15	7.82E-06	4.38E-02
cg20228119	*ANKS1B*	Body	-0.31	0.07	7.99E-06	4.38E-02
cg03149565	*LEF1-AS1*	TSS1500; Body	-0.48	0.11	8.19E-06	4.38E-02
cg06801569	*HLA-DQA1*		0.92	0.21	8.23E-06	4.38E-02
cg26086731	*PHC3*	TSS1500	0.39	0.09	8.42E-06	4.38E-02
cg11203156	*OSBPL11*	5'UTR; 1st Exon	0.33	0.07	8.60E-06	4.38E-02
cg22184145	*POLR2B*	Body	-0.43	0.10	8.78E-06	4.38E-02
cg20414512	*MYOZ2*	TSS1500	-0.65	0.15	9.01E-06	4.38E-02
cg22401796	*HELT*		-0.35	0.08	9.08E-06	4.38E-02
cg07942847	*HAUS4*	Body	-0.47	0.11	9.10E-06	4.38E-02
cg00263326	*SEPT7*		0.55	0.12	9.14E-06	4.38E-02
cg20325560	*HEPACAM*	1st Exon; 3'UTR; 5'UTR	0.32	0.07	9.17E-06	4.38E-02
cg08965464	*EPHA4*	1st Exon; 5'UTR	-0.31	0.07	9.20E-06	4.38E-02
cg03105244	*NCK2*	Body	-0.51	0.12	9.28E-06	4.38E-02
cg24951140	*DUSP4*		-0.47	0.11	9.32E-06	4.38E-02
cg11414415	*TNKS1BP1*	Body	-0.52	0.12	9.36E-06	4.38E-02
cg17945358	*IGF2*		-0.34	0.08	9.48E-06	4.39E-02
cg12020639	*AHCYL1*	TSS200	0.33	0.07	9.78E-06	4.49E-02
cg02286008	*SMG1P2*	Body	-0.37	0.08	9.99E-06	4.53E-02
cg14206898	*PRKACG*	3'UTR; 1st Exon	-0.52	0.12	1.02E-05	4.58E-02
cg03946530	*PARP16*		-0.34	0.08	1.07E-05	4.74E-02
cg03761210	*NECAB3*	Body	0.30	0.07	1.08E-05	4.74E-02
cg00009834	*MRPL20*		0.24	0.05	1.10E-05	4.78E-02
cg05080566	*MIIP*	TSS200	-0.26	0.06	1.14E-05	4.86E-02
cg06206603	*SEC24C*	5'UTR	0.34	0.08	1.14E-05	4.86E-02
cg26974500	*GPBP1*	TSS1500	-0.30	0.07	1.19E-05	4.86E-02
cg06296151	*CMTM6*	3'UTR	-0.55	0.13	1.20E-05	4.86E-02
cg22396353	*GTSE1*	5'UTR; 1st Exon; TSS200	0.96	0.22	1.20E-05	4.86E-02
cg11823235	*PRR29*		-0.34	0.08	1.20E-05	4.86E-02
cg21229079	*COL4A2*	Body	0.31	0.07	1.21E-05	4.86E-02
cg04253453	*SMARCA2*	5'UTR	0.37	0.08	1.22E-05	4.86E-02
cg15077087	*COPS9*	Body	0.51	0.12	1.23E-05	4.86E-02
cg06765909	*AGO3*	1st Exon; 5'UTR	0.42	0.10	1.23E-05	4.86E-02
cg12900942	*THRAP3*	TSS1500	0.32	0.07	1.24E-05	4.86E-02
cg23374762	*TXNL1*	Body	-0.25	0.06	1.28E-05	4.96E-02
cg23090607	*MS4A7*		-0.36	0.08	1.29E-05	4.96E-02
cg03115444	*CLIP1*	Body	0.38	0.09	1.30E-05	4.97E-02

table 7.

Position	Gene	Region	# probes	*P*	Šidák
chr11:134152195-134152203	*GLB1L3*	Intron	2	1.64E-07	8.78E-03
chr10:8006646-8006678	*TAF3*	CDS	2	6.98E-07	9.35E-03
chr11:67381142-67381193	*DOC2GP*	Intron	3	9.11E-07	7.66E-03

TABLE 7. DMRs of the group by time interaction methylome-wide association analysis.

ABBREVIATIONS: CDS, coding DNA sequence; chr, chromosome; DMR, differentially methylated region; Šidák, Šidák-corrected *p*-values.

table 8.

Probe	Gene	Region	ES	SE	*P*	FDR
cg26215113	*DGKD*	Body	0.48	0.11	2.89E-05	3.26E-03
cg00009834	*MRPL20*		0.28	0.08	3.60E-04	1.94E-02
cg05194545	*ARHGAP12*	3'UTR	0.67	0.19	5.15E-04	1.94E-02
cg07934604	*LINC00616*		0.34	0.10	7.27E-04	2.06E-02

table 9.

Probe	Gene	Region	ES	SE	*P*	FDR
cg13654276	*GRAMD1C*	TSS1500	0.64	0.14	4.11E-06	4.64E-04
cg00005861	*SMNDC1*		0.58	0.14	4.07E-05	2.30E-03
cg14915854	*ARHGAP1*	TSS200	-0.97	0.25	9.29E-05	2.91E-03
cg16838132	*MIEF1*	3'UTR	0.98	0.26	1.19E-04	2.91E-03
cg10664768	*ZBTB46*	Body	-1.24	0.32	1.29E-04	2.91E-03
cg17945358	*IGF2*		0.43	0.12	2.30E-04	4.33E-03
cg23374762	*TXNL1*	Body	0.30	0.09	4.54E-04	7.33E-03
cg20325560	*HEPACAM*	1st Exon; 3'UTR; 5'UTR	-0.37	0.11	6.56E-04	9.24E-03
cg25750404	*VAMP1*	Body	0.29	0.09	7.77E-04	9.24E-03
cg25554183	*COBL*	Body	0.58	0.18	1.03E-03	9.24E-03
cg03101580	*TOLLIP*	Body	-0.41	0.12	1.04E-03	9.24E-03
cg27487704	*CYLD*		-0.33	0.10	1.06E-03	9.24E-03
cg16475558	*GNAO1*	Body	0.46	0.14	1.06E-03	9.24E-03
cg04905421	*IFT140*	Body	0.38	0.12	1.51E-03	1.22E-02
cg26827033	*ADGRD1*	Body	0.37	0.12	1.62E-03	1.22E-02
cg24251448	*AGO2*	Body	-0.56	0.18	1.73E-03	1.22E-02
cg00734760	*WBSCR16*	TSS200	-0.36	0.12	2.15E-03	1.43E-02
cg26974500	*GPBP1*	TSS1500	0.30	0.10	3.36E-03	2.05E-02
cg10540754	*FAM49A*	5'UTR	-0.35	0.12	3.69E-03	2.05E-02
cg14337324	*PACRG*	Body	0.31	0.11	3.70E-03	2.05E-02
cg12764704	*PCNX2*		0.25	0.09	3.90E-03	2.05E-02
cg19820921	*ATP11B*	Body	0.58	0.20	3.99E-03	2.05E-02
cg21104351	*GLB1L3*	Body	0.26	0.09	4.67E-03	2.29E-02
cg11203156	*OSBPL11*	5'UTR; 1st Exon	-0.31	0.11	5.19E-03	2.44E-02
cg14206898	*PRKACG*	3'UTR; 1st Exon	0.48	0.17	5.73E-03	2.59E-02
cg03049303	*C10orf76*	TSS1500	-0.34	0.13	6.57E-03	2.86E-02
cg13477253	*MIR548G*	Body; TSS1500	-0.29	0.11	7.30E-03	3.06E-02
cg10960920	*CPQ*	Body	0.43	0.16	7.71E-03	3.11E-02
cg11642909	*TRIM59*		0.27	0.10	8.40E-03	3.20E-02
cg12020639	*AHCYL1*	TSS200	-0.29	0.11	8.49E-03	3.20E-02
cg27614376	*PLCL2*		0.59	0.23	9.15E-03	3.34E-02
ch.16.1667936F	*PSMD7*		0.42	0.16	1.03E-02	3.59E-02
cg00483886	*HLA-DRB5*	5'UTR; 1st Exon; Body	-0.38	0.15	1.06E-02	3.59E-02
cg26554699	*WFIKKN2*	Body	-0.23	0.09	1.08E-02	3.59E-02
cg20228119	*ANKS1B*	Body	0.25	0.10	1.39E-02	4.50E-02

TABLE 8. DMPs of the group by time interaction methylome-wide association analysis also observed to change over time for converters specifically.
ABBREVIATIONS: DMPs, differentially methylated positions; ES, effect size; FDR, false discovery rate adjusted *p*-values; SE, standard error; UTR, untranslated region.

TABLE 9. DMPs of the group by time interaction methylome-wide association analysis also observed to change over time for non-converters specifically.
ABBREVIATIONS: DMPs, differentially methylated positions; ES, effect size; FDR, false discovery rate adjusted *p*-values; SE, standard error; TSS, transcription start site; UTR, untranslated region.

9.4. Discussion

The present work aimed to identify methylomic markers associated with conversion to AD dementia at a preclinical stage, as well as dynamic markers showing different time-related changes in converters and non-converters. A methylome-wide association study at baseline and a group by time interaction analysis revealed several DMPs and DMRs, associated with known AD risk genes, genes part of pathways previously implicated in AD, as well as novel candidate genes that merit further investigations.

Past investigations into blood DNA methylation in relation to AD is limited, mainly focusing on the direct comparison of AD cases and healthy controls [33–35]. Di Francesco et al. [33] focused on global DNA methylation levels, and observed these to be increased in late-onset AD patients. Although we did not detect differences in global methylation between converters and controls, these outcomes cannot really be compared due to the difference in methodology. The luminometric methylation assay used by Di Francesco et al. is geared towards the global quantification of DNA methylation, whereas the beadchip array used for the present work covers only a minor fraction of all possible methylation sites, but does so at a single-site resolution [36].

Tannorella et al. [37] performed a candidate-based comparison of blood DNA methylation between AD cases and healthy controls in six genes (*PSEN1*, *BACE1*, *DNMT1*, *DNMT3A*, *DNMT3B*, and *MTHFR*), related to AD pathology or DNA methylation itself, but did not find a difference in methylation levels between groups. This is in line with the current findings, as no DMPs or DMRs associated with conversion to AD were found in these genes. It may be interesting to point out that even when looking at the nominal *p*-values of all the probes (188) in these six genes, only 2 probes, both in *MTHFR*, had a *p*-value below 0.05 when comparing converters with controls at baseline, which would not survive FDR correction for 188 probes. Similarly, while looking at the group by time interaction analysis there were more probes with a nominal *p*-value below 0.05 (2 in *PSEN1*, 2 in *BACE1*, 1 in *DNMT1*, 5 in *DNMT3A*, 3 in *DNMT3B*, and 2 in *MTHFR*), none of these survive FDR correction for 188 probes.

Lunnon et al. [34], also utilizing the 450K BeadChip, identify several DMPs related to clinical AD in blood, but with minimal overlap with the present study. Both studies find a DMP in a COP9 signalosome subunit gene, although they find it in *COPS8*, and we in *COPS9*. In either case, COP9 signalosome dysfunction may be involved in dendritic spine deterioration [38], one of the early hallmarks of AD [39]. Of note, the main focus of Lunnon et al. [34] is the brain, where they find strong

evidence for the epigenetic dysregulation of *ANK1*, but they do not find evidence for altered DNA methylation of *ANK1* in the blood. We also did not detect any DMPs or DMRs in *ANK1* surviving multiple testing correction, but there were some sites in *ANK1* and *ANK2* within the top 1000 CpGs, with a nominal *p*-value below 0.05, included in the gene set enrichment analysis and occurring in various enriched terms, including GO:0045202 ("synapse"), GO:0007267 ("cell-cell signaling"), GO:0055085 ("transmembrane transport"), GO:1903522 ("regulation of blood circulation"), and GO:0042391 ("regulation of membrane potential").

Adding to the evidence of a disturbed immune system in AD, we found a DMP at baseline in *TRIM63*, and a DMP in *TRIM59* showing differential changes in methylation between controls and converters. These genes encode tripartite motif-containing proteins important for innate immunity [40]. While different *TRIM* variants, Lunnon et al. [34] find a DMP in *TRIM26* in blood of AD cases, and another study by Niikura et al. [41] implicates *TRIM11* in AD.

Several members of the solute-carrier (*SLC*) gene superfamily have been detected in relation to AD. *SLC* genes encode all manner of membrane transporters, responsible for the transmembrane transport of a wide array of compounds, including amino acids, peptides, sugars, ions, lipids, vitamins, and neurotransmitters [42]. Before the development of clinical AD, we observed a DMR in *SLC44A4*, considered to be a choline transporter [43], and in the group by time interaction analysis a DMP in *SLC39A10*, a zinc transporter in the blood-brain barrier [44], was found. Additionally, many of the GO terms found to be enriched in converters at baseline included differentially methylated *SLC* genes, including GO:0099536 ("synaptic signaling"), GO:0007267 ("cell-cell signaling"), GO:0055085 ("transmembrane transport"), GO:0050877 ("neurological system process"), GO:1903522 ("regulation of blood circulation"), and GO:0043679 ("axon terminus"), as well as the KEGG pathway hsa04724 ("Glutamatergic synapse") (Table 4 and Table 5). Comparing AD cases with controls, Lunnon et al. [34] found *SLC15C4* and *SLCO3A1* to be differentially methylated, and differentially expression in blood. Moreover, a SNP in SLC24H4 has been identified as a risk factor for AD [45].

Interestingly, *SLC44A4* is located within the human leukocyte antigen (*HLA*) super-locus and may contain an enhancer region that is also associated with *HLA-DRB5* [46, 47]. *HLA-DRB5* is one of the major genes with differential methylation found in the current study, with 4 DMPs at baseline, and 1 DMP with a different time-related pattern for converters and controls. Differential methylation of *HLA-DRB5* was also observed in the AD brain [48] and a SNP in this gene has been established as a susceptibility factor for AD [49]. Additional support for a role of *HLA*

genes in AD [50] comes from the identification of a DMP in *HLA-DQA1* in the group by time interaction analysis, and from multiple enriched GO terms at baseline including HLA genes, such as GO:0098609 (“cell-cell adhesion”), GO:0050877 (“neurological system process”), GO:0042611 (“MHC protein complex”), GO:0004888 (“transmembrane signaling receptor activity”), and in all but 2 out of the 12 enriched KEGG pathways (Table 4 and Table 5).

OXT is another gene associated with altered epigenetic regulation in AD, previously identified in the superior temporal gyrus [51] and by our group in the middle temporal gyrus (MTG) (Chapter 7), whereas now a blood DMR associated with conversion to AD was observed. Although the possible role of *OXT* in the etiopathogenesis of AD remains unknown, the identification of a DMR in this gene, identical to the one identified in the MTG, before the development of clinical symptoms indicates it may serve as a valuable early diagnostic marker.

It is thought that the first steps in the etiopathogenesis of AD start years, possibly decades before any clinical symptoms can be observed [6, 52]. The present study captures the methylomic changes associated with the final stages of disease progression, just before the development of clinical symptoms. Especially the group by time interaction analysis is, to our knowledge, a first attempt to map which genes, as far as can be detected in the blood, show altered methylation levels during the onset of dementia. The results indicate that over a period of about 4.5 years many genes show a different methylation pattern in converters and non-converting healthy controls. With a very high mean age of 81.80, both the control and converter groups fall within the extreme risk group for the development of AD [53], allowing for two, likely overlapping, interpretations of the methylomic differences between controls. They may reflect pathological changes leading up to the manifestation of dementia in the converters, or, in contrast, may represent protective mechanisms in the control group, making them resilient to the development of dementia. Both interpretations may be worthwhile for future investigations, as it may prove to be more difficult to halt disease progress, than to bolster innate mechanisms that delay the onset of clinical symptoms. Especially those DMPs also identified in the separate converter and non-converter comparisons between baseline and follow-up may be of particular interest for future studies into markers for conversion to dementia or resilience to such a conversion.

Even though the post-hoc selection design of the current study allowed for the inclusion of a sizeable group of converters, it remains a relatively small sample size for a genome-wide approach. However, to lack of similar studies focusing on the preclinical blood methylome of AD

precluded a targeted approach. Additionally, the design could have benefitted from the inclusion of clinical data at multiple timepoints to match the changes in methylation to changes in cognition, or other clinical hallmarks of AD. DNA from the blood originates from a heterogenous population of cell types, the proportions of which change during aging and may also be affected by disease, and each with their distinct epigenetic profile [27, 54, 55]. It has therefore been noted that disease- or age-related epigenetic changes in the blood may be explained by shifts in the white blood cell composition [27, 35]. The current study adjusts for these changes through the inclusion of covariates representing the most prominent white blood cell types into the model [28], even though this cannot guarantee changes in blood cell type composition had absolutely no effect on the observed methylomic changes. It should also be kept in mind that even though the 450K BeadChip covers most known genes, it actually only covers only 1.5-2% of all CpG sites, and practically none of the CpA, CpT, and CpC sites [36], meaning that it cannot be considered as truly 'genome-wide'.

Taken together, the present work offers a unique window into the methylomic profile of AD before the onset of clinical symptoms, and the critical methylomic changes that have occurred after the onset of symptoms. Thereby the results provide a compelling basis for the use of blood methylomic markers for the pre-clinical diagnosis and prognosis of AD, and provides candidate sites that can be investigated in this respect, as well as potential markers of resilience to AD dementia.

Acknowledgments

Funds have been provided by the Internationale Stichting Alzheimer Onderzoek (ISAO) grant 11532 (D.L.A.vdH.), by the ISAO grants 09552 and 13515, and the Netherlands Organization for Scientific Research (NWO), grant 916.11.086 (Veni Award) (B.P.F.R.), and by a fellowship as part of NWO grant 022.005.019, (R.L.). The funding agencies were not involved in the study design, data collection, analysis and interpretation, writing of the report, and the decision to submit the article for publication. The authors declare no conflicts of interest.

REFERENCES

[1] Yates D, McLoughlin DM. The molecular pathology of Alzheimer's disease. *Psychiatry* 2008; 7: 1–5.

[2] Godyń J, Jończyk J, Panek D, et al. Therapeutic strategies for Alzheimer's disease in clinical trials. *Pharmacol Reports* 2015; 68: 127–138.

[3] Tanzi RE. The genetics of Alzheimer disease. *Cold Spring Harb Perspect Med*; 2. Epub ahead of print 2012. DOI: 10.1101/cshperspect.a006296.

[4] Robinson M, Lee BY, Hane FT. Recent progress in Alzheimer's disease research, part 2: genetics and epidemiology. *J Alzheimers Dis* 2017; 57: 317–330.

[5] Lardenoije R, Iatrou A, Kenis G, et al. The epigenetics of aging and neurodegeneration. *Prog Neurobiol* 2015; 131: 21–64.

[6] Iatrou A, Kenis G, Rutten BPF, et al. Epigenetic dysregulation of brainstem nuclei in the pathogenesis of Alzheimer's disease: looking in the correct place at the right time? *Cellular and Molecular Life Sciences*, 2016, pp. 1–15.

[7] van den Hove D LA, Kenis G, Rutten BP. Epigenetic dysregulation in Alzheimer's disease: cause or consequence? *Epigenomics* 2014; 6: 9–11.

[8] St-Amour I, Cicchetti F, Calon F. Immunotherapies in Alzheimer's disease: Too much, too little, too late or off-target? *Acta Neuropathol* 2016; 131: 481–504.

[9] Sperling R, Mormino E, Johnson K. The evolution of preclinical Alzheimer's disease: implications for prevention trials. *Neuron* 2014; 84: 608–622.

[10] Guidotti A, Auta J, Davis JM, et al. Toward the identification of

peripheral epigenetic biomarkers of schizophrenia. *J Neurogenet* 2014; 28: 41–52.

[11] Cacabelos R, Torrellas C. Epigenetic drug discovery for Alzheimer's disease. *Expert Opin Drug Discov* 2014; 9: 1059–1086.

[12] Wen K-X, Miliç J, El-Khodor B, et al. The role of DNA methylation and histone modifications in neurodegenerative diseases: a systematic review. *PLoS One* 2016; 11: e0167201.

[13] Luck T, Riedel-Heller SG, Luppa M, et al. Risk factors for incident mild cognitive impairment - results from the German Study on Ageing, Cognition and Dementia in Primary Care Patients (AgeCoDe). *Acta Psychiatr Scand* 2010; 121: 260–272.

[14] Zaudig M, Hiller W, Geiselmann B, et al. SIDAM - Handbuch, strukturiertes Interview für die Diagnose einer Demenz vom Alzheimer-Typ, der Multiinfarkt-(oder vaskulären) Demenz und Demenzen anderer Ätiologie nach DSM III R, DSM IV and ICD 10http://pubman.mpdl.mpg.de/pubman/faces/viewItemFullPage.jsp?itemId=escidoc%3A1629566%3A1&view=EXPORT (1995, accessed 20 April 2017).

[15] McKhann G, Drachman D, Folstein M, et al. Clinical diagnosis of Alzheimer's disease: report of the NINCDS-ADRDA Work Group under the auspices of Department of Health and Human Services Task Force on Alzheimer's Disease. *Neurology* 1984; 34: 939–44.

[16] Reisberg B, Ferris SH, de Leon MJ, et al. The Global Deterioration Scale for assessment of primary degenerative dementia. *Am J Psychiatry* 1982; 139: 1136–1139.

[17] Hughes CP, Berg L, Danziger WL, et al. A new clinical scale for the staging of dementia. *Br J Psychiatry* 1982; 140: 566–72.

[18] R Core Team. R: A language and environment for statistical computing.https://www.r-project.org/ (2016).

[19] van Iterson M, Tobi EW, Slieker RC, et al. *MethylAid*: visual and interactive quality control of large Illumina 450k datasets. *Bioinformatics* 2014; 30: 3435–3437.

[20] Aryee MJ, Jaffe AE, Corrada-Bravo H, et al. Minfi: a flexible and comprehensive Bioconductor package for the analysis of Infinium DNA methylation microarrays. *Bioinformatics* 2014; 30: 1363–1369.

[21] Pidsley R, CC YW, Volta M, et al. A data-driven approach to preprocessing Illumina 450K methylation array data. *BMC Genomics* 2013; 14: 293.

[22] Zhou W, Laird PW, Shen H. Comprehensive characterization, annotation and innovative use of Infinium DNA methylation BeadChip probes. *Nucleic Acids Res* 2016; 15: gkw967.

[23] van Iterson M, Tobi E, Slieker R, et al. *DNAmArray*. Epub ahead of print 2017. DOI: https://doi.org/10.5281/zenodo.158908.

[24] Fortin J-P, Labbe A, Lemire M, et al. Functional normalization of 450k methylation array data improves replication in large cancer studies. *Genome Biol* 2014; 15: 503.

[25] Müllner D. *fastcluster*: Fast hierarchical, agglomerative clustering routines for R and Python. *J Stat Softw* 2013; 53: 1–18.

[26] Price ME, Cotton AM, Lam LL, et al. Additional annotation enhances potential for biologically-relevant analysis of the Illumina Infinium HumanMethylation450 BeadChip array. *Epigenetics Chromatin* 2013; 6: 4.

[27] Jaffe AE, Irizarry RA. Accounting for cellular heterogeneity is critical in epigenome-wide association studies. *Genome Biol* 2014; 15: R31.

[28] Houseman E, Accomando WP, Koestler DC, et al. DNA methylation arrays as surrogate measures of cell mixture distribution. *BMC Bioinformatics* 2012; 13: 86.

[29] Du P, Zhang X, Huang C-C, et al. Comparison of Beta-value and M-value methods for quantifying methylation levels by microarray analysis. *BMC Bioinformatics* 2010; 11: 587.

[30] Du P, Kibbe WA, Lin SM. *lumi*: a pipeline for processing Illumina microarray. *Bioinformatics* 2008; 24: 1547–1548.

[31] Ritchie ME, Phipson B, Wu D, et al. *limma* powers differential expression analyses for RNA-sequencing and microarray studies. *Nucleic Acids Res* 2015; 43: e47.

[32] van Iterson M, van Zwet EW, BIOS Consortium BT, et al. Controlling bias and inflation in epigenome- and transcriptome-wide association studies using the empirical null distribution. *Genome Biol* 2017; 18: 19.

[33] Di Francesco A, Arosio B, Falconi A, et al. Global changes in DNA methylation in Alzheimer's disease peripheral blood mononuclear cells. *Brain Behav Immun* 2015; 45: 139–144.

[34] Lunnon K, Smith R, Hannon E, et al. Methylomic profiling implicates cortical deregulation of *ANK1* in Alzheimer's disease. *Nat Neurosci* 2014; 17: 1164–1170.

[35] Li H, Guo Z, Guo Y, et al.

Common DNA methylation alterations of Alzheimer's disease and aging in peripheral whole blood. *Oncotarget* 2016; 7: 19089–98.

[36] Clark C, Palta P, Joyce CJ, et al. A comparison of the whole genome approach of MeDIP-seq to the targeted approach of the Infinium HumanMethylation450 BeadChip(®) for methylome profiling. *PLoS One* 2012; 7: e50233.

[37] Tannorella P, Stoccoro A, Tognoni G, et al. Methylation analysis of multiple genes in blood DNA of Alzheimer's disease and healthy individuals. Epub ahead of print 2015. DOI: 10.1016/j.neulet.2015.06.009.

[38] Djagaeva I, Doronkin S. Dual regulation of dendritic morphogenesis in *Drosophila* by the COP9 signalosome. *PLoS One* 2009; 4: e7577.

[39] Knobloch M, Mansuy IM. Dendritic spine loss and synaptic alterations in Alzheimer's disease. *Mol Neurobiol* 2008; 37: 73–82.

[40] Ozato K, Shin D-M, Chang T-H, et al. TRIM family proteins and their emerging roles in innate immunity. *Nat Rev Immunol* 2008; 8: 849–60.

[41] Niikura T, Hashimoto Y, Tajima H, et al. A tripartite motif protein TRIM11 binds and destabilizes Humanin, a neuroprotective peptide against Alzheimer's disease-relevant insults. *Eur J Neurosci* 2003; 17: 1150–8.

[42] He L, Vasiliou K, Nebert DW. Analysis and update of the human solute carrier (SLC) gene superfamily. *Hum Genomics* 2009; 3: 195–206.

[43] Mattie M, Raitano A, Morrison K, et al. The discovery and preclinical development of ASG-5ME, an antibody-drug conjugate targeting SLC44A4-positive epithelial tumors including pancreatic and prostate cancer. *Mol Cancer Ther* 2016; 15: 2679–2687.

[44] Huntley MA, Bien-Ly N, Daneman R, et al. Dissecting gene expression at the blood-brain barrier. *Front Neurosci* 2014; 8: 355.

[45] Karch CM, Goate AM. Alzheimer's disease risk genes and mechanisms of disease pathogenesis. *Biol Psychiatry* 2015; 77: 43–51.

[46] Shiina T, Hosomichi K, Inoko H, et al. The *HLA* genomic loci map: expression, interaction, diversity and disease. *J Hum Genet* 2009; 54: 15–39.

[47] GeneCards Human Gene Database. *SLC44A4*. http://www.genecards.org/cgi-bin/carddisp.pl?gene=SLC44A4 (2017, accessed 30 April 2017).

[48] Yu L, Chibnik LB, Srivastava GP, et al. Association of brain DNA methylation in *SORL1*, *ABCA7*, *HLA-DRB5*, *SLC24A4*, and *BIN1* with pathological diagnosis of Alzheimer disease. *JAMA Neurol* 2015; 72: 15.

[49] Lambert J-C, Ibrahim-Verbaas CA, Harold D, et al. Meta-analysis of 74,046 individuals identifies 11 new susceptibility loci for Alzheimer's disease. *Nat Genet* 2013; 45: 1452–1458.

[50] Steele NZR, Carr JS, Bonham LW, et al. Fine-mapping of the human leukocyte antigen locus as a risk factor for Alzheimer disease: A case-control study. *PLoS Med* 2017; 14: e1002272.

[51] Watson CT, Roussos P, Garg P, et al. Genome-wide DNA methylation profiling in the superior temporal gyrus reveals epigenetic signatures associated with Alzheimer's disease. *Genome Med* 2016; 8: 5.

[52] Lahiri DK, Maloney B. The 'LEARn' (Latent Early-life Associated Regulation) model integrates environmental risk factors and the developmental basis of Alzheimer's disease, and proposes remedial steps. *Exp Gerontol* 2010; 45: 291–296.

[53] Xu W, Ferrari C, Wang H-X. Epidemiology of Alzheimer's Disease. In: *Understanding Alzheimer's Disease*. InTech. Epub ahead of print 27 February 2013. DOI: 10.5772/54398.

[54] Reynolds LM, Taylor JR, Ding J, et al. Age-related variations in the methylome associated with gene expression in human monocytes and T cells. *Nat Commun* 2014; 5: 5366.

[55] Shad KF, Aghazadeh Y, Ahmad S, et al. Peripheral markers of Alzheimer's disease: Surveillance of white blood cells. *Synapse* 2013; 67: 541–543.

supplementary figure 1.

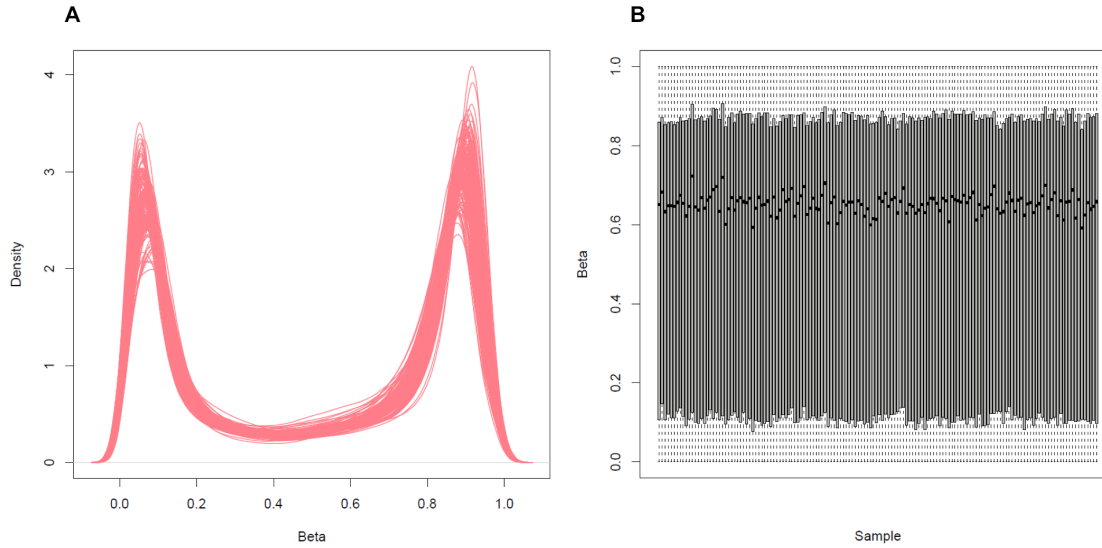

supplementary figure 2.

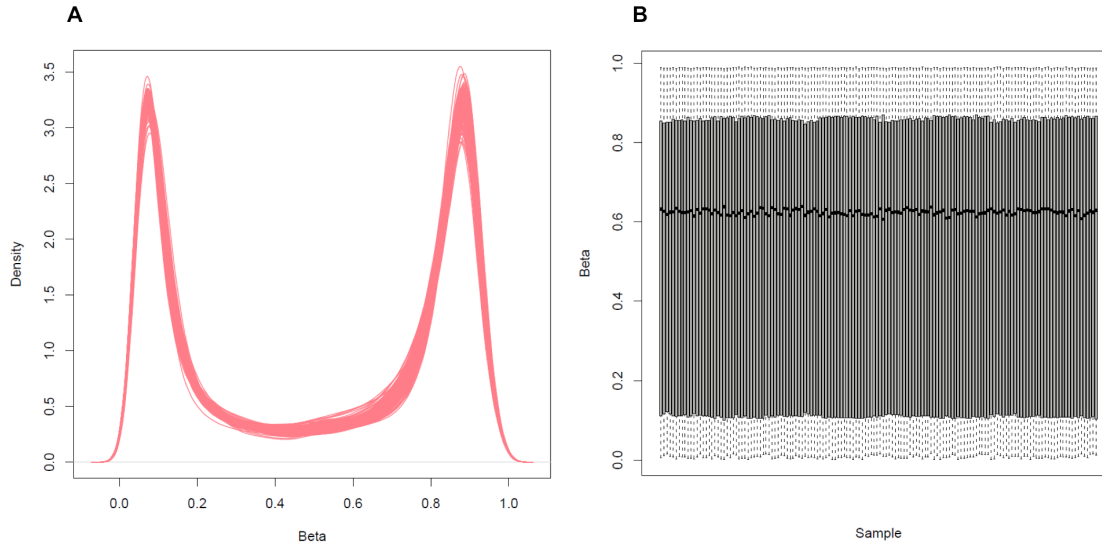

SUPPLEMENTARY DATA

SUPPLEMENTARY FIGURE 1. Density plot (A) and boxplot (B) of raw beta values. Plots include all DNA methylation probes on the Illumina HumanMethylation450 BeadChip, plotted for each sample separately.

SUPPLEMENTARY FIGURE 2. Density plot (A) and boxplot (B) of normalized beta values. Plots include DNA methylation probes passing the filtering steps, plotted for each sample separately.

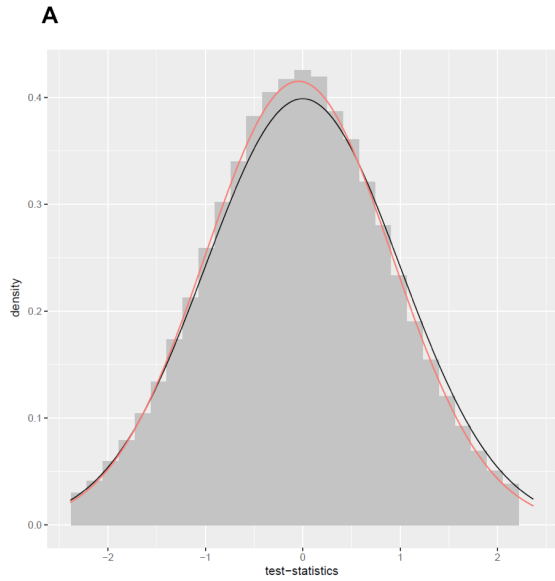

supplementary figure 3.

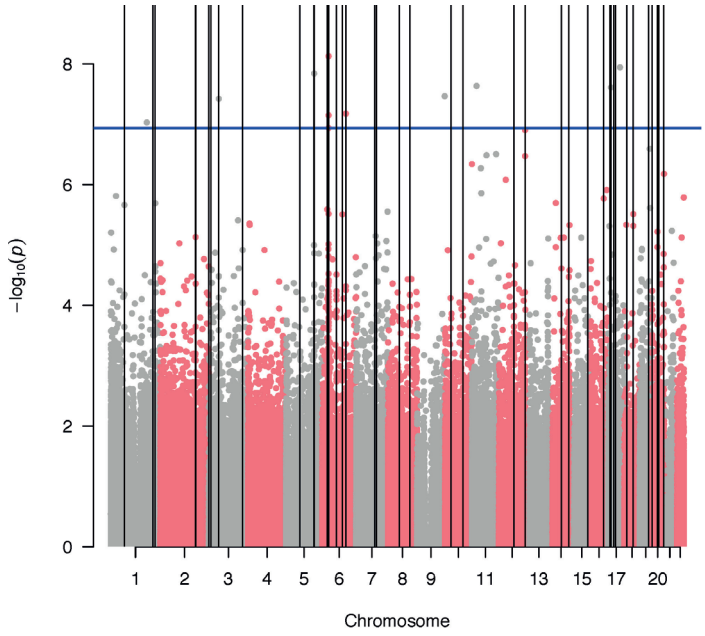

supplementary figure 4.

SUPPLEMENTARY FIGURE 3. Histogram of test-statistics showing potential bias (A) and quantile-quantile (QQ) plot showing potential inflation (B) of the methylome-wide association study results at baseline. The pink line in A represents the fit of the empirical null distribution and the black line the fit of the mixture of the empirical null distribution, the proportion of positively associated features, and the proportion of negatively associated features, both estimated as described in [32]. The estimated bias and inflation was -0.042 and 0.96, respectively.

SUPPLEMENTARY FIGURE 4. Manhattan plot of the methylome-wide association study at baseline. The blue horizontal line indicates the genome-wide significance threshold (0.05 / # probes in analysis). Vertical black lines indicate differentially methylated regions as determined with *comb-p*, using a seeding *p*-value threshold of 0.05 and an extension window of 200 base pairs, and with more than two probes and a Šidák-adjusted *p*-value below 0.05.

supplementary figure 5.

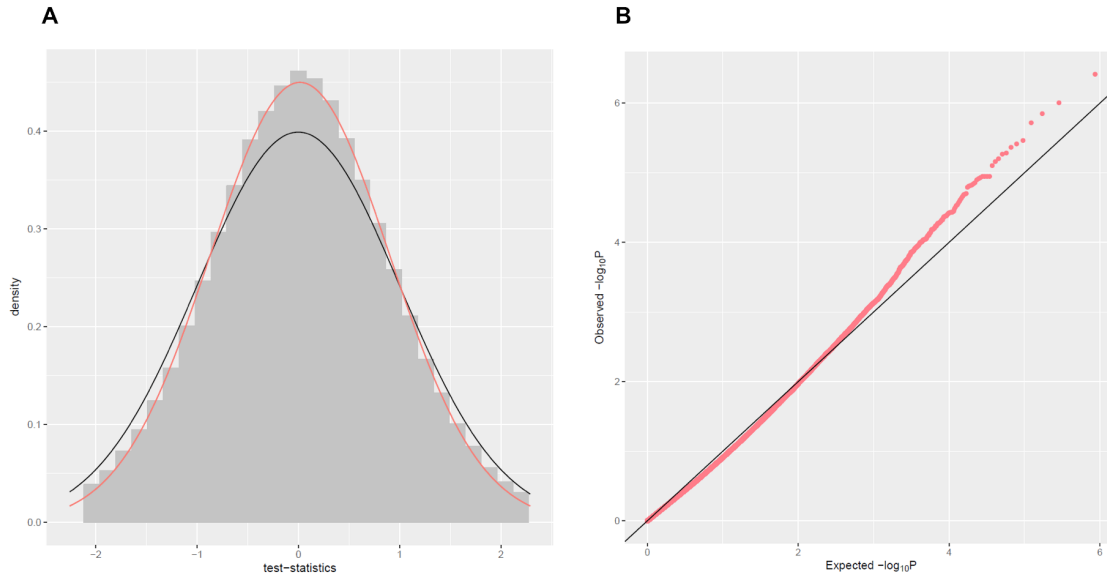

SUPPLEMENTARY FIGURE 5. Histogram of test-statistics showing potential bias (A) and quantile-quantile (QQ) plot showing potential inflation (B) of the group by time methylome-wide association analysis. The pink line in A represents the fit of the empirical null distribution and the black line the fit of the mixture of the empirical null distribution, the proportion of positively associated features, and the proportion of negatively associated features, both estimated as described in [32]. The estimated bias and inflation was 0.16 and 0.89, respectively.

supplementary figure 6.

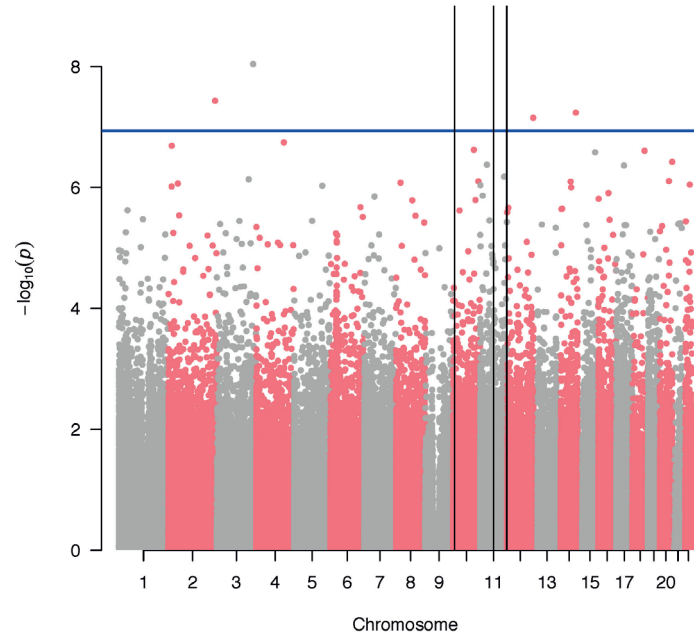

SUPPLEMENTARY FIGURE 6. Manhattan plot of the group by time interaction methylome-wide association analysis. The blue horizontal line indicates the genome-wide significance threshold (0.05 / # probes in analysis). Vertical black lines indicate differentially methylated regions as determined with *comb-p*, using a seeding *p*-value threshold of 0.05 and an extension window of 200 base pairs, and with more than two probes and a Šidák-adjusted *p*-value below 0.05.

GENERAL DISCUSSION

10.1. Summary of key findings

This thesis commences with a broad exposition of the current status of epigenetics research in relation to aging and neurodegeneration in Chapter 2. Starting with a description of the various layers of epigenetic regulation of transcription and translation, from DNA and chromatin modifications, to non-coding RNAs, followed by a discussion of the epigenetic dysregulation observed in aging and neurodegenerative diseases Alzheimer's disease (AD), Parkinson's disease, and Huntington's disease. From this it followed that epigenetic dysregulation in neurodegeneration may be the result of other pathological processes, such as the proposed interaction between amyloid-β (Aβ) and DNA methylation in AD, leading to an exacerbation of pathology. Alternatively, epigenetic cascades leading to pathology may be set in motion in response to environmental factors, such as the apparent effect of insufficient vitamin B12 and B6, folate, and S-adenosylmethionine intake on the development of dementia. The potential of epigenetics-based therapies was also discussed, including the off-label use of existing drugs that impact epigenetic regulation, usually on a global level, and the development of novel, more targeted and disease-specific approaches. Such therapies may directly target epigenetic dysregulation observed in relation to a disease, or may be aimed at improving symptoms associated with the disease, for instance in order to enhance cognitive function in AD. The perspective ended with a critical appraisal of the limitations of current epigenetics studies and supplied suggestions for future research.

As animal models are crucial for validation and for investigation of the functional impact of disease-related factors in a strictly regulated experimental setting, and as half of the studies included within this thesis rely on animal models, Chapter 3 provides a concise overview of animal models used for studying cognitive impairment as seen in neurodegenerative diseases such as AD. In addition to the animal models used in the three chapters following Chapter 3, pharmacological models and models used for other neurodegenerative diseases were also described.

In contrast to the later AD-centered studies, the study in Chapter 4 focused on epigenetic changes associated with healthy aging, and how these may be influenced to prolong the lifespan. Specifically, global levels of DNA methylation and hydroxymethylation were measured in the nuclei of mouse cerebellar Purkinje cells and analyzed with respect to age, caloric restriction, and endogenous antioxidant overexpression. It was found that both DNA methylation and hydroxymethylation increase with age in Purkinje cells, and that caloric restriction, but not overexpression of antioxidant, was able to prevent these age-related epigenetic changes. Although caloric restriction was associated with an increased lifespan, it

remains to be established exactly what the role of epigenetic alterations is in prolonging the lifespan.

Chapter 5 moved from normal aging to aging in animal models of AD, looking at age-related changes of DNA methylation and hydroxymethylation, and DNA methyltransferase 3A (DNMT3A) in the hippocampus. Animals with different genetic mutations related to AD pathology were included to investigate the differences in age-related epigenetic changes; a transgenic mouse model expressing human mutant *APP* (J20), a transgenic mouse model expressing both human mutant *APP* and *PS1* (APP/PS1dE9), a transgenic mouse model expressing mutant *APP*, *PS1* and *MAPT* (3xTg-AD), and a non-human primate model (Caribbean vervets), naturally exhibiting sporadic AD-like pathology with aging. A great discrepancy was observed between the different models, with the J20 model showing a decrease of global DNA methylation levels in the hippocampus, the 3xTg-AD model displaying an age-related increase in DNA methylation levels, and the APP/PS1dE9 and vervets showing no significant age-related changes. Accordingly, a negative correlation between DNA methylation and plaque load was observed in the J20 model, while this correlation was positive in the 3xTgAD model. No significant age-related change in DNA hydroxymethylation and DNMT3A were observed in any of the models. This study showed that the selection of an animal model for epigenetic studies may have a profound effect on the outcome, although it remains to be elucidated what the exact relationship is between the different genetic mutations and the observed epigenetic differences. Additionally, due the discrepancy in observations regarding global levels of epigenetic markers in AD it may be more fruitful to use targeted approaches, focusing on specific AD-related genomic regions.

The dynamic relationship between Aβ pathology and markers of DNA methylation and hydroxymethylation, as well as DNMT3A, was investigated and covered in Chapter 6. Making use of hippocampal tissue from APP/PS1dE9 mice that underwent active anti-Aβ immunotherapy, the epigenetic impact of lowering Aβ levels at an advanced disease stage could be studied. It was found that global DNA hydroxymethylation and DNMT3A levels were decreased in the vaccinated group, while global DNA methylation levels remained the same. Interestingly, DNA methylation and hydroxymethylation, but not DNMT3A, correlated with behavioral outcomes related to cognition. Additionally, Aβ pathology and markers of synaptic integrity correlated with DNA hydroxymethylation and DNMT3A levels, but not DNA methylation. This study showed that lowering Aβ levels by anti-Aβ immunotherapy has a profound effect on epigenetic markers, and that DNA methylation and hydroxymethylation levels may be an indicator of cognitive performance in the transgenic APP/PS1dE9 model of AD.

For Chapter 7 the methylomic and hydroxymethylomic profiles associated with AD were investigated using a genome-wide microarray with tissue from the human middle temporal gyrus, one of the brain regions affected by AD pathology. Using bisulfite (BS)- and oxidative bisulfite (oxBS)-treated DNA, the combined DNA methylation and hydroxymethylation signal, and the isolated DNA methylation signal could be determined, respectively. Subtracting the signal from the oxBS-treated DNA from the BS-treated DNA signal yielded the DNA hydroxymethylation signal. Changes in levels of unmodified cytosines could also be determined by subtracting the beta values of the BS converted DNA from 1. This novel approach, separating the different DNA modifications, led to the detection of genes previously associated with AD, such as *RHBDF2*, *ANK1*, and *C3*, but also *OXT*, which has only very recently been associated with AD. Inspection of *OXT* methylation and hydroxymethylation as a function of Braak stage indicated progressive hyperhydroxymethylation and hypomethylation with advancing Braak stages. This study illustrates the importance of separating DNA methylation and hydroxymethylation signals when studying the epigenome in the brain where DNA hydroxymethylation is enriched.

The explorative study described in Chapter 8 assessed the blood methylomic profile of AD. Additionally, it looked at the overlap between the AD methylomic profile and that observed in individuals with mild cognitive impairment (MCI), and the association of the AD methylomic profile with other measures of clinical AD dementia, including cognitive performance, Aβ and phosphorylated tau in the cerebrospinal fluid, and hippocampal volume. The identified blood methylomic profile of AD, comprising various genes with differentially methylated positions (DMPs) and regions (DMRs), showed limited overlap with previously reported methylomic profiles of the AD brain, including *HLA-DRB5*. Nonetheless, multiple affected genes which may play a role in AD etiopathogenesis were identified, such as *PCDHA1*, *CDH13*, *CLSTN2*, *NEFL*, and *MAD1L1*, some of which already showed differential methylation at the MCI stage or also showed associations with other markers of clinical AD dementia. These markers may therefore be investigated as early markers of AD dementia and could represent dysregulated pathways part of the etiopathogenesis of AD.

Chapter 9 presents a seminal study exploring the pre-clinical AD blood methylome in a sample of individuals without signs of dementia at baseline, but part of which had converted to AD dementia at follow-up 4.5 years later. Comparing the baseline methylome of converters and non-converters led to the identification of multiple genes with DMPs and DMRs associated with conversion to AD dementia, including *HLA-DRB5* and *OXT*, candidates from previous investigations of the AD methylomic

profile in the brain. In addition, using the methylome at baseline and follow-up, a group by time interaction analysis was performed to identify positions and regions showing differences in time-related alterations in methylation levels between converters and non-converters. The candidates from this analysis were subsequently analyzed for age-related changes in converters and non-converters separately, to establish in which group they were mainly affected. Epigenetic regulation of the resulting set of genes may be used as an indication for conversion to clinical dementia, or resilience to such a conversion.

10.2. Limitations

The most important limitations encountered in epigenetics studies are described in Chapter 2, and the studies presented in this thesis are also subjected to some of these limitations. One of the most critical limitations may be the small to moderate sample size of most of the studies, limiting their power to detect significant changes, in particular at the level of DMPs. This is exemplified by some of the *p*-values reported in Chapters 4-6 being close to the 0.05 threshold. These findings would greatly benefit from a replication study followed by a meta-analysis. Also the results of Chapter 7 should be interpreted with caution, as none of the identified DMPs survived correction for multiple testing. Generally, as it may be difficult to gather large samples, as well as the funds to perform epigenome-wide analyses on them, it is crucial for the field to collaborate and merge assets, perform replication studies, and attempt meta-analyses of existing observations.

A limitation inherent to epigenetic studies is their interpretability regarding causality. When comparing a diseased group with a healthy group and epigenetic differences are detected, it is impossible to say whether the epigenetic dysregulation caused the pathology, or whether it is a consequence of it, or an epiphenomenon. However, as, for instance, environmental exposures and Aβ can both have an effect on epigenetic regulation, the observed epigenetic changes in relation to AD are likely a combination of early, potentially causal changes, and changes that are caused by other pathological hallmarks of the disease. Disentangling these processes will require highly regulated longitudinal *in vitro* and animal model studies, involving, for example, *in vitro* and *in vivo* epigenetic editing.

Another difficulty of epigenetics research is the dynamic nature of epigenetic regulation, meaning that experimental procedures themselves may induce epigenetic changes. Thus, while it is crucial to determine the behavioral impact of epigenetic alterations, it should be taken into

account that, for instance, behavioral testing in animal models may be stressful and induce epigenetic changes [1], or repeated testing may induce epigenetic processes related to learning and memory [2].

It is also important to be aware of the extent of the epigenetic regulatory machinery and the limitations of the tools used to investigate it. For instance, the studies described in Chapters 4-6 use immunohistochemistry for the detection of epigenetic markers. This allows for the study of these markers in a highly localized manner, focusing on a small sub-region or even a specific cell-type as in Chapter 4. However, this method, especially when using 3,3'-diaminobenzidine tetrahydrochloride (DAB) as chromogen, cannot be used for absolute quantification of the targets, as there is no strictly linear relationship between staining intensity and antigen levels. Additionally, while in principle the immunohistochemical detection of DNA methylation and hydroxymethylation targets the whole genome, it obviously cannot distinguish between genes or genomic regions, something which can be achieved through sequencing techniques.

To investigate single CpG resolution changes in DNA methylation the Illumina HumanMethylation450 BeadChip (450K BeadChip) was used in Chapters 7-9. While overcoming some of the limitations of the immunohistochemical approach, it comes with its own set of restrictions. The probes of the 450K BeadChip are spersed over the genome, covering most of the known genes, but just a small fraction of all CpGs in the genome, let alone CpA, CpT, and CpC sites [3]. This array thus cannot be truly considered 'genome-wide', and its use to determine global DNA methylation levels (to compare with immunohistochemical observations) is thus also limited due to its sparse and biased coverage of the genome. Another important consideration when using the 450K BeadChip is the need for BS conversion of the input DNA. This procedure does not distinguish between DNA methylation and hydroxymethylation [4], which particularly hampers the interpretation of observations in the brain, which is enriched in DNA hydroxymethylation [5]. This limitation can be overcome through the use of oxBS conversion, which results in the 'true' DNA methylation signal, as opposed to the combined DNA methylation and hydroxymethylation signal gained from only BS treated DNA [6], as was applied in Chapter 7. However, the more recently discovered DNA formylation and carboxylation modifications are not taken into account using the oxBS approach, which actually converts 5-hydroxymethylcytosine (5-hmC) to 5-formylcytosine (5-fC) [6, 7]. Due to the low presence of 5-fC and 5-carboxylcytosine (5-caC), even when compared to 5-hmC, they are not likely to have a strong impact on DNA methylation and hydroxymethylation readings [7]. A possibly larger limitation of the indirect approach of determining DNA hydroxymethylation

levels used in Chapter 7 is its vulnerability to noise, which is already relatively high due to the much higher abundance of DNA methylation in relation to DNA hydroxymethylation, but becomes even higher due to the subtraction procedure to obtain 5-hmC levels [6]. This is exemplified by the large amount of negative 5-hmC beta values observed in Chapter 7, which required the implementation of strict detection thresholds.

While the work in this thesis focused on epigenetic DNA modifications, it is important to keep in mind the biological relevance of the findings. Global changes in epigenetic markers detected by immunohistochemistry are likely to reflect significant changes in cellular physiology, although it cannot be said which pathways are affected. On the other hand, significant changes in DNA methylation at a single CpG site may not result in a change in gene expression and may not have a subsequent functional outcome. Therefore, the studies in Chapters 7-9 are complemented by gene set enrichment analyses, identifying sets of genes with altered epigenetic regulation, which are more likely to have biological relevance. Nevertheless, such studies would benefit from secondary measures, such as gene expression.

Cell-type and tissue specific epigenetic profiles may limit the use of material not extracted directly from the main site of pathology, and which may explain the limited overlap between the AD methylomic profiles determined from the brain and those from the blood [8, 9]. This becomes particularly important for longitudinal studies, where age-related changes in epigenetic markers could be explained by a shift in the cell-type composition of tissues with age [10], and therefore this was corrected for in the study of Chapter 9.

10.3. Future perspectives

One of the main limitations of genome-wide studies in the epigenetics field remains sample size, which makes studies often underpowered and limits the reproducibility of findings. Tissue banks, ideally also recording antemortem phenotypic data, may constitute an important source to increase sample sizes or of replication cohorts for simple designs. Nevertheless, as it may not be possible to gather large samples in practice, other approaches may be employed to strengthen observations. For instance, multiple tissues can be investigated, independent cohorts can be used to replicate findings, and alternative techniques can be employed to reproduce observations [9, 11]. Additionally, the detection of changes in epigenetic regulation should be followed-up by investigating changes in transcription and protein levels, and may be complemented by other ‘omics’ data [12, 13]. As for diagnostic purposes it may be

necessary to investigate tissues, such as blood, when the main site of pathology is not readily accessible, such as the brain in case of AD, it is important to determine how representative the investigated tissue is for pathological processes occurring at the site mainly affected by disease. It should also be noted that, while more expensive and more difficult to process, the field may greatly benefit from truly genome-wide sequencing approaches, as opposed to microarray techniques, which remain limited and biased in their coverage of the genome [3]. Furthermore, the use of tissue homogenates may dilute effects due to the inclusion of cell-types not relevant for the investigation, which may be overcome by advances in single-cell sequencing techniques [14].

Even though the research covered within this thesis covers a range of species, tissues, and techniques, and even looking at the broader perspective offered by Chapter 2, the current status of our understanding of the epigenetics of AD and aging barely scratches the surface of its full complexity. Thus, while solutions can be offered to address the specific limitations mentioned above, a more radical shift in approach may be needed to truly evolve the field. With advances in microarray and sequencing techniques of recent years, the generation and sharing of big 'omics' datasets has become easier and easier, but the field seems to lag behind in how to deal with these datasets. For instance, harnessing the computational power of the current era and advances in computational modelling and machine learning, it may be possible to generate predictive models based on epigenetic profiles that may aid in the diagnosis and prognosis of AD [15]. This may be crucial for the implementation of personalized medicine, which can benefit the development of effective treatment strategies for complex multifaceted diseases such as AD [16].

The World Health Organization (WHO) stated that early diagnosis and the identification of modifiable risk factors is pivotal for the optimal management of AD [17]. With the suspected gene-environment interactions at the bedrock of sporadic AD [18, 19], and epigenetics as mediator [20], it may be necessary to apply a systems biology approach to fully grasp the etiopathogenesis of AD and identify novel therapeutic targets [21]. Furthermore, as AD etiopathogenesis is thought to start long before the onset of clinical symptoms, longitudinal study designs such as employed in Chapter 9, but spanning a larger timeframe and including more follow-ups, are crucial to elucidate the early pre-clinical stages of AD, to disentangle healthy aging from pathological aging, and distinguish between epigenetic cascades driving disease progression from epigenetic epiphenomena [22].

REFERENCES

[1] Ryan J, Chaudieu I, Ancelin M-L, et al. Biological underpinnings of trauma and post-traumatic stress disorder: focusing on genetics and epigenetics. *Epigenomics* 2016; 8: 1553–1569.

[2] Molfese DL. Advancing neuroscience through epigenetics: molecular mechanisms of learning and memory. *Dev Neuropsychol* 2011; 36: 810–827.

[3] Clark C, Palta P, Joyce CJ, et al. A comparison of the whole genome approach of MeDIP-seq to the targeted approach of the Infinium HumanMethylation450 BeadChip(®) for methylome profiling. *PLoS One* 2012; 7: e50233.

[4] van den Hove DLA, Chouliaras L, Rutten BPF. The role of 5-hydroxymethylcytosine in aging and Alzheimer's disease: current status and prospects for future studies. *Curr Alzheimer Res* 2012; 9: 545–9.

[5] Skvortsova K, Zotenko E, Luu P-L, et al. Comprehensive evaluation of genome-wide 5-hydroxymethylcytosine profiling approaches in human DNA. *Epigenetics Chromatin* 2017; 10: 16.

[6] Booth MJ, Ost TWB, Beraldi D, et al. Oxidative bisulfite sequencing of 5-methylcytosine and 5-hydroxymethylcytosine. *Nat Protoc* 2013; 8: 1841–1851.

[7] Ito S, Shen L, Dai Q, et al. Tet proteins can convert 5-methylcytosine to 5-formylcytosine and 5-carboxylcytosine. *Science*; http://science.sciencemag.org/content/333/6047/1300 (2011, accessed 3 April 2017).

[8] Davies MN, Volta M, Pidsley R, et al. Functional annotation of the human brain methylome identifies

tissue-specific epigenetic variation across brain and blood. *Genome Biol* 2012; 13: R43.

[9] Lunnon K, Smith R, Hannon E, et al. Methylomic profiling implicates cortical deregulation of *ANK1* in Alzheimer's disease. *Nat Neurosci* 2014; 17: 1164–1170.

[10] Li H, Guo Z, Guo Y, et al. Common DNA methylation alterations of Alzheimer's disease and aging in peripheral whole blood. *Oncotarget* 2016; 7: 19089–98.

[11] De Jager PL, Srivastava G, Lunnon K, et al. Alzheimer's disease: early alterations in brain DNA methylation at *ANK1*, *BIN1*, *RHBDF2* and other loci. *Nat Neurosci* 2014; 17: 1156–1163.

[12] Lunnon K, Mill J. Epigenetic studies in Alzheimer's disease: current findings, caveats, and considerations for future studies. *Am J Med Genet B Neuropsychiatr Genet* 2013; 162B: 789–99.

[13] Dong HK, Gim J-A, Yeo SH, et al. Integrated late onset Alzheimer's disease (LOAD) susceptibility genes: Cholesterol metabolism and trafficking perspectives. *Gene* 2017; 597: 10–16.

[14] Grün D, van Oudenaarden A. Design and analysis of single-cell sequencing experiments. *Cell* 2015; 163: 799–810.

[15] Goldstein BA, Navar AM, Carter RE. Moving beyond regression techniques in cardiovascular risk prediction: applying machine learning to address analytic challenges. *Eur Heart J* 2016; ehw302.

[16] Tebani A, Afonso C, Marret S, et al. Omics-based strategies in precision medicine: toward a paradigm shift in inborn errors of metabolism investigations. *Int J Mol Sci* 2016; 17: 1555.

[17] World Health Organization. Dementia. *WHO Media Centre*. http://www.who.int/mediacentre/factsheets/fs362/en/ (2016, accessed 29 July 2016).

[18] Lahiri DK, Maloney B, Zawia NH. The LEARn model: an epigenetic explanation for idiopathic neurobiological diseases. *Mol Psychiatry* 2009; 14: 992–1003.

[19] Iatrou A, Kenis G, Rutten BPF, et al. Epigenetic dysregulation of brainstem nuclei in the pathogenesis of Alzheimer's disease: looking in the correct place at the right time? *Cellular and Molecular Life Sciences*, 2016, pp. 1–15.

[20] Vineis P, Chatziioannou A, Cunliffe VT, et al. Epigenetic memory in response to environmental stressors. *FASEB J* 2017; fj.201601059RR.

[21] Parikshak NN, Gandal MJ, Geschwind DH. Systems biology and gene networks in neurodevelopmental and neurodegenerative disorders. *Nat Rev Genet* 2015; 16: 441–458.

[22] van den Hove D LA, Kenis G, Rutten BP. Epigenetic dysregulation in Alzheimer's disease: cause or consequence? *Epigenomics* 2014; 6: 9–11.

SUMMARY

The work in this thesis explores the involvement of epigenetics in aging and Alzheimer's disease (AD), using various techniques, animal models, and tissues.

CHAPTER 2 presents a thorough overview of epigenetic regulation and its involvement in aging and neurodegeneration. It covers the various layers of the epigenetic apparatus, including the mechanisms operating at the DNA level, the chromatin level, and the RNA level. Following this is a critical literature review of investigations implicating epigenetic mechanisms in aging and the neurodegenerative diseases AD, Parkinson's disease, and Huntington's disease. From this review, it followed that epigenetic processes may be disturbed due to genetic variation, environmental exposures, or due to interactions with disease-related pathology, in which case establishing causality remains a major challenge of the field. The implication of epigenetic processes in these neurodegenerative diseases provides novel therapeutic options that target these processes. While epigenetics-based treatments targeting specific disease-associated genes are still in their infancy, there are also investigations into the off-label use of existing drugs that have a widespread impact on epigenetic regulation. Furthermore, there are therapies being developed that aim to counteract certain symptoms, such as cognitive decline, but that do not necessarily target disease-related pathways, while other therapies directly aim to counter pathological cascades. Finally, the limitations of the field were discussed, such as the problem of causality in epigenetics research, and the challenge of replicating findings, complemented with suggestions for future studies, including the utilization of novel techniques and integration of multiple data modalities.

In **CHAPTER 3** a selection of the most used rodent models to study cognitive impairments are described. Various modes of achieving cognitive impairment are covered, including pharmacological models, models based on aging, and transgenic disease models, among which transgenic models of AD.

The first experimental part of this thesis starts off with an investigation into epigenetic changes associated with normal aging in **CHAPTER 4**. For this study, global levels of DNA methylation and hydroxymethylation, two pivotal epigenetic markers, were determined at two ages in the nuclei of mouse cerebellar Purkinje cells. These cells are known for their vulnerability to age-related deterioration. Additionally, the impact on these epigenetic changes of caloric restriction and endogenous antioxidant overexpression, two strategies previously reported to extend the lifespan, were studied. It was observed that both global DNA methylation and hydroxymethylation increased with age in Purkinje cells, that caloric

restriction was able to reduce this age-related increase, but that antioxidant overexpression did not have a significant effect on age-related epigenetic changes. These observations suggest that the life-prolonging effects of caloric restriction may be mediated through epigenetic processes, the exact nature of which remains to be established.

CHAPTER 5 covers a similar study as the previous chapter, but instead of healthy aging focuses on age-related epigenetic changes in models of AD. This study included three transgenic mouse models, expressing human mutant genes *APP* and *PS1*, associated with familial AD, or related to AD pathology in case of the tangle-inducing mutant *MAPT* gene. One model only expressed mutant *APP* (J20), another both *APP* and *PS1* (APP/PS1dE9), and the third model expressed mutant *APP*, *PS1* and *MAPT* (3xTg-AD). Additionally, Caribbean vervets, a non-human primate model which may naturally develop early AD-like pathology with age, were included in the study. Global levels of DNA methylation and hydroxymethylation, as well as DNA methyltransferase (DNMT) 3A, responsible for *de novo* DNA methylation, were investigated in the hippocampus, a brain region related to memory heavily afflicted by AD. Curiously, the models showed divergent age-related changes in global DNA methylation levels; the J20 model exhibited decreases, the APP/PS1dE9 and vervets showed no changes, whereas the 3xTg-AD presented increases. Global DNA hydroxymethylation and DNMT3A levels, however, did not change significantly between ages in any of the models. Correlation analyses with plaque load, which, as expected, increased with age, detected a negative correlation with DNA methylation in the J20 model, and a positive correlation with DNA methylation in the 3xTg-AD model, while no significant correlations were observed for the other epigenetic markers. These results indicate that, on a global level, AD-related pathology mainly appears to be associated with DNA methylation, but that the choice of animal model may profoundly affect this association. It may thus be more insightful for future studies into the relationship between genetic mutations and epigenetic dysregulation to focus on specific disease-related genes and pathways to complement the observations on a global level.

For **CHAPTER 6**, the impact of lowering amyloid-β (Aβ) levels through active immunotherapy on epigenetic DNA modifications was investigated. Global levels of DNA methylation, DNA hydroxymethylation and DNMT3A were determined in the hippocampus of APP/PS1dE9 mice, which were distributed between a vaccinated and a vehicle control group. Anti-Aβ immunotherapy was associated with lower levels of DNA hydroxymethylation and DNMT3A. Looking at correlations between the epigenetic markers and previously established markers of AD pathology, including behavioral outcomes related to cognition, indicated

that DNA hydroxymethylation and DNMT3A levels correlated with Aβ pathology and synaptic integrity. Interestingly, both DNA methylation and hydroxymethylation, both not DNMT3A levels, correlated with the behavioral scores. These results offer a first glimpse into the epigenetic component of anti-Aβ immunotherapy, although it remains to be elucidated whether the epigenetic differences stem from lowering Aβ level or from immunologic processes associated with active immunization.

The second experimental part of this thesis focuses on human AD patients, and switches from global immunohistochemical enquiries to a genome-wide, and site-specific, microarray approach. For **CHAPTER 7** the methylome and hydroxymethylome were interrogated in the middle-temporal gyrus, a brain region affected by AD pathology. A novel approach integrating readings from bisulfite (BS)- and oxidative bisulfite (oxBS)-treated DNA was used to determine differences in the proportion of methylated, hydroxymethylated, and unmodified signals between AD patients and controls for each of the over 450,000 investigated CpG sites. Correlations between nearby CpG sites were also investigated to determine differentially methylated regions associated with AD. This implicated several genes known to be associated with AD, including *RHBDF2*, *ANK1*, and *C3*, but also *OXT*, which was only very recently found in relation to AD. Interestingly, *OXT* showed hyperhydroxymethylation and hypomethylation with increasing Braak stages. These findings underpin the importance of separating the DNA methylation and hydroxymethylation signals when studying the epigenome of the brain, which is highly enriched in DNA hydroxymethylation.

CHAPTER 8 can be seen as a more clinically oriented extension of the previous chapter, exploring the methylomic profile of AD in blood. For this study, the blood methylome was determined in AD patients, individuals with mild cognitive impairment (MCI), and a group of healthy controls. Sites associated with AD were also investigated in relation to other determinants of clinical AD dementia, such as mini-mental state examination (MMSE) scores, Aβ and phosphorylated tau in the cerebrospinal fluid, and hippocampal volume. Several differentially methylated positions (DMPs) and regions (DMRs) were observed in relation to AD, including some in AD risk gene *HLA-DRB5*, which was previously observed to also exhibit altered DNA methylation in the brain of AD patients. Implicated genes such as *PCDHA1*, *CDH13*, *CLSTN2*, *NEFL*, and *MAD1L1*, which already presented with altered methylation profiles in the MCI group or showed associations with other markers of AD dementia, may reflect disturbed pathways in the etiopathogenesis of AD and could be further investigated as early blood markers of AD dementia.

For **CHAPTER 9** the pre-clinical methylome associated with conversion to AD dementia was determined. Using samples from a large aging cohort including only healthy subjects at baseline and monitoring their conversion to AD dementia, it was possible to compare the methylome of individuals converting to AD dementia after an interval of 4.5 years, with that of controls still cognitively sound after 4.5 years, at a stage both groups did not yet show signs of dementia. This comparison led to the identification of multiple DMPs and DMRs, including the AD risk gene *HLA-DRB5* and, once more, *OXT*, which may represent prime candidates for the pre-clinical diagnosis of AD. Additionally, to gain insight into the differences in dynamic epigenetic regulation between converters and non-converters, a group by time interaction analysis was performed. DMPs from this analysis were further investigated for time-related alterations in converters and non-converters separately to identify in which group they were significantly altered. Differences in methylation of top genes, such as *DGKD*, *MRPL20*, and *ARHGAP12* from this analysis associated with converters may signify vulnerability to convert to AD dementia. Conversely, methylation levels of top genes associated with non-converters, including *GRAMD1C*, *SMNDC1*, and *ARHGAP1* may reflect resilience to AD dementia.

SAMENVATTING

Het werk in dit proefschrift verkent de rol van epigenetica in het verouderingsproces en de ziekte van Alzheimer (ZvA), en maakt hierbij gebruik van verschillende technieken, diermodellen en weefsels.

HOOFDSTUK 2 presenteert een gedetailleerd overzicht van epigenetische regulatie en de rol hiervan bij veroudering en neurodegeneratie. Het hoofdstuk omvat de verschillende lagen van het epigenetische systeem, inclusief de mechanismen die actief zijn op het DNA niveau, het chromatine niveau en het RNA niveau. Dit overzicht wordt gevolgd door een kritische evaluatie van de huidige literatuur omtrent de implicatie van epigenetische processen in de neurodegeneratieve ziektes van Alzheimer, Parkinson en Huntington. Hieruit blijkt dat epigenetische processen kunnen worden verstoord door genetische factoren en omgevingsfactoren, almede door interacties met ziekte-gerelateerde pathologie, waardoor causaliteit een van de grote uitdagingen van het onderzoeksveld is. De implicatie van epigenetische processen in deze ziektes kan leiden tot de ontwikkeling van nieuwe behandelingsstrategieën, die op deze processen inspelen. Momenteel staat de ontwikkeling van epigenetische behandelingen nog in de kinderschoenen, al wordt er ook onderzoek gedaan naar bestaande medicijnen die invloed kunnen hebben op epigenetische regulatie. Nieuwe behandelingen proberen symptomen zoals cognitieve achteruitgang tegen te gaan, of om direct pathologische cascades te onderbreken en zo ziekte te voorkomen. Als laatste worden de beperkingen van het huidige epigenetica onderzoek aan de tand gevoeld en worden suggesties gegeven voor toekomstige studies in dit veld. Bijvoorbeeld het gebruik van nieuwe technieken en de integratie van verschillende datatypes, zoals genetische en expressie data om de epigenetische data te complementeren.

In **HOOFDSTUK 3** wordt een selectie van de meest gebruikte knaagdier-modellen voor cognitieve stoornissen beschreven. Verschillende modellen worden behandeld, waaronder farmacologische modellen, modellen gebaseerd op natuurlijke veroudering en transgene modellen, waaronder modellen voor ZvA.

HOOFDSTUK 4, het eerste onderzoek in dit proefschrift, focust op epigenetische veranderingen tijdens normale veroudering. Voor deze studie werd het globale niveau van DNA methylatie en hydroxymethylatie, twee belangrijke epigenetische indicatoren, bepaald in de kernen van cerebellaire Purkinje cellen van twee lijftijdsgroepen muizen. Deze cellen staan bekent om hun gevoeligheid voor verouderingsprocessen. Ook was de invloed van calorische restrictie en overexpressie van endogene antioxidanten, twee strategieën waarvan men denkt dat deze de levensduur kunnen verlengen, op deze epigenetische

veranderingen onderzocht. Hieruit bleek dat globale DNA methylatie en hydroxymethylatie toeneemt met veroudering in Purkinje cellen, dat calorische restrictie deze toename tegengaat en dat antioxidant overexpressie geen significante invloed heeft op de geobserveerde epigenetische veranderingen. Deze observaties suggereren dat de levensduur-verlengende effecten van calorische restrictie gemedieerd worden door epigenetische processen. Het onderliggende mechanisme van deze mediatie zal nog verduidelijkt moeten worden in toekomstig onderzoek.

HOOFDSTUK 5 betreft een soortgelijk onderzoek als het vorige hoofdstuk, maar bestudeerd verouderings-gerelateerde epigenetische veranderingen in diermodellen van ZvA. In deze studie werd gebruik gemaakt van drie transgene muismodellen met transgenen die geassocieerd zijn met de familiale vorm van ZvA (*APP* en *PS1*) of pathologische kenmerken van ZvA (*MAPT*). Het eerste model (J20) was alleen gebaseerd op een gemuteerde variant van het *APP* gen, het tweede model (APP/PS1dE9) op mutanten van *APP* alsmede *PS1* en het derde model (3xTgAD) bracht drie gemuteerde genen tot expressie; *APP*, *PS1* en *MAPT*. Ook werd een non-humaan primaat model bestudeerd, de Caribische vervet, die van nature pathologie kan ontwikkelen die lijkt op de vroege stadia van ZvA. Het globale niveau van DNA methylatie en hydroxymethylatie, maar ook DNA methyltransferase (DNMT) 3A, het enzym verantwoordelijk voor de novo DNA methylatie, werd op verschillende leeftijden in de hippocampus bepaald. De hippocampus speelt een belangrijke rol bij het geheugen en is ernstig aangetast bij ZvA. Opmerkelijk was de observatie dat de modellen verschillende ouderdoms-gerelateerde veranderingen in DNA methylatie lieten zien; in het J20 model ging het methylatie niveau omlaag, bij de APP/PS1dE9 muizen en de vervetten was er geen verandering en bij de 3xTgAD muizen ging de methylatie juist omhoog. Daarentegen lieten DNA hydroxymethylatie en DNMT3A geen significante veranderingen zien bij veroudering in alle modellen. De aanwezigheid van amyloïde plaques nam, zoals verwacht, toe met veroudering en deze liet een negatieve correlatie zien met DNA methylatie in het J20 model en een positieve correlatie in het 3xTg-AD model, maar correleerde niet met de andere epigenetische indicatoren. Deze resultaten lijken erop te wijzen dat, op een globaal niveau, Alzheimer pathologie vooral geassocieerd is met DNA methylatie, maar dat het gekozen diermodel een grote invloed kan hebben op deze associatie. Voor toekomstige onderzoeken naar de relatie tussen genetische mutaties en epigenetische misregulatie kan het dus gunstig zijn als globale metingen gecombineerd worden met relevante gen-specifieke observaties.

Voor **HOOFDSTUK 6** werd de impact van een vermindering van bèta-amyloïd (Aβ) door middel van actieve immunotherapie op epigenetische DNA modificaties onderzocht. De globale aanwezigheid van DNA methylatie, DNA hydroxymethylatie en DNMT3A werd bepaald in de hippocampus van APP/PS1dE9 muizen, verdeeld over een gevaccineerde en een controle groep. Anti-Aβ immunotherapie werd geassocieerd met een vermindering van DNA hydroxymethylatie en DNMT3A. Met behulp van bestaande gegevens met betrekking tot Alzheimer pathologie en cognitie, werd een correlatie gevonden met Aβ pathologie en synaptische integriteit voor DNA hydroxymethylatie en DNMT3A. Verder correleerde DNA methylatie en hydroxymethylatie, maar niet DNMT3A, met gedragsscores. Deze resultaten bieden een eerst blik op de epigenetische component van anti-Aβ immunotherapie, al is vervolgonderzoek nodig om uit te wijzen of de epigenetische veranderingen een gevolg zijn een vermindering van Aβ, of van immunologische processen die onderdeel uitmaken van de actieve immunisatie.

Het overige experimentele deel van dit proefschrift verplaatst de focus van modellen van ZvA naar menselijke patiënten en van globale immunohistochemische epigenetische metingen naar genoomwijde, plaats specifieke, microarray bepalingen. Voor **HOOFDSTUK 7** was het methyloom en hydroxymethyloom van de *gyrus temporalis medius* bepaald, een hersengebied aangetast door ZvA. Een nieuwe methode die metingen van bisulfiet (BS)- en oxidatief BS-behandeld DNA integreert werd gebruikt om verschillen in de proporties gemethyleerd, gehydroxymethyleerd en ongemodificeerd signaal te bepalen tussen patiënten met ZvA en controles voor meer dan 450.000 CpG plekken in het genoom. Correlaties tussen nabijgelegen CpG plekken werd ook onderzocht voor de bepaling van differentieel gemethyleerde regio's (DGRs) geassocieerd met ZvA. Dit leidde tot de identificatie van enkele genen die geassocieerd zijn met ZvA, waaronder *RHBDF2*, *ANK1* en *C3*, maar ook *OXT*, waarvan afwijkende epigenetische regulatie nog maar zeer recentelijk geïmpliceerd is in ZvA. *OXT* laat hypomethylatie en hyperhydroxymethylatie zien met toenemende Braak stadia. Deze bevindingen onderstrepen het belang van het scheiden van DNA methylatie en hydroxymethylatie signalen bij het bestuderen van het epigenoom van het brein, welke sterk verrijkt is met hydroxymethylatie.

HOOFDSTUK 8 kan gezien worden als een wat meer klinisch georiënteerde extensie van het vorige hoofdstuk, waarvoor het methylomische profiel van ZvA werd verkent in het bloed. Voor deze studie werd het methyloom van bloed bepaald voor patiënten met ZvA, personen met een milde cognitieve beperking (MCB) en gezonde controles. Posities in het methyloom die geassocieerd werden met

ZvA, werden vervolgens verder onderzocht in relatie tot indicatoren van Alzheimer dementie, zoals *mini-mental state examination* (MMSE) scores, Aβ en gefosforyleerd tau in de cerebrospinale vloeistof en hippocampaal volume. Verscheidene genen met differentieel gemethyleerde posities (DGPs) en/of DGRs werden gedetecteerd in verband met ZvA, waaronder het risico gen voor ZvA *HLA-DRB5*, waarvan in een andere studie de methylatie status in het brein van patiënten met ZvA ook anders was bevonden ten opzicht van gezonde controles. Andere genen zoals *PCDHA1*, *CDH13*, *CLSTN2*, *NEFL* en *MAD1L1* toonden al differentiële methylatie in de MCB groep, of werden naast ZvA ook geassocieerd met andere indicatoren van dementie. Deze genen reflecteren mogelijk verstoorde processen die onderdeel zijn van de pathogenese van ZvA en die, na verder onderzoek, gebruikt zouden kunnen worden als vroege indicatoren van ZvA in het bloed.

Voor **HOOFDSTUK 9** werd het preklinische methylomisch profiel bepaald, dat geassocieerd is met conversie naar Alzheimer dementie. Door gebruik te maken van DNA, geïsoleerd uit bloed van een groot verouderingscohort waarbij gezonde personen werden geincludeerd en waarvan conversie naar Alzheimer dementie werd bijgehouden, was het mogelijk om individuen te vergelijken die na 4,5 jaar Alzheimer dementie hadden ontwikkeld, met individuen die binnen deze tijd geen dementie ontwikkelden. Deze vergelijking leidde tot de identificatie van enkele DGPs en DGRs, waaronder ook weer *HLA-DRB5* en *OXT*, die mogelijk gebruikt kunnen worden voor de preklinische diagnose van ZvA. Om inzicht te verkrijgen in verschillen in de dynamische epigenetische regulatie tussen geconverteerde en niet geconverteerde personen, was een interactie analyse uitgevoerd voor groep en tijd. De DGPs uit deze analyse waren vervolgens verder onderzocht voor veranderingen tussen de twee tijdpunten voor de geconverteerde en niet geconverteerde groep apart om te bepalen voor welke groep de verandering over tijd significant waren. Verschillen in methylatie in de geconverteerde groep, in genen zoals *DGKD*, *MRPL20* en *ARHGAP12*, kunnen een teken zijn van conversie naar Alzheimer dementie. Anderzijds, in de niet geconverteerde groep, zouden verschillen in de methylatie van genen zoals *GRAMD1C*, *SMNDC1* en *ARHGAP1*, juist een indicatie kunnen zijn van bescherming tegen conversie naar Alzheimer dementie.

VALORIZATION

As society becomes more critical about what science feeds it, it is a logical requirement to dedicate a chapter to the societal impact of my research. However, before I present my view, let us first take a look at what 'non-scientists' think the impact of my research is. When someone asks me what I do, I usually just say "I do research into aging and Alzheimer's disease". For this chapter, I asked a few people what they think the societal impact of my research is (admittedly, they have not much to go on):

"Immense. You are able to scientifically show how many people get Alzheimer's in these times with many elderly. More years to live; live longer at home, economic target, save money on healthcare; people are able to live longer independently, etc."

"I have no knowledge of the actual content of your research, but I myself have no urge to further extend the lifespan, something many strive for. Your research seems part of this and I think it may eventually contribute to this in the future."

"I think it has a positive influence, as our careers get longer these days. Additionally, the quality of life can, especially at advanced ages, be drastically improved for many people when aging can be slowed and Alzheimer's can be detected/treated earlier."

"The research will lead to a better understanding of Alzheimer's disease, and because of this a better treatment can be provided or the symptoms can be managed better."

"If you succeed, you will profoundly increase the quality of life for the elderly, but especially for those close to the otherwise affected individuals."

Now, how do the findings of this thesis compare with these steep expectations? In short, unfortunately there still is no cure for Alzheimer's disease and our life expectancy remains the same. On the one hand, it should be recognized that, especially the first chapters of this thesis involving animal research, are very fundamental and exploratory in nature. The research presented in this thesis will likely not have a direct impact on society in the short run, but mainly offers insights important for other scientists and is able to guide future studies. On the other hand, the research covered in **CHAPTER 4** offered new insights into caloric restriction, which is known to prolong life in rodents. As a life-long reduction in calorie intake may not sound attractive to many people to extend their lifespan a bit, my research and that of others in our group, investigated the mechanisms behind the effects of caloric restriction so

that these processes may in the (far) future be targeted through e.g. pharmaceutical intervention instead of reducing calorie intake. Although most responses above do not address aging directly, promoting healthy aging, or even 'curing' aging would have the largest impact on society imaginable (only one responder seems to realize this!).

The research of **CHAPTER 5** may be the furthest from society. Comparing different animal models, its main conclusions are about how to tackle future studies in the field of epigenetics[1] and Alzheimer's disease. Useful for fellow researchers, but not so much for society at large. Or is it? It is easy to diminish the usefulness of a single study when viewed separately, but it may play a pivotal role in directing future research into more fruitful avenues. As the study in **CHAPTER 5** indicates, current animal models do not capture Alzheimer's disease very well, and findings are not easily translated to the human situation. Indeed, while Alzheimer's disease has been cured over and again in animal models (see e.g. [1] for an overview), it should not be forgotten the end goal is to treat human patients. Thus, although animal models are extremely important for fundamental research (see e.g. [2]), it needs to be complemented with human-oriented studies to ensure the clinical validity of the observations.

Starting from **CHAPTER 7**, the research focuses on humans and gets closer to society. In this chapter, we offer novel insights into epigenetic dysregulation associated with Alzheimer's disease, comparing brain tissue from patients and healthy controls. While for this type of study replication is crucial, the affected markers identified can be further investigated as potential diagnostic markers or treatment targets in future studies. Note that many of the findings of epigenome-wide association studies (i.e. covering the epigenetic regulation of most known genes), such as those described in Chapters 7 through 9, are often not easily replicated, making the selection of viable targets for mechanistic and functional follow-up studies a major challenge. Nevertheless, expanding our knowledge of the disease is already a merit on itself, as a greater understanding is crucial for the development of effective treatment strategies, whereas a lack of knowledge may explain why there currently is no cure for Alzheimer's disease.

The final scientific efforts described in this thesis, in **CHAPTERS 8 AND 9**, are similar in nature to **CHAPTER 7**, but focus on the blood instead of the brain. While it may seem strange at first, to investigate the blood in relation to a neurodegenerative disease, this actually makes the findings much more relevant for clinical purposes in the shorter run. Brain tissue can in most cases only be obtained postmortem, but blood can be easily obtained from patients, and importantly, possible future patients. Even though blood markers may thus indirectly represent

[1] Wonder what epigenetics is? In short, epigenetic regulation supervises gene expression; it dynamically determines which genes are expressed (and to which extent) and which are not in response to your diet, physical activity and other environmental factors. For a more detailed, but still accessible explanation of epigenetics see: http://www.whatisepigenetics.com/what-is-epigenetics/.

what happens in the brain, they can be directly used for diagnostic and prognostic applications. In fact, this is what my future research will focus on ; using machine learning to make predictions about the development of Alzheimer's disease based on blood markers and identify novel candidates for therapy, such as oxytocin. Even though the identification of Alzheimer's disease at a pre-clinical stage has currently, without the availability of an effective treatment, not much clinical use, it may be fundamental for the development of such treatments, as it is thought past clinical trials have focused on a disease stage where damage to the brain is too advanced to reverse [3]. Furthermore, to fully grasp the etiology of complex diseases like Alzheimer's disease it will be necessary for future research to embrace advances in computer modelling and systems biology to integrate genomic, epigenomic, transcriptomic, proteomic, and other data modalities. This will also allow for a better informed development of treatment strategies.

Looking again at what others think the impact my research has on society, it seems many people[2] think of what the impact could be. This is indeed what is traditionally described in, say, a grant proposal, as this is perhaps what people want to hear. Therefore, I decided to write about the toned-down, in my view more realistic impact my research may have on society, as you see above. Notably, apart from the societal impact of the research performed by PhD students, it is in my opinion extremely important to look at the societal impact of successful PhD students themselves (i.e. the most important outcome of a PhD project is not the research, but the researcher). While I cannot speak for all PhD students, going through the PhD trajectory has allowed me to explore a field of research in depth, identify gaps and weaknesses in the current body of knowledge and related approaches. During the latter part of my project, I have expanded my capabilities in my specific field of study beyond the strong foundation provided by my supervisors to meet the requirements to advance this field. I now feel ready and confident to design my own studies, write my own grant proposals, and supervise my own team. In short, now, I am ready to make a real impact on society.

[2] Please forgive me the crude extrapolation of 5 people's opinion to that of many.

REFERENCES

[1] Franco R, Cedazo-Minguez A. Successful therapies for Alzheimer's disease: why so many in animal models and none in humans? *Front Pharmacol* 2014; 5: 146.

[2] Granholm A-C. Why do we need to use animal models to study cognition and aging? *Neuropsychopharmacology* 2010; 35: 1621–2.

[3] Sperling RA, Jack CR, Aisen PS. Testing the right target and right drug at the right stage. *Sci Transl Med* 2011; 3(111):111cm33.

CURRICULUM VITAE

Roy Lardenoije was born on the 11th of April 1990 in Leiderdorp, the Netherlands. He grew up and went to school in Leiden. In 2006, he got his first chance to work in a laboratory, during a high school internship at PharmaCell BV in Maastricht, where he studied the differentiation of muscle stem cells. He obtained his high school diploma *cum laude* (VWO, Nature & Health profile) in 2008 at the Marecollege in Leiden. After a country-wide search for a suitable Bachelor program that could satisfy his broad interests, he moved to Maastricht and entered University College Maastricht (UCM). There, he sculpted his own curriculum, blending molecular biology, computer science, psychology, philosophy, and with towards the end, a focus on neuroscience. This cumulated in a study on the functional organization of the visual cortex for his bachelor thesis, supervised by Dr. Vincent van de Ven at the Cognitive Neuroscience department of Maastricht University. Shortly after this, in 2011, he was granted his *cum laude* Bachelor of Science degree. After another arduous search for a Master program, it was the friendly and welcoming interview with Dr. Daniël van den Hove and Dr. Jos Prickaerts for the Fundamental Neuroscience specialization of the Cognitive and Clinical Neuroscience Research Master that convinced him to stay in Maastricht. For his Master thesis Roy investigated the epigenetics of aging under supervision of Dr. Daniël van den Hove and Dr. Bart Rutten, and he obtained his Master of Science degree *cum laude* in 2013. For his thesis, he received the Studentprize 2013 for the best Master thesis of the Faculty of Psychology and Neuroscience. He was able to continue the research of his Master internship as a research and education assistant with a Kootstra Talent Fellowship, until he obtained an NWO Graduate School of Translational Neuroscience Fellowship in 2014 to fund a PhD position under the supervision of Prof. dr. Bart Rutten , Prof. dr. Harry Steinbusch, and Dr. Daniël van den Hove. Apart from his work in Maastricht, Roy visited the lab of Dr. Cynthia Lemere at Harvard Medical School in Boston (USA) for half a year. He also shortly visited the group of Dr. Alfredo Ramirez, at both the University of Bonn and the University of Cologne. Additionally, he presented his research at numerous national and international conferences, including the Society for Neuroscience Annual Meeting and the Dutch Neuroscience Meeting. In addition to research, Roy has also taken on the roles of internship coordinator and meeting organizer for the Translational Neuropsychiatry / Neuroepigenetics group and was a PhD representative of the Neuroscience division and member of the educational committee of the School for Mental Health and Neuroscience (MHeNS). During his PhD, Roy has also been tutor and practical supervisor in several Bachelor and Master courses at Maastricht University and has supervised many Bachelor and Master students during their internship. Next to teaching others, Roy also kept on expanding his own skills, taking courses and workshops in statistics, bioinformatics, and programming to evolve his research. Since 2016 Roy also operates as a

freelance programmer and writer, including a collaboration with graphic designer Eric Lardenoije as Brave Monkeys. Currently, Roy is a postdoc fellow in the group of Dr. Daniël van den Hove and Prof. dr. Bart Rutten, further expanding his work on the epigenetics of aging and Alzheimer's disease through the implementation of machine learning and systems biology approaches.

LIST OF PUBLICATIONS

Published

Pishva E, Kenis G, Hannon E, Viechtbauer W, Jeffries A, **Lardenoije R**, Sienaert P, van OS J, Stek ML, Rutten BPF. Genome-wide meta-analysis of DNA methylation changes associated with antidepressant effects of Electroconvulsive Therapy. *Brain Stimulation* 2017; 10:388.

Bey K, Wolfsgruber S, Karaca I, Wagner H, **Lardenoije R**, Becker J, Milz E, Kornhuber J, Peters O, Frölich L, Hüll M, Rüther E, Wiltfang J, Riedel-Heller S, Scherer M, Jessen F, Maier W, van den Hove DLA, Rutten BPF, Wagner M, Ramirez A. No association of the variant rs11887120 in *DNMT3A* with cognitive decline in individuals with mild cognitive impairment. *Epigenomics* 2016; 8(5):593-8.

Lardenoije R, van den Hove DLA, Vaessen TSJ, Iatrou A, Meuwissen KPV, van Hagen BTJ, Kenis G, Steinbusch HWM, Schmitz C, Rutten BPF. Epigenetic modifications in mouse cerebellar Purkinje cells: effects of aging, caloric restriction, and overexpression of superoxide dismutase 1 on 5-methylcytosine and 5-hydroxymethylcytosine. *Neurobiology of Aging* 2015; 36:3079-89.

Lardenoije R, Iatrou A, Kenis G, Kompotis K, Steinbusch HWM, Mastroeni DF, Coleman P, Lemere CA, Hof PR, van den Hove DLA, Rutten BPF. The epigenetics of aging and neurodegeneration. *Progress in Neurobiology* 2015; 131:21-64.

Fitzsimons CP, van Bodegraven E, **Lardenoije R**, Kompotis K, Kenis G, Chouliaras L, Biojone C, Joca S, Steinbusch HWM, Lunnon K, Mastroeni DF, Mill J, Coleman P, van den Hove DLA, Rutten BPF. Epigenetic regulation of neural stem cells: Implications for Alzheimer's disease. *Molecular Neurodegeneration* 2014; 9:25.

Van den Hove DLA, Kompotis K, **Lardenoije R**, Kenis G, Mill J, Steinbusch HW, Lesch KP, Fitzsimons CP, De Strooper B, Rutten BPF. Epigenetically regulated microRNAs in Alzheimer's disease. *Neurobiology of Aging* 2014; 35(4):731-45.

Lardenoije R*, Van Goethem N*, Kompotis K, Rutten BPF, Prickaerts J, Steinbusch HWM. Cognitive disorders: aging, impairment and dementia cognitive deficit models, In: In Vivo *Models for Drug Discovery*, Wiley-VCH Verlag. 2014: 349-366.

Lardenoije R*, Brasnjevic I*, Schmitz C, Van Der Kolk N, Dickstein DL, Takahashi H, Hof PR, Steinbusch HWM, Rutten BPF. Region-specific neuron and synapse loss in the hippocampus of APPSL/PS1 knock-in mice. *Translational Neuroscience* 2013; 4:8-19.

Submitted and in preparation

Lardenoije R, van den Hove D, Havermans M, van Casteren A, Le K, Palmour R, Lemere CA, Rutten BPF. Age-related epigenetic changes in hippocampal subregions of four animal models of Alzheimer's disease. *Submitted*.

Pishva E, Kenis G, Viechtbauer W, Arts B, Jeffries A, Hannon E, **Lardenoije R**, Burrage J, Murphy T, van den Hove DLA, Sienaert P, Bouckaert F, Mill J, Stek M, van Os J, Dols A, Rutten BPF. Longitudinal changes in genome-wide DNA methylation associated with electroconvulsive therapy. *Submitted*.

Chouliaras L, **Lardenoije R**, Kenis G, Mastroeni DF, Hof PR, van Os J, Steinbusch HWM, van Leeuwen FW, Rutten BPF, van den Hove DLA. Age-related disturbances in DNA methylation and hydroxymethylation in the hippocampus of transgenic APPswe/PS1ΔE9 mice. *Submitted*.

Lardenoije R, van den Hove DLA, Jung SE, Havermans M, Liu B, Rutten BPF*, Lemere CA*. Active amyloid-β immunotherapy results in epigenetic changes in the hippocampus of an Alzheimer's disease mouse model. *In preparation*.

Lardenoije R*, Roubroeks JAY*, Pishva E*, Iatrou A, Smith AR, Smith RG, Eijssen LMT, Kenis G, Mastroeni DF, Delvaux E, Coleman PD, Mill J, Rutten BPF, Lunnon K, van den Hove DLA. The DNA methylome and hydroxymethylome in Alzheimer's disease; Cortical dysregulation of *OXT*, *C3*, *ANK1* and *RHBDF2*. *In preparation*.

Lardenoije R, Pishva E, Jacobs H, Ramakers I, Visser PJ, Steinbusch HWM, van den Hove DLA, Rutten BPF. Detection of blood methylomic markers associated with clinical features of Alzheimer's disease; An exploratory approach. *In preparation*.

Lardenoije R, Leber M, Pishva E, Rutten BPF, van den Hove DLA, Ramirez A. Identification of preclinical methylomic blood markers associated with conversion to Alzheimer's disease. *In preparation*.

* Equal contribution

ACKNOWLEDGMENTS

First and foremost I would like to thank my promotion team, Prof. dr. Bart Rutten, Prof. dr. Harry Steinbusch, Dr. Daniël van den Hove, and Dr. Cynthia Lemere, who made it possible for me to embark on the wondrous journey that led to this thesis.

Daniël, I first met you for the Fundamental Neuroscience interview. I had gone through interviews for two other Master programs, but there the people felt indifferent, like I was being interrogated. However, the interview with you and Jos was very welcoming and it was more like we were having a friendly chat. I believe this is characteristic for you, and what makes you such an amazing supervisor; I always had the feeling I could walk into your office and discuss anything, even things not related to my research. You treat the people under your supervision with interest and respect and not just as workhorses and also give them the opportunity to grow in the direction they want. Having talked with many other PhD students about their supervision, I truly believe you are one of the best daily supervisors around and that I was very lucky to end up under your care.

Bart, I got introduced to you by Daniël as my second supervisor for my Master internship because I wanted to do aging research. During this first meeting you asked me the classic question of what I wanted to do next, after my Master, and further in the future. A normal question at the time, but I like how you always think about 'the next thing'. It seems every time I talk to you, you have a new exciting opportunity to be explored and I greatly enjoy the challenges this provides. You always seem to have a cheerful spark in your eyes and have an infectious optimistic attitude towards science. While the meetings with you at the beginning of my PhD were a bit overwhelming, leaving me with so many new things to delve into, I have learned to be more selective so I can better appreciate the opportunities you have to offer. Together with Daniël, I think you two strike an excellent balance between realism and idealism; daring to explore novel fields, but without getting lost.

Dear Cindy, I am extremely grateful that you gave me the opportunity to work with you and your wonderful group. It was my first time going so far from home for an extended period of time, and if not for your warm and welcoming personality and the amazing people in your group I would not remember my time in Boston as one of the greatest highlights of my PhD and as a pivotal milestone in my personal development. I not only got to learn a different approach to research, but also learned a lot about American culture such as by experiencing an absolutely delightful Christmas dinner at your home, witnessing a baby shower at work, and you even organized a surprise birthday party in your office!

Harry, although we did not meet that often during my time as a PhD student, when we did you always had some valuable input for my research. Even though my specific field of study was not your specialization, you were still able to always provide quick and useful feedback on my work.

Apart from my promotion team, I also would like to thank another very important team, the wonderful technician team, Hellen, Marjan, and Denise. Hellen greatly helped me to enhance my skills in the lab at the start of my PhD and was always ready to share her expertise when setting up new experiments. Marjan and Denise have always been friendly and helpful, even when I needed some last-minute materials. Without them, many experiments would not have run so smoothly as they did!

Barbie, a special thank you goes out to you, as you are a special technician from a different world (the lab upstairs truly feels like a different world). You have thought me some of the most elementary basics, such as running a gel, without which my lab work would likely have been doomed. You act with a certain pragmatism which makes it easy to work with you and to get things done.

Rachelle, we started around the same time at the department and ever since your assistance has been invaluable. Whether it was making a simple copy, planning a meeting, or making sure I didn't go broke in Boston, I could always rely on you to help out with a smile!

Kostas, although we technically were rivals during our Master internship, vying for a PhD position, it never felt that way. Although we stayed many evenings and weekends at the lab, there was always some time for fun; from deep technical discussions to just watching some anime in the MPR. Thanks for being the funniest IHC instructor I ever met, your instructions lay at the foundation of this thesis!

Leo, as my predecessor, your work forms the pillars upon which my thesis is build. You have always greatly helped me when I had questions, even though you did not work in Maastricht anymore. The few times we met were a pleasure, so much so that I believe we spend the majority of this time in bars.

Julie, as I am myself not the most socially skilled person, your kind and caring nature were integral for my integration in the broader PhD student community in Maastricht. You were always ready to help out when needed and it was always a delight chatting with you in the lab or the office.

Ehsan! Hoi. One of the few veterans remaining in the group from before I started, you have been an inspiring mentor, as well as a great friend. You were introduced to me as 'the freezer guy' who knows where stuff is, and I think we have both grown a lot since then. I greatly enjoy our discussions and highly value your thoughts on subjects that go beyond the expertise of my supervisors. Your modesty and realistic view of science is refreshing and your cooking is enrapturing. Be sure to let me know when you start your own group!

Jo, the first impression I got of you was as a strict tutor for FN. However, when I started as a PhD student I quickly learned you were the true embodiment of "work hard, party harder"! Bringing life to the department, while also delivering inspiring work, you are truly a living legend and the department will never be the same without you.

Yara, you had your setbacks at work, but you did not let this influence your life outside the office and you were always fun to be around. You were the only true match for Jo in the partying department, and I will never forget the crazy trip to Munich for the Startbierfest that you organized!

Nicole, while we have not worked a lot together, your grant-obtaining skills are truly legendary and reading them has thought me a lot for writing my own proposals. Your cheerfulness and dedication to science is very inspiring, and you are great to chat with to boot!

Mark, you offered some well-needed male presence in our female-dominated office and it was great to have a sparring partner also going trough the trials of becoming an R master. You also introduced the department to CrossFit and avocados, leading to some fascinating discussions!

Marion, you are one of the nicest persons I ever met and your cheerfulness and enthusiasm always brightened up the room. It was great to have an even greater geek as myself in the group, to share some of life's delights only understood by a select few. I also have you to thank for introducing me to the glorious raclette tradition, those tasty movie nights at your place were truly something to look forward to!

Magda, I really appreciate your directness and honesty and enjoyed our critical discussions. You were a nice fresh breath in a lab where most people accepted the status quo. You introduced me to some great German beers, a great treat in the Netherlands! And I hope to try some more; maybe when we watch Black Sheep?

Lars, you were a great help to get me started with some of my bioinformatic analyses. However, your true expertise shines as a fellow whisky connoisseur. Did you already catch a Kelpie?

Laurence, you were the first postdoc joining our group since I started as a PhD and it was really nice to have a 'heavyweight' researcher in the lab to discuss and do experiments with. As the seniors focus more on the planning aspect of research, I think your more pragmatic approach of not only planning but also executing research really pushed things forward. Additionally, I must say being a tutor in your course at the Maastricht Science Programme was one of the best tutoring experiences I had.

Gunter "The Big G" Kenis, while not officially part of my promotion team, you are a crucial member of the triad at the head of our TNP group. We worked more together at the start of my PhD, when I still worked on miR-137, and later I had the honor of disturbing the peace in your office while meeting with Ehsan. Nonetheless, I have gotten to know you as a scientific mastermind, with a great sense of humor to match.

Koen, you were one of my first interns and I hope that elective didn't scar you as me eating a banana did. While our scientific collaboration was of a short duration, we had many memorable moments, such as in Indonesia and Berlin, where I thoroughly got to enjoy your great sense of humor. And how do you manage to always look good in a picture!?

Britt, I think you were actually my first intern, definitely the first to do lab work, so you thought me possibly more about supervising a student than I thought you about immunohistochemistry. After that, you became a great colleague, especially our time in San Diego with the great performance of Artemis was unforgettable.

I also would like to thank all the other wonderful people (past and present) at our department and beyond, for many memorable occasions during my time as a PhD student in Maastricht. Especially the great group of guys, Ehsan, Jo, Koen, Maarten, and Pim, for the epic Berlin experience. Gerard for some excellent beer, whisky and coffee experiences. Gisela, for your great enthusiasm, and fun conversations in and outside the lab. Nick, it was a pleasure working on the book chapter together, and it is always fun talking to you. Simone for some hilariously fun moments in Braga. Marina for the fantastic Spanish flair you bring to the department, as well as your hospitality and the great events you host, bringing the department closer on a social level together with Artemis. The same can be said about Shannon, organizer of the best Christmas dinners. Shengua, for the fun we had organizing the lab day out. Carolin, although we never really worked together, I feel we have a certain bond, going

through the same trials and getting the same fellowships. An, I hope you have by now memorized all the distilleries on Islay. Your dedication to learn Dutch is amazing, goed zo! Fred, even though we don't talk often, it always ends with a laugh.

I also owe thanks to many of the senior scientists at our department. Especially, Jos, for being the perfect FN coordinator, not only teaching prospective scientists to work hard, but also to party harder. Mario for helping with my microscope image analyses. Fred van Leeuwen for the insightful discussions.

Obviously, I would not have been able to achieve so much during my PhD without the help of some wonderful students. Bhavana, you thought me more than you can imagine, but unfortunately I was not able to instill some sense of responsibility in you. Thomas, you showed a critical mind and a great dedication to the project, showing a greater independence and responsibility than expected of an intern. I hope you finish all your studies and find a way to combine them in your future career. Nathalie, thanks to your efficient and independent work we were able to run many PCR experiments, but alas, they did not make it into this thesis even though these experiments were crucial to move my project forward. Kirsten, you had barely set a foot in the lab before you started, but your cautious approach to the lab work resulted in brilliant gels, which were fundamental for the LR-PCR experiments, which sadly, did not make it into this thesis. Büsra, you had a bit of a rough start, but it was a delight to have you visit our lab and I think you really grew as a scientist during your stay. Anne and Sophie, you really helped me out by daring to take on an internship with long distance supervision while I was in Boston! Sophie, as your report stood out in quality, I am happy you could further help me with turning the data you generated into a chapter of this thesis. Sabine, you were a great help to make sense of my first EWAS results. Monique, when I came back from Boston you were a godsend for the quick processing and analysis of the immunohistochemistry image data, while also assisting with other projects, quickly learning new techniques. I dare you to give more of your own input during your future endeavors, as you have a lot of potential! Renzo, even though the results were not earth-shattering, you achieved something amazing for your elective; setting up and running your own little study, with only minimal guidance. I look forward to see what you can achieve during a full PhD project! Floris, you also did your own pilot study and delivered great work considering the not so ideal state of the tissue you had to work with. Narek, you were my last intern during my PhD period and it was a breeze. Despite the sketchy content of your internship, you quickly mastered the laboratory techniques, especially admirable considering you never took notes. It was great getting to know you and I hope you have become a Pokémon Master by now!

Special thanks go out to Bert Smeets, Jo Vanoevelen and Wanwisa Dijkstra, who were pivotal in setting up the next-generation sequencing study, which unfortunately had to be cancelled. Especially Wanwisa thought me a lot about LR-PCR, kept answering my incessant stream of questions, and went above and beyond to get the experiment to work.

Apart from Cindy, it was also thanks to her amazing group that my time in Boston was such a success. Particularly, Helen, your welcoming and fun personality made me immediately feel accepted in the group, and it was extremely kind of you and Qiaoqiao to scout my room before I arrived in Boston! And that Boston Beer Summit we went to really made me fall in love with the contemporary US brewing styles. Kevin and Emmett, it was great working with you and exploring the lunch options that the American cuisine has to offer was delightful, especially that “All the Way” hotdog/hamburger monster from Tasty Burger was a delicious challenge, and that sushi place Kevin took us remains the stuff of dreams! Saba, your cheerful demeanor and our chats made those countless hours behind the microscope much more enjoyable than they had the right to be. Finally, I would like to thank Allison Roper for helping me through the bureaucratic maze required to work in the US, without you I would likely not have been able to even enter the country!

Frank, having you as a roommate at the beginning of my stay in Boston was hilarious (you know what time it is!), and we had some great moments with other Dutchies Nadine, Nienke and Anouk, and your labmate Gea. I still haven’t found a place here that can compete with that Thai in Boston!

Alfredo, your collaboration with our group gave me an exciting new project to work on at the end of my PhD, and our collaboration will likely continue into the future. Thanks for showing me Bonn and I must agree a couple of beers form the perfect foundation for invigorating scientific discourse. Markus, working with you in Cologne and your continued support was invaluable for finishing Chapter 9 of this thesis, and thanks for curing my fear of the terminal.

Artemis. You have probably been the most important person in making my time as a PhD student so memorable. Without you I would probably have had a very sober life outside the lab. I think if someone else had been my roommate it might have been painfully awkward, but your wonderfully sociable character, open mind, and great intellect has made you a precious friend. I really miss our culinary exploits, late night chats, the marvelous gatherings at our place, and we still have to finish Gears of War 3... But also at work you have always been a reliable friend, when I needed your expert opinion or an ever important coffee break. I could think of no other person better suited to be my paranymph!

Janou, I also got to know you as my intern, and you immediately struck me as very kind, charming and hardworking. It was delightful to work with you on the same project, but we also had lots of fun outside the R environment, such as during the epic quiz nights. As fellow whisky lovers, you and Artemis are the perfect paranymphs!

My brother and good friend Eric, thank you for your amazing dedication to this project and for turning the physical thesis into something truly unique! Be sure to check him out at ericlardenoije.com if you also want an exceptional thesis or have any other undertaking that requires some designer flair.

Mom and dad, you are at the genesis of this thesis. Your views on life and how you raised me have always inspired me to think about what I am doing and to make sure I enjoy it; to always explore beyond perceived boundaries. Whatever choices I made and will make in the future, I feel I can always rely on your love and support; truly, what else can a son wish from his parents? I brewing buddy perhaps?

Sophie, my other (better) half, and only person that not only ‘knows me longer than today’, but also knows me today. You have been instrumental in the completion of this thesis. You are the one it is always worth for to take a break. Especially during that final push to complete this thesis, you were there to pull me out of the thesis haze when needed. Now as a PhD veteran, I hope to be of service to you in your journey as a PhD student, especially for the extracurricular activities!

ABBREVIATIONS

12SOD-CD: 12-months-old SOD1 mice on the CD

12SOD-CR: 12-months-old SOD1 mice on the CR diet

12WT-CD: 12-months-old WT mice on the CD

12WT-CR: 12-months-old WT mice on the CR diet

24SOD-CD: 24-months-old SOD1 mice on the CD

24SOD-CR: 24-months-old SOD1 mice on the CR diet

24WT-CD: 24-months-old WT mice on the CD

24WT-CR: 24-months-old WT mice on the CR diet

3NP: 3-nitropropionic acid

3R-tau: tau with 3 microtubule-binding repeats

3xTg-AD mice: triple transgenic mouse model of AD expressing human mutant APPK670N/M671L, PS1M146V, and TauP301L

450K BeadChip: Illumina Infinium HumanMethylation 450K BeadChip

4PBA: 4-phenylbutyrate

4E-BP: eukaryotic translation initiation factor 4E-binding protein

4R-tau: tau with 4 microtubule-binding repeats

5-caC: 5-carboxylcytosine

5-fC: 5-formylcytosine

5-hmC: 5-hydroxymethylcytosine

5-hmU: 5-hydroxymethyluracil

5HT: serotonin

5HTR3: type 3 serotonin receptor

5-mC: 5-methylcytosine

5xFAD mice: transgenic mouse model overexpressing mutant human APP (695) with the Swedish (K670N and M671L), Florida (I716V), and London (V717I) mutations, and mutant human PS1 with the M146L and L286V fAD mutations

7-mG: 7-methylguanine

A: acetyl modification / adenosine (depending on context)

A3SS: alternative 3' splice site

A5SS: alternative 5' splice site

Aβ: amyloid-β

Aβ42: Aβ 1-42

ABCA1: ATP binding cassette subfamily A member 1

ac: acetylation (as in H3K9ac)

ACh: acetylcholine

ACI: annulus crossing index

AD: Alzheimer's disease

ADAM: a disintegrin and metalloproteases domain

ADAR: adenosine deaminases that act on RNA

ADP: adenosine diphosphate

AFE: alternative first exon

AgeCoDe: German Study on Ageing, Cognition and Dementia in Primary Care Patients

AGK2: 2-cyano-3-(5-(2,5-dichlorophenyl)-2-furanyl)-N-5-quinolinyl-2-propenamide

AICDA: activation-induced cytidine deaminase

ALDH: aldehyde dehydrogenase

ALE: alternative last exon

ALKBH: alkylation repair homolog

Alu: *Arthrobacter luteus elements*

AMPA: alpha-amino-3-hydroxy-5-methyl-4-isoxazolepropionic acid

ANOVA: analysis of variance

antagomirs: anti-miRNAs conjugated to cholesterol molecules

APOBEC: apolipoprotein B mRNA editing enzyme, catalytic polypeptide-like protein

APOE: apolipoprotein E

APP: amyloid-β precursor protein

APP23 mice: transgenic mouse model with a 7-fold overexpression of APPswe

APP/PS1 mice: transgenic mouse model expressing mutant human APPK670N/M671L and PS1M146V

APP/PS1-21 mice: transgenic mice overexpressing APPswe and human PS1 with the L166P mutation, line 21

APP/PS1dE9 mice: transgenic mice overexpressing APPswe and PS1dE9

APPind: human APP with the V717F Indiana mutation

APPswe: human APP isoform 695 with the double KM670/671NL Swedish mutation

α-Syn: α-synuclein

ATC: anterior temporal cortex

ATP: adenosine triphosphate

AU: arbitrary units

BACE: β-secretase

BACE1-AS: BACE1-antisense

BAF: Brg1/hBrm associated factor

BAG2: B-cell chronic lymphocytic leukemia/lymphoma 2-associated athanogene 2

BBB: blood-brain barrier

BC200: brain cytoplasmic RNA 200

BDNF: brain-derived neurotrophic factor

BER: base excision repair

BP: biological process

BS: bisulfite

BSeq: bisulfite sequencing

C: cytosine

C57BL/6 mice: C57 black 6 inbred mouse strain

CA: cornu ammonis

CAG: cytosine-adenine-guanine

cAMP: cyclic adenosine monophosphate

caspase: cysteine-dependent aspartate-directed protease

CBP: cAMP response element-binding protein binding protein

CD: control diet

Cdk5cKO mice: cyclin-dependent kinase 5 conditional knock-out mouse model

CDR: Clinical Dementia Rating

CDS: coding DNA sequence

CE: cassette exon

CEC: cerebral endothelial cell
CiEC: circulating endothelial cells
C. elegans: *Caenorhabditis elegans*
CER: cerebellum
CFC: contextual fear conditioning
CGI: CpG island
CHD: chromodomain, helicase, DNA binding
ChIP: chromatin immunoprecipitation
ChIP-Seq: chromatin immunoprecipitation sequencing
chr: chromosome
CHRM1: muscarinic acetylcholine receptor 1
CI: confidence interval
CK-p25 mice: transgenic mouse model overexpressing p25 under control of an inducible calcium/calmodulin-dependent protein kinase II a promoter
CLU: clusterin
CNE: constitutive exon
CNS: central nervous system
Co-IP: protein complex immunoprecipitation
COX: cyclooxygenase
CpG: cytosine-phosphate-guanine
CR: caloric restriction
CREB: cAMP response element-binding protein
CREBBP: CREB binding protein
CSF: cerebrospinal fluid
DAB: 3,3'-diamino benzidine tetrahydrochloride
DAC: 5-aza-2'-deoxycytidine (decitabine)
DAF-16/FOXO: dauer 16/forkhead box O
DAPI: 4',6-diamidino-2-phenylindole dihydrochloride
DG: dentate gyrus
DHbE: dihydro-beta-erythroidine
DHP: differentially hydroxymethylated position
DHR: differentially hydroxymethylated region
Dicer cKO mice: conditional Dicer1 knock-out mouse model
DMP: differentially methylated position
DMR: differentially methylated region
DNAm age: DNA methylation age
DNMT: DNA methyltransferase
DNMT3L: DNMT3-like
DP: differentiation regulated transcription factor protein (chapter 2)
DP: distal promotor (chapter 7)
DS: downstream region
dsRNA: small double-stranded RNA
DT: diphtheria toxoid
DUP: position with differentially unmodified cytosine levels
DUR: region with differentially unmodified cytosine levels
E1A: adenovirus early region 1A
E2F1: E2F transcription factor 1
EC: entorhinal cortex
ECA: enzyme complementation assay
ECD: electrochemical detection
EDAR: Early Diagnosis of AD and as marker for treatment Response
EI: exon isoforms
EID1: EP300 interacting inhibitor of differentiation 1
ELISA: enzyme-linked immunosorbent assay
EP300: E1A-binding protein P300
ERK: extracellular signal-regulated kinase
eRNA: enhancer RNA
ES: effect size
EWAS: epigenome-wide association studies
EZH: enhancer of zeste homolog (Drosophila)
f6A: N6-formyladenosine
fAD: familial AD
FAIRE: formaldehyde-assisted isolation of regulation
FC: frontal cortex
FDA: Food and Drug Administration
FDR: false discovery rate
FTD: frontotemporal dementia
FTLD: frontotemporal lobar degeneration
FTO: fat mass and obesity-associated protein
fPD: familial PD
FRM-0334: Forum Pharmaceuticals compound 0334
GABA: gamma-aminobutyric acid
GABRA: γ-aminobutyric acid receptor subunit alpha
GAD-3: gastrulation defective 3
GADD45: growth arrest and DNA damage 45
GB: gene body
GCF: granulocyte chemotactic factor
GCN: general control of amino acid synthesis
gDNA: genomic DNA
GDNF: glial cell line-derived neurotrophic factor
GDS: Global Deterioration Scale
GFAP: glial fibrillary acidic protein
GFPT: glutamine-fructose-6-phosphate transaminase
GluR: glutamate receptor
GO: Gene Ontology
GR: glucocorticoid receptor
GSK: glycogen synthase kinase
GWAS: genome-wide association studies
GWES: genome-wide epistasis study
H: histone protein, always followed by a number (for example, H3 in H3K4)
H2AX: histone protein H2A member X
hAD-MSC: human adipose tissue-derived MSC
HAEC: human aortic endothelial cells
HAT: histone acetyltransferase
HCAEC: human coronary artery endothelial cells
Hcy: homocysteine
HD: Huntington's disease
HDAC: histone deacetylase
HDACI: HDAC inhibitor
HdhQ150/Q7 mice: transgenic mouse model expressing one mutant HTT copy with 150 CAG repeats and a normal HTT copy with 7 CAG repeats

HEK293 cells: human embryonic kidney 293 cell line
HeLa cells: cell line established from cervical cancer cells
Hip: hippocampus
His: histidine
HKDM: histone lysine demethylase
HKMT: histone lysine methyltransferase
HLA: human leukocyte antigen
hm6A: N6-hydroxymethyladenosine
HMW: high molecular weight
hnRNP: heterogeneous nuclear ribonuclear protein
HPLC: high-performance liquid chromatography
HRDM: histone arginine demethylase
HSP: heat shock protein
HTS: high-throughput sequencing
HTT: huntingtin
hUCB-MSC: human umbilical cord blood-derived MSC
HuR: human antigen R
HUVEC: human umbilical vein endothelial cells
HV: hippocampal volume
I: inosine
IBA1: ionized calcium-binding adapter molecule 1
ICC: immunocytochemistry
IF: immunofluorescence
IG: intergenic region
IGF: insulin-like growth factor
IHC: immunohistochemistry
II: intron isoforms
IKK: inhibitor of kappaB kinase
i.n.: intranasally
INO: inositol requiring 80
iNPC: induced neural progenitor-like cell
i.p.: intraperitoneally
iPSC: induced pluripotent stem cell
IR: immunoreactivity
IR: intron retention (chapter 7)
IRAK: interleukin-1 receptor-associated kinase
ISH: in situ hybridization
ISWI: imitation SWI
J20 mice: transgenic mouse model expressing mutant human APP (APPK670N/M671L, V717F)
JMJD: jumonji domain containing
K: lysine (as in H3K9ac)
KAT: lysine acetyltransferase
KEGG: Kyoto Encyclopedia of Genes and Genomes
KI: knock-in
L-DOPA: L-3,4-dihydroxy-phenylalanine
lincRNA: large intergenic non-coding RNA
LINE-1: long interspersed element 1
lncRNA: long ncRNA
LRRK2: leucine-rich repeat kinase 2
LT: Escherichia coli heat-labile enterotoxin
M: methyl modification
m1A: N1-methyladenosine
m1G: N1-methylguanine
m6A: N6-methyladenosine
MALDI-TOF: matrix assisted laser desorption/ionization time-of-flight
MAP: microtubule-associated protein
MAPK: mitogen-activated protein kinase
MAPT: microtubule-associated protein tau
MAS-1: Mercia's Th2-biased adjuvant
MAT: methionine adenosyltransferase
MBP: methyl-CpG-binding domain protein
MCI: mild cognitive impairment
me: methylation (as in H3K4me3)
MeCP: methyl CpG-binding protein
MeDIP-Seq: methylated DNA immunoprecipitation sequencing
MedFG: medial frontal gyrus
MetH: methionine synthase
METTL: m6A methyltransferase-like protein
MFG: middle frontal gyrus
miR: microRNA
miRNA: microRNA
MLA: methyllycaconitine
MMSE: mini-mental state examination
MPP+: 1-methyl-4-phenyl-pyridinium ion
MPTP: 1-methyl-4-phenyl-1,2,3,6-tetrahydropyridine
MRI: magnetic resonance imaging
mRNA: messenger RNA
MSC: mesenchymal stem cells
MSK: mitogen- and stress-activated protein kinase
MS-PCR: methylation-specific PCR
mtDNA: mitochondrial DNA
mtDNMT: mitochondrial DNMT
MTG: middle temporal gyrus
MTHF: methylenetetrahydrofolate
MTHFR: MTHF reductase
MWM: Morris water maze
MXE: mutually exclusive exon
N171-82Q mice: transgenic mouse model expressing the first 171 amino acids of HTT with 82 CAG repeats
N2a: Neuro-2a
NA: not applicable
nAChR: ionotropic nicotinic ACh receptor
NAD: nicotine adenine dinucleotide
Nano-LC: nano liquid chromatography
NAT: natural antisense transcript
NB: northern blot
NC: non-CGI
ncRNA: non-coding RNA
NDM29: neuroblastoma differentiation marker 29
NEFL: neurofilament light
NeuN: Neuronal nuclei
NF-κB: nuclear transcription factor kappa B
NFT: neurofibrillary tangle
NGF: nerve growth factor
NIH: National Institutes of Health
NINCDS-ADRDA: National Institute of Neurological and Communicative Disorders and Stroke and the Alzheimer's Disease and Related Disorders

Association
NMDA: N-methyl-D-aspartic acid
NS: not specified
NS20Y cells: mouse cholinergic neuroblastoma cell line
NSE: neuron-specific enolase
NuRD: nucleosome remodeling and histone deacetylase
OR: odds ratio
oxBS: oxidative BS
p: phosphorylation (as in H3S10p)
P300: E1A-binding protein P300
PAR: promoter-associated RNA
PARP: poly[ADP]-ribose polymerase
PASR: promoter-associated short RNA
P-bodies: processing bodies
PBS: phosphate-buffered saline
PC: principal component
PC12 cells: rat pheochromocytoma-derived cell line
PCAF: P300/CBP-associated factor
PCDH: protocadherin
PcG: Polycomb-group
PCP: phencyclidine
PCR: polymerase chain reaction
PD: Parkinson's disease
PDAPP mice
transgenic mice overexpressing AP-Pind
PFC: prefrontal cortex
PGC1-α: peroxisome proliferator receptor gamma coactivator-1 alpha
piRNA: piwi-interacting RNA
PKCδ: protein kinase Cδ
PMI: postmortem interval
POLG: DNA polymerase gamma
PP: proximal promoter
PP2A: protein phosphatase 2A
PPT: protein phosphatase
PRC1: polycomb repressive complex member Bmi1
PRC2: polycomb repressive complex member EZH2
pre-miRNA: precursor miRNA
PRMT: protein arginine methyltransferase
PROMPTS: promoter upstream transcripts
PS: presenilin
PS1dE9: human PS1 deleted in exon 9 mutation
PSD: postsynaptic density protein
ptau: phosphorylated tau
PTBP: polypyrimidine tract binding protein
QQ plot: quantile-quantile plot
r: Pearson' s correlation coefficient
R: arginine (as in H3R2me)
R6/2 mice: transgenic mice overexpressing exon 1 of human HTT with an expanded CAG repeat length
RAN: Ras-related nuclear protein
Ras: rat sarcoma
rasiRNA: repeat-associated small interfering RNA
RFLP: restriction fragment length polymorphism
RISC: RNA-induced silencing complex
RNAi: RNA interference
RNAP: RNA polymerase
ROI: region of interest
ROS: reactive oxygen species
RRBS: reduced representation bisulfite sequencing
rRNA: ribosomal RNA
RT: room temperature
RT-PCR: real-time PCR
S: serine (as in H3S10p)
sAD: sporadic AD
SAH: S-adenosylhomocysteine
SAHA: suberoylanilide hydroxamic acid
SAHF: senescence-associated heterochromatin foci
SAHH: SAH hydrolase
SAM: S-adenosylmethionine
SAMP8 mice: senescence-accelerated prone mouse model
SAT-α: satellite-α
SB: sodium butyrate
SB: Southern blot (in table)
scaRNA: small Cajal body-specific RNA
SD: standard deviation
SE: standard error
SET: Drosophila Su(var)3-9 and enhancer of zeste proteins
SETDB1: SET domain bifurcated 1
SFG: superior frontal gyrus
SHE: shelf
SHMT: serine hydroxymethyltransferase
SHO: shore
SH-SY5Y cells: human neuroblastoma cell line
shRNA: short hairpin RNA
SIDAM: Structured Interview for Diagnosis of Dementia of Alzheimer Type, Multi-infarct Dementia, and Dementia of Other Etiology
siRNA: small interfering RNA
SIRT: sirtuin
SI-SD: Stereo Investigator Confocal Spinning Disk
SK-N-SH, SK-N-BE: human neuroblastoma cell lines
SLC: solute-carrier
SLK: Stouffer-Liptak-Kechris
smRNA: small modulatory RNA
SN: substantia nigra
sncRNA: small ncRNAs
snoRNA: small nucleolar RNA
SNP: single nucleotide polymorphism
snRNA: small nuclear RNA
SOD: copper-zinc superoxide dismutase
SOD1 mice: transgenic mouse model with 7 copies of the human SOD1 gene
SP: specificity factor
sPD: sporadic PD
SPF: specified pathogen free
spliRNA: splice junction-associated RNA
SPT: serine palmitoyltransferase
ss-siRNA: single-stranded siRNA
STC: superior temporal cortex
SUV39H: suppressor of variegation 3-9 homologue

SWI/SNF: switching defective/sucrose nonfermenting
SYP: synaptophysin
T: thymine
Th: threonine
TACE: TNF-α converting enzyme
TDG: thymine DNA glycosylase
TDP: TAR DNA-binding protein
TE: transposable element
TET: ten-eleven translocation
Tg19959 mice: transgenic mice over-expressing a combination of APPswe and APPind
Tg2576 mice: transgenic mice overex-pressing APPswe
THF: tetrahydrofolate
TIP60: human immunodeficiency virus type 1 transactivating protein interactive protein
tiRNA: transcription initiation RNA
TNF-α: tumor necrosis factor alpha
TOF MS: time-of-flight mass spec-trometry
tRNA: transfer RNA
TSA: trichostatin A
TSS: transcription start site
TSSa-RNA: TSS-associated RNA
U: uracil
U373 cells: human glioblastoma astro-cytoma-derived cell line
UC: unmodified cytosine
UTR: untranslated region
VPA: valproate/valproic acid
WB: western blot
WHO: World Health Organization
WT: wild-type
WTAP: Wilm's tumor-associated protein
Y: tyrosine
YAC128 mice: transgenic mouse model expressing mutant human HTT with 128 CAG repeats
YTHDF: YTH domain family

A

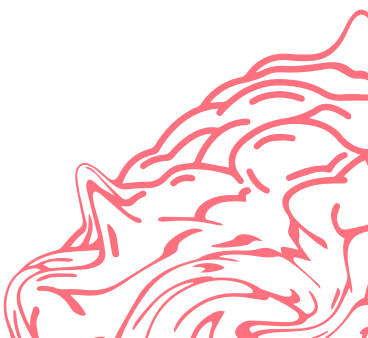

VENTURE

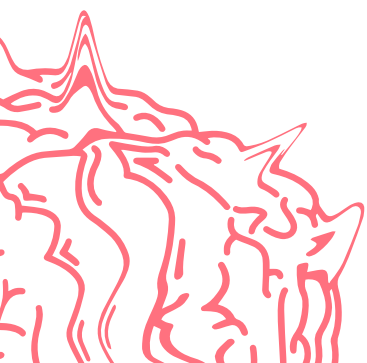

INTO

THE

EPIGENETICS

OF

AGING

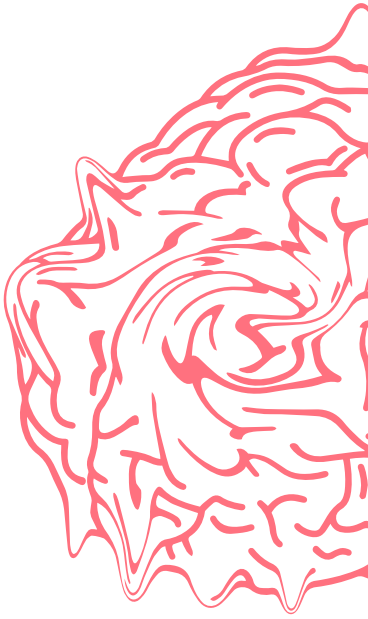

AND

ALZHEIMER’S

DISEASE